A study of linear synchronous motors in the tractive and levitative modes

Dunn, R. W.

Award date:
1988

Awarding institution:
University of Bath

A STUDY OF LINEAR SYNCHRONOUS MOTORS IN THE TRACTIVE AND LEVITATIVE MODES

A thesis submitted by

R. W. DUNN, BSc. (Hons)

For the Degree of

DOCTOR OF PHILOSOPHY

of the

UNIVERSITY OF BATH

1988

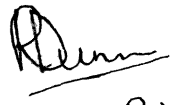

R.W.DUNN

ProQuest LLC
789 East Eisenhower Parkway
P.O. Box 1346
Ann Arbor, MI 48106-1346

SUMMARY

The work contained in this thesis describes research carried out during the development of a one quarter size (500kg) MAGLEV vehicle. The MAGLEV vehicle described differs from existing, more conventional, MAGLEV vehicles in that the type of motors used are Linear Synchronous Motors (LSMs). These motors give better power efficiency and improved compactness of the power electronics circuitry than is achieved with the linear induction motors that are conventionally used for traction in MAGLEV systems.

New power electronics circuitry is described that maintains the optimal torque angle of 90^{o} in the four corner LSMs at all times and at all tractive velocities within the design constraints of the vehicle.

New transducers for both traction and levitation are described that overcome the problems imposed by the form of the LSMs discontinuous track structure. Contactless air gap transducers have been developed and contactless pole position transducers are described.

A microprocessor based controller/data logger has been developed so that a variety of control laws could be easily investigated. This computing system provides a range of data

analysis tools which are necessary to help with the interpretation of the experimental results.

A software environment is described that allows the multi-tasking disc based microprocessor operating system, TRIPOS, to be subordinated to the time critical control programs whilst the vehicle is levitated.

Control of a single degree of freedom motor is described as a precursor to the development of the final four motor, six degree of freedom levitation controller. This allowed the validation under well defined conditions of accurate simulation programs. These simulations include an accurate representation of the power electronics current chopping action, digital transducer quantisation, digital sampling effects and the non-linear electro-magnetic force characteristics of the LSMs.

The digital implementation of a variety of linear and non-linear controllers are investigated as possible candidates for overall control of the non-linear multivariable dynamics of the levitation and guidance functions of the vehicle.

A theoretical treatment of the non-linear multivariable interactions due to unbalanced mass distribution is given. A

method involving only knowledge of the values of the steady state magnet currents for deriving a fixed gain decoupling matrix that greatly reduces interaction in the system is described. Preliminary simulation results of the decoupling effect achieved using these theoretical results are encouraging.

The practical problems of using a Variable Structure Control System (VSCS) as a possible non-linear controller that reduces interaction between the degrees of freedom are investigated. The results of this work highlights the implementation problems of this form of controller in this type of system. Many of the problems have been solved, however, as a result of this work.

Although the work contained within this thesis is oriented towards the control of a MAGLEV vehicle, some of the hardware and software developed has wider application. The results of the work on VSCS may help future use of this technique in systems where non-linear power electronics (choppers) are involved.

CONTENTS

CONTENTS CONTINUED PAGE

CONTENTS CONTINUED PAGE

CONTENTS CONTINUED PAGE

CONTENTS CONTINUED PAGE

CONTENTS CONTINUED PAGE

LIST OF SYMBOLS

da	acoustic path distance to track
dh	distance between air gap transducer and track
dw	ultra-sonic transmitter and receiver separation
EXP()	exponential function
F1-F4	linear force actuators
Ff	field coil attractive force
Fz	force in the heave direction or equivalent force at centre of geometry
Fz"	equivalent force in heave direction at centre of mass
G1-G4	corner air gaps
$G_c(s)$	linearised chopper transfer function
$G_m(s)$	linearised levitated magnet transfer function
h_0	integrator gain
h_1	proportional feedback gain
h_2	velocity feedback gain
h_3	acceleration feedback gain
Δh_1	proportional feedback switching gain
Δh_2	velocity feedback switching gain
Δh_3	acceleration feedback switching gain
hs	track sag between supports
ht	track height w.r.t. inertial frame of reference
I	current
If	LSM field coil current
Imax	maximum field coil current

LIST OF SYMBOLS

Io	mean field coil current
Is	chopper slit-width current
Iz	heave current demand
Izo	steady state heave current demand
I_ψ	roll current demand
$I_{\psi o}$	steady state roll current demand
I_θ	pitch current demand
$I_{\theta o}$	steady state pitch current demand
J_ψ	second moment of inertia about roll axis
J_θ	second moment of inertia about pitch axis
$J_\emptyset$	second moment of inertia about yaw axis
K	forward path controller gain
Ki	linearised current to force gain
Km	magnet force constant
k_r	reference signal gain
Δk_r	reference signal switching gain
Kt	vehicle structure stiffness constant for torsional twisting mode
Kz	linearised air gap positive feedback term
Lf	LSM field coil inductance
Lt	track section length
Md	multivariable decoupling matrix
Mc(s)	forward path controller matrix
Mh(s)	feedback path controller matrix
Mt	total mass of MAGLEV vehicle
Rf	LSM field coil resistance

LIST OF SYMBOLS

s	the Laplace operator
t	time
Td	time delay between ultra-sonic wave edges
Tt	asymetric torsional twisting torque
Tψ	total roll torque
Tθ	total pitch torque
TØ	total yaw torque
Tψ"	equivalent torque in roll direction at centre of mass
Tθ"	equivalent torque in pitch direction at centre of mass
TØ"	equivalent torque in pitch direction at centre of mass
V	voltage
Vf	LSM field coil voltage
Vmax	maximum battery voltage
Vt	tractive velocity of vehicle
Xl	Half of the length of the vehicle
Xw	Half of the width of the vehicle
ΔXl	distance between centre of geometry and centre of mass along the Y axis
ΔXw	distance between centre of geometry and centre of mass along the X axis
Z	air gap of vehicle or equivalent air gap at centre of geometry
Z"	equivalent air gap at centre of mass

LIST OF SYMBOLS

Zi	inertial frame of reference position of magnet
Zo	working point air gap
Zr	track relative position of magnet or air gap
Øf	LSM field coil magnetic flux
θ	angular changes in vehicle pitch about centre of geometry
ψ	angular changes in vehicle roll about centre of geometry
Ø	angular changes in vehicle yaw about centre of geometry
θ"	angular changes in vehicle pitch about centre of mass
ψ"	angular changes in vehicle roll about centre of mass
Ø"	angular changes in vehicle yaw about centre of mass
w_n	natural frequency of operation
w_t	natural frequency of oscillation of asymetric torsional twisting mode
μ_r	relative permeability
ζ	damping ratio
ζ_t	damping ratio of asymetric torsional twisting mode

LIST OF DIAGRAMS

LIST OF DIAGRAMS

LIST OF DIAGRAMS

LIST OF DIAGRAMS

LIST OF DIAGRAMS

LIST OF DIAGRAMS

LIST OF DIAGRAMS

LIST OF DIAGRAMS

LIST OF DIAGRAMS

LIST OF DIAGRAMS

LIST OF DIAGRAMS

LIST OF DIAGRAMS

LIST OF DIAGRAMS

1. INTRODUCTION

1.1. Introduction

The history of the civilised world has been shaped through the centuries by the ability of nations to transport goods and personnel efficiently. In earlier centuries there was a tendency towards personal transportation in the form of privately owned horses and other beasts of burden. With the invention of the steam engine and the subsequent development of the steam driven train guided by steel tracks along set routes, the concept of mass transportation evolved. At around this period in the development of the industrial civilisations the general population was moving away from the land, which had been the heart of the traditional agricultural economy, towards the major cities. Networks of railway tracks and canals were set up in order to improve the efficient flow of traffic between these now more centralised pockets of commerce. Outside the cities raw materials and food products were moved in bulk from the surrounding lands using commercial shipping companies rather than private transportation.

Around the beginning of this century the development of a new power unit for mechanically propelled vehicles, the internal combustion engine, had a great effect upon this move towards organised public transportation. The internal combustion engine was compact, yet powerful enough to form the basis of a motorised vehicle. This property was exploited to create a cheap form of personal and private transportation. These engines were clean, easy to run and physically small when compared to steam engines. This allowed the owner a new freedom, and they enjoyed considerable success. The petroleum by which they were powered appeared to be in ample supply and cheap.

Perhaps the major effect of the 'automobile', or 'car' as it was later called, was the reinstatement of the prevalence of private transportation as opposed to forms of mass transportation such as trains which ran on rails. This wasteful form of mobility, with hundreds more individual vehicles than necessary all travelling in the same direction, was for many years backed up by the cheap price of oil. This situation persisted until the early nineteen-seventies.

In the years leading up to the nineteen-seventies growing fears about pollution of the Earth's atmosphere, acid rain, high levels of lead in inner city areas, carbon

dioxide and carbon monoxide emissions started considerable public debate about the long term effects of the use of hundreds of millions of cars for private transportation all over the world. Added to this was the effect of the oil crises of 1973 and 1978. These crises removed, for a time, one of the prime economic arguments for the use of private cars, namely cheap oil. In some quarters these changes caused renewed interest in more efficient public mass transportation systems.

The possibility of producing an efficient and reliable means of transportation for the future was investigated simultaneously around the world, primarily in West Germany, Britain, Canada, the U.S.A., France and Japan. In Japan and West Germany the challenge has been taken up by private industry and has made steady progress throughout the last decade. The U.S.A. has had a less consistent interest and no significant practical system has resulted. Britain and France have both improved the design of their existing conventional wheeled rail mass transportation systems.

In Japan, Britain and West Germany one field in which there has been a steady growth of interest over the past fifteen years is that of magnetically levitated or suspended vehicles [1,2,3].

This thesis describes a complete strategy for both levitation and traction of a new form of magnetically levitated vehicle. In the past fifteen years many practical vehicles have been based on the use of d.c. electromagnets for electrodynamic control of levitation together with a separate set of linear induction motors for propulsion [4]. More recently it has been shown that new forms of linear synchronous motors can be used to provide both of these functions from one motor [5]. Another useful property of these new linear synchronous motors is that they provide better power factor and efficiency figures [6] than the corresponding linear induction motor based systems.

In the following section a short history of the development of the field of magnetic levitation will be given so that it can be clearly seen where the work contained in this thesis fits in.

1.2. History Of Magnetic Levitation

Basic research into the understanding of the interaction of forces between bodies was carried out by Earnshaw [7] in 1842. His work showed that two bodies could not stay in stable equilibrium if the force between them obeyed an inverse square law with respect to the distance separating them. Later, in the mid-twentieth century

Earnshaw's theorems were applied to electrostatic and magnetostatic systems. In particular Braunbek's work [8] in 1939 showed that it was possible to provide stable suspension with a permanent magnet only if part of the magnetic circuit contained materials with relative permeability 'μ_r' less than or equal to unity. From this work it can be deduced that diamagnetic materials with 'μ_r' less than unity, or superconductors with 'μ_r' equal to unity could be used to produce a stable magnetic levitation system.

Indeed, permanent magnet levitation is possible but only if some of the natural degrees of freedom of the magnets used are held steady. The principle of operation of such a system is best understood by considering a setup containing two magnets, one placed above the other, with the lower one fixed and with like poles facing one another. The repulsive force set up between the lower and upper magnet will levitate the upper magnet above the lower. However, the system is unstable unless the upper magnet is only able to move in the vertical degree of freedom. Figure 1.2.1 shows this basic configuration for permanent magnet levitation systems.

It is also possible to produce levitating forces using induced eddy currents. If a magnet is moved over a

conducting surface then Lenz's law states that an eddy current will be induced in the conductor surface such as to oppose the change of magnetic flux introduced by the magnet's motion. The interaction between the eddy current set up and the magnetic flux of the magnet will provide a repulsive force between the magnet and the conducting surface. This force may be used to overcome the downward force due to gravity to produce levitation [9].

Alternating currents in an electromagnet can be used to induce eddy currents in a conducting surface even when the electromagnet is not in motion. Figure 1.2.2 shows a system that will give a repulsive force between an electromagnet and a conducting plate.

Another method of producing levitating forces is to use controlled d.c. electromagnets. An energised d.c. electromagnet has properties similar to a permanent magnet. If unlike poles of two electromagnets are placed so that they can attract one another, or a single magnet is placed below a fixed steel support, and the excitation of the electromagnet is appropriately varied using information about the air gap between the members and also the rate of change of the air gap then stable suspension can be achieved [10]. The major difference between this and the permanent magnet system is that attractive rather than

repulsive forces are used. In addition to achieving a stable system, this arrangement allows the air gap to be varied at will by changing the equilibrium point of the control system.

Similar results can be acheived using alternating rather than direct currents in the electromagnets.

1.3. Transportation Systems

High speed, pollution free, noise free and low maintenance transportation systems have been the subject of extensive research [11,12].

A system using permanent magnets was patented by Polgreen in 1958 [13]. This was known as 'Magna rail'.This consisted of a continuous row of magnetised Barium Ferrite blocks for the track. The vehicle body had permanent magnets mounted under it which reacted against the track magnets. This system is shown in figure 1.3.1 One of the major problems with systems of this kind is the need for mechanical constraints to guide the vehicle. More complex arrangements of permanent magnets may also be used to overcome this problem. However, there are two basic drawbacks with this concept. Firstly, a permanent magnet track would be prohibitively expensive to build, and

secondly, any disturbance of the system would be followed by a long period of settling due to the lack of natural damping in the suspension system. From the passenger comfort and overall control points of view the second drawback is particularly unacceptable.

In 1966 Powell [14] suggested using cryogenic superconducting magnets and a rocket propelled sledge was built by Guderjahn in 1969 [15]. Unfortunately, this system can only levitate the vehicle once it has attained a certain velocity. This velocity is too great to be consistent with low speed urban transportation applications. In addition, as with the permanent magnet configurations, lateral and yaw disturbance recovery has been observed to be underdamped.

Electrodynamic levitation utilising a.c. excitation magnets was developed by Laithwaite [16] into the 'Magnetic River' concept. This system used a three phase induction motor with the stator unwrapped to form a linear motor. The long, linear stator with the windings along its length formed the track down which the short secondary, made of a conducting material, moved. Unfortunately, any practical magnetically levitated vehicle of this type requires relatively large air gaps which, as Eastham [17] showed, makes this dual levitation and propulsion system unreasonably expensive to run. The technology has however

been developed into a propulsion only system by providing a long secondary as the track, made from aluminium, and a short stator which is mounted on the moving vehicle. The vehicle is then levitated by other means, such as a d.c. electromagnetic system with the linear induction motor only providing propulsion.

In the last few decades, the major effort of research into magnetically levitated vehicles has been in electrodynamic d.c. magnet systems. These systems provide a reasonable air gap for a relatively low running cost. In addition, the damping of the disturbance response can be controlled, giving better ride quality and guidance. Some of the first successful efforts were made in West Germany, Japan, and Britain [1,2,3]. The basic layout of a controlled d.c. magnet suspension system is shown in figure 1.3.2. In Japan and West Germany the work has been confined to high speed intercity links and the Germans have demonstrated vehicles that can travel in excess of 400 km/hr. As previously stated, Britain has developed high speed wheeled vehicles and so has been more interested in low speed urban transportation as an application for MAGLEV. The main recent research effort in Britain has been undertaken by The University of Sussex, British Rail and The University of Bath.

1.4. Vehicle Propulsion

So far, propulsion methods have not been discussed in any great depth. In conventional vehicles, wheels are used to convert rotary motion into linear motion. Researchers have tried to develop new machines to produce linear motion so that wheels could be replaced with a non-contact propulsion system such as is required by levitated vehicles. In the past fifteen years linear induction motors [18] have received much attention. More recently, linear synchronous motors [19] have been found to be capable of producing both propulsion and levitation simultaneously.

Linear synchronous motors require only plain mild steel segments to be built into the track, instead of a continuous aluminium reaction rail as is needed with linear induction motors. The tractive forces produced by linear synchronous motors is described in reference [20]. Linear synchronous motors can operate with larger air gaps than corresponding linear induction motors [21]. The larger air gap allows greater tolerance on the track alignment and the use of cheaper steel track sections. The track for a linear synchronous motor based system should be considerably less expensive to construct and maintain.

1.5. Research At The University Of Bath

At The University of Bath a transverse flux heteropolar linear synchronous motor was built and tested [22] and its steady state characteristics were evaluated. The control of the propulsion mechanism provided by this motor was investigated by Ng [23]. This thesis describes the implementation of a complete vehicle which produces both levitation and propulsion on a real linear track. In addition, the interaction problems between the various degrees of freedom inherent in the low cost, low strength vehicle are investigated in depth and various solutions are proposed and tested. It is shown that the levitation function of the motors is adequately decoupled from the propulsion function, even though the same magnetic circuits are used for both.

The construction of a complete working vehicle has necessitated the development of specialised power electronics, digital control and data logging and analysis tools. It has also been essential to develop new forms of non-contact feedback transducers in order to obtain measurements of system variables for control of both propulsion and suspension. All these vital parts of the system are described in this thesis.

2. GENERAL DESCRIPTION OF THE LSM VEHICLE

2.1. Introduction

The study explained in this thesis is the result of the continuation of work carried out at the University of Bath that investigated a single corner simulation of a full LSM MAGLEV vehicle (SERC grant GR/A/71240). This work studied a rotating drum equivalent of the linear synchronous motor (LSM). The study described here first transferred that work into a true linear system. This used new transducers developed to measure air gap parameters and the linear position of the LSMs with respect to the track pole positions. The study was then extended to include two LSMs at one end of a full four cornered vehicle. This allowed algorithms for control of the multivariable aspects of the system to be produced. Finally, the full four cornered LSM vehicle was controlled using one LSM at each corner of the 500kg vehicle. When levitated, side position of the vehicle was controlled using d.c. side magnets for lateral guidance. These side magnets were designed to produce similar forces to those of the levitating magnets of the LSMs, producing a more balanced multivariable system.

2.2. Overall Vehicle Description

A general block diagram describing the control scheme is given in figure 2.2.1. This chapter will describe the LSMs and power electronics in some detail. The microcomputing system and the new transducers are described in chapters three and four although a summary giving the reasons for the need for new transducers is given in this chapter.

The relevant feedback control signals used to control each of the four motors and the lateral or side position were all wired back to a central control system.

The overall system controller was based on a microcomputing system. This allowed the digital implementation of a number of different control algorithms giving a flexibility of control law not achievable using any form of analogue controller. This controller was placed within the vehicle so that it was known from the outset that it could work within the electro-magnetically noisy environment. Apart from controlling the system levitation, the microcomputer was also capable of storing and helping with the analysis of the large amounts of data produced by the many transducers placed on the system. The computer ran

a software environment known as the TRIPOS operating system which could directly control large disc filing systems and had many utilities available to the user. The computing system, then, acted as a combined controller, data logger and system health monitor.

2.3. The Transverse Flux Homopolar LSM

The original design specification of the one quarter size vehicle was such that the four LSMs were to be able to levitate, in stable equilibrium, a vehicle of some 350kg in mass with a static air gap of ten millimetres. In the final vehicle which was constructed the mass had increased to nearer 500kg due to placing a lot of the control equipment on board. To compensate for this, the air gap was reduced to some seven or eight millimetres. The levitation force produced by the field coils of the LSMs was designed to balance the vehicle weight when levitating. Linear tractive accelerations of up to 0.15g ($1.5\ m.s^{-2}$) with a maximum velocity of $3m.s^{-1}$ were allowed for. This specification was thought to be consistent with a scale model of a small (2 tonne) urban passenger carrying MAGLEV vehicle. The design of the field coils was such that transient forces of up to three times that needed for stable equilibrium would be available to the controller for disturbance recovery at the maximum expected air gap of fifteen millimetres. Appendix

one gives details of the winding arrangements of the LSMs used.

A diagram of the transverse flux homopolar LSM is shown in figure 2.3.1. The motor consisted of two main iron sections and two sets of coils. These motors were designed by Dr. M.J.Balchin and constructed at the University of Bath within the School of Electrical Engineering.

The first iron part consisted of the primary flux carrying short stator, on which all the coils were wound. This component, with its coils, made up the mobile LSM that moved with the MAGLEV vehicle along the track. The track was made up of the secondary iron components, the pole pieces. These static parts were placed at a precise pole pitch apart from each other along the whole length of the two tracks towards which the whole vehicle was levitated. Figure 2.3.2. shows the complete vehicle with its full set of four LSMs. It can be seen that two tracks were required, one on each side of the vehicle and each one supporting two LSMs.

2.3.1. Tractive Mode of Operation

When the d.c. field coils were energised the flux path created produced magnetic poles of opposing polarity at either end of each pole piece. This is shown in figure

2.3.3. The polyphase current inputs to the a.c. armature windings resulted in a sinusoidally varying current magnitude along the length of each side of the LSM, that is, along each limb of the primary iron parts. These current waveforms had wavelengths that were exactly equal to the spacing of the secondary iron pieces, the pole pieces, in space. Two wavelengths were produced along the forty centimetre length of the LSM.

Thrust was produced by the interaction of the d.c. field flux and the a.c. armature winding current so that in order to produce a steady thrust the peak of the a.c. coil current waveform had to have a fixed relationship to the secondary members. As the motor operated at a constant torque angle of 90^{o} then a maximum thrust would be produced for a given magnitude a.c. current waveform in the armature coils. This fixed 90^{o} torque angle was achieved by using closed loop control with the aid of a transducer that measured the spacial position of the pole pieces with respect to the LSM. The output from this transducer was used to control the operation of the static power converter (inverter) used to supply variable frequency currents to the a.c. armature windings of the LSM.

2.3.2. Levitative Mode of Operation

The flux linking the primary and secondary members produced an attractive force. This force could be used to balance the force downwards due to gravity if the motors were positioned under the track. This provided a levitation force for the vehicle.

One of the advantages of operating the LSM at a constant torque angle of 90° was that the tractive trust and the levitating force were effectively decoupled. This was because the zero crossing point in the current waveform in the armature coils was directly under the pole pieces. This then produced no net change in the levitating force as the magnitude of the a.c. current was varied, see figure 2.3.4.

With feedback from appropriate air gap transducers it was possible to control a fast power converter (chopper) using the system controller, see figure 2.3.5. These air gap transducers measured the levitated height of the vehicle with respect to the two tracks. The current in the d.c. field winding was controlled so as to change the force/distance characteristic of the field magnet such that a stable equilibrium was reached at a particular air gap, see figure 2.3.6. This fixed the air gap between the primary

and secondary members of the LSM giving a controlled magnetic circuit such that stable contactless levitation was achieved. The mechanisms for control of the chopper are described in more detail in chapters five onwards of this thesis.

2.4. Lateral Guidance of the LSM Vehicle

Side motion of the MAGLEV vehicle was achieved using a d.c. magnet at each of the corner points of the vehicle as shown in figure 2.4.1. These small d.c. magnets were specifically designed to produce the same attractive force towards the side rails as the LSMs produced towards the pole pieces of the track. This was important when considering the multi-variable interaction aspects of the overall vehicle for control purposes and gave a more balanced system making it easier to control. These magnets were controlled using the microcomputer controller in the same way as the LSM field current. The same air gap transducers were used here as were used for levitation in order to maintain a system standard throughout the vehicle. Appendix 1. gives details of the winding arrangements of the side magnets and figure 2.4.2. shows their physical dimensions.

2.5. The Need for New System Transducers

With the introduction of the LSM as the main levitative and tractive element in a practical MAGLEV vehicle it was necessary to develop new types of system transducers. It was envisaged that the pole pieces of a full size vehicle would be mounted on the under side of concrete supports as shown in figure 2.5.1. and that for reasons of simplicity and economy these would form the only metal parts along this face.

This arrangement however would lead to problems with the non-contact transducers that have been developed over the years to supply air gap information in other MAGLEV systems. The majority of these transducers [24] used either inductance, capacitance or eddy current effects to determine the air gap and gap rate between the track and LSM. These all required a continuous metal surface from which to work so that they could measure at any point along the track as the vehicle moved. In the system described, no such continuous rail existed and it was thought better to design new transducers that did not need such constraints rather than compromise the simplicity of the basic design shown in figure 2.5.1.

In addition to the air gap transducers it was necessary to supply information about the spacial position of the track pole pieces with respect to the LSMs in order that the correct torque angle (90^{o}) of the LSM could be maintained. This also needed to be a non-contact device as the vehicle would not touch any part of the track once levitated.

Both of these transducers and other system transducers are discussed in more detail in chapter four.

2.6. System Power Electronics.

In order that full control of both levitation and propulsion could be achieved, each of the LSMs had to be supplied with a controlled field current. This current had to have a fast response on both the rising and falling edges so that adequate control of the field current could be maintained. Also, a three-phase sinusoidal armature current of controlled amplitude, with frequency and phase locked to the output of the pole position transducer, was required so that an efficient control of tractive thrust with minimal interaction with the levitation force could be produced.

2.6.1. The D.C. Field Current Chopper

The LSM field coil current was obtained from a 48V battery source which allowed unrestricted regeneration. The power converter used was a pulse width modulated (P.W.M.) chopper that used current feedback and slit-width modulation [25]. The demand signal into this chopper was an analogue voltage produced by a digital-to-analogue converter that was part of the microcomputer controller system.

Four of these choppers were used with the LSMs in order to give each LSM an independent field current. This was necessary to obtain control of all the degrees of freedom of the vehicle. These degrees of freedom are more thoroughly described in chapter five of this thesis. In addition, a further four choppers were used to control the four side magnets used for lateral guidance.

Current choppers were used as they had a faster response to changes in current demand than the alternative voltage choppers, although it was recognised that voltage choppers would give a more linear response.

The basic chopper configuration is shown in figure 2.6.1. The full battery voltage of 48V was applied across

the magnet windings such that either +48V or -48V appeared across the field coil. The field windings were found to exhibit considerable stray capacitance that could upset the operation of the slit-width modulation and so some additional inductance was added at the chopper output to ensure a predominantly inductive reactance in the chopper load.

This inductance, Lf, and the resistance of the field winding, Rf, produced the first order lag that was necessary for operation of the current chopper. The current flowing in the field coils of the LSM was measured using a Hall effect device rather than a shunt resistance so as to provide full isolation of the low voltage control circuitry from the high voltage power circuits.

The transistors of figure 2.6.1. were controlled such that the mean current in the field coils of the LSM was that required by the microcomputer controller. This was achieved by comparing the field coil current with the current demand signal from the controller and either switching the battery voltage one way or the other, +48V or -48V, using the chopper transistors.

The dynamics of the field coil, with the extra inductance, may be modelled in the Laplace domain using the

standard Laplace transform method such that the load, shown in figure 2.6.2., is given by:-

$$\frac{If(s)}{Vf(s)} = \frac{1}{(Rf+Lf.s)} \qquad 2.6.1$$

Because of the chopper action the voltage input in the Laplace domain, V(s), may either be:-

$$Vf(s) = \frac{+Vmax}{s}$$

when the battery is switched on, where Vmax=48V, or:-

$$Vf(s) = \frac{-Vmax}{s}$$

when the coil regenerates.

The chopper action may now be described in the Laplace domain so that:-

$$If(s) = \frac{\pm\ Vmax}{Lf.s(s + \frac{Rf}{Lf})} \qquad 2.6.2$$

This may be transformed to the time domain so that, starting with an initial condition of zero current in the field windings of the LSM, we have:-

2-13

$$If(t) = \frac{Vmax}{Rf}.(1-EXP(-\frac{Rf}{Lf}.t)) \qquad 2.6.3$$

This shows that the current rises exponentially towards the aiming current Imax, where:-

$$Imax = \frac{Vmax}{Rf} \qquad 2.6.4$$

with a time constant of Lf/Rf seconds. The operation of the slit width modulator was such that a window was set around the current demanded by the controller. If the current in the field coils, as detected by the Hall effect sensor, ever became greater than the maximum limit of this window, then the transistors switched so that the field coil regenerated into the battery. This effectively placed -Vmax volts across the field coil. Then the coil current would fall exponentially towards the negative aiming current of -Vmax/Rf until the lower limit of the slit width was reached. When the lower limit was reached, the battery was again switched across the coil causing the process described above to be repeated ad infinitum.

If the upper limit of the slit width is Io+Is and the lower limit is Io-Is then it can be seen that from the point when the coil regenerates into the battery the current time history is given by:-

$$If(t) = Io+Is-(Imax+Io+Is).(1-EXP(-\frac{Rf}{Lf}.t)) \qquad 2.6.5$$

Similarly, when the lower limit is reached and the battery is switched across the coil then:-

$$If(t) = Io-Is+(Imax-Io+Is).(1-EXP(-\frac{Rf}{Lf}.t)) \qquad 2.6.6$$

Figure 2.6.3 shows the time domain response of the field coil current to a step demand. From this it can be seen that the current in the coil reaches the required level much sooner than it would if a voltage chopper were used. A voltage chopper would have require approximately five field coil time constants to settle to the demand current.

The block diagram of the complete chopper system is shown in figure 2.6.4 with the circuit diagram of the base drive controller shown in figure 2.6.5. These choppers were designed specially for the LSM vehicle.

2.6.2. The A.C. Armature Current Inverter

The three phase armature currents needed by the LSMs was supplied by two current source inverters, one for each side of the vehicle. These devices employed six transistors in a conventional bridge arrangement. The inverters operated in a current feedback slit-width modulation mode. This form of inverter had been chosen for two reasons:-

1. The control circuit had to operate the LSM in a constant torque angle mode. This meant that the current waveform, particularly around the zero crossing point, was more important than the voltage waveform.
2. The LSM's air gap could vary under certain conditions. This could change the coil dynamics quite significantly. The chosen form of inverter was relatively insensitive to these parameter changes.

The primary purpose of the inverter was to produce a fixed output current waveform at a given phase angle and magnitude. A block diagram of the inverter is shown in figure 2.6.6. The use of a three wire output scheme allowed the control to be applied to only two phases, with the third current phase being obtained from the summation of these two controlled currents. This arrangement reduced the amount of

control electronics required by one third and also reduced the complexity of the task of setting up the inverter.

In order to reduce the power device switching rates, and hence keep down the power dissipation, three state operation (class ABD) was used. In this mode each of the output stages rectified, inverted or flywheeled. The algorithm for this was placed into read only memory (ROM) within the inverter switching logic. Each of the slit-width modules of figure 2.6.7 gave two outputs which provided information about the sign and magnitude of the error between the input reference, produced in response to the output from the pole position transducers, and the a.c. armature current.

The inputs to the slit-width modulators were provided by two digital sine tables held in ROMs on the control board. The addresses of these ROMs were driven by the digital outputs of the pole position transducers. The data output from the ROMs was passed through two digital-to-analogue converters. The outputs from the digital-to-analogue converters was then passed onto the modulators for comparison with the armature coil currents.

The action of each of the slit-width modulators was similar to that already described for the chopper modulators

in the previous section.

The most significant data bits of the outputs from the sine lookup tables, and the most significant bit of the digital pole position transducer output were also used in the switching logic. These signals defined the sign of the three phase currents and were used to fully describe the necessary switching function.

This type of inverter produced an output which was a close replica of the reference voltage. Thus for sinusoidal output currents, a sinusoidal reference of controllable amplitude was required. For operation of the LSM the frequency and phase angle of this sinusoidal reference had to be controlled from the output of the pole position transducer if successful synchronous operation was to be achieved.

It was also necessary for the inverter to operate at zero frequency at any point in the sinusoid (standing wave) in order that the vehicle could pull away from a standing start. Hence the sine lookup tables were driven from the pole position sensor outputs. The two lookup tables were phase shifted by 120^{o} with respect to each other as shown in figure 2.6.8.

The magnitude of the three phase currents in the a.c. armature coils was ultimately to be controlled by the central control computer. This would allow closed loop control of the vehicle velocity. This magnitude control was provided by supplying an external reference to the digital-to-analogue converters. Thus controlling the magnitudes of the three sine waves going into the slit-width modulators and hence the magnitudes of the three phase currents in the armature coils.

Only two inverters such as that described above were needed to control the tractive mode of operation of the whole vehicle. This was true, despite the fact that four LSMs were used, as the two LSMs on one side of the vehicle could be driven from one inverter so long as the phase relationship of the armature windings with respect to the track pole pieces was the same for both motors. This was achieved by accurately fixing the distance between the centres of motors on each end of the vehicle to be exactly a whole number of pole pitches. Figure 2.6.9 shows this relationship.

It was not possible to derive the supply for all four LSMs from only one inverter as the phase relationship between pole pieces of the two tracks, one on each side of the vehicle, would alter whenever a curve in the track was

encountered. This was due to the different radii of curvature of the tracks and the need to maintain a pole pitch of exactly twenty centimetres on each track as shown in figure 2.6.10.

The tractive force acting on the vehicle is determined by both the field flux density in the LSM air gaps and the three phase armature coil current magnitude. Because of this there is a coupling effect from the levitative mode of the LSM on the tractive mode. Under normal operating conditions the field flux density would not change in each of the four corner LSMs. However, if for example the mass distribution on board the vehicle were to change, or a track irregularity should occur, then the field flux density in the LSM air gap would vary. This variation in field flux density would cause a disturbance to the tractive mode force.

There are two methods available to reduce this coupling effect. Firstly, the central control computer could directly compensate the three phase armature coil current magnitude to account for the change in field coil current at each LSM. This is essentially an open loop method and does not take into account variations in other system parameters such as the air gap at each corner. Secondly, a closed loop tractive velocity or position controller could be used to maintain constant tractive performance and hence reduce the coupling

effect. Chapter 4 describes some results that show that closed loop control of the tractive mode can provide adequate decoupling of the this mode of operation of the LSM from the levitative mode of operation.

2.7. Conclusions

This chapter has described the general layout of the LSM vehicle that was designed during this research project. It has shown that there were several design constraints that were specific to the use of LSMs. It has been necessary to design specialised transducers and power electronics circuitry.

Each of the components described in the block diagram of figure 2.2.1 has been fully developed and made operational. In particular the transducers used for air gap measurement were novel, these devices are described in detail in chapter four. Chapter four also gives a detailed description of the pole position transducer and its design. This transducer allowed effective decoupling of the levitative and tractive modes of operation of the LSMs that were used.

It has been shown that a microcomputer controller was chosen as the system central control element. The reasons

for this lay in the increased flexibility that this allowed with quick and easy implementation of new control laws being simply a matter of running a different control program. The microcomputer was also ideally placed to collect and analyse all the system data. This computing system and the choice of operating system and programming language are fully discussed in the next chapter.

3. THE SYSTEM CONTROLLER AND DATA RECORDER

3.1. Introduction

When considering a suitable controller for the research LSM vehicle there were several important points to take into account:-

1. The system plant was very non-linear, which meant that any controller had to have the ability to adapt so that it could cope with variable operating conditions.
2. The dynamics of the system were relatively fast, making it necessary for the controller to arrive at quick decisions if it was non-continuous (sampled).
3. In the simplest practical magnetically levitated vehicle there were four levitation motors. However, it was likely that in a future vehicle there may be eight or more to cope with increased size and mass. Therefore, the basic structure of the controller had to be expandable.

In the past researchers have used a variety of controller types with magnetically levitated vehicles. These controllers fall into four main categories:-

1. Hardwired analogue control circuitry.
2. Analogue computer controllers.
3. Hybrid analogue / digital computer controllers.
4. Digital computer controllers.

The first two options had the disadvantage that it would have been necessary to either change the physical wiring arrangement, or at least alter the potentiometer and switch settings, in order to change the control parameters.

The hybrid analogue / digital controller offered a more automated control element, where these functions would be carried out by the digital computer component of the controller. The other advantage of the hybrid option was that it provided fast acting continuous circuitry which could be used in an adaptive controller configuration. Hybrid computers were costly, however, in comparison to the fourth possibility, that of the digital controller.

The main advantages of digital computer controllers were that they were flexible, they could be used to store and analyse data simultaneously while carrying out the control functions and they could be easily upgraded to accommodate future expansion of the LSM vehicle concept.

3.1.1. The Digital Computer As A Controller

There were several forms that a digital controller could take, these included:-

1. Mainframe computers.
2. Minicomputers.
3. Microprocessor systems.

The first two options were very expensive relative to the third possibility. Also, it was unreasonable to expect to be able to mount either of these devices locally on board the LSM vehicle. In addition, while the central processing elements of both devices were very fast, of the order of 10 million instructions per second (MIPS)), it would often be necessary to run a complex operating system (OS) to handle file storage etc. The overheads of such an OS would exclude precise event timing, and severely reduce the percentage of the central processor available to the control task. Only on the smaller mini-computers was there any access to the machine code of the processor to allow the production of high speed, efficient, low level, software.

The third option represented a field that was undergoing many advances at the time when the work described

in this thesis was done. The few years prior to this time had seen the introduction of fast, 16 and 32 bit, microprocessors. These processors could be used in single processor microcomputers, which rivalled the minicomputers in terms of raw processing speed, or as elements in multi-processor configurations that attained processing power comparable to the smaller mainframe computers. The real advantage, however, was in the vastly reduced size and cost of these devices.

The microprocessor was chosen as the central control element in the realisation of the LSM vehicle because of the flexibility, the speed and the cost effectiveness mentioned above. The limitations of using digital computers as controllers are restricted to two main areas:-

1. Limited arithmetic word size leading to quantisation error.
2. Processor speed limitation causing a reduction in the possible controller bandwidth, which might decrease the complexity of the calculations that could be processed in the given sample period.

The increased word length of the modern microprocessor overcame the first problem to a large extent, and the ever increasing processor speed (approximately 2 MIPS at the

time, with expected future increases to 8 MIPS within a year or so) made the investigation of the use of these devices, as the main control element in a system as complex as the LSM vehicle, a logical step.

3.1.2. The Digital Computer As A Data Recorder

One of the immediate advantages to be gained from the use of a digital computer as a control element was that, while controlling, it could also be instructed to collect relevant information on the performance of the LSM vehicle under various test conditions. This data could then be analysed 'on line' and conclusions drawn before further test runs were started.

There was available a range of compact hardware, SASI 'Winchester' hard disc drives and floppy disc drives, that could be used with the modern microprocessor to facilitate the collection and storage of large amounts of experimental data. Small, portable operating systems (OSs), that could maintain tens of Megabytes of hard disc existed. These OSs also supported a widening range of application software, which could be used in the observation and analysis of data taken from the research rig. Software could be developed by the researcher, using the programming languages supported by the OS, to analyse data in a variety of ways. Having these

facilities locally on the LSM vehicle with immediate access, had obvious advantages over transmitting the data to a minicomputer or mainfrain for analysis 'off line'.

3.1.3. The Choice Of Microprocessor

At the time when the choice of microprocessor was taken, there were several processors with 16 and 32 bit data word lengths in the marketplace. The best of these processors are listed below:-

		External Data Bus	Internal Data Bus	Clock Speed MHz.
1.	TMS9900	16 Bits	16 Bits	4.0 [26]
2.	TMS99000	16 Bits	32 Bits	24.0 [27]
3.	MC68000/10	16 Bits	32 Bits	8.0 [28]
4.	Z8001/2	16 Bits	16 Bits	6.0 [29]

The Texas TMS9900 had already been successfully used as a controller, to control the vehicle speed [23], in the earlier stages of the LSM development. However, the levitation function was more complex and required a more powerful processor, with a longer arithmetic word length. The TMS99000 was not in full production and also was not much of an advance on the TMS9900. The main effort had gone into increasing the bus access time, but little regard had

been given to improving upon the inferior instruction set of this processor. In order to utilise the full speed of the TMS99000 processor, it would have been necessary to use small capacity static memory chips. However, it had been decided to use large capacity dynamic memory arrays in order not to severely limit the storage capacity of the computer.

The Zilog Z8001/2 had only a 16 bit internal data bus. However, its registers were constructed so that it was possible to link them and carry out arithmetic operations of up to 64 bits accuracy. Unfortunately, the basic structure of the processor, from a software point of view, was not as good as that of the Motorola MC68000/10. The main problem arose from the lack of generality of the addressing modes available for use with different instructions. In addition, the internal state machines of the Z8001/2 were not as efficient as those of the MC68000/10, and were not microcoded to allow for future efficiency improvements. Finally, the MC68000/10 employed instruction fetch pipe-lining to improve the efficiency of the data bus usage by fetching the next instruction in parallel with the execution of the current instruction.

So, despite the apparent greater word length of the Z8001/2 a comparison previously carried out by a researcher with similar needs to the author [30], concluded that the

MC68000/10 was a better choice.

The MC68000 offered well structured machine code, with most addressing modes available with all instruction types. The internal state machines were microcoded which allowed for the possibility of future speed enhancements being carried out by the manufacturers, MOTOROLA. The basic hardware interface to the processor was well suited to running a good operating system. The processor was capable of detecting system faults, such as illegal addresses and memory protection violations, within hardware and taking appropriate action in such circumstances. This last feature was very important if the controller was to allow for the possibility of later expansion in to a multi-processor system, utilising redundancy or majority voting protection techniques for robustness.

3.1.4. The MC68000 Microprocessor System

The LSM vehicle was controlled by a digital computer in the form of a MOTOROLA MC68000 based system. The computer consisted of a set of printed circuit cards. These were developed within the Control section of the School of Electrical Engineering at the University of Bath. This system was constructed specifically for use in control and simulation applications.

The particular system configuration used, shown in figure 3.1.1, was a single processor microcomputer. It carried out three functions:-

1. Control of levitation and traction of the LSM vehicle.
2. On line recording and analysis of experimental data.
3. Software development, to produce code to carry out the above two functions.

Each of the above functions had specific hardware and software requirements. The control function required transducer and power electronics interfacing hardware, along with a good interrupt structure to achieve efficeint use of the processor power. The multi card system was based around a fast bus structure. This bus was designed to maintain maximum operating speed of the 8.0 MHz. MC68000 when running programs in the main memory.

The data recording facility required a good filing system, and the ability to execute simultaneously with the control code without significantly affecting the operation of this code. In addition, high resolution colour graphics, in the form of a graphics system based on the EF9965 colour graphics processor (EFCIS) [31], was used for visual representation and analysis of the experimental results.

Mass data storage was supplied by a SASI [32] hard disc interface, driving a 5.25 inch disc drive giving 5.5 Megabytes of hard disc storage. Removable data storage was achieved with a SHUGART [33] 8 inch floppy disc drive interface, based around a Western Digital Disc Controller chip the WD1793 [34], giving an additional 2.4 Megabytes of storage on two disc drives.

The large main memory requirements of both the above functions and the OS were met using 0.5 Megabyte Dynamic Memory cards. The memory carried out transparent error checking in order to maintain system integrity. The whole system was further enhanced by the use of transparent memory refresh for the dynamic memory cards.

The system used Direct Memory Access (DMA) between the memory cards and the disc interfaces. This function was carried out by a DMA controller card to minimise processor involvement in these repetative tasks, thus leaving the processor free to proceed, unhindered, with the control algorithm.

The whole processing system was small and portable, and was capable of being placed on board the LSM vehicle. The system could directly drive digital plotters, printers etc., situated at a distance from the LSM rig.

The plotters, printers and graphical output devices were controlled by a range of application software that was specifically developed for this processing system, the software running asynchronously to the control code as a 'background' task.

The following section looks at the requirements of the control and data logging software for support from the OS, and explains how these restrictions led to the specific choice of OS, 'TRIPOS'.

3.2. Real Time Control Software Requirements

It was envisaged that the computing system should be able to implement a wide range of fundamental controller types. Throughout the project these controllers would be compared with one another for various performance advantages and suitability for running the LSM vehicle under a variety of conditions. The forms of controller being considered at the start of the project were:-

1. Classical Full State Feedback.
2. Various forms of Partial State Feedback, with Complimentary Filtering and Forward Path Compensation.
3. Classical fixed gain matrix multi-variable

controllers.

4. Classical adaptive controllers, using multi-variable control techniques.

5. Variable Structure Control Systems (VSCS). [35]

Each of the above techniques could be implemented in software on a computer, but they each had different specific requirements. The simple classical state feedback method required no event timing, and only needed the processor to collect the transducer data and produce a current demand that was a linear combination of the instantaneous values of the transducer outputs.

However, if not all the higher states of each of the controlled outputs were available it would become necessary to implement a partial state feedback controller. This could also employ dynamic forward path observer networks. Dynamic components implemented in computer software to control real plants had to be simulated using 'Real Time' simulation techniques which required system event timing.

As the system, in practice, represented a coupled multi-variable problem, multi-variable controllers were investigated. This sort of controller required several matrix operations during each sample period, and so it was important that the software be structured to carry out

efficient matrix operations.

It was necessary that the OS that was chosen could compile, load and run code to the above specification. The OS also had to be able to support and develop the user interface, so that different test conditions could be applied by the experimenter during the test runs.

3.2.1. The Choice Of The Operating System

At the time when the control code was run, the OS that was used to develop and compile the code had to become of secondary importance. Hence, one of the major requirements of the OS was that it had to be capable of being pushed into the background giving the control code as much of the processor power as it needed during time critical control runs.

Another prime requirement was that the user should have direct access to the input / output (IO) addresses in the processor memory map. This was necessary so that transducer data could be read and current demands set for the power electronics exactly when required.

As the system was to carry out simultaneous tasks, such as data recording and terminal input the OS had to be able

to support a multi-tasking environment so that these tasks could be made to run transparently to the control programs.

One of the advantages of choosing the MC68000 microprocessor was the fast growing number of software packages available. This was due to the high interest in the capabilities of this device. At the time when the choice of support software was taken there were three main contenders as OSs for the MC68000 microprocessor, these were:-

1. CP/M-68K [36]
2. UNIX Version 7 [37]
3. TRIPOS [38]

CP/M-68K was a MC68000 version of the standard OS CP/M, designed for the older 8 bit processor, the Intel 8080. Over the years, CP/M had been ported to the newer microprocessors. However, this OS was basically only a file server for running floppy discs. Even the CP/M-68K version did not contain the structures for running a multi-tasking operating environment. In addition, it did not make good use of the interrupt structure of the MC68000.

UNIX Version 7, like all other UNIXs, was a very elegant OS for microprocessors. Unfortunately, such elegance placed demands on the system which put UNIX at a

disadvantage when it was being considered as a candidate for real time control purposes. These restrictions included:-

1. The multi-user protection, implemented under UNIX, required the use of hardware memory management [39] in order to guard against memory access violations etc. This would have slowed down the bus cycles, taking typically 1.5 times as long to complete each memory access when compared with full speed memory cycles. This reduced the effective processor speed.
2. The system IO was very highly protected under UNIX, and so to gain access to the transducers and power electronics it would have been necessary to make system requests that would have been processed in due course, but not necessarilly immediately.
3. It would have been exceptionally difficult to make UNIX take a secondary role, and would have required major alterations in the way the OS worked, which would have defeated the object of using a standard OS.

The third OS mentioned is TRIPOS, a little known OS designed at Cambridge University and latterly ported to the MC68000 system by the University of Bath Computer Science Department, in the School of Mathematics. This OS was some way between the first two OSs discussed in terms of its capabilities and represented a good compromise.

3.2.2. The TRIPOS Operating System

TRIPOS was a single user multi-tasking OS, the kernel of which contained all the necessary code to schedule a time sharing set of simultaneously active tasks. On TRIPOS all the scheduling was triggered either by hardware interrupts or packets being sent from the presently executing task to other tasks. This meant that all that was required in order to force the TRIPOS OS into the background was to withhold the interrupts and send no inter-task packets. Under these conditions the current task could maintain use of the processor for as long as it wished. Using these techniques a controlled amount of the processor power could be allowed to execute all background tasks.

TRIPOS had been developed over a number of years, and offered the features of much larger OSs, such as UNIX, without the associated overheads. Only the kernel was written in MC68000 assembly code, while all the utilities and system commands were written in the system programming language, BCPL [40]. This language will be described in more detail later, as it was used to code the user interface to the control programs run on the MC68000. The system also supported a range of programming languages including:-

1. FORTRAN
2. PASCAL
3. BASIC
4. PROLOG
5. LISP
6. ALGOL
7. BCPL

Also, there were assemblers available for a variety of microprocessors including the MC68000. The system provided a simple method of linking machine code segments to BCPL, so that high and low level code could easily be mixed.

In addition to this, application software of a high quality was available, such as REDUCE [41], a symbolic mathematics processor. This was useful for some of the theoretical work on the representation of the non-linear system developed in chapter 5 of this thesis.

Finally, the operating system provided a comprehensive 'de-bugging' task that could be used during the early stages of the control code design to check functionality.

TRIPOS's flexibility allowed the full power of the MC68000 to be released for use in the control code, while also being a powerful research tool. This led to the choice

of TRIPOS as the microprocessor OS for real time control work.

3.2.3. BCPL As A System Programming Language

In many ways BCPL bore a marked resemblance to 'C' (the system programming language of UNIX). This was because the two languages had a common evolution. Both had been derived from 'B' which was used with very early versions of UNIX, in the late 1960's and early 1970's.

BCPL, the system programming language of TRIPOS, was a block structured language and offered the advantages of formal parameter passing between the component blocks of the programs. This form of structuring gave clear definition of which blocks of code had access to which variables. BCPL had no inherent concept of data typing which at first may appear to be a serious disadvantage. For instance, there was no automatic checking on the variable types being used in a floating point operation. However, BCPL also had many positive advantages. Programming in BCPL produced very efficient, fast code and was considered as being similar to programming in assembler, except with many of the basic structures having already been written. For example, outputting a string to the console was a library routine etc. This provided an efficient environment for a programmer

to produce fast and easily maintained code.

It was felt that BCPL would be a useful language in which to write the user interface and data collection routines for the control code of the LSM vehicle. As BCPL was closely associated with the TRIPOS system it had standard routines which were available from within the language to directly access disc files.

However, BCPL did not represent a good environment in which to write the control code itself. This section of code needed accurate event timing and BCPL, unlike 'C', could not directly handle hardware interrupts. (from the system timer, for instance). For this reason it was decided to use assembly code to write the main synchronous control code which could utilise timer interrupts directly. Fortunately, interfacing BCPL to MC68000 assembly code was straight forward and relevant information could be passed from assembly code back to the BCPL user interface and data collection routines.

3.2.4. The Use Of Assembly Code, Interrupt Driven Control Programs

It was envisaged that the main control code would be written in MC68000 assembly code and that this would run at

a set sample rate which was triggered by the system timer interrupts. For this purpose the TRIPOS hardware timer interrupts were redirected. This was achieved by altering the interrupt vector in the initialisation code to go to the machine code routines that carried out the control function.

The timer interrupts on TRIPOS normally occurred once every twenty milliseconds. However, because of the fast dynamics of the LSM field coils and power electronics it was necessary to run at a much higher sample rate (of the order of one millisecond period). To deal with this, the system clock frequency was altered by the machine code to produce the required sample rate. The code then kept count of interrupts and every twenty milliseconds this code passed on an interrupt to the TRIPOS operating system, which was still resident in the main memory. This procedure allowed TRIPOS to continue operating in the background with the assembly coded LSM control routines coming in as high priority interrupt routines.

The operation of the LSM control code was observed as a percentage slow down of the OS, this percentage can be approximated to:-

(Control loop execution time / The sample period).100%

3.2.1

At the end of the test run the 'uninitialisation' code was run by the asynchronous BCPL user interface program. This caused the interrupts to be redirected back to TRIPOS and the interrupt rate to be slowed down to a rate of once every twenty milliseconds. As the control code was not receiving any more interrupts it had ceased operation and so was unloaded by the OS via the BCPL user interface. The OS once more had full control of the processor at this stage.

The software associated with the various controllers and user interfaces, together with methods of data collection will now be explained in more detail.

3.3. The Control And Data Recording Software

This section of the chapter will explain how the TRIPOS OS was used to load and run the MAGLEV control and data recording programs. It will also explain how TRIPOS was then effectively pushed into the background to release the whole computing power of the MC68000 for use with the control program structure. The section will then show how the processing priorities of the various sections of MAGLEV programs (user interface, data collection, event timing and synchronous control code) were set up to create a hierarchical structure of time sharing processes.

3.3.1. The TRIPOS Multi-Tasking Environment

During normal operation the multi-tasking TRIPOS OS ran a minimum of four tasks using a time sharing principle, namely:-

1. A Command Line Interpreter, CLI, which recognised and executed commands input via the console task, COHAND.
2. A Console Handler, COHAND. This task interfaced to the machine code interrupt routine that responded to characters sent to and received from the console.
3. A Filing System task, FILSYS, which was responsible for interfacing to the machine code driver that stored and retrieved data held on the mass storage device.
4. A Debugging task, DEBUG, used for program debugging. This task also handled major system faults such as accesses to invalid memory locations.

Each of the above tasks had a unique priority level which was used to determine whether it should be scheduled to run or not. Only one task could actually run on the processor at any one time in the time sharing environment. The basic rule used to determine which task should run was that a task could run until one of two conditions occurred.

1. The task was pre-empted by a higher priority task, that is, either a high priority task that had just been entered into the system or a higher priority task that had just received an information packet that it had been waiting for before continuing.
2. The task had sent out an information packet and was suspended awaiting the return of this packet.

In the event of the second option occurring, the next highest priority task in the task table would be run until one of the above two conditions was met again. If there were no runable tasks then the 'IDLE' task would run. This was a kernel routine generally doing nothing more than looping back on itself. This would happen, for instance, if all tasks were waiting on information packets.

A new task such as the MAGLEV control code would be run by typing the request into the console. The console handler task COHAND would package the line and send it to the CLI task which would decode the command and request the FILSYS task to collect the runable object module from the disc device. A new CLI task would then be created under which the MAGLEV program may be run, thus entering a new task into the time sharing system at a low priority. All the system tasks, CLI, COHAND and FILSYS, having completed their operations would then be suspended waiting on another interrupt or

information packet requesting more work. This would leave the MC68000 free to execute the new task. This set of events is shown in figure 3.3.1.

3.3.2. The User Interface

The basic structure of the MAGLEV software that was used with the experimental rig is shown in figure 3.3.2. As was mentioned in the previous section, and may also be seen in this diagram, the program forked at point 'A' when the User Interface software had been loaded by the TRIPOS OS. The BCPL user interface code then performed a series of operations that set up the relevant control code depending on which control law was under investigation. The code was then set running as an interrupt driven task working at a higher processing level than all other currently loaded tasks, including the user interface code.

The user interface program is responsible for the following functions:

1. It prompted the user for control code parameters.
2. It asked relevant questions of the user so that inputs to the control loops could be programmed to give specified disturbances at set times during the experimental run.

3. It loaded and initialised the interrupt driven control code, setting the control loops running. This initialisation code set all chopper outputs to zero Amperes, loaded the initial control loop parameters, altered the timer interrupt vector to point to the control code interrupt routine and set the interrupt to the correct sample period for the control program being run.

4. The BCPL user interface then entered the main loop keeping count of time and performing both automatic reference changes and keyboard controlled reference signal alterations. Thus it allowed a variety of test conditions to be investigated.

5. It detected the 'end of run' signal which could occur from a variety of sources and effect the return of the test rig to a safe condition before stopping the control code.

6. At the end of a run the 'uninitialisation' code was run. This redirected the timer interrupts once more to TRIPOS and slowed down the interrupts to the normal operating system period of twenty milliseconds. All the choppers were then switched off.

7. The recorded experimental data from the run was then converted to graphical format. This was scaled and stored to specified file locations on the mass storage disc device for later analysis.

8. The option was then given to the user of performing another experiment or exiting the program causing the unloading of both the control code and the user interface. If the latter was chosen then at this point only TRIPOS would be running on the MC68000 processor, and could be used either for further program development or experimental data analysis.

The general structure of the user interface is shown diagrammatically in figure 3.3.3. It can be seen that after point 'B' the interrupt driven control code took up a portion of the MC68000's processing time as determined by relationship 3.2.1. Also note that at point 'B' a new task running asynchronously to the user interface had been created and ran at a higher priority than the BCPL user interface due to the fact that it used high priority timer interrupts to trigger events that then ran to completion before giving up the processor for interface code execution.

The main control loop was implemented in MC68000 assembly code. A number of different programs were available depending on the control law being implemented and the experiment in progress.

The main control loop was executed once every millisecond. In this time transducer inputs were collected

and processed, the control algorithm was calculated and new current demands sent out to all the system choppers. In addition, data on the air gaps, inertial accelerations and air gap rate for all the controlled variables was logged. Any spare time left over after all these actions was the given back to the operating system for its own execution.

The later chapters in this thesis will describe particular control programs and there results in more detail.

3.4. Conclusions

This chapter has described the requirements for the controller on the experimental LSM vehicle. It has been shown that in the research environment a digital computer based controller is both possible and desirable.

In particular, the additional flexibility that the computer allows provides a good environment for investigating the properties and usefulness of various control laws.

It has been shown that a good compromise was reached to supply an operating system environment for program development and results analysis that still allowed the

execution of time critical control programs.

A method for achieving the above involving the interception of operating system timer interrupts has been discussed. This method allowed the control code to decide how much of the processor power should be allowed for the running of the operating system. During this process all operating system functions were maintained, but at a reduced speed.

4. SYSTEM TRANSDUCERS

4.1. Introduction

One of the major considerations in any control system is the method by which information about the state of the plant is to be collected. This chapter will look at the transducers that were used to provide the dynamic information with which the control laws involved made calculations to bring about adequate dynamic performance of the overall system. It will be shown that practical considerations restrict the choice of available methods of transduction and that in particular the new form of the proposed track, figure 4.1.1., made it necessary to develop a completely new set of transducers for this novel motor configuration.

Two areas are examined and are essentially treated as being independent of one another at this stage. These are, firstly, levitation transducers and, secondly, traction transducers. The latter were necessary in order to control the torque angle and speed of the linear synchronous motors under tractive conditions.

4.2. Levitation Transducers

This section will look at the possible choice of state variables and their usefulness in the control laws discussed in later chapters. It will show that there was an optimum choice of the possible feedback states that enabled the conflicting requirements of guide rail following and passenger comfort to be met. Then the techniques used to physically obtain the required system information will be discussed. Finally, the methods of synthesis of the transducers used on the experimental rig and the designs of these transducers will be described.

4.2.1. The Choice of Levitation State Variables

The parameters concerned with the levitation of a single magnet towards a track are shown in figure 4.2.1. At first it was not obvious that this single magnet model was useful for a multi-magnet structure such as a levitated platform. However, it can be assumed that to a good approximation each of the degrees of freedom on a full six degree of freedom vehicle exhibited the same open loop form as the single levitated magnet.

Given that the above was true, then it was possible to determine what was likely to lead to a good control system for the whole vehicle by examining the response of just one degree of freedom when a range of different feedback states were used. This gave an insight into the needs of the complete levitation control system.

The system had three energy storage elements. These consisted of the field coil inductance and the second order suspended mass. It was seen that the track height ht and the force Fz in the heave direction could be considered to be disturbance inputs and that several possible choices of state variables arose that could be used to control the third order levitated magnet dynamics, for instance:-

1. (Zr, $\dot{Z}r$, $\ddot{Z}r$)
2. (Zr, $\dot{Z}i$, $\ddot{Z}i$)
3. (Zr, $\dot{Z}r$, If)
4. (Zr, $\dot{Z}i$, $\emptyset f$)

Where Z represents an air gap, If a field current and $\emptyset f$ a field flux according to the list of symbols given at the front of this thesis.

The various options given by these sets of state variables were considered. The lowest order terms reflected

the prime output that was to be controlled, and so it was obvious that some measurement of the air gap, Zr, between the track and the LSM surface was necessary. The inertial position, quite apart from being difficult to measure, had no meaning when the vehicle traversed an incline or negotiated a curve. Therefore a transducer that could measure air gap relative to the track position was required.

There was more freedom of choice in the first order feedback state, as under steady state conditions $\dot{Z}r = \dot{Z}i = 0$ and for force disturbances not involving positional changes in the track surface with respect to the inertial frame of reference then $\dot{Z}r = \dot{Z}i$. However, when the various possibilities of a disturbance involving ht were considered it was found that these fell into two broad categories:-

1. Trends in track position that had to guide the vehicle over some obstacal such as a hill or a curve.
2. Inherent ht variations caused by the basic construction of the track, but with no long term trend.

The former category had to be followed by the vehicle, and so if a constant incline was followed then at steady state, $\dot{Z}r = 0$, but, $\dot{Z}i \neq 0$. In this case it appeared that $\dot{Z}r$ was the correct one to follow because as the track must be followed then the air gap had to settle to a fixed value.

This however led to a dilemma with the second category. In this case the type of disturbance was not due to a long term trend, but instead was due either to track roughness, which gave stocastically varying rate of change of air gap noise, or periodic effects such as those caused by inter-support sagging of the guide rails. For example if the vehicle had a certain tractive velocity 'Vt' and the distance between the supports was 'Lt' with a sag at the centre point between the supports of 'hs' (see figure 4.2.2.) then the vehicle would experience a periodic input disturbance even when traversing flat ground. The fundamental frequency of this disturbance would produce an input to the system described by:-

$$ht(t) = hs.SIN(\frac{2.\pi.Vt.t}{Lt}) \qquad 4.2.1$$

The problem with allowing such a disturbance to be followed by the vehicle was that passenger comfort would have been compromised. It had been shown [42] that human passengers find accelerations of greater than about 1 $m.s^{-2}$ uncomfortable. If the sag in the vehicle track described was the only disturbance applied to a MAGLEV vehicle and the vehicle was so well controlled for following the track that the effect were passed on to the occupants then the peak acceleration experienced by the passengers would have been:-

$$4\text{-}6$$

$$\frac{(2.\pi.Vt)^2.hs}{2.Lt^2} \qquad 4.2.2$$

Thus using track relative higher state feedback signals the passenger of a typical vehicle of this kind with, say, a speed of 20 $m.s^{-1}$ and a 5 millimetre sag at the mid-point of each track section of 5 metres length would have experienced accelerations of up to 1.6 $m.s^{-2}$. This would be 60% more than the acceptable maximum vibration for passenger comfort.

Similar effects could be experienced due to the stocastic roughness of the track surface. A solution to this would be to reduce the bandwidth of the controller and so reduce the high frequency following characteristics of the vehicle. However, this could lead to inadequate disturbance rejection of things like cross winds etc. It had been shown [43] that by using inertial frame of reference transducers for acceleration and velocity feedback signals a greater degree of isolation from track characteristics such as those mentioned above could be achieved. Such a system would have good disturbance rejection properties as the higher state feedback signals would try to hold the vehicle steady with respect to the inertial frame of reference. The track referenced air gap transducers together with these higher state transducers would provide good track following characteristics.

4.2.2. The Air Gap Transducer

The first concern when developing an air gap transducer was to ensure that the device would work with the envisaged track design. Figure 4.2.3 shows the manner in which the pole blocks would be supported in concrete in a full scale linear synchronous motor based vehicle. As has already been mentioned, it was important that the type of transducer chosen would work as well on the concrete parts of the track as it would on the iron parts.

Many investigators had in the past used air gap transducers that relied on eddy current effects or capacitive effects. These studies are well described in reference 44. Primarily, such transducers had been used because the guidance rails for the more commonly used linear induction motor contained continuous stretches of aluminium. No such rail existed in the track structure used in this investigation and so such devices were of no use. Alternative technologies had to be used and several were investigated by the author. These included:-

1. Light sensitive arrays.
2. Laser.
3. Ultra-sonics.

Light sensitive arrays had been used in many applications such as road texture measurement [45]. However it was considered that the designs used had a number of drawbacks. The primary problem was due to the large number of elements that had to form an array that satisfied two conflicting requirements of high resolution and large operating range (several centimetres). Studies had shown that these devices produce a quite high 'drop out' rate due to spurious reflections. They also required some considerable regularity from the reflective surface. As the intention was to differentiate the output from this transducer it was felt that the large quantisation effects caused by the limited size of a practical array precluded this form of transducer.

Various ideas involving laser light were investigated, the most elegant of which was perhaps that given in figure 4.2.4. In this proposal a servo mechanism was to be used to place the maximum reflection into the centre of a small array of light sensitive devices. This device was discarded as it was unreasonably complex for reliable use and would have led to a host of implementation problems.

The third technique that was considered was ultra-sonics. Figure 4.2.5 shows two possible ways of using

ultra-sound as a distance measuring device. In the first, the transducer is used both to transmit and receive the coaxial reflection. As the ultra-sonic medium was air, frequencies much above 100 KHz would be considerably attenuated and so relatively low frequency ultra-sonics was required. The problem with this was that using, say, a standard 40 KHz ultra-sonic transducer, the wavelength in air was approximately 8.125 mm. Sending a pulse and waiting for a return was difficult because the air gap, being around 1 cm, was less than two wavelengths. This made it difficult to stop the ultra-sonic device from transmitting in time for it to receive the reflection. One solution was to increase the gap between the transducer and the guide rail. However, this then left the further problem of transducer latency (i.e. transport lag). If, for instance, the transducer was placed 0.5 m from the guide rail then a delay of 1/330 seconds would be experienced which would have affected the usefulness of the signal in controlling a fast dynamic system such as the basically highly unstable elecro-magnetic system.

The second option shown circumvented the pulsing problem of the first transducer by using continuous ultra-sound. This device used two ultra-sonic transducer parts, one transmitted continuously and one received continuously. The basis of the method was to measure the

phase difference between outgoing and incoming waveforms. This would, as shown in figure 4.2.6, give a good measure of air gap. The only remotely mounted components had to be the two transducers and a small amount of comparator electronics used to generate a return square wave for digital comparison by purpose built circuitry situated within the MC68000 computer controller itself. The obvious objection to the device described was that if the vehicle had moved more than one half wavelength, of 40 KHz sound in air, from the track then the device output would have been ambiguous, not able to distinguish one wavelength from the next. This was indeed true, but, as will be shown, the design took this into account, producing a complete result once every 50 μs. In order to confuse the device the air gap had to decrease at a rate of one half wavelength in less than 50 μs (a closing velocity of 82.5 $m.s^{-1}$), or experience a step change of more than one half wavelength (4.125 mm). As the device was mounted typically 2 cm from the track, then the settling time of the signal after some disturbance of the air gap was approximately 0.1 ms. This is given by the speed of sound in air over the distance of 4 cm.

4.2.3. Physical Realisation of an Ultra-sonic Contactless Air Gap Measurement Transducer

A prototype transducer based on the idea described in figure 4.2.7 was constructed. Figure 4.2.8 shows the remotely mounted driving circuitry that was used to send and receive the ultra-sound. In the first prototype this consisted of a simple ultra-sonic transmitter and an ultra-sonic receiver with a comparator that transformed the 40 KHz sinusoidal received signal into a digital compatible 40 KHz TTL square wave. The circuit described is a.c. coupled at point 'A' so that any drift in the mean voltage from the ultra-sonic receiver is lost giving a zero crossing sine wave that can be turned into a square wave using a zero crossing detector in the form of an comparator.

The 40 KHz return signal was originally directly connected to the phase comparator circuitry of figure 4.2.8. However, as this circuitry was edge triggered it was very sensitive to electrical noise or 'glitches' on the digital signal. Such noise spikes occurred in the return wires that were several metres long and had to traverse parts of the vehicle that had large electro-magnetic noise levels created by the linear synchronous motors being driven by high speed current choppers.

The main effect of the noise was to cause momentary glitches on the position signal. These glitches had little effect on the main control loop by themselves. However, occasionally they would cause the digital wave boundary crossing logic to indicate that the vehicle had moved a half wavelength from the actual position at which it was situated.

The noise problem was solved by replacing the return signal wire with an optical fibre that was immune to the electro-magnetic noise. The additional circuitry of figure 4.2.9 was thus required to convert the digital signal to an optical signal and then transform it back to a standard Transistor Transistor Logic (TTL) signal at the phase comparison circuitry.

4.2.4. The Ultra-sonic Phase Detector

As has already been mentioned, with the type of technique used it was necessary to have some extra logic to extend the active range of the device to further than one wavelength. This was achieved by the use of a wave boundary crossing detector, the principle of operation of which shall now be described.

Figure 4.2.10 shows a typical set of transmitted and received ultra-sonic signals produced by a transducer such as that described. During most of the operation of the transducer, small changes in the relative phase of the two signals were detected by digitally measuring the time between corresponding rising edges on the two waveforms. This was carried out with the aid of a digital clock running at a frequency of 10.24 MHz. Problems occurred due to the fact that a movement of one whole wavelength (corresponding to an air gap change of 4.125mm) was indistinguishable from no movement at all, as shown by the dotted lines. In order to overcome this, a wave boundary detector was added to detect movements across any number of wave boundaries and to count how many wavelengths the airgap changed by as well as the position within each wavelength. Using this technique the only limitation on the range of the transducer was the attenuation of the magnitude of the return signal through the air gap medium.

It was necessary to detect the rising edge of the return signal going past either end point (i.e. a rising edge) of the transmitted signal. This was achieved by first dividing the frequency of each signal by two to give them a 1:1 mark space ratio. Figure 4.2.11 shows this situation. The period of each signal was now 50 μs, and this represented the measurement time between valid results

produced by the electronics of the transducer. Every 50 μs the time, Td, was measured as a number of pulses of the 10.24 MHz clock and this count represented the air gap being measured to an accurracy of 16 μm.

A state machine was used to detect a rising edge of the return signal which occurred before that of the reference signal. If this situation occurred then the sonic path length had decreased in size through a wave boundary. Having detected this, the wave count was decreased by one and the reference signal inverted so that the method of counting from rising edge to rising edge could be maintained. Similarly, if no rising edge in the return signal was detected before the falling edge of the reference then the sonic path length had increased by one wave length, in which case the wave counter was incremented and the reference signal was again inverted.

The state diagram of the state machine is shown in figure 4.2.12. In this case the diagram consists of four symmetric parts. This was because the reference signal was only inverted internally to the state machine and this condition was remembered by the position within the machine and not by actually inverting the reference signal. The state machine shown produced count up and count down signals for the wave counter as well as a count pulse for the phase

comparator counters. The necessary inputs were the reference and return signals and also the end count signal from the phase comparator.

The output from the sets of counters were available to the microprocessor at any time through a generalised MC68000 bus interface that was used for all of the system transducers. This circuitry will be shown later.

4.2.5. Linearity Testing of the Ultra-sonic Transducer

The remote part of the ultra-sonic transducer described in the previous section was mounted inside a metal box of dimensions as shown in figure 4.2.13. One of these devices was mounted at each air gap that was required to be measured. The devices were bolted onto brackets on the vehicle with the optic fibre return signals going to the transducer card within the microprocessor system. Initially four devices were used in the configuration so that all four lift magnets could be used to give four corner levitation but no side motion or yaw control.

It was initially thought that only one non-linearity would manifest itself. This was that due to the angular path of the acoustic path lengths as opposed to the vertical air gap that was actually being measured. The equation

describing the relationship between these two quantities is:-

$$da^2 = \frac{dw^2}{4} + dh^2 \qquad 4.2.3$$

Where 'dw' is the distance between the centres of the ultra-sonic transmitter and receiver, 'dh' is the distance from the centre point of the line joining the transmitter and receiver to the track and 'da' is the acoustic path length measured by the transducer.

It can be seen that as the ratio of dw:dh was kept reasonably small then this effect was minimal and the observed air gap dh approached the transducer output da. To test this, the transducers were given linearity tests by using accurately measured distances as references. The results of these tests are shown in figure 4.2.14. As can be seen, there was a very considerable linearity problem. It was decided that this probably originated from one of two sources:-

1. Ultra-sonic transmitter reflection interference.
2. Multiple reflection interference at the ultra-sonic receiver.

The first of these was caused when a considerable proportion of the transmitted ultra-sonic sound energy returned to the ultra-sonic transmitter and upset its oscillations. This was less likely than the second fault caused by interference which produced nulls in the wave pattern at the receiver by secondary reflections which came primarily from the centre parts between the two transducer components. This situation is shown in figure 4.2.15.

The linearity problems were overcome by using a specially designed foam rubber damper to damp out all but the primary reflection pathway. A new set of linearity results, as shown in figure 4.2.16, showed that these measures were successful and that a good linearity was achieved.

The transducers described above were used for all air gap measurement for control and data logging purposes in all subsequent work described throughout this thesis.

4.2.6. The Acceleration Transducer

Several forms of accelerometer were investigated. The considerations that were made were:-

1. Bandwidth.
2. Dynamic range.
3. Interface capabilities.
4. Compactness.
5. Power requirements.

Because of the fast chopper pole (situated around s = -200 in the s-domain) and the system poles of the vehicle being at approximately s = ±40 it was necessary to have an accelerometer that had a flat frequency response over a large frequency range. The dynamic range of the devices would have to be at least ±1.0 g in order to cover the case when the field windings in the magnets were switched off. However, the accelerations experienced during levitation should not be greater than $\pm 1 m.s^{-2}$ for any length of time. Another important consideration was the interface capabilities and power requirements. These tended to affect the compactness of the transducer. This was important because it was intended that the transducers should be mounted within the four inch square section of the vehicle structure below the motors. This is shown in figure 4.2.17

The accelerometers available fell into two main categories:-

4-19

1. Mass restoring types.

2. Piezo-electric effect types.

The devices in the first categcry used a solenoid to return a mass on a spring to a fixed position. A control circuit produced the necessary current and this current was itself a measure of the force necessary to hold the mass in the correct position. Hence the output current from the integral control loop was used as the output from the mass restoring accelerometer. Unfortunately this type of transducer did not have a very wide bandwidth as it relied on a mechanical spring arrangement to restore the mass.

The second category had a mass fixed to the surface of a piezo-electric crystal which produced a voltage proportional to acceleration when the mass was disturbed. This voltage change was amplified and presented at the output of the transducer. These devices generally had very high bandwidth, typically of the order of between 1 and 2 KHz. The output could be a.c. coupled with a very long time constant a.c. coupling filter to remove any d.c. offset. A compact version of this type of transducer was obtained from 'BRUEL and KJAER', the LOW-G ACCELEROMETER TYPE 8306. The power requirements of these devices was a single 24 volt supply. An output of 1 volt/m.s^{-2} was available with a typical bandwidth chart as shown in figure

4.2.18.

The interface to the device was simple as shown in figure 4.2.19. This circuit took the output from the co-axial lead from the transducer and converted it via an analogue-to-digital converter to a digital signal. The 8 bit signal covered a range of ± 10m.s^{-2} giving a resolution of 0.08m.s^{-2} per least significant bit. An output was produced by the accelerometer transducer circuitry once every 16 μs for use by the microprocessor. This circuitry was placed on the same circuit board as the air gap transducer and accessed via the same generalised bus interface.

Four accelerometers were provided for the stages of the research which are described in this thesis.

4.2.7. The Transducer and Chopper Interface Card

All the interface circuitry described so far as well as the chopper reference voltage generators were located in one specially designed digital interface card. The function of this card was to present the signals to the MC68000 microprocessor whenever they were required by it. It also had to allow the MC68000 to update the chopper reference voltages and hence control the field coils of the magnets used for levitation.

Each interface card was designed to have four sets each of the following:-

1. Air gap transducer phase detector.
2. Accelerometer interface.
3. Chopper output drivers and digital to analogue converters.

The first two pieces of this circuitry have been described in full. Figure 4.2.20. shows the chopper digital to analogue converter and driver circuitry. As the screened leads from this circuitry to the chopper control cards were long it was necessary to limit the bandwidth at the driver stage in order to stop the lines from ringing.

A block diagram of the interface card is given in figure 4.2.21. The interface between the various pieces of circuitry so far described and the MC68000 interface bus will now be given.

4.2.8. The MC68000 Hardware Interface

The MC68000 microprocessor implemented a standard asynchronous interlocked handshake technique in order to communicate with memory and peripheral devices. Figure

4.2.22. shows a basic read and write cycle that would be observed taking place using such a bus mechanism. It can be seen that the peripheral had to respond in order both to acknowledge that it had put the data on the data bus (read cycle) and that it had finished with the data on the bus (write cycle), and also to acknowledge its existence when an access was requested by the MC68000.

The MC68000 was a 16 bit microprocessor as far as its bus interface was concerned, although internally most operations were 32 bit operations and so it was generally known as a 32/16 bit processor. In order to allow for the possibility of 8 bit peripheral devices the manufacturers, MOTOROLA, presented two data strobes, $\overline{UDS}$ and $\overline{LDS}$. This was so that the upper and lower halves of the 16 bit memory and peripheral bus could be used independently. Figure 4.2.23. shows how this worked for a read cycle. This then allowed the interface to the 8 bit devices described in the previous sections.

An address strobe, $\overline{AS}$, was provided by the processor to indicate that the address on the address bus was valid. Also a read/write signal, R/$\overline{W}$, was used to indicate whether the access taking place was a read or write cycle.

Using this information an interface was developed as shown in figure 4.2.24 to interface the air gap transducers, accelerometers and chopper drivers to the processor for control and data logging. The devices appeared to the processor as a set of registers that could be written to (in the case of the chopper drivers) or read from at any time (for the air gap transducers and the accelerometers).

Figure 4.2.25 gives the memory map of all the devices on the interface card. The base address of the card was switch selectable so that it was possible to insert any number of cards each with its own unique address giving the capability of using an exactly similar card for side control and yaw control in a later stage of the project.

As well as air gap and/or vehicle attitude control it was also necessary to control the torque angle and possibly velocity and acceleration in the traction direction. As with the levitation transducers it proved necessary to develop a new form of transducer to do this.

4.3. Traction Transducers.

The following sections deal with the design of the contactless pole position transducer for the measurement of the physical position of a set of pole blocks with respect

to the physical position of the linear synchronous motor surfaces. This was necessary in order that a constant torque angle could be maintained during operation of the tractive mode of the linear synchronous motor.

It was important to maintain a constant torque angle of 90^{o} so that two properties of the linear synchronous motor were utilised to the full. These were:-

1. Maximum torque production.
2. Minimum interaction with the heave force produced by the field coil.

It was also desirable that the pole position transducer could provide a velocity sign to help with speed control of the vehicle in the tractive direction.

The transducer was required to operate under the following hostile conditions:-

1. Noisy electro-magnetic environment, with choppers and inverters switching continuously.
2. Outdoor environment with adverse weather conditions.
3. Operation over an air gap range of at least two centimetres.

Figure 4.3.1 gives a schematic of the track poles and their dimensions.

4.3.1. Initial Design Ideas for the Pole Position Transducer

Several different possible contactless pole position transducer types were investigated. These included:-

1. An array of coils on 'U' core formers as shown in figure 4.3.2. As the pole piece passed over the formers the coil inductance would change and give an indication of the pole position.
2. An array of coil pairs with one excited from an oscillator and the other used as a detector. As the pole piece passed over the pair the coupling would increase giving a signal in the detector dependent on the amount of coupling, see figure 4.3.3.
3. An array of coils, positioned so that they were not coupled, with a large exciter coil below them. When the edge of the pole piece passed over the top of the array the magnetic field produced by the large coil would be rotated through 90^{o} thus exciting the array at the point just below the pole piece. This is shown in figure 4.3.4.

All three of the above methods were tried. The first proved to be very insensitive except when a gap of less that 1mm was used. This technique was also prone to interference from general electro-magnetic noise. The second technique produced only small increases in coupling with air gaps of the order of two centimetres and was believed to be of no value on an electro-magnetically noisy environment. The third technique, after some modification, proved to be quite acceptable.

4.3.2. Principle of Operation of the Pole Position Transducer

The layout of the transducer developed is shown in figure 4.3.5. The source coil was excited with a 100KHz oscillator and by using a high frequency modulated signal it was observed that with proper filtering at the receiver a high degree of noise immunity resulted.

The sense coil axis was at 90^{o} to the source coil axis. Thus without the presence of a pole piece the signal picked up at the sense coil was relatively small. The construction of the transducer was such that the sense coils could have their positions individually fine tuned so that as little signal as possible was received without the presence of a pole piece.

As a pole piece traversed the coils from above, eddy currents were induced in the pole piece by the excited source coil. A secondary field was then created at the pole end that, due to the fringing effects at the edge of the pole piece, was rotated through 90^{o} with respect to the source field. As the sense coils were sensitive to a field in this direction a signal was then received by the elements in the array that lay directly beneath the pole piece.

An array of twenty sense coils placed one centimetre apart were used. This covered exactly one pole pitch of the test rig. Thus there would always be a pole piece lying at some point along the sensor array.

Each sensor coil had an associated conditioning and amplification circuit which filtered, amplified and returned a binary signal the sense of which depended on either the presence or absence of a pole piece above the sensor. Thus at any time most of the sensor outputs would be logic '0' indicating that no pole piece was currently above the sensor, whilst a small section of contiguous sensors would have a logic '1' indicating that a pole piece was directly above them.

The number of sensors indicating that a pole piece was present would vary with the air gap produced by the levitation control circuitry and possibly with perturbations in the height of the track. The centre of the contiguous section of logic '1's was taken to always represent the centre point of a pole piece.

In order to make this set of twenty signals useful to the main inverter circuitry and the MC68000 control processor, it was necessary to carry out a small amount of local signal processing. This signal processing at all times gave the centre position of the pole piece to an accuracy of one fourtieth of a pole pitch. The sensor array was fixed relative to the vehicle structure and so the pole piece position relative to the linear motor armature coils was able to be determined by this local processor.

The overall schematic of the transducer operation is shown in figure 4.3.6.

4.3.3. Pole Piece Transducer Analogue Circuitry

As is suggested by figure 4.3.5. the output from each sense coil went into an individual card in a rack of twenty signal conditioning cards. The function of each of these cards was to extract the information from its corresponding

sensor as to the presence, or otherwise, of a pole piece. The circuit used for this is shown in figure 4.3.7. The first part of the circuit was a high pass filter to reject 'mains hum' etc. This was followed by a high-Q filter with a peak at 100kHz, the oscillation frequency of the excited source coil. There was then a gain stage before the signal was rectified and passed through a low pass filter to produce a d.c. level dependent on the magnitude of 100kHz signal picked up by the sense coil. The final stage was a magnitude comparator with an adjustable input for setup purposes so that the transducer could be calibrated.

Each sense coil was tuned to 100 KHz by use of a parallel capacitor placed across the sense coil. The output from each of the twenty sensor cards was connected to both the local processor card and also an array of light emitting diodes for quick visual display during setup. Figure 4.3.8. shows the interface circuitry for both these functions. In the case of the local processor a TTL compatible signal is produced.

4.3.4. Pole Piece Position Transducer Local Processor

The main function of the local processor was to release the central MC68000 control processor from the time

consuming task of signal processing so that it could get on with the system control and data logging tasks. It was the task of the small local processor system to collate the outputs from the twenty transducers and produce a single six bit binary number that always represented a valid pole position along with a validation bit to qualify the result as being true. This output was used to directly control the phase angle of the inverters and thus maintained a constant torque angle in the linear synchronous motor. As was decribed in chapter two, this led to the condition where the linear synchronous motor was always in synchronism. This essentially provided self commutation thus producing a very efficient tractive mode of operation.

4.3.5. Local Processor Hardware

A block diagram of the local processor hardware is shown in figure 4.3.9. This shows a very basic processor system of minimal configuration. Almost any small 8-bit microprocessor would have been powerful enough to do the task necessary. The RCA1802 was chosen primarily because, being of CMOS technology, it was unlikely to generate significant magnitudes of power rail noise that would have upset the sensitive sense coil circuitry. The RCA1851 parallel input/output (PIO) device was used to collect the twenty inputs from the sensor detection circuitry. The

RCA1852 output port was used to indicate the value of the processed pole piece position result and also to indicate the validity of the result. One kilobyte of Random Access Memory (RAM) and two kilobytes of Erasable Programmable Read Only Memory (EPROM) were provided for work space and permanent program store respectively. One switch pack was used to allow a manual input of the torque angle offset of the linear synchronous motor with respect to the pole piece position. The processor would read this switch pack and use it to give a fixed offset to the transducer output, thus allowing manual setup.

4.3.6. Local Processor Software

The software implemented on the RCA1802 local processor for the pole piece position transducer had three basic functions to carry out:-

1. Collect and collate the twenty logic levels on the input port.
2. Determine that a valid configuration was present.
3. Produce a valid position of the centre point of the pole detector and set the 'valid' flag, or, use the last valid result and reset the 'valid' flag if an invalid patterm existed on the sensor returns.

The set of twenty pole piece sensor coils could be conceptually thought of as being in a continuous ring, see figure 4.3.10. This was achieved by 'rolling' up a track section so that sensor one was adjacent to sensor twenty. It could now be seen that the only valid configuration was with a single group of one or more sensors detecting a pole piece in their vicinity and all other sensors in the 'off' state. This requirement formed the basis of the 'health monitoring' that was continually carried out during the operation of the transducer. If at any stage more than one group of sensors was 'on' then the last recorded valid result was returned instead of faulty data and the 'valid' flag was reset to indicate both that there was a fault and that the present result was out of date. A result obtained from ambiguous data was never returned. Likewise, if all sensors were 'on' or all sensors were 'off' then the data was invalid.

If an odd number of sensors were 'on', then the pole piece position was assumed to be the central sensor position. As it was also quite possible for an even number of transducers to be 'on', then the pole position could be given as the midway point between two sensors. This gave a total of fourty possible pole piece positions for the data returned from the twenty sensors. The minimum resolution of the device was therefore one fourtieth of 20cm i.e. 0.5cm. Figure 4.3.11. shows a variety of transducer states and the

associated outputs from the local processor.

The first version of the transducer software that was developed is shown in block diagram form in figure 4.3.12. This figure shows all the features described at the beginning of this section. The program formed an endlessly cycling loop that was continuously executed, with an initialisation portion that was only executed once. Sections 3 to 6 formed the intelligent health monitoring, sections 7 and 8 calculated the pole piece position and made one final check for ambiguous groups of sensors being 'on'. Finally, the 'valid' flag was set and a new set of data was produced.

There were several problems with this initial approach to the software, which were:-

1. The program took more than 4ms to operate.
2. The calculation time was very variable depending on the validity of the sensor output.
3. No allowance was made for an external offset to be made to the result so that the distance between transducer and linear synchronous motor face could be adjusted for.

There were two basic problems associated with the above. Firstly, the slow calculation time, in excess of 4ms,

meant that, given the designed maximum velocity of 20 metres per second, the vehicle could have moved by up to 80mm during the period of calculation. This could have been overcome by adjusting the transducer output using a vehicle velocity signal to correct for the delay. However, the second problem of variable calculation time of the transducer output precluded this possibility. Thus, over the range of velocities experienced by the vehicle, the torque angle could shift by up to 40% of one pole pitch. This was not acceptable.

An alternative program was developed which utilised a very fast technique to collect and collate the data from the RCA1851 PIO. This alternative approach is shown in figure 4.3.13. In this case, rather than reading the bits from the input port one by one and carrying out expensive processing on each, the data was read in in parallel 8 bit batches on to a stack. Then a very efficient sub-program was used to extract the data from the stack and count the 'on' sensors and their positions. By this technique, only three machine code instructions were used on each of the sensor values except when an 'on' to 'off' or an 'off' to 'on' transition occurred in the sequence. If a transition occurred a separate routine was used that remembered the position and detected invalid signal returns. This program always took the same time to calculate the result and was quite fast,

taking only 0.25ms to run. This approach meant that even at the top vehicle speed the calculation time would still give a result to within 1cm accuracy.

The result was scaled up from a number between 0 and 39 to a 6 bit number between 0 and 63 so that it could be more easily used with the hardware of the inverter. An additional section in this program was used to add an offset of between 0 and 63 into the final result.

A full listing of the program used in the final transducer local processor is given in Appendix two.

4.3.7. Pole Piece Position Transducer Testing and Performance.

The amplifier, filter and comparator card used with each of the twenty sense coils have been frequency response tested up to 150Hz using a vibrating aluminium plate with no detection of failure. This repesented 150 pole pieces passing a given point in 1 second, i.e. a vehicle speed of 30 metres per second.

The excitation frequency of 100kHz, used for the excitation coil, was chosen so that it was both well removed from significant inverter and chopper harmonics as well as

being well above the maximum pole speed of 100 pole pieces per second on a vehicle moving at 20 metres per second with a pole pitch of 20cm.

The transducer has been operated in the presence of high electro-magnetic noise generated by the MAGLEV vehicle choppers and field coils, with no sign of deterioration in the accuracy of the result produced. No invalid configurations of sensors reporting 'on' conditions were registered during these test that were attributable to the electro-magnetic environment.

It was determined that an extended excitation coil was necessary in order to achieve consistantly good results at the leading and trailing edges of the transducer. It was also necessary to mount two 'dummy' sense coils at the ends of the array of sensor coils in order to maintain a uniform flat field at these points.

Also, it was necessary to introduce an aluminium plate covering half of each sense coil to shield it from spurious 100kHz modulated magnetic fields set up in various metallic parts of the test rig that were in close proximity to the transducer. The final dimensions of the sense coils and its fixture to the MAGLEV vehicle is shown in figures 4.3.14. and 4.3.15.

4.3.8. Pole Piece Position Transducer Conclusions

A new form of contactless pole piece position transducer has been developed which allows the linear synchronous motors to be used in the design of a magnetically levitated vehicle. The problems of reliability in a noisy electro-magnetic environment have been overcome using modulated eddy current effects. The transducer speed has been improved by the development of a very efficient data processing program. The transducer used a local CMOS microprocessor to pre-process the collected data, thus removing this task from the main MC68000 MAGLEV control processor. A signal was produced that was compatible with both the digital armature coil inverter and the MC68000 microprocessor.

This transducer is one of the final building blocks for the practical implementation of the linear synchronous motor based MAGLEV vehicle described in this Thesis. Appendix three gives the setting up procedures used.

In order to test the effectiveness of the decoupling between the levitative and tractive modes of operation of the MAGLEV vehicle that should have been provided by maintaining the torque angle at 90° a series of experiments

were conducted. Firstly, a simple tractive control loop was implemented by feeding back the pole piece position signal to the main control computer. The position signal and a digitally differentiated velocity signal were used to form a tractive position control loop. When a continuous ramp was demanded at the reference input to the control loop the MAGLEV vehicle was to attain a constant velocity along the track. The field flux during these tests was provided by levitating the vehicle to an air gap of 7 millimetres. The levitation control loops are discussed in depth in chapters 5, 6 and 7. The field flux provided the reaction field against which the armature coils pulled. The main control computer produced an output signal that was fed to the inverter to control its current magnitude thus controlling the tractive force of the vehicle. The closed loop dynamics of the tractive controller were set so that the loop had a natural frequency of oscillation of 10 radians per second and a damping ratio of 1.0.

The first set of tests involved requesting the MAGLEV vehicle to track two different velocity demands while the levitated height was maintained constant at 7 millimetres by the levitation controllers. The results of these tests are presented in figures 4.3.16 and 4.3.17. It can be seen from figures 4.3.16(b) and 4.3.17(b) that the MAGLEV vehicle's tractive position accurately kept pace with the input

demands shown in figures 4.3.16(a) and 4.3.17(a). Figures 4.3.16(c) and 4.3.17(c) show that the levitated air gap remained constant as the vehicle travelled first one way and then the other way along the track. This showed that the 90^{o} torque angle was maintained by the pole piece position transducer and that this effectively decoupled the levitative mode of operation of the vehicle from changes in the tractive velocity, i.e. changes in the armature coil currents.

Significant amounts of noise were observed on the tractive position of the vehicle as measured by the pole position transducer. This was due to the use of the noisy digitally differentiated velocity signal derived from the pole position transducer output. These velocity signals are shown in figures 4.3.16(d) and 4.3.17(d).

It was also noted that while there was always some noise present on the levitated air gap measurement, the noise was more severe when the vehicle was at a stand-still. This effect was due to the excitation of track harmonics by the levitation control loop. The noise reduced while the vehicle was in motion because the resonant frequencies of various sections of the track were different and so when the vehicle was moving it never spent long enough near a particular resonance to excite it. This effect is discussed

along with the levitation controllers in the later chapters of this thesis.

The tests were then repeated, but with a change in the levitated air gap of 1 mm introduced while the MAGLEV vehicle was moving. This was representative of a step disturbance caused by a 1 millimetre misalignment of the track. The results of this experiment are shown in figures 4.3.18 and 4.3.19. The effect on the tractive performance due to the changes in air gap were observed to be minimal. This demonstrated that the introduction of a controller for tractive position had decoupled the effects of levitation disturbances from the tractive mode of operation of the MAGLEV vehicle.

4.4. Conclusions

A new set of system transducers have been developed to meet the needs of the new motors and track structure used in the development of a Linear Synchronous Motor based MAGLEV vehicle.

An ultra-sonic air gap transducer that produced a digitally compatible result once every 50 μs to a resolution of 16 μm and with a range of several metres has been developed. These devices made no special requirements on the

properties of the surface that they were measuring the distance from.

Shaft mounted accelerometers, again digitally compatible, giving a result every 16 μs to an accuracy of $0.08 m.s^{-2}$ have been used to provide absolute second derivative feedback signals. Digital integration of this signal produced an inertial frame of reference first derivative (velocity) feedback signal of exceptional quality. Digital differentiation of the air gap transducer output gave a poorer quality gap rate signal with a resolution of $0.016 m.s^{-1}$ that was relative to the track position.

Traction transducer needs have been met with the development of the contactless pole position transducer that used eddy current effects to detect pole pieces.

These transducers were considered adequate for this initial research work into the practical implementation of a MAGLEV vehicle using Linear Synchronous Motors.

5. THE NATURE OF THE CONTROL PROBLEM

5.1. Introduction

This chapter investigates the form of the control problem with particular reference to the choice of control variables and the inherent coupling between controlled parameters. Initially, a simple linear force actuated model with three spacial degrees of freedom is presented and it is shown that the coupling between the controlled modes of a rigid four cornered vehicle is dependent on both the mass distribution and the location of the force actuators.

The discussion then considers similar effects in a more practical six degree of freedom model, with force actuators for levitation, guidance and traction. The effects of variable mass distribution and the location of the plane of action of the force actuators is investigated and it is also shown that there are further vehicular degrees of freedom that need to be considered.

It is shown that at least one of the vehicular degrees of freedom, due to asymmetric torsional twisting of the vehicle body, is open loop unstable and therefore must be

included in the control scheme, thus increasing the scope of the model to seven controlled degrees of freedom.

The effect of replacing the idealised force actuators with practical electro-magnets is then investigated. It is shown that these non-linear devices again complicate the multi-variable coupling in the plant. It is demonstrated that these problems may be overcome, maintaining sufficient isolation between the controlled modes, by use of classical multi-variable design techniques. Further to this, a general solution is presented that may be used as the basis for an adaptive multi-variable controller that can adjust to suit a wide range of operating conditions. This makes the possibility of a centralised controller dealing purely in terms of vehicle attitude a practical proposition.

5.2. Linear Models

Before any specific method for levitation of the whole vehicle is developed it is necessary to produce an accurate description of the open loop plant. In the past, several research teams have published work in this area and an accurate summary of this work is given in reference 44. However, by far the majority of these works concentrated on controlling the corner air gaps and did not try to treat the vehicle as one centralised control problem. In doing this

the problem is simplified from the design point of view, but the multi-variable interactions of the control loops, brought about by conflicting demands, cause the system to be less stable than the design would otherwise predict.

5.3. The Rigid Vehicle Model

The simplest possible representation of a vehicle is that of a rigid four cornered structure, using idealised linear force actuators to control the levitation. Initially it was useful to restrict the vehicle so that it could not move in the two translational degrees of freedom in the plane of the force actuators (side and forward motion). It was then possible to investigate basic mechanical coupling in the plant structure. Such a structure is shown in figure 5.3.1. At this stage in the analysis a set of restrictions was imposed on the model to allow this fundamental coupling to be observed. The effects of relaxing these conditions is demonstrated as the model is extended towards the end of this chapter.

5.3.1. Coincident Centre of Geometry and Centre of Mass

Consider the schematic of figure 5.3.1 with the following set of preconditions:-

1. The centre of geometry and the centre of mass of the vehicle are coincident.
2. The vehicle is assumed to tilt (roll and pitch) through only small angles.
3. The structure is suspended from a rigid and flat track.
4. Only three degrees of freedom exist. These are heave, roll and pitch.
5. The vehicle is symmetric and actuated by four idealised force actuators, F1-F4, one placed at each corner.
6. The total mass of the vehicle, Mt, is concentrated in four equal portions, one at each corner.

The first analysis looks at the natural response of the air gaps, G1-G4, to the applied forces from the actuators, F1-F4. The motion at the corners of the rigid structure may be described by a transformation of the motion of the vehicle body about the centre of mass. Using assumption 1 and 2 from the above list, it is easily shown that for small angular changes in pitch, 'θ', the effect on the air gap G1 is given by:-

$$\Delta G1 = -X1.\mathrm{Sin}(\theta) \qquad \ldots\ldots 5.3.1$$

As 'θ' in any practical system will not be greater than a few milli-radians, it is possible to approximate and say that for small pitch changes:-

$$\Delta G1 = -X1.\theta \quad (\text{as } \text{Sin}(\theta) \rightarrow \theta \text{ for small } \theta) \qquad \ldots\ldots 5.3.2$$

The same argument may be applied for small changes in roll angle, 'ψ', and extended to include all four air gaps G1-G4. Therefore, by also taking into account heave mode changes in position of the centre of mass, it can be stated to a good approximation that:-

$$G1 = Z - Xw.\psi - X1.\theta \qquad \ldots\ldots 5.3.3$$

$$G2 = Z + Xw.\psi - X1.\theta \qquad \ldots\ldots 5.3.4$$

$$G3 = Z + Xw.\psi + X1.\theta \qquad \ldots\ldots 5.3.5$$

$$G4 = Z - Xw.\psi + X1.\theta \qquad \ldots\ldots 5.3.6$$

Alternatively represented in matrix form as:-

$$\underline{G} = \begin{bmatrix} 1 & -Xw & -Xl \\ 1 & Xw & -Xl \\ 1 & Xw & Xl \\ 1 & -Xw & Xl \end{bmatrix} . \underline{G}' \qquad \ldots\ldots 5.3.7$$

Where

$$\underline{G} = [\ G1 \quad G2 \quad G3 \quad G4\ ]^T$$

and

$$\underline{G}' = [\ Z \quad \psi \quad \theta\ ]^T$$

If the vehicle mass is 'Mt', and the second moments of inertia about the two rotational axes, 'ψ' and 'θ', are '$J\psi$' and '$J\theta$' respectively, then the principles of linear and angular momentum yield three second order differential equations relating to the coordinate system placed at the centre of mass, such that:-

$$Mt.\frac{\delta^2 Z}{\delta t} = -(F1 + F2 + F3 + F4) + Mt.g \qquad \ldots\ldots 5.3.8$$

$$J\psi.\frac{\delta^2 \psi}{\delta t} = (F1 - F2 - F3 + F4).Xw \qquad \ldots\ldots 5.3.9$$

$$J\theta.\frac{\delta^2\theta}{\delta t} = (F1 + F2 - F3 - F4).X1 \qquad \ldots\ldots 5.3.10$$

Where 'g' is the gravitational constant.

Using the Laplace transform method, the above three equations may be re-written as:-

$$Z(s) = \frac{-1}{s^2.Mt}.(F1(s) + F2(s) + F3(s) + F4(s) - Mt.g) \qquad \ldots\ldots 5.3.11$$

$$\psi(s) = \frac{Xw}{s^2.J\psi}.(F1(s) - F2(s) - F3(s) + F4(s)) \qquad \ldots\ldots 5.3.12$$

$$\theta(s) = \frac{X1}{s^2.J\theta}.(F1(s) + F2(s) - F3(s) - F4(s)) \qquad \ldots\ldots 5.3.13$$

Or:-

$$\underline{G}'(s) = \frac{1}{s^2}.\left[\begin{bmatrix} \frac{-1}{Mt} & \frac{-1}{Mt} & \frac{-1}{Mt} & \frac{-1}{Mt} \\ \frac{Xw}{J\psi} & \frac{-Xw}{J\psi} & \frac{-Xw}{J\psi} & \frac{Xw}{J\psi} \\ \frac{X1}{J\theta} & \frac{X1}{J\theta} & \frac{-X1}{J\theta} & \frac{-X1}{J\theta} \end{bmatrix}.\underline{F}(s) + \begin{bmatrix} g \\ 0 \\ 0 \end{bmatrix}\right] \qquad \ldots\ldots 5.3.14$$

Where

$$\underline{G}'(s) = [\ Z(s)\ \ \psi(s)\ \ \theta(s)\ ]^T$$

And

$$\underline{F}(s) = [\ F1(s)\ \ F2(s)\ \ F3(s)\ \ F4(s)\ ]^T$$

From equations 5.3.7. and 5.3.14. it may be shown that:-

$$\underline{G}(s) = \frac{1}{s^2}\left[\begin{bmatrix} 1 & -Xw & -Xl \\ 1 & Xw & -Xl \\ 1 & Xw & Xl \\ 1 & -Xw & Xl \end{bmatrix}\begin{bmatrix} \frac{-1}{Mt} & \frac{-1}{Mt} & \frac{-1}{Mt} & \frac{-1}{Mt} \\ \frac{Xw}{J\psi} & \frac{-Xw}{J\psi} & \frac{-Xw}{J\psi} & \frac{Xw}{J\psi} \\ \frac{Xl}{J\theta} & \frac{Xl}{J\theta} & \frac{-Xl}{J\theta} & \frac{-Xl}{J\theta} \end{bmatrix}.\underline{F}(s) + \begin{bmatrix} g \\ g \\ g \\ g \end{bmatrix}\right]$$

..... 5.3.15

By application of the restrictive conditions 5. and 6, as set out above, it can be seen from figure 5.3.1 that:-

$$J\psi = Mt.Xw^2$$

..... 5.3.16

and

$$J\theta = Mt.Xl^2 \qquad \ldots\ldots 5.3.17$$

Substituting these values into 5.3.15. the equation reduces to:-

$$\underline{G}(s) = \frac{1}{Mt.s^2}.\left[\begin{bmatrix} -3 & -1 & 1 & -1 \\ -1 & -3 & -1 & 1 \\ 1 & -1 & -3 & -1 \\ -1 & 1 & -1 & -3 \end{bmatrix}.\underline{F}(s) + \begin{bmatrix} Mt.g \\ Mt.g \\ Mt.g \\ Mt.g \end{bmatrix}\right] \qquad \ldots\ldots 5.3.18$$

It may now be seen that even with all the restrictive conditions imposed there is a large cross-coupling effect between the gaps at given corners and the forces applied at other corners, as indicated by the non-zero off-diagonal elements in equation 5.3.18. Furthermore, the above matrix is singular indicating that it is not possible to control the air gaps independently from one another. In practical terms it can be seen why this is so; if the track is flat and a change in only one of the air gaps is required then it would be necessary to bend the vehicle chassis in order that the other three air gaps remain the same. The rigid body analysis does not allow for such bending. Likewise, if the track were warped, the vehicle would also have to warp in order to maintain the fixed air gaps at each corner. Some

investigators [44] have worked around this problem using a variety of techniques including:-

1. Using a non-rigid vehicle body, allowing the vehicle to warp dynamically on uneven track sections.
2. Mounting the levitation magnets onto a secondary suspension system, allowing this to dynamically take up any warping.
3. Using only nominal air gaps with a type zero controller so that the steady-state errors that the controller achieves reduces the chassis warp.

The problems with using the above techniques are two-fold. Firstly, moving mechanical parts are introduced into the system causing an increase in failure due to long term stress. Secondly, the suspension systems used improve the steady-state coupling at the expense of complicating the dynamic air gap coupling terms. It would be better if a set of control variables were chosen such that adequate track following is maintained and the variables are mechanically independent of each other at steady-state.

There were several possible choices of control variables. One fundamental point to notice was that at this point in the discussion, as there were only three degrees of freedom, it was necessary to chose only three variables

for control. This condition was broken in the previous attempt to look at four air gaps and so led to the singular matrix of equation 5.3.18. Possible candidates for control of the levitation were:-

1. Three air gaps, leaving one uncontrolled.
2. Two average air gaps at each end, and the pitch angle of the vehicle.
3. The centre of geometry coordinates, heave, roll and pitch.

Only one of these is discussed here, the control of the centre of geometry coordinates. For these parameters the action of the force actuators is easily understood, as is the effect of the removal of restrictive condition 1.

Equation 5.3.14. may be rearranged by replacing the force vector, $\underline{F}(s)$, by a transformed vector of forces and torques about the centre of geometry coordinates, such that:-

$$Fz(s) = -(F1(s) + F2(s) + F3(s) + F4(s)) \quad \ldots\ldots 5.3.19$$

$$T\psi(s) = Xw.(F1(s) - F2(s) - F3(s) + F4(s)) \quad \ldots\ldots 5.3.20$$

$$T\theta(s) = Xl.(F1(s) + F2(s) - F3(s) - F4(s)) \quad \ldots\ldots 5.3.21$$

So that:-

$$\underline{F}(s) = \frac{1}{4}\begin{bmatrix} -1 & \frac{1}{Xw} & \frac{1}{Xl} \\ -1 & \frac{-1}{Xw} & \frac{1}{Xl} \\ -1 & \frac{-1}{Xw} & \frac{-1}{Xl} \\ -1 & \frac{1}{Xw} & \frac{-1}{Xl} \end{bmatrix}.\underline{F}'(s) \quad \ldots\ldots 5.3.22$$

Where

$\underline{F}'(s) = [\ Fz \quad T\psi \quad T\theta\ ]^T$

$T\psi$ is the torque about the Y-axis, and

$T\theta$ is the torque about the X-axis.

Using equation 5.3.22. with equation 5.3.14. then:-

$$\underline{G}'(s) = \frac{1}{s^2}.\left[\begin{bmatrix} \frac{1}{Mt} & 0 & 0 \\ 0 & \frac{1}{J\psi} & 0 \\ 0 & 0 & \frac{1}{J\theta} \end{bmatrix}.\underline{F}'(s) + \begin{bmatrix} g \\ 0 \\ 0 \end{bmatrix}\right] \quad \ldots\ldots 5.3.23$$

This matrix represents a totally decoupled system so long as the force actuators are operated through the matrix

given in 5.3.22. Furthermore, relaxing restrictive condition 6. will now only affect the effective gains of the three independent control loops, as it will adjust the ratio of Mt, $J\psi$ and $J\theta$ with respect to one another. The control vector $\underline{G}'(s)$ is a linear function of the air gaps as given by equation 5.3.7. In any closed loop control system for this vehicle each element of the force vector $\underline{F}'(s)$ will be a suitable linear function of the states of the elements of the control vector $\underline{G}'(s)$.

It has been shown that by choosing the centre of geometry variables for the control vector it is possible to accommodate any ratio of vehicle mass to second moment of inertia about the rotational axis, which eliminates the restriction that the mass be concentrated at the corners in order to maintain reduced coupling. A vehicle designed along these principles need not bend in order to traverse an uneven track section.

5.3.2. The Effects of Non-coincident Centre of Geometry and Centre Of Mass

Now consider the effects of the relaxation of restrictive condition 1., as mentioned above. This may be expected to occur due to the movement of passengers or uneven loading of cargo. The system that arises is given in

figure 5.3.2, which shows that the centre of mass, Cm, has now moved away from the centre of geometry, Cg, by an amount ΔXw along the X-axis and $\Delta X1$ along the Y-axis. The vehicle inertia matrix about the centre of geometry is now non-diagonal leading to system coupling about the chosen control vector $\underline{G}'$, placed at the centre of geometry. It is now necessary to introduce a further coordinate system based at the centre of mass, at which point the inertia matrix is diagonal, such that:-

$$\underline{G}''(s) = \frac{1}{s^2}.\left[\begin{bmatrix} \frac{1}{Mt} & 0 & 0 \\ 0 & \frac{1}{J\psi} & 0 \\ 0 & 0 & \frac{1}{J\theta} \end{bmatrix}.\underline{F}''(s) + \begin{bmatrix} g \\ 0 \\ 0 \end{bmatrix}\right] \quad \ldots\ldots 5.3.24$$

Where

$$\underline{G}''(s) = [\ Z'' \quad \psi'' \quad \theta''\ ]^T$$

And

$$\underline{F}''(s) = [\ Fz'' \quad T\psi'' \quad T\theta''\ ]^T$$

The force vector $\underline{F}''(s)$, however, no longer obeys equations 5.3.19.-5.3.22., but is now given by figure 5.3.2. as:-

$$\underline{F}''(s) = \begin{bmatrix} -1 & -1 & -1 & -1 \\ Xw1 & -Xw2 & -Xw2 & Xw1 \\ X12 & X12 & -X11 & -X11 \end{bmatrix} . \underline{F}'(s) \qquad \ldots\ldots 5.3.25$$

Where

$$Xw1 = Xw + \Delta Xw, \qquad Xw2 = Xw - \Delta Xw$$

$$X11 = X1 + \Delta X1, \qquad X12 = X1 - \Delta X1$$

The transformation from centre of mass coordinates to centre of geometry coordinates may be written as:-

$$\underline{G}'(s) = \begin{bmatrix} 1 & -\Delta Xw & \Delta X1 \\ 0 & 1 & 0 \\ 0 & 0 & 1 \end{bmatrix} . \underline{G}''(s) \qquad \ldots\ldots 5.3.26$$

Equations 5.3.24-26 show that the extent of the system coupling that will occur due to non-coincident centre of mass and centre of geometry for the open loop plant described in the last section is:-

$$\underline{G}'(s) =$$

$$\frac{1}{s^2}.\left[\begin{bmatrix} 1 & -\Delta Xw & \Delta Xl \\ 0 & 1 & 0 \\ 0 & 0 & 1 \end{bmatrix}\begin{bmatrix} \frac{1}{Mt} & 0 & 0 \\ 0 & \frac{1}{J\psi} & 0 \\ 0 & 0 & \frac{1}{J\theta} \end{bmatrix}\begin{bmatrix} -1 & -1 & -1 & -1 \\ Xw1 & -Xw2 & -Xw2 & Xw1 \\ X12 & X12 & -X11 & -X11 \end{bmatrix}.\underline{F}(s)\right.$$

$$\left. + \begin{bmatrix} 1 & -\Delta Xw & \Delta Xl \\ 0 & 1 & 0 \\ 0 & 0 & 1 \end{bmatrix}\begin{bmatrix} g \\ 0 \\ 0 \end{bmatrix}\right]$$

..... 5.3.27

Using equation 5.3.22. to create the force vector $\underline{F}'(s)$ yields the final coupled system equations. This analysis assumes that the system is to be controlled about its centre of geometry, so that:-

$$\underline{G}'(s) =$$

$$\frac{1}{s^2}.\left[\begin{bmatrix} \frac{1}{Mt} & \frac{-\Delta Xw}{J\psi} & \frac{\Delta Xl}{J\theta} \\ 0 & \frac{1}{J\psi} & 0 \\ 0 & 0 & \frac{1}{J\theta} \end{bmatrix}\begin{bmatrix} 1 & 0 & 0 \\ -\Delta Xw & 1 & 0 \\ \Delta Xl & 0 & 1 \end{bmatrix}.\underline{F}'(s) + \begin{bmatrix} g \\ 0 \\ 0 \end{bmatrix}\right]$$

..... 5.3.28

Therefore:-

$$\underline{G}'(s) =$$

$$\frac{1}{s^2}\cdot\left[\begin{bmatrix} \frac{1}{Mt}+\frac{\Delta Xw^2}{J\psi}+\frac{\Delta Xl^2}{J\theta} & -\frac{\Delta Xw}{J\psi} & \frac{\Delta Xl}{J\theta} \\ -\frac{\Delta Xw}{J\psi} & \frac{1}{J\theta} & 0 \\ \frac{\Delta Xl}{J\psi} & 0 & \frac{1}{J\theta} \end{bmatrix}\cdot\underline{F}'(s)+\begin{bmatrix} g \\ 0 \\ 0 \end{bmatrix}\right]$$

..... 5.3.29

These equations show that there is interaction from the roll and pitch modes on the heave mode, but there is no coupling between the roll and the pitch modes themselves. As will be shown in the next chapter an open loop system with this relatively simple form of coupling may be totally decoupled by classical multi-variable control techniques. This essentially involves altering the values in equation 5.3.22 so that when it is introduced into equation 5.3.27 the resulting coupling matrix is diagonal. The form of the closed loop multi-variable controller is as shown in figure 5.3.3. In practice it is necessary to know the values 'ΔXw', 'ΔXl', 'Mt', 'Jψ', and 'Jθ' in order to create an adequate decoupling matrix, 'Md'. It is possible either to make 'Md' a fixed gain decoupling matrix or use an adaptive controller that is able to identify the above parameters 'on line' and continually adjust the decoupling matrix to cope with changing variables in the system. In the case given it can

be shown[41] from equation 5.3.29 that the suitable fixed gain decoupling matrix is:-

$$Md = \begin{bmatrix} 1 & \frac{\Delta Xw Mt}{J\psi} & \frac{-\Delta Xl Mt}{J\theta} \\ \Delta Xw & 1+\frac{\Delta Xw^2 Mt}{J\psi} & \frac{-\Delta Xw \Delta Xl Mt}{J\theta} \\ -\Delta Xl & \frac{-\Delta Xw \Delta Xl Mt}{J\psi} & 1+\frac{\Delta Xl^2 Mt}{J\theta} \end{bmatrix} \quad \ldots\ldots 5.3.30$$

To give an idea of the approximate values in this decoupling matrix that are associated with a practical system, consider a system with the following parameters:-

$Mt = 400$ Kg $Xw = 0.5$ m

$J\psi = 75$ Kg.m^2 $Xl = 1.0$ m

$J\theta = 300$ Kg.m^2 $\Delta Xw = 0.3$ m

$\Delta Xl = -0.3$ m

These closely resemble the parameters of the experimental rig, except the ΔXw and ΔXl values introduced to simulate an off-centred mass in the system. Using equation 5.3.29 this gives a coupled system such that:-

$$\underline{G}'(s) = \frac{1}{s^2}.\left[\begin{bmatrix} 0.004 & -0.004 & -0.001 \\ -0.004 & 0.013 & 0.0 \\ -0.001 & 0.0 & 0.003 \end{bmatrix}.\underline{F}'(s) + \begin{bmatrix} g \\ 0 \\ 0 \end{bmatrix}\right] \quad \ldots\ldots 5.3.31$$

The values in the decoupling matrix, Md, are:-

$$Md = \begin{bmatrix} 1.0 & 1.6 & 0.4 \\ 0.3 & 1.48 & 0.12 \\ 0.3 & 0.48 & 1.12 \end{bmatrix} \quad \ldots\ldots 5.3.32$$

As the system between the force vector [Fz, Tψ, Tθ]^T and the output vector [Z, ψ, θ]^T is dynamically decoupled by the introduction of the above matrix, Md, the forward path controller matrix and feedback matrix, Mc(s) and Mh(s), may be designed for the individual performance of each of the three systems.

A simulation of the simple force actuated platform was used to demonstrate the effect of this decoupling, each control loop having been designed to be predominately second order with a damping ratio of 0.5 and a natural frequency of oscillation of 20 radians per second. The roll and pitch controllers were set to have a steady state value of 0.0 radians at their outputs. Figure 5.3.4 shows that the effect on the roll and pitch for this system was slight when a step disturbance was applied to the air gap. Such a response would result from the vehicle passing onto a track irregularity. The effect of the small roll and pitch movements on each of the four air gaps at the vehicle corners was also slight. This would tend to indicate that

although there is some system coupling, it is small and would not cause either instability or unacceptable transient responses. However, it may be seen that if the three control loops are not matched, as is shown in figure 5.3.5 then this results in a considerable transient cross coupling from the heave mode onto the roll and pitch modes. It may also be seen from this diagram that the air gap responses were considerably different. This was due to the slower roll and pitch control loops being unable to respond quickly enough to the independent forces applied by the faster heave mode controller. In this case the control loops were designed for the following responses:-

$\zeta z = 0.5 \quad Wnz = 20.0 \text{ rad.s}^{-1}$

$\zeta \psi = 0.5 \quad Wn\psi = 10.0 \text{ rad.s}^{-1}$

$\zeta \theta = 0.5 \quad Wn\theta = 10.0 \text{ rad.s}^{-1}$

Where

ζz is the damping ratio for the heave mode.

$\zeta \psi$ is the damping ratio for the roll mode.

$\zeta \theta$ is the damping ratio for the pitch mode.

Wnz is the natural frequency of oscillation for the heave mode.

$Wn\psi$ is the natural frequency of oscillation for the roll mode.

$Wn\theta$ is the natural frequency of oscillation for the pitch mode.

The control loops implemented were based on full state feedback with an additional integrator in the forward path as shown in figure 5.3.6. The feedback parameters for each of the control loops formed the elements of the diagonal feedback matrix Mh(s). A further linear lag was added to give a simulation of the dynamics of the magnet coils that would form the force actuators in any real system. Also, a force disturbance due to the effects of gravity was added to the heave mode as shown by equation 5.3.29.

Figure 5.3.7 shows the responses of the system under the same conditions as that of figure 5.3.5 except that the decoupling matrix specified by equation 5.3.32 has been added into the system as Md. It may now be seen that all the system coupling has ceased to exist, although there is an off-centred mass and the control system is attempting to control the centre of geometry such that the lift forces are apportioned correctly so that they do not excite the roll and pitch modes.

At this stage in the analysis the value of decoupling the relatively small coupling effects may not be clear. However, it should be considered that this analysis assumes idealised force actuators which do not have non-linearities due to air gap changes. In reality, the small mismatches in the air gaps caused by the roll and pitch disturbances will

affect the force actuators and therefore must be minimised. Indeed, as is shown later, even in a non-linear system this decoupling matrix will reduce coupling.

It has been shown that for a general three degrees of freedom model of a levitated vehicle, with random mass distribution, there exists a simple decoupling matrix that can be used to enhance the performance of the force actuated model. In reality, however, the vehicle is to be totally free and so all six spacial degrees of freedom must be controlled.

5.4. Extension of the Model to Six Spacial Degrees of Freedom

The previous section showed a form of analysis that led to an accurate model for a rigid levitated platform using linear force actuators. This analysis may be extended to cover the more practical case when restriction 4 of section 5.3.1. is eliminated. It is necessary to decouple the natural mechanical interaction present in the six degrees of freedom case so that the practical vehicle may respond to the many types of disturbance that it is likely to meet in any real environment. These disturbance types include:-

1. Centripetal forces due to cornering.
2. Heave forces due to guide rail irregularities.
3. Tractive interaction with levitation during acceleration.
4. Cross winds and drag effects.

The system under these conditions may be more accurately modelled by the schematic shown in figure 5.4.1. Notice that the centre of mass is allowed to move with respect to the centre of geometry and that it is also able to move away from the plane of the heave force actuators. Also notice that now instead of four force actuators there are eight. In the complete MAGLEV vehicle there would be twelve actuators. However, in this analysis, the four tractive forces of the practical system have been combined into two pairs as it is envisaged that they would always be driven in this manner. Similarly, the side forces at each end of the vehicle would in practice be produced by the four side magnets, one facing outwards on each corner and pulling on the side rails. These would always be driven in pairs, one pair at each end of the vehicle. The tractive forces, then, are modelled by F7 and F8. The side forces are F5 and F6 which act horizontally at the centre of each end of the vehicle at a vertical displacement of ΔXs from the plane of action of the vertical lift forces F1, F2, F3 and F4.

As in the previous sections of this chapter, the actual measured parameters will be the air gaps G1-G4 for heave, roll and pitch and G5-G6 for side motion at each end of the vehicle. A hypothetical measurement device, G7, measures the motion along the guide rail in the 'Y' direction. For the purposes of levitation there is no need to control this motion, although it is necessary to include the effect of F7 and F8 in the analysis in order to allow the coupling effect of the tractive forces on the levitation control to be understood. There is one more additional parameter, JØ, which represents the second moment of inertia of the vehicle about the 'Z"' axis.

Firstly, it is necessary to define some coordinate system vectors that apply to the diagram shown. These are:-

$$\underline{G} = [\ G1\ \ G2\ \ G3\ \ G4\ \ G5\ \ G6\ \ G7\ ]^T$$

$$\underline{G}' = [\ Z\ \ X\ \ Y\ \ \psi\ \ \theta\ \ \emptyset\ ]^T$$

$$\underline{G}'' = [\ Z''\ \ X''\ \ Y''\ \ \psi''\ \ \theta''\ \ \emptyset''\ ]^T$$

There are corresponding force vectors given by:-

$$\underline{F} = [\ F1\ \ F2\ \ F3\ \ F4\ \ F5\ \ F6\ \ F7\ \ F8\ ]^T$$

$$\underline{F}' = [\ Fz\ \ Fx\ \ Fy\ \ T\psi\ \ T\theta\ \ T\emptyset\ ]^T$$

$$\underline{F}'' = [\ Fz''\ \ Fx''\ \ Fy''\ \ T\psi''\ \ T\theta''\ \ T\emptyset''\ ]^T$$

Where Fz, Fx and Fy are forces along the three axes Z, X and Y. $T\psi$, $T\theta$ and $T\phi$ are torques about the three rotational axes Z, X and Y with origin at the centre of geometry Cg. Similarly, the components of $\underline{F}''$ relate to the coordinate system with an origin at the centre of mass of the vehicle Cm.

Now it is seen from figure 5.4.1. that there exists a transformation matrix between $\underline{G}'$ and $\underline{G}$. A transformation matrix between $\underline{G}''$ and $\underline{G}'$ also exists such that:-

$$\underline{G} = Mgg'.\underline{G}' \qquad \ldots\ldots 5.4.1$$

and

$$\underline{G}' = Mg'g''.\underline{G}'' \qquad \ldots\ldots 5.4.2$$

Where

$$Mgg' = \begin{bmatrix} 1 & 0 & 0 & -\Delta Xw & -\Delta Xl & 0 \\ 1 & 0 & 0 & \Delta Xw & -\Delta Xl & 0 \\ 1 & 0 & 0 & \Delta Xw & \Delta Xl & 0 \\ 1 & 0 & 0 & -\Delta Xw & \Delta Xl & 0 \\ 0 & 1 & 0 & -\Delta Xs & 0 & \Delta Xl \\ 0 & 1 & 0 & -\Delta Xs & 0 & -\Delta Xl \\ 0 & 0 & 1 & 0 & \Delta Xs & 0 \end{bmatrix} \qquad \ldots\ldots 5.4.3$$

and

$$Mg'g'' = \begin{bmatrix} 1 & 0 & 0 & -\Delta Xw & \Delta Xl & 0 \\ 0 & 1 & 0 & \Delta Xh & 0 & -\Delta Xl \\ 0 & 0 & 1 & 0 & -\Delta Xh & \Delta Xw \\ 0 & 0 & 0 & 1 & 0 & 0 \\ 0 & 0 & 0 & 0 & 1 & 0 \\ 0 & 0 & 0 & 0 & 0 & 1 \end{bmatrix}$$

..... 5.4.4

It is also possible to extend, to six degrees of freedom, equation 5.3.24, such that:-

$$\underline{G}''(s) = \frac{1}{s^2}.(Mg''f''.\underline{F}''(s) + \underline{g})$$

..... 5.4.5

where

$$\underline{g} = [\, g \;\; 0 \;\; 0 \;\; 0 \;\; 0 \;\; 0 \,]^T$$

and g is the gravitational constant, and also:-

$$Mg''f'' = \begin{bmatrix} 1/Mt & 0 & 0 & 0 & 0 & 0 \\ 0 & 1/Mt & 0 & 0 & 0 & 0 \\ 0 & 0 & 1/Mt & 0 & 0 & 0 \\ 0 & 0 & 0 & 1/J\psi & 0 & 0 \\ 0 & 0 & 0 & 0 & 1/J\theta & 0 \\ 0 & 0 & 0 & 0 & 0 & 1/J\emptyset \end{bmatrix}$$

..... 5.4.6

The forcing vector, $\underline{F}''(s)$, may be produced by a linear combination of the force vector $\underline{F}(s)$ so that the force vector about the centre of mass is given by:-

$$\underline{F}''(s) = Mf''f.\underline{F}(s)$$

..... 5.4.7

where

$$Mf''f = \begin{bmatrix} -1 & -1 & -1 & -1 & 0 & 0 & 0 & 0 \\ 0 & 0 & 0 & 0 & 1 & 1 & 0 & 0 \\ 0 & 0 & 0 & 0 & 0 & 0 & 1 & 1 \\ Xw1 & -Xw2 & -Xw2 & Xw1 & Xhs & Xhs & 0 & 0 \\ X12 & X12 & -X11 & -X11 & 0 & 0 & -\Delta Xh & -\Delta Xh \\ 0 & 0 & 0 & 0 & X12 & -X11 & Xw1 & -Xw2 \end{bmatrix}$$

..... 5.4.8

Where

$Xw1 = Xw + \Delta Xw$

$Xw2 = Xw - \Delta Xw$

$X11 = X1 + \Delta X1$

$X12 = X1 - \Delta X1$

and

$Xhs = \Delta Xh - \Delta Xs$

From equations 5.4.2 to 5.4.8 it can now be seen that,

$$\underline{G}'(s) = \frac{1}{s^2}.Mg'g''(Mg''f''.Mf''f.\underline{F}(s) + \underline{g})$$

which reduces to:-

$$\underline{G}'(s) = \frac{1}{s^2}.(Mg'g''.Mg''f''.Mf''f.\underline{F}(s) + \underline{g}) \quad \ldots\ldots 5.4.9$$

In the real system the force signals for each of the elements of the force actuator vector, $\underline{F}$, may be derived from the desired centre of geometry force vector, $\underline{F}'$, without regard for the fact that there is a displacement, ΔXs, from the plane of the X and Y axes of the side forces F5 and F6 or any compensation for the non-coincidence of the centre of mass and the centre of gravity. The conversion from the centre of geometry forces to actuator forces is then given by:-

$$\underline{F} = Mff'.\underline{F}' \quad \ldots\ldots 5.4.10$$

where

$$Mff' = \begin{bmatrix} -1/4 & 0 & 0 & 1/4Xw & 1/4Xl & 0 \\ -1/4 & 0 & 0 & -1/4Xw & 1/4Xl & 0 \\ -1/4 & 0 & 0 & -1/4Xw & -1/4Xl & 0 \\ -1/4 & 0 & 0 & 1/4Xw & -1/4Xl & 0 \\ 0 & 1/2 & 0 & 0 & 0 & 1/2Xl \\ 0 & 1/2 & 0 & 0 & 0 & -1/2Xl \\ 0 & 0 & 1/2 & 0 & 0 & 0 \\ 0 & 0 & 1/2 & 0 & 0 & 0 \end{bmatrix}$$

..... 5.4.11

This matrix, Mff', is an extension of that given in equation 5.3.22 to include the side force and traction actuators. By substituting equation 5.4.11 into equation 5.4.9 the total coupling matrix of the system is obtained such that:-

$$\underline{G}'(s) = \frac{1}{s^2}.(Mg'g".Mg"f".Mf"f.Mff'.\underline{F}'(s) + \underline{g})$$

..... 5.4.12

It should be noted that as the transformation matrix Mff' is not a perfect conversion between the $\underline{F}'$ force vector and the $\underline{F}$ force vector then this will introduce some additional interaction due to the forces F5 and F6 not being in the plane of the levitation forces F1 to F4. It is also seen that this may be corrected for by altering the second

column of Mff', so that the roll torque produced about the Y-axis in response to forces F5 and F6 is corrected for by the co-ordinated action of F1 to F4. Thus:-

$$Mff' = \begin{bmatrix} \frac{-1}{4} & \frac{\Delta Xs}{4Xw} & 0 & \frac{1}{4Xw} & \frac{1}{4Xl} & 0 \\ \frac{-1}{4} & \frac{-\Delta Xs}{4Xw} & 0 & \frac{-1}{4Xw} & \frac{1}{4Xl} & 0 \\ \frac{-1}{4} & \frac{-\Delta Xs}{4Xw} & 0 & \frac{-1}{4Xw} & \frac{-1}{4Xl} & 0 \\ \frac{-1}{4} & \frac{\Delta Xs}{4Xw} & 0 & \frac{1}{4Xw} & \frac{-1}{4Xl} & 0 \\ 0 & \frac{1}{2} & 0 & 0 & 0 & \frac{1}{2Xl} \\ 0 & \frac{1}{2} & 0 & 0 & 0 & \frac{-1}{2Xl} \\ 0 & 0 & \frac{1}{2} & 0 & 0 & 0 \\ 0 & 0 & \frac{1}{2} & 0 & 0 & 0 \end{bmatrix}$$

In the system described, it may now be seen that the total coupling matrix for a six degrees of freedom force actuated model is given by:-

$$\underline{G}'(s) = \frac{1}{s^2}.(Mp\underline{F}'(s) + \underline{g}) \qquad \ldots\ldots 5.4.13$$

and

$Mp = Mg'g".Mg"f".Mf"f.Mff'$

so that

$$Mp = \begin{bmatrix} A & -\frac{\Delta Xh\Delta Xw}{J\psi} & -\frac{\Delta Xh\Delta Xl}{J\theta} & -\frac{\Delta Xw}{J\psi} & \frac{\Delta Xl}{J\theta} & 0 \\ -\frac{\Delta Xh\Delta Xw}{J\psi} & B & -\frac{\Delta Xw\Delta Xl}{J\emptyset} & \frac{\Delta Xh}{J\psi} & 0 & -\frac{\Delta Xl}{J\emptyset} \\ -\frac{\Delta Xh\Delta Xl}{J\theta} & -\frac{\Delta Xw\Delta Xl}{J\emptyset} & C & 0 & -\frac{\Delta Xh}{J\theta} & \frac{\Delta Xw}{J\emptyset} \\ -\frac{\Delta Xw}{J\psi} & \frac{\Delta Xh}{J\psi} & 0 & \frac{1}{J\psi} & 0 & 0 \\ \frac{\Delta Xl}{J\theta} & 0 & -\frac{\Delta Xh}{J\theta} & 0 & \frac{1}{J\theta} & 0 \\ 0 & -\frac{\Delta Xl}{J\emptyset} & \frac{\Delta Xw}{J\emptyset} & 0 & 0 & \frac{1}{J\emptyset} \end{bmatrix}$$

..... 5.4.14

where

$$A = \frac{1}{Mt} + \frac{\Delta Xw^2}{J\psi} + \frac{\Delta Xl^2}{J\theta}$$

$$B = \frac{1}{Mt} + \frac{\Delta Xh^2}{J\psi} + \frac{\Delta Xl^2}{J\emptyset}$$

$$C = \frac{1}{Mt} + \frac{\Delta Xh^2}{J\theta} + \frac{\Delta Xw^2}{J\emptyset}$$

Several points of interest arise from the above result. Firstly, the value ΔXs is not involved in the interaction. This is due to the modified matrix Mff' that now takes the offset into account. Also, it should be recognised that in most practical vehicles ΔXw at least, and in most cases ΔXl,

will be zero as the vehicle will tend to be symmetrically loaded about the Y-axis and the X-axis. The inclusion of ΔXw and ΔXl is maintained only to preserve generality. As in the previous section this matrix, Mp, may be inverted to form a decoupling matrix, Md, the forward path decoupling in a multi-variable form of controller as shown in figure 5.4.2. As in the previous section, Mc(s) and Mh(s) are diagonal forward path controller and state feedback matrices respectively. These may now be designed to give each of the six control loops the desired performance independently of each other.

In the case of the experimental rig, the following parameters are approximately correct and give some idea of the decoupling matrix values that would be necessary.

$\Delta Xw = 0.0$ m $\quad \Delta Xl = 0.0$ m $\quad \Delta Xh = 0.1$ m

Mt = 400.0 Kg $\quad J\psi = 75.0$ Kg.m^2 $\quad J\theta = 300.0$ Kg.m^2

$J\emptyset = 300.0$ Kg.m^2

Therefore:-

$$Mp = \begin{bmatrix} 0.0025 & 0.0 & 0.0 & 0.0 & 0.0 & 0.0 \\ 0.0 & 0.00383 & 0.0 & 0.0013 & 0.0 & 0.0 \\ 0.0 & 0.0 & 0.00283 & 0.0 & -0.0003 & 0.0 \\ 0.0 & 0.0013 & 0.0 & 0.013 & 0.0 & 0.0 \\ 0.0 & 0.0 & -0.0003 & 0.0 & 0.003 & 0.0 \\ 0.0 & 0.0 & 0.0 & 0.0 & 0.0 & 0.003 \end{bmatrix}$$

The matrix of equation 5.4.14, Mp, was inverted using a symbolic arithmetic processing program, REDUCE-3, to give the general six degree of freedom force actuated model decoupling matrix, Md, where:-

$$Md = \begin{bmatrix} 1 & 0 & 0 & \frac{\Delta XwMt}{J\psi} & -\frac{\Delta XlMt}{J\theta} & 0 \\ 0 & 1 & 0 & -\frac{\Delta XhMt}{J\psi} & 0 & \frac{\Delta XlMt}{J\emptyset} \\ 0 & 0 & 1 & 0 & \frac{\Delta XhMt}{J\theta} & -\frac{\Delta XwMt}{J\emptyset} \\ \Delta Xw & -\Delta Xh & 0 & 1+\frac{(\Delta Xh^2+\Delta Xw^2)Mt}{J\psi} & -\frac{\Delta Xl\Delta XwMt}{J\theta} & -\frac{\Delta Xh\Delta XlMt}{J\emptyset} \\ -\Delta Xl & 0 & \Delta Xh & -\frac{\Delta Xl\Delta XwMt}{J\psi} & 1+\frac{(\Delta Xh^2+\Delta Xl^2)Mt}{J\theta} & -\frac{\Delta Xh\Delta XwMt}{J\emptyset} \\ 0 & \Delta Xl & -\Delta Xw & -\frac{\Delta Xh\Delta XlMt}{J\psi} & -\frac{\Delta Xh\Delta XwMt}{J\theta} & 1+\frac{(\Delta Xl^2+\Delta Xw^2)Mt}{J\emptyset} \end{bmatrix}$$

..... 5.4.15

For the particular case of the experimental rig with the parameters shown above, this yields:-

$$Md = \begin{bmatrix} 1 & 0 & 0 & 0 & 0 & 0 \\ 0 & 1 & 0 & -0.5\dot{3} & 0 & 0 \\ 0 & 0 & 1 & 0 & 0.1\dot{3} & 0 \\ 0 & -0.1 & 0 & 1.05\dot{3} & 0 & 0 \\ 0 & 0 & 0.1 & 0 & 1.01\dot{3} & 0 \\ 0 & 0 & 0 & 0 & 0 & 1 \end{bmatrix} \quad \ldots\ldots 5.4.16$$

It is observed from the off-diagonal elements of equation 5.4.14 that the interaction expected on the experimental machine is between side motion and roll, and between traction and pitch. As was shown in the previous section, there are two ways to reduce interaction. The first is to use matched controllers which has the effect of allowing each of the interacting modes to respond at the same rate as the disturbances that are applied by other modes. This method only reduces interaction and in the case of the traction mode interaction with the pitch mode makes it necessary to put a minimum response time for the pitch mode control loop as the traction mode is uncontrolled, and so a steady step force may be applied as in the situation when the vehicle accelerates out of a station. In this case it may be necessary to employ the second technique of introducing the decoupling matrix, Md, into the forward path

to allow complete independence of the design of the pitch mode controller.

The system described was simulated using a digital simulation package developed by Dr. B. A. White at the School of Electrical Engineering at the University of Bath. Initially, a set of matched controllers was used for all the five controlled modes: heave, side, roll, pitch and yaw. Figure 5.4.3 shows the pitch response to the application of a forward traction force along the Y-axis consistant with an acceleration of 1.0 ms^{-2}. This sudden application of force by the force actuators F7 and F8 causes a considerable change in pitch. It would be possible to reduce this change by making the pitch controller faster. However this would then have to be re-matched to all the other control loops in the system so that interactions due to changes in ΔXw and ΔXl would be minimised. Figure 5.4.4 shows the effect of the introduction of the decoupling matrix, Md, given in equation 5.4.15, into the system. Now the interaction is completely suppressed, allowing the design freedom sought for the pitch mode.

It has been demonstrated that for the general force actuated model of a rigid levitated vehicle with six degrees of freedom there is an interaction introduced by both the non-coincidence of the centre of mass and the centre of

geometry, and the non-coincidence of the force actuators at each corner of the vehicle. A general decoupling matrix has been developed that completely decouples the system's controlled modes, and it can be seen that this matrix is an extension of that developed for the three degrees of freedom case of the previous section.

5.5. Vehicular Degrees of Freedom

The analysis has now taken into account all the spacial degrees of freedom of the MAGLEV vehicle. However, it can be shown that there are also vehicular degrees of freedom that must be considered. The most important of these is the assymetric torsional twisting of the non-rigid platform that would result by the relaxation of condition 7 in section 5.3.1. The effect of this degree of freedom on the control system is important and will now be considered.

If constraint 7 in section 5.3.1 is relaxed, then the vehicle may be considered to be of a non-rigid nature. Now several modes of bending may occur in the body of the platform that supports the force actuators. It can be seen that the most important of them is the assymetric torsional twisting about the roll and pitch axes of the vehicle. This is graphically shown in figure 5.5.1

The twisting will tend to close the air gap of two of the corners and increase it at the other two corners. Because of the fact that roll, pitch and heave are symmetric functions of the four air gaps as given by equation 5.3.7., then the torsional twist will not register as a change in any of these feedback signals. Hence, it can easily be seen that this is an unobserved degree of freedom. Likewise, as the forces are symmetrically applied, it is an uncontrolled degree of freedom.

In the real vehicle this mode can be unstable due to the fact that the idealised force actuators are replaced by electromagnets. This causes a problem as the upward force will increase on the two corners which have reduced air gaps due to the reduction in air gap. Likewise, the force upwards will decrease on the two corners that have larger air gaps. This will increase the force tending to bend the vehicle and so twist it still further.

If left unchecked, this uncontrollable, unobserved degree of freedom could cause a weak structure to bend until two of the corners touched the track. This is unacceptable. There are two solutions:-

1. Increase the structural strength of the vehicle.
2. Control this vehicular degree of freedom as is done

with the other six degrees of freedom.

Some systems rely on structural strength. However, this increases the mass thus increasing both the construction costs and the running costs of the vehicle. It is more rewarding to control this seventh degree of freedom. This will now be considered in the context of a multivariable seven degrees of freedom model.

The most important point to notice about the asymetric torsional twist is that it occurs about the centre of geometry of the vehicle. This indicates that it does not interact significantly with the six spacial degrees of freedom which are also centred about the centre of geometry even when an off-centred centre of mass is present. This makes it possible to control this degree of freedom independently of the other six so that equations 5.4.14 and 5.4.15 still hold true. It can be seen that the torsional twisting torque about the roll axis of the vehicle, Tt, may be controlled using the four force actuators F1 to F4 so that:-

$$Tt = (F1 - F2 + F3 - F4).Xw \qquad \ldots\ldots 5.5.1$$

and also that the torsional twist, T, may be observed as:-

$$T = \frac{G1 - G2 + G3 - G4}{Xw} \qquad \ldots\ldots 5.5.2$$

It should be noted that the dynamics of the vehicle structure are unlikely to be similar to that of the spacial degrees of freedom. The spacial degrees of freedom may be treated as the motion of free masses in space, whereas the vehicle under torsional strain will resemble a sprung mass to a first approximation, so that in the Laplace domain,

$$T(s) = \frac{Kt.Tt(s)}{(s^2+2.\zeta_t.w_t.s+w_t^2)} \qquad \ldots\ldots 5.5.3$$

where w_t represents the natural frequency of oscillation of the vehicle body and ζ_t represents the damping factor. Kt is proportional to the inverse of the vehicle body stiffness.

This seventh degree of freedom may be controlled separately from the other six as shown in figure 5.5.2.

In the practical system the idealised force actuators were replaced by real magnets which are far from ideal and introduce further problems. The next section extends the analysis to that of a current controlled d.c. magnet actuated model and studies the effects on the coupling

problem.

5.6. The Effect of Magnet and Air Gap Non-Linearities on the System

It has already been shown that the force generated by a magnet across an air gap is proportional to the square of the current, and inversely proportional to the square of the air gap, such that,

$$F = -\frac{Kmi^2}{z^2} \qquad \ldots\ldots 5.6.1$$

This section will look at the effect of using this non-linear force actuator at each corner of the three degrees of freedom rigid body model developed in section 5.3.2. In the following analysis it will be assumed that each of the four chopper time constants are identical, and may be represented by a single linear lag.

The block diagram of the non-linear multi-variable system is shown in figure 5.6.1. In this diagram, N1-N4 refer to non-linearities in the relationship between the forces F1-F4 and the currents I1-I4 and the air gaps at each corner, G1-G4. For the case of a rigid vehicle it is possible to say that the currents I1-I4 and gaps G1-G4 are

linear functions of the current demands Iz, $I\psi$, $I\theta$ and the vehicle attitudes Z, ψ, θ respectively, such that, at steady state,

$$I1 = Iz + I\psi + I\theta \quad \ldots\ldots 5.6.2$$

$$I2 = Iz - I\psi + I\theta \quad \ldots\ldots 5.6.3$$

$$I3 = Iz - I\psi - I\theta \quad \ldots\ldots 5.6.4$$

$$I4 = Iz + I\psi - I\theta \quad \ldots\ldots 5.6.5$$

and

$$G1 = Z - Xw.\psi - Xl.\theta \quad \ldots\ldots 5.6.6$$

$$G2 = Z + Xw.\psi - Xl.\theta \quad \ldots\ldots 5.6.7$$

$$G3 = Z + Xw.\psi + Xl.\theta \quad \ldots\ldots 5.6.8$$

$$G4 = Z - Xw.\psi + Xl.\theta \quad \ldots\ldots 5.6.9$$

Using the non-linear relationship of equation 5.6.1 it is possible to quantify the value of the corner forces F1-F4 such that:-

$$F1 = \frac{-Km.I1^2}{G1^2} \qquad \ldots\ldots 5.6.10$$

$$F2 = \frac{-Km.I2^2}{G2^2} \qquad \ldots\ldots 5.6.11$$

$$F3 = \frac{-Km.I3^2}{G3^2} \qquad \ldots\ldots 5.6.12$$

$$F4 = \frac{-Km.I4^2}{G4^2} \qquad \ldots\ldots 5.6.13$$

Also, the forces and torques acting about the centre of mass of the physical system as described in figure 5.3.2 are given by:-

$$Fz' = F1 + F2 + F3 + F4 + Mt.g \qquad \ldots\ldots 5.6.14$$

$$Ty' = -(F1+F4)(Xw+\Delta Xw) + (F2+F3)(Xw-\Delta Xw) \qquad \ldots\ldots 5.6.15$$

5-43

$$T\theta' = -(F1+F2)(X1-\Delta X1) + (F3+F4)(X1+\Delta X1) \quad \ldots\ldots 5.6.16$$

This set of non-linear equations may be linearised about operating points for the vehicle attitude and steady state currents to yield a linearised multi-variable system as shown in figure 5.6.2.

From figure 5.6.2 it should be noted that the linearised gains of the forward path gain matrix, Mki, are in terms of the steady state currents Izo, Iψo and Iθo, which are purely conceptual currents, the physical values of I1-I4 being linear functions of these values as dictated by equations 5.6.2-5.6.5. It is necessary to work in terms of Iz, Iψ and Iθ as these values will be produced as demands from any control system used to stabilise the plant shown. Also included into the diagram is the matrix Md. This matrix is not inherent to the plant, but is added specifically to try to decouple the system coupling caused by the forward path linearised current gain matrix, Mki. As a result, this correcting matrix will be the fixed gain inverse matrix of the Mki matrix at the operating currents. Alternatively, the decoupling matrix, Md, could be made part of an adaptive system by adjusting the values used depending on the long term average of these currents.

The aim of this exercise, then, is to produce expressions for the values in the matrix Mki in terms of known system constants and the steady state control current demands Izo, Iψo and Iθo, and hence attempt to produce a usable decoupling matrix Md.

The current gain matrix Mki is produced using three sets of partial differential equations for Fz', Tψ' and Tθ', differentiated with respect to Iz, Iψ and Iθ. The operating air gap, assuming a rigid structure and track, is Zo, so that G1-G4 are set to this operating point. The symbolic maths processor, REDUCE-3, previously mentioned, was used with the set of equations given above to yield the set of nine differential equations, such that for operating points of current of Izo, Iψo and Iθo it was found that:-

$$\frac{\delta Fz'}{\delta Iz} = -Ka.Izo \qquad \ldots\ldots 5.6.17$$

$$\frac{\delta Fz'}{\delta I\psi} = -Ka.I\psi o \qquad \ldots\ldots 5.6.18$$

$$\frac{\delta Fz'}{\delta I\theta} = -Ka.I\theta o \qquad \ldots\ldots 5.6.19$$

$$\frac{\delta T\psi'}{\delta Iz} = Ka.(Izo.\Delta Xw+I\psi o.Xw) \qquad \ldots\ldots 5.6.20$$

$$\frac{\delta T\psi'}{\delta I\psi} = Ka.(Izo.Xw+I\psi o.\Delta Xw) \qquad \ldots\ldots 5.6.21$$

$$\frac{\delta T\psi'}{\delta I\theta} = Ka.I\theta o.\Delta Xw \qquad \ldots\ldots 5.6.22$$

$$\frac{\delta T\theta'}{\delta Iz} = Ka.(-Izo.\Delta Xl+I\theta o.Xl) \qquad \ldots\ldots 5.6.23$$

$$\frac{\delta T\theta'}{\delta I\psi} = -Ka.I\psi o.\Delta Xl \qquad \ldots\ldots 5.6.24$$

$$\frac{\delta T\theta'}{\delta I\theta} = Ka.(Izo.Xl-I\theta o.\Delta Xl) \qquad \ldots\ldots 5.6.25$$

where

$$Ka = \frac{8.Km}{Zo^2} \qquad \ldots\ldots 5.6.26$$

this gives the gain matrix Mki as

$$Mki = Ka.\begin{bmatrix} -Izo & -I\psi o & -I\theta o \\ Izo.\Delta Xw+I\psi o.Xw & Izo.Xw+I\psi o.\Delta Xw & I\theta o.\Delta Xw \\ -Izo.\Delta Xl+I\theta o.Xl & -I\psi o.\Delta Xl & Izo.Xl-I\theta o.\Delta Xl \end{bmatrix}$$

..... 5.6.27

This matrix is not yet useful as there are still two unknown and possibly variable quantities in some of the terms, ie. ΔXw and ΔXl. The steady state values of currents would depend on the mass of the vehicle and the position of the centre of mass with respect to the centre of geometry, and so it would seem likely that ΔXl and ΔXw may be expressed in terms of Izo, $I\psi o$, $I\theta o$ and Mt, the vehicle mass. Consider that at steady state,

$Fzo' = -Mt.g$ where g is the gravitational constant

$T\psi o' = 0$

$T\theta o' = 0$

Then from equations 5.6.14-5.6.16 and using equations 5.6.2-5.6.5 and 5.6.10-5.6.13 for steady state air gaps G1-G4=Zo with steady state currents of Izo, $I\psi o$ and $I\theta o$ it is shown that

$$Fzo' = \frac{4.Km}{Zo^2}.(Izo^2+I\psi o^2+I\theta o^2) = Mt.g$$

..... 5.6.28

$$T\psi o' = \frac{4.Km.(Izo^2+I\psi o^2+I\theta o^2).\Delta Xw}{Zo^2} + \frac{8.Km.Izo.I\psi o.Xw}{Zo^2} = 0 \quad \ldots\ldots 5.6.29$$

$$T\theta o' = -\frac{4.Km.(Izo^2+I\psi o^2+I\theta o^2).\Delta Xl}{Zo^2} + \frac{8.Km.Izo.I\theta o.Xl}{Zo^2} = 0 \quad \ldots\ldots 5.6.30$$

Now substituting 5.6.28 into both 5.6.29 and 5.6.30 the result for ΔXw and ΔXl is given as

$$\Delta Xw = -\frac{8.Izo.I\psi o.Xw.Km}{Mt.g.Zo^2} \quad \ldots\ldots 5.6.31$$

and

$$\Delta Xl = \frac{8.Izo.I\theta o.Xl.Km}{Mt.g.Zo^2} \quad \ldots\ldots 5.6.32$$

Finally, the matrix Mki is transformed to centre of geometry co-ordinates by using the transformation matrix developed in equation 5.3.26 such that the total coupling matrix due to the steady state values of motor currents and mechanical interaction may be given as Mc, where:-

$$Mc = \begin{bmatrix} 1 & -\Delta Xw & \Delta Xl \\ 0 & 1 & 0 \\ 0 & 0 & 1 \end{bmatrix} . Mki$$

..... 5.6.33

It is now possible, using the inverse of the coupling matrix as Md, to greatly reduce the interaction between the controlled degrees of freedom. The symbolic maths processor REDUCE-3 was again employed to generate the inverse matrix with elements such that:-

$$Md_{1,1} = Izo^2.Xw.Xl.\left(1 - \frac{8.Km}{Mt.g.Zo^2} (I\theta o^2 + I\psi o^2) \right)$$

$$Md_{1,2} = Izo.I\psi o.Xl.\left(1 - \frac{8.Izo^2.Xw^2.Km}{Mt.g.Zo^2} \left(1 - \frac{8.Km}{Mt.g.Zo^2} (I\theta o^2 + I\psi o^2)\right) \right)$$

$$Md_{1,3} = Izo.I\theta o.Xw.\left(1 - \frac{8.Izo^2.Xl^2.Km}{Mt.g.Zo^2} \left(1 - \frac{8.Km}{Mt.g.Zo^2} (I\theta o^2 + I\psi o^2)\right) \right)$$

$$Md_{2,1} = Izo.I\psi o.Xw.Xl.\left(\frac{8.Izo^2.Km}{Mt.g.Zo^2} - 1 \right)$$

$$Md_{2,2} = Xl.\left((I\theta o^2 - Izo^2) + \frac{8.Izo^2.I\psi o^2.Xw^2.Km}{Mt.g.Zo^2}.\left(1 - \frac{8.Izo^2.Km}{Mt.g.Zo^2}\right)\right)$$

$$Md_{2,3} = I\psi o.I\theta o.Xw.\left(\frac{8.Izo^2.Xl^2.Km}{Mt.g.Zo^2}.\left(1 - \frac{8.Izo^2.Km}{Mt.g.Zo^2}\right) - 1 \right)$$

$$Md_{3,1} = Izo.I\theta o.Xw.Xl.\left(\frac{8.Izo^2.Km}{Mt.g.Zo^2} - 1 \right)$$

$$Md_{3,2} = I\psi o.I\theta o.Xl.\left(\frac{8.Izo^2.Xw^2.Km}{Mt.g.Zo^2}.\left(1 - \frac{8.Km.Izo^2}{Mt.g.Zo^2}\right) - 1 \right)$$

$$Md_{3,3} = Xw.\left((I\psi o^2 - Izo^2) + \frac{8.Izo^2.I\theta o^2.Xl^2.Km}{Mt.g.Zo^2}.\left(1 - \frac{8.Izo^2.Km}{Mt.g.Zo^2}\right)\right)$$

or

$$Md = \begin{bmatrix} Izo^2.Xw.Xl.A & Izo.I\psi o.Xl.(1-BA) & Izo.I\theta o.Xw.(1-CA) \\ -Izo.I\psi o.Xw.Xl.D & Xl.(I\theta o^2-Izo^2+I\psi o^2.BD) & -I\psi o.I\theta o.Xw.(1-CD) \\ -Izo.I\theta o.Xw.Xl.D & -I\psi o.I\theta o.Xl.(1-BD) & Xw.(I\psi o^2-Izo^2+I\theta o^2.CD) \end{bmatrix}$$

..... 5.6.34

where

$$A = 1 - \frac{8.Km.I\theta o^2+I\psi o^2}{Mt.g.Zo^2} \qquad B = \frac{8.Izo^2.Xw^2.Km}{Mt.g.Zo^2}$$

$$C = \frac{8.Izo^2.Xl^2.Km}{Mt.g.Zo^2} \qquad D = 1 - \frac{8.Izo^2.Km}{Mt.g.Zo^2}$$

Also from equation 5.6.28

$$\frac{8.Km}{Mt.g.Zo^2} = \frac{2}{(Izo^2 + I\psi o^2 + I\theta o^2)}$$

In order to demonstrate the usefulness of this result a three degrees of freedom non-linear simulation was developed which complied with the system schematic shown in figure 5.6.1. Firstly, three control loops were designed with the assumption of no interaction using the following values as system constants:-

$Km = 6.13x10^{-4}$ $J\psi = 75.0\ Kg.m^2$

$Zo = 0.01$ m $\quad J\theta = 300.0$ Kg.m^2

$Mt = 400.0$ Kg

$Xw = 0.5$ m $\quad X1 = 1.0$ m

$\Delta Xw = 0.3$ m $\quad \Delta X1 = -0.3$ m

The set of results shown in figure 5.6.3 demonstrates the interaction that exists between the three control modes when a small step change in attitude is demanded of each mode in turn. This set of results indicate that the main coupling occurs on the roll and pitch modes excited by the change in the heave mode demand. This is expected as the heave mode is a faster acting control loop and can therefore hold its position when roll and pitch disturbances occur. It can be seen from figure 5.6.3(b) that a significant divergence in the corner gaps occur due to this heave mode disturbance. This occurs even though the pitch and roll modes should remain steady.

The results of two other forms of disturbance were also considered. Figure 5.6.4 shows the effect of demanding a vehicle attitude change. Here the input step demands were applied simultaneously at 0.5 seconds such that there was a 1mm step for the heave mode, a 0.25 milli-radian step for the roll mode and a 0.5 milli-radian change for the pitch. As with the first test, it can be seen that the system's multi-variable interactions cause unacceptably long

transients on the roll and pitch responses. Finally, the system response to a step change in the heave mode disturbance force is shown in figure 5.6.5. The force used simulates the effect of a 1.0 ms^{-2} acceleration change applied to the heave mode. Such a thrust can be expected on the curved approach to an incline in the track. As before, the unacceptable transient response of the roll and pitch degrees of freedom can be clearly seen. Some form of decoupling matrix, Md, is needed in the system to reduce the interaction between the control loops.

The first type of multi-variable compensation that may be used is the fixed gain mechanical coupling compensation matrix developed in the earlier sections of this chapter. The same set of responses with this matrix inserted as Md is shown in figures 5.6.6, 5.6.7 and 5.6.8. It is readily observed that no great advantage has been gained as this decoupling matrix fails to take into account the non-linear force actuators in the form of the field coils of the linear synchronous motors used in this realistic simulation. In fact, the matrix has over compensated, and the long term transients on both pitch and roll are still observable in these responses. Figure 5.6.7 shows the system responses to an attitude change on all three modes simultaneously. The effect of the roll and pitch control loops conflicting is now very noticeable in the long settling time of gaps G1 and

G3. Finally, figure 5.6.8 shows the disturbance generated on each of the three controlled modes when a step acceleration of 1.0 ms^{-2} is applied to the heave mode.

Now consider figure 5.6.2 and figures 5.6.9, 5.6.10 and 5.6.11. In this system the decoupling matrix Md is composed of the fixed gains calculated for the operating points of the currents Izo, Iψo and Iθo. It can be seen that although the interaction has not all gone it is significantly reduced and, of primary importance, the slow transients on the roll and pitch responses has disappeared. However, there are still some undesirable side effects. There is now a greater interaction between the roll and pitch modes as shown in figures 5.6.9 (c) and (d). Also, these modes appear to be somewhat underdamped. A similar effect is observed on the results given in figure 5.6.10 for the simultaneous disturbance on all three controlled modes, although, as before, the slow time constants have been erradicated. Figure 5.6.11 shows that this multivariable fixed gain compensation matrix is sufficient to stop roll and pitch disturbances due to an applied heave mode step acceleration.

The above set of results indicates that significant advantages may be gained by including a fixed gain decoupling matrix that is fixed by the operating currents in the magnet windings. The actual effect of the compensation

is to correct for the off-centred centre of mass, taking into account that now the force actuators each have different operating gains, these gains being dependent on the steady state current in the magnets as shown in the linearised equation 5.6.27. It is also seen, however, that the performance of the roll and pitch loops is not correct and appears to be underdamped. In addition, there is some direct interaction between these two loops.

This continued interaction is due to the fact that no attempt has been made to decouple the effects due to the Mkz matrix. This causes coupling due to the air gap non-linearity. However, it should be noted that figure 5.6.2 can be reduced to the form of figure 5.6.12 and that Mkz may be compensated for in this system by synthesising Mkz within the controller so that the system shown in 5.6.13 is obtained. Then the coupling due to air gap non-linearity is removed. Mkz can be calculated in a similar fashion to Mki so that a coupling equation purely in terms of Izo, $I\psi o$ and $I\theta o$ and the known parameters of the vehicle can be produced. Mkz may be used within the controller for air gap non-linearity compensation.

Figures 5.6.14, 5.6.15 and 5.6.16 show the results obtained when this additional decoupler is used in the system. Initially, it appears that this set of results is

even worse. However, it should be noted that this is due to the lack of compensation for the first order lag due to the field coils used in the real system. In order to allow for this, the compensator Mkz' must also have some velocity signal applied to it in order that the forward path poles due to the field coil of the LSMs are fully compensated for. This is shown in the block diagram of the fully compensated system shown in figure 5.6.17. The inverse of the field coil matrix is used in the feedback path to fully compensate for Mkz so that the full feedback compensator is given by

$$Mm'(s) = Mm(s) + Mkz'.Mfc(s)^{-1}$$

where Mm(s) is a diagonal matrix containing the compensation for each of the decoupled control loops. Mkz' is a model of the gains in the Mkz linearised gain matrix of the MAGLEV vehicle and Mfc(s) is a diagonal matrix where each diagonal element represents the dynamics of the LSM field coils.

It should be noted that because of the form of $Mfc(s)^{-1}$, the system requires velocity feedback signals to obtain the first order feedback term in s. This is no problem, as Mm(s) requires these signals already because of the form of each decoupled control loop.

The set of results that are obtained when the field coil is compensated for are given in figures 5.6.18 to

5.6.20. These results show that all the non-linearities have been compensated for adequately.

5.7. Conclusions

A thorough examination of the control problems associated with the non-linear multi-variable MAGLEV vehicle has been presented. This analysis is not specific to the LSM type of vehicle but is generally applicable to the problems of levitating a four cornered plate of the sort described using non-linear actuators such as d.c. magnets.

The mechanical coupling due to off-centred masses has been dealt with along with treatments that give a symbolic solution to the decoupling matrices necessary for eradicating interactions due to current/force non-linearities. It has been shown that it is also necessary to take the air gap/force non-linearities into account and that an acceptable decoupling can only be obtained when all three of the above interactions are catered for.

Simulation results for three degrees of freedom gave very encouraging results showing that the coupling can be greatly reduced.

5-57

It has also been shown that it is necessary to control at least one vehicular degree of freedom, that of asymetric transitional twisting. Control of this degree of freedom can lead to cheaper running costs and construction costs for a MAGLEV vehicle.

6. SINGLE DEGREE OF FREEDOM DIGITAL CONTROLLER

6.1. Introduction

An initial study was carried out using a single magnet setup. The purpose of this study was to investigate the problems of using a digital controller in the system that was described in chapter 2. In this system a single magnet driven by a chopper produced a plant that was taken to be of third order when linearised. There were three main sources of non-linearity in the system. These were:-

1. The coil current response to changing input current demands.
2. The change in the linearised parameters due to fluctuations in the current in the motor coils.
3. The change in the linearised parameters due to fluctuations in the air gap.

This section of the thesis looks at how the problems due to non-linearities were overcome in the single magnet setup. As has already been stated, the various degrees of freedom of the whole vehicle could each be modelled as having the same basic dynamics as this single degree of

freedom setup.

6.2. The Single Magnet Rig.

The setup used is shown in figure 6.2.1. A single d.c. magnet was positioned at the top of a restraining cylinder. The function of the cylinder was to restrain the magnet from motion in all but the vertical direction. Under these conditions it was possible to investigate a single degree of freedom of a practical rig.

The magnet was positioned at a distance of about one centimetre from a mild steel pole piece when the current in the coil was at zero. The various control loops that will be described were used to control the single magnet to a certain demanded air gap at a distance 'Zo' below the pole piece lower surface.

6.3. The Linearised Model

The action of the chopper circuit used as a current drive device in the system described was very non-linear. Figure 6.3.1. shows the time response of the current in the LSM field coils when a step change in the current is demanded. If the initial current is ΔI less than the demanded current Id then the full battery voltage Vmax is

placed across the field coil at time t_1 (when the change in demand is applied). The current in the coil then rises following an exponential response towards a maximum coil current, Imax, such that:-

$$Imax = \frac{Vmax}{Rf} \qquad \ldots\ldots 6.3.1$$

Where Rf is the field coil resistance. The initial slope of this exponential response is determined by the coil time constant. A full description of the operation of the chopper is given in chapter 2. From this it can be seen that the time constant of the exponential is given by:-

$$T_c = \frac{Lf}{Rf} \qquad \ldots\ldots 6.3.2$$

Where Lf is the coil inductance. The initial slope, Si, is then given by noting that at the initial rate of current rise the aiming current, Imax, would be reached in one time constant such that:-

$$S_i = \frac{Vmax}{Rf}.\frac{1}{T_c} = \frac{Vmax}{Rf}.\frac{Rf}{Lf} = \frac{Vmax}{Lf} \text{ Amperes/second} \qquad \ldots\ldots 6.3.3$$

It can be seen that when the vehicle initially levitated from the resting air gap of around 1 cm the current would have risen from zero to the current necessary to produce the force that countered the downward pull of gravity. This current would have been greater than the actual steady state current needed to maintain the magnet in stable equilibrium at the smaller levitated air gap Zo. The design of the vehicle was such that it levitated from a rest air gap of 1.5 times the nominal levitated air gap. So under these circumstances 1.5 times the normal steady state current was flowing in the field coil at the moment of 'lift-off'. It was therefore possible to obtain an approximate estimate of the steady state levitating current for the LSM before the controllers were designed by manually measuring the current at which the LSM started to lift towards the track under open loop conditions. It was found that a current of 33 Amperes was required for 'lift-off' at an air gap of 1.0 cm. This indicated that at the levitated height of 0.7 cm a current of about 23 Amperes would be necessary.

The speed with which this current would be reached by the chopper circuit gave a measure of the effective equivalent Laplace domain pole position of the worst case chopper transient. This pole was non-linear as it changed position on the s-domain as the difference between the

demanded and actual field coil currents, ΔI, varied. The initial slope can be seen to only depend on the battery voltage and the chopper load inductance. As was stated in chapter 2, it was found that the LSM did not present a pure inductance as a load and it had been necessary to insert a series inductance into the drive circuitry. This meant that the chopper load inductance was known to a high degree of accuracy, with Lf = 0.05 H. Thus Si = 960.0 Amperes/Second for the battery voltage of 48.0 V. This rate of current rise took 23.0/960.0 seconds to reach the steady state levitation current of 23.0 Amperes. This rise time was then a measure of the worst case equivalent chopper time constant, giving an equivalent s-domain pole position of s = -41. So the worst case linearised transfer function for the chopper was taken to be:-

$$G_c(s) = \frac{41}{(s + 41)} \qquad \ldots\ldots 6.3.4$$

The other non-linear element in the levitation system was the magnet current and air gap non-linearities. The magnet, when energised, gave a non-linear force function so that a set of second order non-linear differential equations resulted. The field coil for each LSM produced an attractive force, F, such that:-

$$F = \frac{Km.Io^2}{Zo^2} \qquad \ldots\ldots 6.3.5$$

This can be linearised as shown in appendix 4, so that it can be shown that:-

$$G_m(s) = \frac{-\frac{2.g}{Io}}{(s^2 - \frac{2.g}{Zo})} \qquad \ldots\ldots 6.3.6$$

Where g is the gravitational constant, Io is the steady state levitation current and Zo is the steady state levitated air gap. So that at steady state the system could be represented as two poles in the s-domain such that one was in the stable half plane and one in the unstable half plane.

From the above the complete linearised model of the system was given by the worst case conditions such that:-

$$G(s) = \frac{-41.(\frac{2.g}{Io})}{(s + 41).(s^2 - \frac{2.g}{Zo})} \qquad \ldots\ldots 6.3.7$$

With this linearised model for the plant it was possible to continue with the design of the controller for the single magnet system.

6.4. The Linear Controller Development

The initial attempts to control the above linearised system were carried out using the small single magnet rig described in section 6.2. In this case, the initial rest air gap was measured as 1.1 cm and controllers were to be developed to try to levitate this magnet so that an air gap, Zo, of 0.6 mm was achieved. For this the current necessary for lift off at 1.1 cm was measured in the same way as it was for the LSM. It was found that 22 Amperes were necessary. This indicated that Io should be 12 Amperes for Zo = 0.6 cm.

From this the linearised plant transfer function for the small magnet was calculated using equation 6.3.6 to give:-

$$G_m(s) = \frac{-1.64}{(s^2 - 3270)} \qquad \ldots\ldots 6.4.1$$

When the worst case chopper pole was added in, a complete system was obtained such that:-

$$G(s) = \frac{-41 * 1.64}{(s+41).(s^2-3270)} = \frac{67.24}{(s+41).(s^2-3270)} \quad \ldots\ldots 6.4.2$$

The characteristic equation of this system gave s-domain poles at:-

$s = -41$

$s = -57.2$

$s = 57.2$

So it can be seen that the system was fundamentally unstable with an open loop right half pole at $s = 57.2$.

6.4.1. State Feedback

Simple unity feedback would not stabilise this system. The root locus of 6.4.1 shows the effect of applying unity feedback and varying the forward path gain of the system. The system can be seen to remain unstable for all values of forward path gain. It was necessary to apply velocity or air gap rate feedback in order to stabilise this system.

Under these conditions a zero was placed on the negative real axis in the s-domain and as the forward path gain was increased the right hand half plane pole at s = 57.2 moved to the left and stabilised. The velocity feedback had to be such as to achieve an adequately fast response. Figure 6.4.2 shows the block diagram of this simple form of controller. The root loci of figure 6.4.3 show the s-domain poles for forward path gains varying from 0 to 4000 for the following feedback parameters.

1. $h_1 = 1$ $h_2 = 0.1$
2. $h_1 = 1$ $h_2 = 0.05$
3. $h_1 = 1$ $h_2 = 0.03$
4. $h_1 = 1$ $h_2 = 0.01$

The first three systems produced stable poles. However, once the feedback zero moved past the chopper pole position in figure 6.4.3(d) the system became unstable again.

The first three systems produced first order dominated systems with the dominant poles of:-

1. $s = -5.8$ for $h_2 = 0.1$ at $K = 4000$
2. $s = -13.8$ for $h_2 = 0.05$ at $K = 4000$
3. $s = -30.2$ for $h_2 = 0.03$ at $K = 4000$

All four systems were programmed into the digital controller. Figures 6.4.4 to 6.4.7 show the resulting responses for a 'lift-off' for the four systems. These diagrams record air gap (a), digitally differentiated air gap (b) (used as a gap rate signal), magnet coil current (c) and chopper demand (d) (digital controller output). Digitally differentiated air gap rate signals were used because at this point in the study accelerometers were not available.

This first set of results highlighted a number of facts:-

1. The method of digital differentiation was simple involving the difference between successive digital samples scaled by the sample rate. This however produced quantisation error of the sample rate multiplied by the resolution of the air gap transducer. A sample rate of 1000 samples per second was used producing a quantisation error on the gap rate signal of 0.016 ms^{-1}. This produced large current demand noise as can be seen in figures 6.4.4(d) to 6.4.7(d). The magnet coil current response reduced the noise as it presented a first order lag that tended to achieve the mean of the demanded current.
2. The air gap response of figure 6.4.4 exhibited

considerably more noise once a stable levitation height had been achieved than did the air gaps of figures 6.4.5 to 6.4.7. As the velocity feedback was reduced so the air gap noise diminished showing that the noise was caused primarily by the velocity signal.

3. It was necessary to demand an air gap of 3 mm in order to achieve an air gap of 6 mm showing that a large steady state error existed. This steady state error was due to the effect of gravity on the magnet mass as is shown in figure 6.4.8. The basic open loop system described was type zero and so exhibited a fixed steady state error for a step disturbance and an infinite steady state error to a ramp disturbance. Under this system if the magnet mass were to change then the air gap would also change. Also, if a steady force were applied such as that experienced whilst cornering of going onto an incline, then a steady state air gap error would be experienced.

4. The fourth system for $h_2 = 0.01$ was not unstable as the root loci of figure 6.4.3(d) had implied. This was due to the fact that the non-linear chopper pole had moved much further to the left on the root locus diagram once a steady state air gap had been approached. This indicated that the worst case chopper pole was probably too pessimistic. Figure 6.4.9 shows root loci for the systems when the chopper pole was

neglected. The dominant poles for the first three systems showed some shift so that they were now:-

1. $s = -8.1$ for $h_2 = 0.1$ at $K = 4000$
2. $s = -10.4$ for $h_2 = 0.05$ at $K = 4000$
3. $s = -18.4$ for $h_2 = 0.03$ at $K = 4000$

But the system for $h_2 = 0.01$ was now seen to be stable and second order dominated with a natural frequency of oscillation of $w_n = 57.4$ rad.s^{-1} and a damping factor of $\zeta = 0.57$. This set of root loci appeared to better represent the experimental results of figures 6.4.4 to 6.4.7 than those of figure 6.4.3.

The above results showed that the system model of equation 6.4.1 was accurate but pessimistic at the levitated height as the chopper pole position tended to move to the left and hence became less significant. The steady state error problem had to be solved as this was unacceptable for a practical vehicle where mass changes and system parameter changes were unpredictable.

6.4.2. The Use of a Forward Path Integrator for Force Disturbance Restoration

In order to eliminate the steady state air gap error it was necessary to make the system into a type 1 or type 2 system. Two methods of doing this were considered. Firstly, as is shown in figure 6.4.10, a P.I. controller could have been used. This introduced a pole at the origin and a zero on the negative real axis increasing the system order by one to fourth order such that:-

$$G(s) = \frac{-1.64(Kp.s+Ki)p}{s(s+p)(s^2-3270)} \qquad \ldots\ldots 6.4.3$$

where p is the chopper pole position, Ki is the integrator gain and Kp is the proportional gain.

With this system it was possible to apply unity feedback, as is shown in figure 6.4.11, such that for a range of gains the system was stable with all the poles are in the left hand half plane. However, this was undesirable as the system linearised gains may change significantly if the system parameters change and there was only a small range of stable gains on the locus of figure 6.4.11.

6-14

Another possibility was to apply air gap and air gap rate feedback so that two zeros were produced as shown in the root loci in figure 6.4.12. Now the fourth order system was stable for all forward path gains higher than a minimum necessary to get all the poles into the left hand half plane as long as the two zeros were kept between the origin and the first open loop system pole on the negative real axis. However, this system only allowed non-complex zeros to be used for control and also produceed a numerator zero into the transfer function so that the time domain response would have been more 'peaky'.

A more flexible controller that maintained the two zeros but allowed them to be positioned anywhere on the s-domain is shown in figure 6.4.13. This system did not produce any numerator zeros and still provided two closed loop denominator zeros and a type 1 system with zero steady state air gap error.

The closed loop transmittance for this system is given by:-

$$T(s) = \frac{h_0.p.k.(1.64)}{s(s+p)(s^2-3270) + p.k.(1.64)(h_2.s^2+h_1.s+h_0)} \quad \ldots\ldots 6.4.4$$

Figure 6.4.14 shows the root loci for this system for the cases where:-

$p = 41$

$h_2 = 0.01$

$h_1 = 1.0$

for h_0 = 10.0, 15.0, 20.0 and 25.0 with forward path gains ranging from 0 to 4000. All the resulting root loci were seen to produce unstable pole positions at all forward path gains. The chopper pole was then removed from the analysis as this worst case pole was seen to be pessimistic from the previous set of results. Figure 6.4.15 shows the same set of root loci as 6.4.14 but with the chopper pole removed. Four stable systems were obtained. The results showed that the systems would be second order dominated but that as h_0 was increased the systems became less stable with the dominant closed loop poles for k = 4000 approaching the right hand half plane.

Experimental results for the above systems are shown in figures 6.4.16 to 6.4.19. It can be seen from these results that the systems did achieve zero steady state error with the integrator (shown in 6.4.16(a) to 6.4.19(a)) taking up the force offset due to the downward pull of gravity. In addition, the second order dominated responses did appear to

become less stable as the integrator gain, h_0, was increased. Figures 6.4.18(a) and 6.4.19(a) show underdamped air gap responses as predicted by the root loci of figure 6.4.15(c) and 6.4.15(d).

The root loci of figure 6.4.15 suggested that the use of a higher forward path gain, k, would lead to better damped second order responses. Another notable point was that the use of very low velocity feedback gains had led to a noise free steady state air gap response. This meant that the raising of the forward path gain would not cause unacceptable variations in the air gap.

Figure 6.4.20 shows the root loci for the above systems, with the chopper pole ignored, but for a higher forward path gain range of k = 0 to 10000. It can be seen that these tended to produce more heavily damped systems than the loci of figure 6.4.15. However, for the lower h_0 values of h_0 = 10.0, 15.0 and 20.0 the systems were first order dominated with a high frequency second order component superimposed.

Figures 6.4.21 to 6.4.24 show the experimental results for the above systems with the forward path gain set to k = 10000. These results confirmed the root loci predictions of figure 6.4.20 producing four stable systems, each with

zero steady state error in the air gap. The higher forward path gains used stabilised the systems that used higher integrator gains, h_0, so that figures 6.4.23 and 6.4.24 now show acceptable levitation controllers.

The higher forward path gain did have the effect of producing more steady state air gap noise than the previous set of results for k = 4000. This was again due to the velocity signal noise shown in figures 6.4.21(b) to 6.4.24(b).

It was considered from these results that the best form of linear levitation controller for the maglev vehicle was that shown in figure 6.4.13. The next section describes the results of implementing this form of controller on a single corner of the LSM MAGLEV vehicle.

6.5. Single Corner LSM Vehicle Results

The controller that was developed in the previous section was chosen for implementation on the MAGLEV vehicle LSMs. This section describes some of the results obtained when a single motor on the vehicle was controlled using this form of controller. The remaining three corners of the vehicle were left inactive. The structure of the vehicle was sufficiently flexible so that the levitated corner was not

significantly affected by the other three corners which remained immobile.

The linearised model for the system was derived by using the techniques already employed for the single magnet rig and described in sections 6.3 and 6.4 of this thesis. The chopper current of the open loop system was slowly increased until the LSM began to lift. The current that was reached was assumed to be the steady state current necessary for levitation at the rest air gap of 1.0 cm. The steady state current necessary for levitation at other air gaps could now be approximated as the levitation current was directly proportional to the air gap. It was found that 33.0 Amperes were necessary for the LSM to lift at 1.0 cm.

By using the linear model obtained in section 6.3 the system could be modelled as shown in figure 6.5.1. Two studies for the single LSM are described here. The first was for a steady state air gap of 0.7 cm and the second for a steady state air gap of 0.8 cm. These two systems gave the following steady state currents:-

Zo = 0.7 cm, Io = 23.1 Amperes

Zo = 0.8 cm, Io = 26.4 Amperes

such that the linearised current to force gain, Ki, and the linearised air gap positive feedback gain, Kz, for the open loop system shown in figure 6.5.1 were given by:-

$$Ki = \frac{2.g}{Io} = \frac{2.g}{26.4} = 0.866, \quad \text{for } Zo = 0.7 \text{ cm}$$

$$Kz = \frac{2.g}{Zo} = \frac{2.g}{0.007} = 2857, \quad \text{for } Zo = 0.7 \text{ cm}$$

$$Ki = \frac{2.g}{Io} = \frac{2.g}{23.1} = 0.758, \quad \text{for } Zo = 0.8 \text{ cm}$$

$$Kz = \frac{2.g}{Zo} = \frac{2.g}{0.008} = 2500, \quad \text{for } Zo = 0.8 \text{ cm}$$

This produced open loop systems of:-

$$G(s) = \frac{-p * 0.866}{(s + p)(s^2 - 2857)} \quad \text{for } Zo = 0.7 \text{ cm} \qquad \ldots\ldots 6.5.1$$

And

$$G(s) = \frac{-p * 0.758}{(s + p)(s^2 - 2500)} \quad \text{for } Zo = 0.8 \text{ cm} \qquad \ldots\ldots 6.5.2$$

Where 'p' is the chopper linearised pole position. Figure 6.5.2 shows the control loop used in both cases. The results for control of the single magnet rig of section 6.4 suggested that the following set of control parameters would

produce a stable system with zero steady state error in the air gap:-

$k = 10000$

$h_0 = 20.0$

$h_1 = 1.0$

$h_2 = 0.04$

Notice that a higher value of velocity feedback was used to add more damping to the system as the open loop forward path gains, Ki, of the LSM systems were smaller than that of the single magnet rig and so the system was expected to be less well damped.

Figure 6.5.3 shows the root loci for both of the above systems over the controller gain range of k = 0 to 10000. Figure 6.5.3(a) and 6.5.3(b) shows the loci for Zo = 0.7 cm with and without the chopper pole. Likewise, figures 6.5.3(c) and 6.5.3(d) show the loci with and without the chopper pole for the case where Zo = 0.8 cm.

It was immediately seen from these plots that the systems were insensitive to the location of the chopper pole. However, a non-dominant pair of poles that were not well damped was produced for the cases where the worst case chopper pole was included. These closed loop poles would go

unstable of the chopper pole was to come much closer to the origin or the closed loop zeros were to move further to the left. This indicated that the chopper pole position set a limit on the maximum speed of response that was achievable by the system.

This set of control parameters were set into the digital controller and two results were recorded for a 'lift-off' of one corner of the vehicle. Figure 6.5.4 shows the results for a 0.7 cm air gap and figure 6.5.5 shows the results obtained for a 0.8 cm air gap.

Notice that the velocity signal in both of these cases was derived using the digitally integrated output from an accelerometer as was described in chapter 4 of this thesis. The accelerometer was mounted on the vehicle at the levitated corner under the LSM. As can be seen this gave much less noisy velocity feedback signals (shown in figure 6.5.4(b) and 6.5.5(b)).

As was predicted by the root loci of figure 6.5.3 both the above systems produced stable levitation. A short time was seen to elapse before the main 'lift-off' transient occurred in figures 6.5.4(a) and 6.5.5(a). Up until 0.2 seconds into the test the vehicle was building up to the 'lift-off' current of 33.0 Amperes, see figures 6.5.4(d) and

6.5.5(d). This slow current build up was caused by the controller integrator reaching the required system offset due to the effects of gravity. After the 'lift-off' current was reached there was a second order dominated response with a natural frequency of about 20 to 25 rad.s^{-1} and damping factor of around 0.5. This is exactly what was expected from the root loci of figure 6.5.3.

This set of results showed that the linear controller developed in section 6.4 was successfully transferred to the real LSM MAGLEV vehicle. The levitation dynamics produced were insensitive to the chopper pole position. The use of a forward path integrator in the controller produced a type 1 system that could adapt to a variety of system parameter changes to maintain the desired air gap during levitation. This form of controller was used as the basis for the two and four LSM levitation results discussed in chapter 7. The next section describes the results obtained as an outcome of attempting to use a non-linear controller with the LSM.

6.6. The Non-Linear Controller Development

As the MAGLEV system was controlled by a digital computer, and the system was both non-linear and multivariable, non-linear controllers were investigated as possible candidates for vehicle levitation control.

Variable structure control systems (VSCS) [35] were investigated. This form of controller was thought to be particularly suitable as it could cope with a wide variation in system parameters. Figure 6.6.1 shows the basic form of the controller. From this diagram it can be seen that the feedback gains are switched. This enables the system dynamic response to be modified dynamically by the controller so that a precise linear response can be maintained.

The theory of VSCS also provides zero steady state error for a step input for type zero systems [47]. This is achieved by modifying the basic form of the controller to that shown in figure 6.6.2. It can now be seen that the input demand to the system also has a gain that is switched by the controller.

There follows a description of the results of the design and implementation of a VSCS for the single corner of the LSM MAGLEV vehicle discussed in the last section. It will be shown that the VSCS did not work properly on this MAGLEV system. In order to investigate this problem a computer simulation was set up so that the effects on the controller of the various non-linearities in the system could be studied.

6.6.1. The Full Order VSCS Controller

The single corner LSM system linearised model of equation 6.5.1 was used to design a VSCS controller so that the LSM could be levitated with well defined closed loop dynamics. The system was designed so that the response to disturbances would have a natural frequency of $w_n = 15.0$ with a damping ratio of $\zeta = 0.7071$ and switching function dynamics that were first order and fast with respect to w_n. The switching function pole position was chosen to be at $\lambda_n = -600$ in the s-domain. This gave the desired closed loop fixed gain characteristic equation of the VSCS as:-

$$(s - \lambda_n)(s^2 + 2.\zeta.w_n.s + w_n^2) = 0 \qquad \ldots\ldots 6.6.1$$

For the LSM the closed loop fixed gain characteristic equation was given by:-

$$(s + 41)(s^2 - 2857) + 35.5(h_3s^2 + h_2s + h_1).k = 0 \qquad \ldots\ldots 6.6.2$$

It should be noted that acceleration feedback was included in this system. Equating coefficients of the powers of 's' in the above two equations gave the fixed controller gains as:-

$$k.h_3 = \frac{621.2 - 41}{35.5} = 16.3 \qquad \ldots\ldots 6.6.3$$

$$k.h_2 = \frac{12945 + 2857}{35.5} = 445.1 \qquad \ldots\ldots 6.6.4$$

$$k.h_1 = \frac{135000 + 117137}{35.5} = 7101.2 \qquad \ldots\ldots 6.6.5$$

The forward path gain, k, was chosen so that the air gap feedback gain, h_1, would remain at 1.0. This gave k = 7101.2 setting the VSCS fixed feedback gains as:-

$h_3 = 0.0023$

$h_2 = 0.063$

$h_1 = 1.0$

The switched gains were calculated using the full order VSCS theory such that:-

$$k.\Delta h_3 > \left|\frac{\lambda_n}{Ki.p}\right| = \left|\frac{600}{35.5}\right|, \text{ where } \lambda_n \text{ is the switching pole position} \qquad \ldots\ldots 6.6.6$$

$$k.\Delta h_2 > \left|\frac{\lambda_n.2.\zeta.w_n}{Ki.p}\right| = \left|\frac{12727.8}{35.5}\right| \qquad \ldots\ldots 6.6.7$$

$$k.\Delta h_1 > \left|\frac{\lambda_n.w_n^2}{Ki.p}\right| = \left|\frac{135000}{35.5}\right| \quad \ldots\ldots 6.6.8$$

which gave the minimum allowable switching gains required as:-

$\Delta h_3 = 0.0024$

$\Delta h_2 = 0.05$

$\Delta h_1 = 0.54$

The theory also gave a value for the input switching gain such that:-

$k_r = 0.5$

$\Delta k_r = 0.54$

The fixed gain K_r was set so that it compensated for the steady state error due to the effect of the downward pull of gravity at the levitated height. The VSCS was programmed into the digital controller and the VSCS gain switching parameters were set to the value calculated above. It was found that this system would not levitate from the rest air gap of 1.0 cm. The reason for this was not clear.

In order to study this further a hybrid controller was programmed which would levitate the corner LSM using the

stable levitation controller of section 6.5. Then at a set time, once the system was stable at the required 0.7 cm air gap, the VSCS would be substituted as the controller. A set of the results of such a study are shown in figure 6.6.3. It can be seen that when the VSCS controller took over, at 0.1 seconds on the plots shown, the system began to act abnormally. The system remained stable but the air gap drifted aimlessly by more than one millimetre. This aimless drift was observed on all VSCS studies with both the real LSM and the single magnet rig described earlier in section 6.4.

The cause of the drift was not immediately apparent. In order to determine the cause a simulation of the levitation system including non-linear choppers, non-linear magnets, transducer quantisation and noise was set up. It was expected that if the same effect could be generated during simulation then the ability to remove the non-linearities, quantisation and noise effects individually in the simulation would clarify the cause.

The results of a simulation including all the non-linear effects are shown in figure 6.6.4. It could be seen that the aimless variation in air gap did occur in the simulation as it had in the real system. The plot of the switching function output, figure 6.6.4(b), showed a d.c.

offset. This signal should have been mean zero. This eliminated the possibility that some software fault in the control program was the cause as two totally different pieces of software were used for the simulation and the real system.

Figure 6.6.5 shows a later result that was obtained when the transducer quantisation and system noise was removed from the simulation. Although the air gap plot of figure 6.6.5(a) still showed a drift, this time it was no longer aimless. A stable system with a fixed steady state error was produced. Again figure 6.6.5(b) showed that a d.c. offset had occurred in the switching function, sigma. It could also be seen from this plot that sigma had a large quantisation effect imposed on it. It was this quantisation that was causing the d.c. offset as the sigma curve was forced to drift until a quantisation boundary was reached which could then supply control information. The source of the quantisation was not obvious as all digital tranducer quantisation had been removed. When the feedback signals were observed it became apparent that the accelerometer output was the cause. Figure 6.6.6 shows the acceleration transducer output. The quantisation effect seen on this signal was observed to be a direct effect due to quantised changes in LSM coil current, also shown in this diagram.

The explanation for this is that because the VSCS controller tended to cause very large changes in the demand current to the chopper from sample to sample then the chopper current window effectively was no longer used. Because of this the chopper tended to switch the coil voltage from +Vmax To -Vmax on almost every sample. As the current ramp rate in the coil was fixed at the levitated air gap then the coil current would change by a fixed amount each sample period. These fixed current changes caused fixed air gap force changes and hence fixed air gap acceleration changes from sample to sample. The accelerometer was read once every sample period and so the small current changes were quantised by the sample rate. The small changes on current caused large changes in acceleration as seen in figure 6.6.6(a) which then dominated the switching function, sigma. In order to obtain a switching boundary sigma was forced to drift to a quantisation boundary. The only way this could occur was by the compensation for the accelerometer quantisation by an air gap drift.

In the real LSM system with digital tranducer quantisation and system noise this effect became less determinable and so the air gap drifted aimlessly. The system did not become unstable because that would have caused large sigma transients and the above effect would have disappeared as the chopper current window came back

into effect.

So, this effect transformed acceleration quantisation into air gap drift. The amount of drift was determined by the amount of quantisation and the relative values of the coefficients of acceleration and position used in the VSCS switching function. When this was understood it was possible to propose several solutions:-

1. Reduce the quantisation by decreasing the rate of change of chopper coil current. This could be achieved by increasing the chopper load inductance. Unfortunately, this would move the chopper pole closer to the origin in the s-domain producing a less stable system.
2. Redesign the system for a faster dynamic response. This would change the relative values of the coefficients of acceleration and position in the switching function in a favourable manner. There was a limit to which this could be achieved while maintaining a stable system.
3. Increase the digital controller sample rate, thus reducing the current ramp time and the acceleration quantisation proportionately. Unfortunately, this method required more digital controller computer power as the controller calculations would have to be

completed more quickly for a higher sample rate.

4. Remove the acceleration term from the switching function altogether. The theory of VSCS allows for this with 'reduced order VSCS'. The disadvantage was that the switching function dynamics of sigma became second order with greater possibility of instability.

The proposed solutions were simulated. Figure 6.6.7 shows the effect of redesigning the system for faster responses while the system sample rate was kept at 1000 samples per second. It can be seen that the air gap drift was reduced until at $w_n = 60$ rad.s^{-1} it was quite small. Figure 6.6.8 shows these systems again but this time with a 2 mm step function applied at 0.5 seconds into a 1.0 second study. Again the $w_n = 60$ rad.s^{-1} case shows a near perfect response for this large air gap change involving large plant parameter changes. Figure 6.6.9 shows the effect of changing the digital controller sample rate. At 10000 samples per second the drift became almost imperceptable.

The proposed solutions had not been implemented on the real LSM vehicle at the time of writing. It is thought that solutions 1,2 and 3 could be used in combination to achieve an acceptable VSCS controller for the single degree of freedom maglev controller.

Before VSCS can be used on the multiple degrees of freedom MAGLEV vehicle a method of implementing multivariable VSCS must be worked out. Any attempt to use two separate VSCS loops with the same choppers by summing the current demands is pointless due to the chopper current limits and the large changes in the VSCS current demands which cause saturation.

This investigation into the use of VSCS as a control system for the MAGLEV vehicle has highlighted the problems of using a non-linear force actuator such as a chopper with a digitally sampled implementation of VSCS. Also, it demonstrated the effect of system state quantisation transference that can occur due to the sigma function and cause steady state output error or drift.

6.7. Conclusions

The results of an investigation of various controller types that could have been used for the control of the whole LSM MAGLEV vehicle has been presented. This initial study was carried out firstly using a single magnet, single degree of freedom, suspension system before moving on to the real LSM.

The best of the controllers tried was a linear state feedback controller with a forward path force restoring integrator which could cope with steady state disturbances that would otherwise have caused steady state errors in the system air gap.

The variable structure control systems (VSCS) discussed in section 6.6 had a number of problems. The main problem was associated with the use of a non-linear current driver, the chopper. A number of solutions were suggested and these require further investigation.

The most promising controller was applied to a single corner of the maglev vehicle, these results being presented in section 6.5. This set of results showed that this form of controller could be made insensitive to the linearised chopper pole position and that even the worst case chopper pole position still produced an adequately controlled system. This form of controller was therefore used for the various multi-motor levitation systems described in chapter seven.

7. RESULTS FOR CONTROL OF THE FOUR MOTOR LSM VEHICLE

7.1. Introduction

The vehicle as described in chapter two of this thesis was constructed. The transducers of chapter four and the digital controller of chapter three were installed. This chapter describes the implementation of the linear control laws developed in chapter six for the full four cornered vehicle with four corner LSMs and four side magnets, one at each corner.

The levitation of the whole vehicle was achieved at the end of a number of intermediary stages. These will be individually described. Firstly, the single magnet, single degree of freedom controller of chapter six was extended to a two LSM controller operating at just one end of the vehicle. This controlled the two motors as though they were each a single degree of freedom problem and so were essentially separate controllers. Secondly, the control law was rearranged such that coordinated control of the two LSMs was achieved so that the centre of goemetery coordinates of heave and roll were controlled instead. This stage was necessary if independent control of each of the degrees of

freedom of the whole vehicle was to be obtained as was discussed in chapter five. Following on from this, the controller was extended to cover both ends of the vehicle so that four of the six unstable degrees of freedom were controlled. This gave coordinated control of the field currents in all four LSMs. Next, the controller for the side magnets was developed. This allowed lateral guidance control thus controlling the remaining two unstable degrees of freedom. The seventh degree of freedom was longitudinal speed and was controlled separately by the armature coil current inverters of the LSMs.

7.2. Two Motor Results

A number of results were taken for two motors used simultaneously. These results are presented in this section. Several different control laws were studied and these will be described.

The first set of results was obtained with one end of the vehicle pivoted so that it did not either help or hinder the operation of the other end. Initially, no acceleration feedback was applied and an attempt was made to determine the sensitivity of the system to changes in position of the pivot.

The first set of results, shown in figures 7.2.1 and 7.2.2, in which the pivot was centrally located, shows that the system achieved stable levitation. However, there was a distinct difference in the response of each of the two motors. Motor 1 gave a slight overshoot before settling. This was due to the higher velocity towards the track during the initial lift-off. Figures 7.2.1(b) and 7.2.2(b) show this difference in transient velocity. Both velocity signals appeared to have a drift associated with them. This was caused by the effect of the integration mechanism by which they were derived. In fact, the design of the conditioning software for the accelerometer was such that this drift would eventually settle out. The drift was compensated for by the forward path integrator in the control loop as shown by figures 7.2.1(c) and 7.2.2(c). In addition to the different responses, it may also be seen from figures 7.2.1(b) and 7.2.2(b) that there was higher frequency noise on the velocity signal for motor 1 than for motor 2. It was noted that the current waveforms shown in figures 7.2.1(d) and 7.2.2(d), whilst being similar in form, had different steady state values. Motor 1 required a steady state current of 26 Amperes and motor 2 required a steady state current of 23 Amperes.

It was initially thought that the pivot may not have been centrally located and that this was causing these

offsets. To test this idea, the pivot was re-positioned 5 cm closer to motor 4 and the results were taken again. Figures 7.2.3 and 7.2.4 show these results. Figures 7.2.5 and 7.2.6 show the results of moving the pivot 5 cm closer to motor 3 than the assumed central position. The position curves, (a), integrator output curves, (c), and current demand curves, (d), show no difference in basic form or steady state values. From this it was concluded that the basic response of the system was only marginally sensitive to the pivotal position. However, it was noted that the velocity waveforms, (b), showed marked differences, particularly those for motor 2. In fact, any movement of the pivot away from the centre seemed to induce high frequency oscillations in the velocity signal and the effects of this may be seen as a small ripple in both the current demands, (d), and position signals, (a).

It was thought that these effects, which have a zero mean effect and do not affect the basic system response, were caused by excitation of vehicular and track modes of vibration. Any imbalance in the structure such as that caused by taking the pivot away from the centre point was likely to excite such vibrations.

With the pivotal position eliminated as the cause of the different responses of motors 1 and 2, the only other

likely causes were either non-concentric mass distribution on the vehicle or a slight difference in the steady state air gaps of the two motors. Motor 1 required a higher steady state current than motor 2 which would indicate that motor 1 was operating with an effectively lower forward path gain. This lower forward path gain would lead to the less damped response observed.

The pivot was returned to the centre position. A set of tests was then performed that investigated the coupling between the two corner motors for this two degrees of freedom situation.

Figures 7.2.7 and 7.2.8 show the results of a test where, during a two second levitation, motor 1 was given a step demand to reduce its air gap by 1 mm at 1 second into the test. The response of motor 1 was noticeably slower for the 1 mm transient than it was for the original 3 mm step which levitated the vehicle. This was due to the effects of the integrator and the chopper non-linearity.

For this controller design, wn = 15 and ζ = 0.5. It may be seen that the air gap settled after 0.4 seconds from the 1 mm step demand and first achieved the desired ride height only 0.2 seconds after the step demand was applied.

The effect on the air gap of motor 2 of the 1 mm step from motor 1 was found to be minimal. Motor 2 moved down by less than 0.1 mm.

Figures 7.2.9 and 7.2.10 show the results of a similar test where motor 2 was given a 1 mm step demand at 1 second into the test and motor 1 was held steady.

The results of this second coupling test were very similar to the first except that less overshoot was obtained from motor 2. This lack of overshoot was consistant with the difference between motors 1 and 2 illustrated in figures 7.2.1 to 7.2.6.

The above two sets of results showed that the two degrees of freedom single ended vehicle was well decoupled for separate air gap control. This was to be expected as virtually all the mass in this case was concentrated in the motors themselves at the two corners.

Figures 7.2.11 and 7.2.12 show a set of results for the same controller when both motors were simultaneously stepped by 1 mm at the 1 second point.

This well decoupled property of the two motor set up with the pivot would not hold for the four cornered vehicle.

A theoretical proof of this has been given in chapter five. In order to maintain well decoupled control loops it was necessary to control centre of geometry co-ordinates instead of corner air gaps. The next set of results record the initial attempts at co-ordinated heave and roll control of the two degrees of freedom set up.

A new control program was written which transformed the output from the air gap transducers into heave and roll signals. In addition, the program also derived the chopper current demands by using the inverse of this transform to convert from heave and roll current demands into current demands for the two corner motors.

Figures 7.2.13 and 7.2.14 show the results of a successful levitation using this new controller. It may be seen that, after an initial slight roll disturbance during 'lift off', the roll controller maintained the roll angle of zero radians and the heave controller achieved the correct ride height of 7 mm.

Figures 7.2.15 and 7.2.16 show results for a 1 milliradian step in roll demand. A very slight heave disturbance of 0.05 mm occurred at this point.

Figures 7.2.17 and 7.2.18 show results for a 2 milliradian step change in roll demand. In this test, a 0.15 mm disturbance was observed in the heave.

Figures 7.2.19 to 7.2.22 show the results of tests where -1 milliradian and -2 milliradian changes were applied to the roll demand. Again, disturbances in the heave loop were observed.

Figures 7.2.23 and 7.2.24 show results for a 1 mm step change in the heave demand. No roll disturbance was recorded. Similarly, a -1 mm step change in heave demand, as shown in figures 7.2.25 and 7.2.26, produced no roll loop interaction.

The preceding set of results demonstrated that when the centre of geometry co-ordinates of heave and roll were controlled some interaction occurred, but it was slight for the set up used. The roll loop affected the heave loop, however, the heave loop did not significantly affect the roll loop. The reasons for this lay in two areas:-

1. Heave mode step demands produced a common mode current change for both motors 1 and 2, and so the magnet non-linearities were balanced causing no roll effect. However, roll mode step demands caused difference mode

current changes in motors 1 and 2 so that an imbalance was set up due to the magnet and air gap non-linearities. This could cause a slight disturbance in the heave control loop.

2. As is illustrated in the recorded curves, the roll response was faster than the heave response so that the heave loop was liable to disturbances from the faster roll loop.

It should be noted that at this point the control program did not attempt any multivariable decoupling and so the interaction recorded was the natural mechanical interaction of the two motor system. The results recorded in chapter five indicated that these interaction effects could be further eliminated by the inclusion of a non-linear decoupling matrix of fixed gains.

7.3. Four Motor Results

The pivot at the second end of the vehicle was removed and the next set of results as shown in figures 7.3.2 to 7.3.6 were recorded for a full four corner levitation. Several points about this study should be noted:-

1. At this point, the lateral position was not controlled as no side magnets were fitted. This will be dealt with

in the following two sections.

2. The controller was somewhat restricted as at the time of the tests only three accelerometers were available. Because of this, the vehicle was controlled as two separate ends using the two motors at each end in pairs as was described in the previous section.

The first end of the vehicle had two shaft mounted accelerometers and so the controller could obtain inertial frame of reference velocity signals for both heave and roll. However, at the second end only one accelerometer was available. The was mounted centrally at the point at which the pivot of the previous section had been placed. The output from this accelerometer could then be used for heave but not roll control of the second end. As the vehicle had a flexible structure the outputs from the accelerometers mounted under the motors at the first end could not be used for control of the second end. Roll control velocity feedback for the second end was obtained by digitally differentiating the air gap signals of the two air gap transducers at the second end of the vehicle as described in some of the earlier controllers of chapter six.

Figure 7.3.1 shows the mounting points of all the transducers for this four motor study.

Figure 7.3.2 shows a successful levitation of the whole four cornered structure. This set of results shows the air gap and roll responses for both ends of the vehicle. It should be noticed that the air gap and the roll signals at end two exhibited more noise than those of end one. This was due entirely to the use of a track relative velocity signal for roll feedback at this end.

Figure 7.3.3 shows the velocity feedback signals obtained in this test. It may be seen from the curve of the roll signal for end two, 7.3.3(d), that a high frequency mode of oscillation in the track had been excited so producing a poor quality velocity signal for this control loop.

Figure 7.3.4 shows the signals returned from the three accelerometers. As before, they contained a large amount of noise due to the chopper action. However, a mean zero acceleration was maintained.

Figure 7.3.6 shows the current demands for all four motors. It may be seen from these that much more noise was present on the current demands for end two. This again was a direct result of having used track relative roll velocity feedback for end two. It also appeared that motors 3 and 4 had lower mean steady state currents than motors 1 and 2.

This was due to the fact that the digital computer, its power supplies and disc drives were mounted mid-way between the centre of the vehicle and end 1 of the vehicle thus producing an off-centred mass distribution. This result showed how the four corner control system coped with off-centred masses.

Figure 7.3.5 shows the integrator outputs for all four control loops. These can be seen to settle once all the imbalances of the system have been dealt with. As may be seen from figure 7.3.2, the desired air gap of 7 mm on both ends was achieved as were the demanded roll angles of 0.0 radians despite the unbalanced rig setup as shown by the disparate currents of figure 7.3.6. This zero steady state error in the system was entirely due to the integrator employed in the forward path as described in chapter six.

7.4. Side Magnet Controller Development

At this point the side magnets as described in appendix 1 were fitted to the MAGLEV vehicle as shown in figure 7.4.1. This section describes the development of the side magnet controller used with the LSM MAGLEV vehicle.

Chopper circuits were built that could control the currents in the coils of the side magnets and the air gap

transducers described in chapter four and already used for vehicle levitation were fitted at the corners. Steel side rails were bolted onto the track structure as shown in figure 7.4.2 so that the side magnets could pull against them. The surfaces of these side rails also provided the reflective surface for gap measurement required by the air gap transducers. No accelerometers were available for side control at the time of the initial work described here. Higher state feedback signals were derived from the digitally differentiated air gap signal.

The location of the side magnets made it possible to control each end of the vehicle individually. A side force was produced whenever an imbalance in the forces generated by opposing sets of magents occurred. Thus the magnets were driven in difference mode.

The design of a controller for side control at one end of the vehicle will be described here. Lateral control of both end of the vehicle was achieved by using two such control loops.

There was a difference between the linearised magnet system for side control and that for heave control. As there was no gravitational effect active in the lateral direction on a level track there was no required steady state current

necessary in the magnets. However, it was noted that it was only possible to derive a linearised equivalent system for a magnet that has steady state current flowing in the coils.

This fact has led some investigators to design in standing currents so that even at steady state with no lateral disturbance the side magnets on opposing corners of the vehicle 'fight' one another. This allows the design of a system using classical linear control techniques, but at the cost of continuously wasting energy in the power dissipation of the side magnets used. Another reason given for standing currents being maintained is that a faster response to lateral disturbances can be achieved as there is no need to wait on the currents to build up in the magnets before they can respond. This argument is less forceful if current choppers rather than voltage choppers are used as only a very short period of time (< 100 ms) will elapse before working currents are reached.

It is possible to show, as is done in appendix 6, that if a stable controller can be achieved at a given standing current, Io, then the side control system will remain stable for any standing current less than Io including Io=0 so long as the feedback parameters and the designed forward path gains are maintained. This then led to a good method of producing a side control system that did not require

standing currents but did have a adequate response.

The method involved firstly designing the system for a given standing current using the linear approximation to the system about this working point. Then a simulation was set up of the system and the designed controller was simulated. In this simulation environment it was possible to observe the effect of reducing the standing current, Io, to zero. Further design of the feedback parameters could then be carried out interactively using the simulator until an adequate system response was obtained. When the desired result was obtained it could be transferred to the real system.

This method provided a means of designing the control parameters for the side control for zero standing current by use of a simulation rather than classical linear controller design techniques.

Appendix 7 gives two designs based on a standing current of Io = 15 Amperes with a nominal side rail to magnet air gap of 7 mm. The design was based on the linearised fourth order model shown in figure 7.4.3. At these working points this diagram reduced to give the model shown in figure 7.4.4.

The first design attempted to achieve a closed loop system that had a second order dominated response with $wn_1 = 20.0$ and $\zeta_1 = 0.5$. The closed loop fourth order system had a linearised transfer function such that:-

$$T(s) = \frac{-3.674.K.h_0}{s.((s+30).(s^2-262.4) + 3.674.K.(h_2.s^2+h_1.s+h_0))} \quad \ldots\ldots 7.4.1$$

This system had a characteristic equation given by:-

$$s^4+30s^3+(3.674.K.h_2-262.4)s^2+(3.674.K.h_1-7822)s+3.674.K.h_0 = 0 \quad \ldots\ldots 7.4.2$$

The design in appendix 7 gave a desired closed loop characteristic equation of

$$s^4 + 30s^3 + 3100s^2 + 54000s + 1000000 = 0 \quad \ldots\ldots 7.4.3$$

Comparing the coefficients of the powers of s in equations 7.4.2 and 7.4.3 and setting the air gap feedback gain, h_1, to 1.0 produced the following control parameters:-

$K = 16843.0$

$h_0 = 16.1624$

h_1 = 1.0

h_2 = 0.05434

Figure 7.4.5 shows a root locus for this system. Unfortunately, this sytem produced two high frequency non-dominant poles that were very underdamped in addition to the dominant pair such that $wn_2 = 50.0$ and $\zeta_2 = 0.1$.

By lowering the specification on the dominant pole pair a better damped non-dominant pair were achievable. Choosing $wn_1 = 5.0$ and $\zeta_1 = 0.5$. Appendix 7 shows a design that gives $wn_2 = 62.5$ and $\zeta_2 = 0.2$. This system had a characteristic equation of:-

$$s^4 + 30s^3 + 4056.25s^2 + 20156.25s + 97656.25 = 0 \quad \ldots\ldots 7.4.4$$

Comparing coefficients gives control parameters for this system of:-

K = 7630.0

h_0 = 3.4842

h_1 = 1.0

h_2 = 0.1541

A root locus of this system up to the gain of K = 7630 is given in figure 7.4.6. It can be seen that in this case the second pair of poles are both fast and better damped than in the previous case.

The designed values for h_0, h_1 and h_2 arrived at due to the limit of stability analysis of appendix 6 suggested that the following feedback parameters would also produce a stable system for zero standing current:-

K > 2143 (designed for Io = 15 Amperes)

$h_0 = 5.0$

$h_1 = 1.0$

$h_2 = 0.06$

Figure 7.4.7 shows the root locus for this set of parameters for K = 0 up to K = 100000. In the next section the results of applying these various designs to the real and simulated systems are presented and discussed.

7.5. Side Magnet Results

Initially, results were obtained from the simulation program based on the following six sets of control parameters:-

Parameter:	K	h0	h1	h2	Standing Current
1.	16843	16.1624	1.0	0.05434	15.0
2.	7630	3.4842	1.0	0.1541	15.0
3.	25000	5.0	1.0	0.06	0.0
4.	50000	5.0	1.0	0.06	0.0
5.	100000	5.0	1.0	0.06	0.0
6.	7630	3.4842	1.0	0.1541	0.0

The control function was a step input of 1.0 mm in magnitude applied at a time of 0.5 seconds.

Having obtained a stable zero standing current set of control parameters, the best of which was set 4, similar results were taken from the real system. Simulation results for this set of parameters incorporating graphs of side position and velocity, air gaps and current demands are given in figure 7.5.1 and the corresponding real results in figure 7.5.2. It was noted that in the real results a current offset had been set up in one magnet of about 7.0 Amperes (as shown in figure 7.5.2(d)). This suggested that the system was compensating for a slope in the track. At a nominal airgap of 7 mm this meant that a force offset was being produced of approximately 20.0 Newtons.

The force offset was incorporated into the simulation to produce the six sets of results given in figures 7.5.3 to 7.5.8.

The six sets of parameters were used to obtain corresponding results from the real system. Graphs of side position and velocity, airgaps and current demands are shown in figures 7.5.2 and 7.5.9 to 7.5.13. The second set of simulation results were seen to give a better corresponance to the real system than those obtained previously.

Several points of note arose from these experimental results. These were:-

1. High forward path gains tended to excite oscillations in the guidance rails. A limit cycle associated with these oscillations can be seen in both responses for a standing current of 15.0 Amperes (figures 7.5.9(a) and 7.5.10(a)) and also for the high gain zero standing current case (figure 7.5.12(a)). The rails are not rigid and may be modelled as a pair of pole-zero combinations as shown in figure 7.5.14 [43]. Increasing the forward path gain of the system, both by increasing the control gain, K, or the system gain, Ki, (by increasing the standing current), pushes the closed loop poles associated with the rails towards the right

hand half-plane thus inducing oscillations.

2. For a standing current of 15.0 Amperes, the design with the lower value of forward path gain produced less oscillations. This is best illustrated by a comparison of the air gap results shown in figures 7.5.9(a) and 7.5.10(a). much higher current deviations were produced by the system with the higher gain (see figures 7.5.9(d) and 7.5.10(d)). This would subject the rails to larger forces and set up larger oscillations. Also, the design procedure adopted in the previous section was such as to ensure better second order dominance in the second design (that is, for a forward path gain of 7630.0) and this can be seen to be the case from figures 7.5.9 and 7.5.10.

3. The zero standing current results shown in figures 7.5.2, 7.5.11 and 7.5.12 suggest that a moderate value of forward path gain gave the response which settled the fastest. Lowering the gain (as in figure 7.5.11) produced a response which was third order dominated. The arrangement of closed loop poles to which this corresponds may be as shown in figure 7.5.15. Putting the gain up to a moderate value (as in figure 7.5.2), produced a highly damped second order dominated response which may be described by closed loop poles as shown in figure 7.5.16. Increasing the gain still further induced oscillations in the rails as can be

seen in figure 7.5.12(a).

4. Generally, zero standing current results, other than those with a high forward path gain, were much less oscillatory as can be seen from figures 7.5.2(a), 7.5.11(a) and 7.5.13(a). With much less current in the magnet windings and smaller current deviations, the rails were subjected to less force and hence oscillations were not set up.

5. A comparison of the side positions shown in figures 7.5.10(a) and 7.5.13(a), which differ only in the standing current in the magnet windings, suggests that the zero standing current system is more stable for a given set of control parameters as suggested in the previous section. It also further illustrates the above point.

The simulation results were less oscillatory than the real results. This was due to the fact that non-rigid rails had not been taken into account in the simulation model of the system. Discrepancies may also be due to parameters which were not well known, such as the saturation curve for the iron parts opf the magnetic circuitry or the true effective mass of the system.

7.6. Conclusions

This chapter has shown the results of applying some of the controllers developed in chapter six to more than one magnet. This has enabled all the degrees of freedom of the LSM MAGLEV vehicle to be controlled using the on-board digital controller.

The two motor studies showed that it was possible to use centre of geometry co-ordinates and that for the experimental rig used, problems of interaction were minimal. The four motor levitation studies of section 7.3 showed that it was possible to levitate the whole vehicle using heave and roll control at each end of the vehicle.

The more elegant roll, pitch, heave and assymetric torsional twist controllers of chapter five were not implemented primarily due to the lack of digital controller computing power. However, in this initial study, the more basic controller used proved to be both reliable and stable.

Side or lateral position at each end of the vehicle was also controlled using a side control loop in addition to the heave and roll control loop at each end of the vehicle.

For the side control, the possibility of only applying side magnet current during disturbances was investigated. It was thought that this could lead to a system that was cheaper to run than a system that maintained opposing side currents in the side magnets. As fast current choppers were in use, standing current was not necessary so long as it was proven that the zero standing current did not lead to an unstable system. This was indeed proven by a study of the factors involved in the limit of stability for the side control system. It was proven that a controller that was stable for any given standing current was stable for any standing current less than the designed standing current including zero standing current. This unfortunately made it difficult to design the system response as the magnets could not be linearised about a working point of zero standing current. As a result, the controller was designed with standing currents of 15 Amperes. Simulations were then carried out with zero standing current to prove that the limit of stability theory held.

The results for side position control showed that zero standing current had a second advantage in addition to the economic argument. The use of zero current in the coils reduced the small disturbance sensitivity of the electromagnet system and this tended to greatly reduce high frequency side rail oscillations that were produced when

15 Amperes standing currents were used. This was important as the side position control used the digitally differentiated air gap relative velocity feedback signals as no accelerometers were available for control of these degrees of freedom of the vehicle at the time at which these results were taken.

The side control loops were used in conjunction with the heave and roll loops at each end of the vehicle to produce a completely controlled vehicle.

When the LSM inverter was used to produce tractive force during levitation no significant interaction was observed on the levitation controllers indicating that the LSM philosophy did indeed decouple the tractive and levitative effects from one another.

8. CONCLUSIONS

A working one-quarter size model of a LSM based MAGLEV vehicle has been designed, constructed and tested. All the required hardware and control theory for a working vehicle, with both levitation and traction simultaneously operational, has been developed.

New types of levitation transducers were developed that could measure the track to motor surface air gap to a high degree of accuracy (16 μm resolution) with a wide bandwidth (>10 kHz) and a large dynamic range (>0.5 m). These transducers did not place any specific restrictions on the materials used for the measurement surface. The only requirement was that a reasonably flat, continuous surface was available that ran along the side of the track pole pieces and had a fixed height relationship to the surfaces of the pole pieces. The ultra-sonic air gap transducer was shown to have good linearity as long as precautions were taken to suppress secondary reflections. Electro-magnetic noise immunity was ensured by using optical fibres to transmit the signals from the remote ultra-sonic transducers (positioned close to the motor faces) to the interface electronics situated centrally in the system digital control

element. It is hoped that these transducers could provide the basis for an environmentally robust contactless air gap measurement device on a full scale vehicle.

It has been shown that shaft mounted accelerometers could be used to provide higher state feedback information and that such feedback was used to improve the levitation control scheme. The use of these inertial frame of reference feedback signals for the higher states gave better isolation from vibration due to rough surfaces on the track as well as isolation from periodic effects due to the structure of the guide rails.

Velocity or air gap rate feedback signals which were used for lateral guidance purposes were derived using digital differentiation of the output from the ultra-sonic air gap transducers. It has been shown that this provided adequate side motion control, although, there was a tendency for high frequency modes of oscillation in the track structure to become excited. This was due in part to the use of track relative higher state feedback, but was added to by the quantisation error produced by the digital differentiation (the velocity transducer is quantised at the sample rate times the air gap transducer quantisation, so the resolution was only 0.016 $m.s^{-1}$). The most common effect of this excitation was to produce a loud buzzing

sound during operation. With adequately stiff side rails the system remained perfectly stable even with this effect.

A new form of contactless pole piece position transducer was developed. This provided information about the position of the guide rail poles pieces with respect to the longitudinal position of the motor surfaces during operation. This transducer was vital to the operation of the LSMs used for traction purposes. The output from this transducer was used to maintain the torque angle of the LSMs at 90^{o} at all times and at all tractive velocities during operation. This transducer provided an output that was accurate to one fortieth (0.5 cm) of a pole pitch and could update the result once every millisecond. Such performance was adequate for the torque angle of the vehicle to remain at 90^{o} to within the transducer accuracy over the whole range of specified tractive speeds. This then provided the most efficient operation of the LSMs and provided maximum electro-magnetic decoupling between the tractive and levitative modes of the motors.

Local signal conditioning and health monitoring was provided for this transducer by a low power, high noise immunity CMOS microprocessor positioned within the transducer electronics. The digital output from this device was available to the inverter's phase control input thus

forming a closed loop that maintained the correct torque angle.

Electro-magnetic noise immunity of the sensors and exciter coil was ensured by using a high frequency modulated input to the tuned exciter coil. The tuned circuits of the sensors then removed all but the modulation frequency, thus avoiding the electro-magnetic noise created by the action of the power electronics and motors.

A highly adaptable form of central controller was developed. This controller was based on a digital computer that provided the control functions, monitored the progress of experiments, logged useful data and, between experiments, provided a complete software development environment and the tools for the analysis of the data that was acquired during the experiments.

A general structure was worked out for the loading and running of the time critical control programs on this digital computer so that the TRIPOS operating system did not cause any timing problems. This structure allowed a number of different control laws to be quickly and efficiently implemented. Results from these different schemes were compared without the need to rewire the control circuitry, as all control was implememted purely in software.

The power of this system was demonstrated by the ease with which Variable Structure Control Systems were investigated on the same LSM MAGLEV vehicle hardware as were more conventional fixed gain state feedback control laws. A stable and adequately decoupled control system for the full eight magnet (four LSM field and four side magnets) levitation and guidance system has been described as the result of the investigation of several different control schemes.

Homopolar Linear Synchronous Motors designed at the University of Bath have been described. A complete vehicle comprising all the preceeding components has been constructed and this vehicle has been shown to function well in the laboratory. In particular it has been shown that adequate decoupling of the levitative and tractive modes of the LSMs has been achieved.

An initial attempt at constructing a guide and support rail has been carried out. The guide rail system described proved to be troublesome for all but these preliminary studies. The problem was identified as being due to the lack of stiffness at certain points along the structure. A better design that would use concrete sections was described which would remove most of the track oscillation problems.

9. FURTHER WORK

There are a number of areas on the LSM MAGLEV vehicle that require extensive further work. The system as described did work and could be used as the basis for a full size vehicle. However, the work so far has not addressed some of the problems involved with placing the vehicle in the less controlled environment outside of the laboratory.

Chapter five of this thesis descrides the theory of some of the problems that would be encountered if the centre of mass of the vehicle were to shift significantly away from the centre of geometry. In a practical vehicle this could of course happen if the vehicle mass comprised independently moving passengers. The simulation results of this situation suggested that a centralised multivariable controller would be required. Also, this work shows that due to the uncertainties caused by the magnet and air gap non-linearities and the possibility of time variable mass distribution any practical controller should be adaptive in nature. Implementation of such a controller was not carried out during the term of the project due to pressure of time. However, it is felt that such work is important if a robust and practical full scale vehicle is to be considered.

Further investigation of the VSCS type of controller described in chapter six should also lead to an adaptive non-linear control mechanism which could provide a vehicle able to respond to large changes in system parameters.

The effects of flexible tracks were observed to significantly affect the levitation and lateral guidance controller performances. Further investigation into either stiffer track or types of controller that are less likely to excite track modes of vibration should be investigated. The use of inertial frame of reference higher state feedback signals rather than track relative signals already shows some improvement in this situation.

The extension of the controllers as mentioned above will require a more powerful digital computer as a central control element. An upgraded computer that runs the same TRIPOS operating system and is capable of running the same software already exists. This computer was designed within the University of Bath for use with real time simulation work [46]. However, it would also suit this application. The main new attribute of this upgraded computer is that it is a parallel computer which would allow the various tasks of the present system to be split off onto individual processors so that each would be able to carry out more complex

calculations in the same time period. For example, one processor could deal with the collection, conditioning and scaling of the transducer inputs to the controller. Another processor could deal with the transformation to and from air gap coordinates and centre of geometry coordinates. A third pocessor could control the chopper outputs. Several other processors could perform the central control law calculations.

It should be noted that unlike the present system the use of a multi-processor system as a controller would support future needs as processor power upgrades could be accommodated by the addition of futher processors. In addition, the multi-processor provides the possibility of the inclusion of reliability features such as multiple redundancy or majority voting systems being employed which could lead to a more robust vehicle design.

The transducers used with the present system could be improved. The operation of the controllers and the LSMs are not directly dependent on the use of these particular transducers and so if necessary other transducer types could be designed. A number of problems might occur if the present transducers were used in the outside environment. The effects of snow, ice and water on the ultra-sonic transducers should be investigated. Similarly, the effects

of these elements on the operation of the pole piece postion transducer should be ascertained. Effects of wind speed and air pressure changes on the ultra-sonic air gap transducers also requires study.

In the system described the power electronics and batteries were situated close to, but outside the vehicle body. The effects of placing these components within the body of the vehicle should be observed. Although it should be noted that no significant problems are expected with this process and the resulting increase in vehicle mass would be within the design specification of the vehicles lifting capability.

Further linearisation of the magnet and air gap non-linearities could be achieved by the use of flux transducers. The problem of measuring the motor pole face flux density as the motor moves along is complicated by the varying phase relationship of the track flux paths with respect to any flux measurement device. It has been shown that the inclusion of an inner flux feedback loop on the chopper circuits can eliminate the non-linearity in the magnetic force actuator [43]. Such a possibility should be investigated.

The ability of the LSM MAGLEV vehicle described to negotiate corners and follow inclines should be tested. This work would require a more complex track than was used for the work discussed in this thesis.

Finally, the possibility of providing secondary suspension of the cargo mass of the vehicle and any effects of this on the controllers already designed should be looked at.

APPENDIX 1. LSM and Side Magnet Details

1.1. LSM Winding Arrangements

1.1.1. D.C. Windings

Turns per coil	91
Conductor cross section	10 mm^2
Current for steady lift (designed)	40 Amperes
Current density for steady lift (designed)	4 A/mm^2
Lift force at designed current	1130 Newtons

When tested the motor produced a steady lift force of 1230 Newtons with 40 Amperes in each field coil. This was achieved by placing a voltage of 21.2 Volts across the coils when hot.

1.1.2. A.C. Windings

Number of poles	4
Pole pitch	100 mm
Number of phases	3
Maximum frequency	15 Hz
Slots per pole and phase	2

Slot width : Slot pitch	6 : 16.7
Slot depth	16 mm
Turns per coil	15
Conductor cross section	1.77 mm^2
Maximum thrust at d.c. winding current of 40 A	129 newtons

When tested the motor produced a thrust of 110 Newtons with an a.c. current of 11 Amperes and a d.c. current of 40 Amperes. The a.c. windings were connected in series star.

1.2. Side Magnet Winding Arrangements

Turns per coil	107
Conductor cross section	4 mm^2
Current for steady force (designed)	13.2 Amperes
Current density for steady force	3.3 A/mm^2
Force at designed current	28 Newtons

When tested each magnet produced a steady force of 32.1 Newtons with a current of 12.2 Amperes when 28 Volts was placed across the coils.

APPENDIX 2. Pole Transducer Program Listing

The following listing is the program used by the RCA1802 local processor for pole piece position detection. The principle of operation of this program is to collect the twenty 'on' or 'off' states of the sensors and then process these to determine where the group of 'on' states are. These sensor outputs are available from a parallel port on the processor board. If the sensor array is in a valid state (not all 'off', all 'on' or with more than one group of 'on' sensors) then the central location of the group of 'on' sensors is calculated and converted into a binary number between 0 and 63. At this stage a validation flag is set to indicate that a new valid result is available for the inverter.

```
REGISTER DEFINITIONS

PC      =       R0      ;R0 IS THE PROGRAM COUNTER
STACK   =       R1      ;R1 IS THE STACK POINTER
POIS    =       R2      ;R2 IS THE PIO STATUS REGISTER
PORTA   =       R3      ;R3 IS THE PIO PORT A
PORTB   =       R4      ;R4 IS THE PIO PORT B
OUTP    =       R6      ;R6 IS THE INVERTER OUTPUT
COUNT   =       R7      ;R7 IS THE SENSOR COUNTER
SWAP    =       R8      ;R8 IS THE SWAP REGISTER
TABLE   =       R9      ;R9 IS THE SENSOR TABLE

CONSTANTS

POI     =       80H     ;UPPER ADDRESS OF PIO
CS      =       1       ;CONTROL REGISTER OF PIO
```

```
A         =         2       ;PORT A ADDRESS
B         =         3       ;PORT B ADDRESS
STK       =         18H     ;UPPER ADDRESS OF STACK 1
TOP       =         0FFH    ;LOWER ADDRESS OF MEMORY
NTOP      =         0FCH    ;UPPER ADDRESS OF STACK 2
LOWZ      =         0       ;ZERO LOWER ADDRESS
POUT      =         10H     ;OUTPUT PORT UPPER ADDRESS
TABLE     =         19H     ;UPPER ADDRESS OF TABLE
SWITCH    =         08H     ;PHASE OFFSET SWITCH ADDR.

ORG       0                 ;PROGRAM IS AT ADDRESS 0

INIT:     DIS
          DC        0H
```

THE NEXT SECTION INITIALISES R8 TO POINT TO THE ROUTINE RSWAP.

```
          LDI       RSWAP(HI);GET THE UPPER ADDRESS OF SWAP
          PHI       R8        ;SET IT TO THE POINTER
          LDI       RSWAP(LO);GET THE LOWER ADDRESS OF SWAP
          PLO       R8        ;SET IT TO THE POINTER
```

THE NEXT SECTION PLACES THE ADDRESS OF THE OFFSET SWITCH INTO R10.

```
          LDI       SWITCH    ;GET THE PHASE OFFSET ADDRESS
          PHI       RA        ;SET IT TO THE POINTER
          LDI       0         ;GET THE LOWER ADDRESS
          PHI       RA        ;SET IT TO THE POINTER
```

NOW THE UPPER ADDRESS OF THE PIO IS PLACED INTO R3, R4 AND R5.

```
          LDI       POI       ;GET THE HIGH PIO ADDRESS
          PHI       R3        ;SET R3 TO POINT TO THE PIO
          PHI       R4        ;SET R4 TO POINT TO THE PIO
          PHI       R5        ;SET R5 TO POINT TO THE PIO
```

THE LOWER ADDRESS OF THE PIO CONTROL REGISTER GOES TO R3.
THE LOWER ADDRESS OF THE PIO PORT A REGISTER GOES TO R4.
THE LOWER ADDRESS OF THE PIO PORT B REGISTER GOES TO R5.

```
          LDI       CS        ;GET THE CONTROL REG. OFFSET
          PLO       R3        ;SET R3 = CONTROL REGISTER
          LDI       A         ;GET THE PORT A OFFSET
          PLO       R4        ;SET R4 = PORT A
          LDI       B         ;GET THE PORT B OFFSET
          PLO       R5        ;SET R5 = PORT B
```

THE NEXT SECTION SETS UP THE POI

```
          LDI       EFH       ;GET THE PIO SETUP DATA
          STR       R3        ;STORE IN THE PIO CONTROL
          LDI       0         ;GET DATA
          STR       R3        ;SET PORT A TO ALL INPUTS
          LDI       F7H       ;GET DATA
          STR       R3        ;SET PORT A CONTROL
          LDI       0         ;GET DATA
          STR       R3        ;SET PORT B TO ALL INPUTS
          LDI       0CH       ;GET DATA
          STR       R3        ;SET ASTR AND ARDY AS INPUTS
          LDI       0EH       ;GET DATA
          STR       R3        ;SET BSTR AND BRDY AS INPUTS

NOW R6 IS POINTED TO THE INVERTER OUTPUT ADDRESS.
R2 IS POINTED AT THE STACK AND R9 AT A TABLE.

          LDI       POUT      ;GET UPPER ADDR. OF OUTPUT
          PHI       R6        ;POINT R6 TO OUTPUT
          LDI       LOWZ      ;SET LOW ADDR TO 0
          PLO       R6        ;SET R6
          LDI       STK       ;GET DATA
          PHI       R2        ;SET THE UPPER STACK ADDR.
          LDI       TABLE     ;GET DATA
          PHI       R9        ;SET THE UPPER TABLE ADDR.

THE INITIALISATION IS NOW OVER, THE MAIN LOOP IS ENTRED.
FIRSTLY, THE STACK AND SENSOR TABLE ARE RESET.

NOGO:     REQ                 ;SET VALID FLAG OFF
REENT:    LDI       TOP       ;GET THE STACK ADDR
          PLO       R2        ;RELOAD STACK POINTER
          SEX       R2        ;SET UP THE DATA
          PLO       R9        ;SET THE TABLE TO TOP

THEN THE PIO DATA FROM THE TRANDUCER SENSORS IS COLLECTED
AND PLACED ON THE STACK.

          LDN       R3        ;GET THE PIO STATUS
          SHLC                ;SAVE S0 TO CARRY
          SHLC                ;SAVE S1 TO CARRY
          STXD                ;PLACE IT ON THE STACK
          LDN       R4        ;GET S2-S9 TO ACCUM.
          STXD                ;SAVE THEM ON THE STACK
          LDN       R5        ;GET S10-S17 TO ACCUM.
          STXD                ;PLACE ON THE STACK
          LDN       R3        ;GET STATUS AGAIN
          BNF       LOOP1     ;BRANCH IF S19=1
          ANI       80H       ;STRIP OUT LOWER 7 BITS
          BR        LOOP2     ;GOTO LOOP2
LOOP1:    ORI       7FH       ;SET 1'S TO LOWER 7 BITS
LOOP2:    SHLC                ;D0 = S19, CARRY = S18
          SHLC                ;D0 = S18, D1 = S19
```

```
          STR       R2          ;STORE ON STACK

NOW THE DATA ON THE STACK IS COLLATED. FIRSTLY, CHECK
IF ALL THE SENSORS ARE OFF -- IF SO THEN INVALID OUTPUT

CHKOFF:   ANI       3H          ;CHECK IF S18=S19=0
          BNZ       ALLON       ;IF NOT CHECK ALL ARE ON
          IRX                   ;INCREMENT THE POINTER
          LDXA                  ;GET S10-S17 TO ACCUM.
          BNZ       ALLON       ;BRANCH IF NOT ZERO
          LDXA                  ;GET S2-S9  TO ACCUM.
          BNZ       ALLON       ;CHECK IF ALL OFF
          LDX                   ;GET S0 AND S1
          ANI       C0H         ;STRIP OUT S0 AND S1
          BZ        NOGO        ;IF ALL ARE OFF GOTO INVALID

NOW CHECK IF ALL THE SENSORS ARE ON -- IF SO THEN THIS
IS AN INVALID SENSOR ARRAY.

ALLON:    LDI       NTOP        ;GO TO THE START OF STACK
          PLO       R2          ;LOAD TO LOWER R2
          LDXA                  ;GET S18-S19 DATA
          XRI       3H          ;FLIP SENSE OF S18-S19
          BNZ       OKSOFAR     ;IF NON-ZERO THEN BRANCH
          LDXA                  ;GET S10-S17 DATA
          XRI       FFH         ;FLIP SENSE OF S10-S17
          BNZ       OKSOFAR     ;IF NON-ZERO THEN OK
          LDXA                  ;GET S2-S9 DATA
          XRI       FFH         ;FLIP THE SENSE
          BNZ       OKSOFAR     ;BRANCH IF NOT ALL ON
          LDX                   ;GET S0 AND S1
          XRI       C0H         ;FLIP ITS SENSE
          ANI       C0H         ;STRIP OUT LOWER BITS
          BZ        NOGO        ;IF ALL ARE ON GOTO INVALID

IF WE GET HERE THEN THE SENSORS ARE NOT REGISTERING EITHER
ALL OFF OR ALL ON SO WE MUST NOW FIND A GROUP OF SENSORS
THAT ARE ON.

OKSOFAR:  LDI       0           ;SET THE COUNTER START VALUE
          PLO       R7          ;TELL THE COUNTER THE VALUE
          LDI       FFH         ;SET R2 TO THE STACK TOP
          PLO       R2          ;LOCATION
          LDX                   ;GET THE S0 AND S1 DATA
          SHLC
          SHLC
          SHLC                  ;D0 = S0, D1 = S1

          LBR       STPOS.OFFDET    ;GOTO START OF CHECK

THE NEXT SECTION IS A CALLABLE SUBROUTINE USED DURING THE
MAIN SENSOR CHECKING LOOP. IT REENTERS THE MAIN CHECK
```

ROUTINE THAT HAS BEEN SET UP BY THE RSWAP ROUTINE.

```
GOBACK:  SEX      R2        ;SET NEW DATA COUNTER POINTER
         SEP      R0        ;SWAP THE PROGRAM COUNTER..GOBACK
```

THE NEXT ROUTINE IS USED WHEN A CHANGE IN THE STATE OF THE SENSORS IS DETECTED. IT MAKES A NOTE OF THE POINT AT WHICH THE STATE CHANGE OCCURRED AND SWAPS THE REGISTERS SO THAT THE COMPEMENTARY ROUTINE WILL BE REENTERED.

```
RSWAP:   PLO      RF        ;USE REGISTER F TO STORE ACC.
         SEX      R9        ;SWAP TO R9 DATA POINTER->TABLE
         GLO      R7        ;GET THE SENSOR COUNT TO ACC.
         STXD               ;STORE THE CURRENT POSITION
         SMI      20        ;SUBTRACT 20 FROM THE COUNTER
         BZ       DONEIT    ;IF ZERO THEN EXIT FROM MAIN.
         GHI      R0        ;ELSE, GET HIGH PROG. COUNTER
         XRI      01H       ;SWAP TO THE OTHER STATE.
         PHI      R0        ;PUT BACK THE PROG. COUNTER
         GLO      RF        ;RETRIEVE THE ACCUMULATOR VALUE
         BR       GOBACK    ;GO TO THE RETURNING ROUTINE.
```

THE FOLLOWING CODE IS ENTERED ONLY WHEN ALL 20 SENSORS HAVE BEEN CHECKED AND STATE CHANGES RECORDED.

```
DONEIT:  GLO      R9        ;GET THE CURRENT STACK POINTER
         SMI      FBH       ;CHECK THE NUMBER OF ENTRIES
         BNF      INVRET    ;IF TOO MANY THEN SET INVALID
         BZ       FOURV     ;IF 3 OR LESS THEN IT IS VALID
         SMI      01H       ;DECREMENT THE ACCUMULATOR
         BZ       VALID     ;GOTO VALID IF IT IS OK.
         LDI      20        ;ELSE, SET THE THIRD RESULT=20
         STXD               ;STORE IT
         BR       VALID     ;NOW GOTO VALID
```

IF FOUR VALUES ARE STORED THEN FUTHER CHECKS TO SEE THAT THE FIRST ONE WAS AT SENSOR ZERO.

```
FOURV:   LDI      FFH       ;GET THE POINTER TO FIRST VALUE
         PLO      R9        ;SET R9 TO POINT AT IT
         LDX                ;GET THE VALUE TO THE ACCUMULATOR
         BNZ      INVRET    ;IF NON-ZERO THEN INVALID
```

THIS SECTION OF CODE IS EXECUTED IF THE 20 SENSORS GIVE A VALID SEQUENCE. THEN TRANSDUCER OUTPUT DATA IS CALCULATED AND PLACED ONTO THE OUTPUT LATCH THE VALID BIT IS SET AND THE MAIN LOOP IS REENTERED.

```
VALID:   LDI      FDH       ;GET THE POINTER TO THIRD VALUE
         PLO      R9        ;SET R9 TO POINT AT IT
         LDXA               ;GET THE FIRST RESULT
         ADD                ;ADD THE SECOND RESULT
```

```
          IRX               ;INCREMENT THE DATA POINTER
          ADD               ;ADD THE THIRD RESULT
          SEX       RA      ;POINT DATA AT THE OFFSET SWITCH
          ADD               ;ADD IN THE OFFSET
          BDF       LOOP4   ;IF CARRY THEN ADD 40
          SMI       40      ;SUBTRACT FOURTY
          BDF       LOOP3   :IF CARRY THEN DONE ADD IT BACK
LOOP4:    ADI       40      ;IF NO CARRY THEN ADD IT BACK
```

THE NEXT SECTION MULTIPLIES THE 0-39 NUMBER UP SO THAT IT COVERS A RANGE OF 0-63. THIS IS DONE BY MULTIPLYING BY 1.10011 IN BINARY

```
LOOP3:    SEX       RB      ;POINT AT A STORAGE LOCATION
          SHL               ;SHIFT LEFT ACCUMULATOR
          STR       RB      ;PUT IT INTO RB POINTER
          SHL               ;SHIFT IT AGAIN
          ADD               ;ADD IT IN TO THE LAST RESULT
          STR       RB      ;PUT IT INTO RB POINTER
          SHR               ;DIVIDE BY TWO
          SHR               ;NOW BY FOUR
          SHR               ;NOW BY EIGHT
          SHR               ;NOW BY SIXTEEN
          ADD               ;ADD IT TO THE ACCUMULATOR
          SHR               ;DIVIDE THE RESULT BY TWO
          SHR               ;TWICE TO COMPENSATE FOR SHL
          STR       R6      ;STORE THE RESULT TO OUTPUT
          SEQ               ;SET THE VALID BIT.
```

SETUP THE REENTRY TO THE MAIN LOOP USING THE GOBACK ROUTINE

```
          LDI       REENT(HI);GET THE REENTRY HIGH ADD.
          PHI       R0      ;POINT R0 HIGH BYTE AT IT
          LDI       REENT(LO);GET THE REENTRY LOW ADD.
          PLO       R0      ;POINT R0 LOW BYTE AT IT
          BR        GOBACK  ;USE THE GOBACK ROUTINE
```

IF AN INVALID RETURN HAS BEEN DETECTED IN THE SENSORS THEN THE FOLLOWING SECTION OF CODE IS CALLED.

```
INVRET:   LDI       NOGO(HI) ;GET THE NOGO HIGH ADDR.
          PHI       R0       ;SET R0 HIGH
          LDI       NOGO(LO) ;GET THE NOGO LOW ADDR.
          PLO       R0       ;SET RO LOW
          BR        GOBACK   ;GO BACK AND SET INVALID BIT
```

THE FOLLOWING TWO ROUTINES ARE VERY EFFICIENT SENSOR STATE CHECKERS. THESE ARE COMPLEMENTARY ROUTINES WHICH HAVE AN EXACT CORRESPONDANCE INSTRUCTION FOR INSTRUCTION. IF THE SENSORS SHOULD CHANGE STATE THEN THE FLOW OF THE PROGRAM JUMPS FROM ONE OF THEM TO TO OTHER AT EXACTLY THE SAME POINT. THE JUMP IS EXECUTED BY THE RSWAP ROUTINE WHICH ALSO

```
STORES THE SENSOR NUMBER AT WHICH THE STATE CHANGE OCCURRED

ORG     200H            ;ADDRESS OF THE OFF DETECTOR
;
OFFTOP: DEC     R2      ;DECREMENT THE DATA COUNTER
        LDX             ;GET THE 8 BITS OF DATA
        INC     R7      ;SENSOR COUNT = COUNT + 1
        SHRC            ;SHIFT THE NEXT SENSOR BIT
        BNF     L1      ;CHECK IF SENSOR IS ON
        SEP     R8      ;IF SO THEN JUMP TO RSWAP
L1:     INC     R7      ;SENSOR COUNT = COUNT + 1
        SHRC            ;SHIFT THE NEXT SENSOR BIT
        BNF     L2      ;CHECK IF SENSOR IS ON
        SEP     R8      ;IF SO THEN JUMP TO RSWAP
L2:     INC     R7      ;SENSOR COUNT = COUNT + 1
        SHRC            ;SHIFT THE NEXT SENSOR BIT
        BNF     L3      ;CHECK IF SENSOR IS ON
        SEP     R8      ;IF SO THEN JUMP TO RSWAP
L3:     INC     R7      ;SENSOR COUNT = COUNT + 1
        SHRC            ;SHIFT THE NEXT SENSOR BIT
        BNF     L4      ;CHECK IF SENSOR IS ON
        SEP     R8      ;IF SO THEN JUMP TO RSWAP
L4:     INC     R7      ;SENSOR COUNT = COUNT + 1
        SHRC            ;SHIFT THE NEXT SENSOR BIT
        BNF     L5      ;CHECK IF SENSOR IS ON
        SEP     R8      ;IF SO THEN JUMP TO RSWAP
L5:     INC     R7      ;SENSOR COUNT = COUNT + 1
        SHRC            ;SHIFT THE NEXT SENSOR BIT
        BNF     L6      ;CHECK IF SENSOR IS ON
        SEP     R8      ;IF SO THEN JUMP TO RSWAP
L6:     INC     R7      ;SENSOR COUNT = COUNT + 1
STPOS:  SHRC            ;SHIFT THE NEXT SENSOR BIT
        BNF     L7      ;CHECK IF SENSOR IS ON
        SEP     R8      ;IF SO THEN JUMP TO RSWAP
L7:     INC     R7      ;SENSOR COUNT = COUNT + 1
        SHRC            ;SHIFT THE NEXT SENSOR BIT
        BNF     OFFTOP  ;CHECK IF SENSOR IS ON
        SEP     R8      ;IF SO THEN JUMP TO RSWAP
        BR      OFFTOP  ;LOOP

AND THE COMPLEMENTERY ROUTINE FOR DETECTING ON SENSORS..

ORG     300H            ;ADDRESS OF THE ON DETECTOR
;
ONTOP:  DEC     R2      ;DECREMENT THE DATA COUNTER
        LDX             ;GET THE 8 BITS OF DATA
        INC     R7      ;SENSOR COUNT = COUNT + 1
        SHRC            ;SHIFT THE NEXT SENSOR BIT
        BDF     L1      ;CHECK IF SENSOR IS OFF
        SEP     R8      ;IF SO THEN JUMP TO RSWAP
L1:     INC     R7      ;SENSOR COUNT = COUNT + 1
        SHRC            ;SHIFT THE NEXT SENSOR BIT
```

```
        BDF     L2      ;CHECK IF SENSOR IS OFF
        SEP     R8      ;IF SO THEN JUMP TO RSWAP
L2:     INC     R7      ;SENSOR COUNT = COUNT + 1
        SHRC            ;SHIFT THE NEXT SENSOR BIT
        BDF     L3      ;CHECK IF SENSOR IS OFF
        SEP     R8      ;IF SO THEN JUMP TO RSWAP
L3:     INC     R7      ;SENSOR COUNT = COUNT + 1
        SHRC            ;SHIFT THE NEXT SENSOR BIT
        BDF     L4      ;CHECK IF SENSOR IS OFF
        SEP     R8      ;IF SO THEN JUMP TO RSWAP
L4:     INC     R7      ;SENSOR COUNT = COUNT + 1
        SHRC            ;SHIFT THE NEXT SENSOR BIT
        BDF     L5      ;CHECK IF SENSOR IS OFF
        SEP     R8      ;IF SO THEN JUMP TO RSWAP
L5:     INC     R7      ;SENSOR COUNT = COUNT + 1
        SHRC            ;SHIFT THE NEXT SENSOR BIT
        BDF     L6      ;CHECK IF SENSOR IS OFF
        SEP     R8      ;IF SO THEN JUMP TO RSWAP
L6:     INC     R7      ;SENSOR COUNT = COUNT + 1
STPOS:  SHRC            ;SHIFT THE NEXT SENSOR BIT
        BDF     L7      ;CHECK IF SENSOR IS OFF
        SEP     R8      ;IF SO THEN JUMP TO RSWAP
L7:     INC     R7      ;SENSOR COUNT = COUNT + 1
        SHRC            ;SHIFT THE NEXT SENSOR BIT
        BDF     ONTOP   ;CHECK IF SENSOR IS OFF
        SEP     R8      ;IF SO THEN JUMP TO RSWAP
        BR      ONTOP   ;LOOP
```

APPENDIX 3. Pole Transducer Setup Procedure

The source frequency of the exciter coil is adjusted to about 100 kHz for peak output from the signal amplifiers.

The sensor array is centred over the source coil. Individual sensors are trimmed by sliding them along their major axis until a minimum pickup is obtained for each sense coil.

The sensitivity of each sensor can be balanced by feeding all amplifiers with the same signal (by replacing the sense coils with a signal generator). The threshold potentiometers can then be adjusted such that the red sensor LEDs all come on at the same signal level.

Once adjusted, when the sense coils are reconnected all the LEDs should be off. Now if the sense coils are all moved together along their major axes they should all come on at the same amount of shift.

When the sense coil array is replaced centrally over the source coil the array is able to detect the position of

the edge of a pole piece. The sensitivity of the transducer may be adjusted by:-

1. Controlling the source coil amplitude.
2. Adjusting the comparator threshold potentiometers.

APPENDIX 4. Magnet Levitation System Linearisation

Applying the equation for the air gap force generated by a levitated magnet about a working point air gap Zo and a working point current Io gives the following equation for small changes in air gap and current:-

$$F = Fo + \Delta F = \frac{Km.(Io + \Delta I)^2}{(Zo + \Delta Z)^2} \qquad \ldots\ldots A4.1$$

Where ΔF, ΔZ and ΔI represent small changes in force air gap and current respectively about the working point. Taking partial derivatives for F with respect to both air gap and current gives:-

$$\Delta F = \frac{\delta F}{\delta I}\Big|_{Io} .\Delta I + \frac{\delta F}{\delta Z}\Big|_{Zo} .\Delta Z \qquad \ldots\ldots A4.2$$

Which using equation A4.1 produces:-

$$\Delta F = \frac{2.Km.Io.\Delta I}{Zo^2} - \frac{2.Km.Io^2.\Delta Z}{Zo^3} \qquad \ldots\ldots A4.3$$

Now, as the steady state levitated working point Fo must be equal to Mt.g where Mt is the mass of the levitated magnet and g is the gravitational constant:-

$$Fo = \frac{Km.Io^2}{Zo^2} = Mt.g \qquad \ldots\ldots \text{A4.4}$$

Equation A4.3 can be rewritten in terms of equation A4.4 such that:-

$$\Delta F = \frac{2.Fo}{Io}.\Delta I - \frac{2.Fo}{Zo}.\Delta Z = \frac{2.Mt.g}{Io}.\Delta I - \frac{2.Mt.g}{Zo}.\Delta Z \qquad \ldots\ldots \text{A4.5}$$

At the working point the incremental force ΔF represents an accelerating force such that:-

$$\frac{\delta^2 \Delta Z}{\delta t^2} = -\frac{\Delta F}{Mt} \qquad \ldots\ldots \text{A4.6}$$

Substituting for ΔF in the above equation gives a linearised second order differential equation in terms of ΔI and ΔZ, such that:-

$$\frac{\delta^2 \Delta Z}{\delta t^2} = -\frac{2.g}{Io}.\Delta I + \frac{2.g}{Zo}.\Delta Z$$

..... A4.7

This differential equation can be expressed using the Laplace operator 's' such that:-

$$\Delta Z(s).s^2 = -\frac{2.g}{Io}.\Delta I(s) + \frac{2.g}{Zo}.\Delta Z(s)$$

..... A4.8

which can be rearranged to give the linearised laplace transfer function for the levitated magnet as:-

$$\frac{\Delta Z(s)}{\Delta I(s)} = \frac{-\frac{2.g}{Io}}{(s^2 - \frac{2.g}{Zo})}$$

APPENDIX 5. Single Magnet Controller Design

The following design was carried out using the linearised single magnet system described in section 6.3. The design is for a second order dominated and critically damped response with $w_n = 5.0$ rad.s^{-1} and $\zeta = 0.7071$. The controller type used is that described in section 6.4.2 which incorporated the integrator for force offset restoration. The open loop linearised system equations are given as:-

$$G(s) = \frac{1.64 * 41.0}{(s + 41.0)(s^2 - 3270)} \qquad \ldots\ldots \text{A5.1}$$

The closed loop transfer function for a system of the type presented in section 6.4.2. is:-

$$T(s) = \frac{1.64 * 41.0 * h_0 * k}{s(s + 41)(s^2 - 3270) + 1.64*41.0*k(h_2.s^2 + h_1.s + h_0)} \qquad \ldots\ldots \text{A5.2}$$

A5-2

This system has a fourth order closed loop characteristic equation given by:-

$$s(s+41)(s^2-3270) + 1.64*41.0*k(h_2.s^2 + h_1.s + h_0) = 0 \quad \ldots\ldots \text{A5.3}$$

For this design the non-dominant pair of poles are calculated to be identical and lie on the negative real axis of the s-domain. This then gives a required characteristic equation for the closed loop system of:-

$$(s^2 + 2.p.s + p^2)(s^2 + 2.\zeta.w_n.s + w_n^2) = 0 \quad \ldots\ldots \text{A5.4}$$

Where 'p' represents the position of the non-dominant closed loop poles. The choice of p is fixed by the s^3 coefficient of equation A5.3 as there is no control over this in the design. This gives:-

$$2.p + 2.\zeta.w_n = 41.0 \quad \ldots\ldots \text{A5.5}$$

which for $w_n = 5.0$ and $\zeta = 0.7071$ gives:-

$$p = 17.0 \quad \ldots\ldots \text{A5.6}$$

This gives two non-dominant poles at s = -17.0 in the s-domain. This sets the required characteriatic equation to:-

$$s^4 + 41s^3 + 552.5s^2 + 2882.5s + 7195 = 0 \qquad \ldots\ldots \text{A5.7}$$

Equating coefficients between the above equation and A5.3 and choosing $h_1 = 1.0$ gives the following set of controller gains:-

$k = 2037$

$h_0 = 0.053$

$h_1 = 1.0$

$h_2 = 0.027$

APPENDIX 6. Side Magnet Stability for Zero Standing Currents

The following analysis considers the effects on stability of reducing the standing currents in the side magnets to zero. In the standard linearised model of the levitated system that was derived in appendix 6 it can be seen that it was necessary to have a non-zero operating point current, Io. If Io was set to zero the system forward path gain vanished making a normal linear design impossible. However, in the side magnet system this would only occur when no disturbance was present. As soon as any disturbance occurs a magnet current would be generated. However, it was not clear that the system would be stable.

If the open loop levitation transfer function is:-

$$G(s) = \frac{-Ki.p}{(s+p)(Mt.s^2 - Kz)} \qquad \ldots\ldots A6.1$$

Where:-

$$Ki = \frac{2.Km.Io}{Zo^2} \qquad \ldots\ldots \text{A6.2}$$

$$Kz = \frac{2.Km.Io^2}{Zo^3} \qquad \ldots\ldots \text{A6.3}$$

Then the closed loop transfer function is:-

$$T(s) = \frac{-k.Ki.h_0.p}{s(s+p)(Mt.s^2 - Kz) + p.k.Ki(h_2s^2 + h_1s + h_0)} \qquad \ldots\ldots \text{A6.4}$$

This gives the closed loop characteristic equation as:-

$$Mt.s^4 + p.Mt.s^3 + (p.k.Ki.h_2 - Kz)s^2 + (p.k.Kih_1 - Kz.p)s + p.k.Ki.h_0 = 0 \qquad \ldots\ldots \text{A6.5}$$

A necessary condition for stability is that all the coefficients of this characteristic equation are finite and have the same sign. This leads to:-

$$p.Ki.k.h_2 > Kz \qquad \ldots\ldots \text{A6.6}$$

and $p.Ki.k.h_1 > p.Kz$ A6.7

Conventionally Kz and Ki are finite and positive when there is a standing current in the magnet windings. This would occur in the side magnet control system if there were a constant lateral force offset (for instance cause by cornering). If a side force of Fo is available then it can be seen that a standing current propotional to the square route of this force will flow in the magnet coils:-

$Io \propto \sqrt{Fo}$ A6.8

From the above definitions for Ki and Kz it is seen that:-

$Ki \propto Kz/Io$ at a nominal air gap Zo A6.9

Using these last two relationships produces the relationship:-

$Ki \propto Kz/\sqrt{Fo}$ A6.10

This last relationship shows that for all steady side forces smaller than Fo the proportion Ki:Kz increases. This

will maintain stability as it will always satisfy relationships A6.6 and A6.7. In fact, decreasing Fo improves these relationships in that the left hand side increases further. This suggests that a true zero standing current controller might have improved stability over one which employed standing currents.

A sufficient condition for stability is to find the points at which the root locus crosses the imaginary axis in the s-plane into the stable left hand half-plane. At the point when the locus cuts the imaginary axis it is possible to put $s = jw$. Putting this into the system characteristic equation and then separating this into real and imaginary components gives:-

$$Mt.w^4 + (Kz - p.k.Ki.h_2).w^2 + p.k.Ki.h_0 = 0$$

For the real component, and

..... A6.11

$$-j.p.Mt.w^3 + j.(p.k.Ki.h_1 - p.Kz).w = 0$$

For the imaginary component

..... A6.12

Solving for w in the imaginary component gives:-

$$w^2 = \frac{k.Ki.h_1 - Kz}{Mt}$$

..... A6.13

Substituting for w^2 using the real component gives:-

$$(Ki^2.h_1{}^2 - p.Ki^2.h_1.h_2).k^2 + (Kz.p.Ki.h_2 + p.Ki.h_0.Mt - Kz.Ki.h_1).k = 0 \quad \ldots\ldots \text{A6.14}$$

The non-trivial solution to this gives the limit of stability for k in terms of the controller feedback gains and system linearised gains:-

$$k = \frac{Kz.h_1 - Kz.p.h_2 - p.h_0.Mt}{Ki.h_1.(h_1 - p.h_2)} \quad \ldots\ldots \text{A6.15}$$

For stability this then requires that:-

$$Ki.k.h_1(h_1 - p.h_2) > Kz.(h_1 - p.h_2) - p.h_0.Mt \quad \ldots\ldots \text{A6.16}$$

This equation shows that if a value of k can be found to give a stable system for a given mass, Mt, then any increase in the mass will improve this inequality in favour of stability. From this it is seen that the worst case is when the mass is zero. For Mt = 0 the above reduces to:-

$$h_1.Ki.k > Kz \quad \ldots\ldots \text{A6.17}$$

It is noticed that the form of this inequality is the same as the necessary condition for stability of equation A6.7 hence the preceeding argument for stability is both necessary and sufficient.

This analysis shows that the form of controller given in figure 6.4.13 should produce a stable system for all standing currents less than the standing current at which the system was designed as long as all other parameters remain the same.

APPENDIX 7. Side Magnet Controller Design

The design recorded here was based on the linearised system model of equation 7.4.1 in chapter 7 of this thesis and shown in block diagram form in figure 7.4.4.

The design approach was to approximate the fourth order characteristic equation to a combination of two second order components so that it took the form:-

$$(s^2 + 2.\zeta_1.w_{n1}.s + w_{n1}^2)(s^2 + 2.\zeta_2.w_{n2}.s + w_{n2}^2) = 0 \quad \ldots\ldots \text{A7.1}$$

The parameters ζ_1, w_{n1}, ζ_2 and w_{n2} were chosen such that ζ_1 and w_{n1} produced dominant closed loop poles describing the desired second order response. There were two possible ways to proceed and these will be described separately.

7.1. Design 1

The first design set w_{n1} to 20.0 rad.s^{-1} and ζ_1 to 0.5. So that this set of closed loop poles could be dominant it was decided to put the other pair at a distance of $5.\zeta_1.w_{n1}$

from the origin in the s-domain. ζ_2 could not be chosen independently because the closed loop characteristic equation for the side magnet system did not allow control over the s^3 coefficient (see equation 7.4.2). This restriction gave rise to the following relationship:-

$$2.\zeta_1.w_{n1} + 2.\zeta_2.w_{n2} = 30.0 \qquad \ldots\ldots \text{A7.2}$$

Using the information above it was possible to derive $\zeta_2 = 0.1$. Substituting for all the variables in equation A7.1 gave the following required closed loop characteristic equation:-

$$s^4 + 30s^3 + 3100s^2 + 54000s + 1000000 = 0 \qquad \ldots\ldots \text{A7.3}$$

Once this had been derived the rest of the design involved equating coefficients between the two equations A7.3 and 7.4.2 so that for $h_1 = 1.0$ this gave:-

$$k = \frac{54000 + 7822}{3.674} = 16843.0 \qquad \ldots\ldots \text{A7.4}$$

$$h_0 = \frac{1000000}{k*3.674} = 16.1624 \qquad \ldots\ldots \text{A7.5}$$

$$h_2 = \frac{3100 + 262.4}{k*3.674} = 0.05434 \qquad \ldots\ldots \text{A7.6}$$

The feedback zeros for this system were given by the solution of:-

$$h_0 + h_1.s + h_2.s^2 = 0 \qquad \ldots\ldots \text{A7.7}$$

7.2. Design 2

An alternative technique that was used was to define the pole pair represented by ζ_1 and w_{n1} to be dominant such that:-

$$\zeta_2.w_{n2} = 5.\zeta_1.w_{n1} \qquad \ldots\ldots \text{A7.8}$$

Now substituting for ζ_2 and w_{n2} in equation A7.2 gave:-

$$12.\zeta_1.w_{n1} = 30.0 \qquad \ldots\ldots \text{A7.9}$$

ζ_1 was chosen to be 0.5 which then gave $w_{n1} = 5.0$ rad.s^{-1} and also:-

$$\zeta_2 . w_{n2} = 12.5 \qquad \ldots\ldots \text{A7.10}$$

ζ_2 was chosen to be 0.2 which gave w_{n2} as 62.5. All these values were substituted into equation A7.1 and gave the required closed loop characteristic equation:-

$$s^4 + 30s^3 + 4056.25s^2 + 20156.25s + 97656.25 = 0 \qquad \ldots\ldots \text{A7.11}$$

Equating coefficients between the above equation and equation 7.4.2 gave the control feedback gains as:-

$k = 7630.0$

$h_0 = 3.4842$

$h_1 = 1.0$

$h_2 = 0.1541$

ACKNOWLEDGEMENTS

The author would like to express thanks to Professor J.F. Eastham for the support and use of the facilities of the School of Electrical Engineering at The University of Bath; Mr. A.R. Daniels for his constant guidance and supervision; Dr. M.J. Balchin for the design of the motors used; Dr. R.T. Lipczynski and Mr. V.S. Gott for their many useful suggestions and help with construction of the vehicle; Dr. B.A. White for his help with the theoretical aspects of the VSCS controllers used; Dr P.F. Whitworth for useful discussions about the design of the microprocessor systems.

Thanks are also due to Miss T.A. Stagg for help with technical proof reading and typing during the writing of this thesis.

REFERENCES

1. JAYAWANT, B.V, SINHA P.K., WHEELER, A.R., WHORLOW, R.J. and WILLSHER J.: 'Development of a 1 ton magnetically suspended vehicle using controlled d.c. electromagnets'.
PROC IEE, Vol 123, No. 9 Sept 1976.

2. JAPAN NATIONAL RAILWAYS: report October 1972.

3. GOTTZEIN, E., BROCK, K., SCHNEIDER, E. and PFEFFERL, J.: 'Control aspects of a tracked magnetic levitation high speed vehicle'.
AUTOMATICA, Vol 13, pp 205-225, 1977.

4. BARWELL, F.T., and LAITHWAITE, E.R.: 'Application of linear induction motors to high speed ground transport'.
PROC IMECHE, Vol 181, 3G, 1967.

5. BALCHIN, M.J. and EASTHAM, J.F.: 'Characteristics of a heteropolar linear synchronous machine with passive secondary'.
IEE Electrical Power Applications, Vol 2, No. 6, pp 213-218, 1979.

6. EASTHAM, J.F., BALCHIN, M.J. and RODGER, D.: 'A comparison of some propulsion methods for magnetically levitated vehicles':
IMECHE C406/84, 1984

7. EARNSHAW, S.: 'On the nature of the molecular forces which regulate the constitution of the luminiferous ether'.
Transactions of the Cambridge Philosophical Society, Vol 7, 1842.

8. BRAUNBEK, W.: 'Free suspension of bodies in electric and magnetic fields'.
Zeitschrift fur Physik, Vol 112, No. 11-12, 1939.

9. LAITHWAITE, E.R.: 'Electromagnetic levitation'
PROC IEE, Vol 112, No. 12, pp 2361-75, 1965

10. GOTTZEIN, E., and LANGE B.: 'Magnetic suspension control systems for the MBB high speed train',
AUTOMATICA, VOL 11, pp 271-284, 1975.

11. POWELL, J.R.: 'The magnetic road',
IEEE, Paper 63-RR-4, April 1963.

12. THORNTON, R.D.: 'Design principles for magnetic levitation',
PROC IEE, Vol 61, No. 5, May 1973.

13. POLGREEN, G.R.: 'Systems of transportation',
BRITISH PATENTS 867,045, August 1958.

14. POWELL, J.R.: 'High speed transport by magnetically suspended trains'
IEEE, Paper 66-RR-5A, SME annual meeting 1966.

15. GUDERJAHN ET AL.: 'Magnetic suspension and guidance for High speed rockets by superconducting magnets',
J.A.Physics VOL 40, 1969.

16. LAITHWAITE, E.R.: 'Linear motion machines'
PROC IEE, Vol 118, 1971.

17. EASTHAM, J.F.: 'The Magnetic River',
Paper presented to the town meeting of the SRC (Advanced Ground Transport Panel), London 24th Feb. 1978.

18. EASTHAM, J.F. and LAITHWAITE, E.R.: 'Linear induction motors and electro-magnetic rivers',
PROC IEE, Vol 121, pp 1099-1107, 1974.

19. EASTHAM, J.F.: 'Iron-cored Linear Synchronous Machines',
Electronics and Power, pp 239-24, March 1977.

20. BALCHIN, M.J., HELANI, M.F. and EASTHAM, J.F.: 'A comparison of the characteristics of the heteropolar and homopolar linear synchronous motors',
IEE coloquium digest, 20 March 1983.

21. LEVI, E.: 'High-speed, iron-cored, symchronously operating linear motors',
IEE conference publication No. 122 pp 155-160

22. BALCHIN, M.J.: 'Design of linear synchronous motors and guidance magnets',
August 1984.

23. NG, P.: 'Control of heteropolar transverse-flux Linear Synchronous Motors',
PhD. THESIS, University of Bath, 1981.

24. JAYAWANT, B.V.: 'Electromagnetic Levitation and Suspension Techniques',
Published by Edward Arnold, ISBN 0 7131 3428 3,
pp 97-105, 1981.

25. GOTT, V.S.: '23-linear thyristor amplifiers', Product Design Engineering, January 1969.

26. TEXAS INSTRUMENTS INC.: '9900 family systems design and data book', 1978.

27. TEXAS INSTRUMENTS INC.: 'Micro systems designers handbook', 1981.

28. MOTOROLA INC.: 'MC68000 16-bit microprocessor user's manual', 1979.

29. ADVANCED MICRO DEVICES INC.: 'AmZ8000 family data book', 1980.

30. TANNER, D.T.: 'Real time simulation of power systems', PhD. THESIS, University of Bath, Appendix A, 1982.

31. THOMPSON CFS.: 'EF9965 application and data sheet', 1981.

32. THAME SYSTEMS LTD.: 'SCSI, Small Computer Systems Interface',
ANSI X379.2/82-2 REV 2, June 1982.

33. DATA RECORDING EQUIPMENT LTD.: 'Technical manual for the diskette drive model 7200',
Document reference 7200/TM, issue A, 1980.

34. WESTERN DIGITAL CORPORATION: '1983 components handbook',
pp 195-211, 1983.

35. UTKIN, V.I.: 'Sliding modes and their applications in variable-structure systems',
MIR Publications, Translated by A. Parakh, 1978.

36. DIGITAL RESEARCH INC.: 'CP/M-68K operating system user's guide',
Second edition, June 1983.

37. WESTERN ELECTRIC: 'User's Guide - UNIX System',
Basic Documentation 301-921, issue 1, June 1982.

38. RICHARDS, M., AYLWARD, A.R., BOND, P., EVANS, R.D., KNIGHT, B.J.: 'TRIPOS - A portable operating system for mini-computers',
Software Practice and Experience, VOL 9, pp 513-526, 1979.

39. MOTOROLA INC.: 'MC68451 data sheet', 1980.

40. RICHARDS, M., WHITLY-STEVENS, C.: 'BCPL, the language and its compiler',
CAMBRIDGE UNIVERSITY PRESS, 1980.

41. THE RAND CORPORATION: 'REDUCE 3 manual', 1983.

42. GOTTZEIN, E., LANGE, B. and OSSENBERG-FRANZES, F.: 'Control system concept for a passenger carrying MAGLEV vehicle',
PROC international conference on high speed ground transportation, pp 435, January 1975.

43. GONDHALEKAR, V.M.: 'Control systems and dynamics of a magnetically suspended vehicle',
PhD. THESIS, University of Sussex, 1980.

44. JAYAWANT, B.V.: 'Electromagnetic Levitation and Suspension Techniques',
Published by Edward Arnold, ISBN 0 7131 3428 3, 1981.

45. STILL, P.B. and WINNET, M.A.: 'Development of a contactless displacement transducer',
T.R.R.L., 1975.

46. DALE, L.A.: 'Real Time Modelling of Multi-Machine Power Systems',
PhD. THESIS, University of Bath, 1986.

47. WHITE, B.A., WONG D.K.K.: 'The response of variable structure systems to reference input demands'
School of Electrical Engineering, The University of Bath, 1982

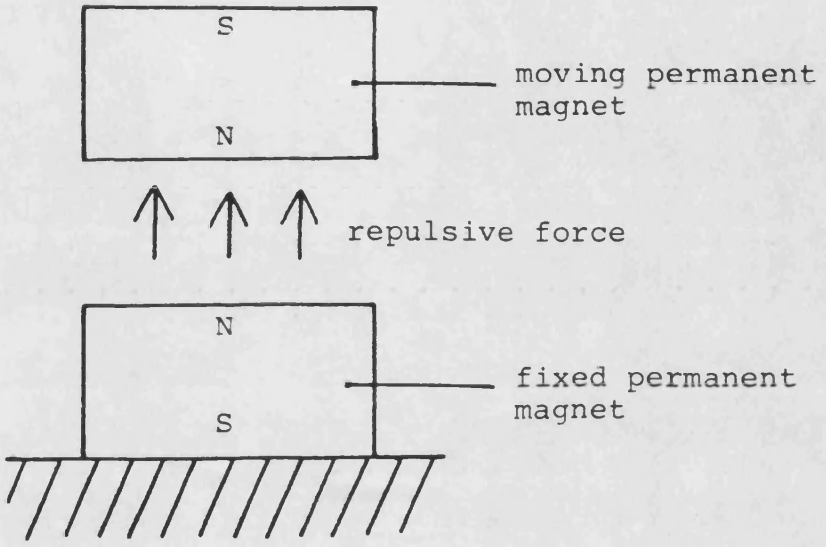

Figure 1.2.1 A permanent magnet levitation system

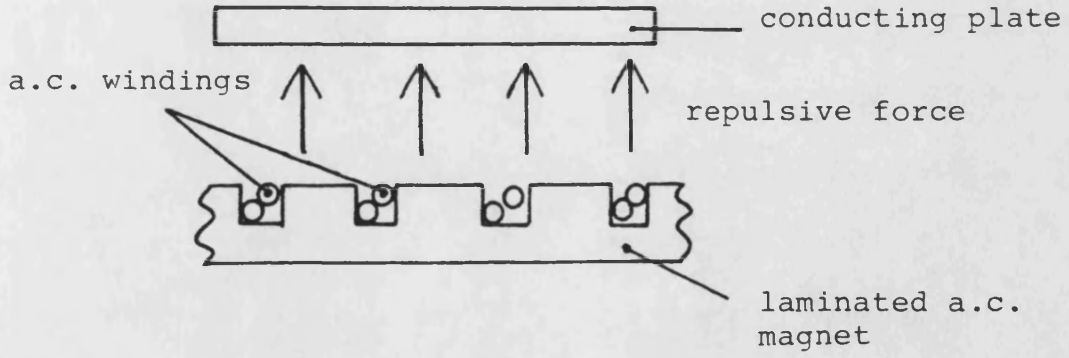

Figure 1.2.2 An induced eddy current levitation system using A.C. current

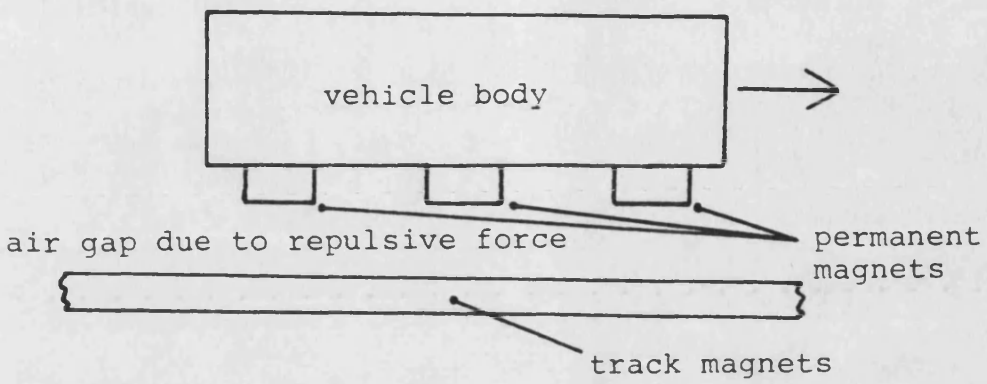

Figure 1.3.1 A permanent magnet levitated vehicle, 'Magna rail'

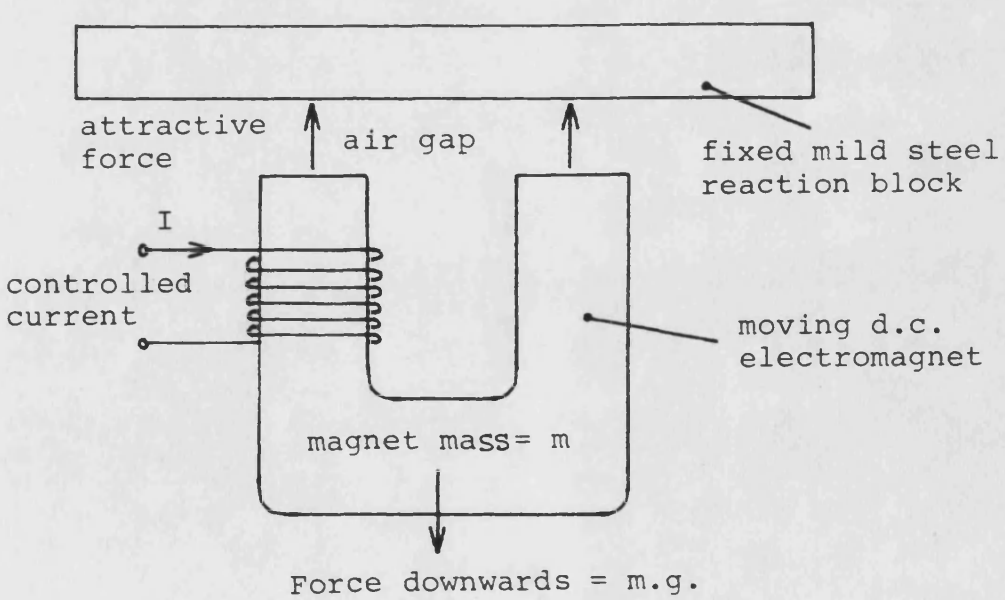

Figure 1.3.2 A controlled D.C. magnet suspension system

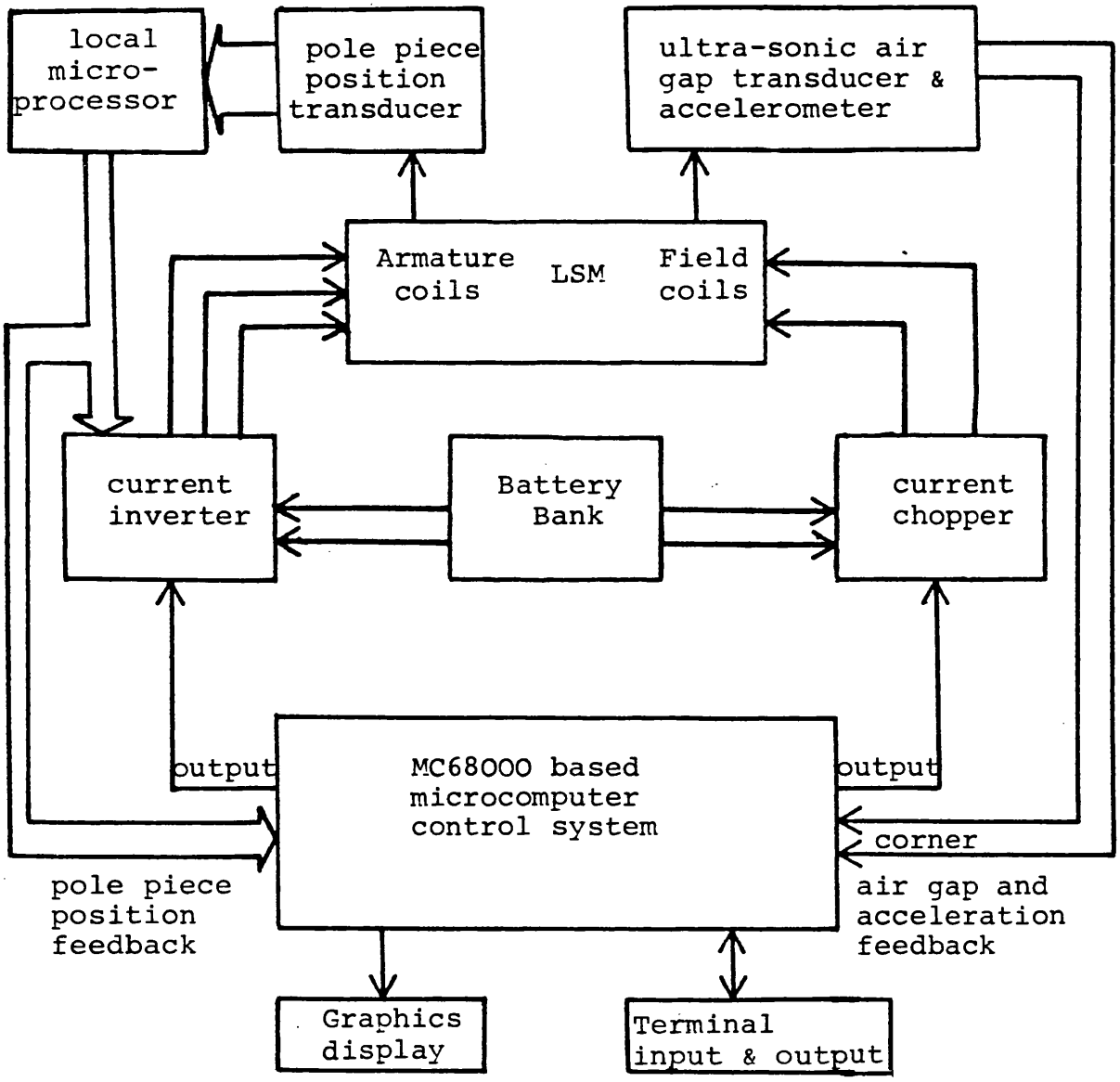

Figure 2.2.1 General block diagram of the LSM control scheme

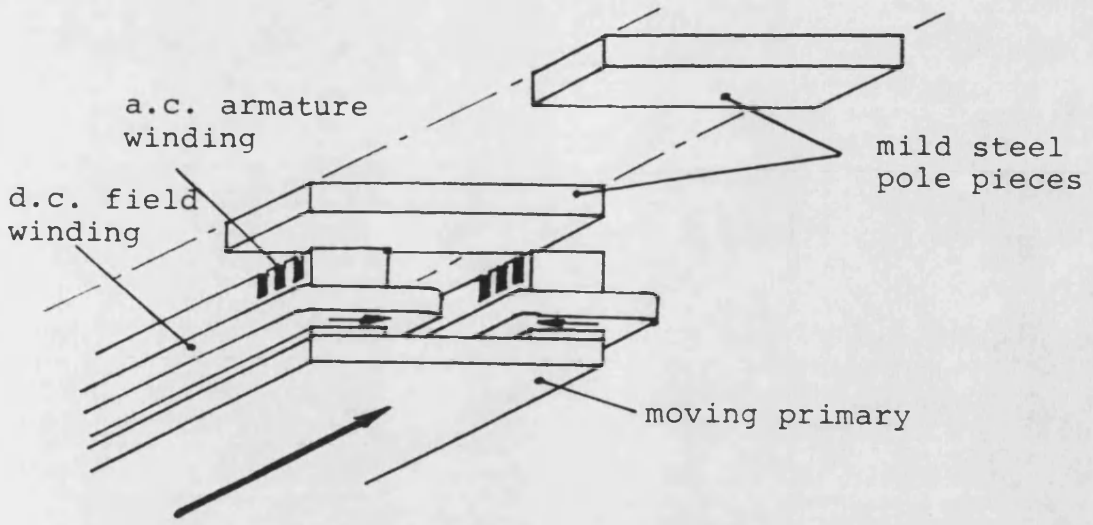

Figure 2.3.1 The Transverse Flux Homopolar L.S.M.

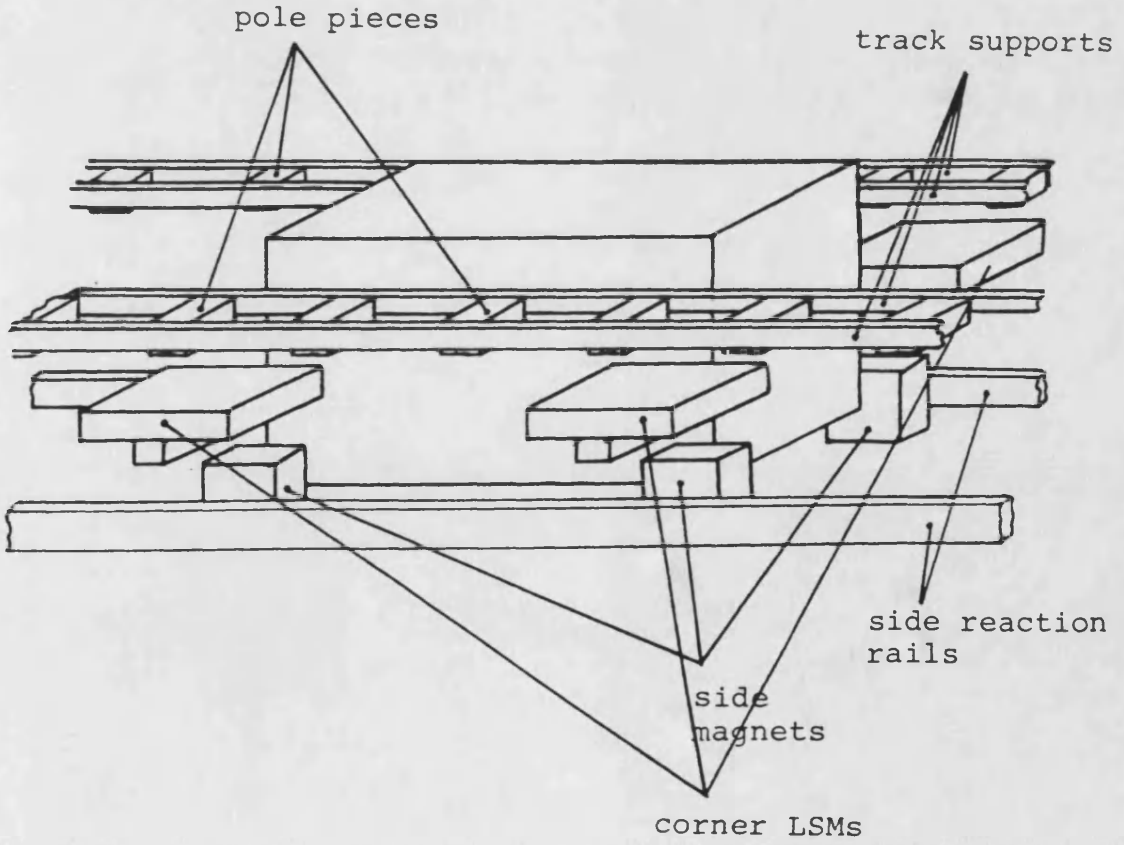

Figure 2.3.2 The L.S.M. vehicle and tracks

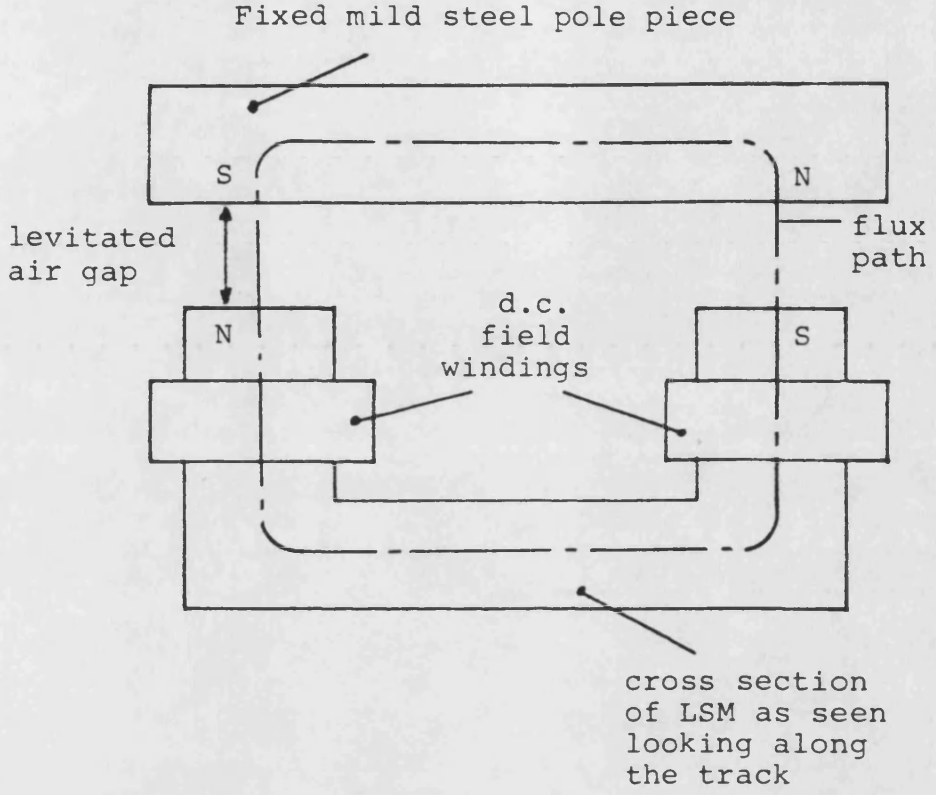

Figure 2.3.3 Magnetisation of the track pole pieces

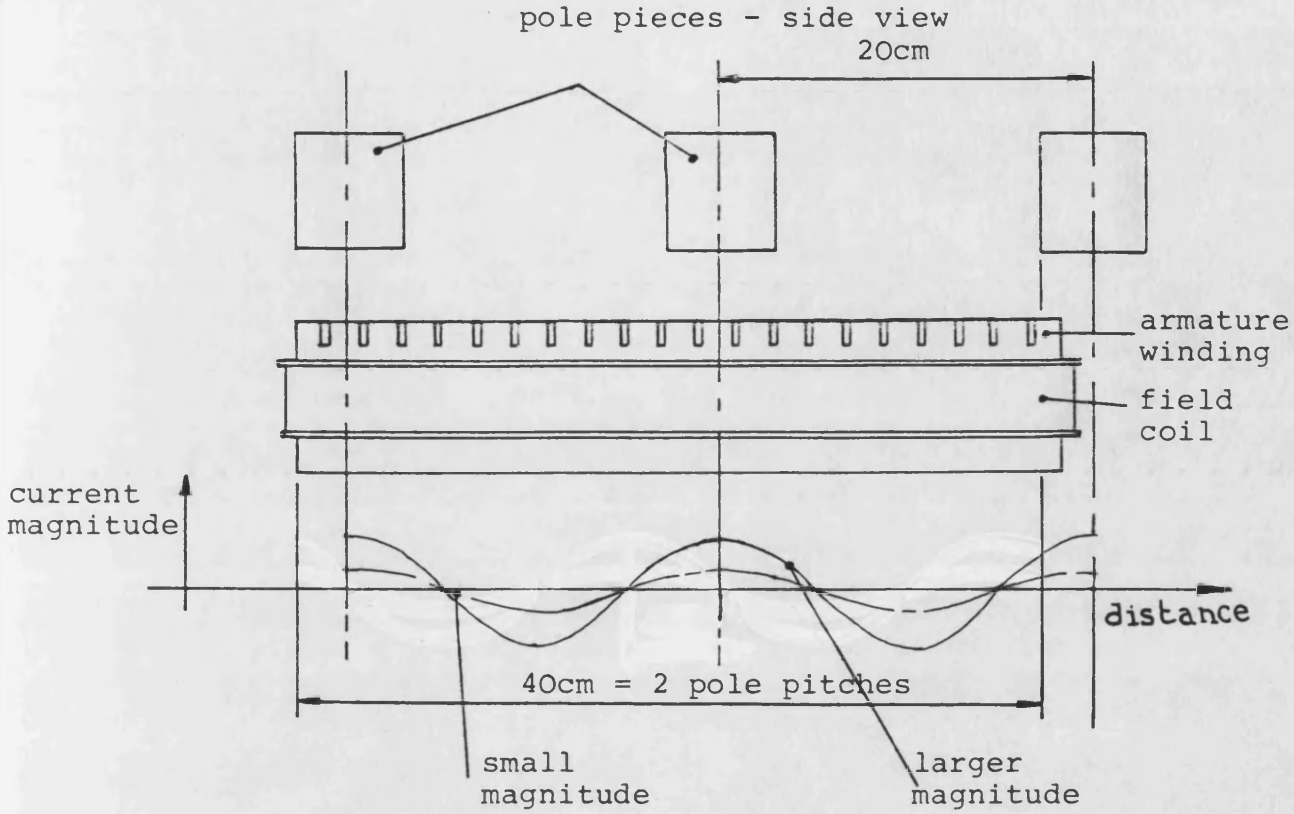

Figure 2.3.4 Decoupling of traction and levitation due to 90° torgue angle operation of the L.S.M.

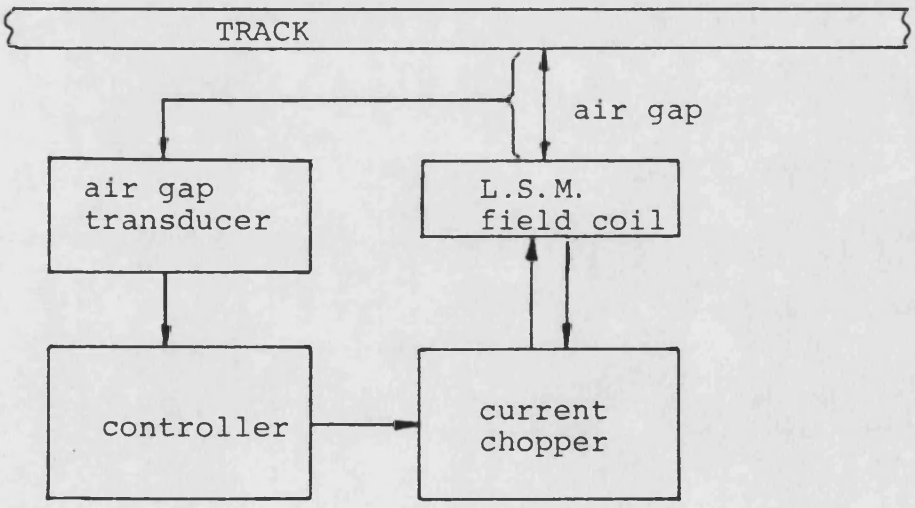

Figure 2.3.5 The basic control loop for levitation

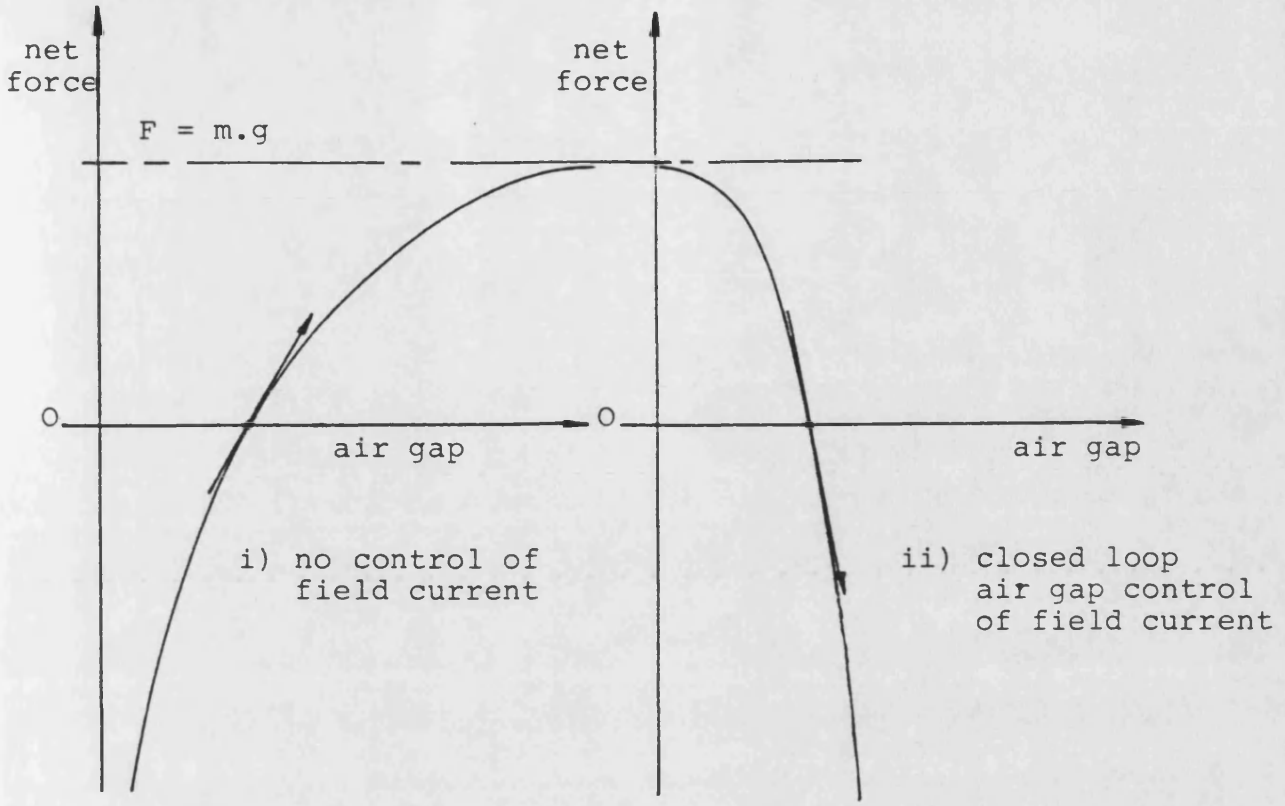

Figure 2.3.6 The effect on the force/distance characteristic when using D.C. controlled electro-magnets

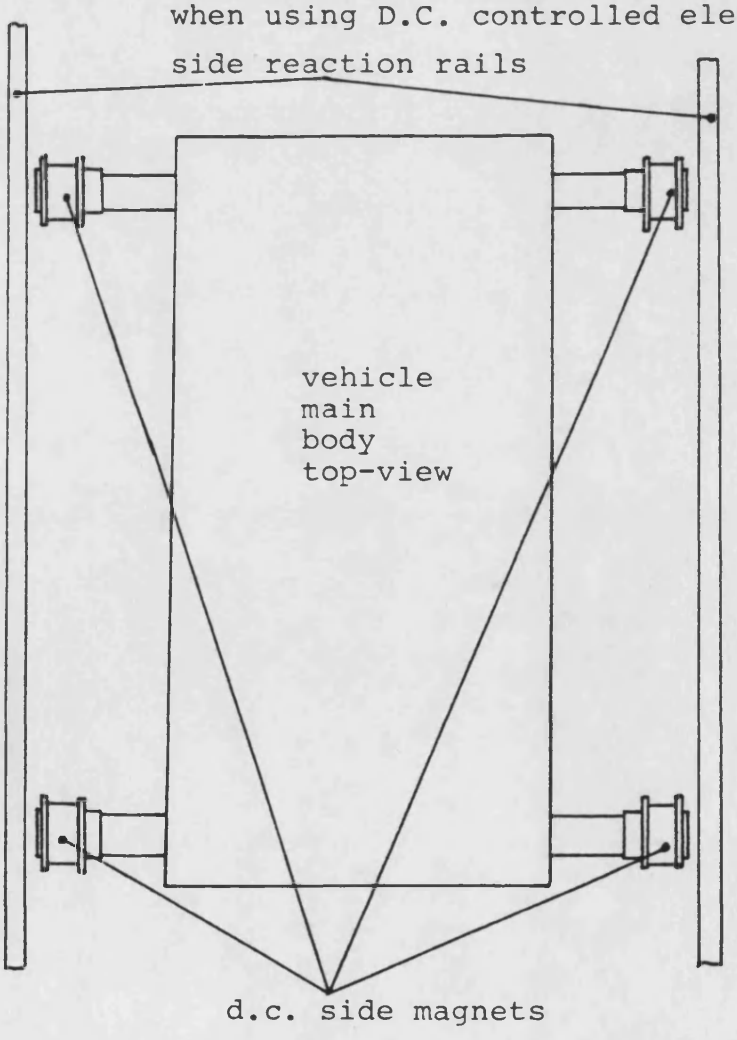

Figure 2.4.1 The use of side magnets for active lateral control

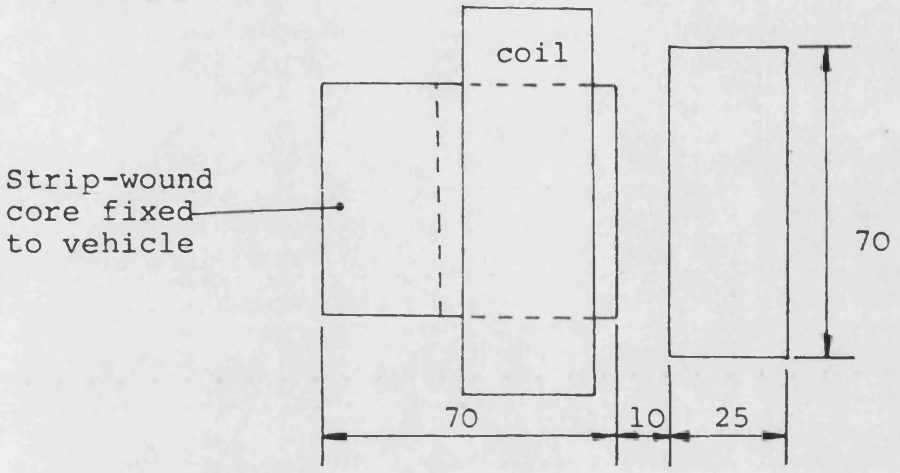

All dimensions are in mm

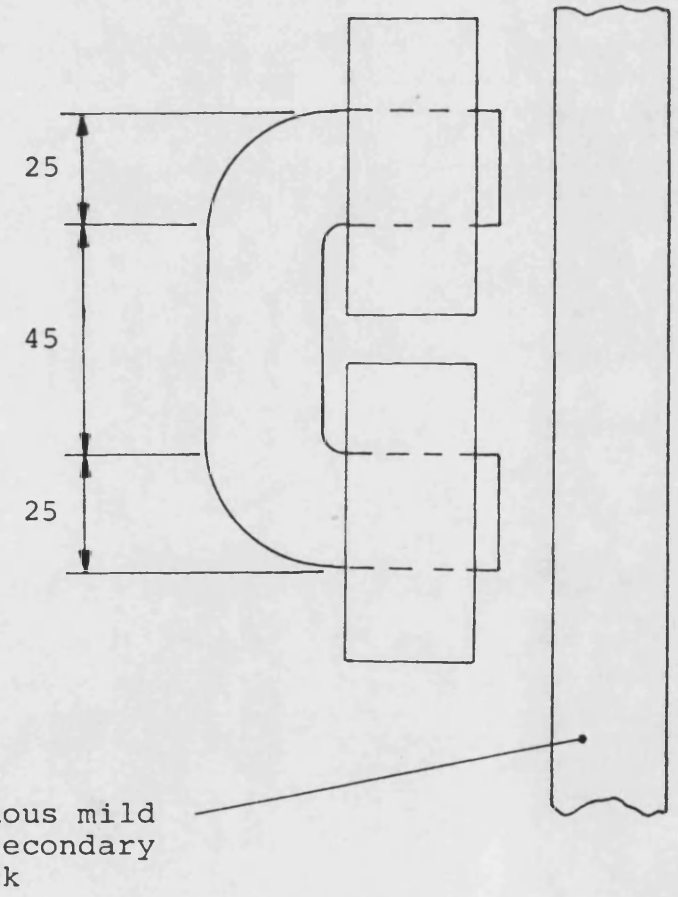

Figure 2.4.2 The dimensions of the side control magnets

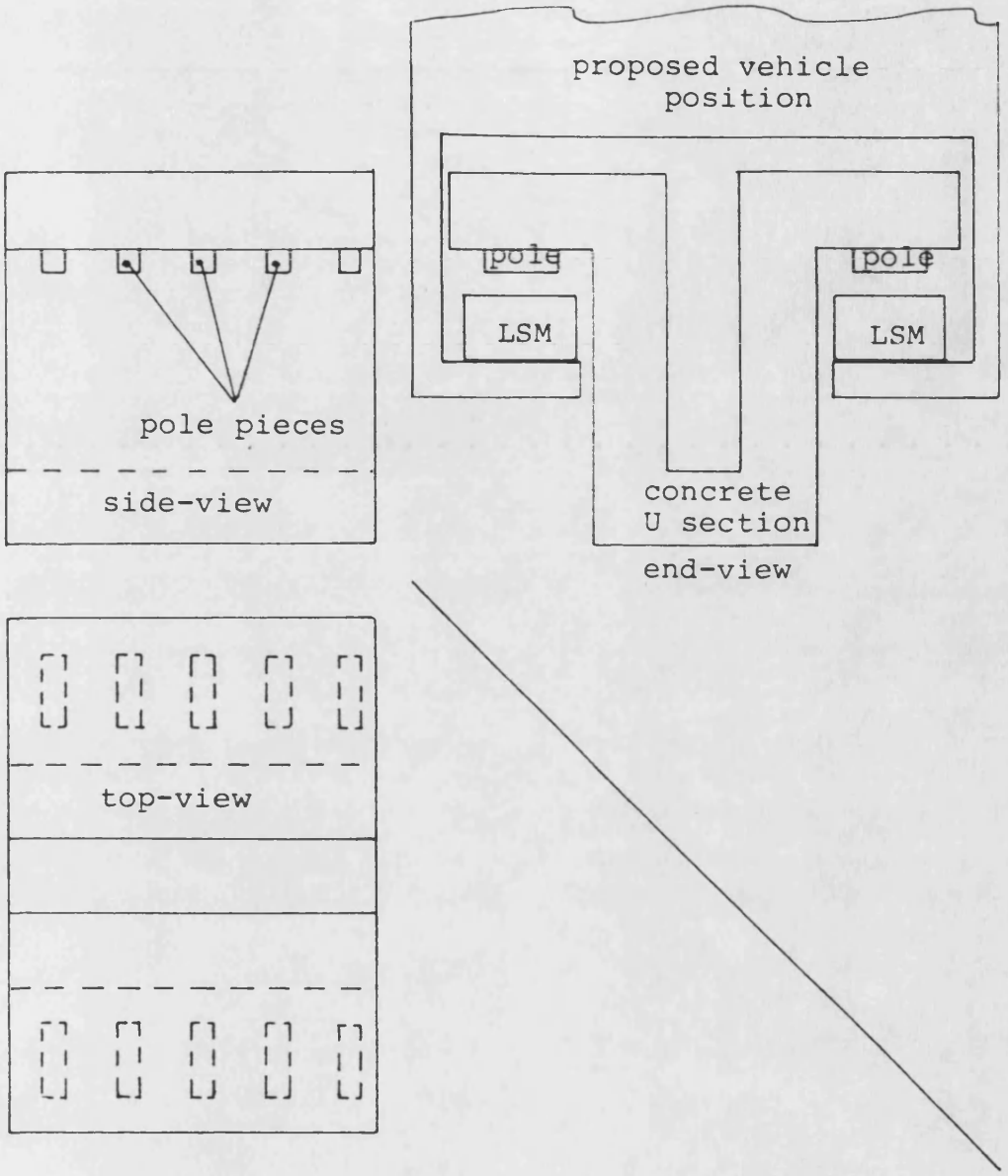

Figure 2.5.1 Envisaged concrete track configuration

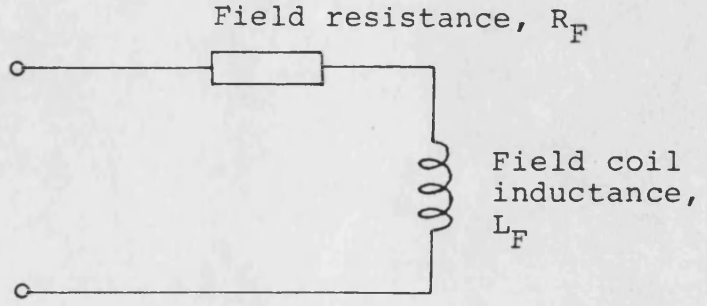

Figure 2.6.2 Chopper load due to the LSM field coil

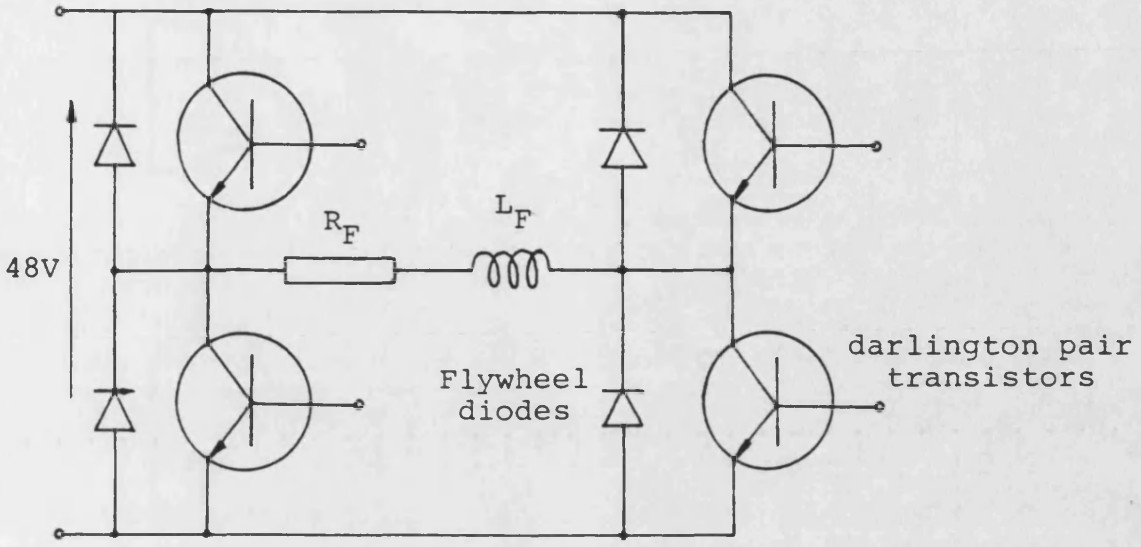

Figure 2.6.1 Basic configuration of the chopper transistors

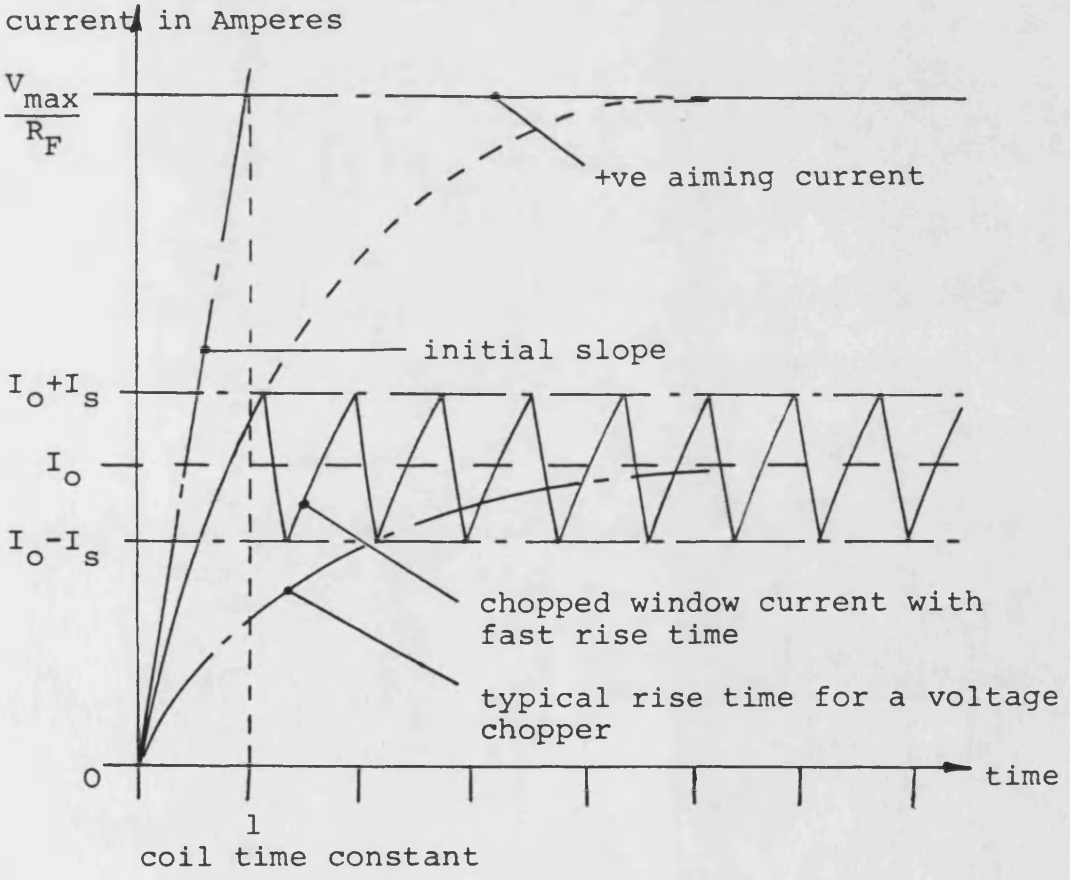

Figure 2.6.3 The time domain response of the field coil current when driven by the chopper

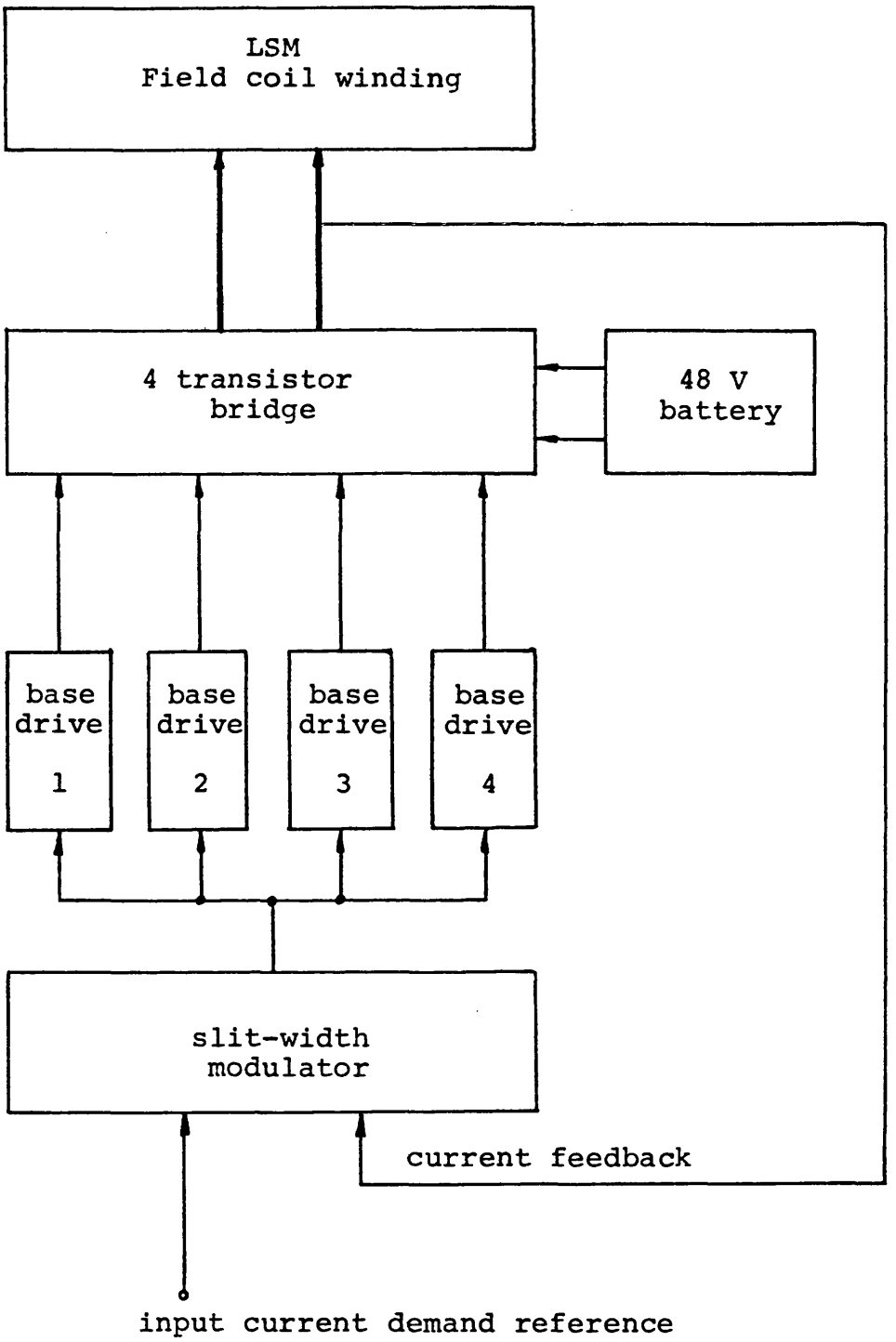

Figure 2.6.4 Block diagram of the complete chopper system

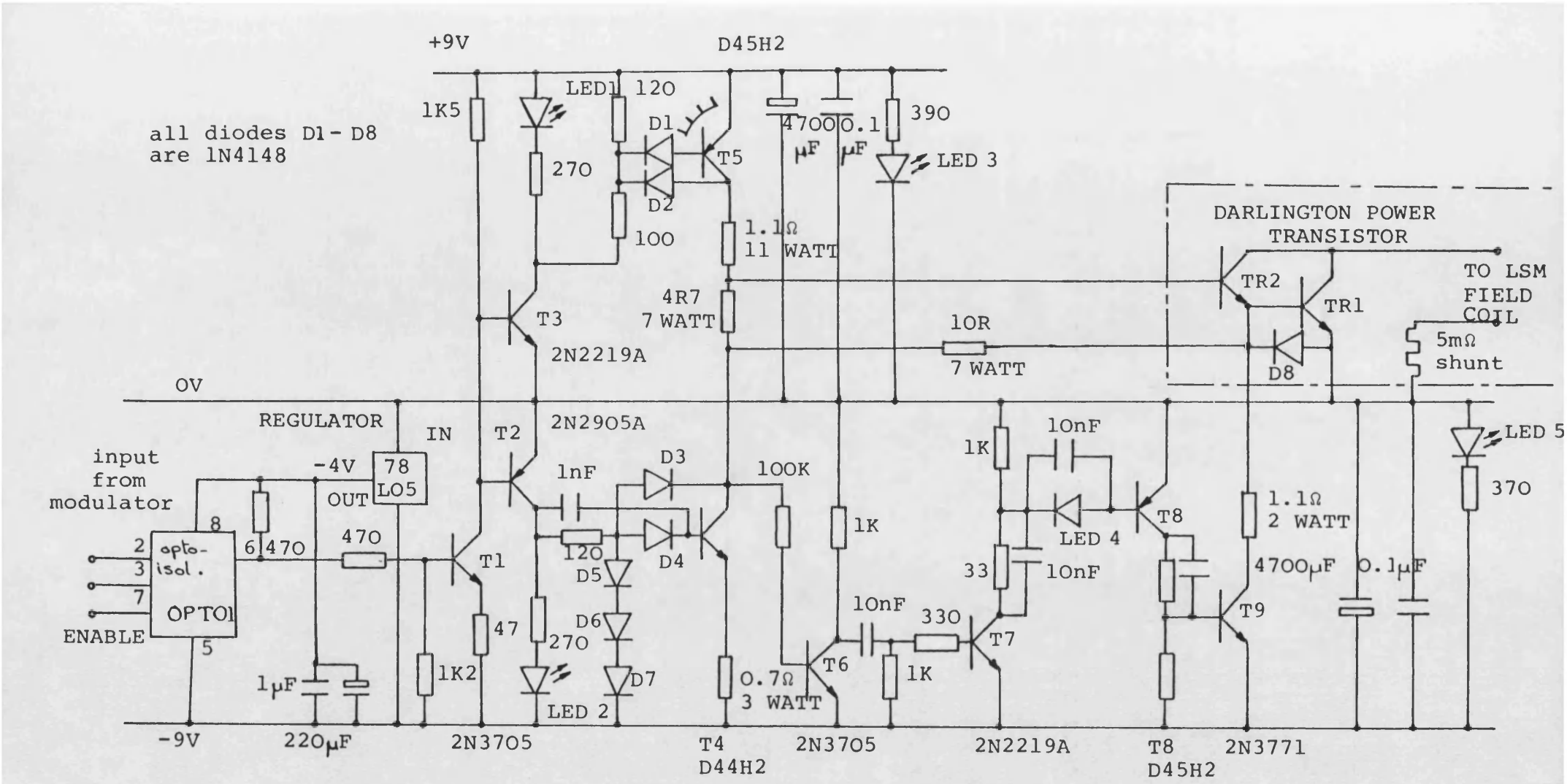

Figure 2.6.5 Base drive controller for the chopper

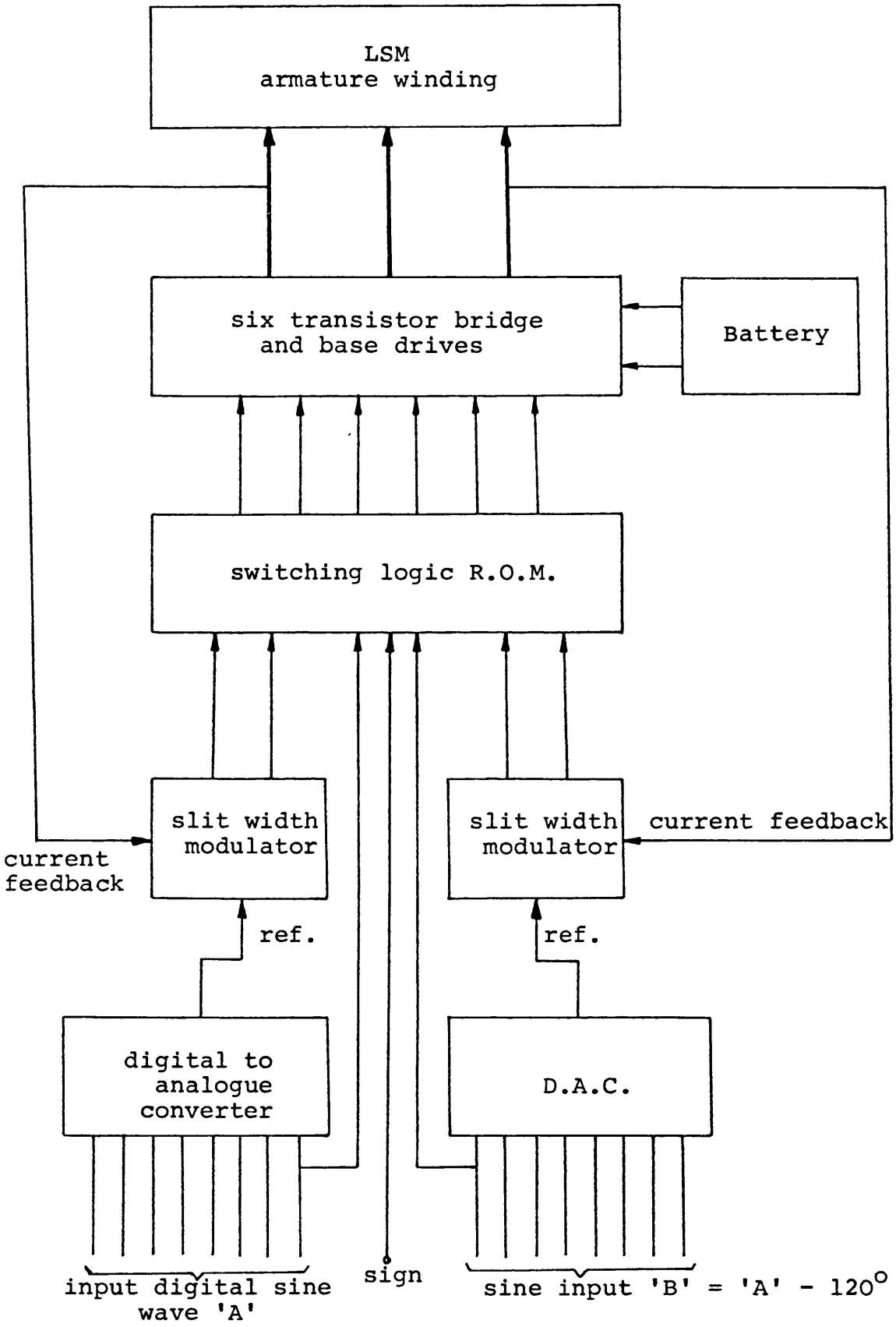

Figure 2.6.6 Block diagram of the A.C. armature current inverter

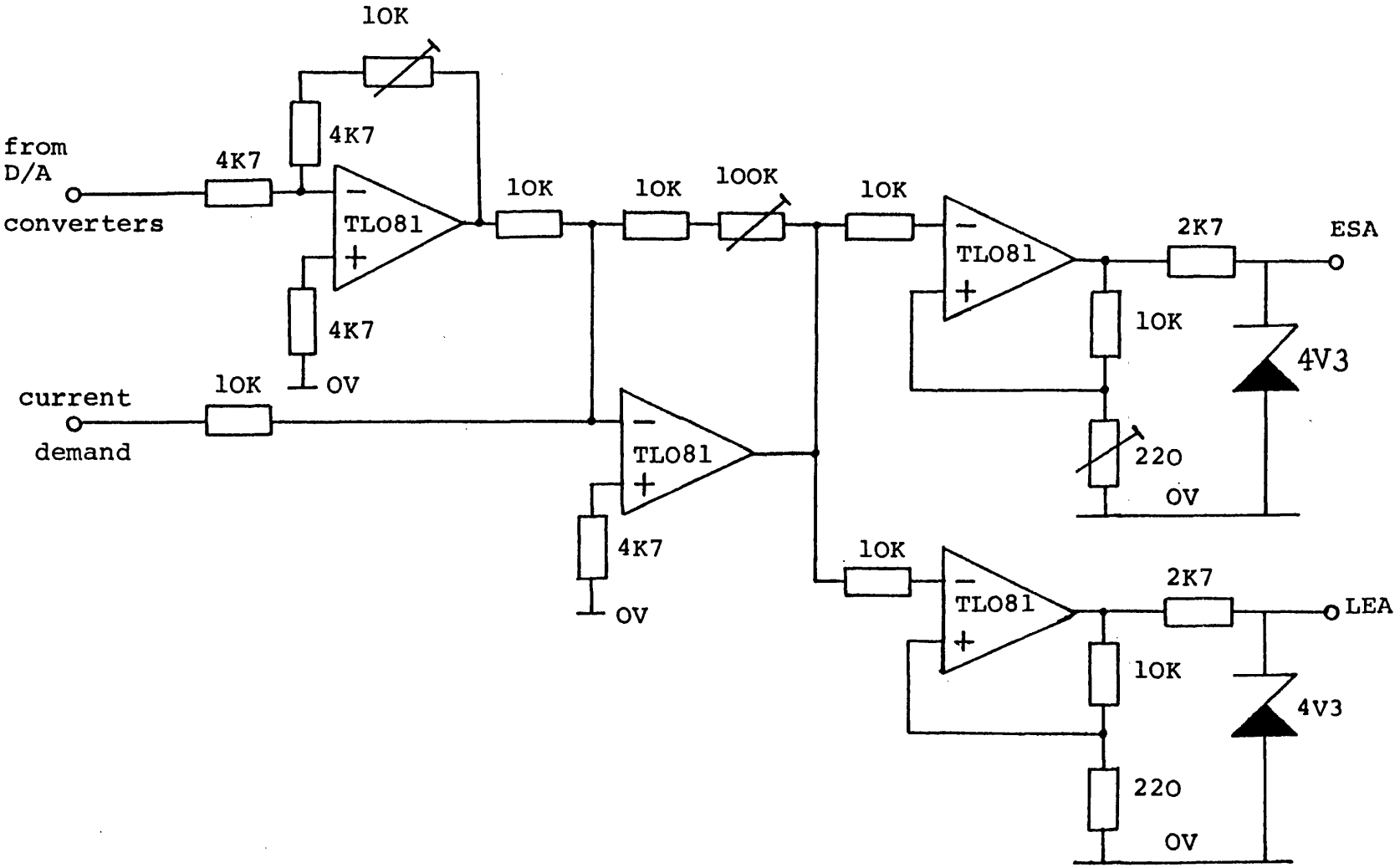

Figure 2.6.7 The slit-width modulator units

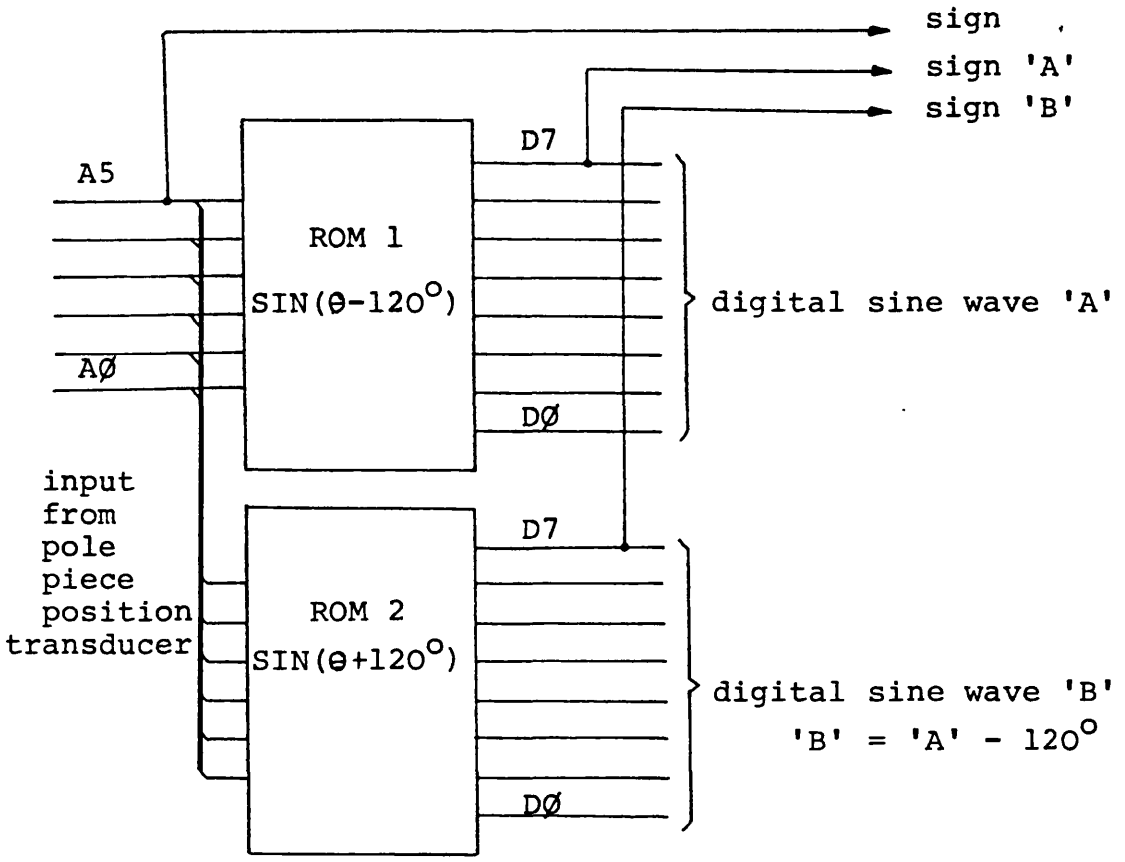

Figure 2.6.8 Sine lookup tables for two phase operation

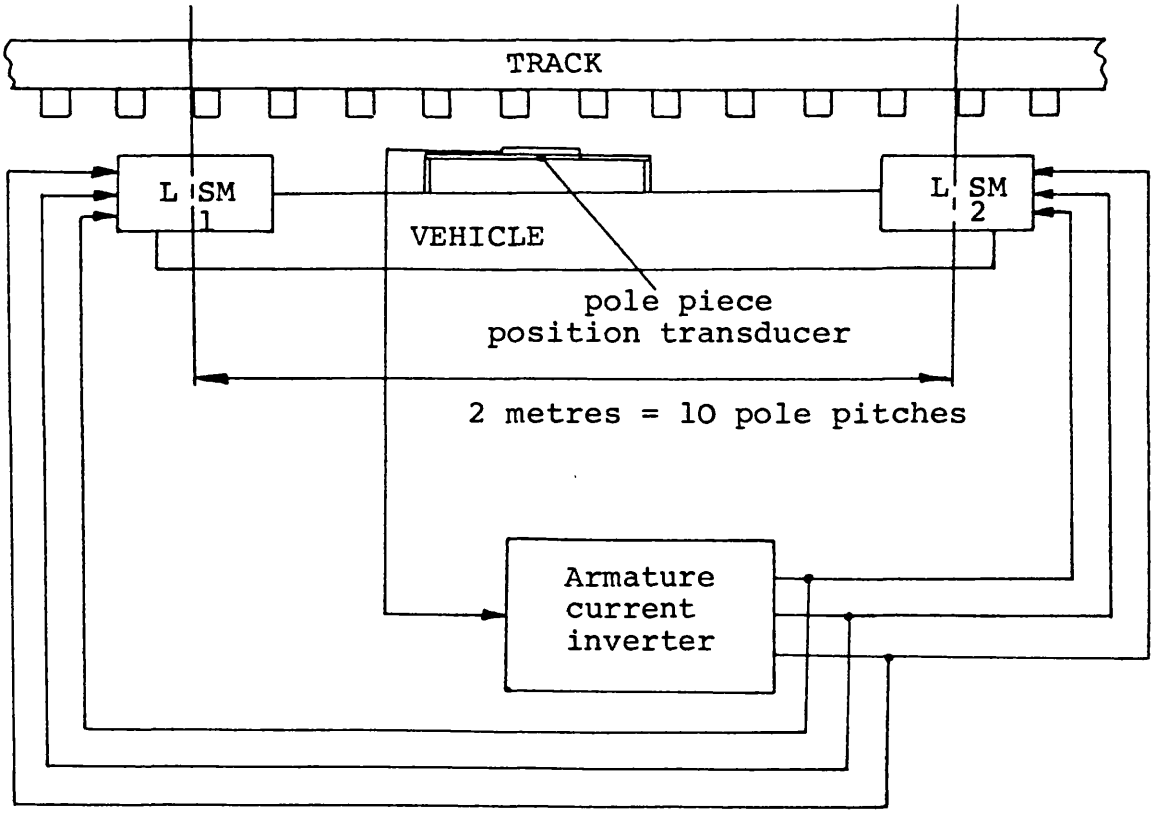

Figure 2.6.9 The use of one inverter to drive two LSM's

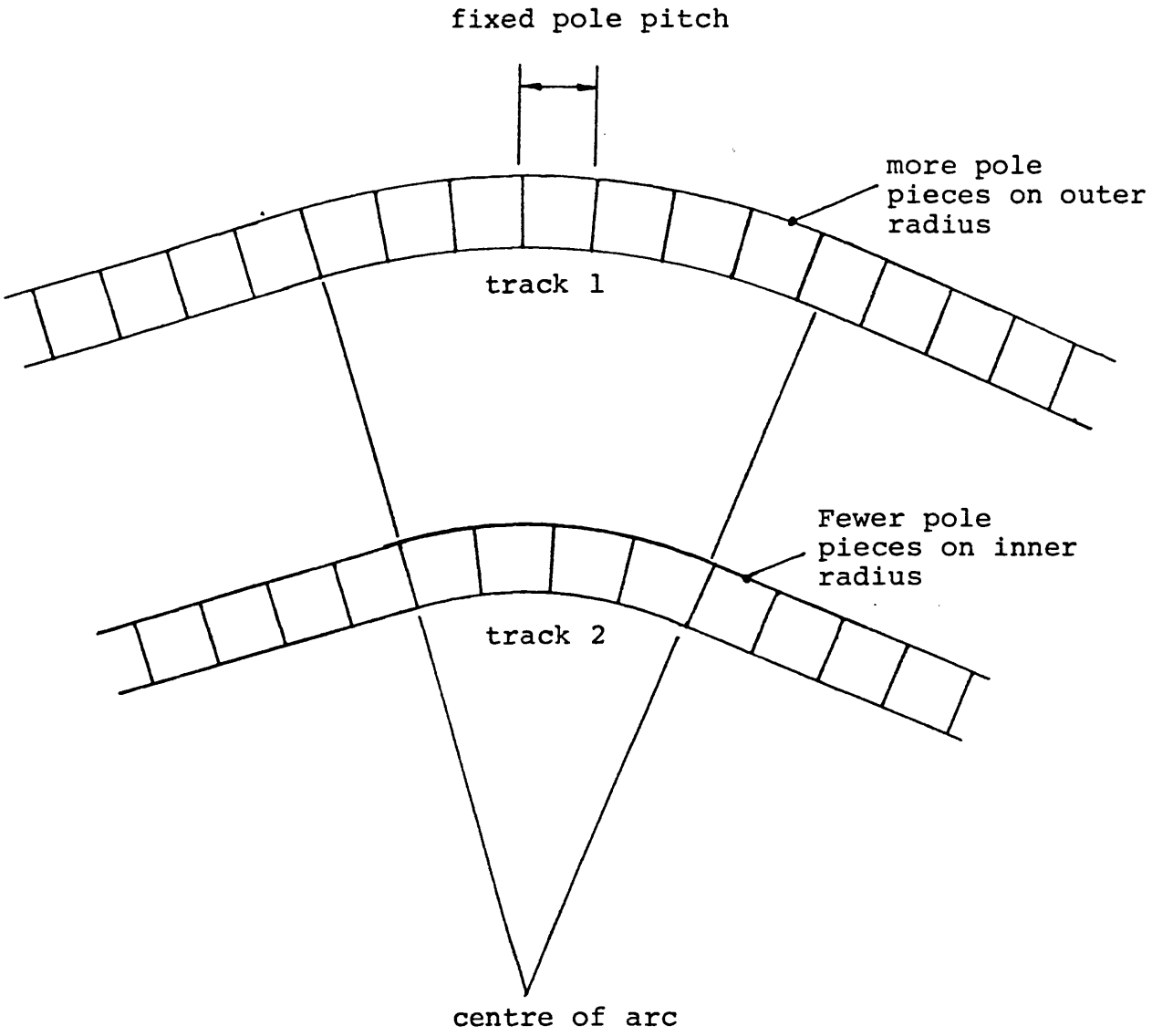

Figure 2.6.10 Cross track pole piece phase shift due to cornering

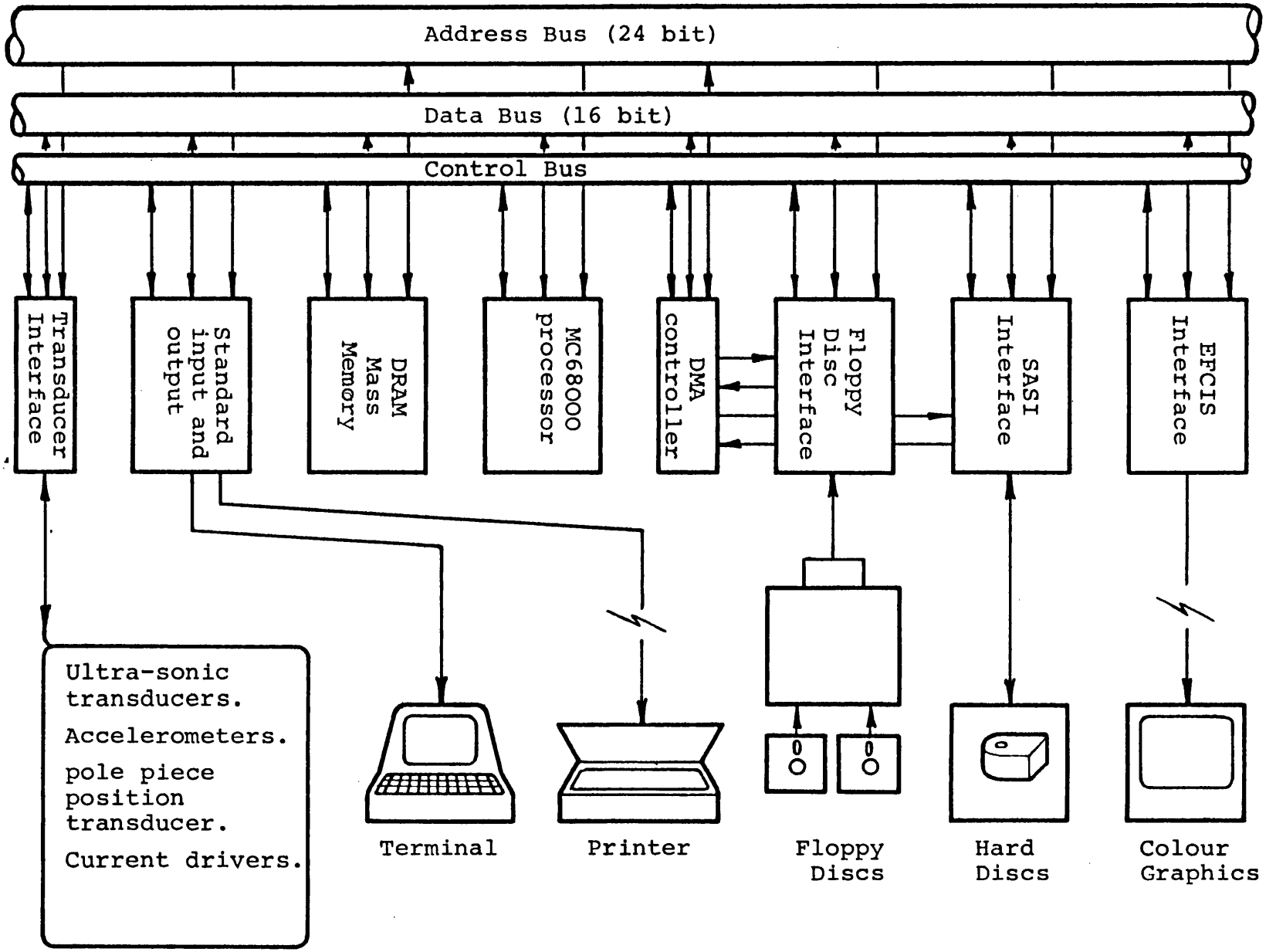

Figure 3.1.1 Computing System Configuration

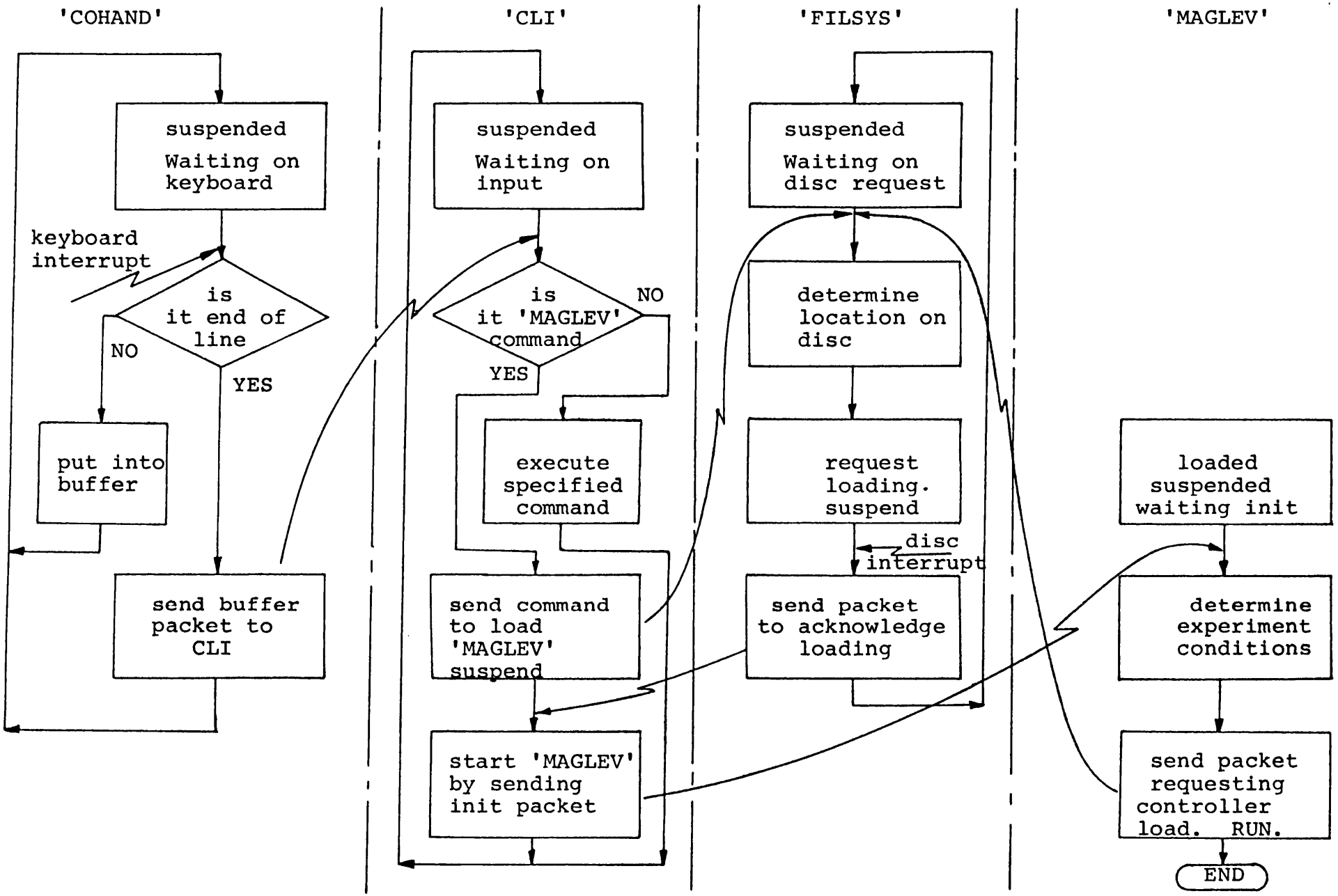

Figure 3.3.1 Loading a new task under the TRIPOS O.S

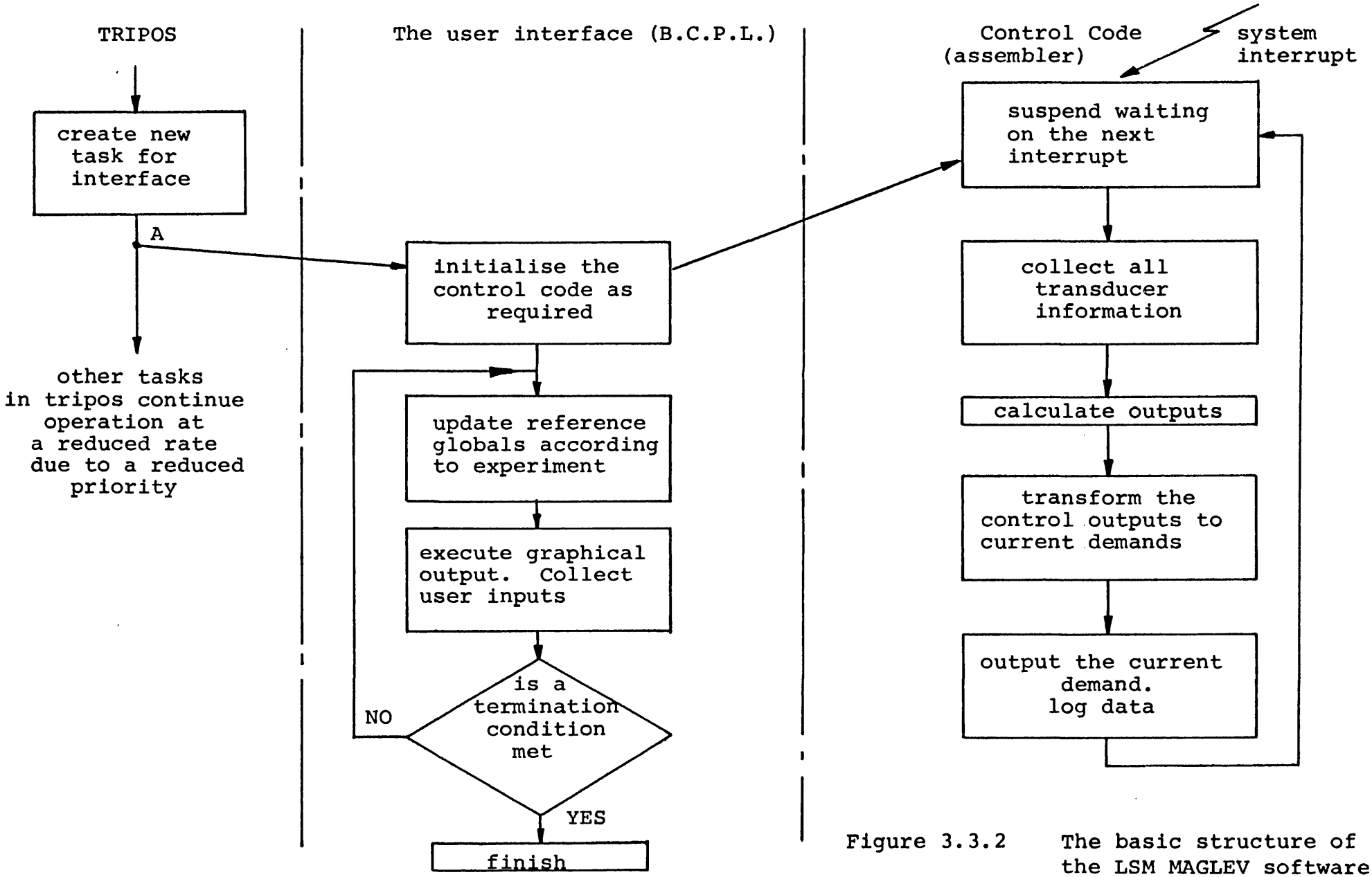

Figure 3.3.2 The basic structure of the LSM MAGLEV software

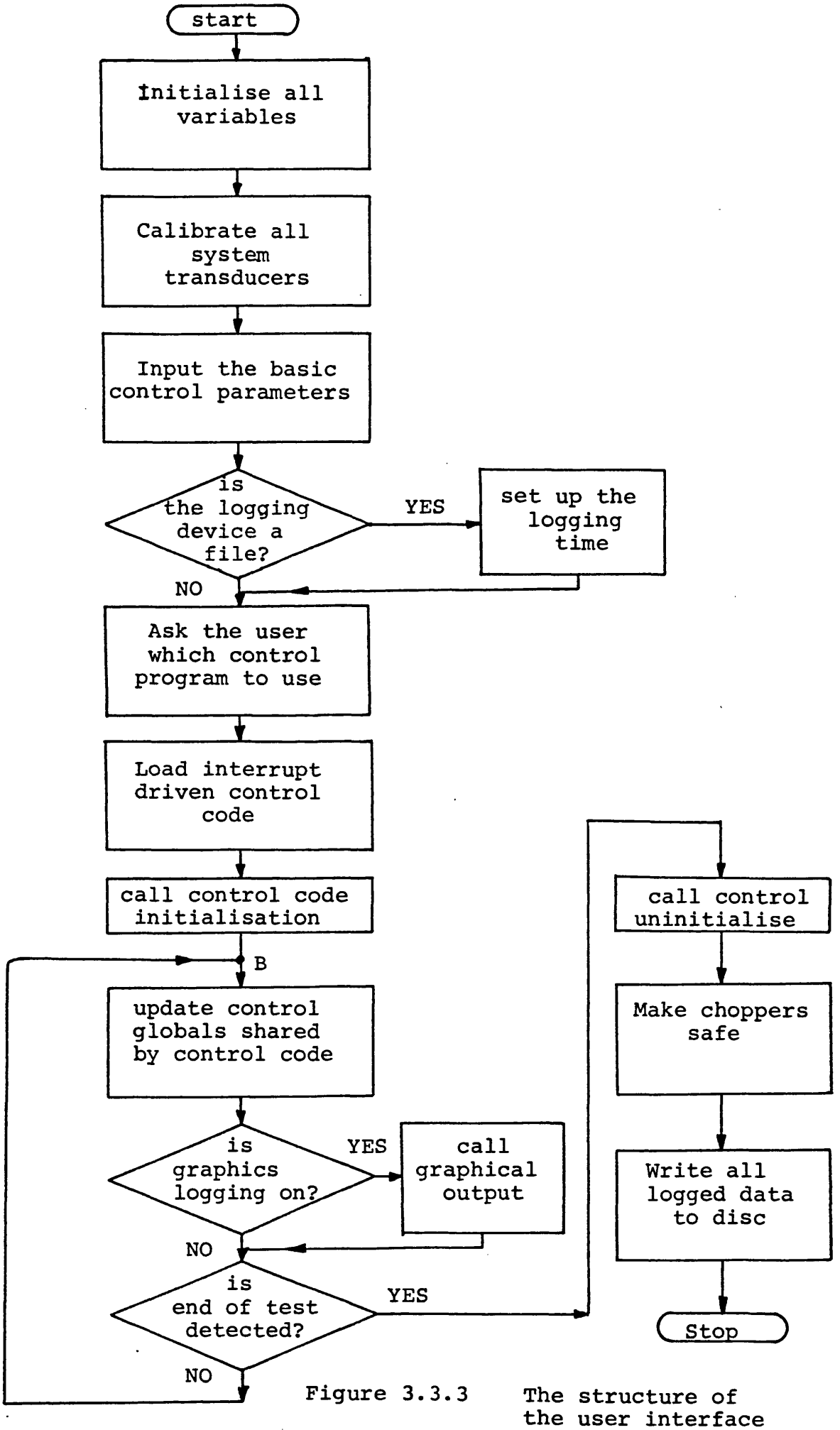

Figure 3.3.3 The structure of the user interface

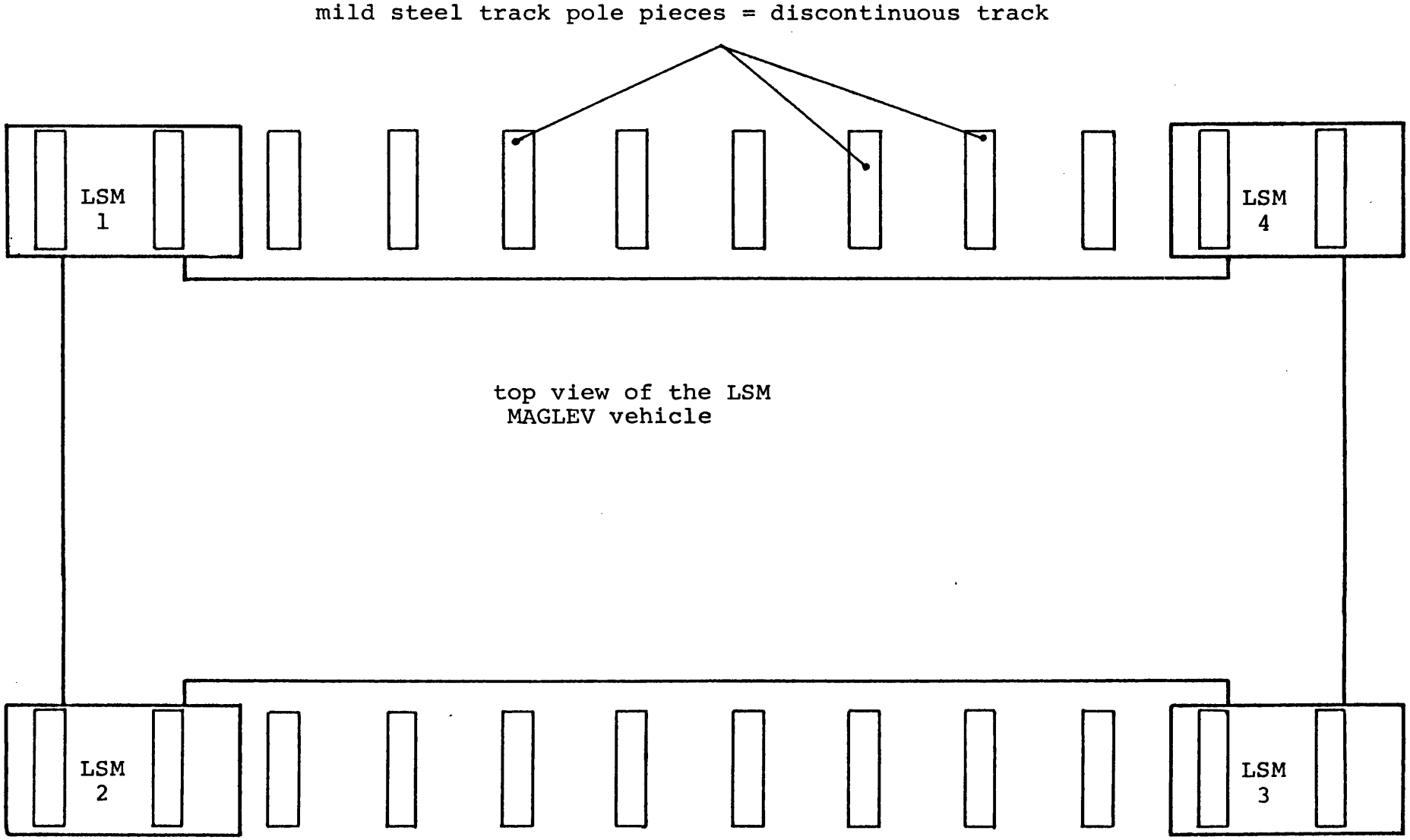

Figure 4.1.1 The form of the linear synchronous motor track

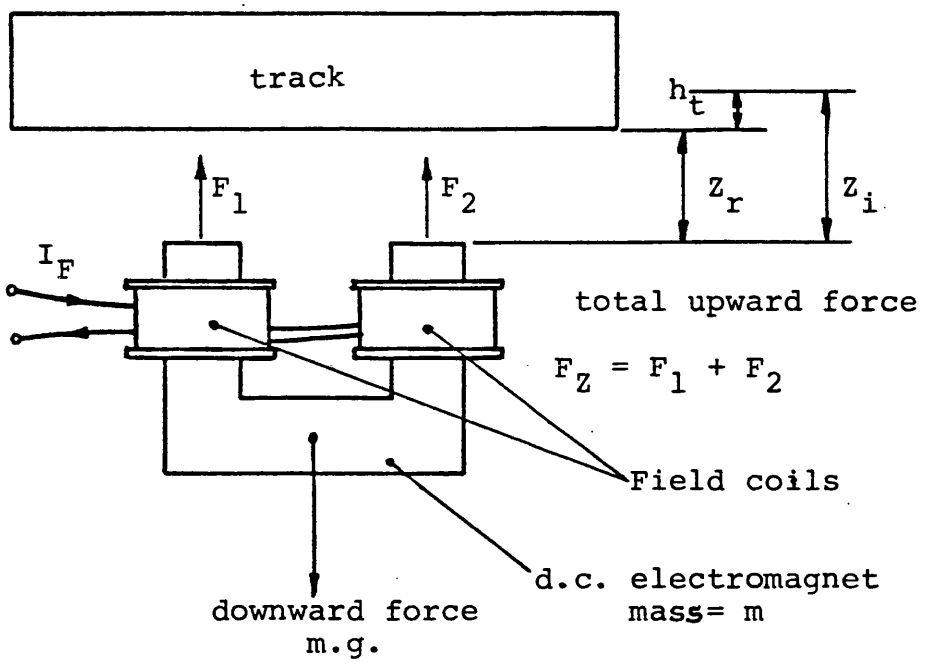

Figure 4.2.1 Definition of levitation variables

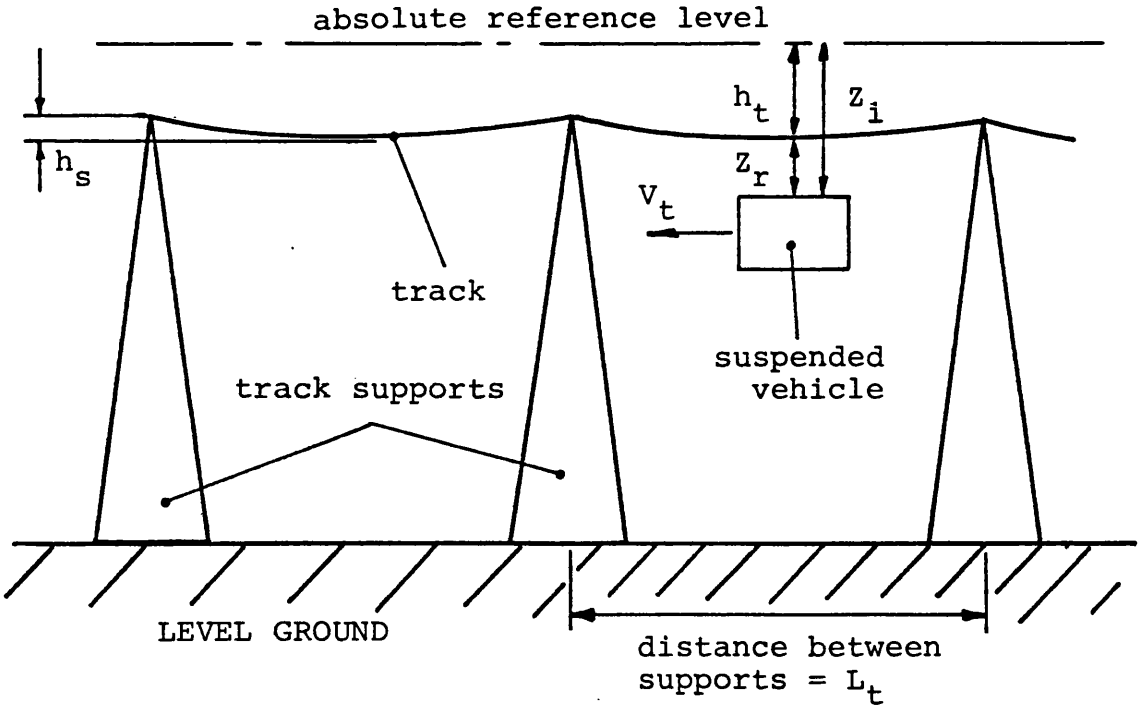

Figure 4.2.2 Periodic disturbance caused by track supports

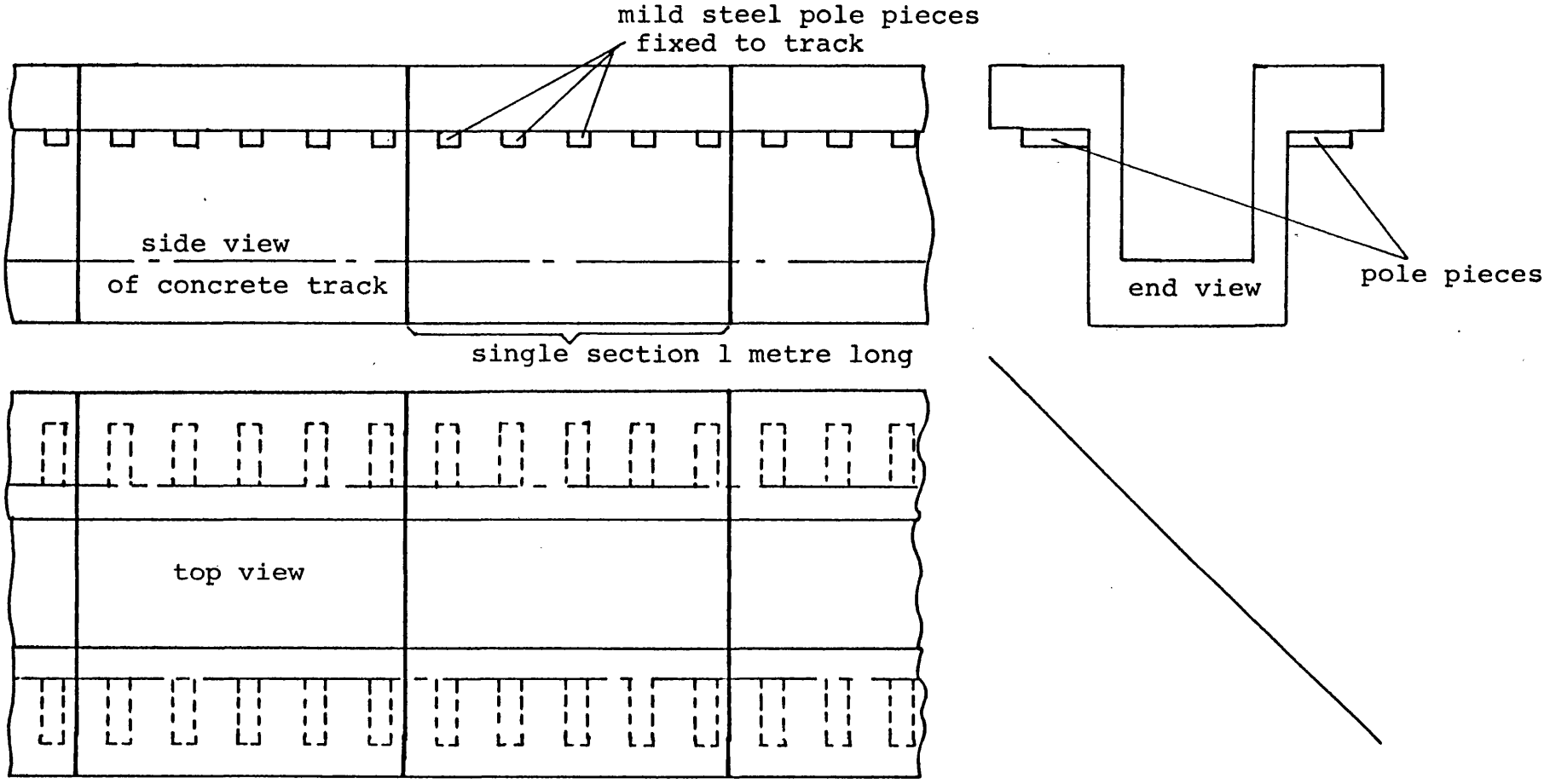

Figure 4.2.3 Pole piece mounting

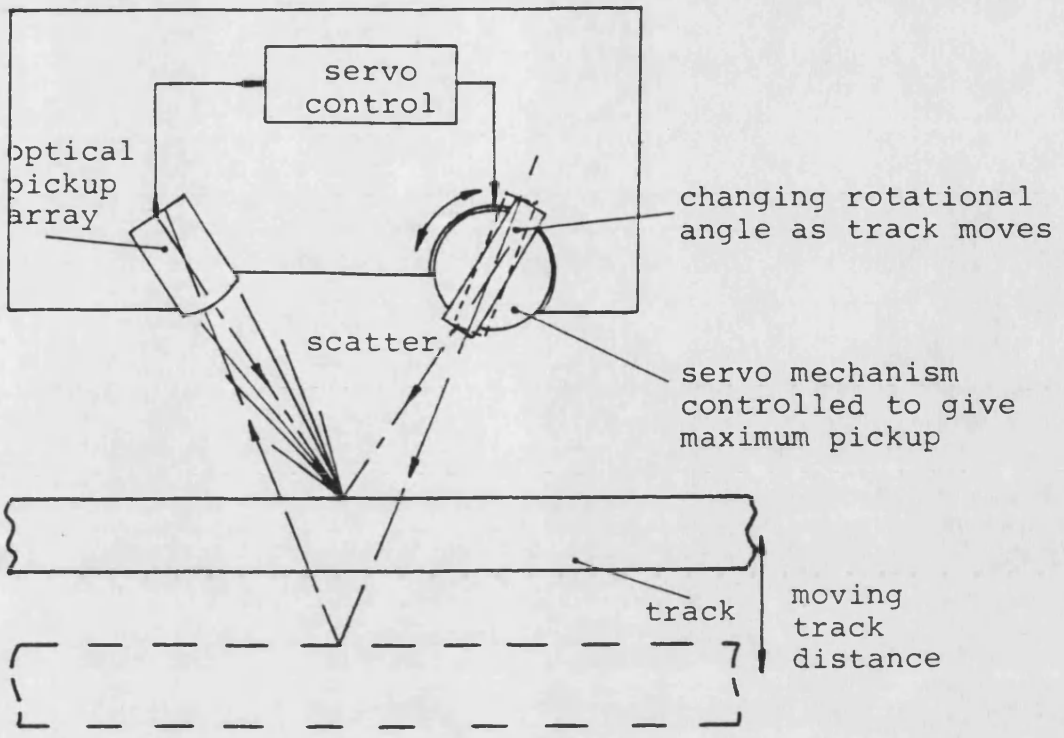

Figure 4.2.4 Laser servo air gap measurement

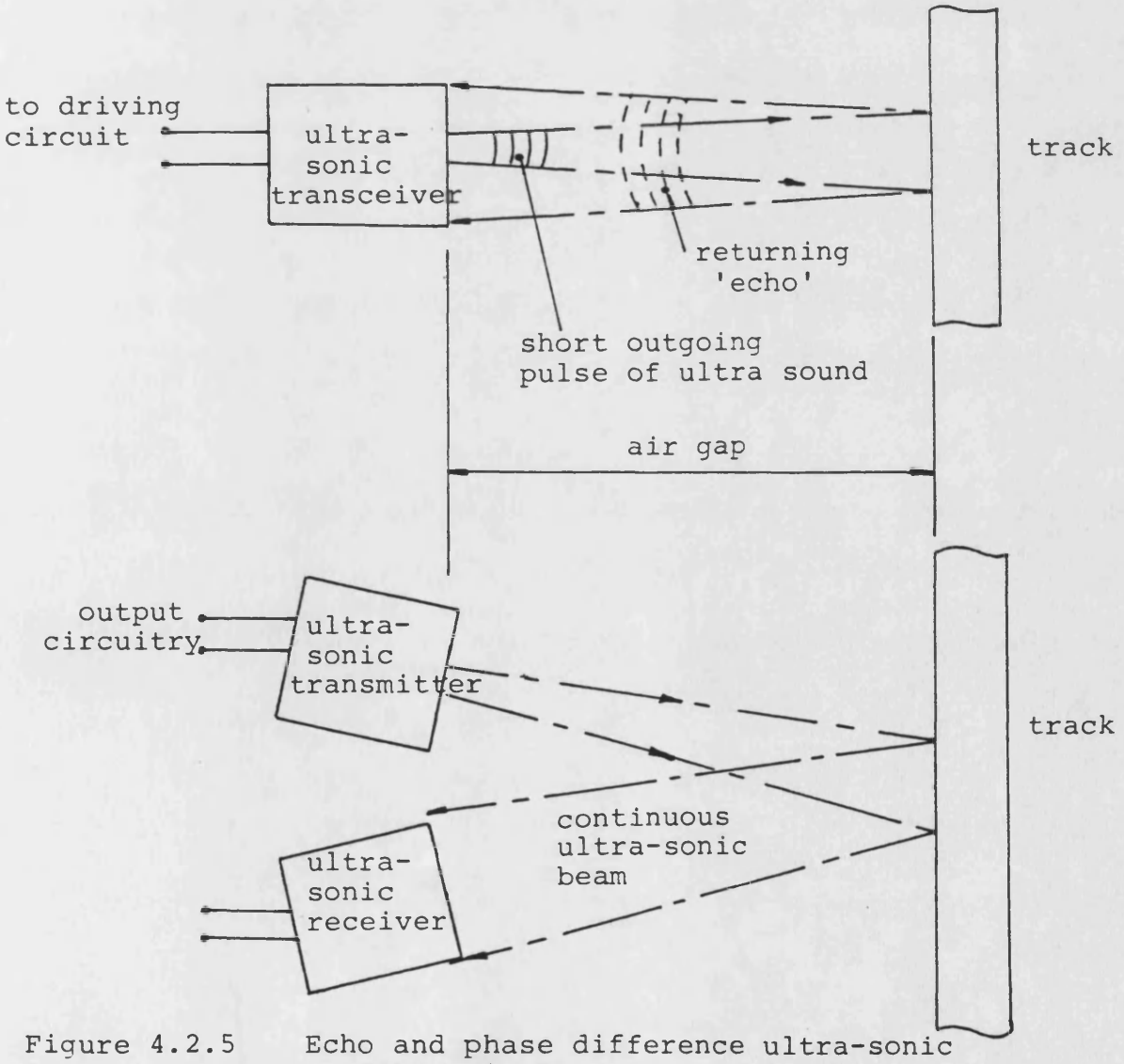

Figure 4.2.5 Echo and phase difference ultra-sonic measurement

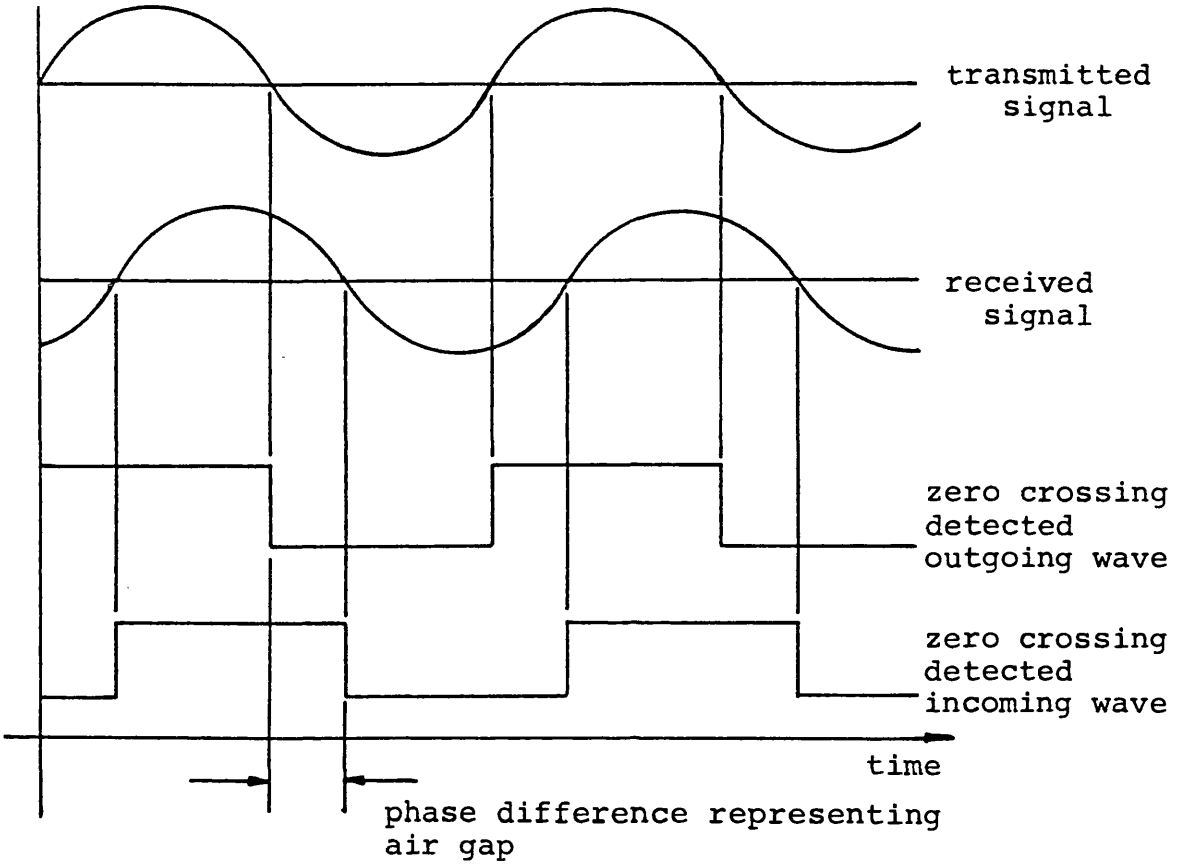

Figure 4.2.6 Phase difference waveforms

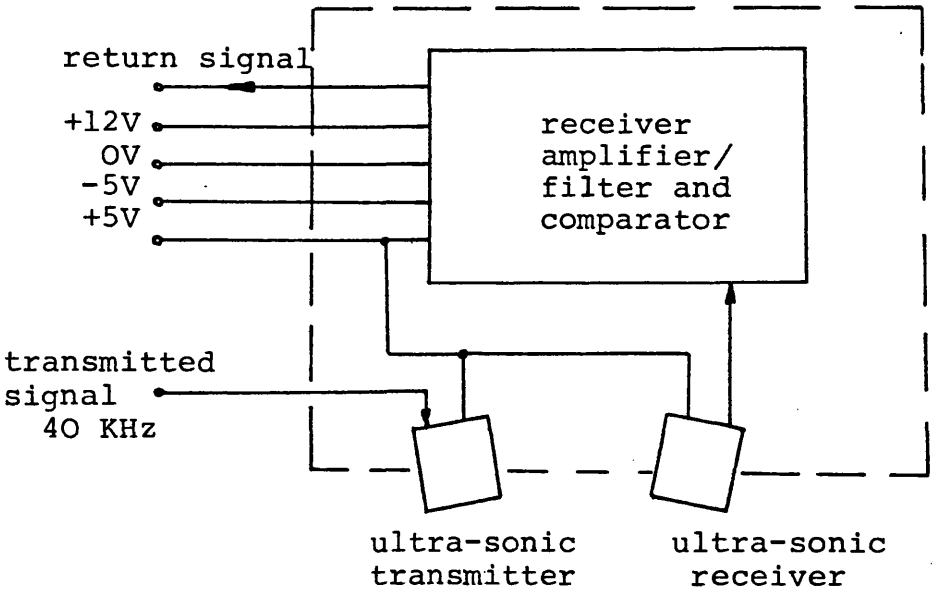

Figure 4.2.7 The remote part of the air gap transducer

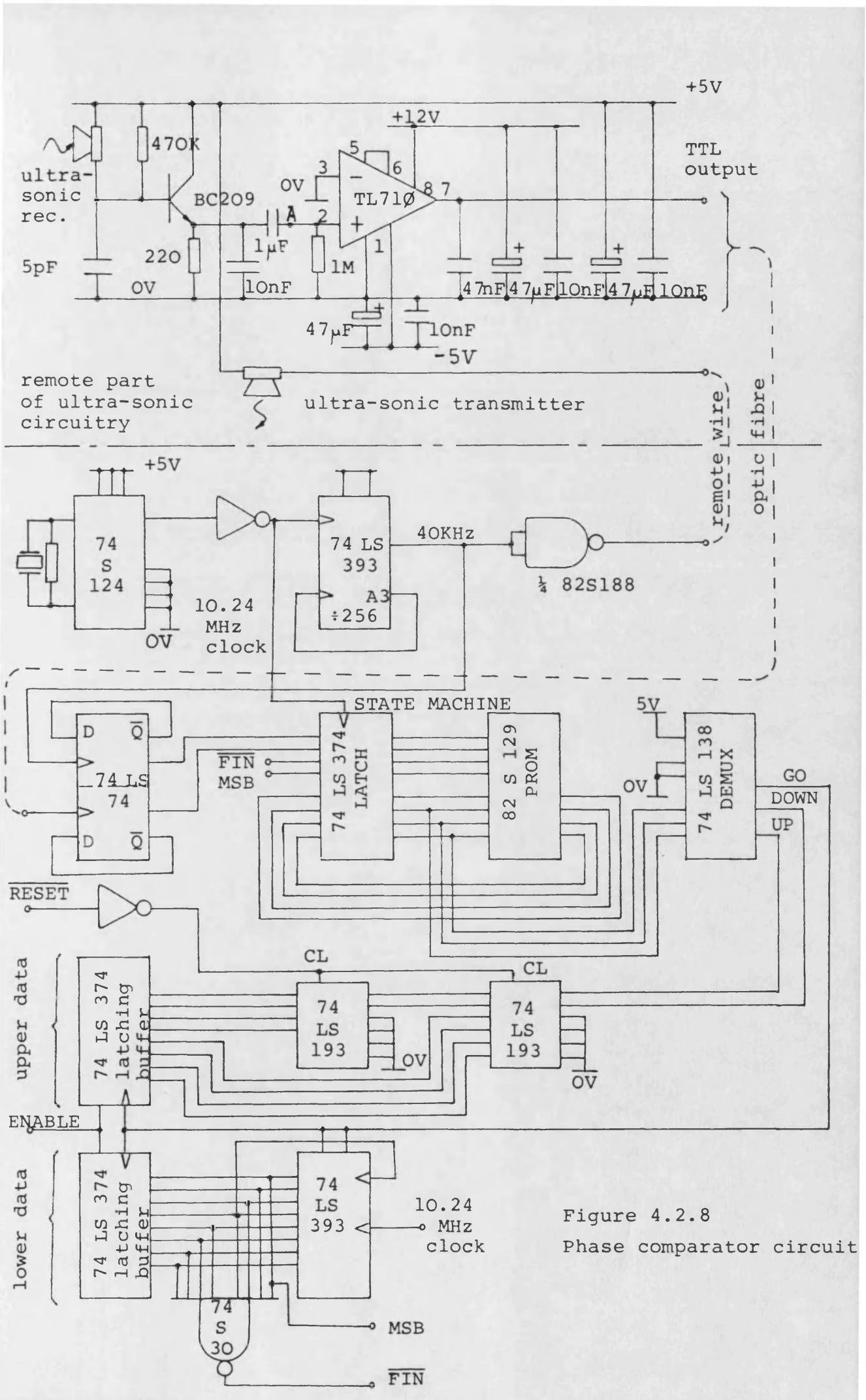

Figure 4.2.8
Phase comparator circuit

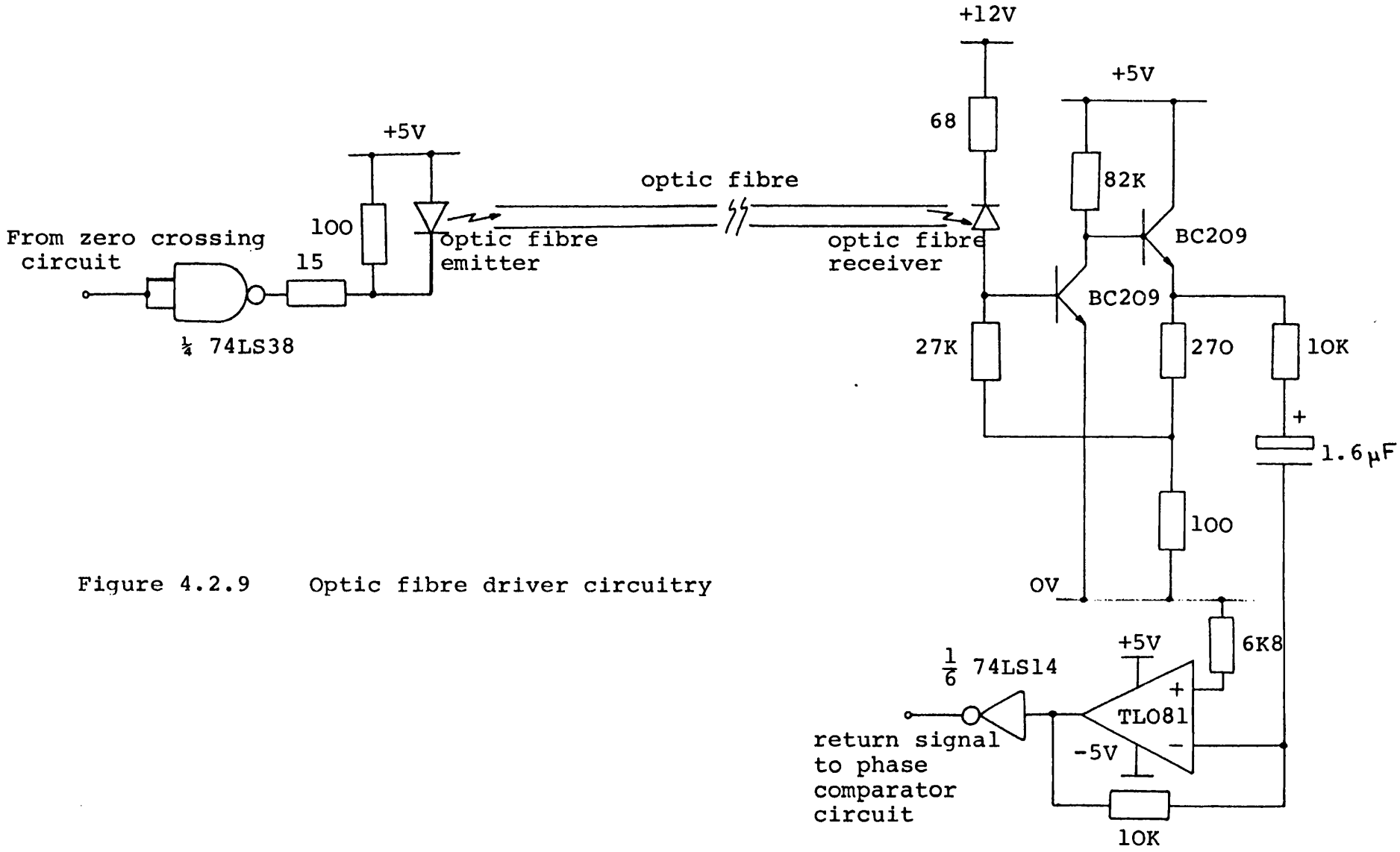

Figure 4.2.9 Optic fibre driver circuitry

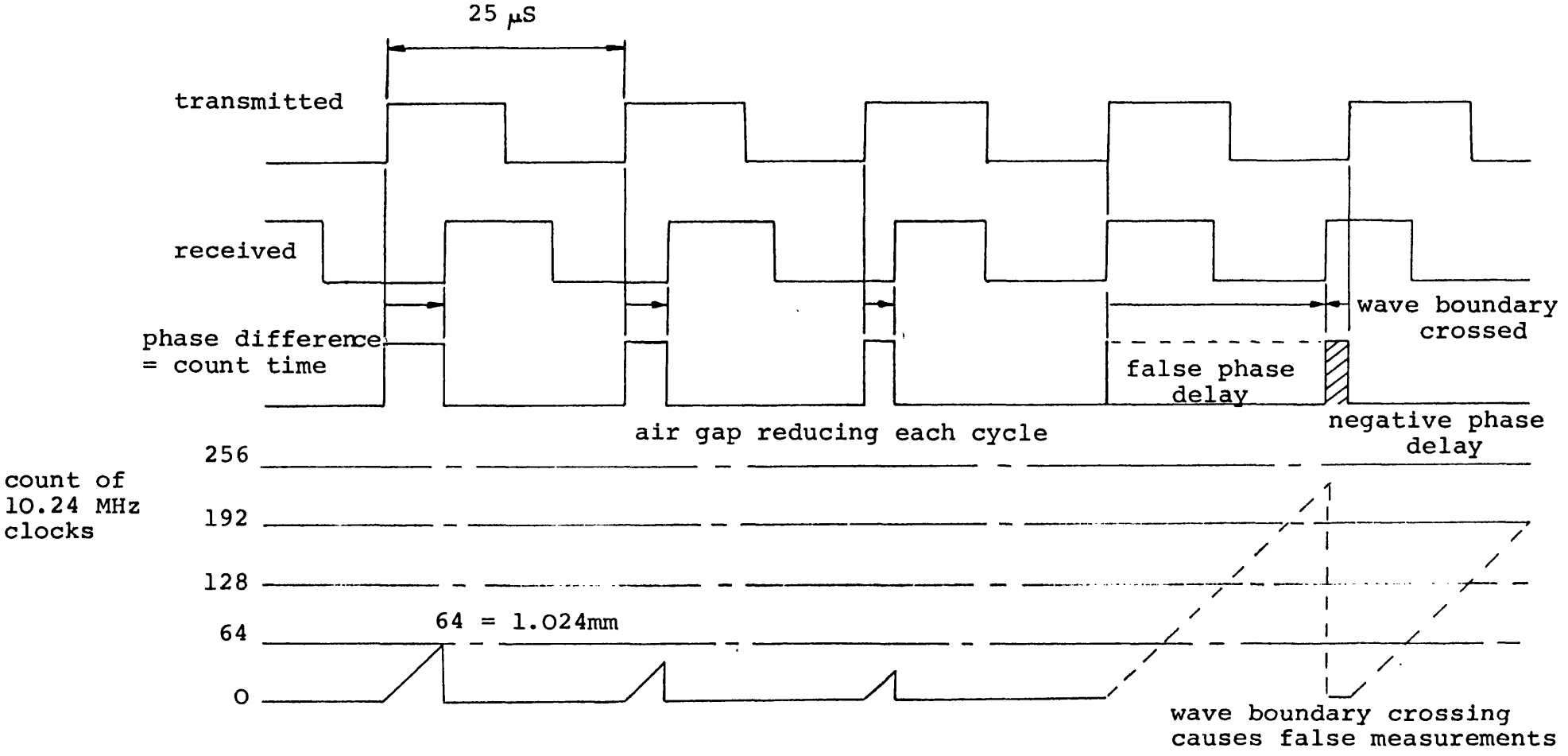

Figure 4.2.10 Transmitted and received ultra-sonic waveforms

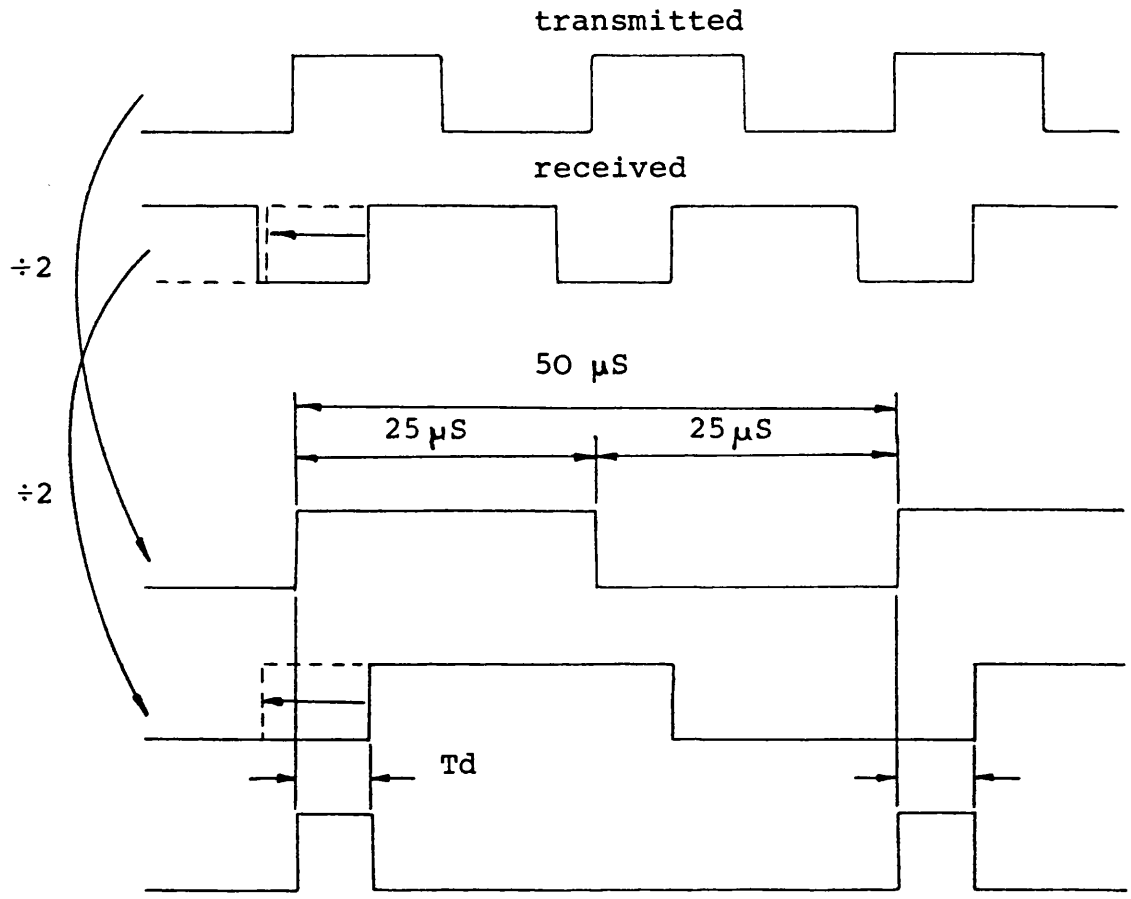

——————— normal phase relationship

– – – – – – – – waveform passed through complete wave boundary

Figure 4.2.11 50/50 duty cycle waveforms

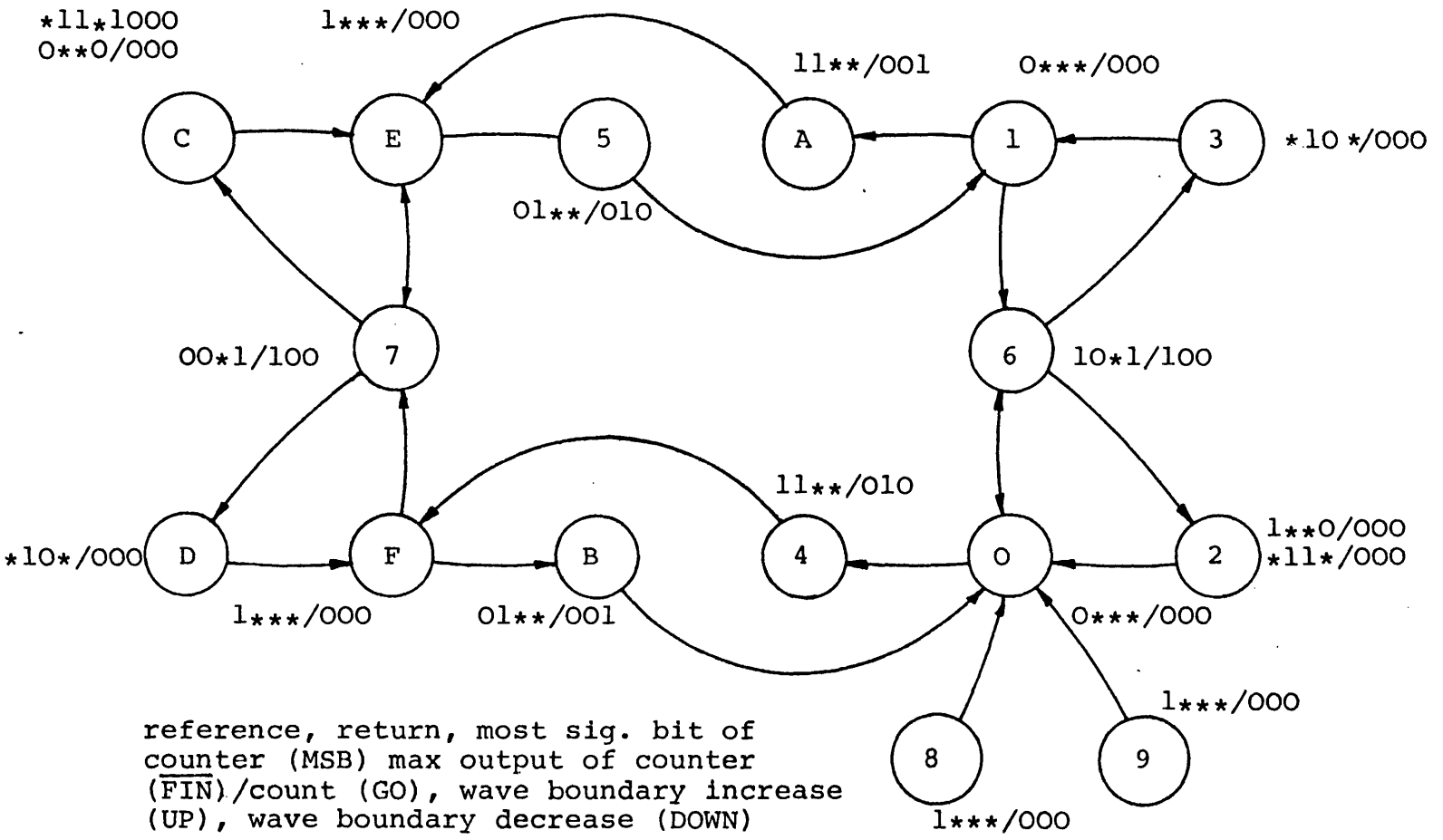

Figure 4.2.12 State diagram of the phase detector

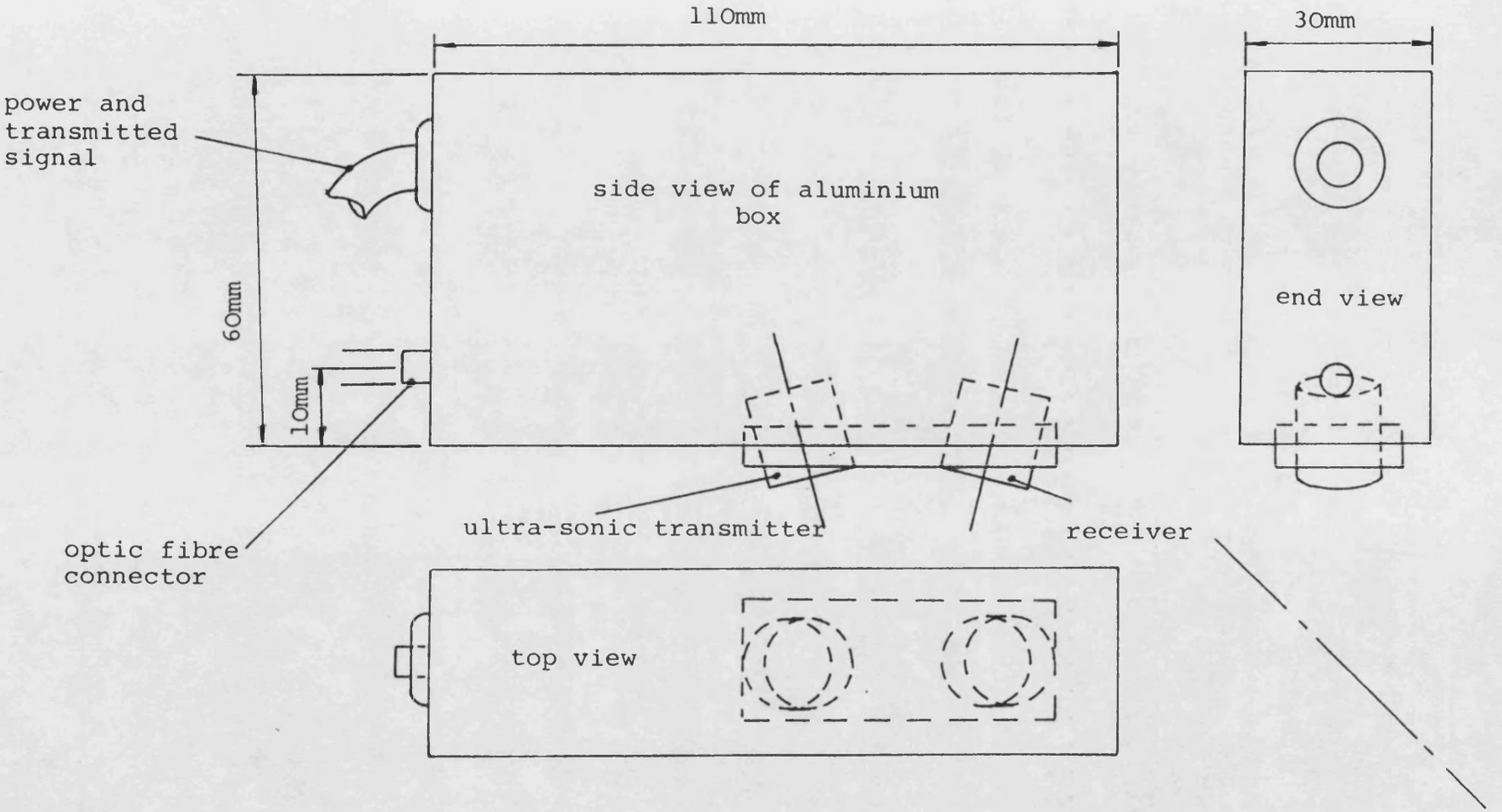

Figure 4.2.13 The remote metal box mounting

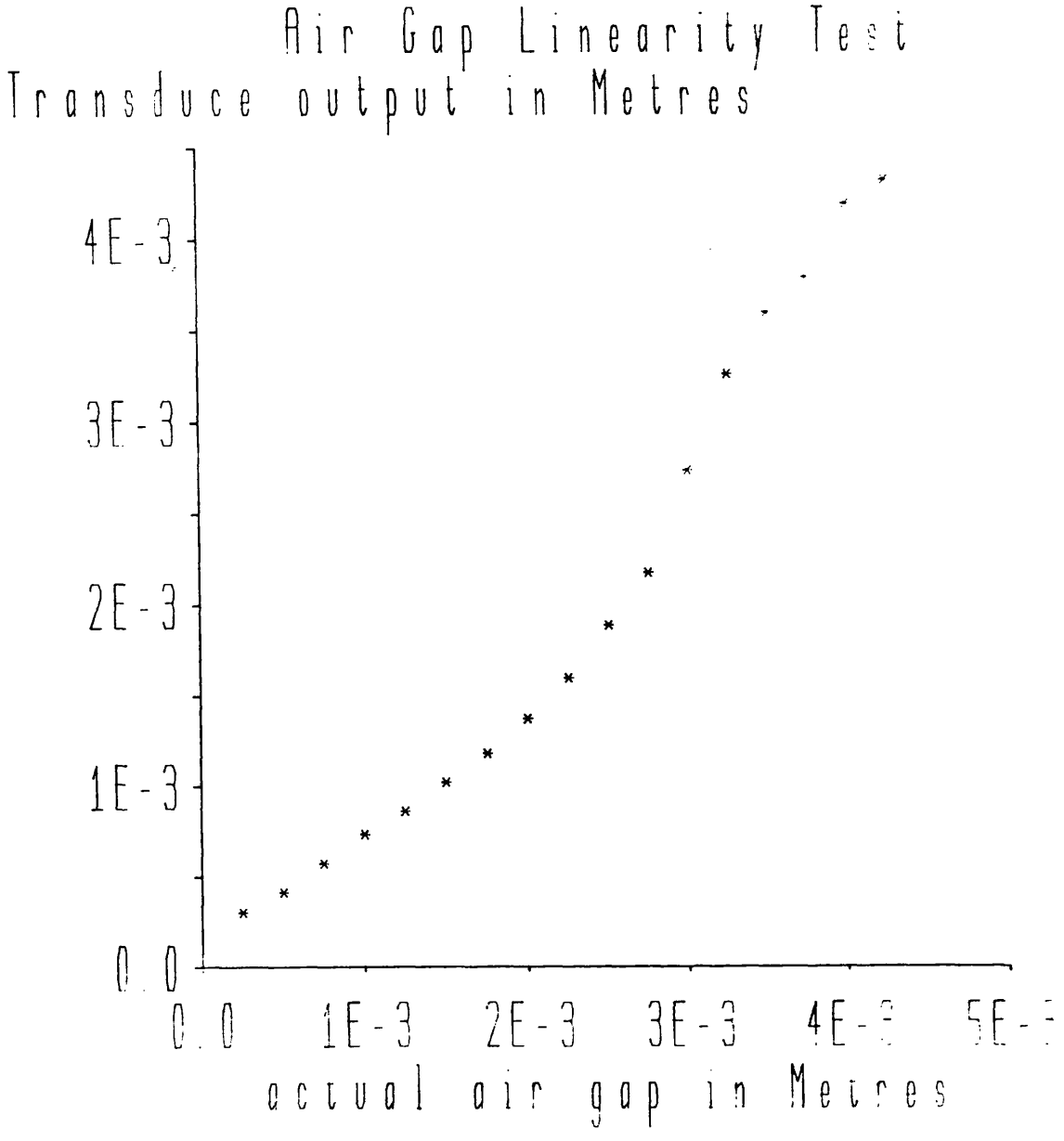

Figure 4.2.14 Initial linearity test results

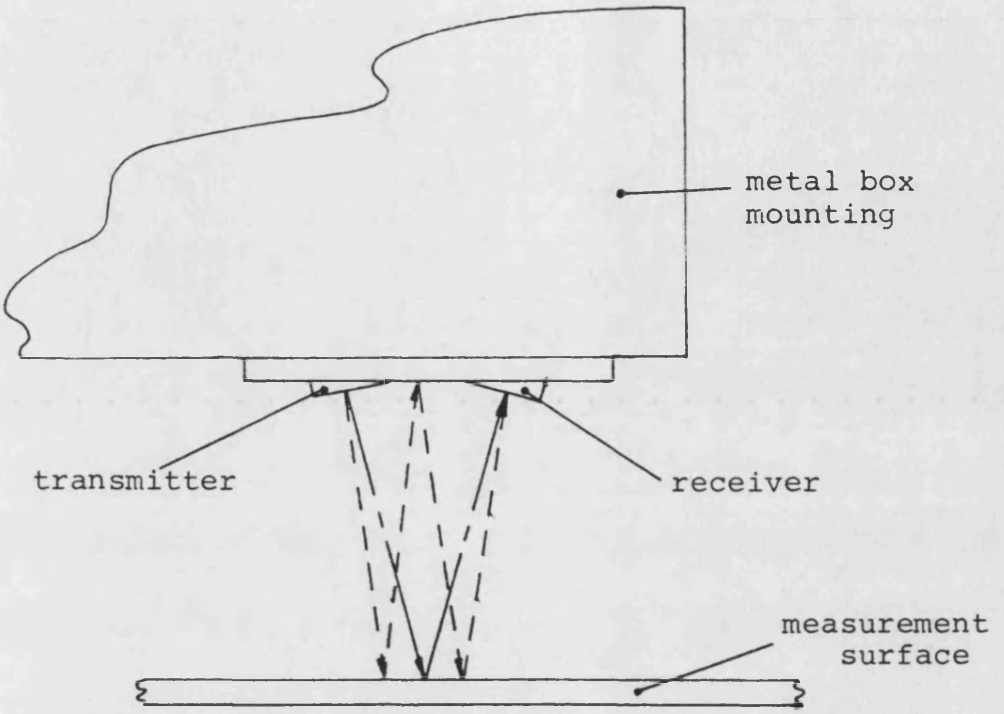

_____ _ _____primary acoustic path

— — — — — — -secondary path

Figure 4.2.15 Secondary reflection paths

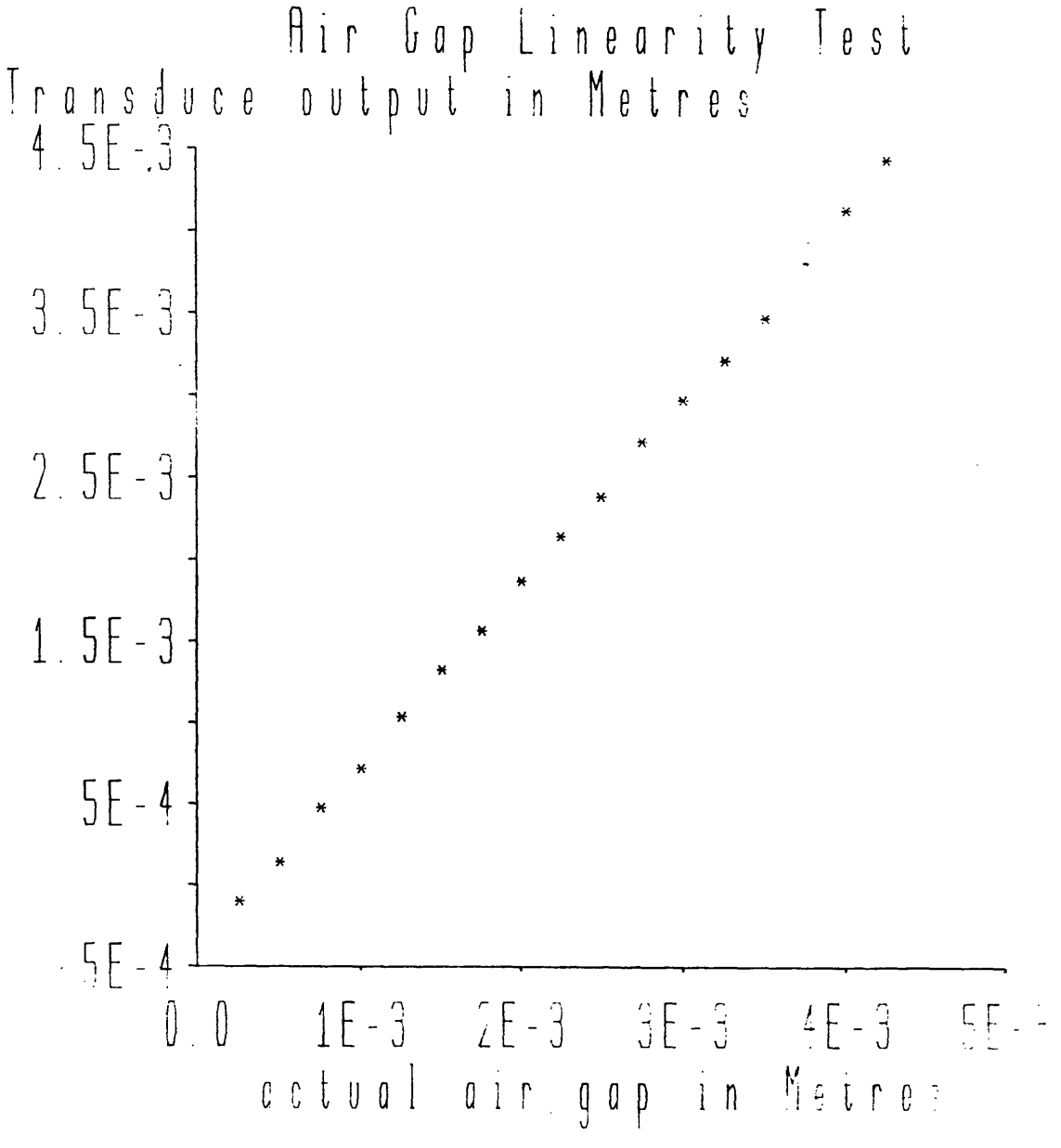

Figure 4.2.16 Improved linearity test results

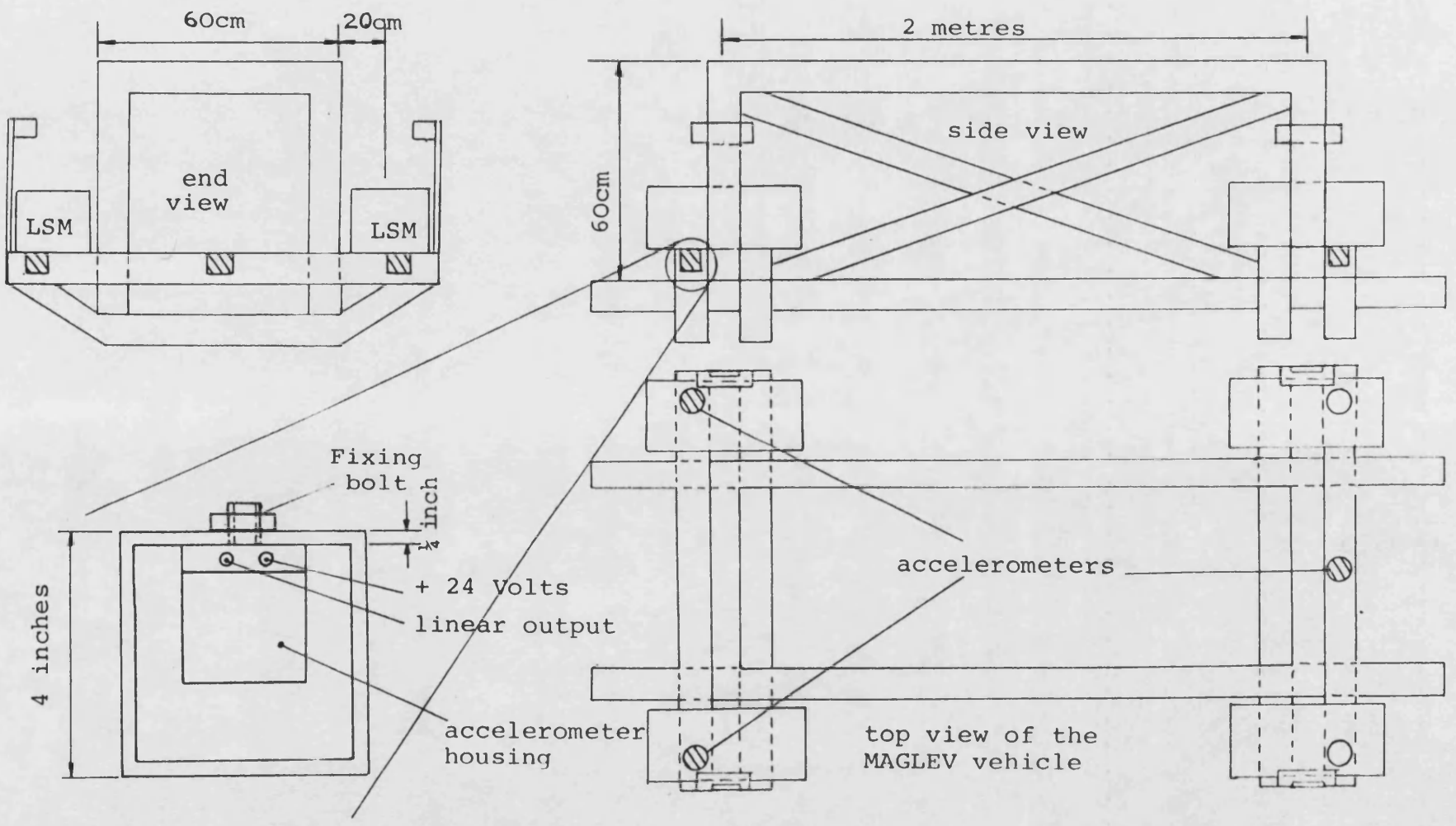

Figure 4.2.17 The accelerometer mounting positions

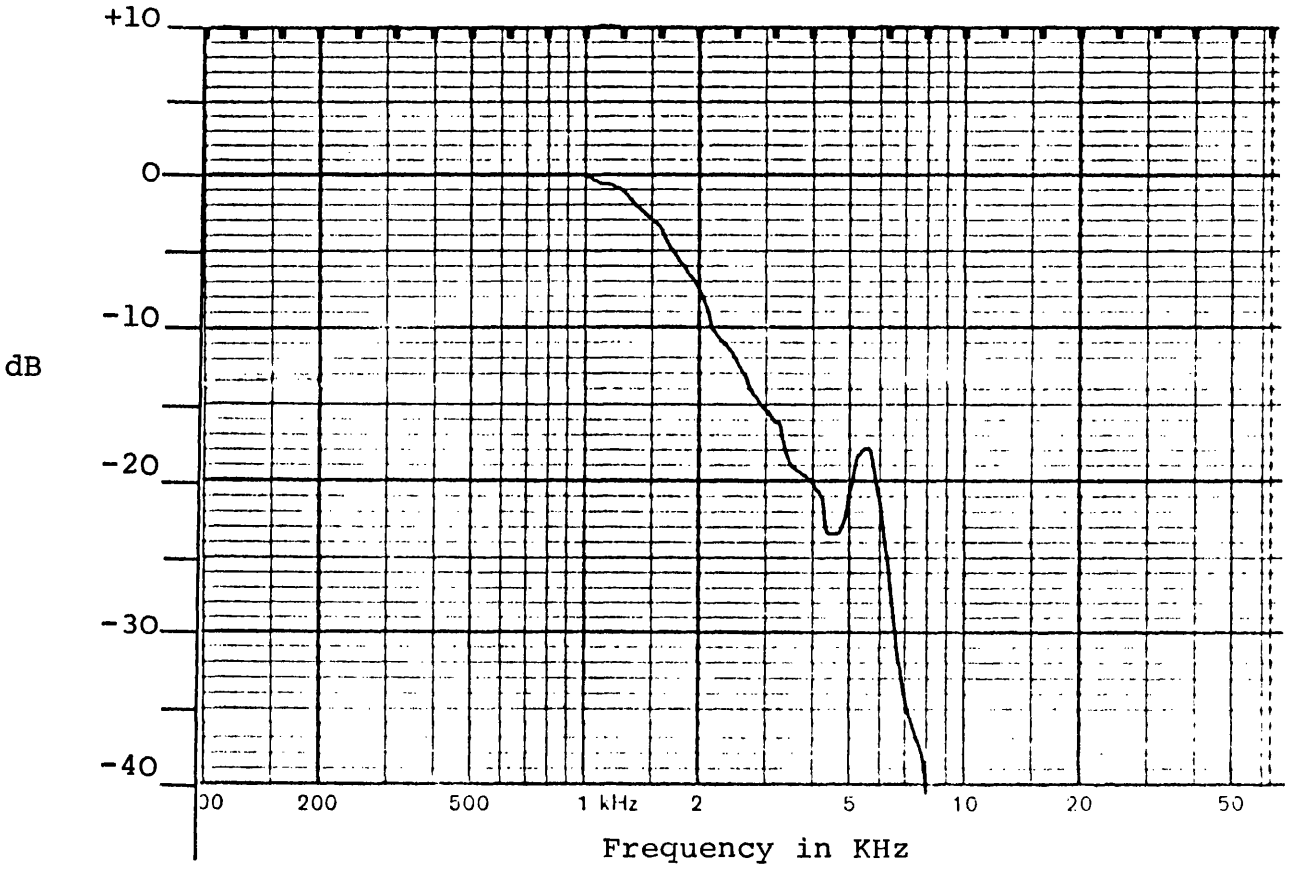

Figure 4.2.18 Bandwidth of the accelerometer used

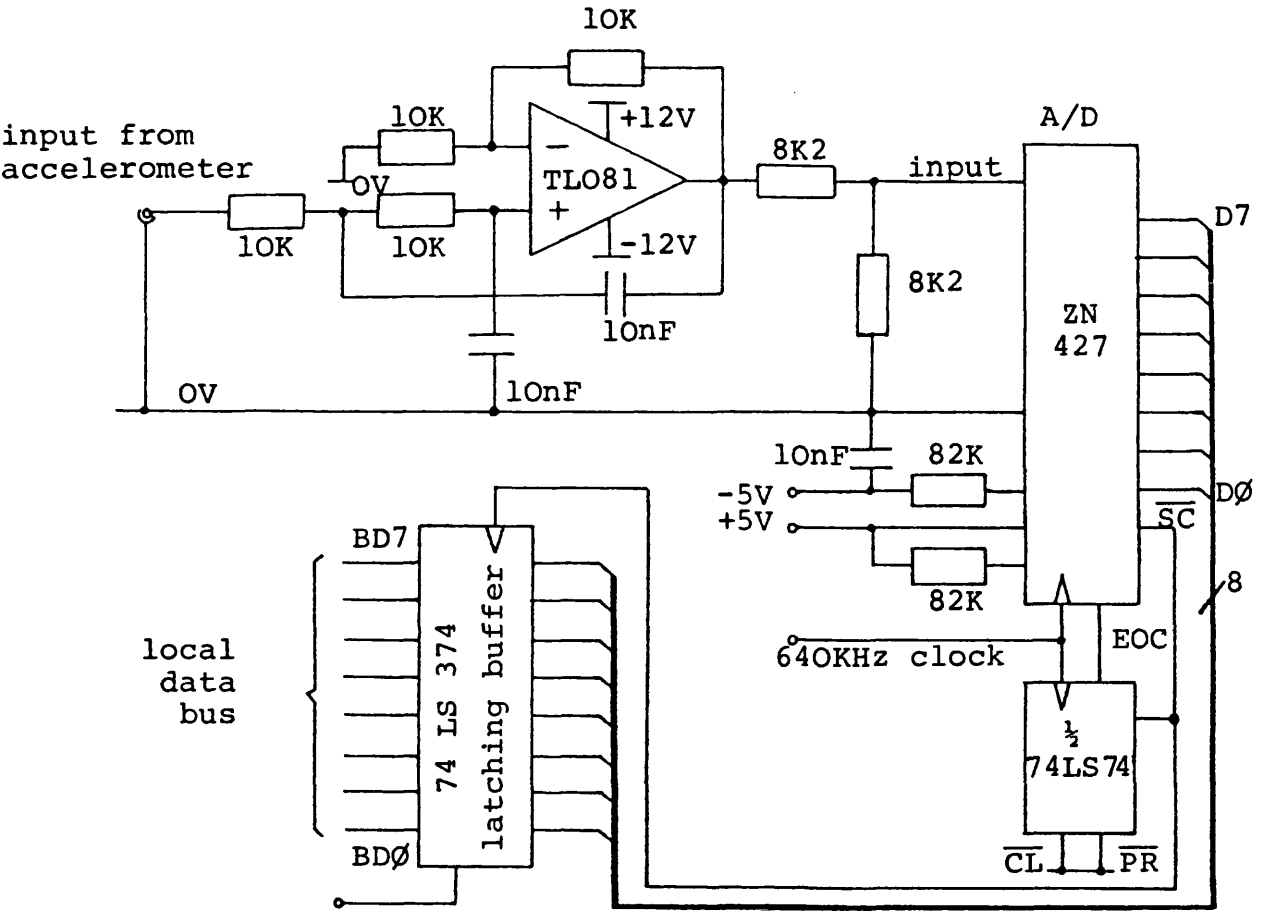

Figure 4.2.19 The interface circuit for the accelerometer

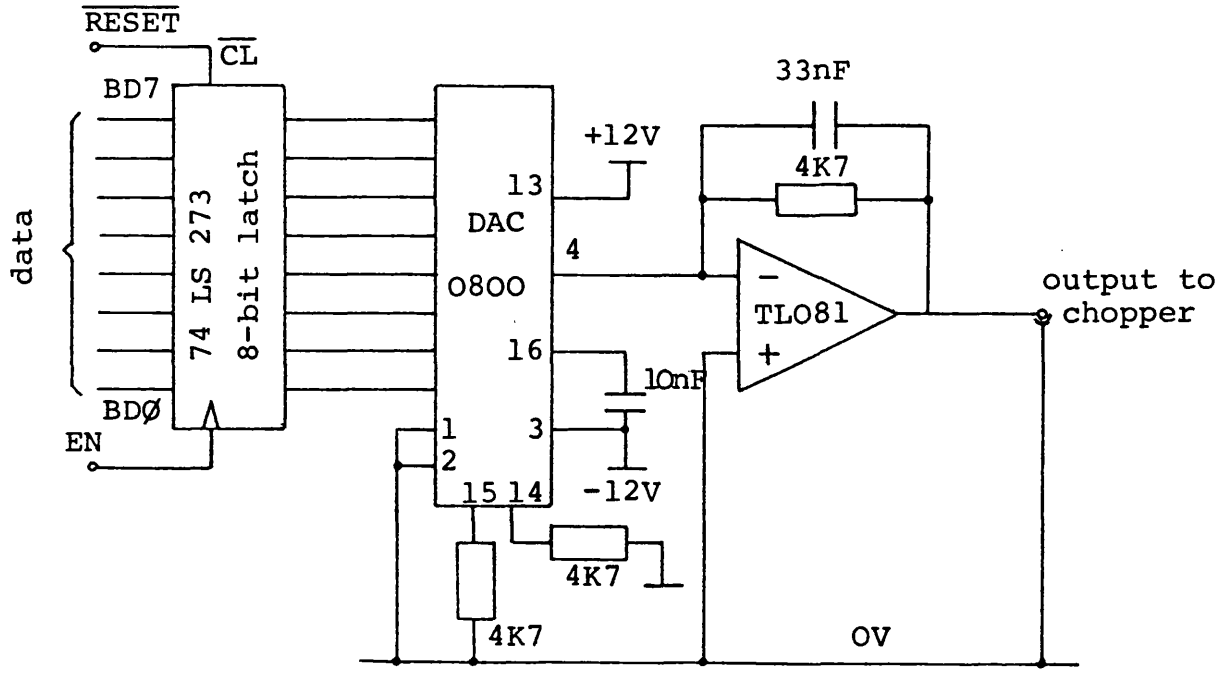

Figure 4.2.20 The chopper control output circuit

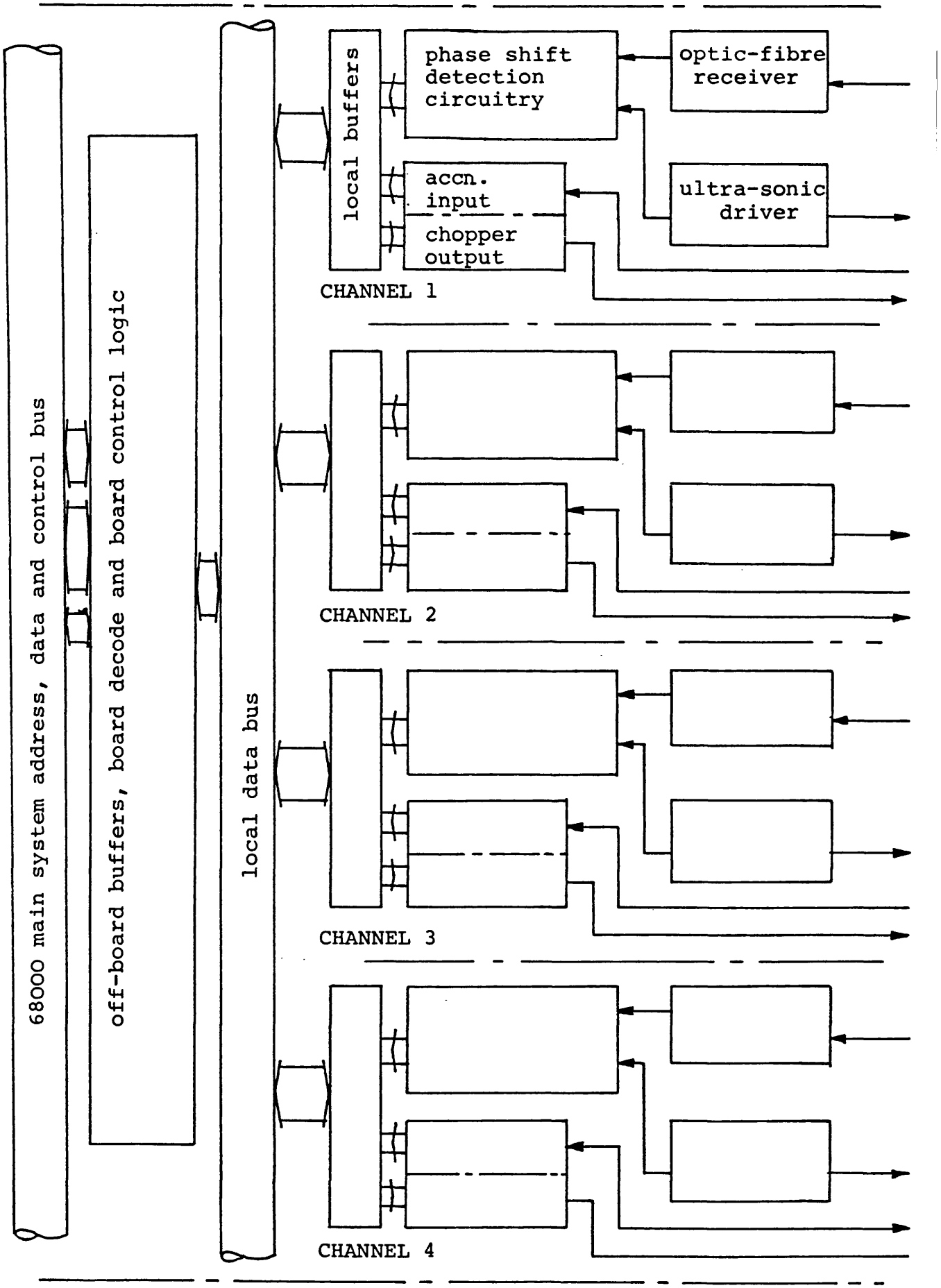

Figure 4.2.21 Block diagram of the interface card

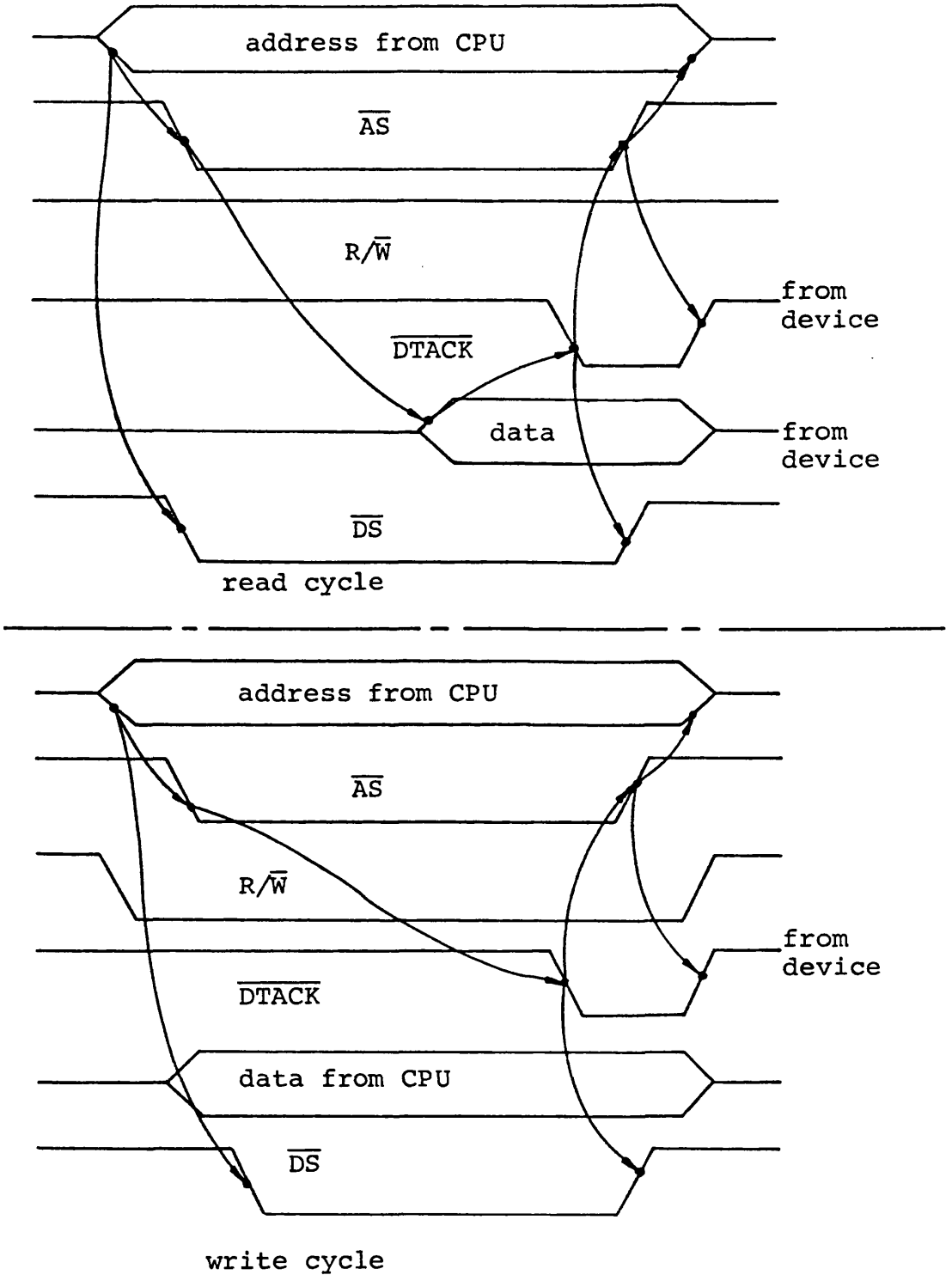

Figure 4.2.22 Motorola MC68000 read/write cycles

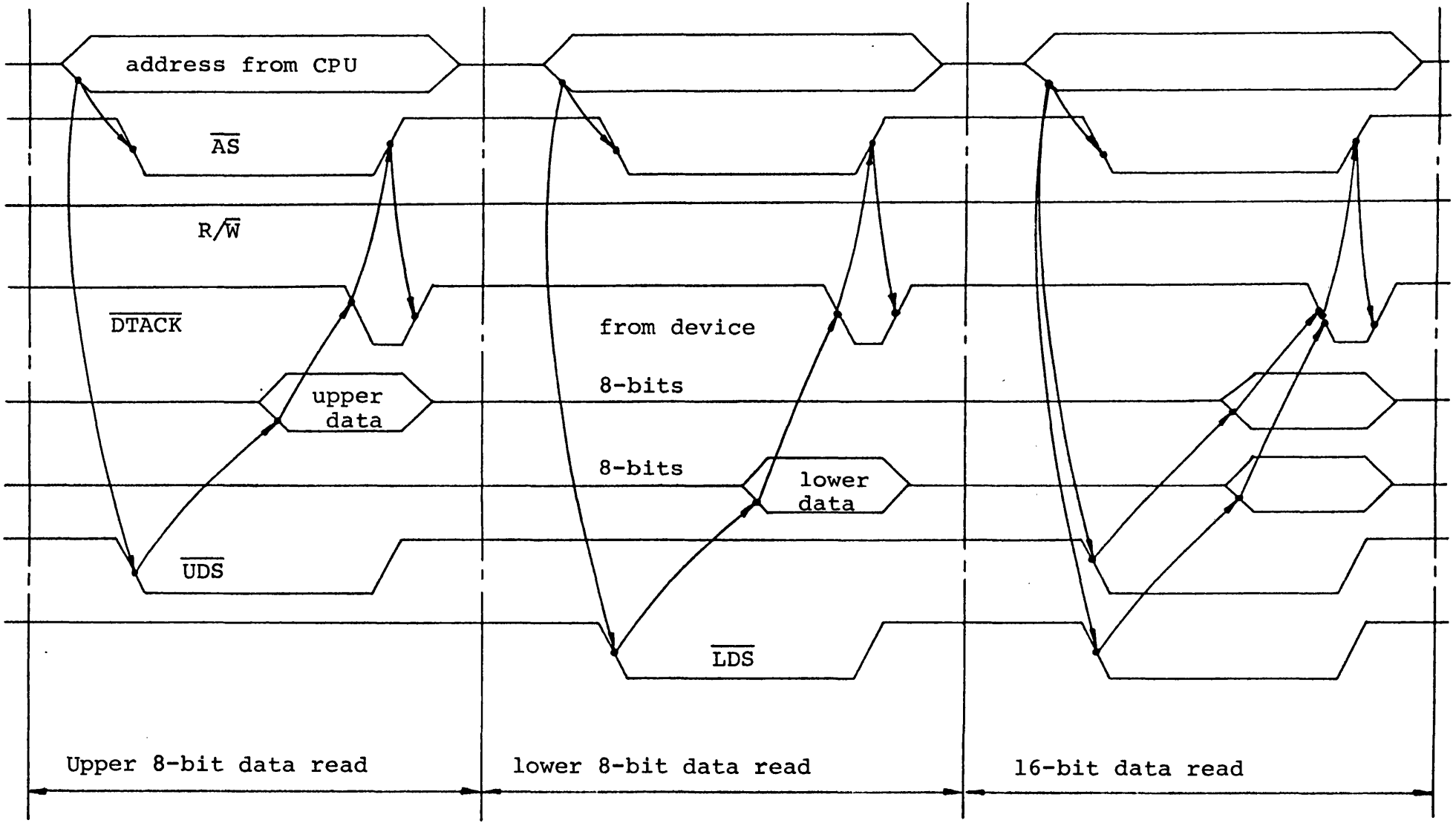

Figure 4.2.23 Upper and lower data byte reads

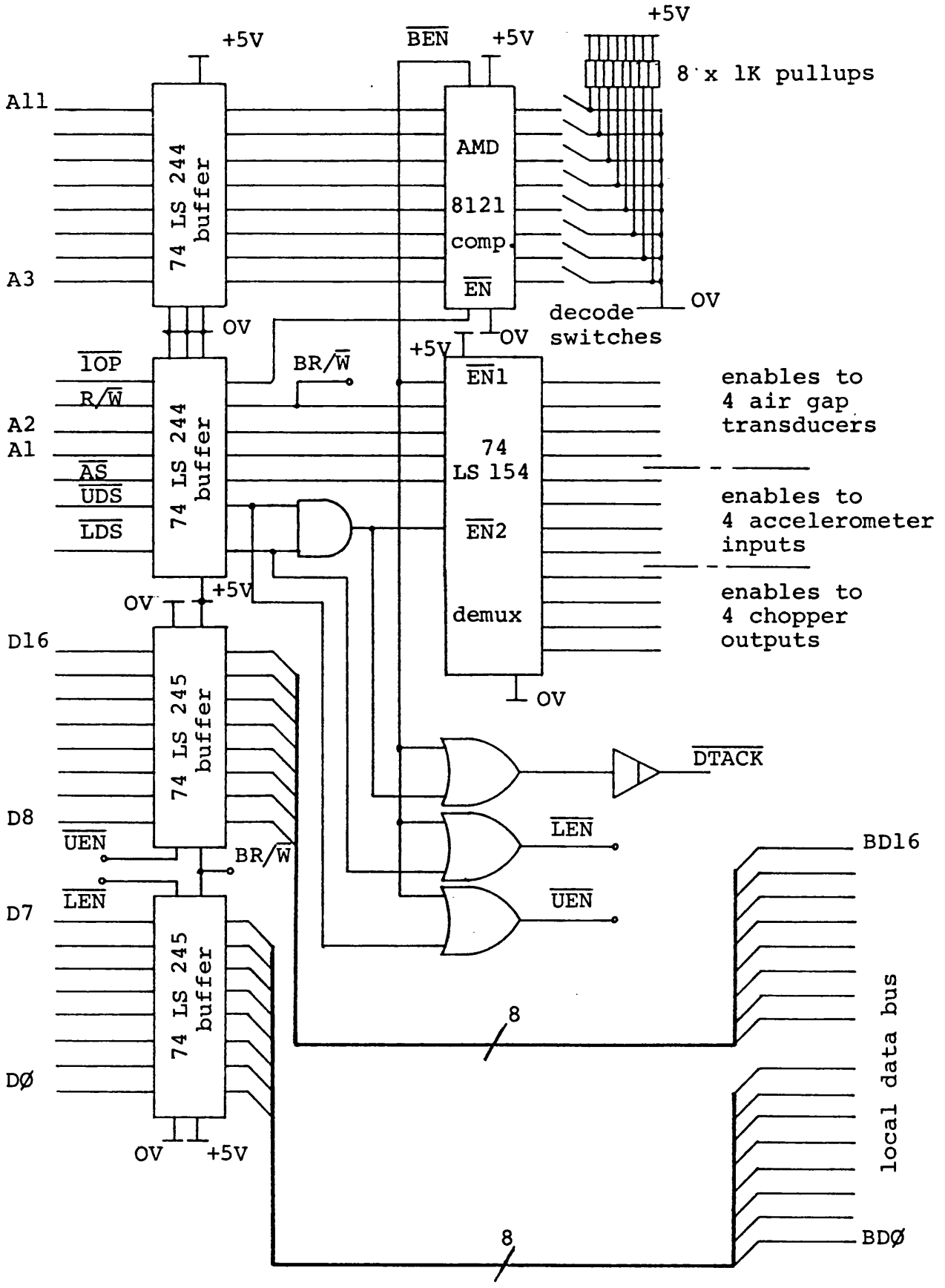

Figure 4.2.24 The interface to the MC68000

address$_{(HEX)}$	Description	READ/ WRITE
8403F1	16-bit air gap transducer 1	READ
8403F3	16-bit air gap transducer 2	READ
8403F5	16-bit air gap transducer 3	READ
8403F7	16-bit air gap transducer 4	READ
8403F9	8-bit, read only accelerometer 1	READ
8403FB	8-bit, read only accelerometer 2	READ
8403FD	8-bit, read only accelerometer 3	READ
8403FF	8-bit, read only accelerometer 4	READ
8403F1	8-bit chopper output 1	WRITE
8403F3	8-bit chopper output 2	WRITE
8403F5	8-bit chopper output 3	WRITE
8403F7	8-bit chopper output 4	WRITE
	n.b. the base address of the card is 84Ø3FØ (HEX), but is relocatable.	

Figure 4.2.25 The memory addresses of the interface devices

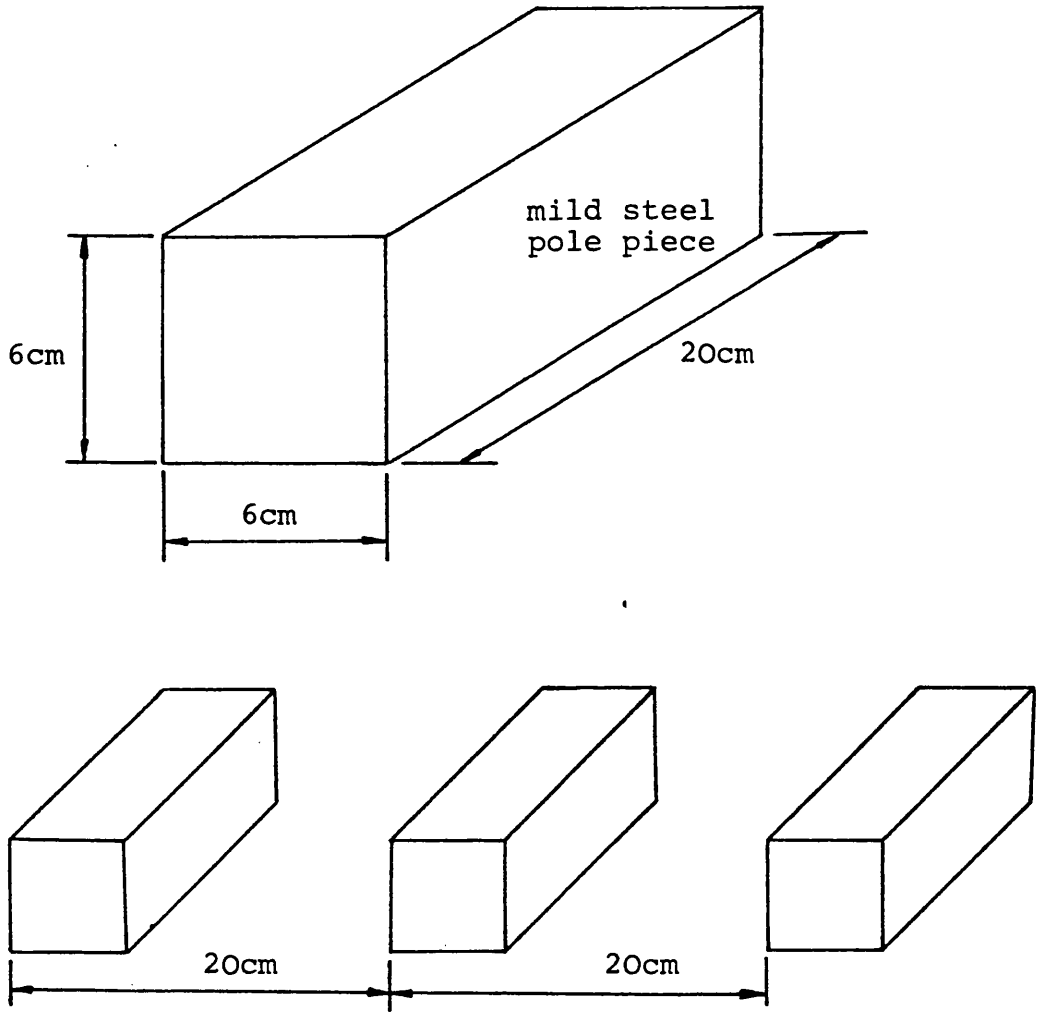

Layout of pole pieces along the track

Figure 4.3.1 The LSM track pole piece dimensions

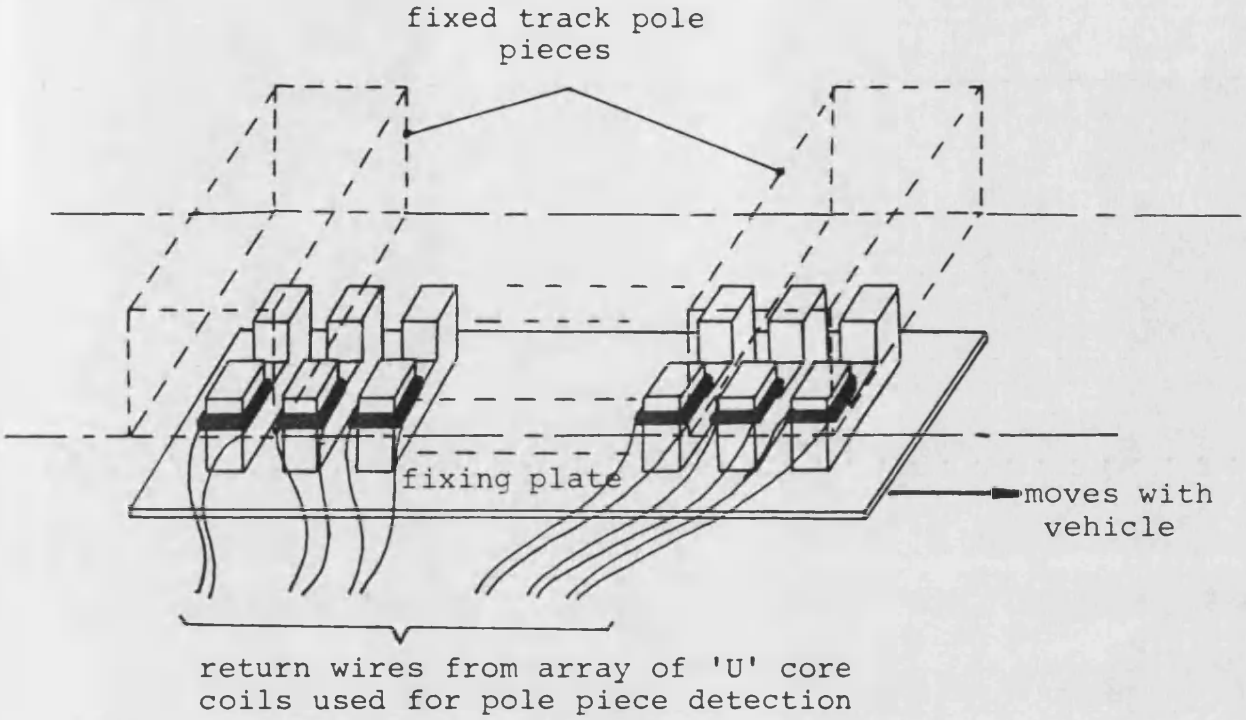

Figure 4.3.2 The use of 'U' core coils for pole detection

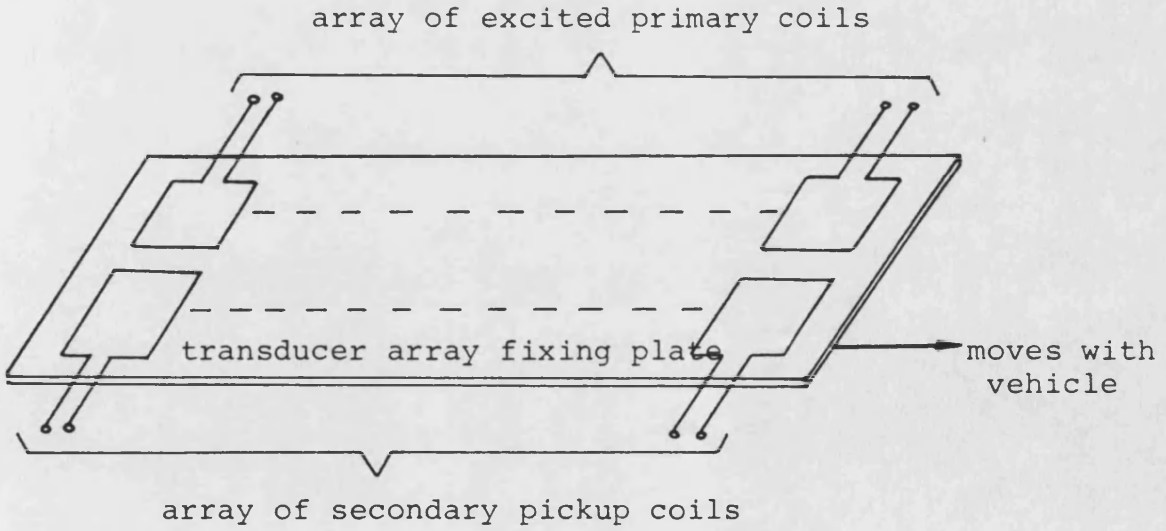

Figure 4.3.3 The use of increased coupling between pairs of coils for pole detection

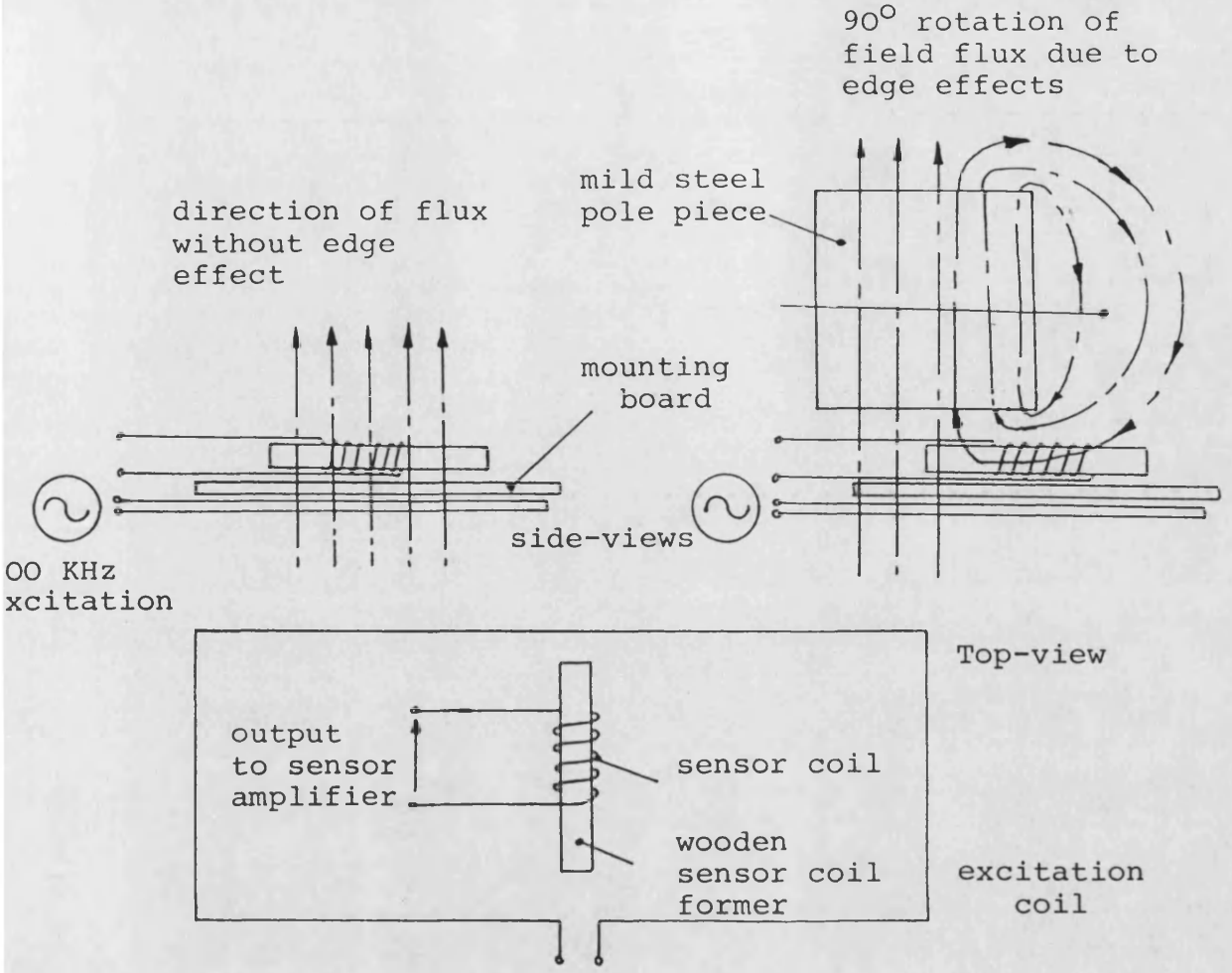

Figure 4.3.4 The use of pole piece edge effects to rotate an exciter field through 90° to increase coupling

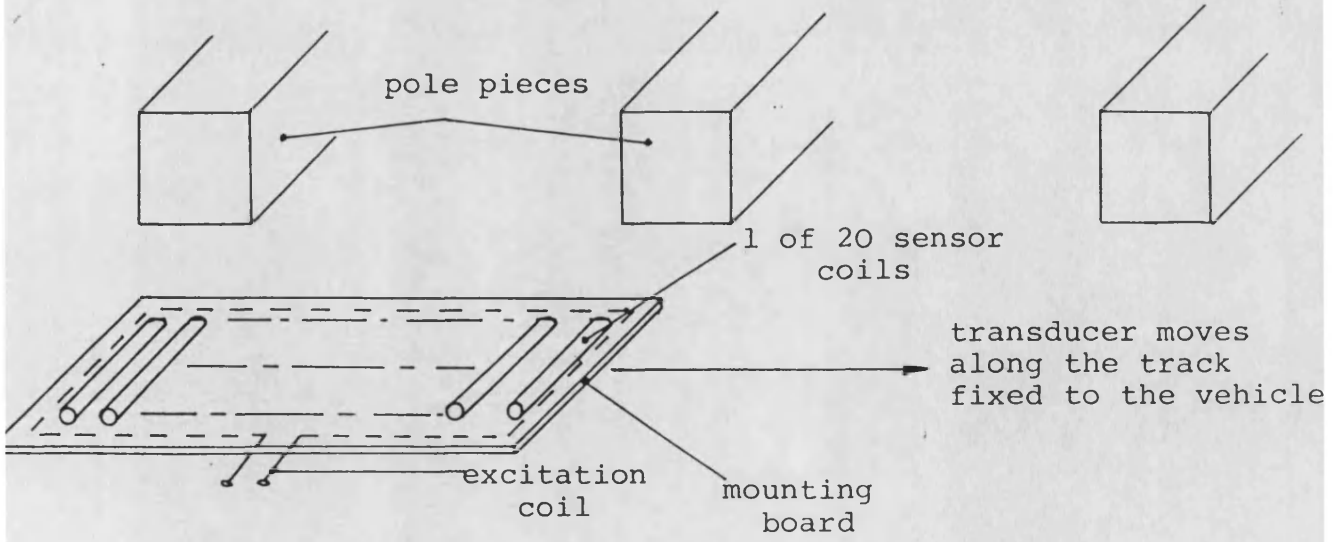

Figure 4.3.5 The layout of the edge detection pole position transducer

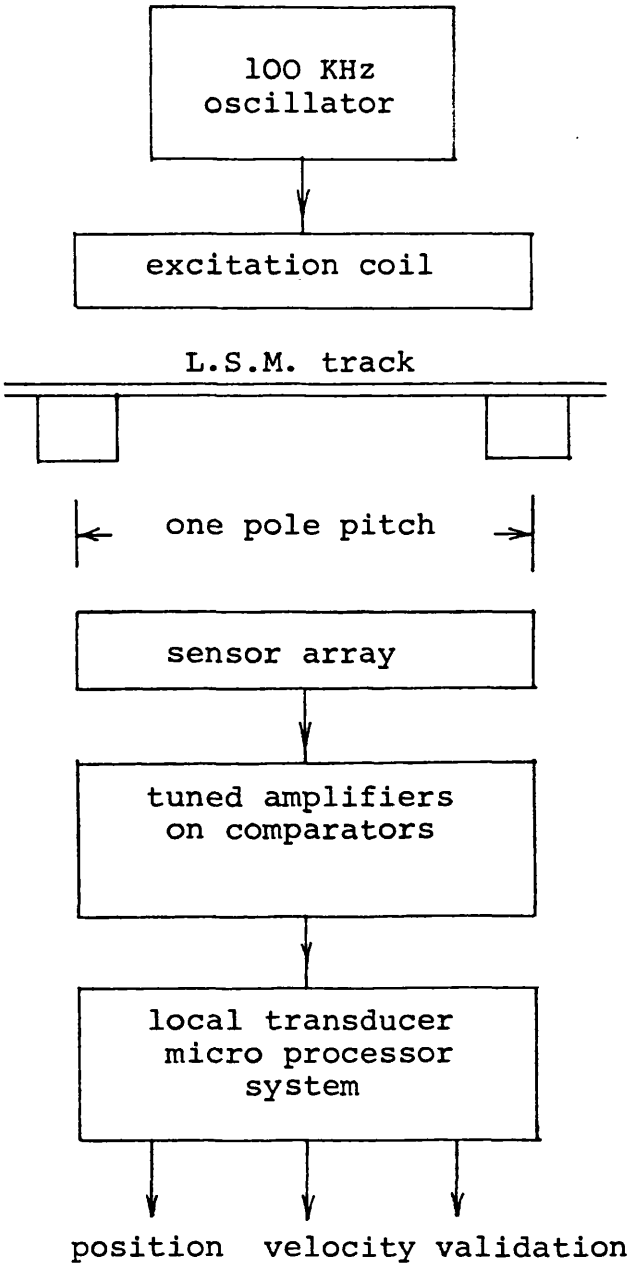

Figure 4.3.6 Schematic of the pole piece position transducer operation

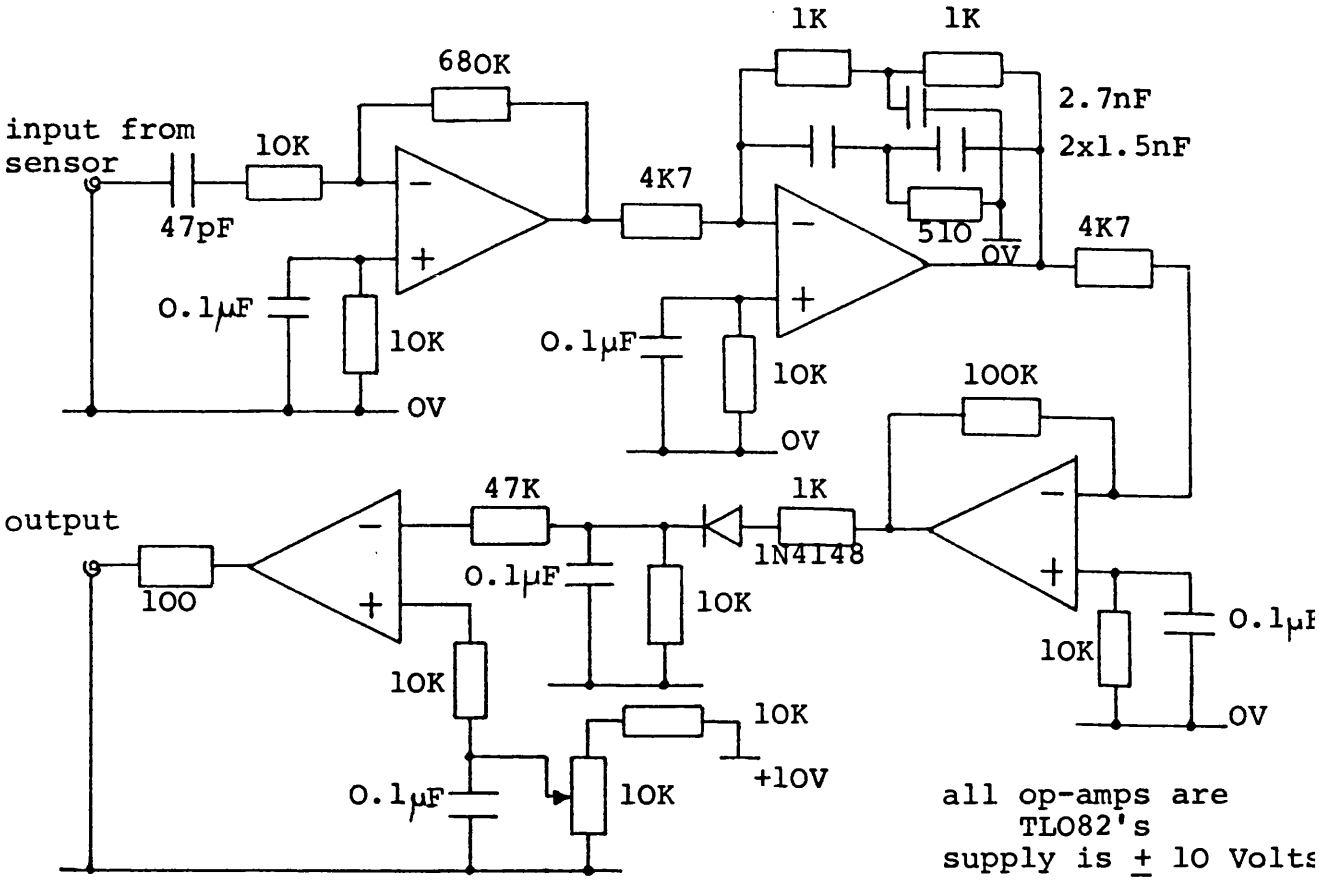

Figure 4.3.7 Pole pieces detection analogue circuitry

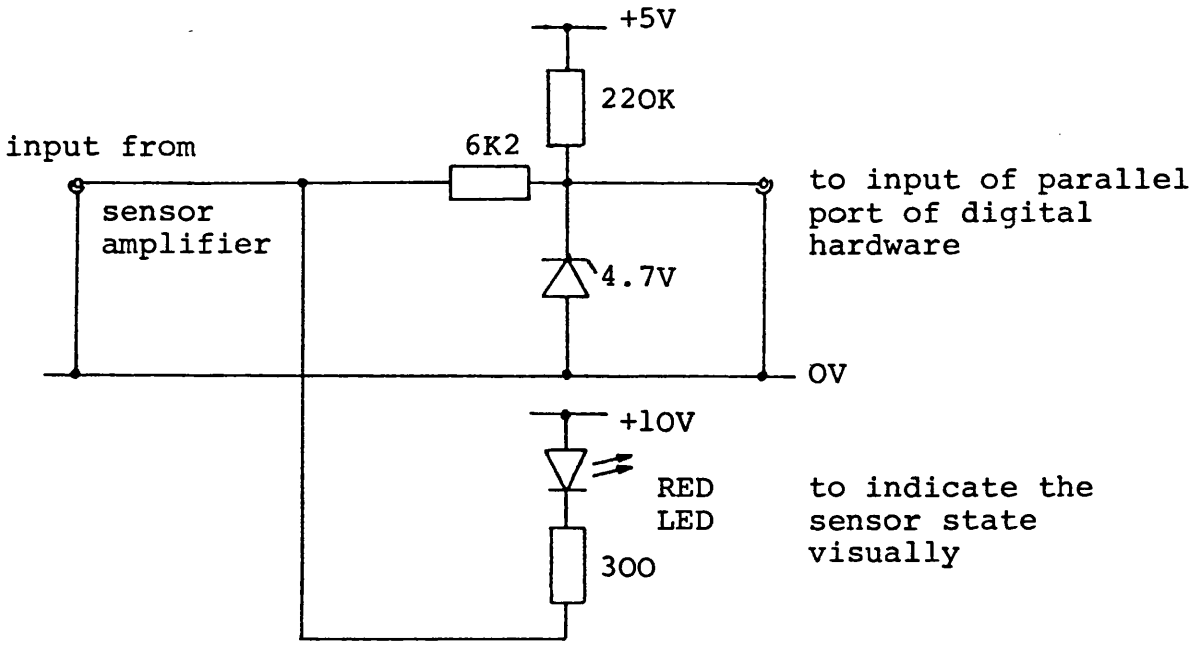

Figure 4.3.8 The interface to the transducer digital circuitry

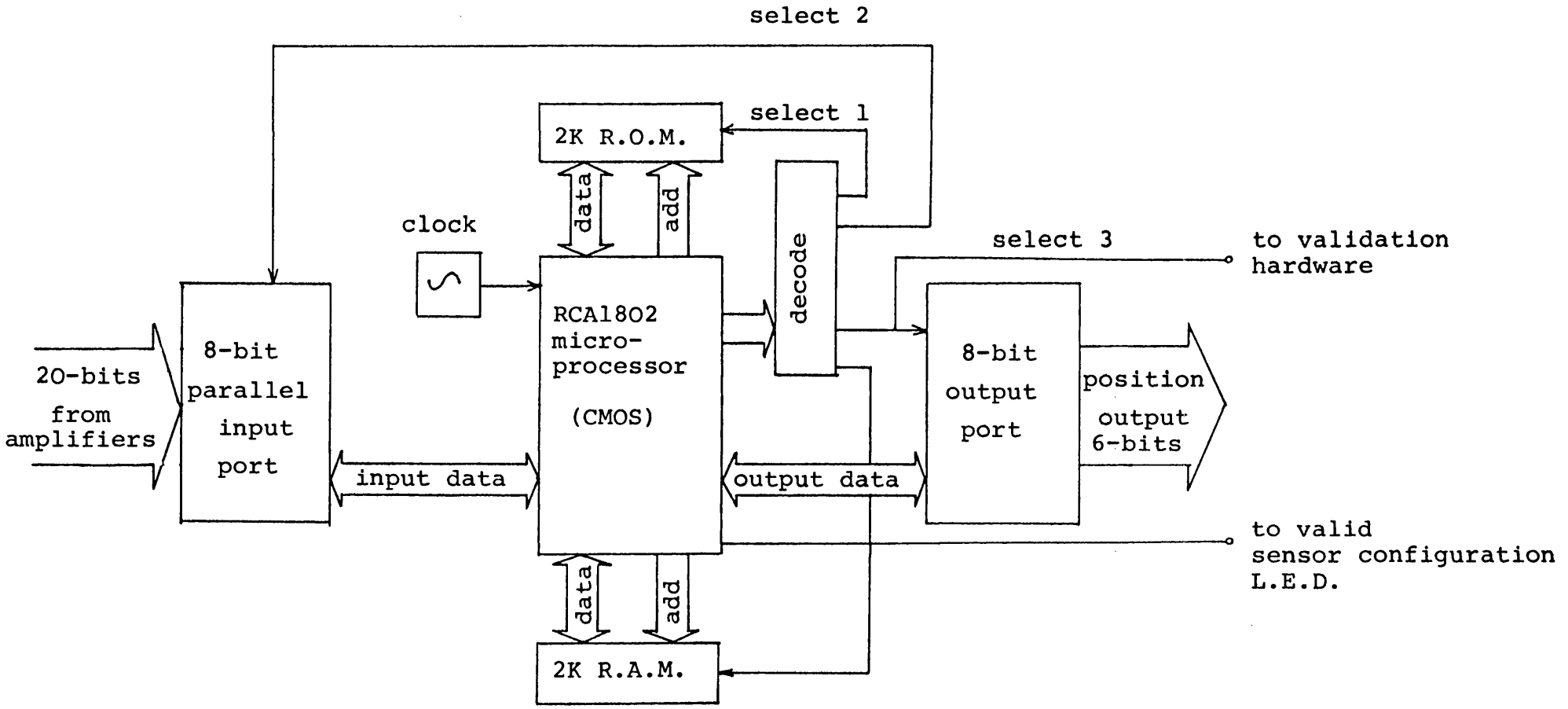

Figure 4.3.9 Block diagram of the local signal processor

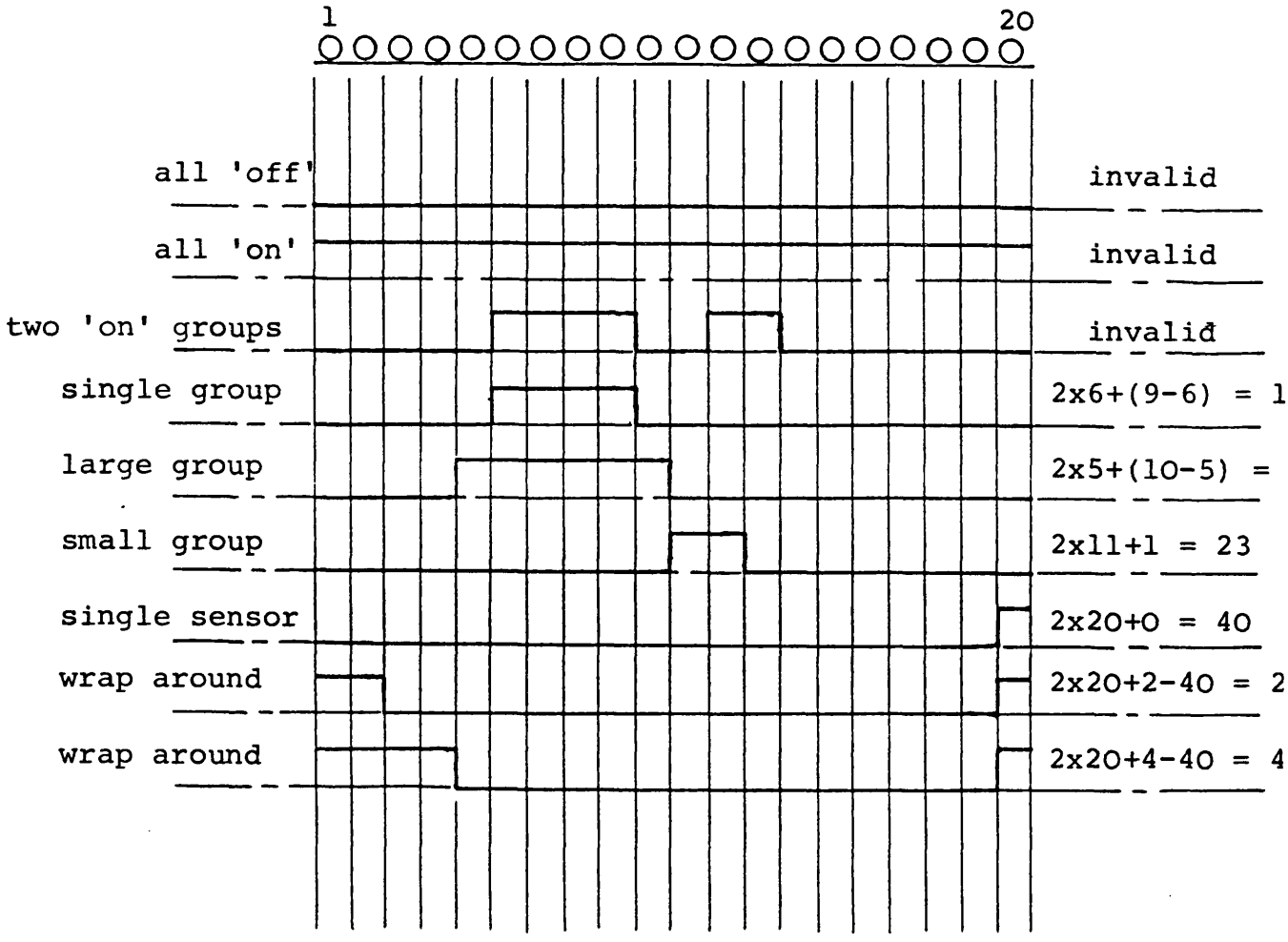

Figure 4.3.11 Possible transducer states and their interpretation

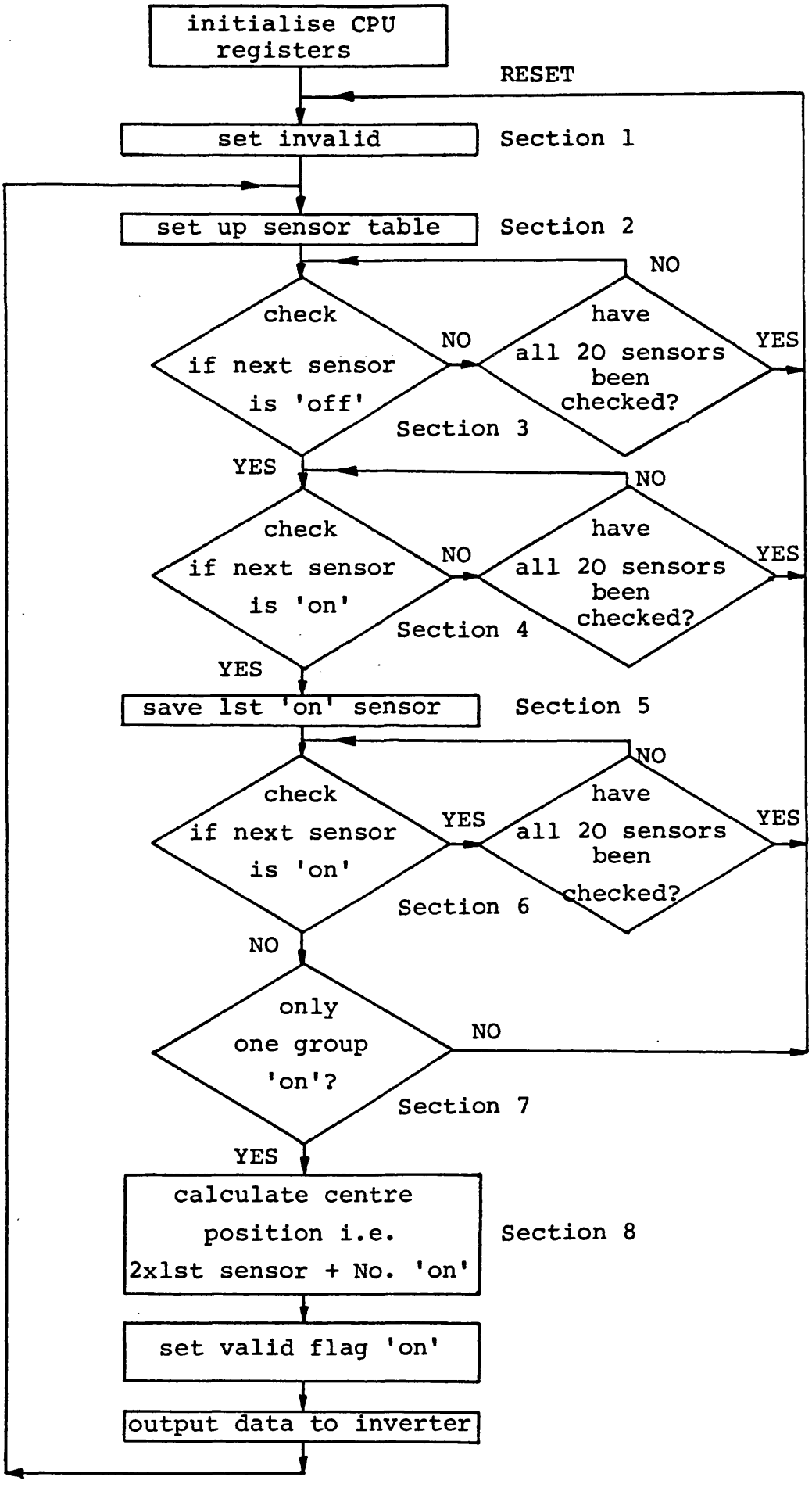

Figure 4.3.12 Block diagram of the original signal processing software

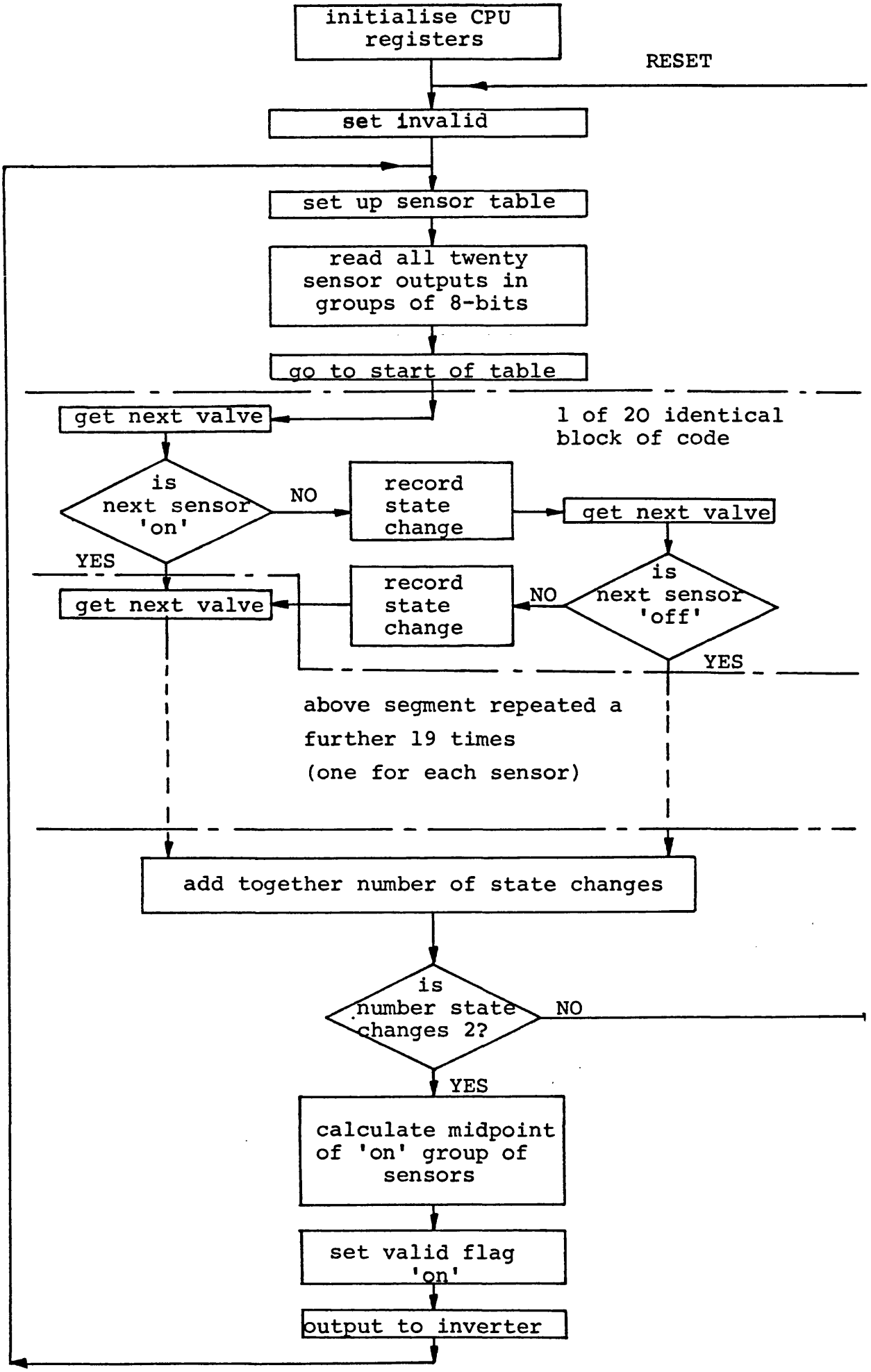

Figure 4.3.13 Block diagram of final approach to the softwa

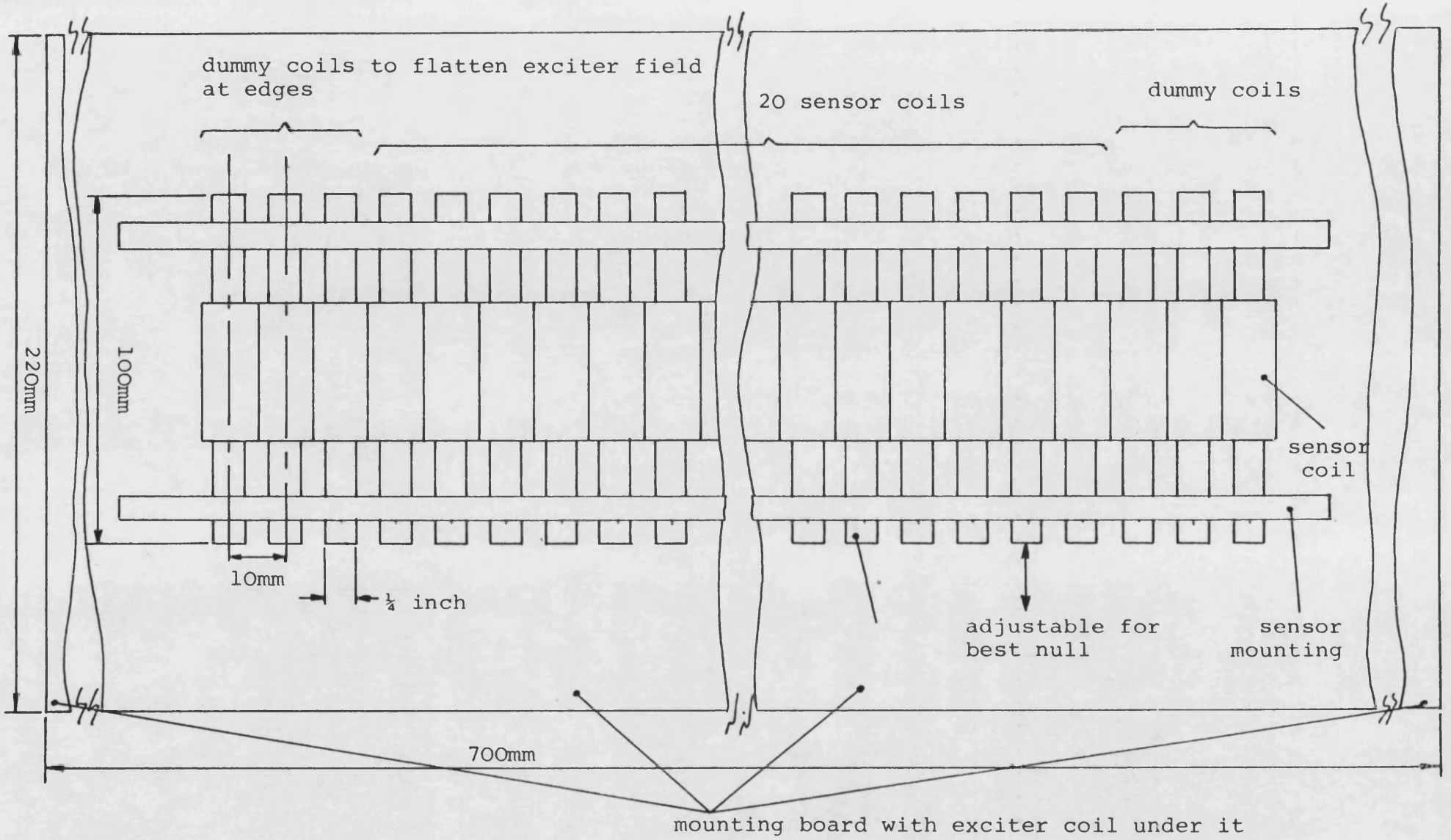

Figure 4.3.14 Sense coil dimensions

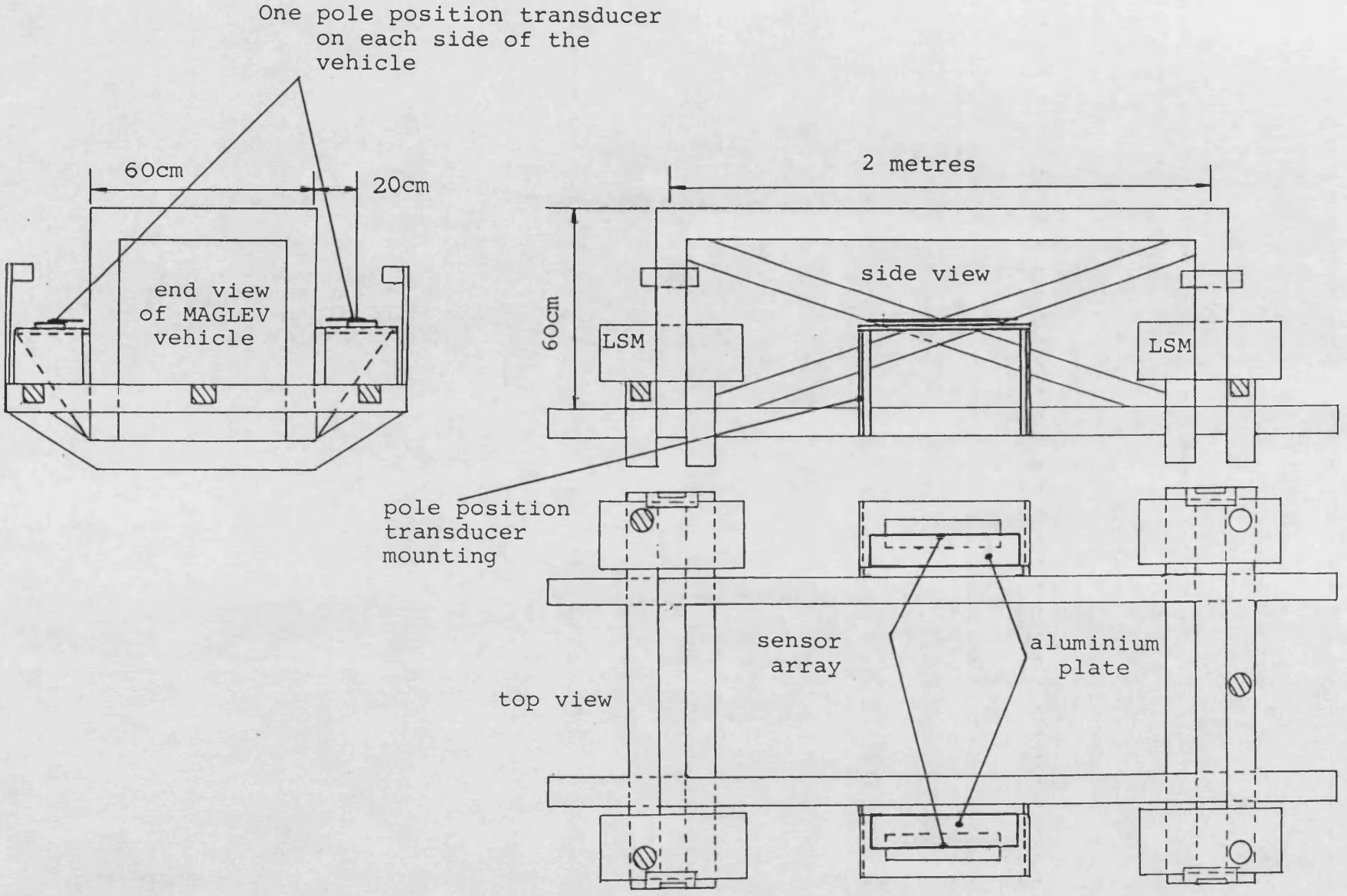

Figure 4.3.15 The fixing position of the pole position transducer on the LSM MAGLEV vehicle

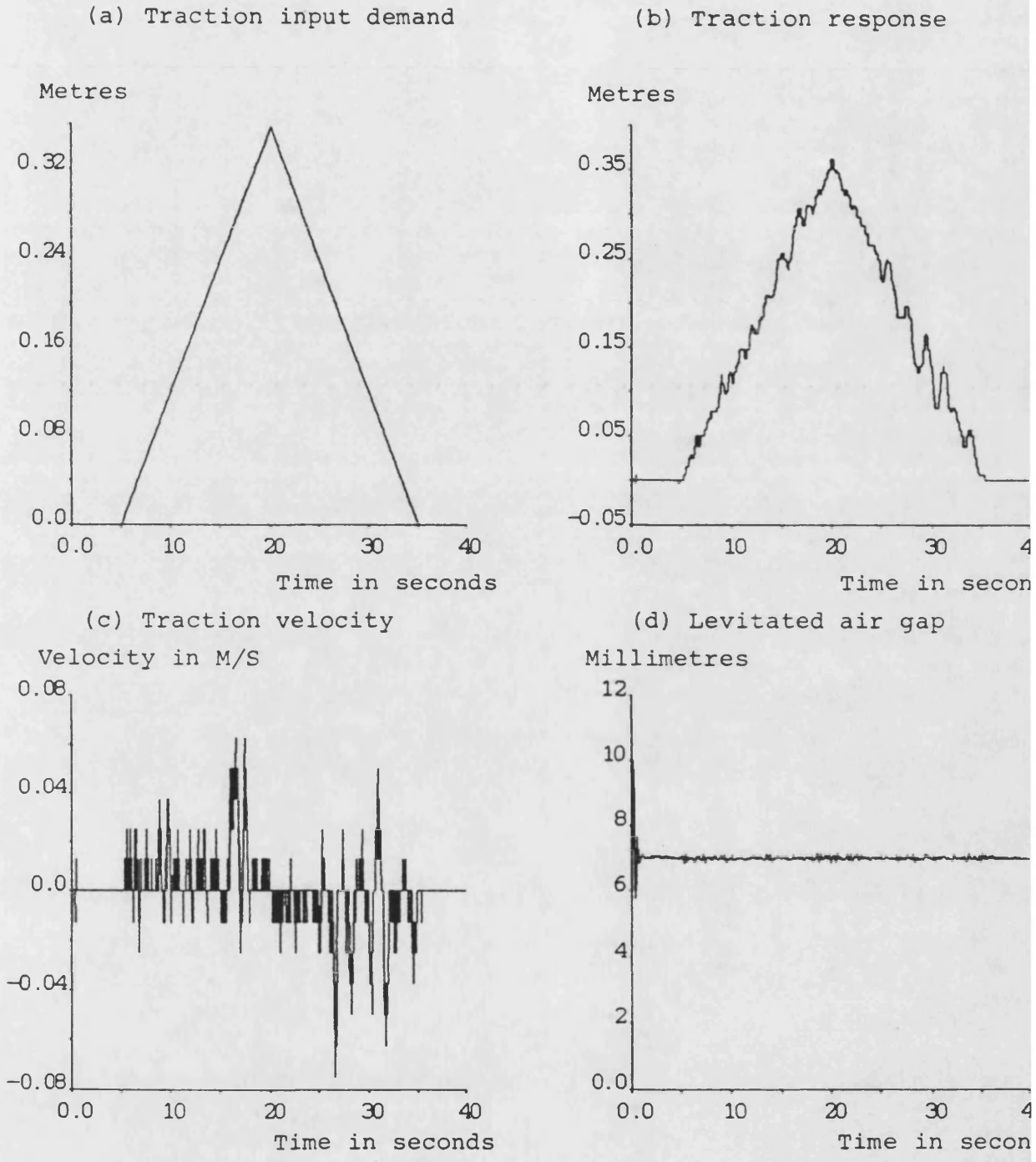

Figure 4.3.16 Tractive control with constant levitated air gap for slow ramp input

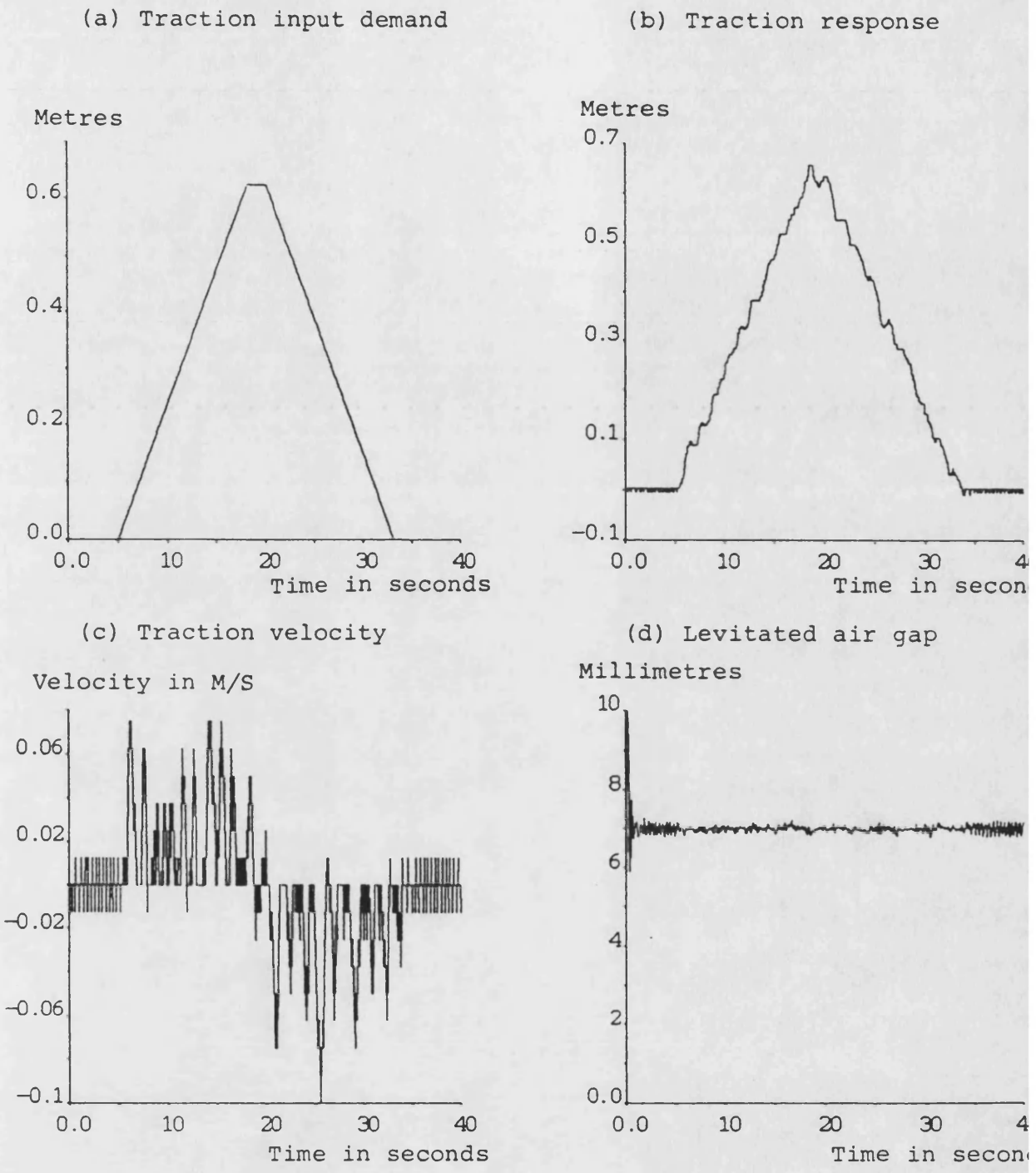

Figure 4.6.17 Tractive control with constant levitated air gap for faster ramp input

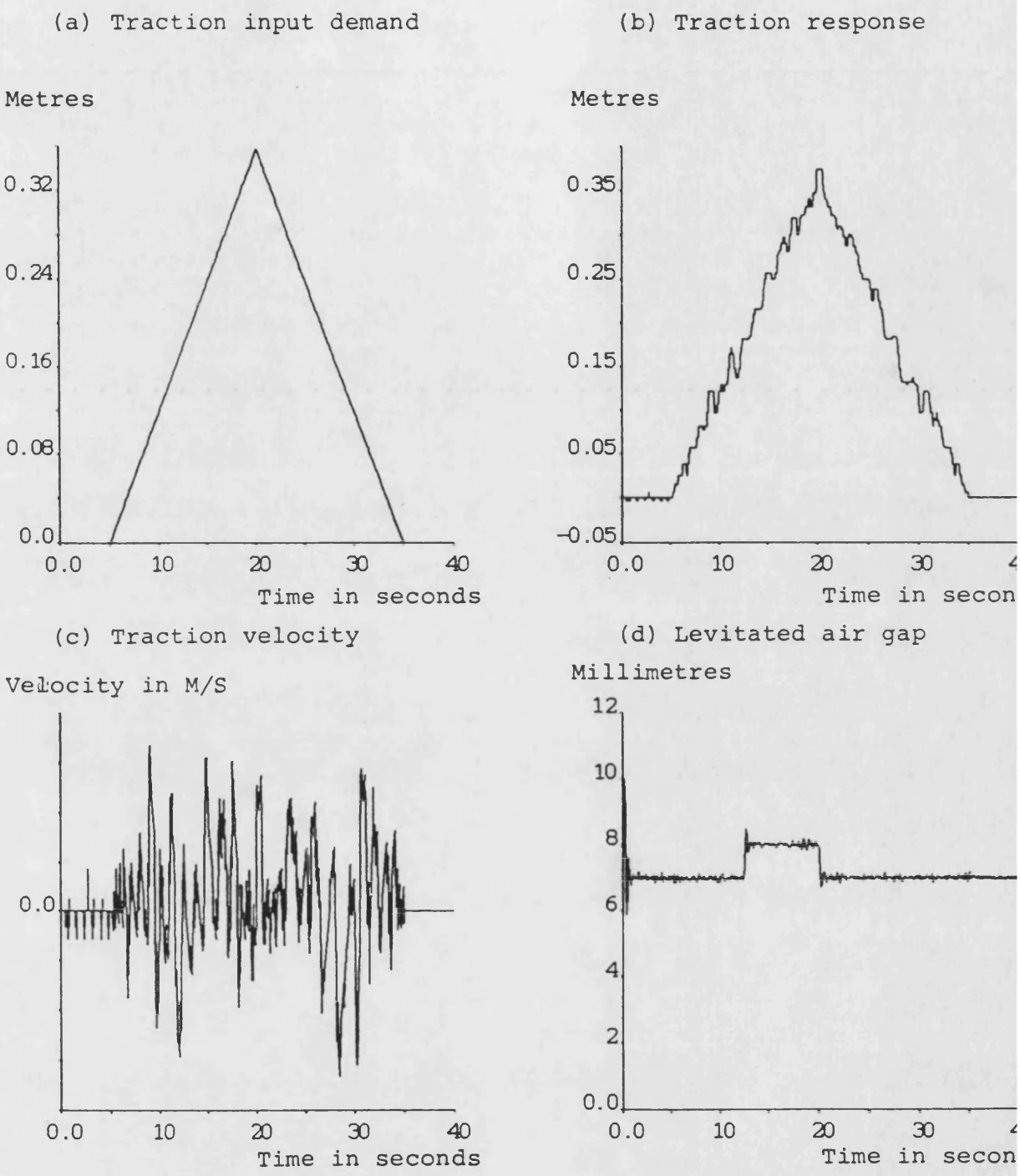

Figure 4.6.18 Tractive control with stepped levitated air gap for slow ramp input

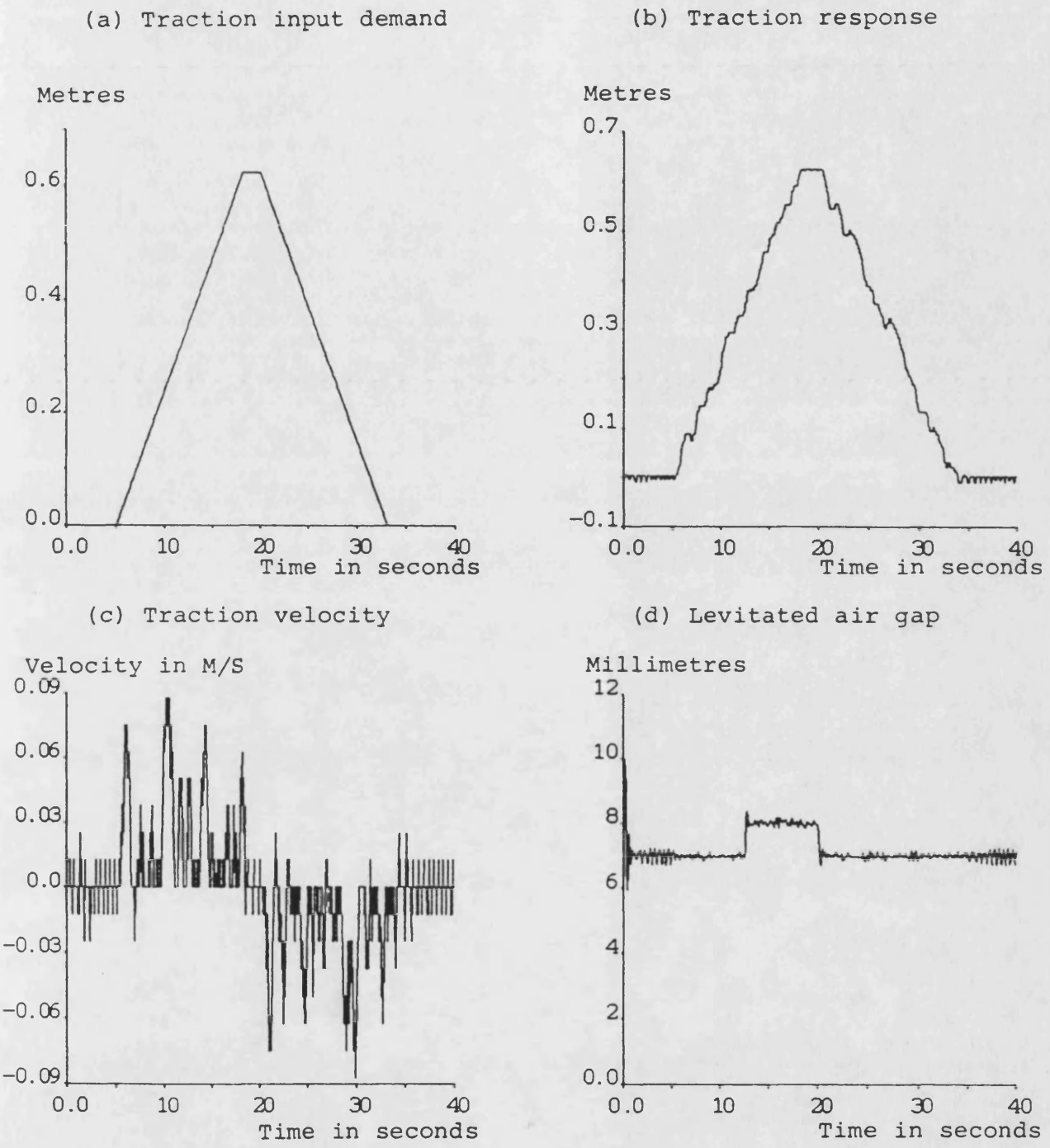

Figure 4.3.19 Tractive control with stepped levitated air gap for faster ramp input

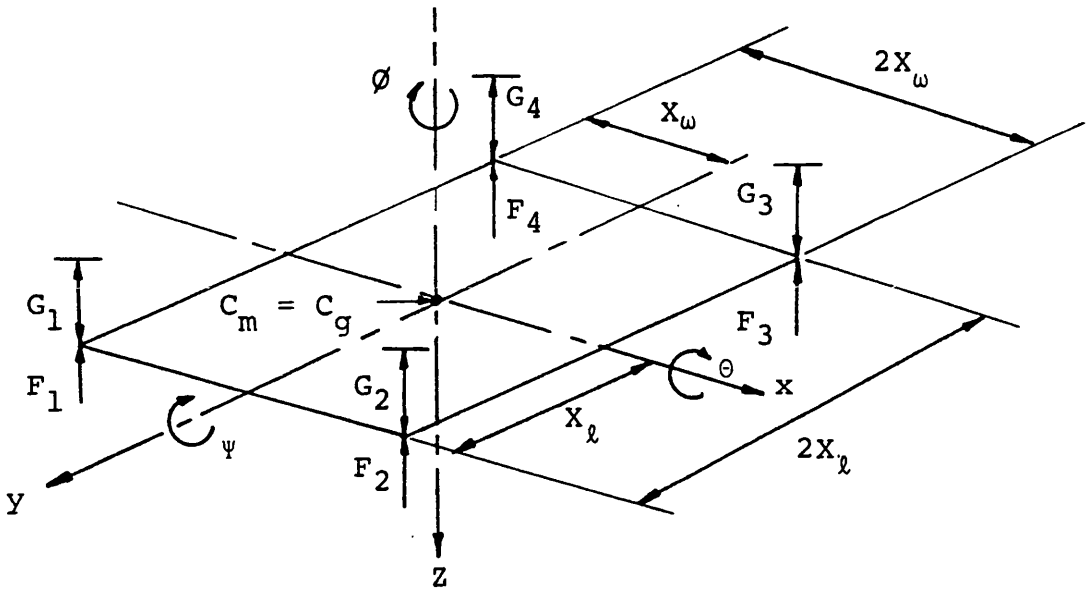

Figure 5.3.1 Three degrees of freedom structure

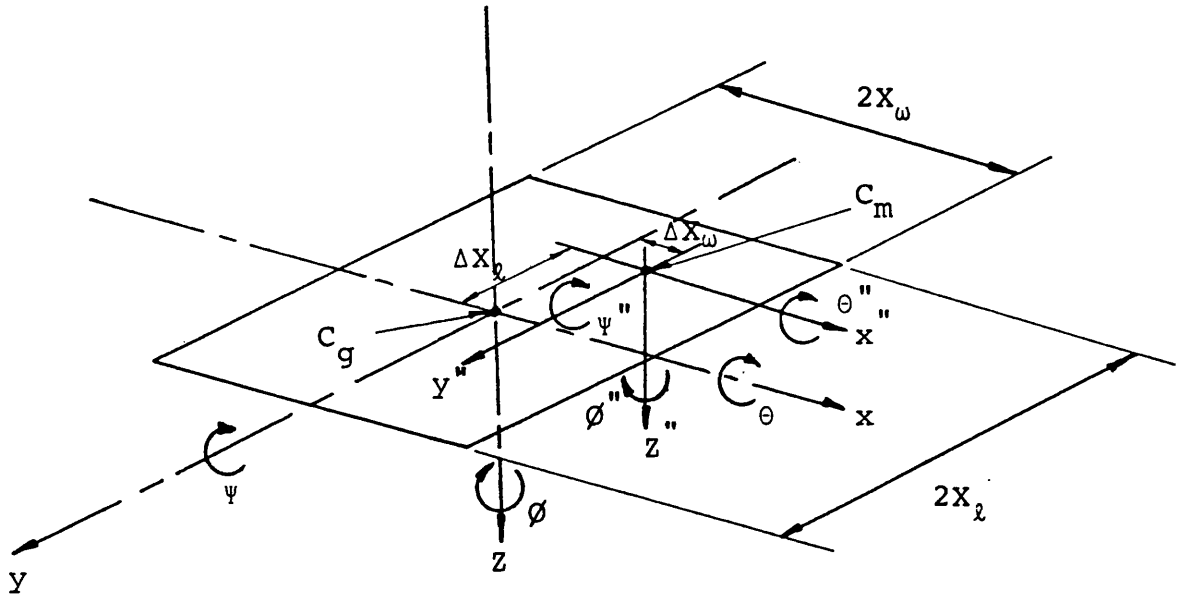

Figure 5.3.2 Three degrees of freedom structure with non-coincident centre of man and centre of geometry

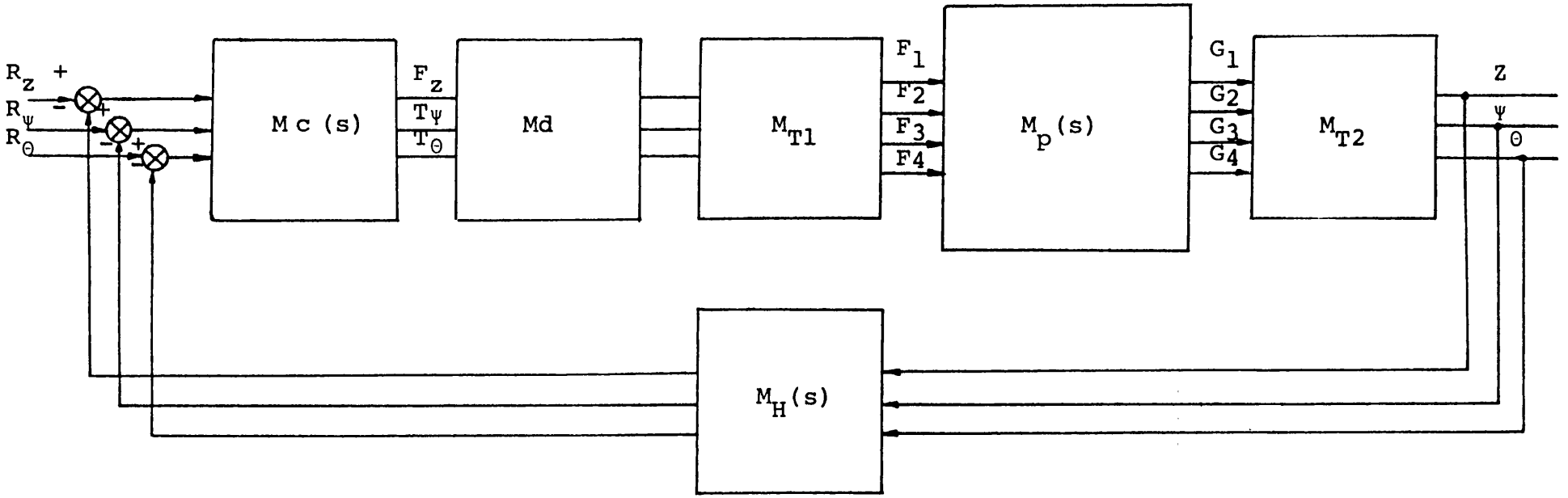

$M_p(s)$ represents the dynamics of the vehicle air gaps when acted on by the corner forces and includes multivariable coupling.

M_{T1} is the transformation matrix from centre of geometry to corner forces.

M_{T2} is the transformation matrix from corner air gaps to centre of geometry coordinates.

Md is the multivariable decoupling matrix.

Mc (s) is some diagonal forward path controller matrix.

$M_H(s)$ is some diagonal feedback path controller matrix.

Figure 5.3.3 Closed loop multivariable controller

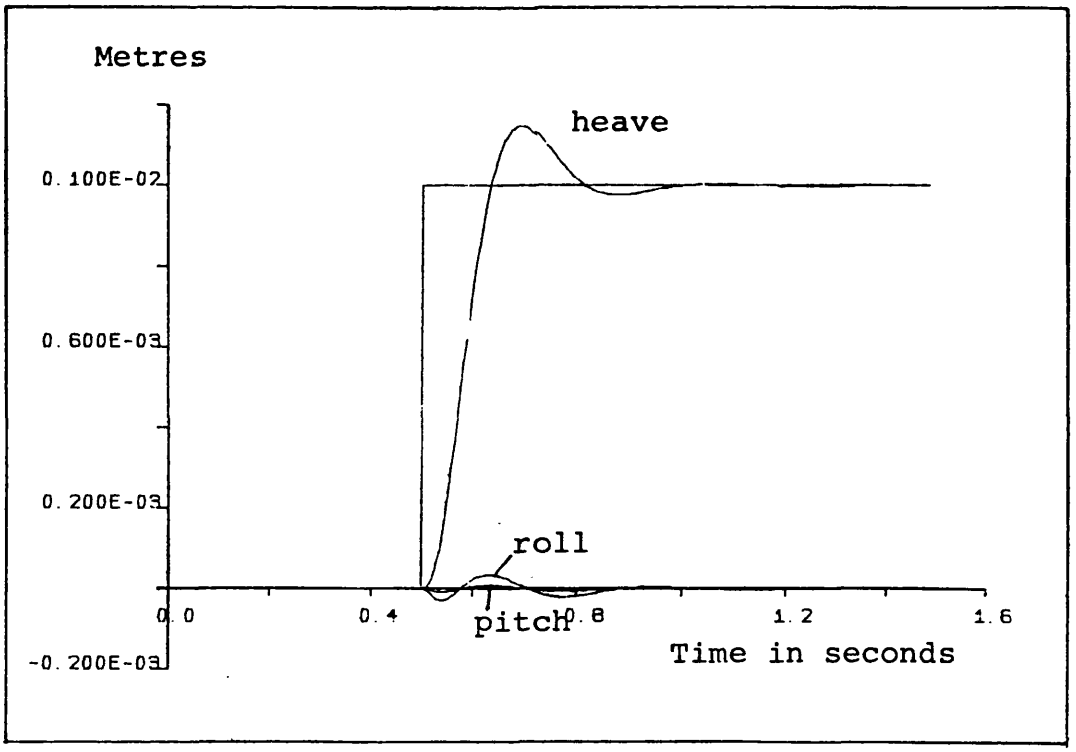

(a) Heave, roll and pitch responses

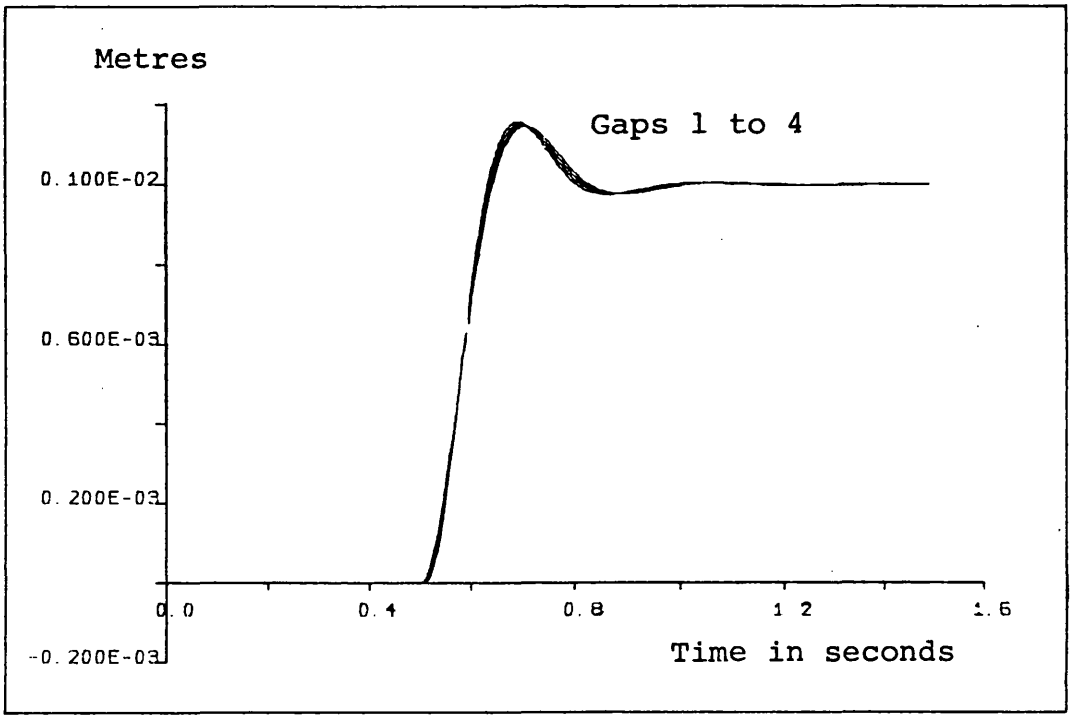

(b) Air gap responses

Figure 5.3.4 Simulation results showing little interaction for matched controllers

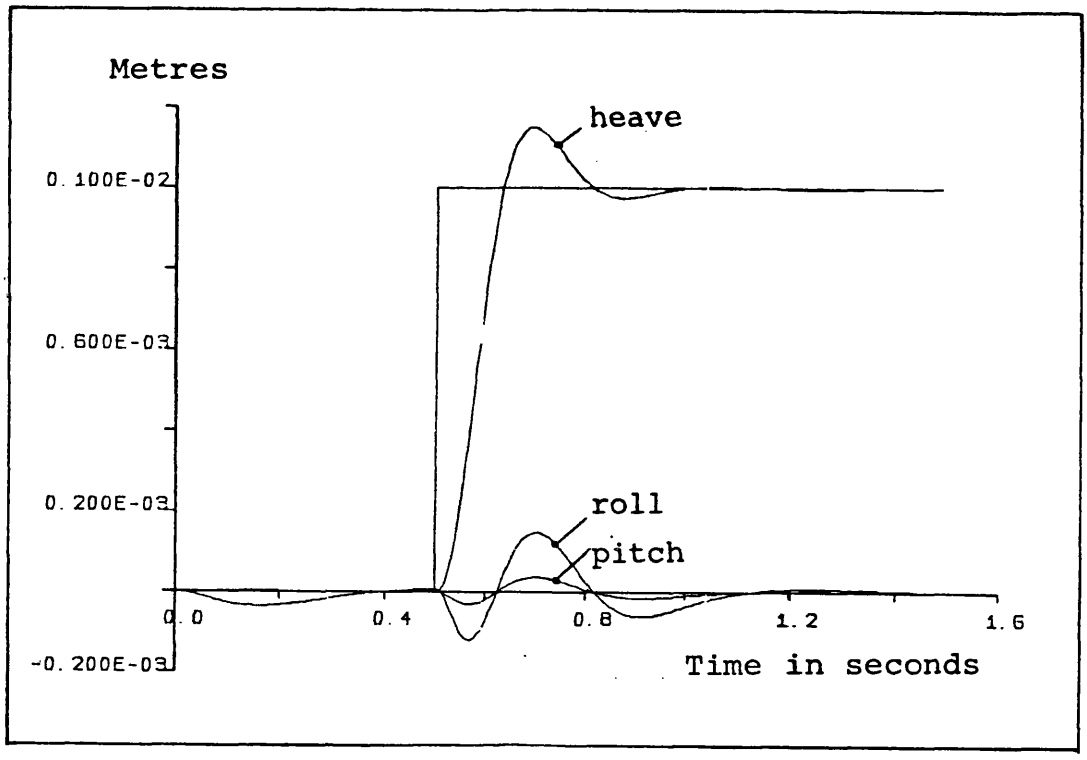

(a) Heave, roll and pitch responses

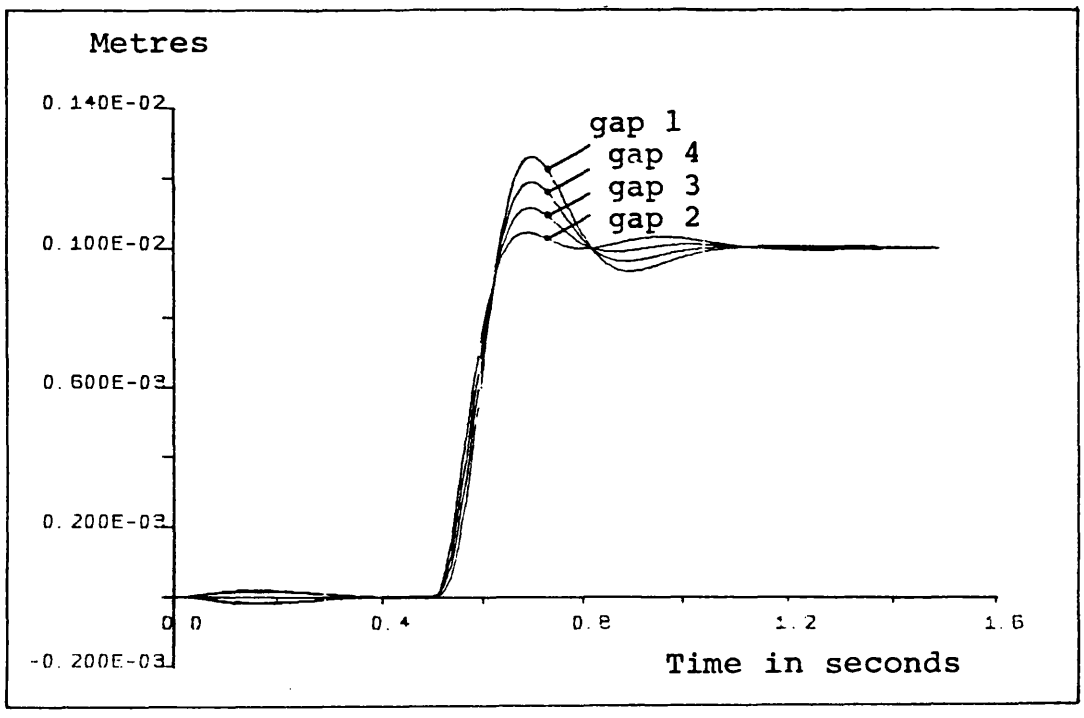

(b) Air gap responses

Figure 5.3.5 Simulation results for mismatched controllers leads to significant interaction

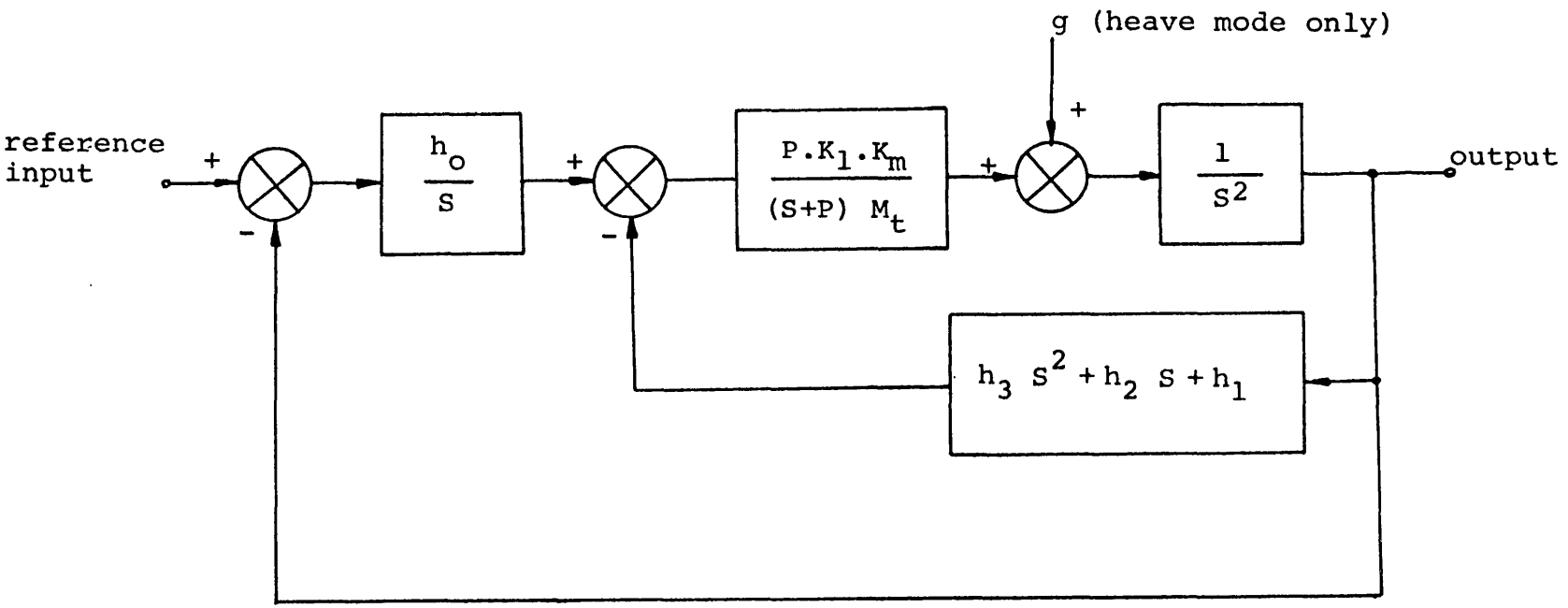

K_m is the effective magnet constant

K_1 is the forward path gain

h_o, h_1, h_2 and h_3 are feedback gains

P is the effective magnet coil pole position

Figure 5.3.6 Simulated control system for three degrees of freedom linear system

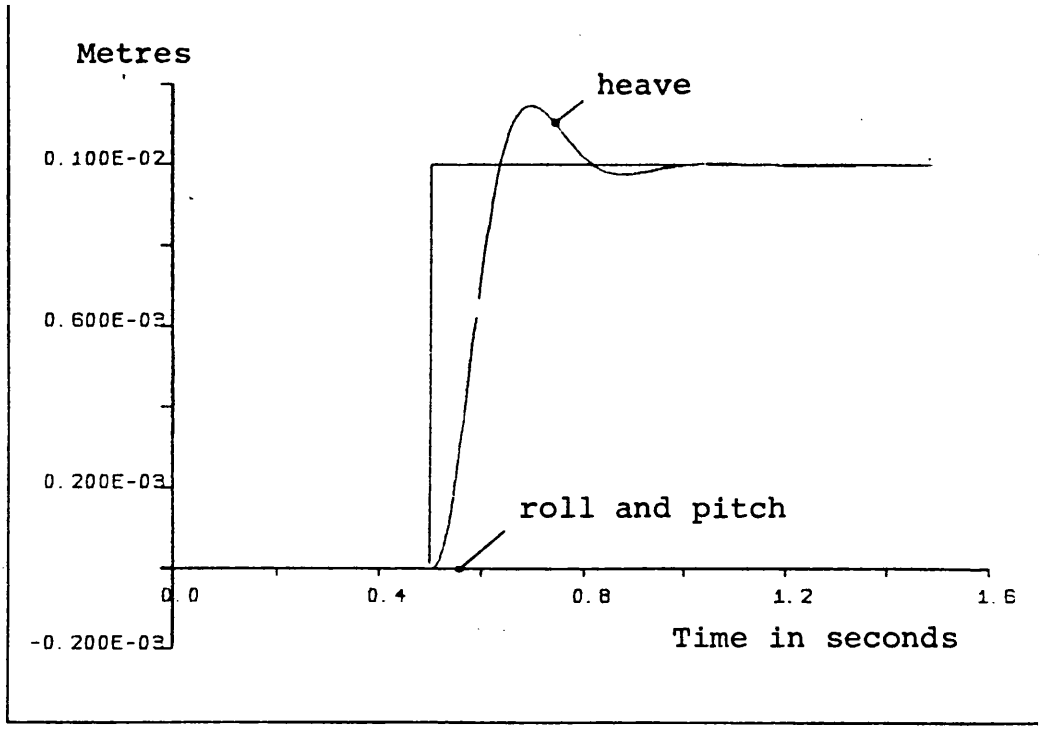

(a) Heave, roll and pitch responses

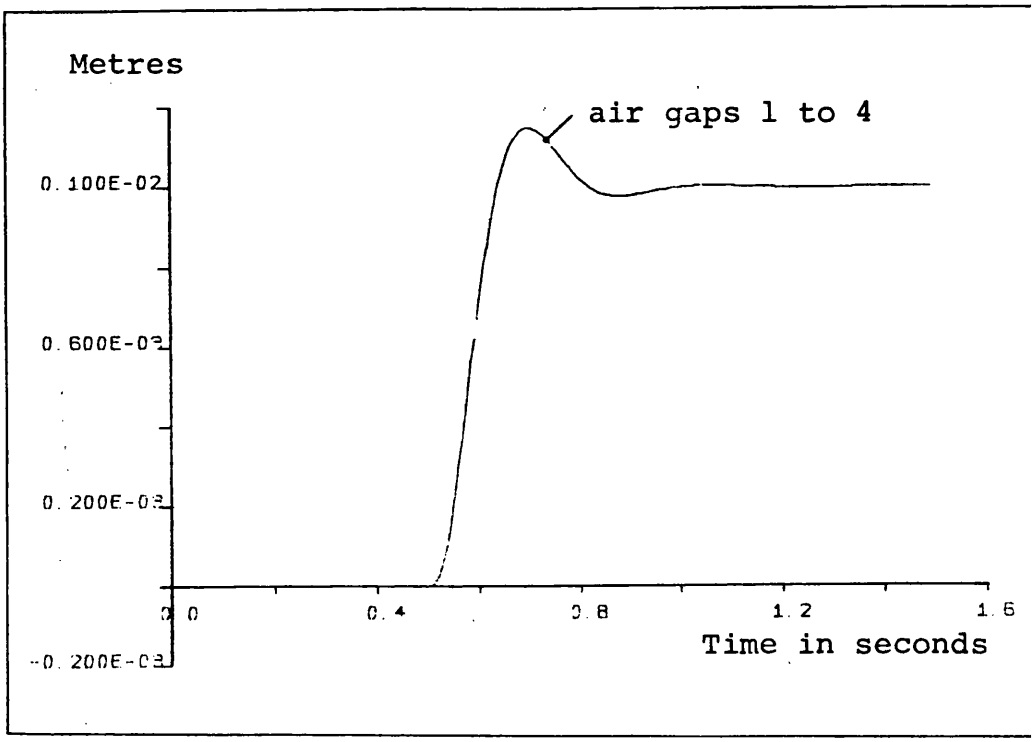

(b) Air gap responses

Figure 5.3.7 Matched controllers with decoupling matrix

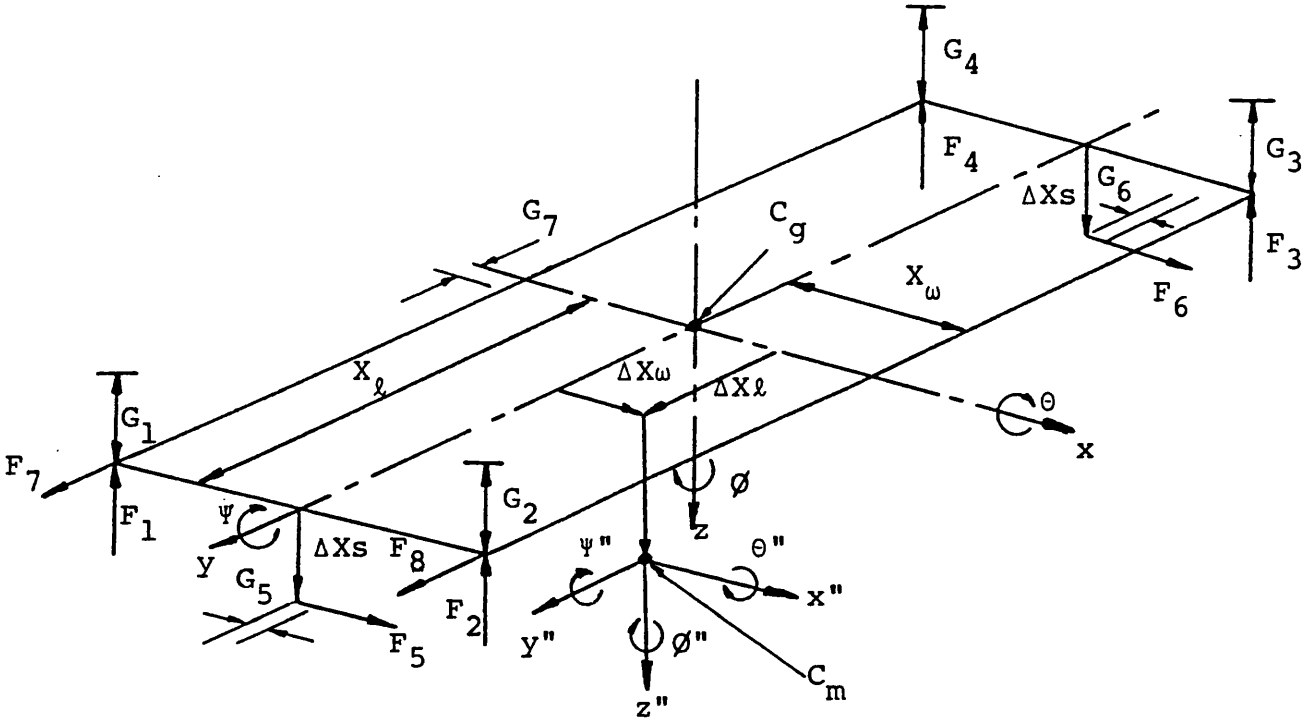

Figure 5.4.1 Six degrees of freedom structure with non-coincident centres of man and geometry

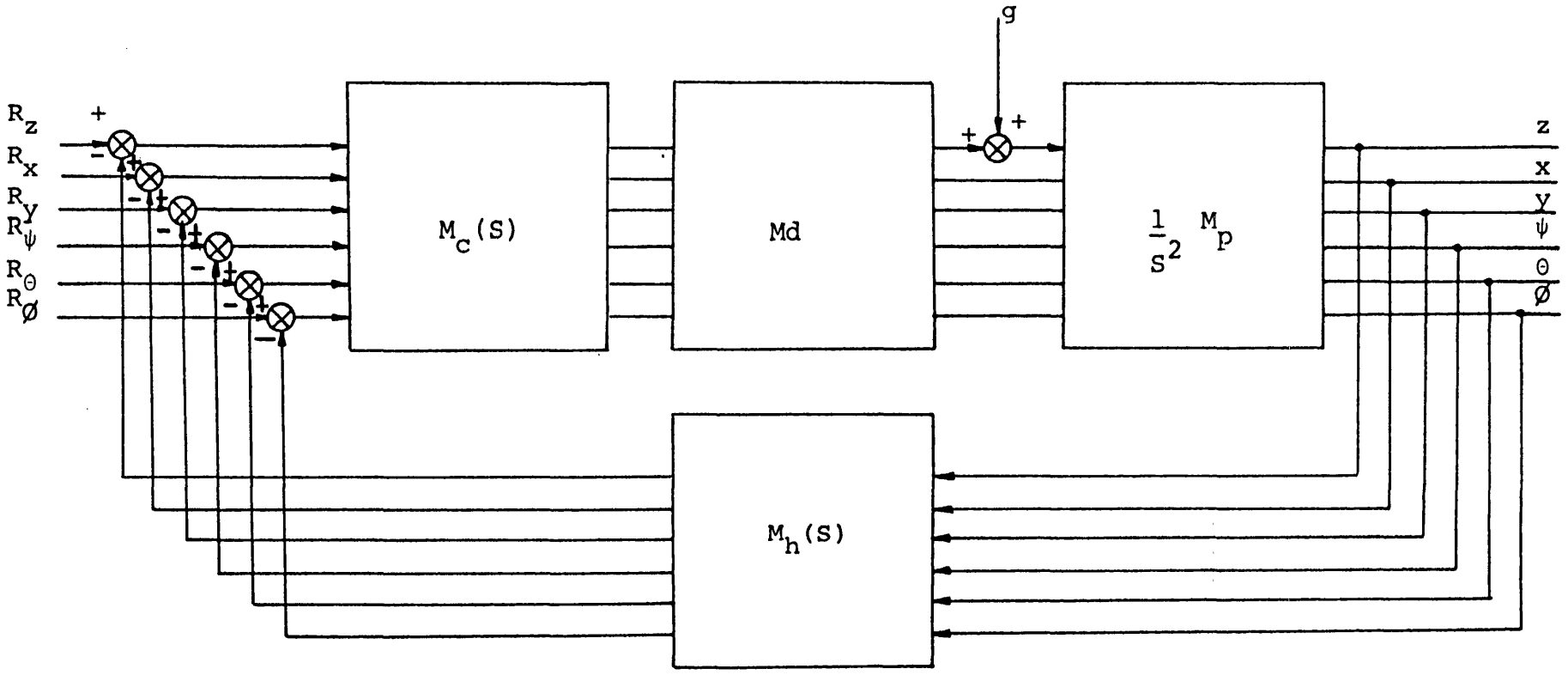

Figure 5.4.2 Decoupled multivariable controller for the six degrees of freedom linear model

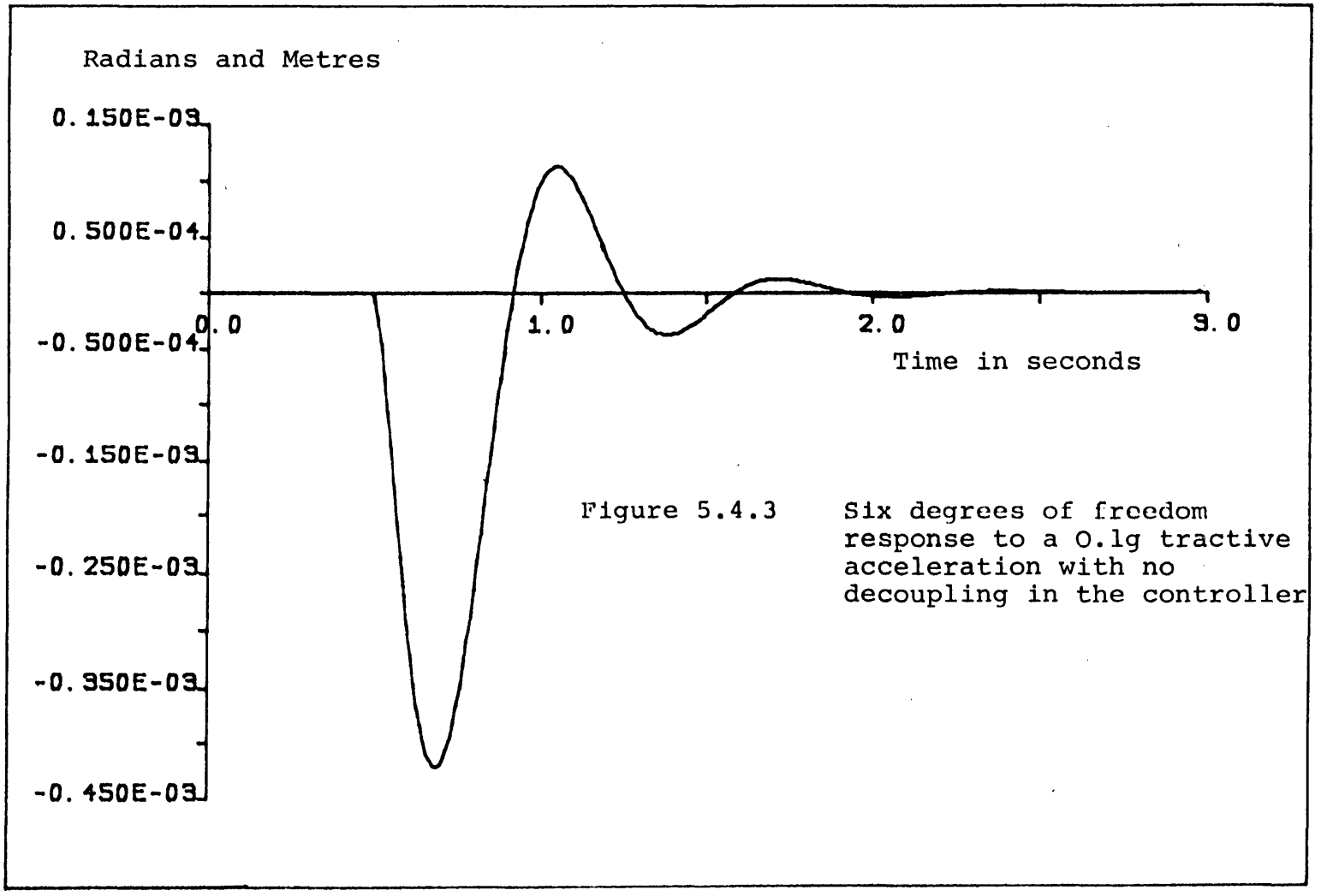

Figure 5.4.3 Six degrees of freedom response to a 0.1g tractive acceleration with no decoupling in the controller

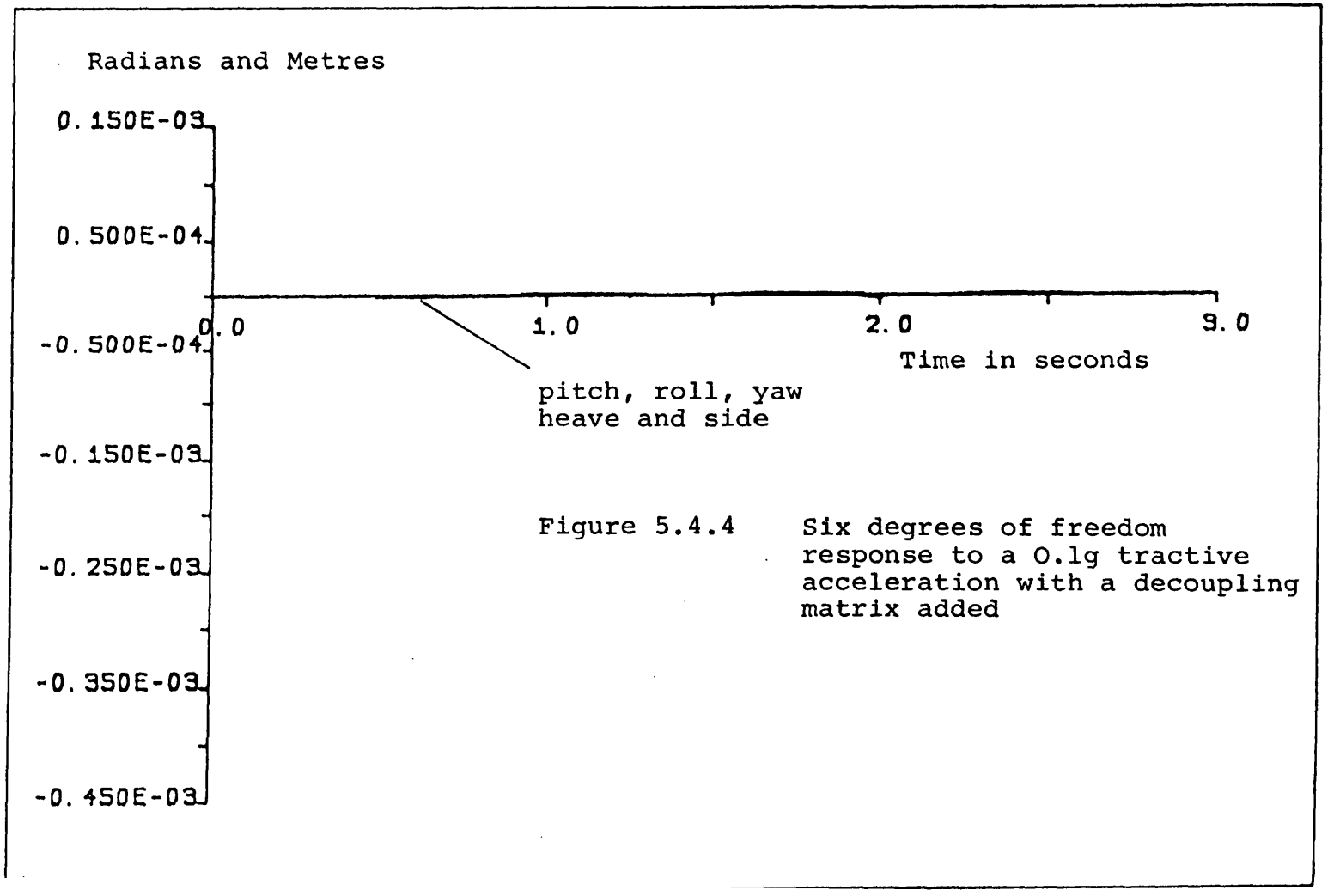

Figure 5.4.4 Six degrees of freedom response to a 0.1g tractive acceleration with a decoupling matrix added

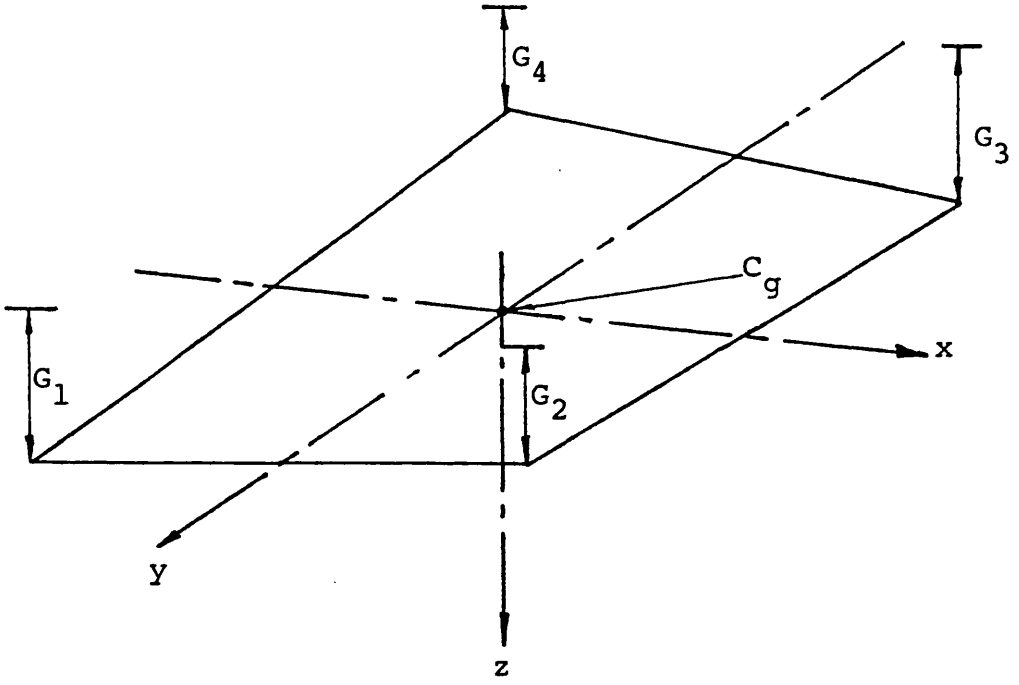

Figure 5.5.1 Asymmetric torsional twisting vehicular degree of freedom

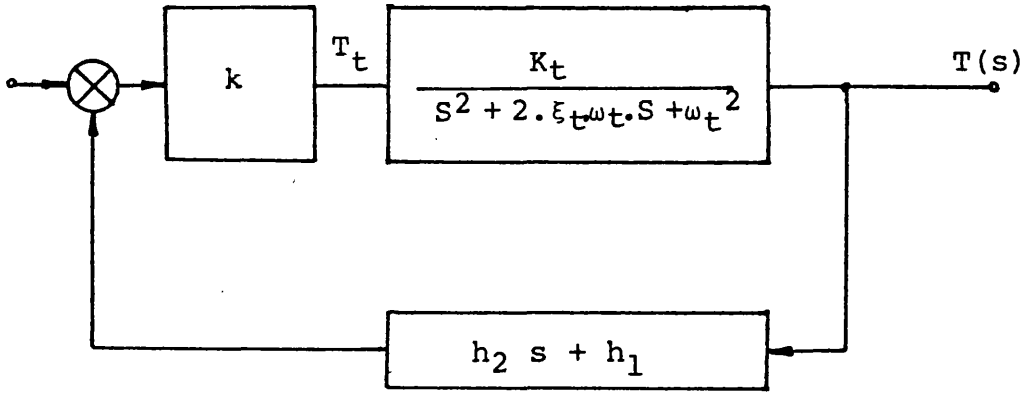

Figure 5.5.2 Control scheme including control of torsional twisting

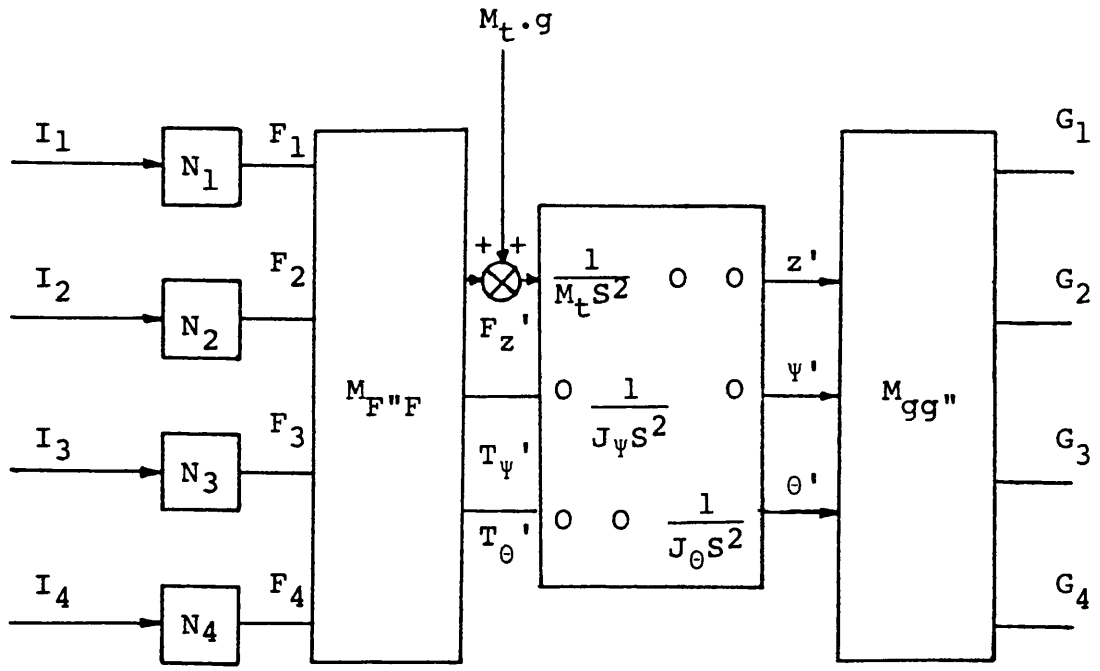

Figure 5.6.1 Three degrees of freedom non-linear rigid vehicle definition

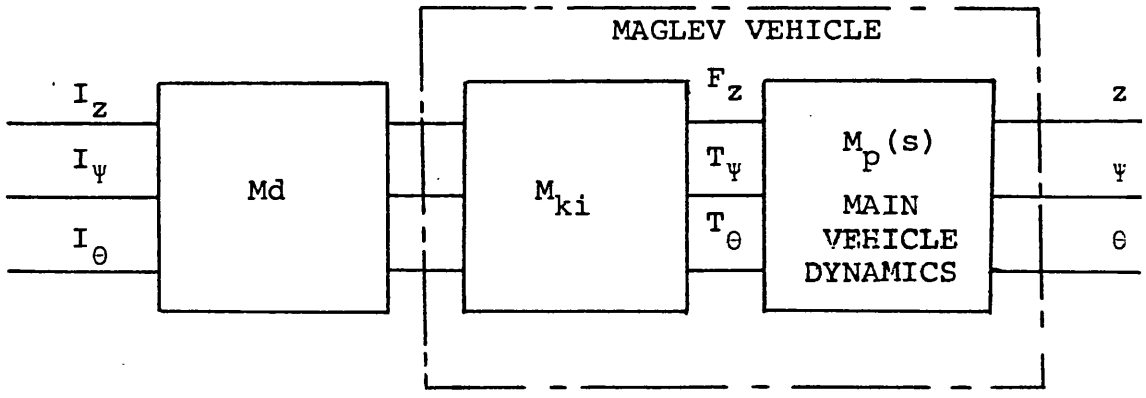

Figure 5.6.2 Linearised three degrees of freedom system

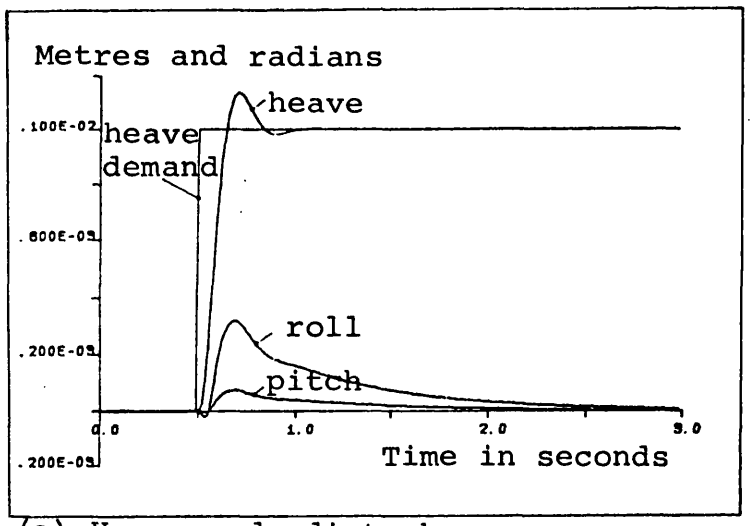

(a) Heave mode disturbance

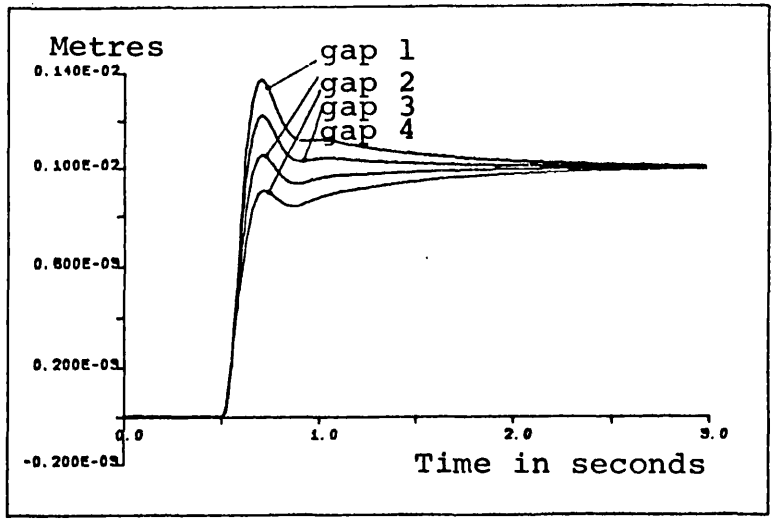

(b) Air gaps for heave mode disturbance

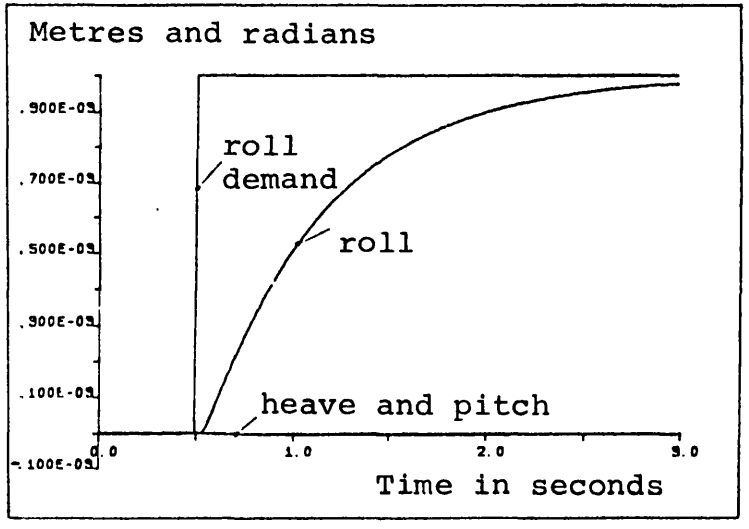

(c) Roll mode disturbance

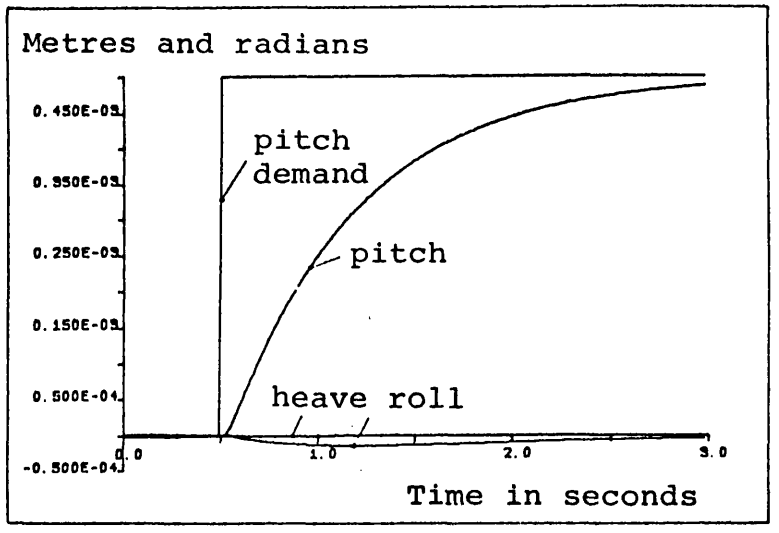

(d) Pitch mode disturbance

Figure 5.6.3 Simulation results showing interaction with non-linear force actuators when disturbances are applied to all modes

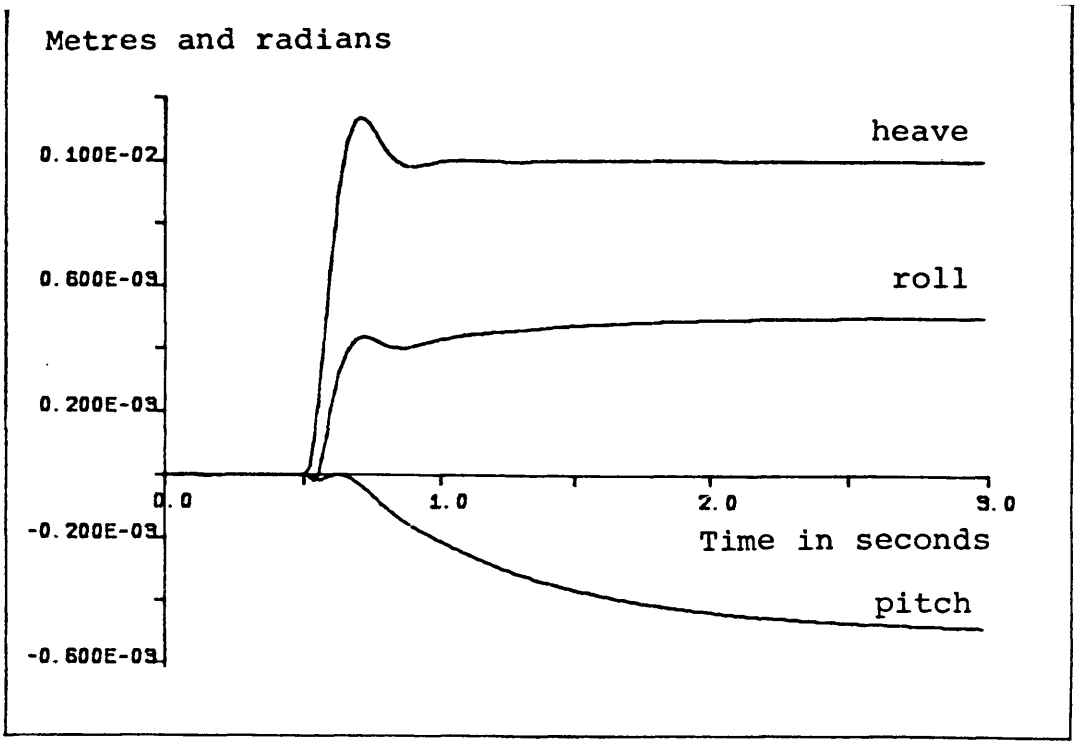

(a) Heave, roll and pitch responses

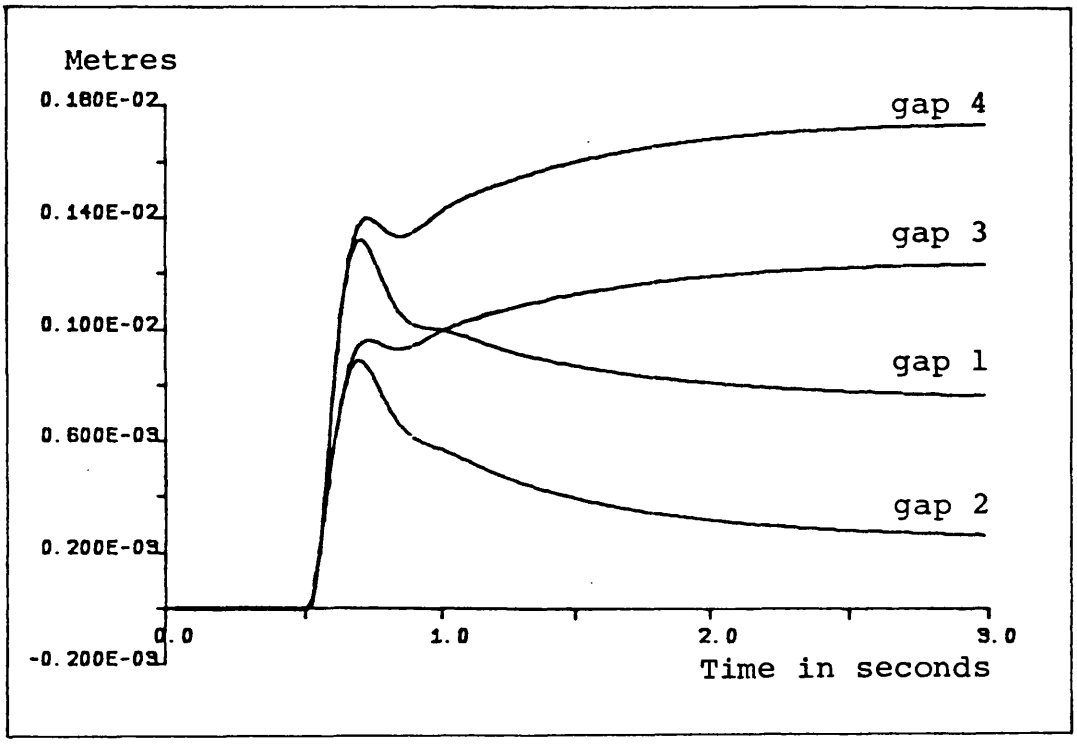

(b) Air gap responses

Figure 5.6.4 Simulation of vehicle attitude change

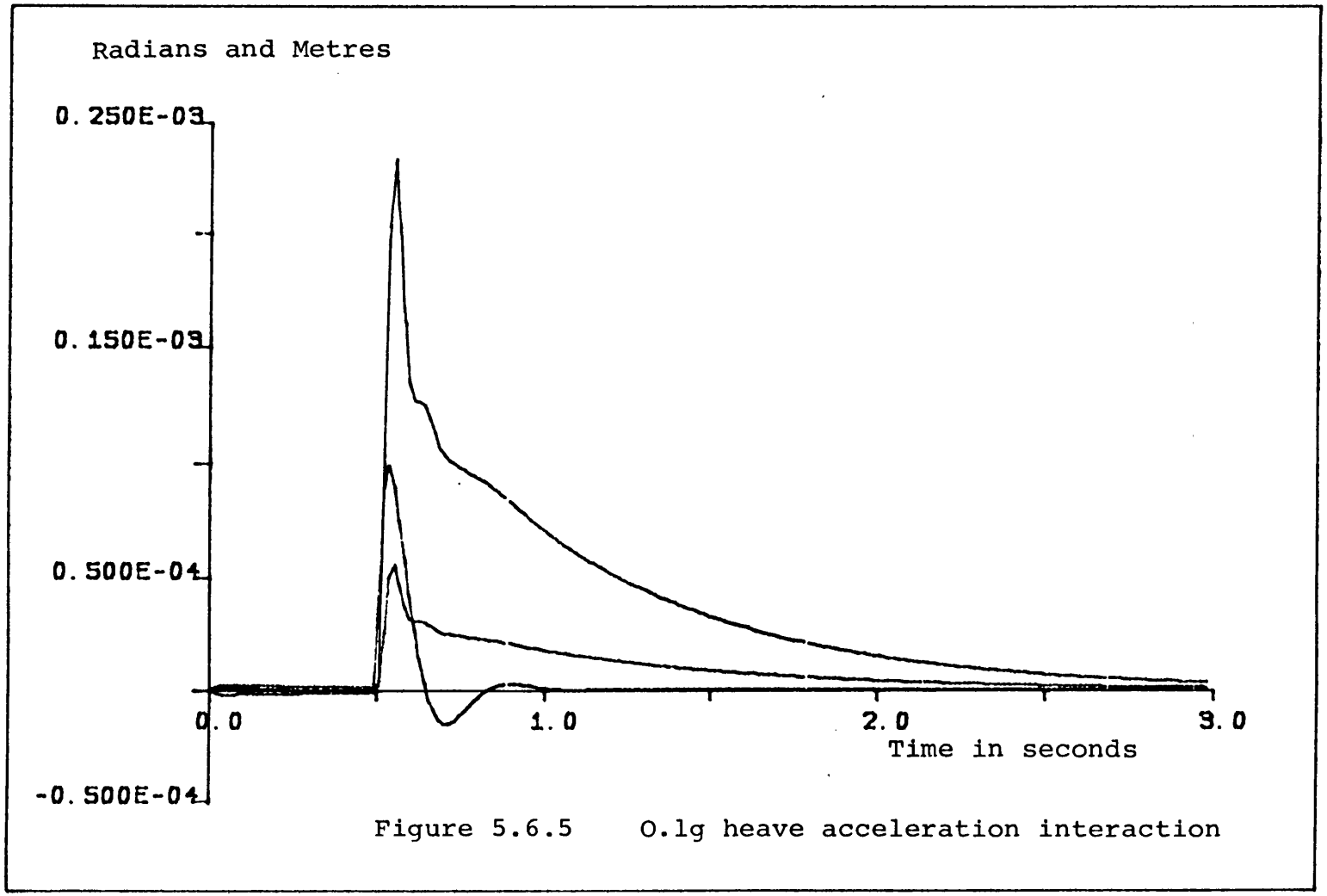

Figure 5.6.5 0.1g heave acceleration interaction

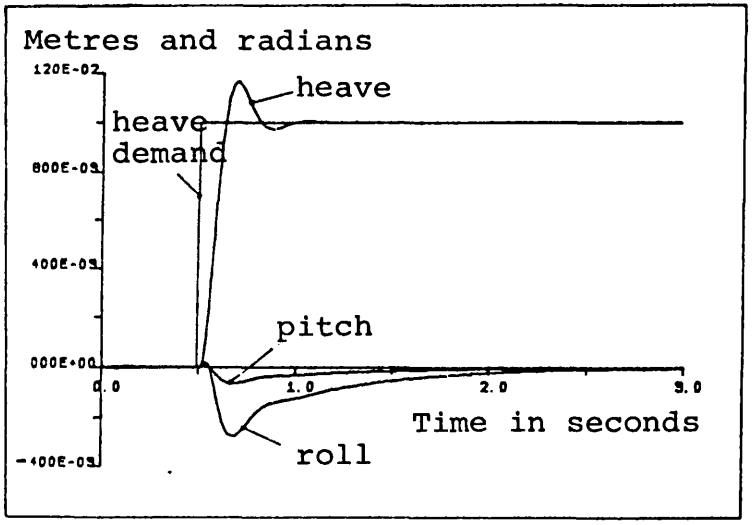

(a) Heave mode disturbance

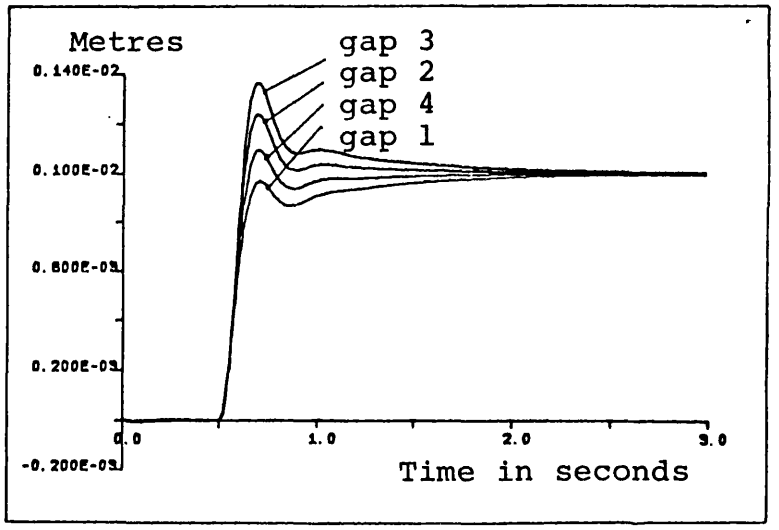

(b) Air gaps for heave mode disturbance

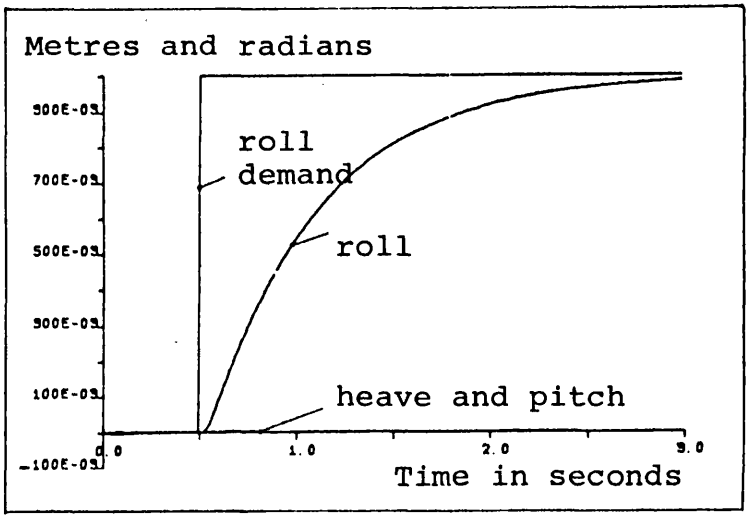

(c) Roll mode disturbance

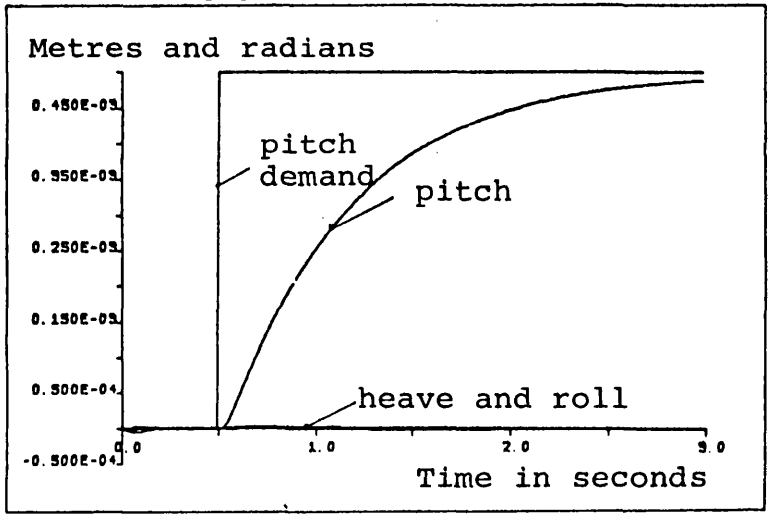

(d) Pitch mode disturbance

Figure 5.6.6 Simulation results showing interaction with non-linear force actuators when disturbances are applied to all modes with linear

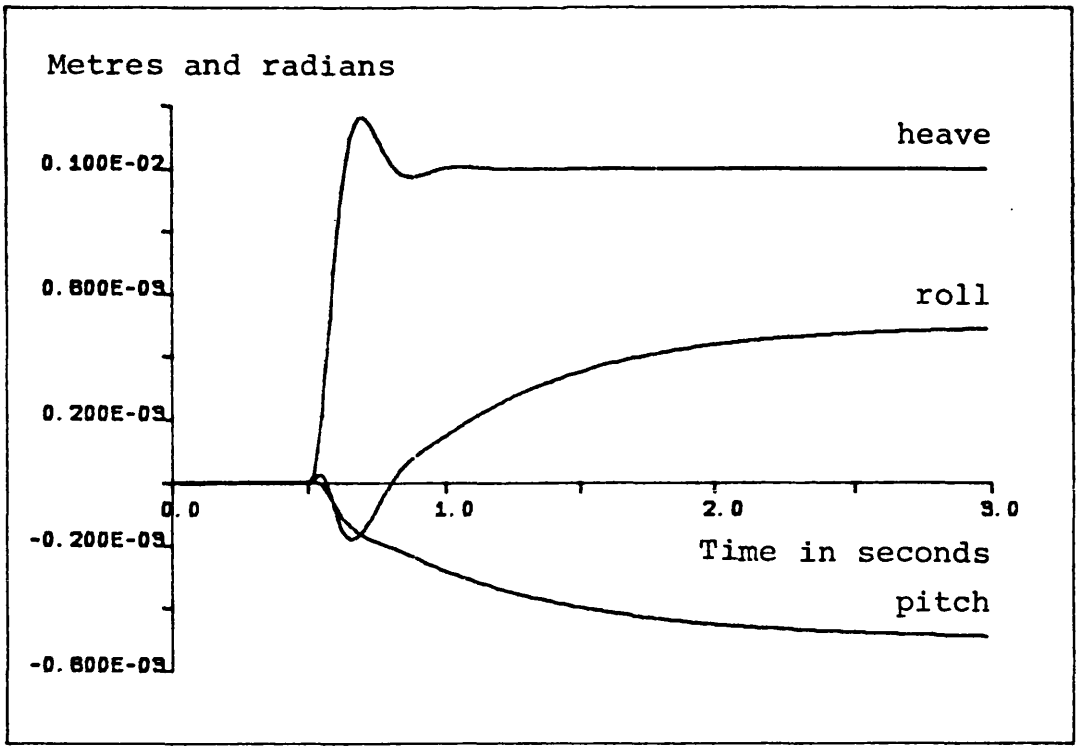

(a) Heave, roll and pitch responses

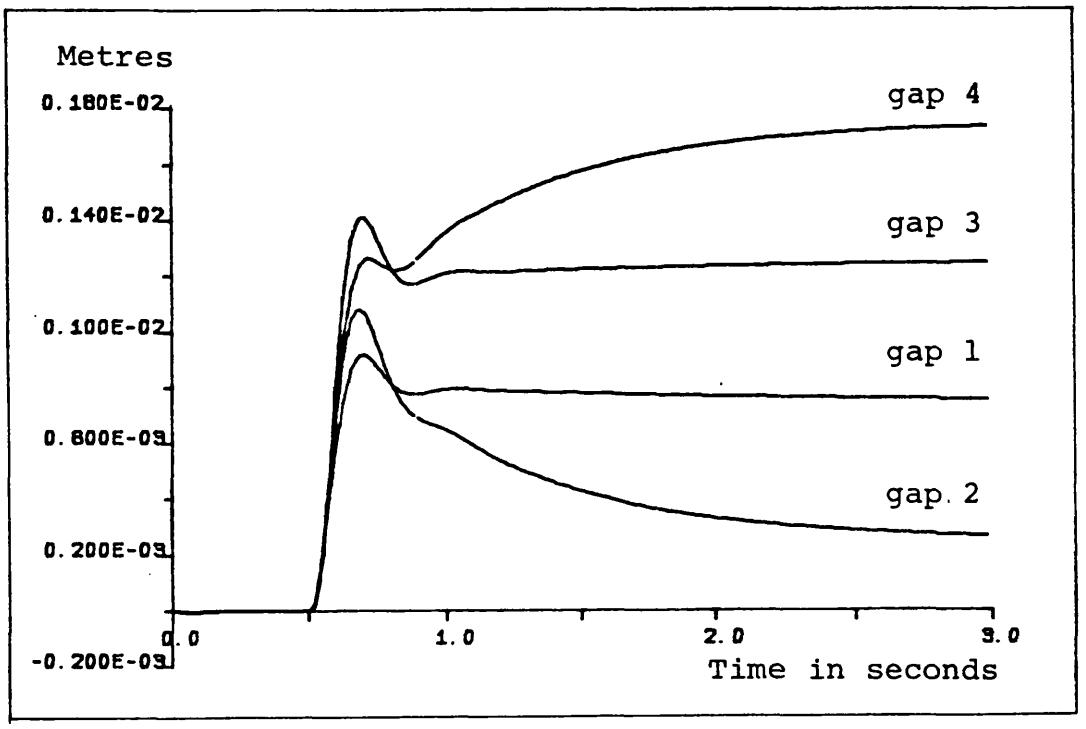

(b) Air gap responses

Figure 5.6.7 Simulation of vehicle attitude change with linear decoupling matrix applied

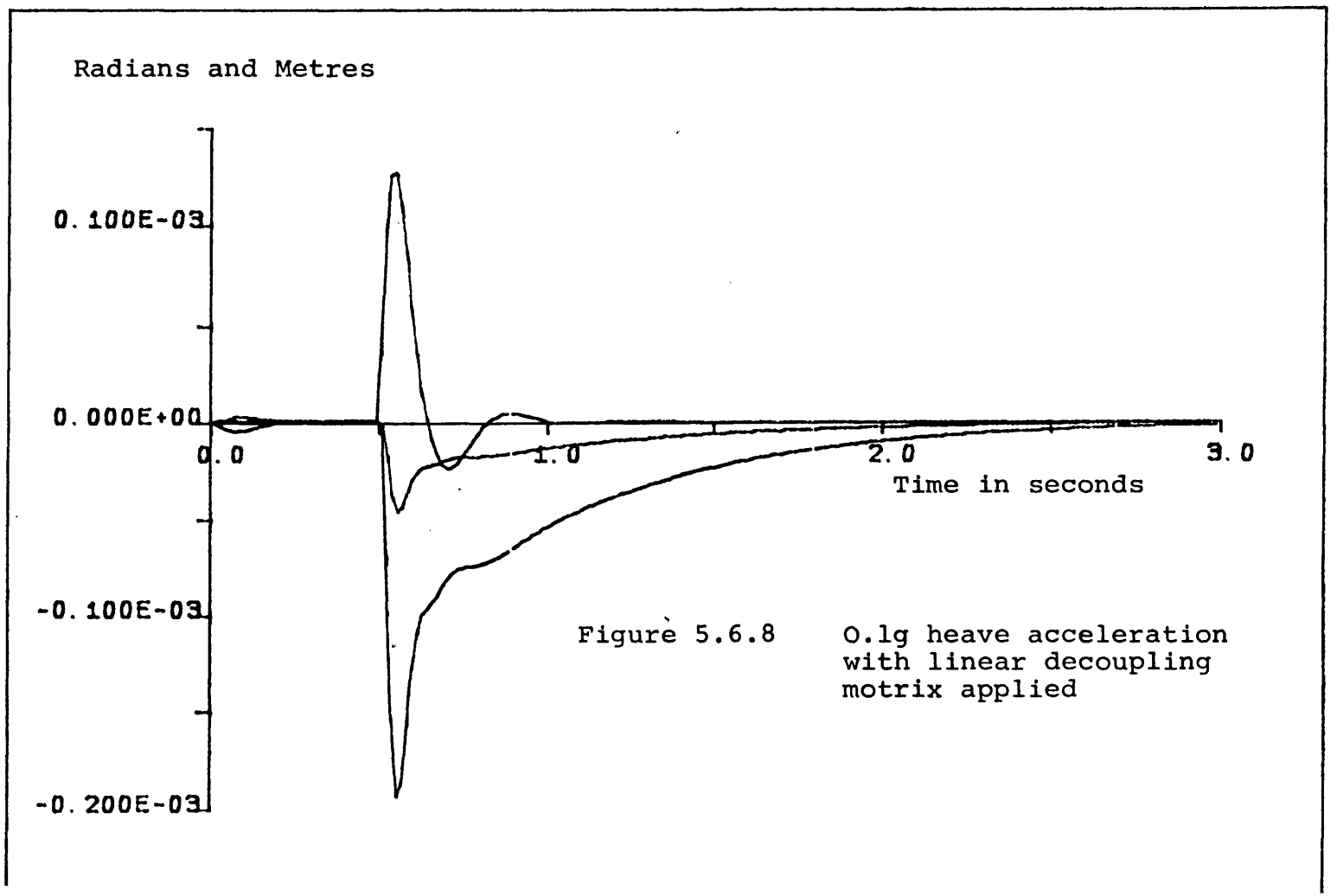

Figure 5.6.8 0.1g heave acceleration with linear decoupling motrix applied

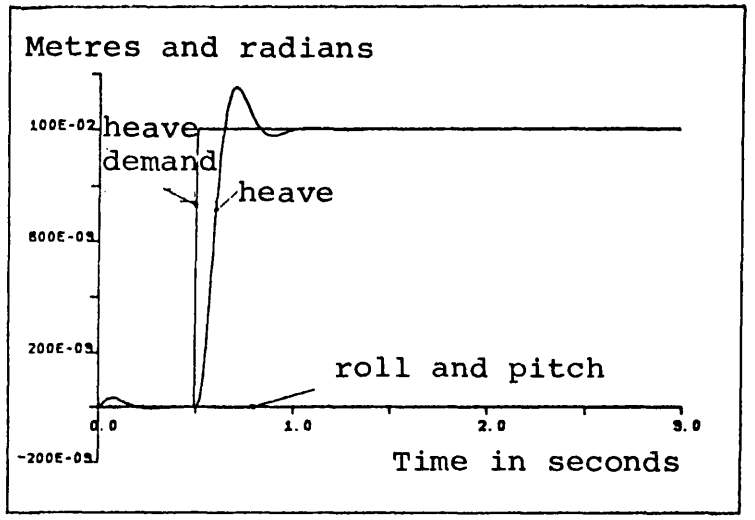

(a) Heave mode disturbance

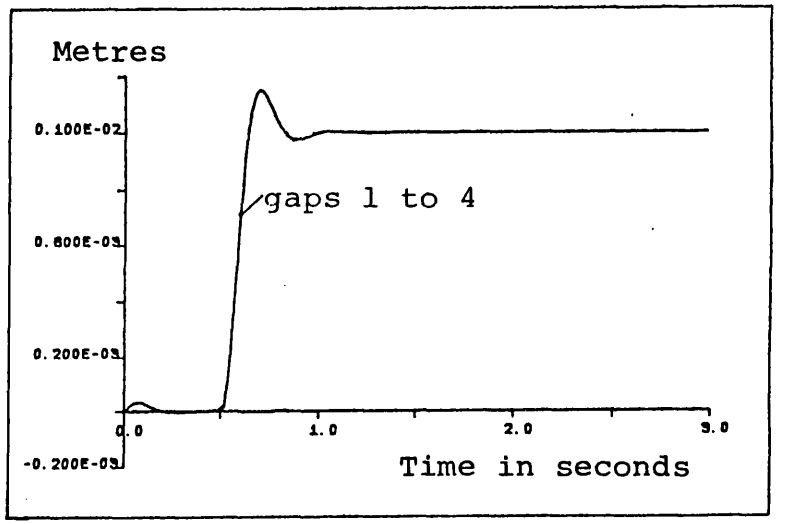

(b) Air gaps for heave mode disturbance

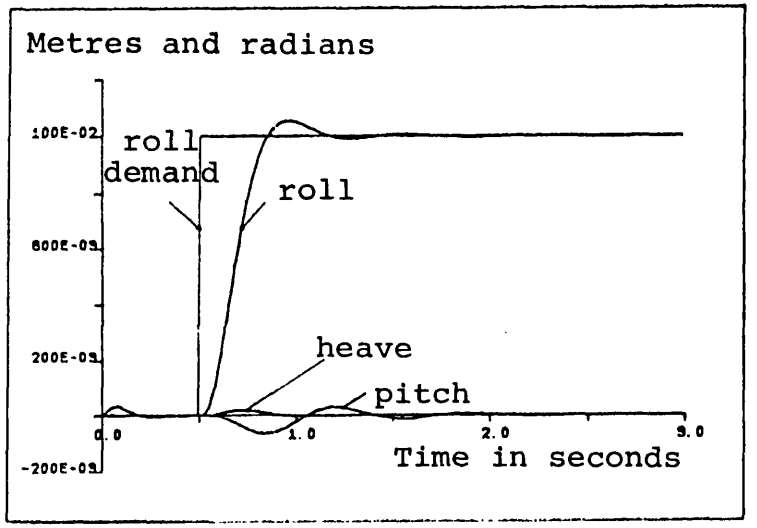

(c) Roll mode disturbance

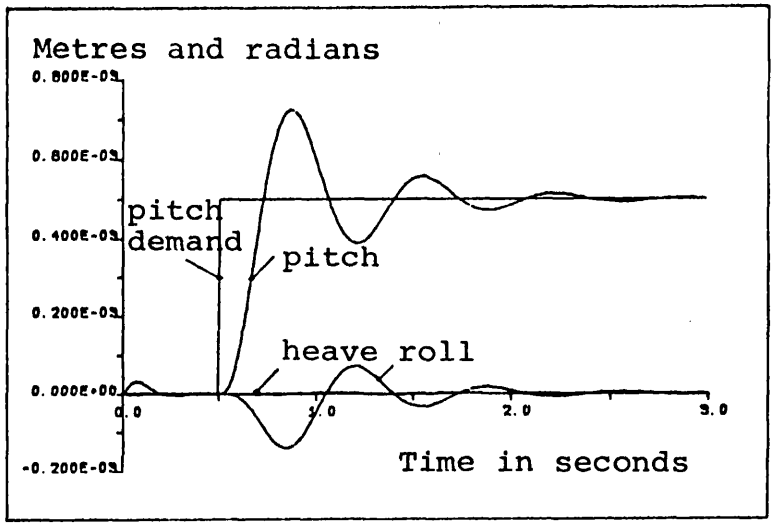

(d) Pitch mode disturbance

Figure 5.6.9 Simulation results showing interaction with non-linear force actuators when disturbances are applied to all modes with a

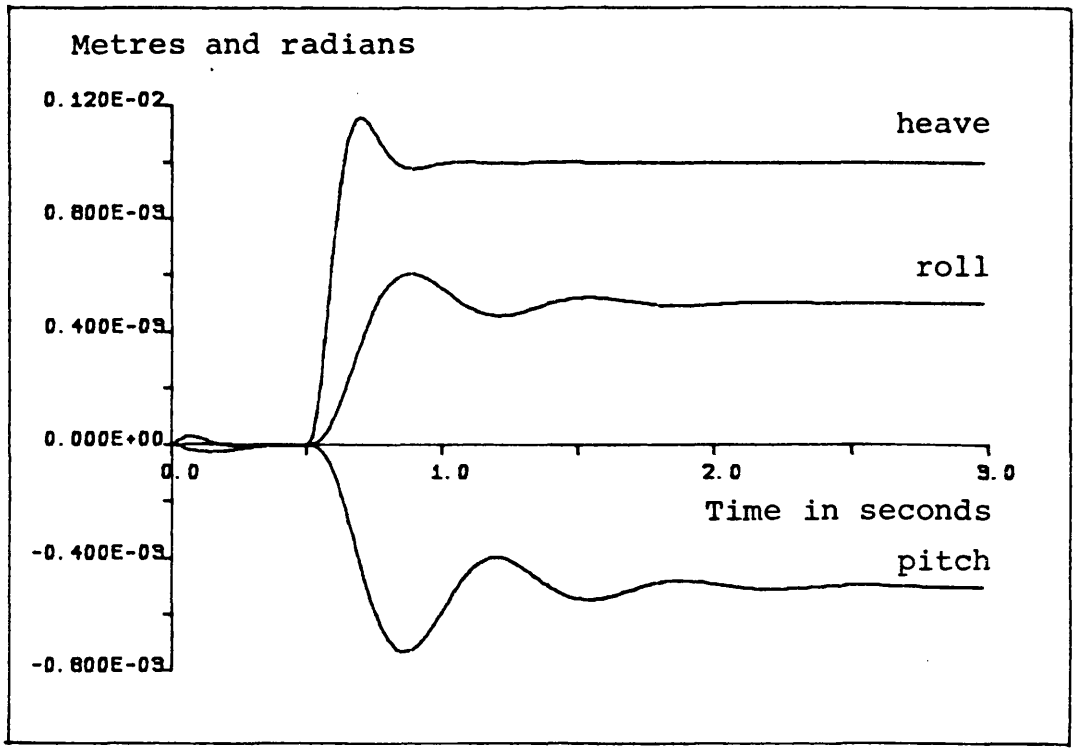

(a) Heave, roll and pitch responses

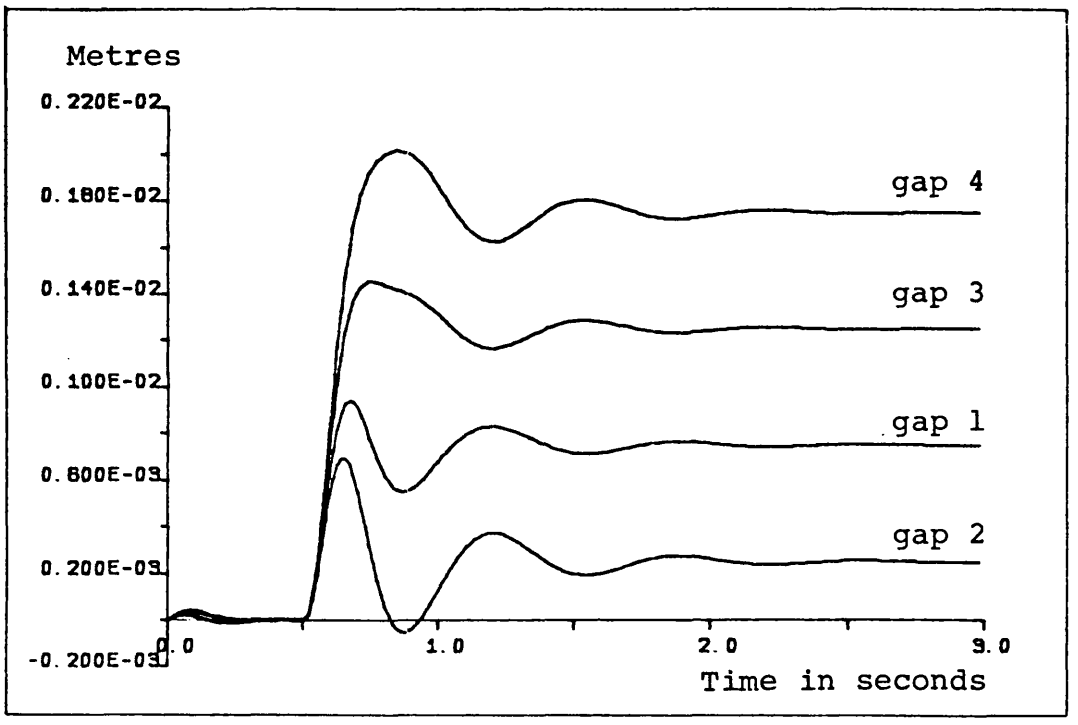

(b) Air gap responses

Figure 5.6.10 Simulation of vehicle attitude change with Md

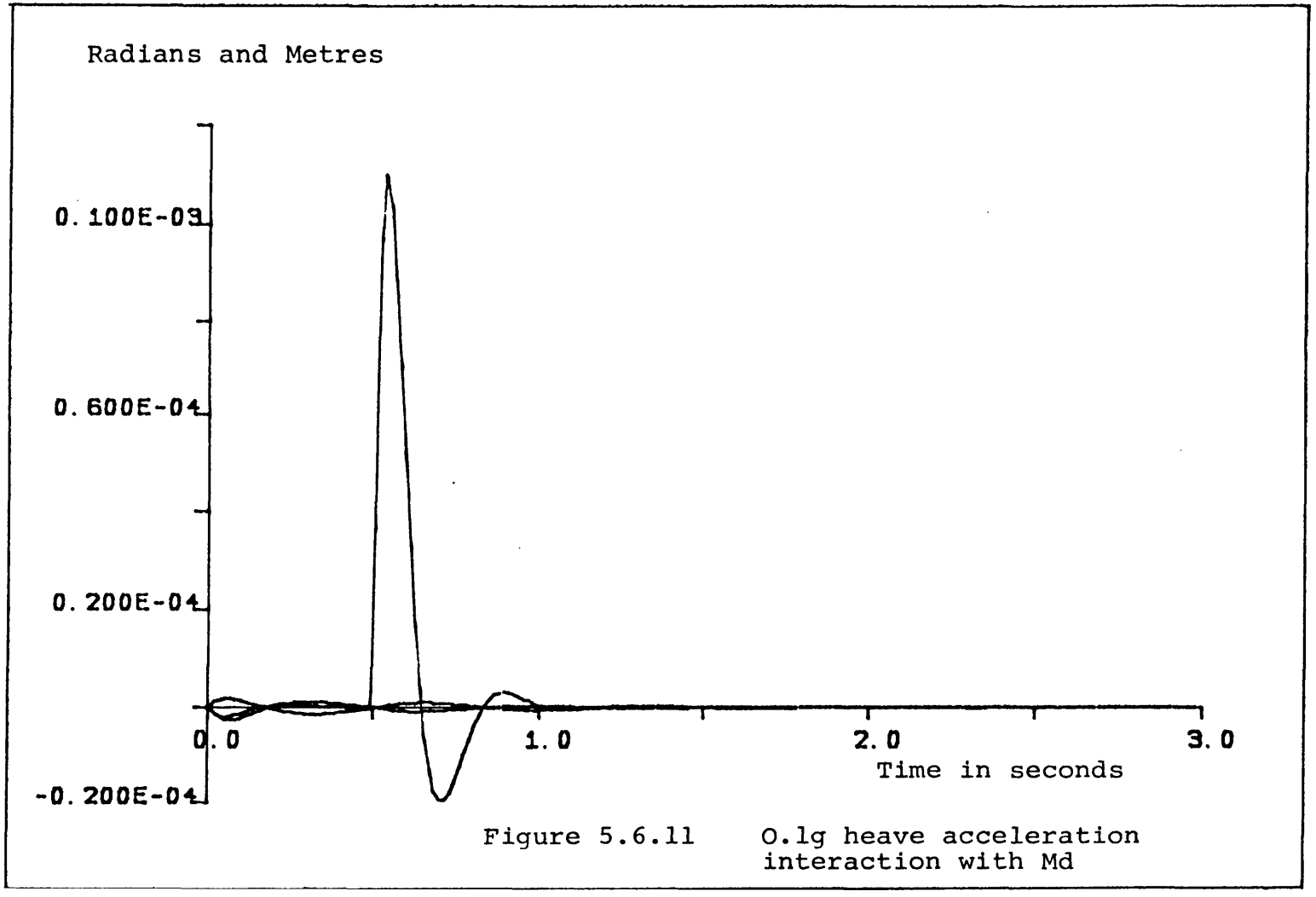

Figure 5.6.11 0.1g heave acceleration interaction with Md

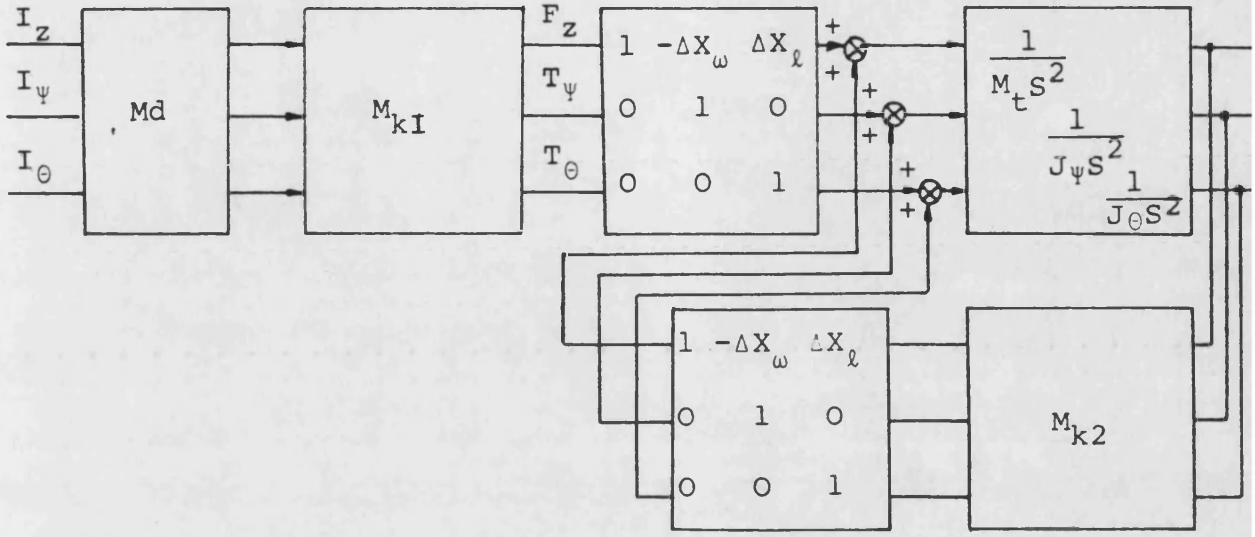

Figure 5.6.12 Reduced linearised block diagram of the non-linear system

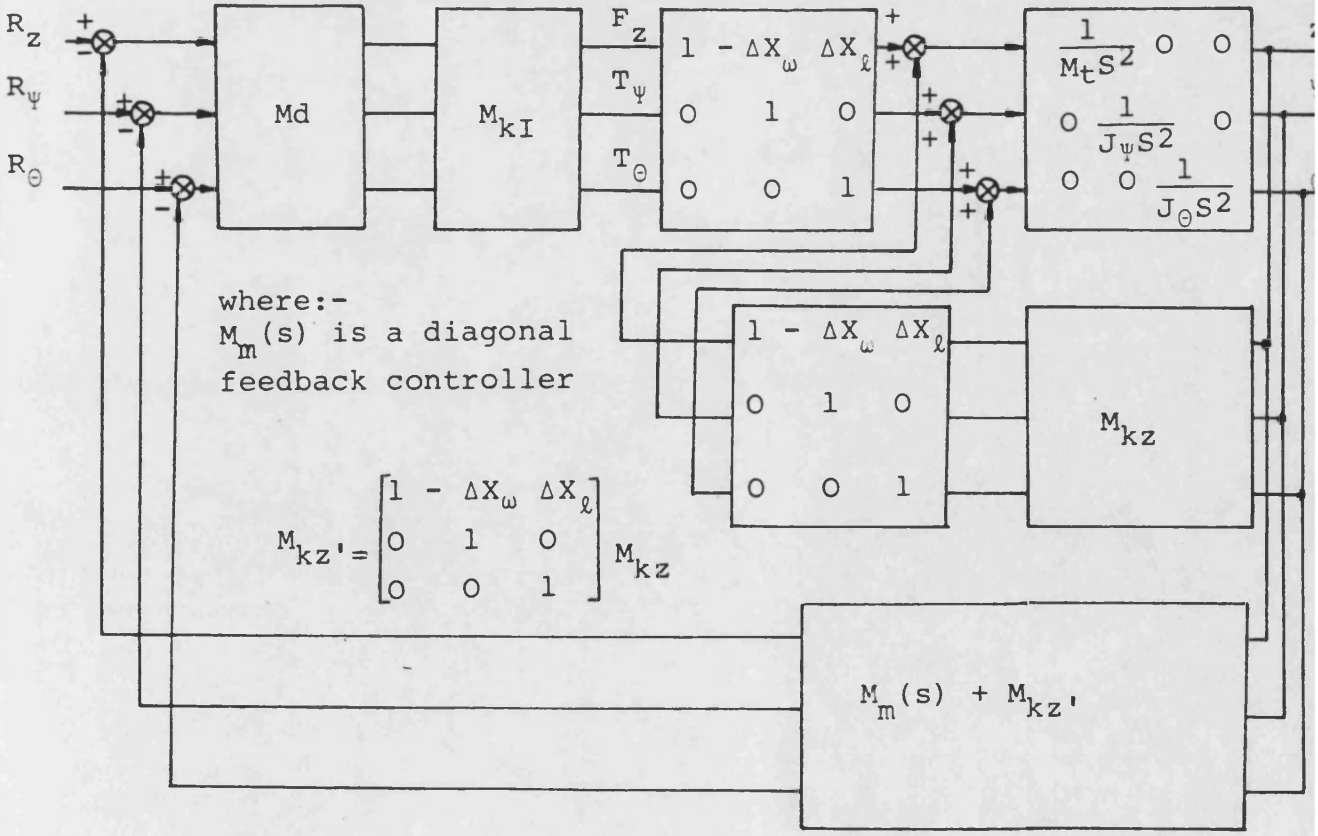

Figure 5.6.13 The application of air gap non-linearity compensation using M_{kz} synthesis

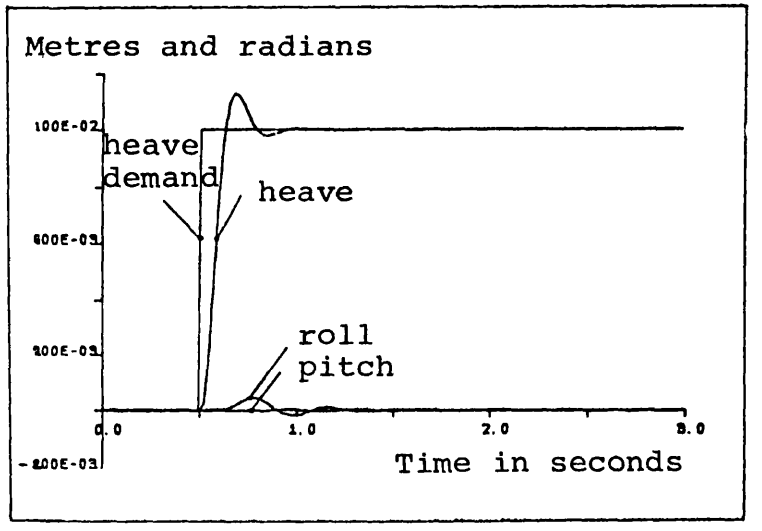

(a) Heave mode disturbance

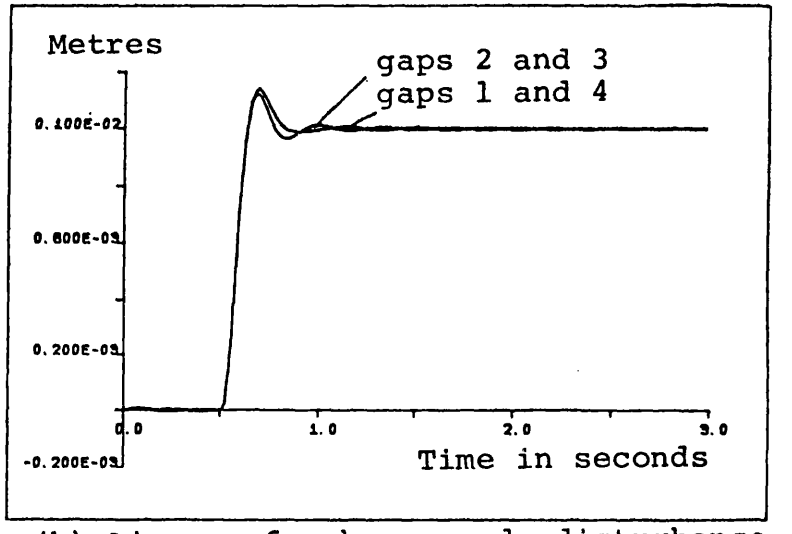

(b) Air gap for heave mode disturbance

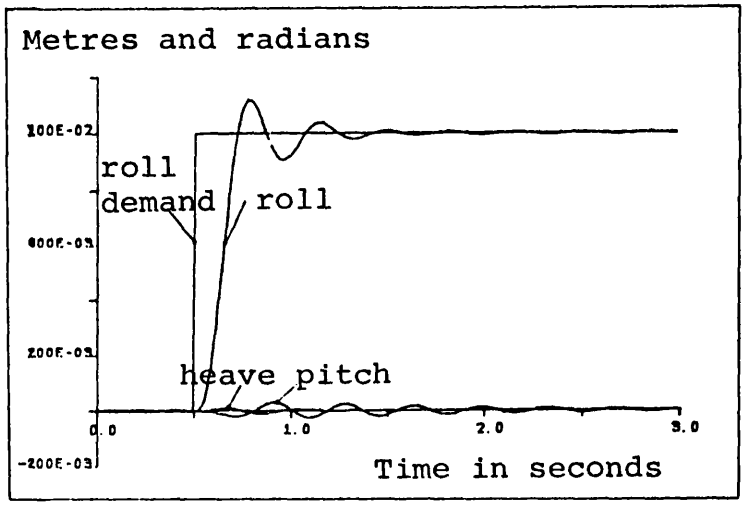

(c) Roll mode disturbance

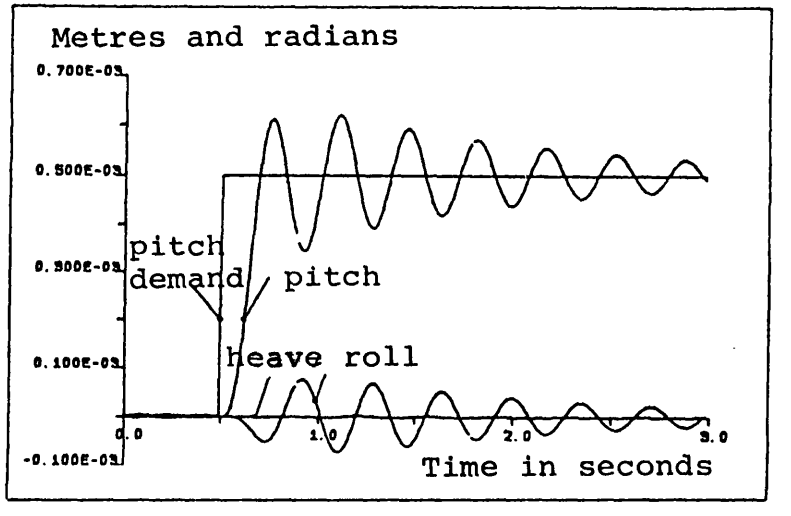

(d) Pitch mode disturbance

Figure 5.6.14 Simulation results showing interaction with non-linear force actuators when disturbances are applied to all modes with Mkz synthesized

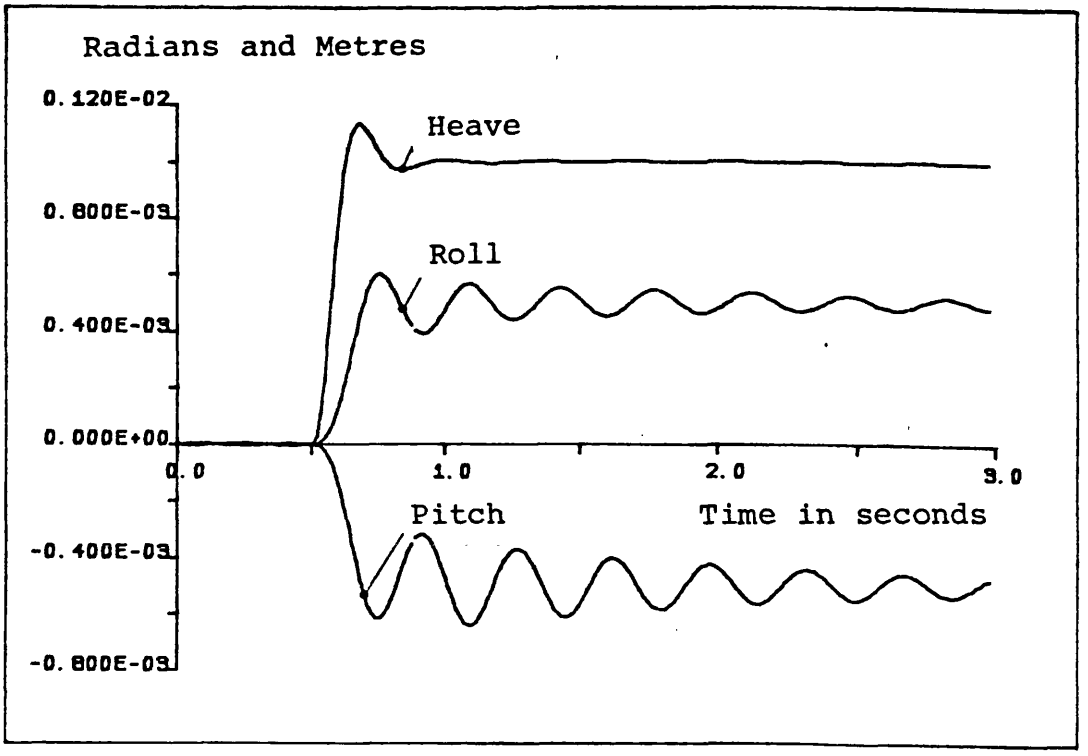

(a) Heave, roll and pitch responses

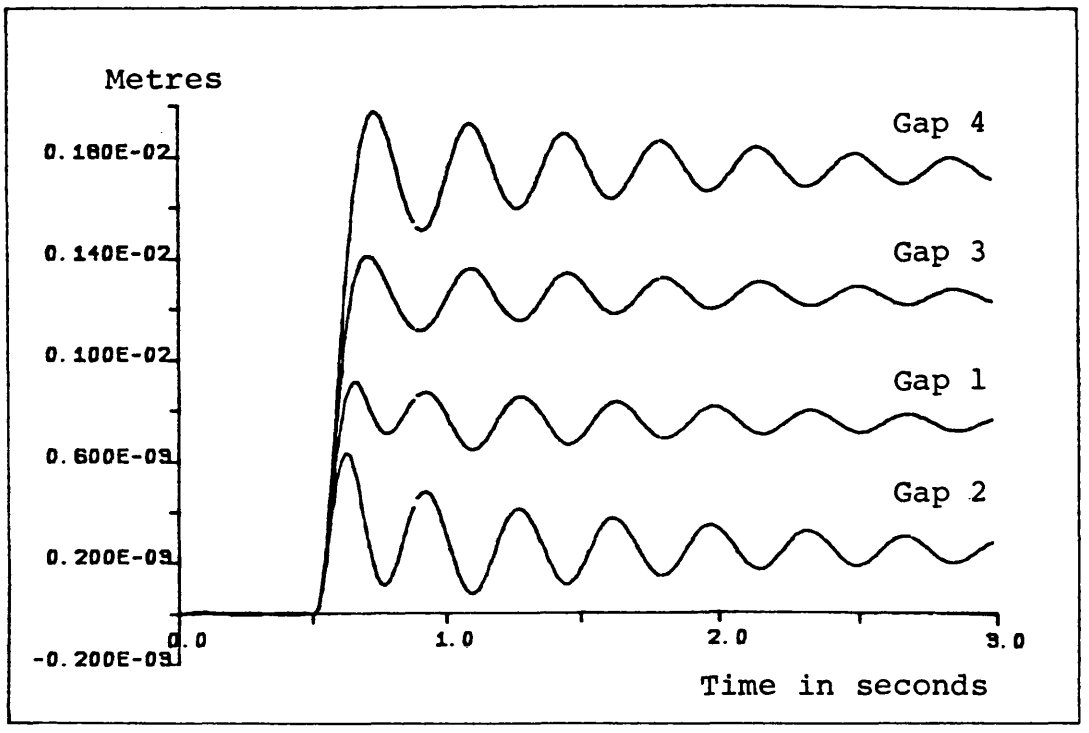

(b) Air gap responses

Figure 5.6.15 Simulation of vehicle attitude change with Mkz synthesized

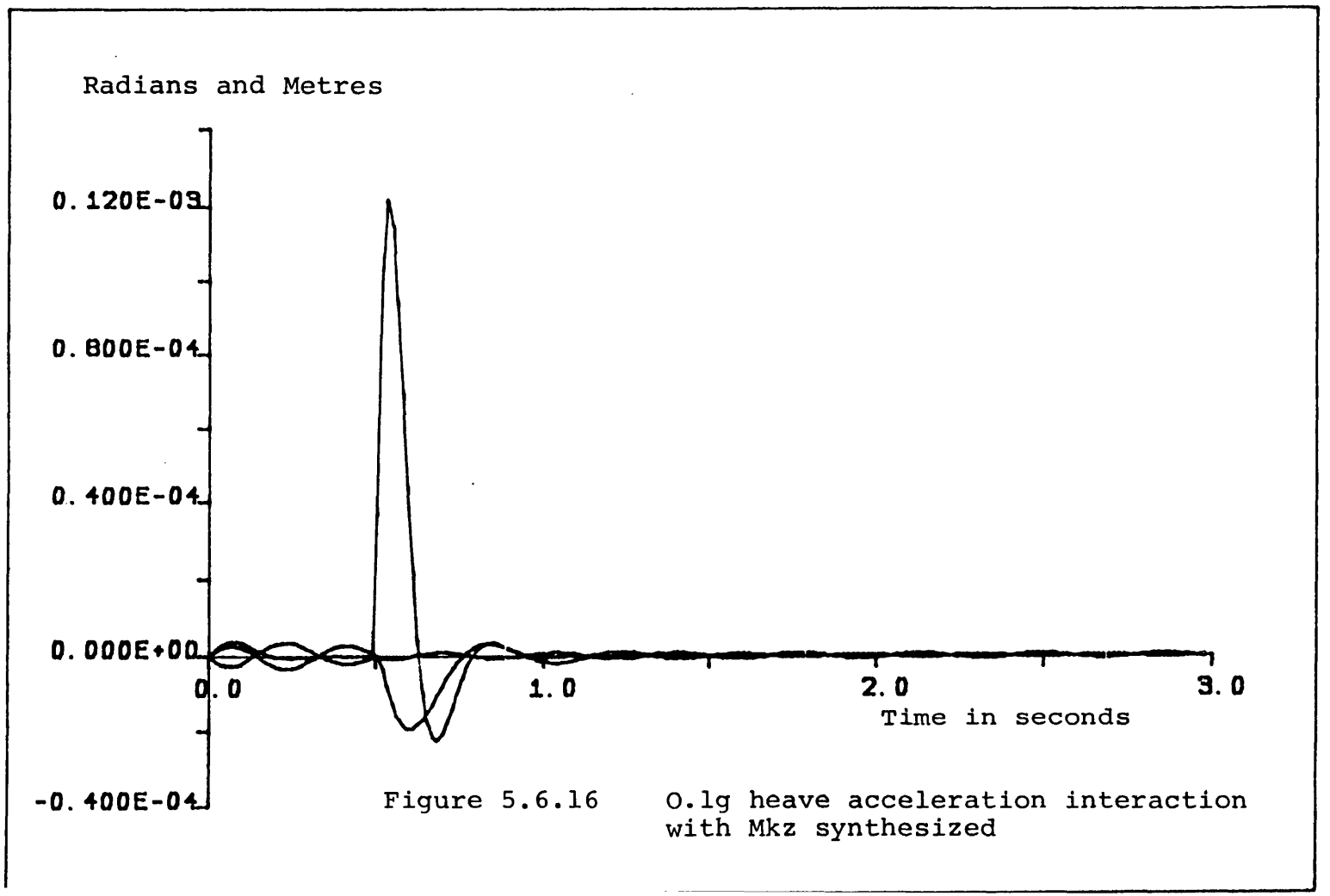

Figure 5.6.16 0.1g heave acceleration interaction with Mkz synthesized

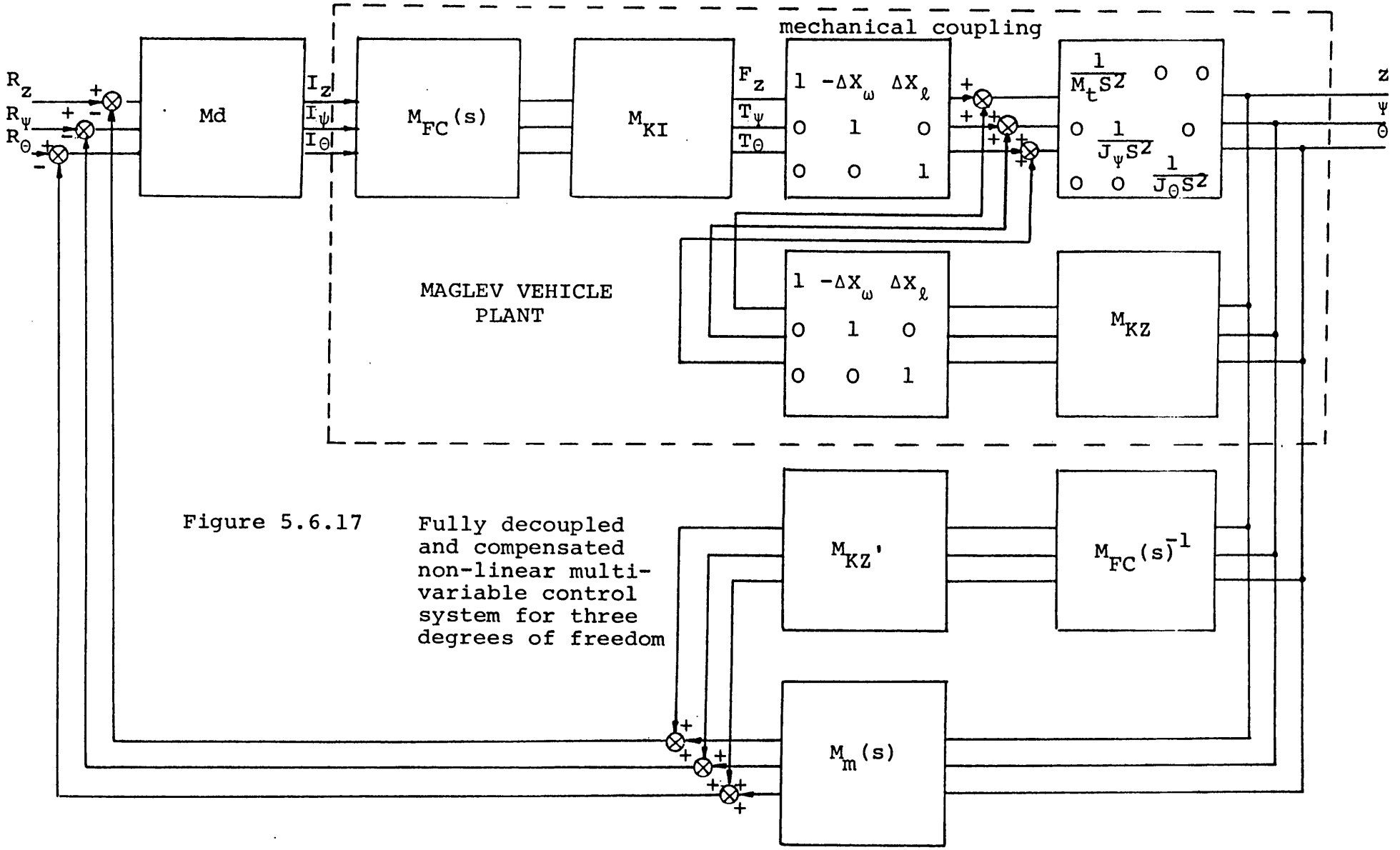

Figure 5.6.17 Fully decoupled and compensated non-linear multi-variable control system for three degrees of freedom

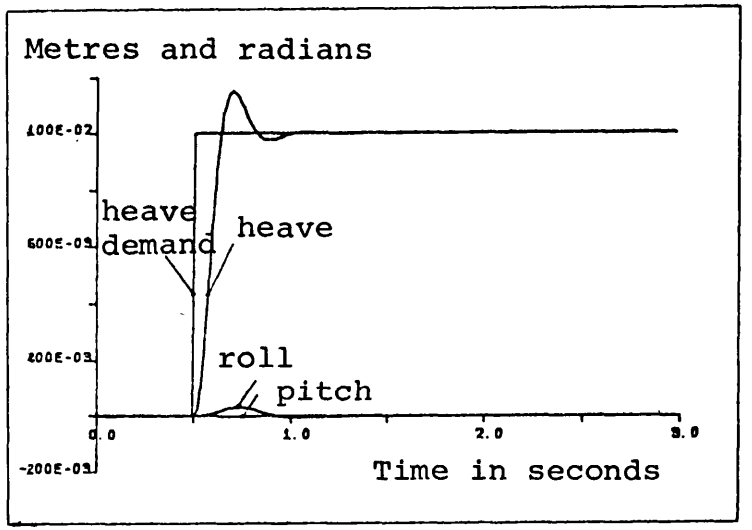

(a) Heave mode disturbance

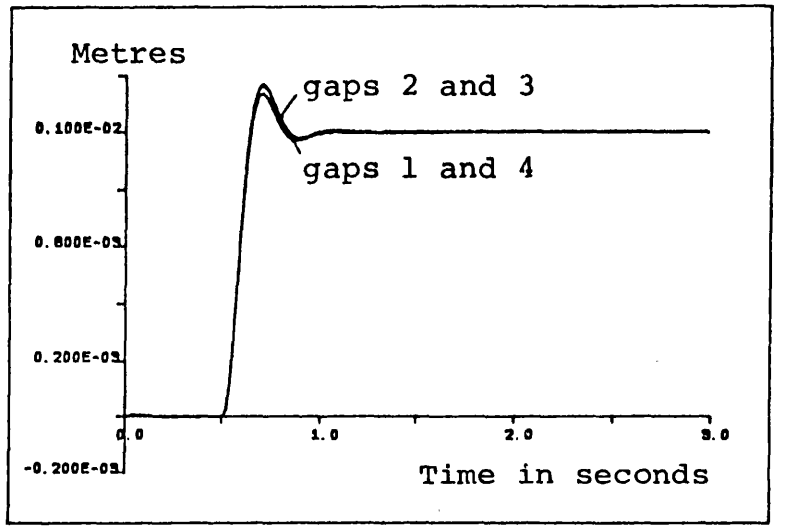

(b) Air gap for heave mode disturbance

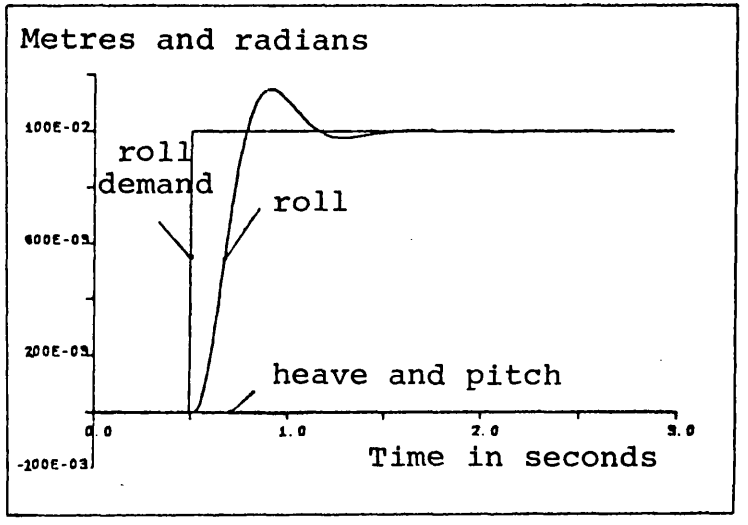

(c) Roll mode disturbance

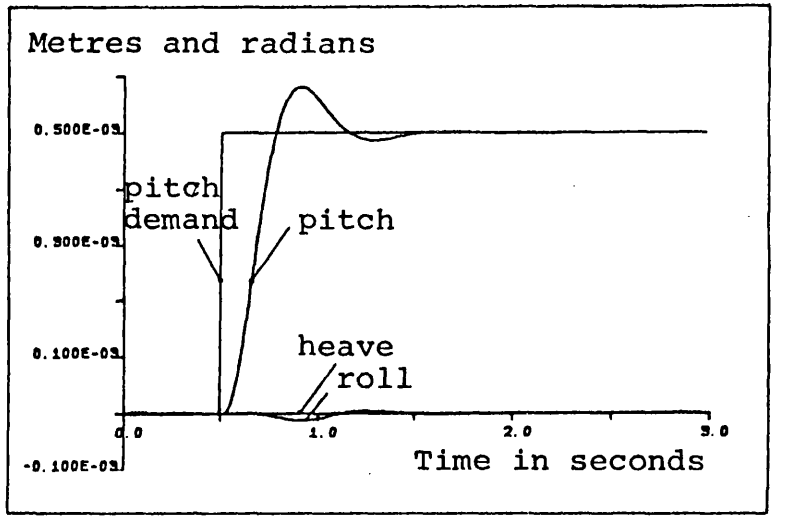

(d) Pitch mode disturbance

Figure 5.6.18 Simulation results showing interaction with fully compensated controller

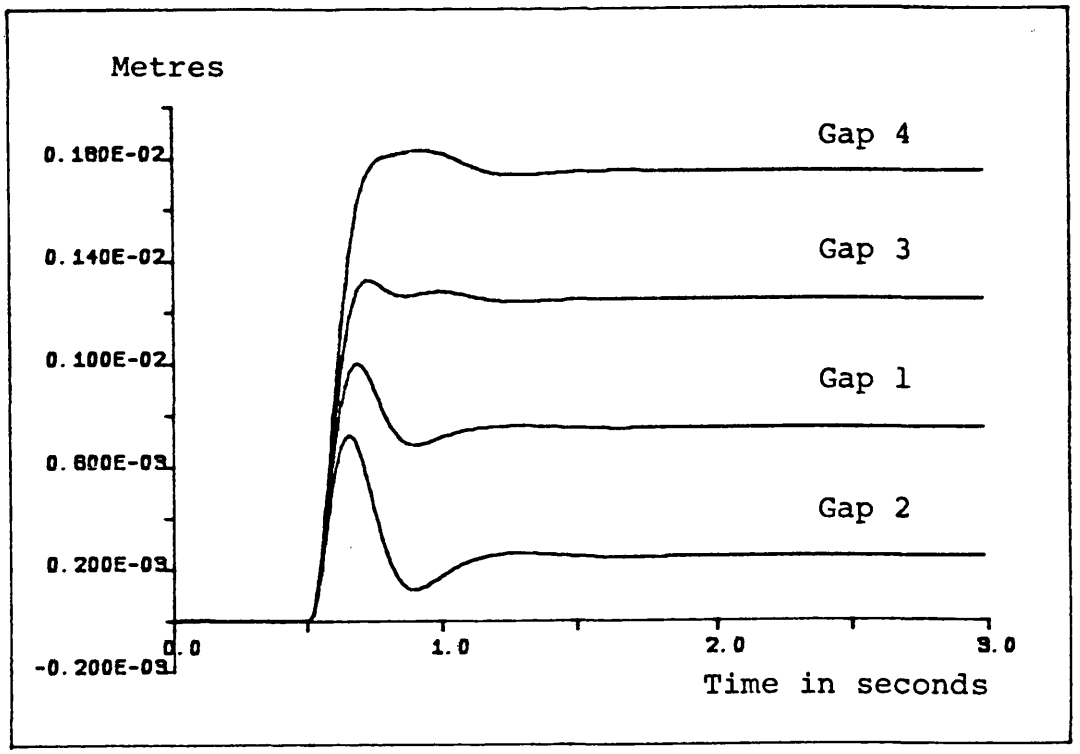

(b) Air gap responses

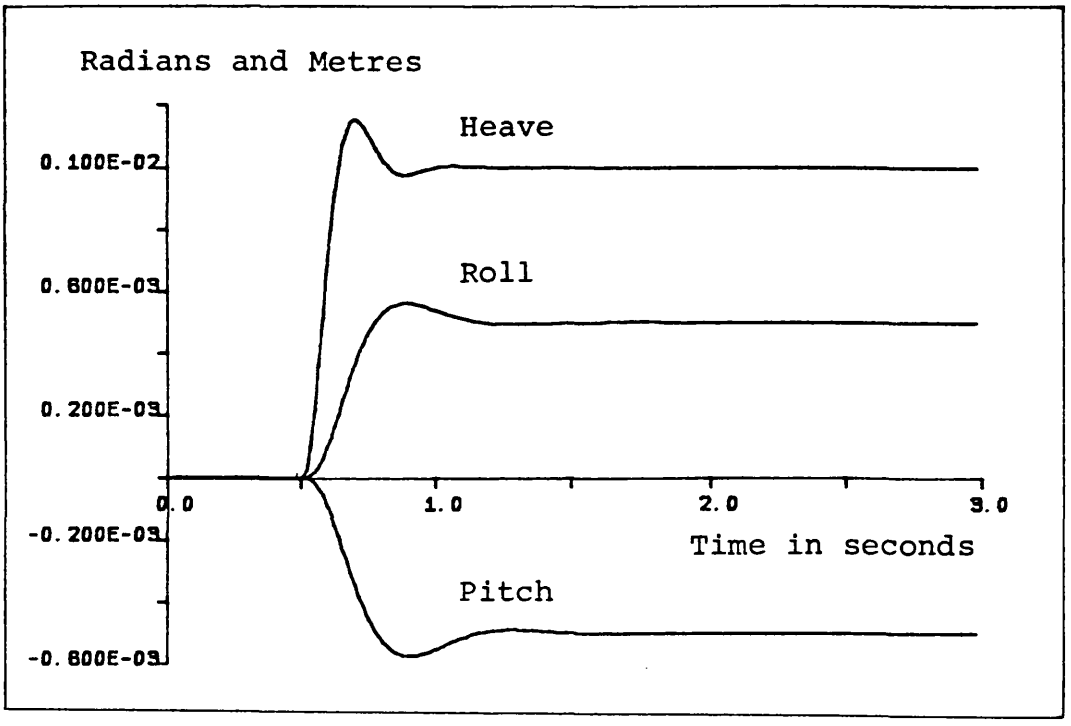

(a) Heave, roll and pitch responses

Figure 5.6.19 Simulation of vehicle attitude change with fully compensated controller

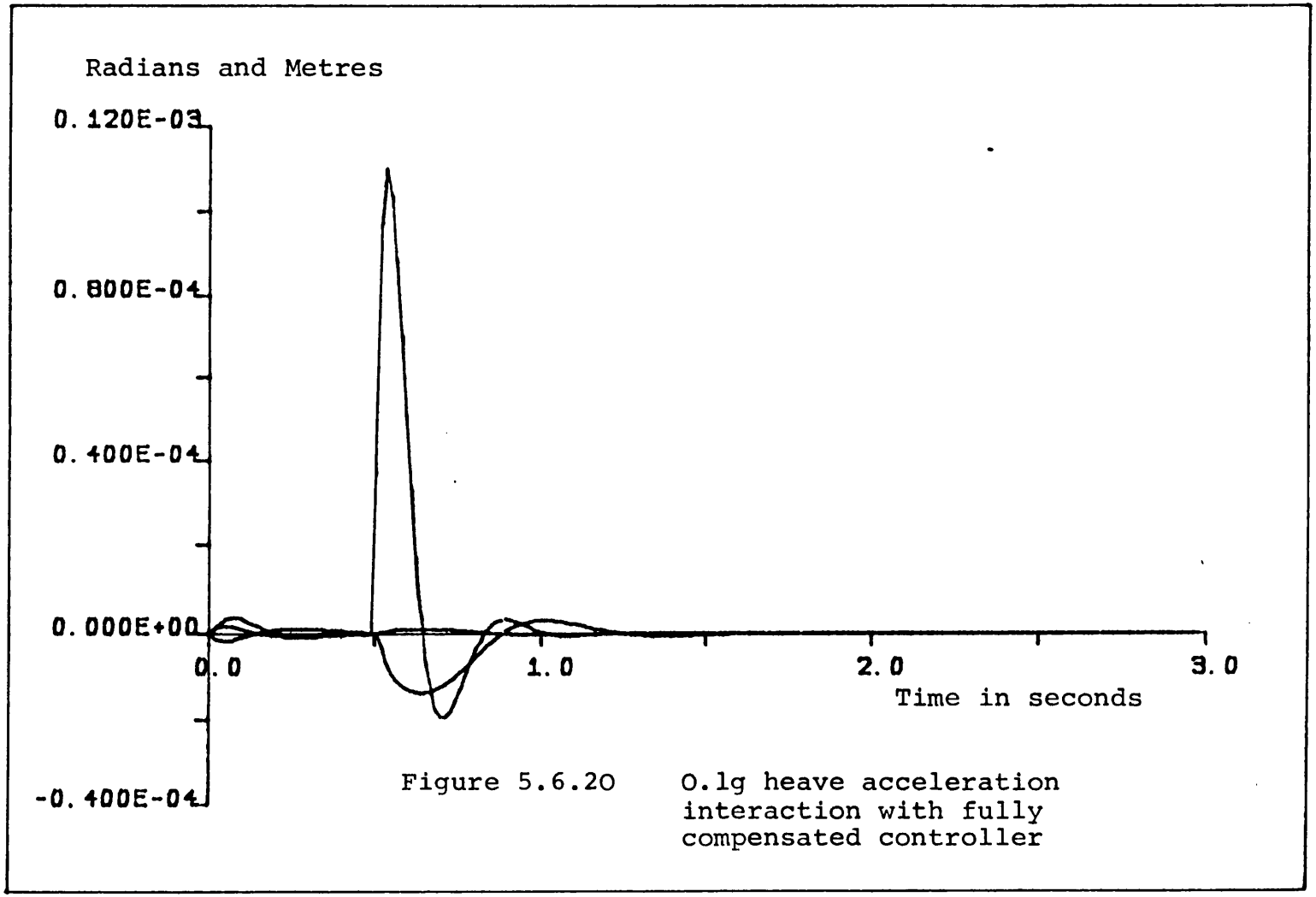

Figure 5.6.20 0.1g heave acceleration interaction with fully compensated controller

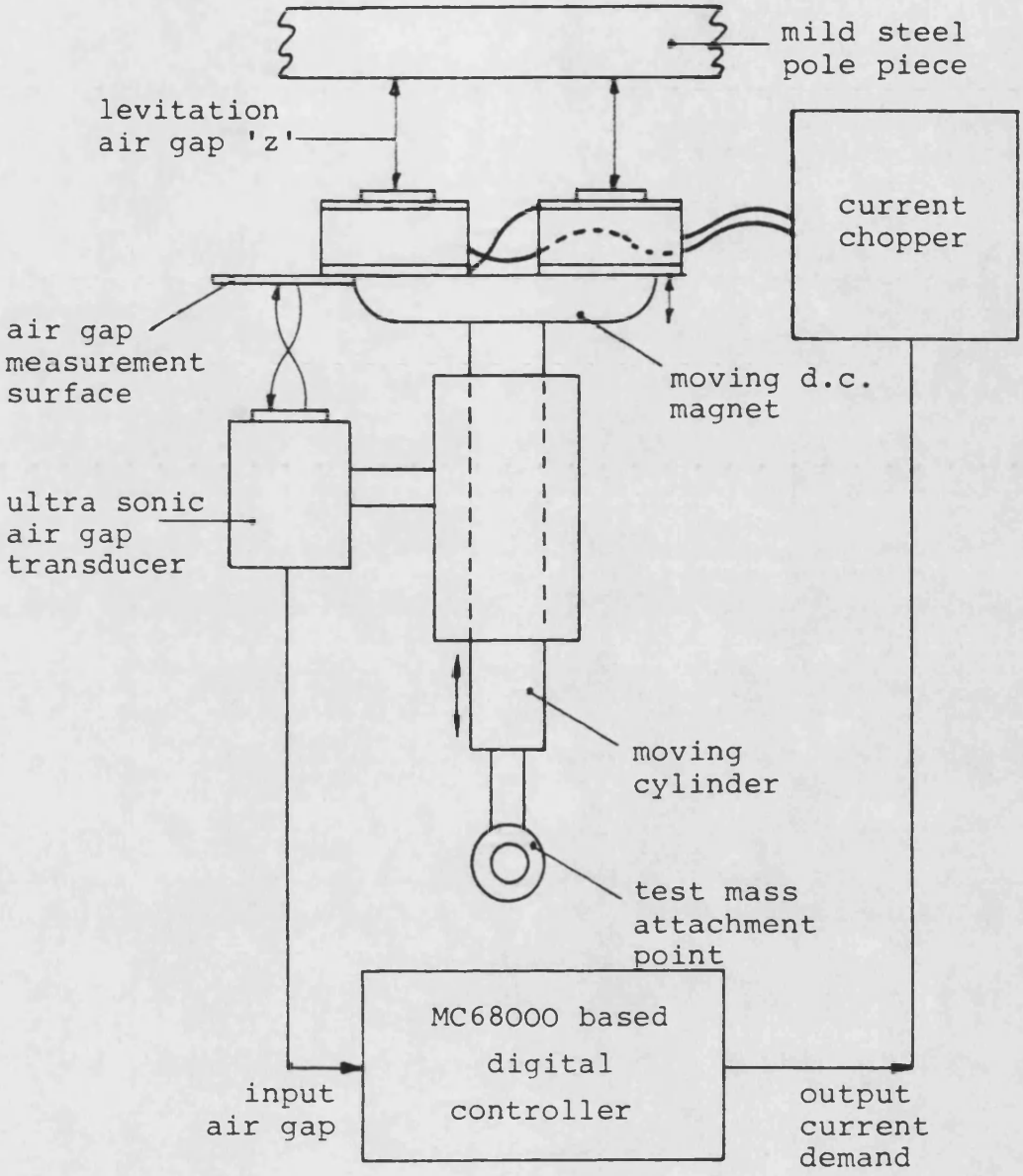

Figure 6.2.1 The single magnet rig

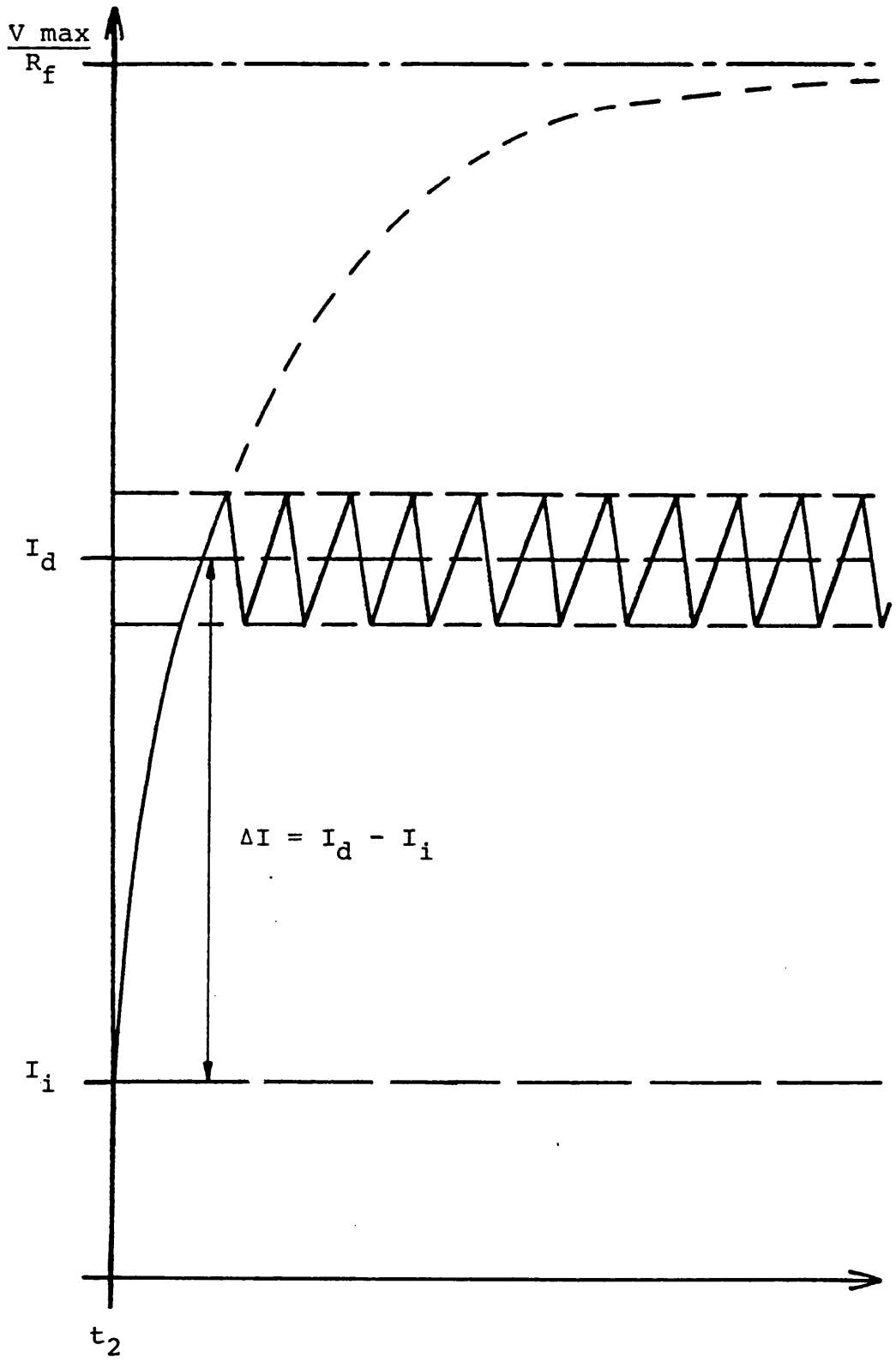

Figure 6.3.1 Time response of chopper current in the LSM field coils

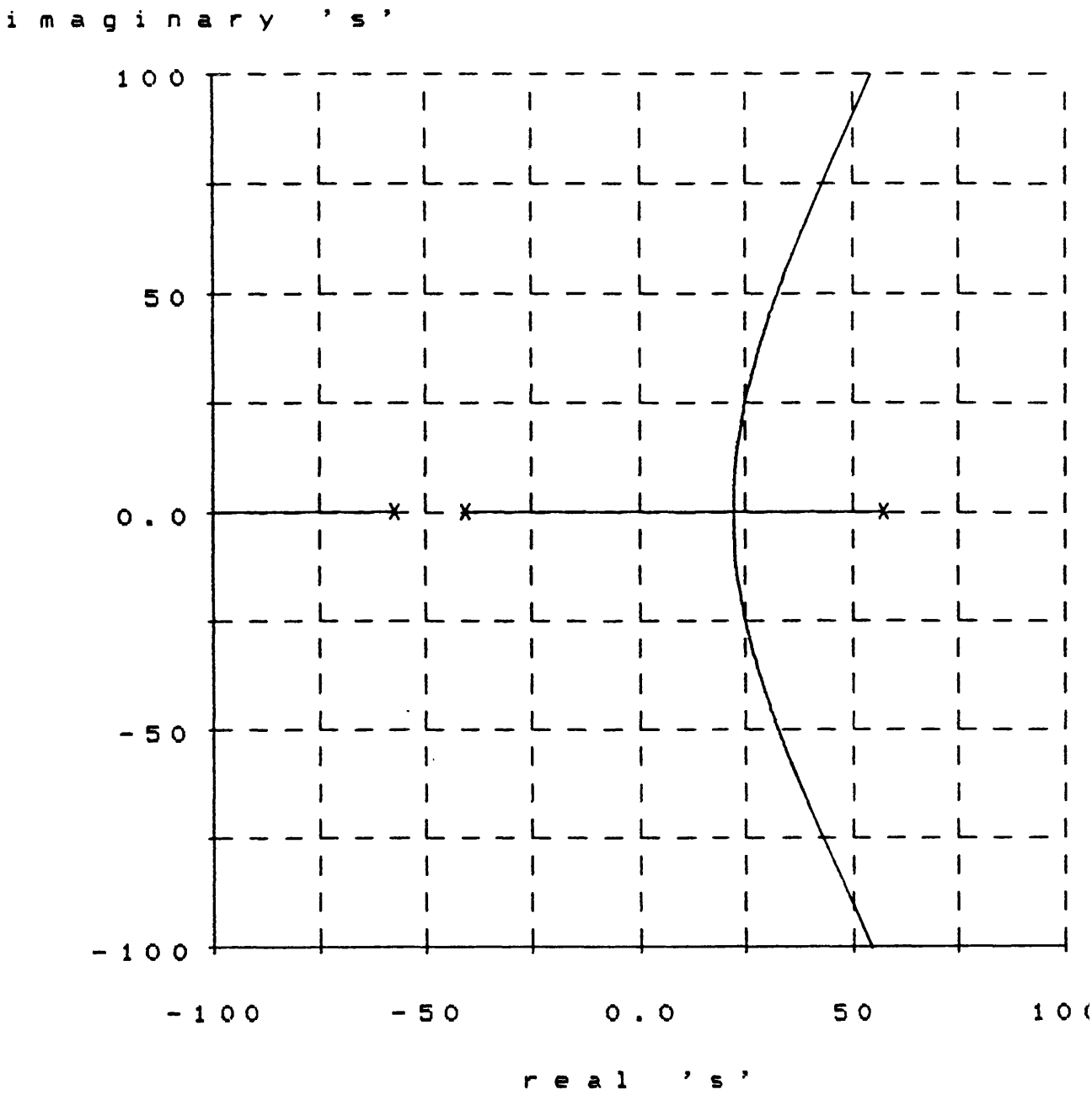

Figure 6.4.1 Root locus of the linearised system for unity feedback

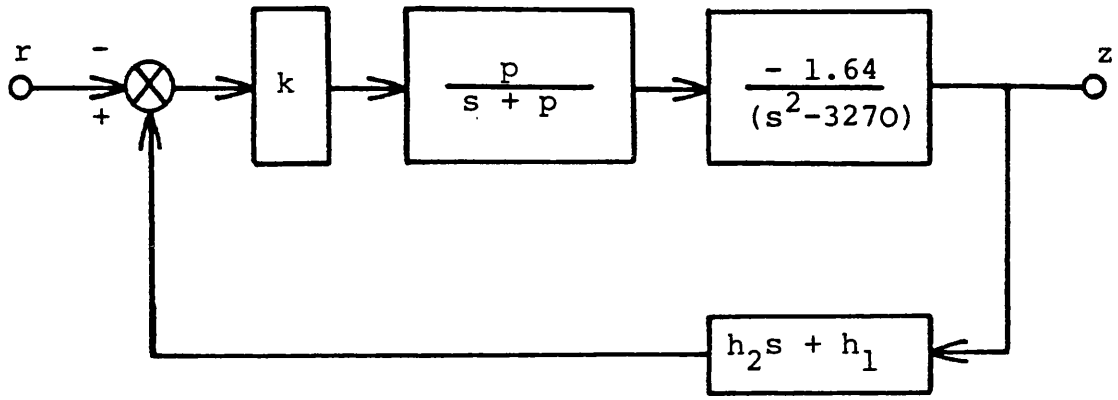

Figure 6.4.2 Block diagram for air gap and air gap rate feedback

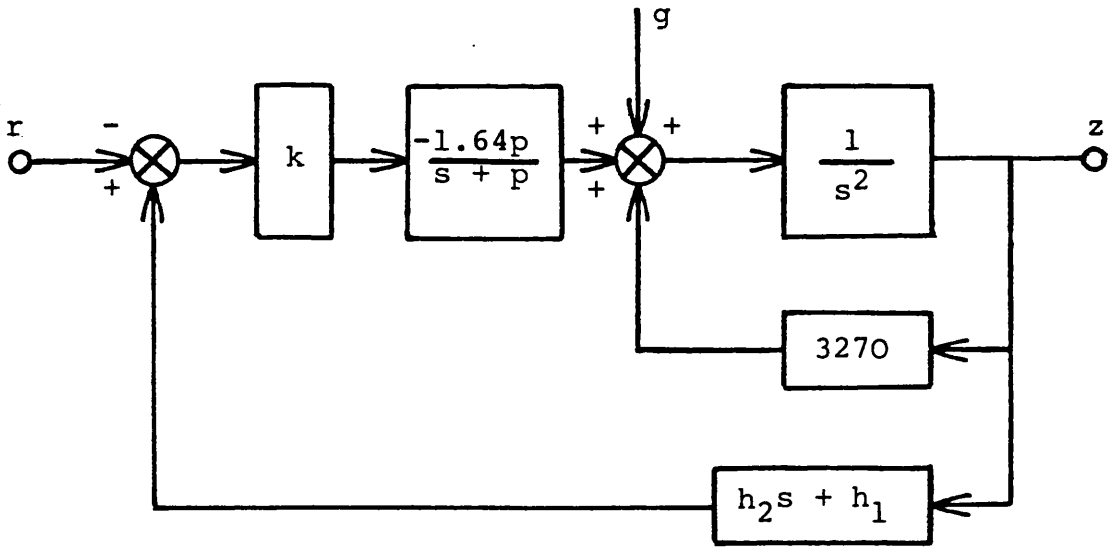

Figure 6.4.8 The effect on the linearised system of gravity acting on the magnet mass

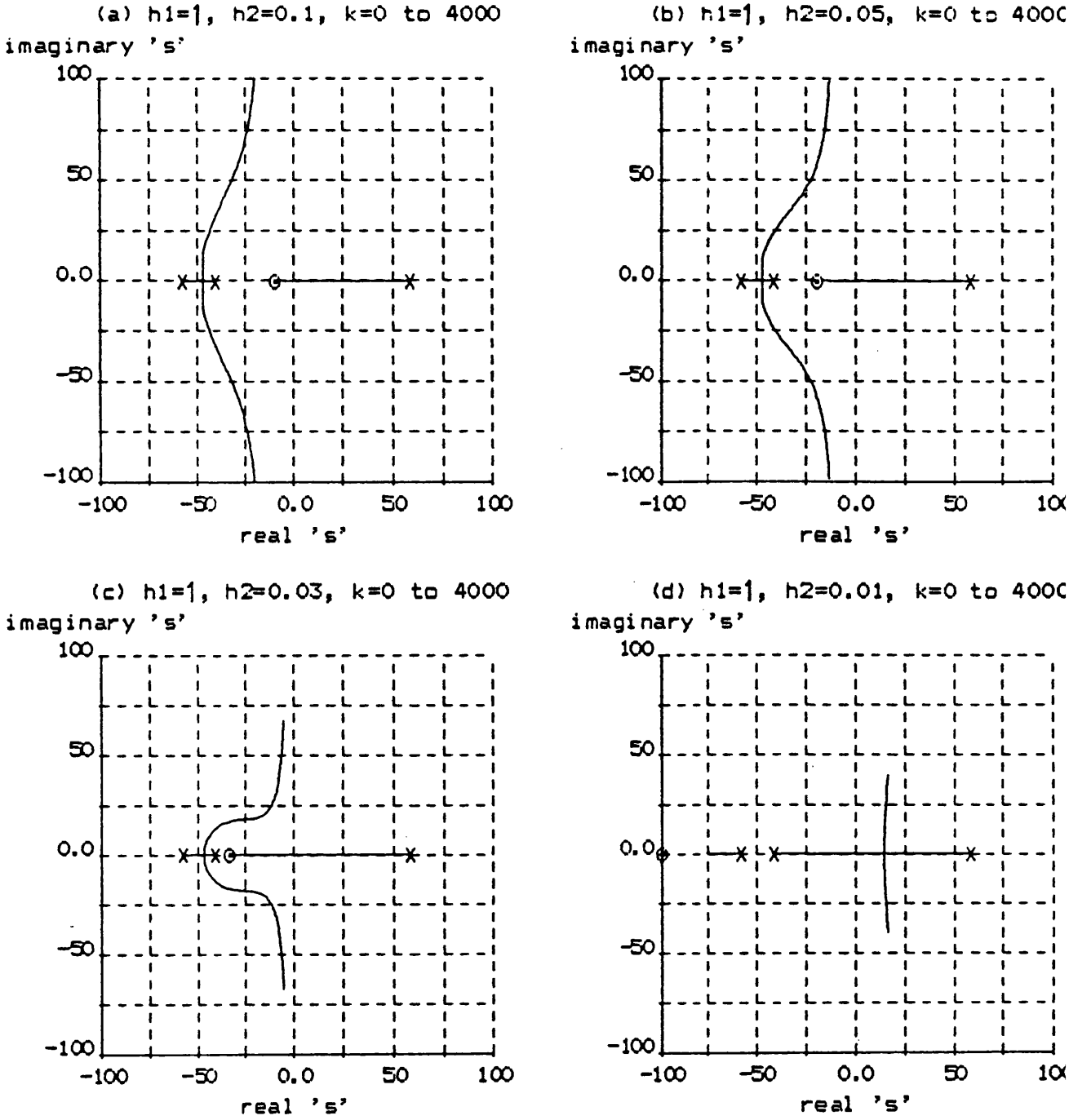

Figure 6.4.3 Root loci showing the effect of various amounts of air gap rate feedback

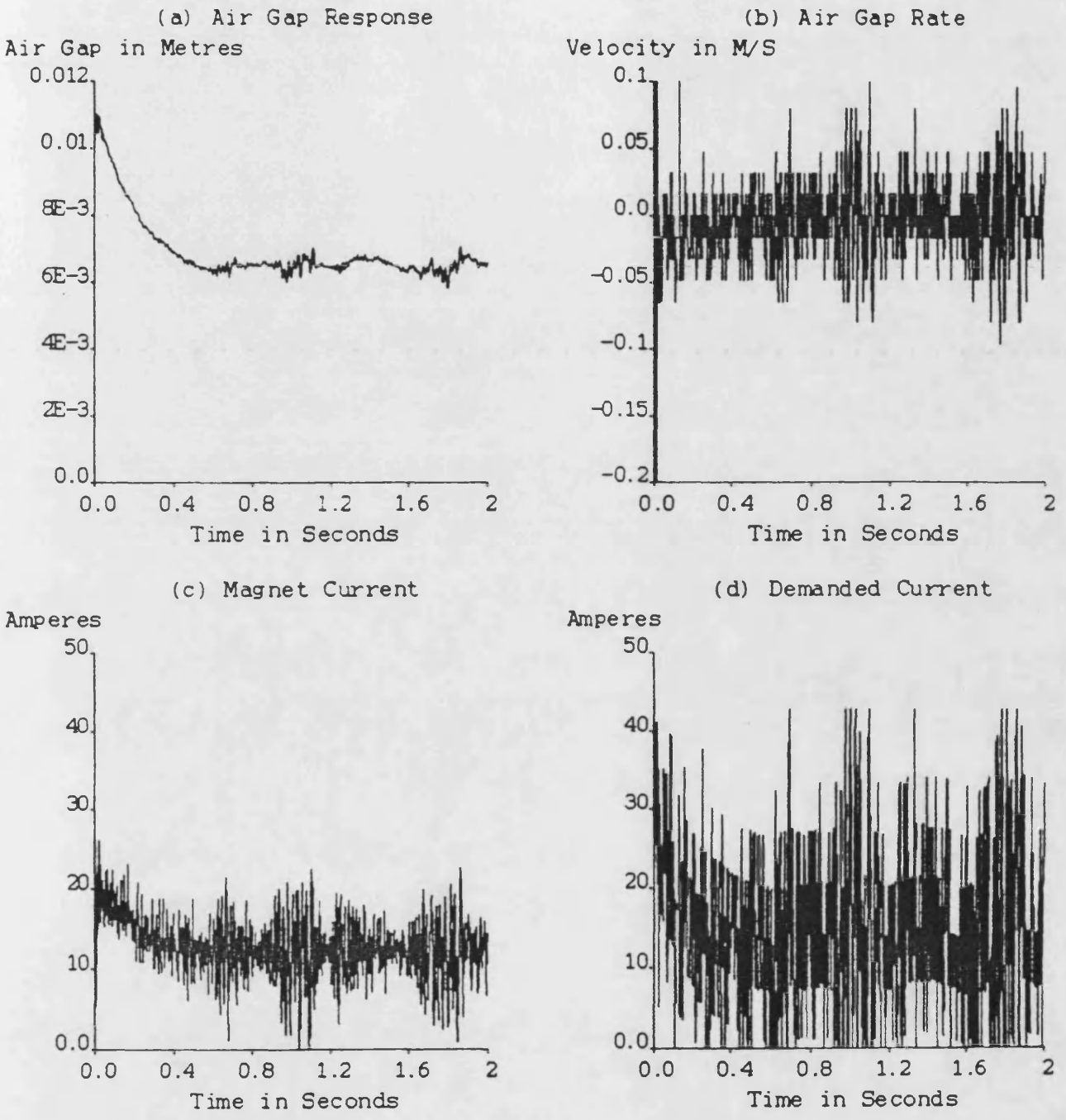

Figure 6.4.4 Levitation results for $h_2 = 0.1$, $h_1 = 1.0$, $k = 4000$

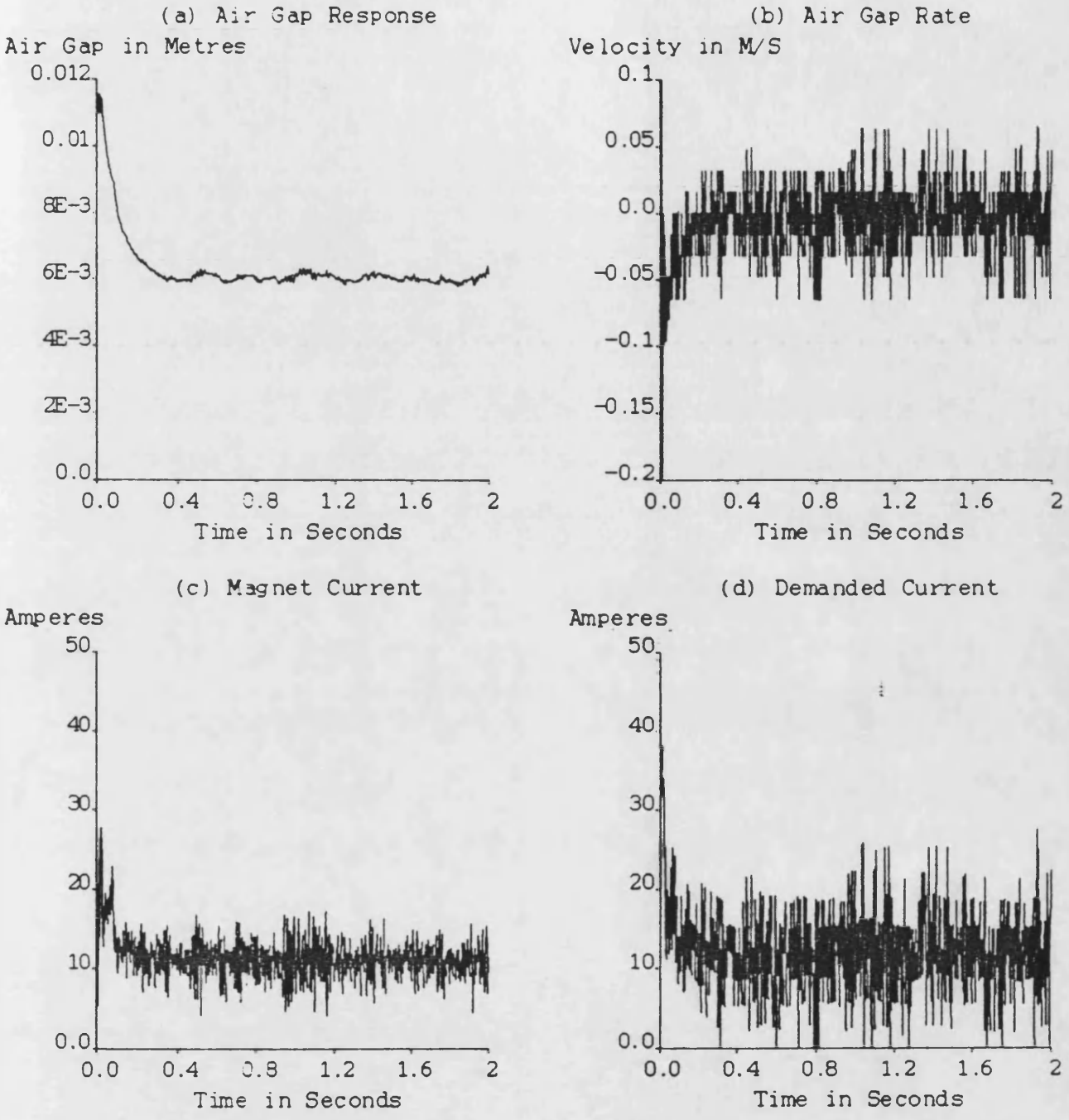

Figure 6.4.5 Levitation results for $h_2 = 0.05$, $h_1 = 1.0$, $k = 4000$

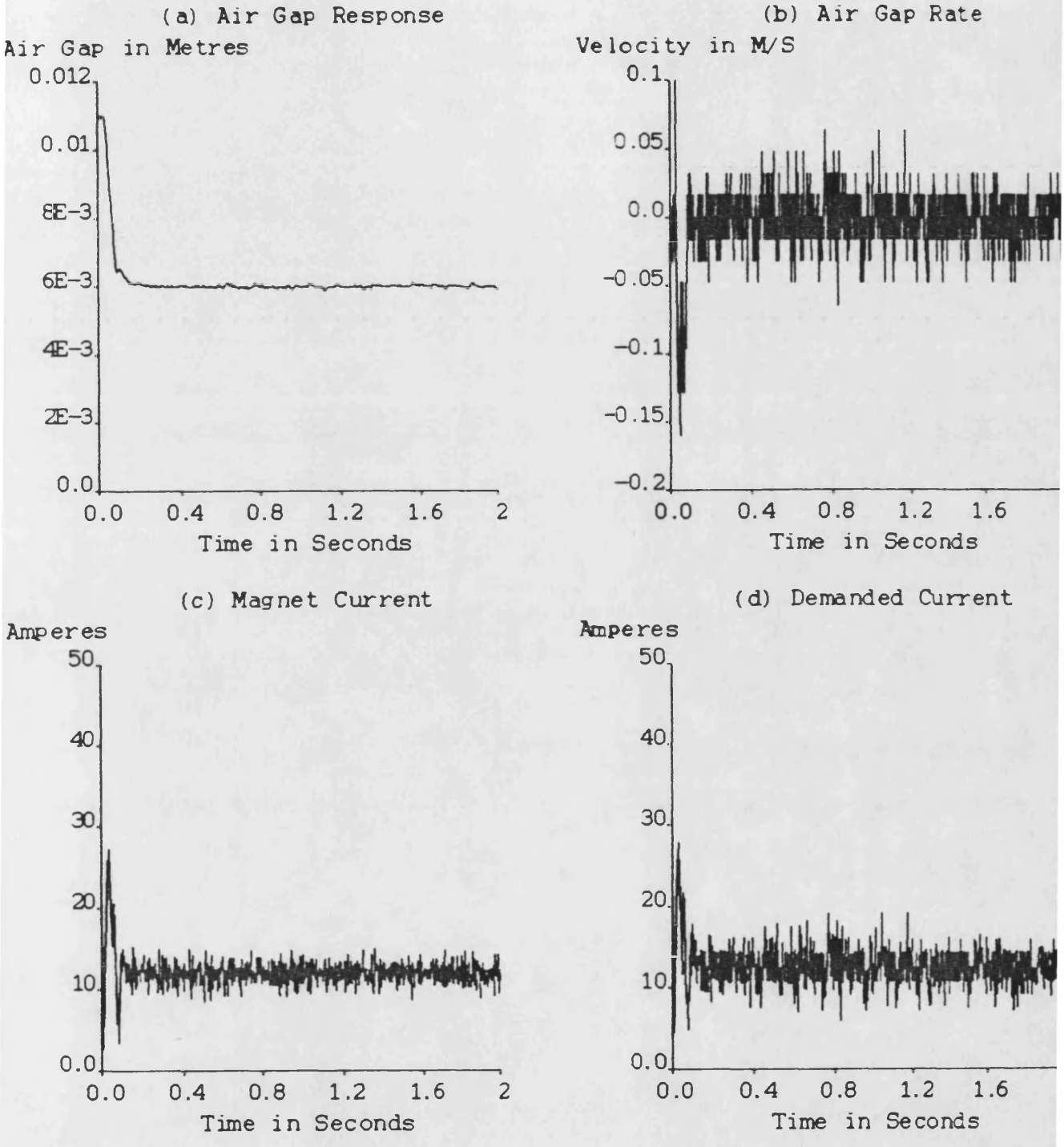

Figure 6.4.6 Levitation results for $h_2 = 0.03$, $h_1 = 1.0$, $k = 4000$

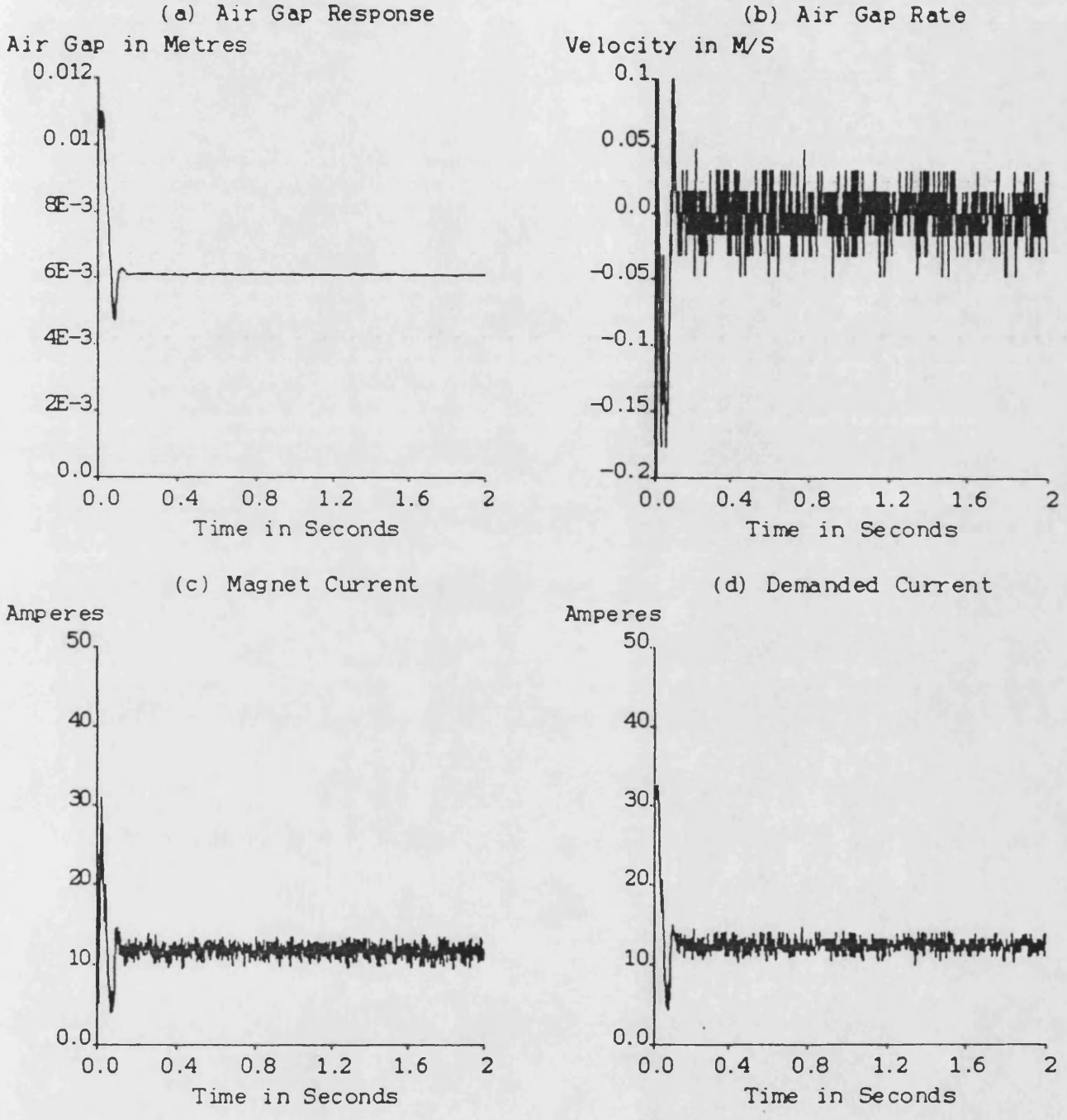

Figure 6.4.7 Levitation results for h_2 = 0.01, h_1 = 1.0, k = 4000

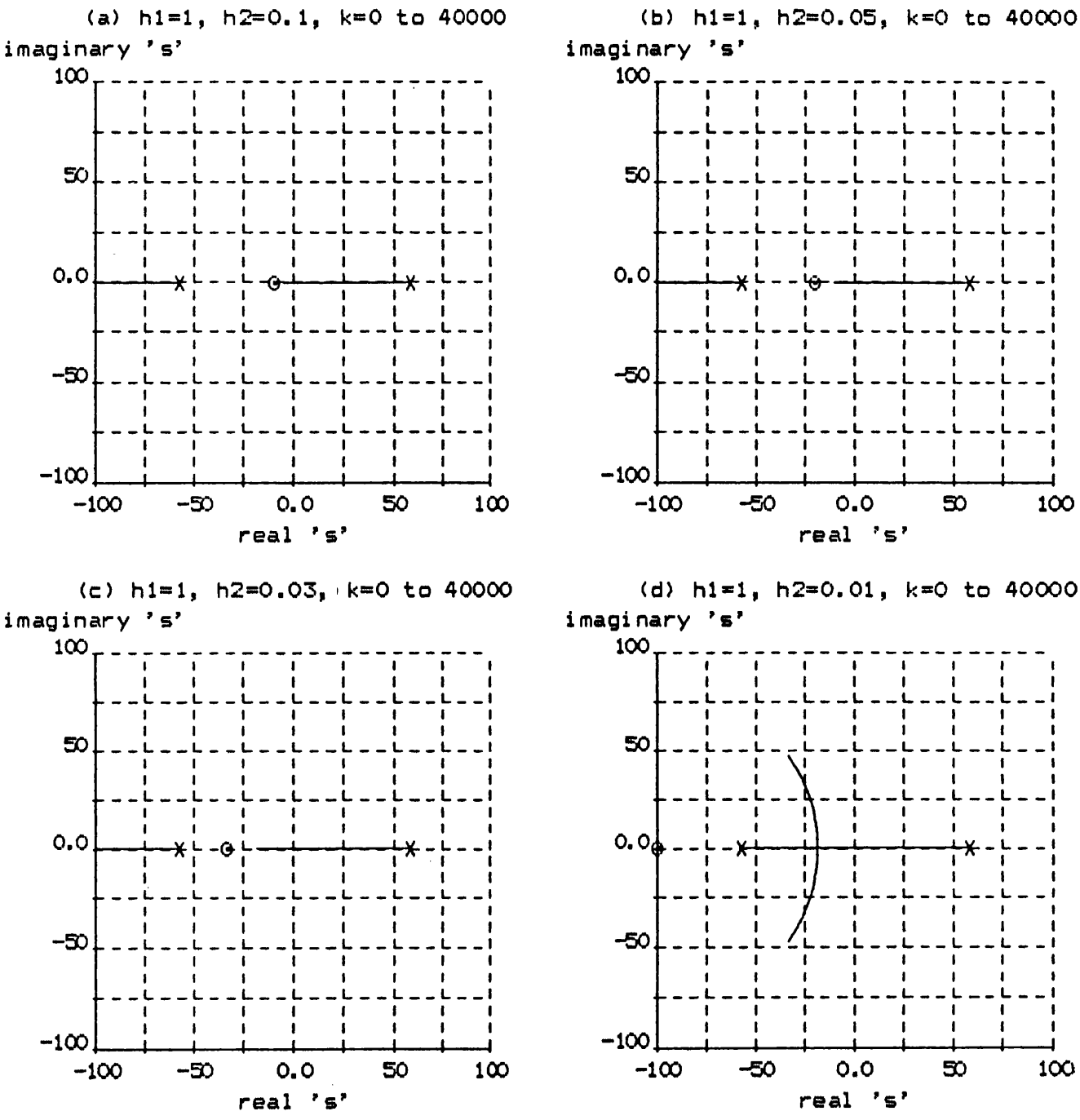

Figure 6.4.9 Root loci showing the effect of removing the linearised chopper pole

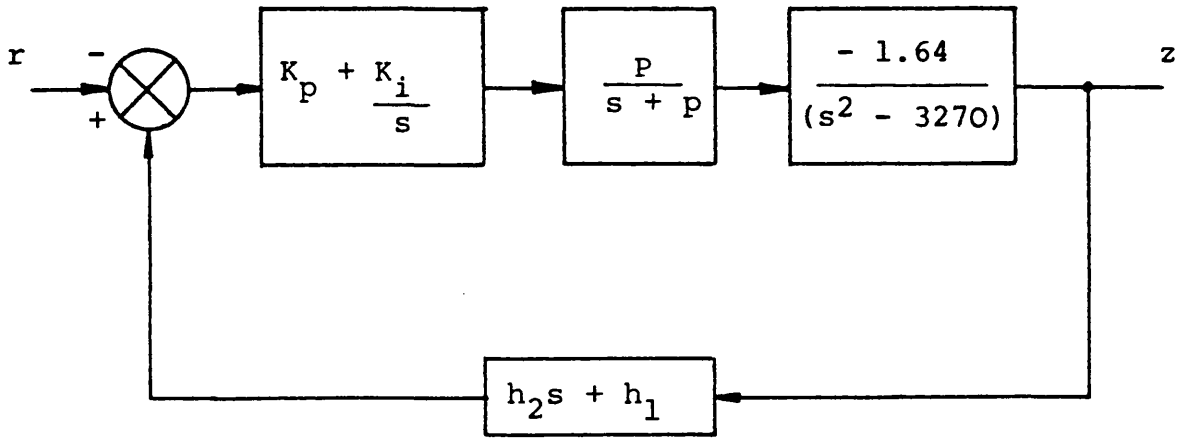

Figure 6.4.10 Block diagram of a P.I. controller for the levitation system

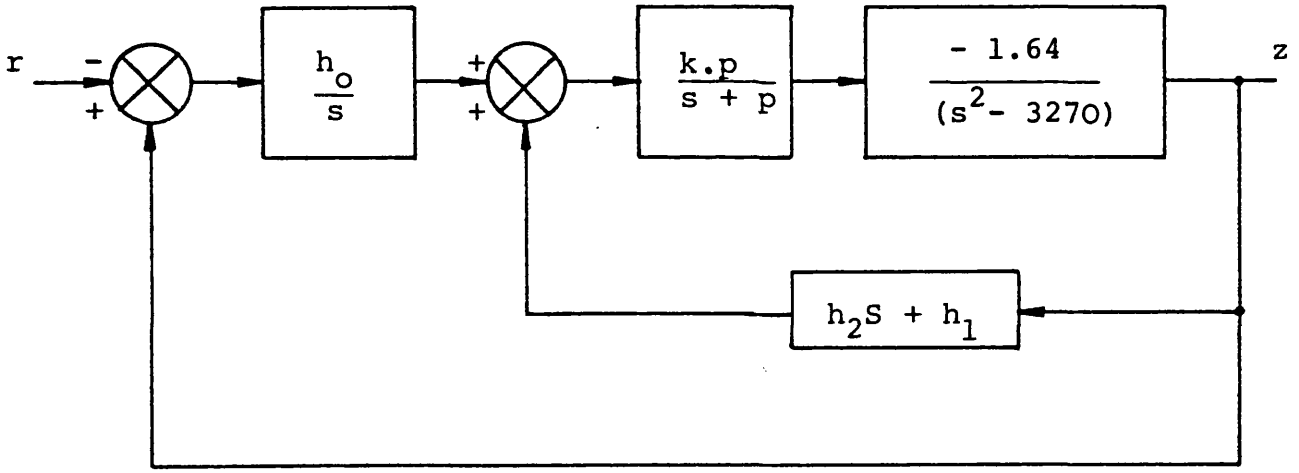

Figure 6.4.13 Block diagram of the linearised system using a state feedback with an outer feedback loop with a forward path integrator

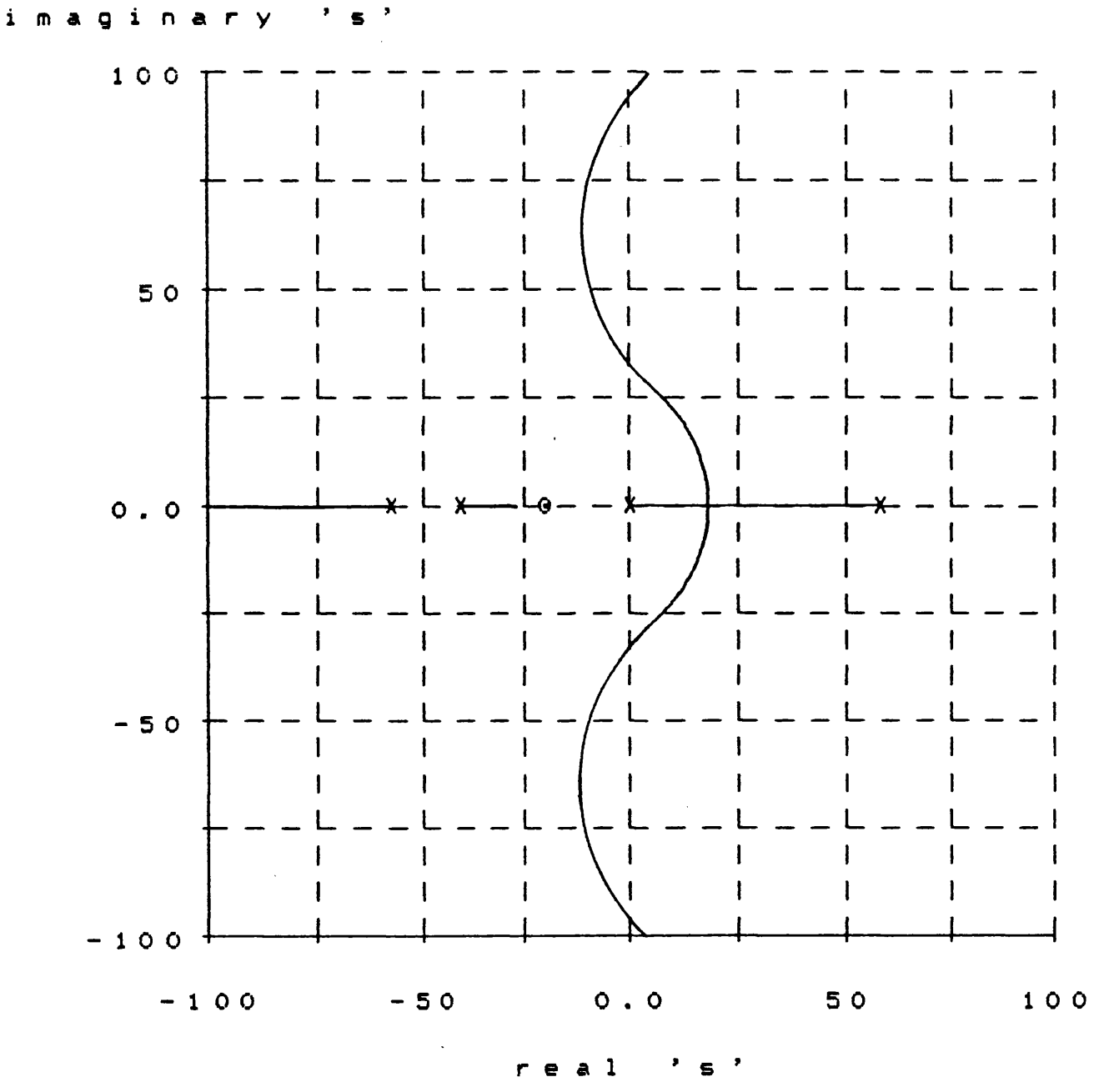

Figure 6.4.11 Root locus for unity feedback with a P.I. controller

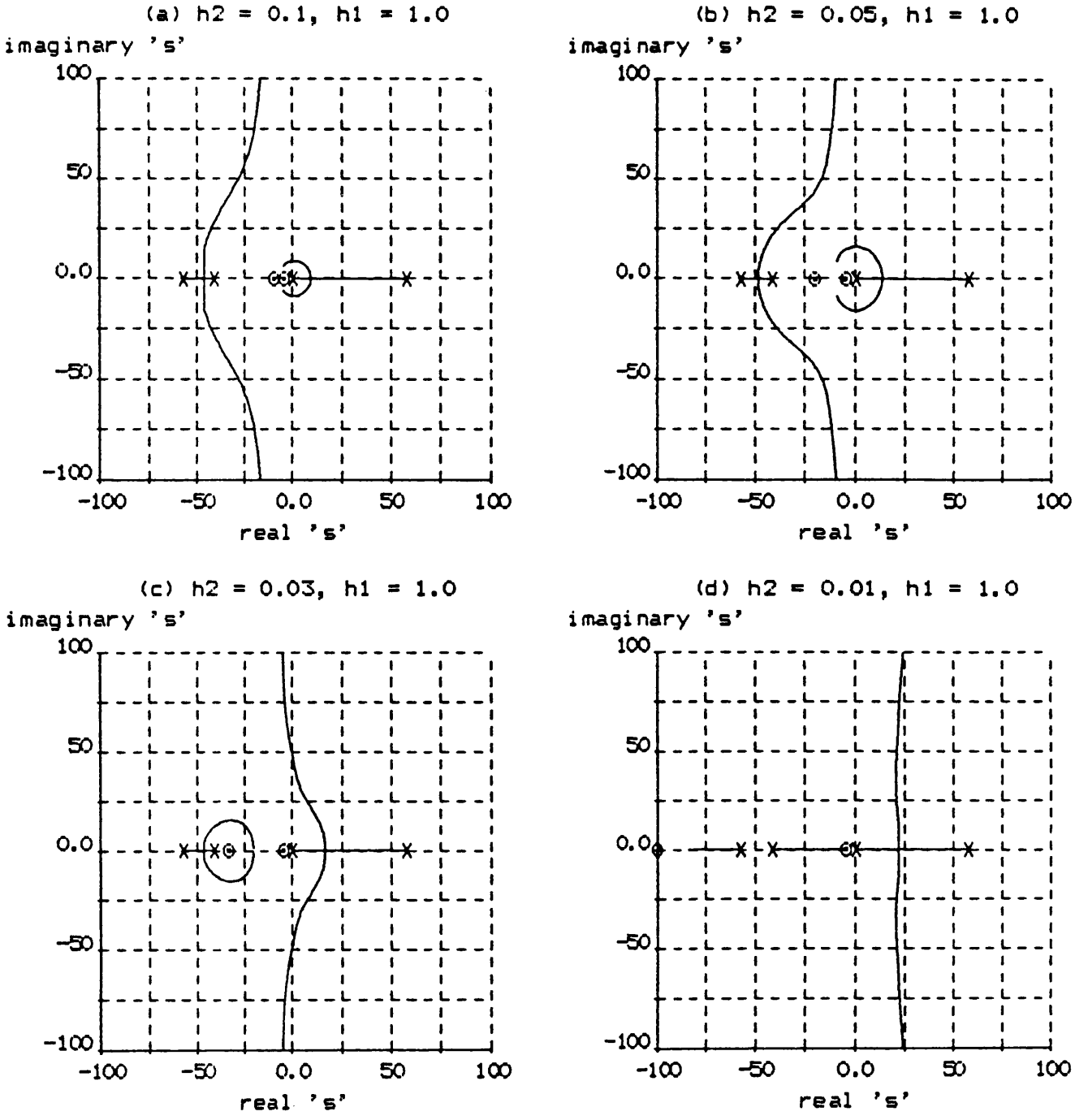

Figure 6.4.12 Various possible root loci for a P.I. controller with air gap rate feedback

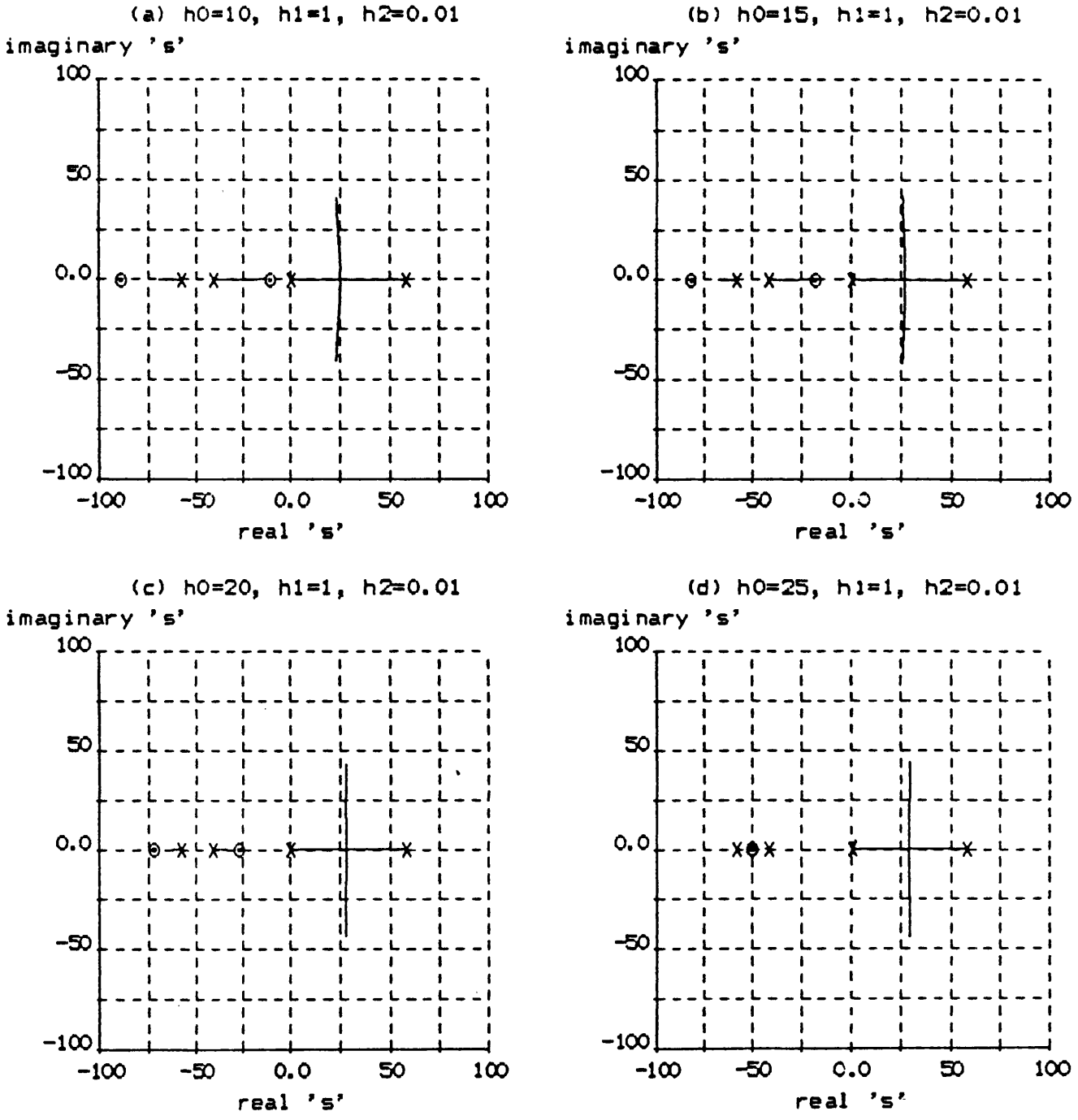

Figure 6.4.14 Root loci for various integrator gains showing the chopper pole caused instability

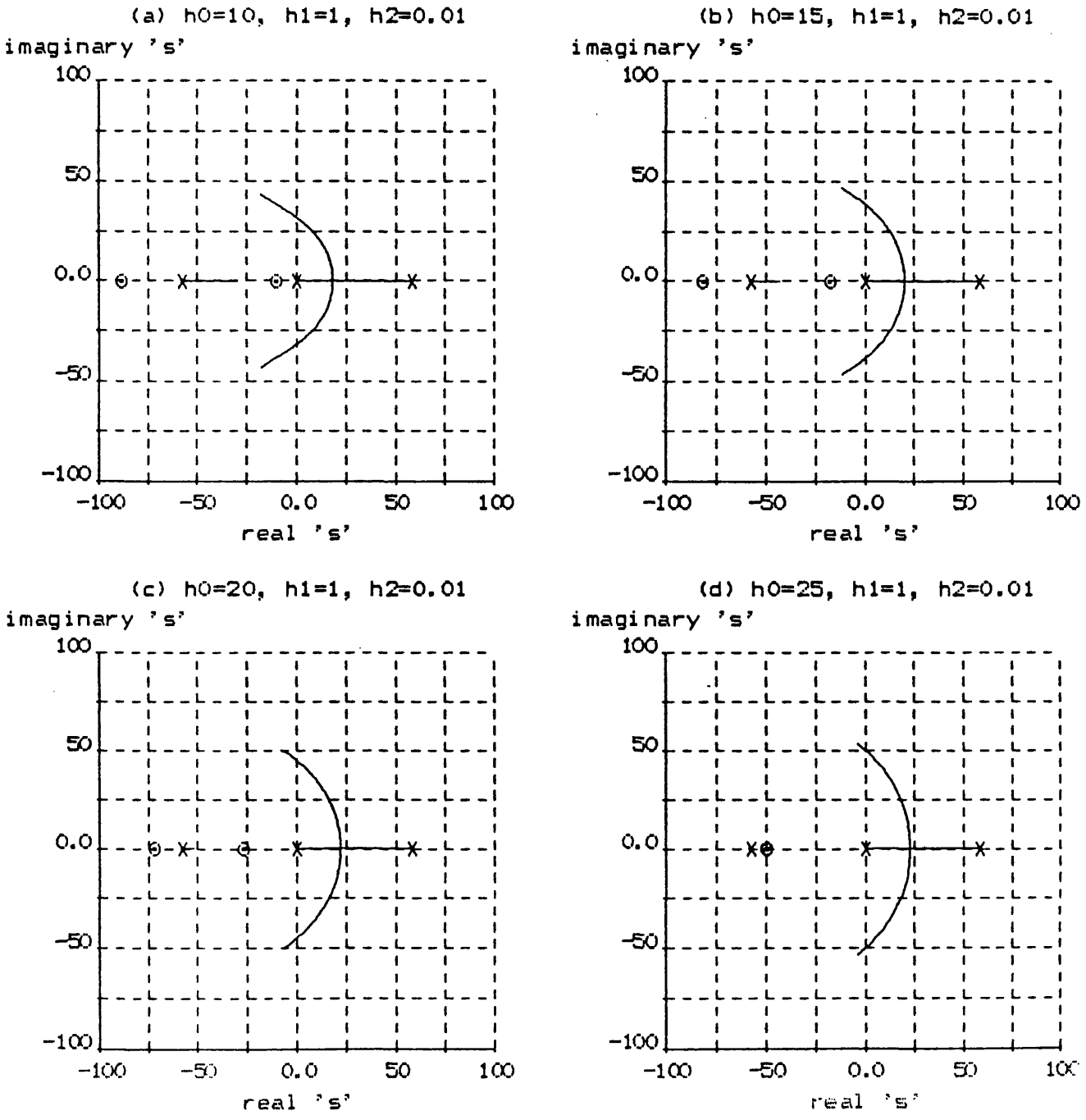

Figure 6.4.15 Root loci for various integrator gains with the linearised chopper pole removed for k = 0 to k = 4000

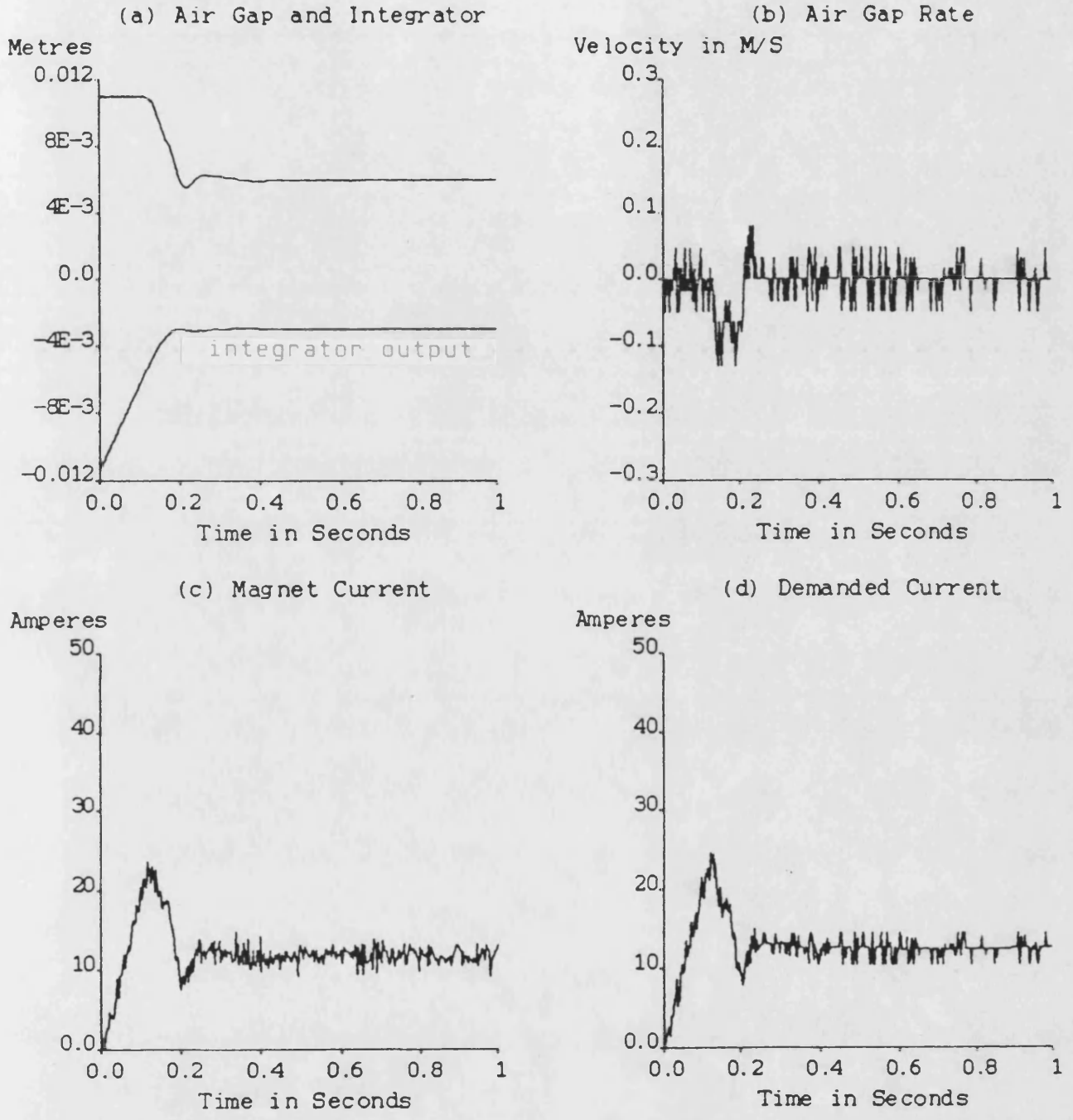

Figure 6.4.16 Levitation results for $h_o = 10$, $h_1 = 1$, $h_2 = 0.01$, $k = 4000$

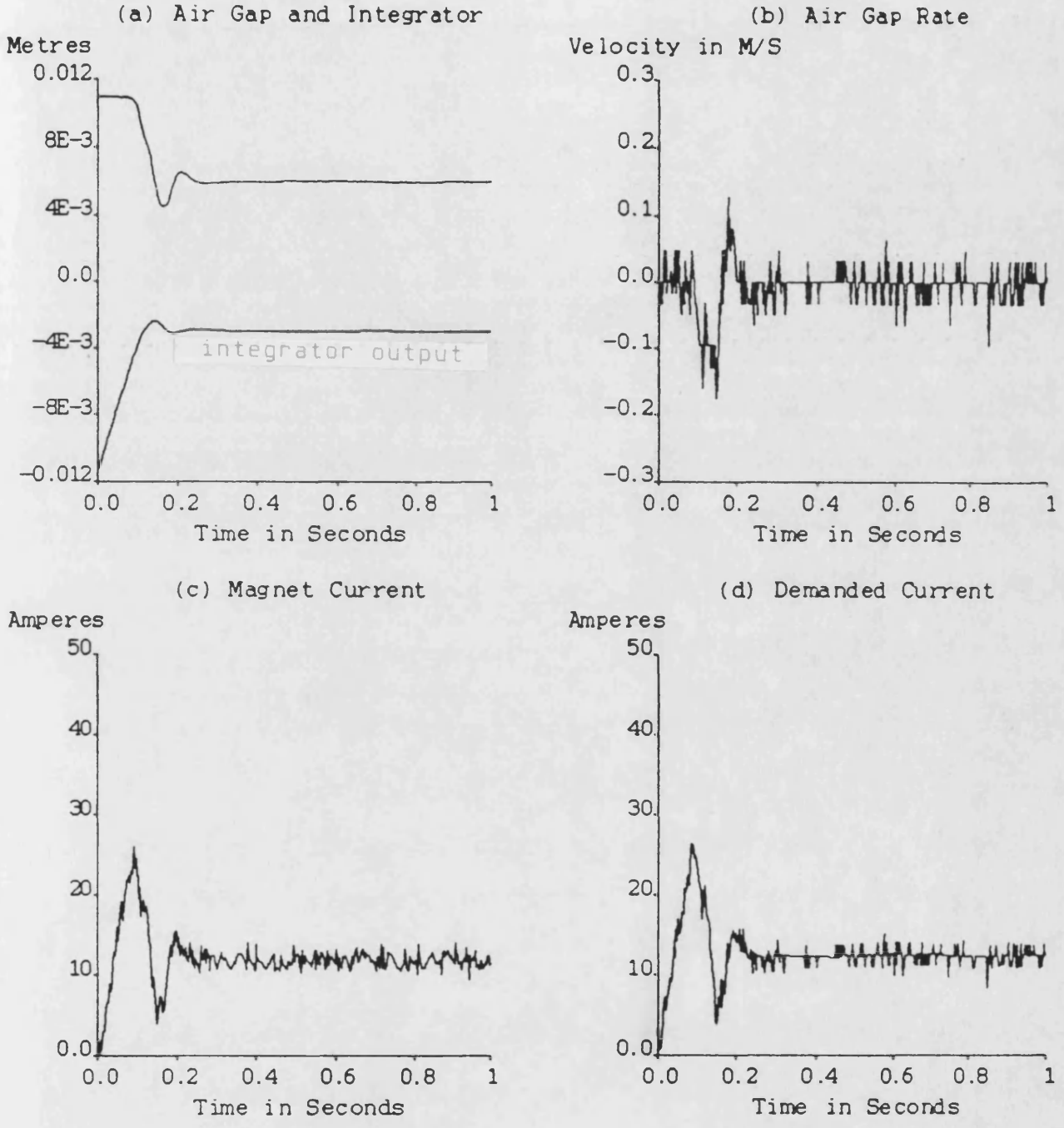

Figure 6.4.17 Levitation results for $h_o = 15$, $h_1 = 1$, $h_2 = 0.01$, $k = 4000$

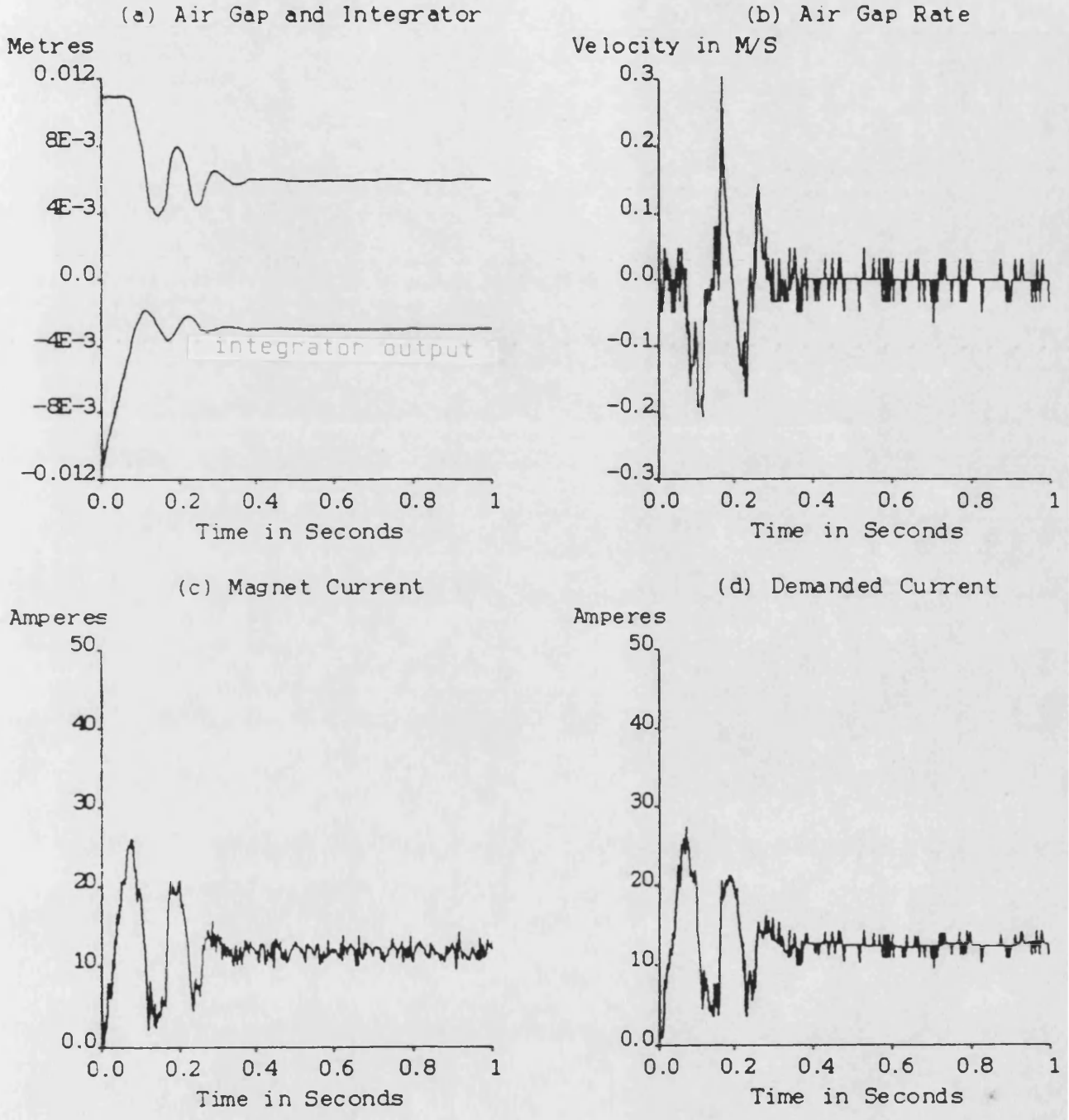

Figure 6.4.18 Levitation results for $h_o = 20$, $h_1 = 1$, $h_2 = 0.01$, $k = 4000$

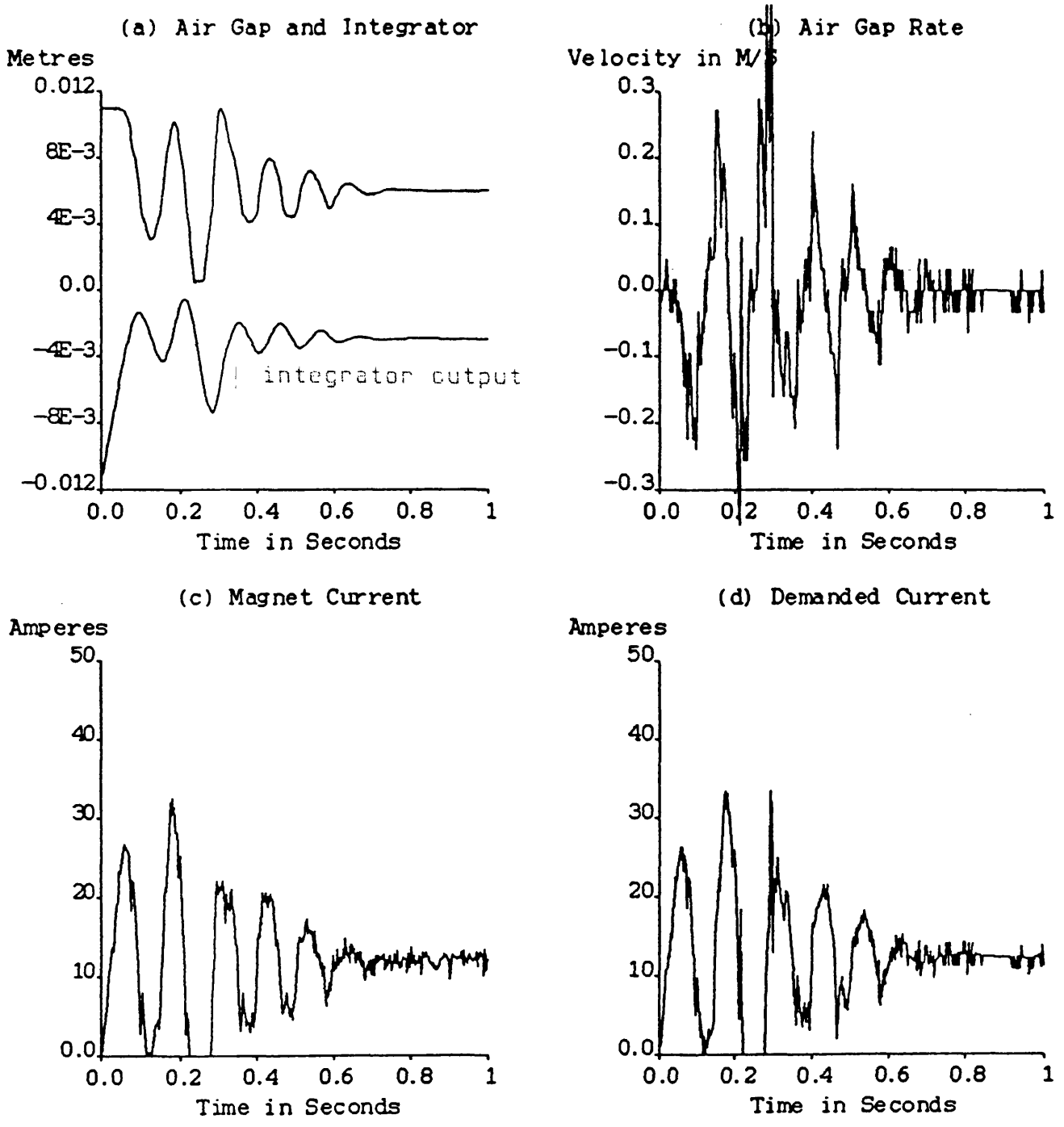

Figure 6.4.19 Levitation results for $h_o = 25$, $h_1 = 1$, $h_2 = 0.01$, $k = 4000$

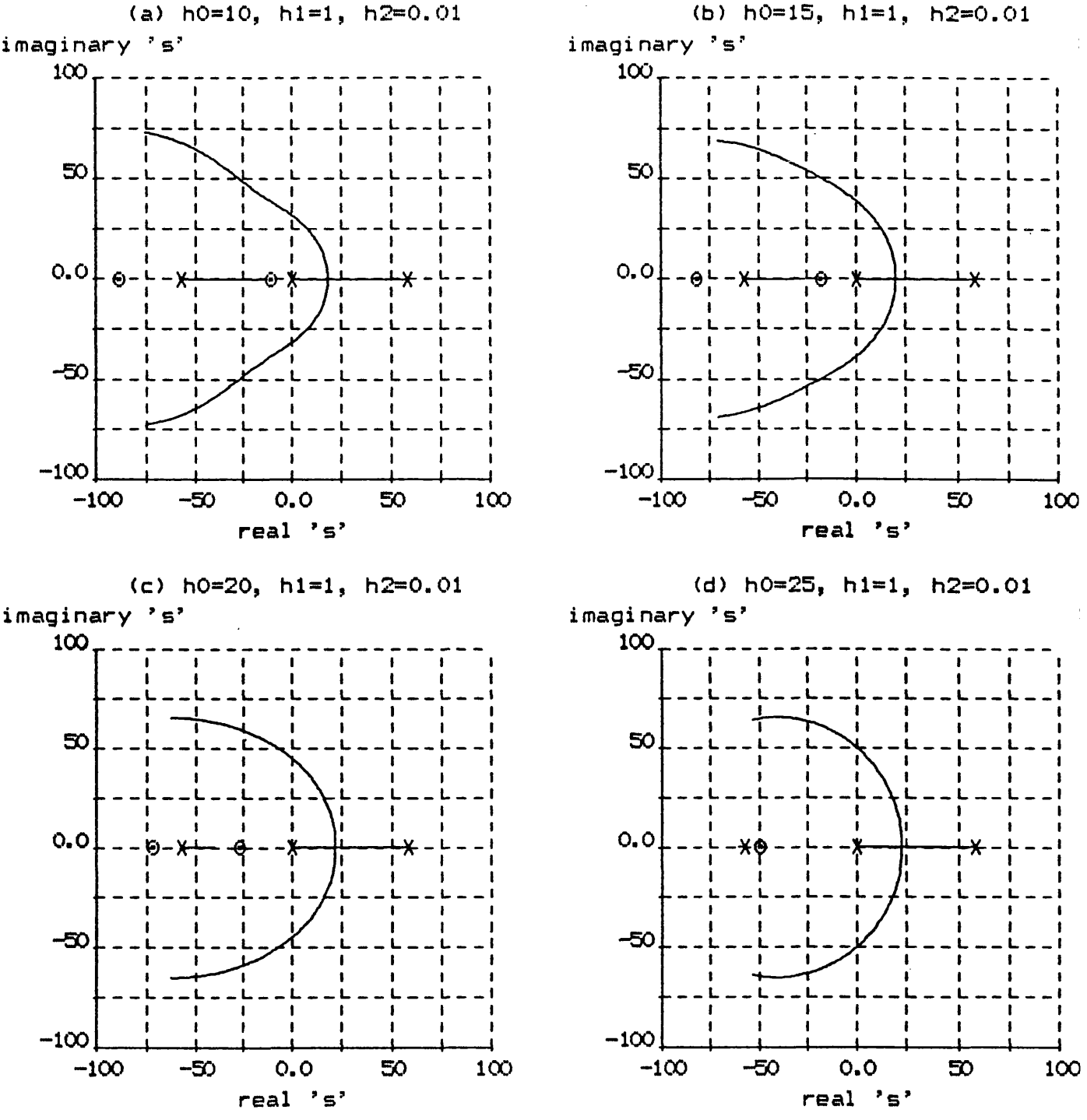

Figure 6.4.20 Root loci for various integrator gains with no chopper pole for K = 0 to K = 10000

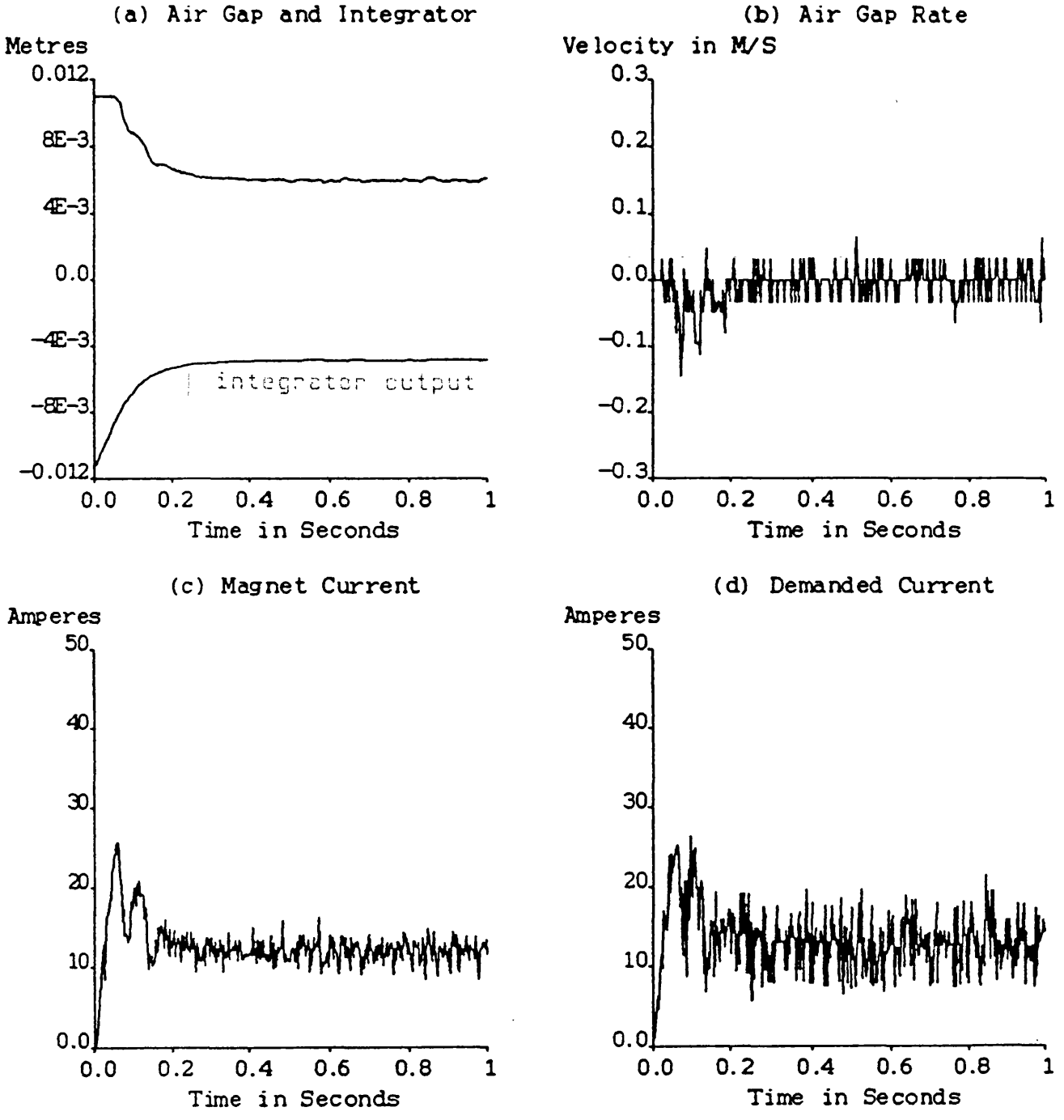

Figure 6.4.21 Levitation results for h_o = 10, h_1 = 1, h_2 = 0.01, k = 10000

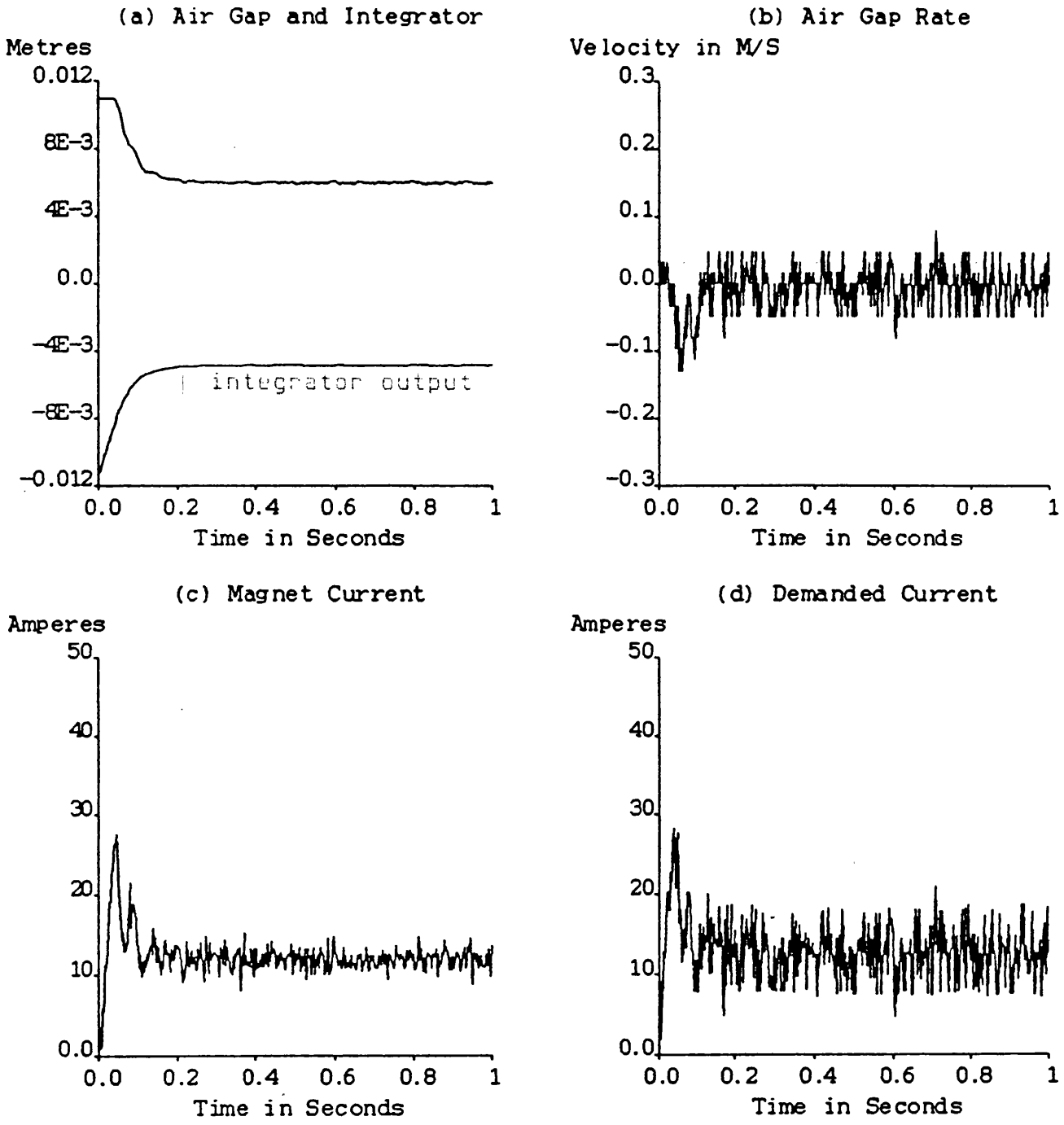

Figure 6.4.22 Levitation results for $h_o = 15$, $h_1 = 1$, $h_2 = 0.01$, $k = 10000$

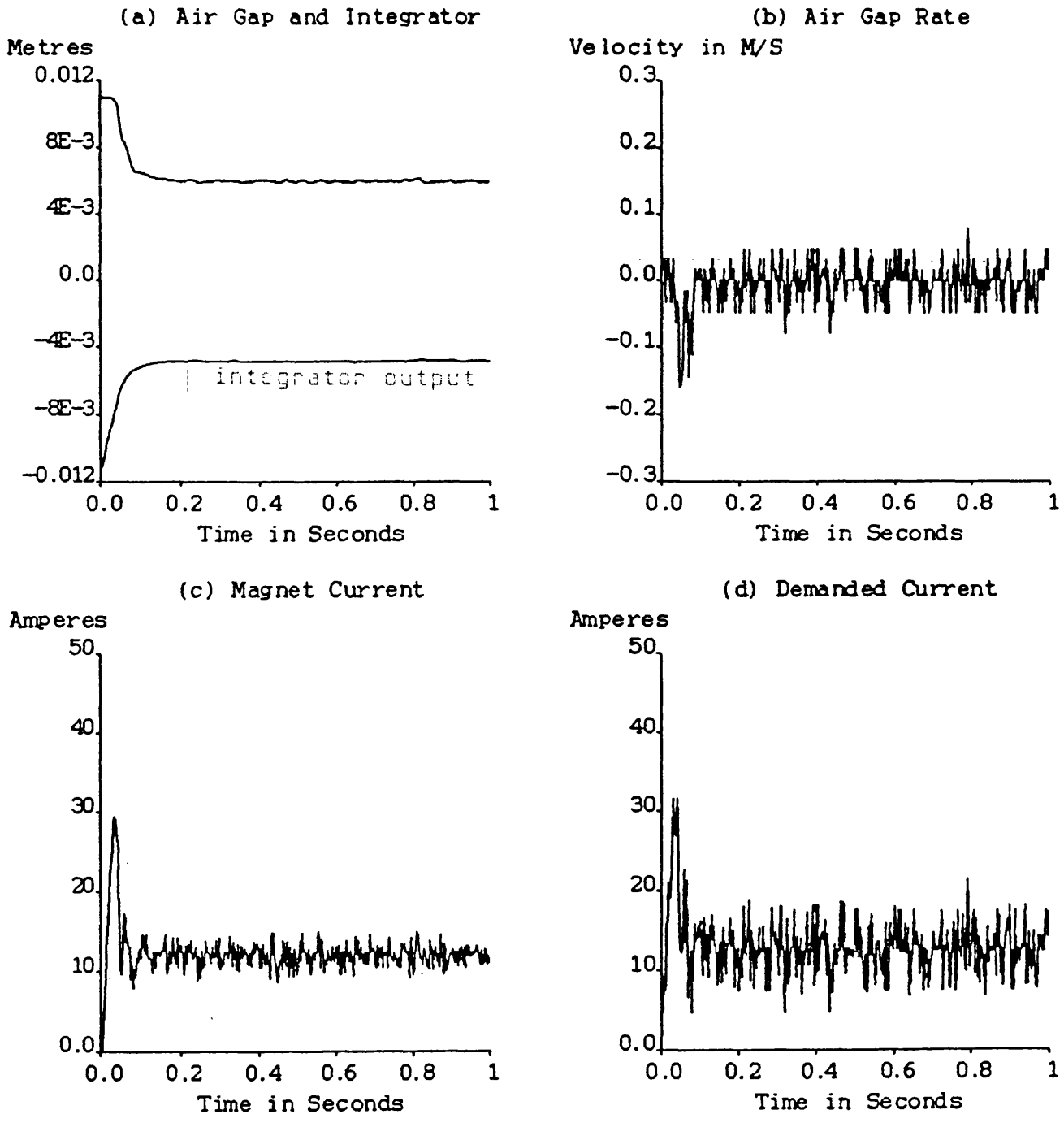

Figure 6.4.23 Levitation results for $h_o = 20$, $h_1 = 1$, $h_2 = 0.01$, $k = 10000$

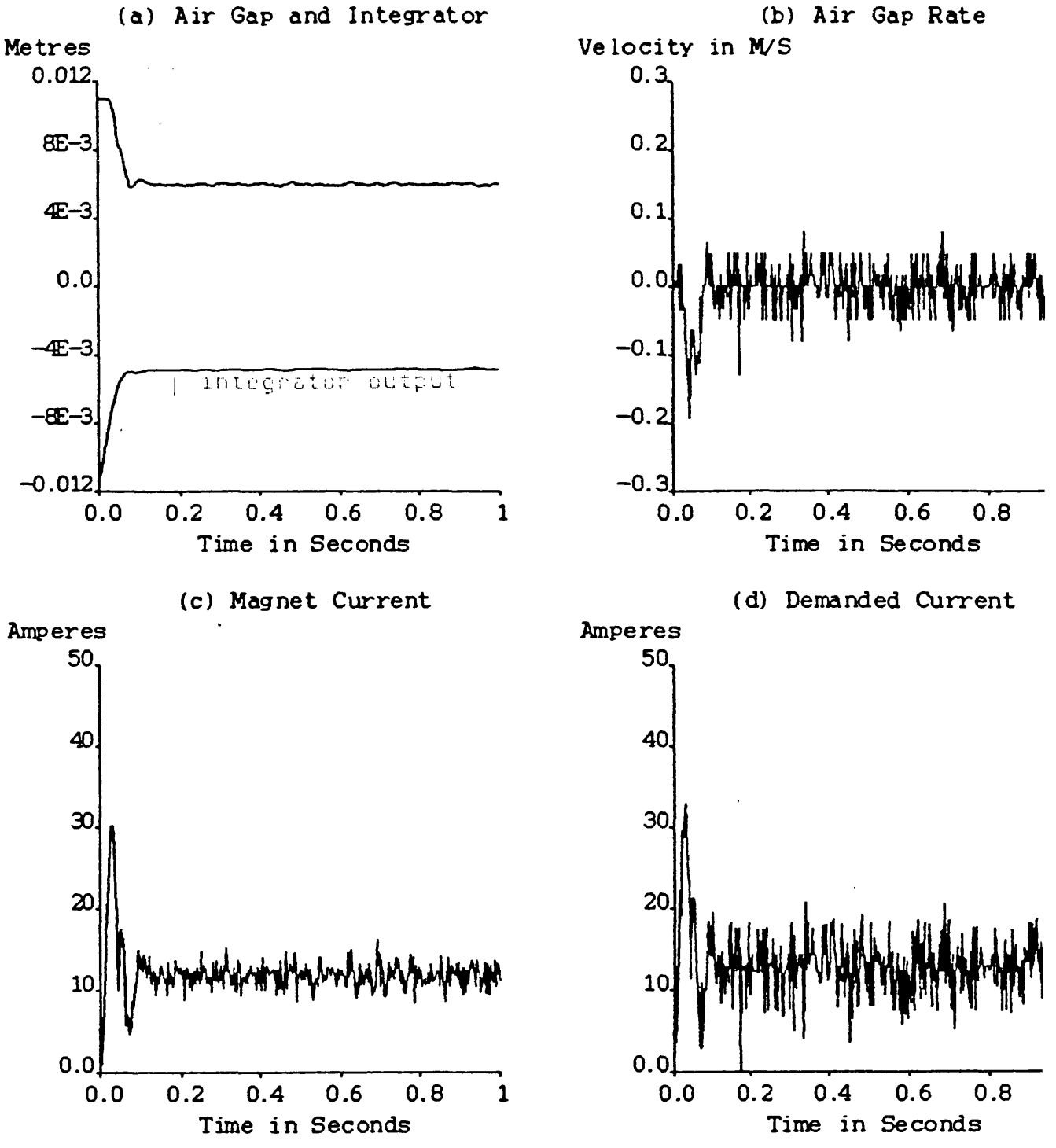

Figure 6.4.24 Levitation results for $h_o = 25$, $h_1 = 1$, $h_2 = 0.01$, $k = 10000$

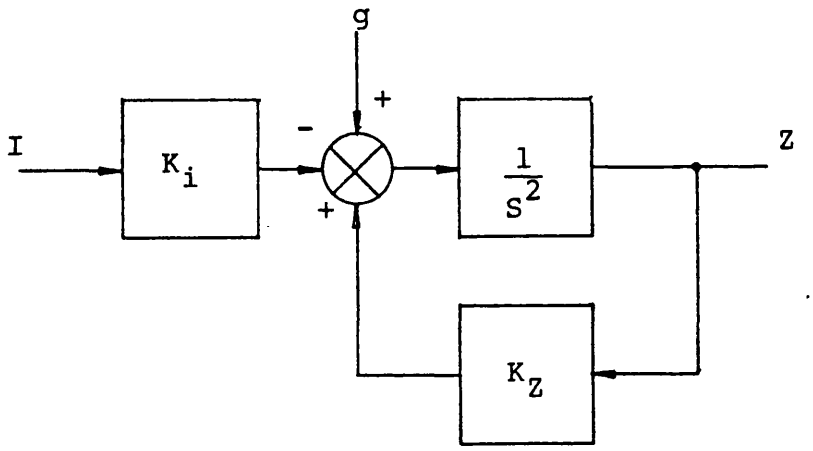

Figure 6.5.1 Block diagram of the open loop single corner LSM linearised system

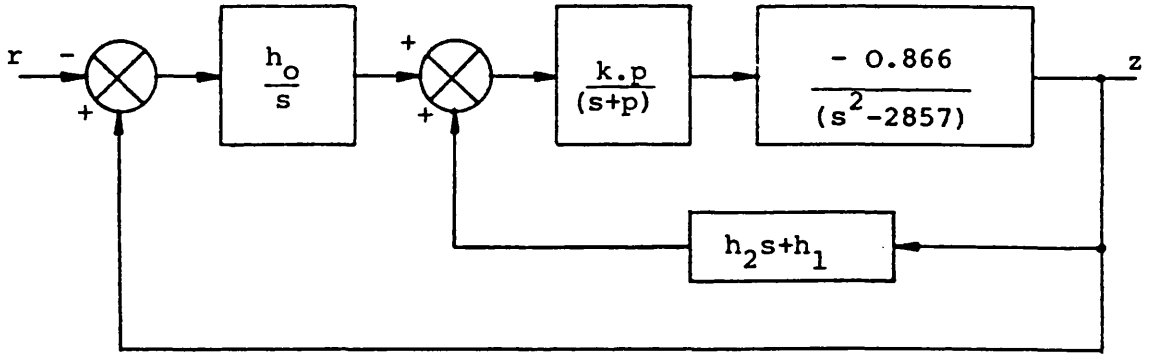

for Z_o = 0.7cm, I_o = 23.1 Amperes

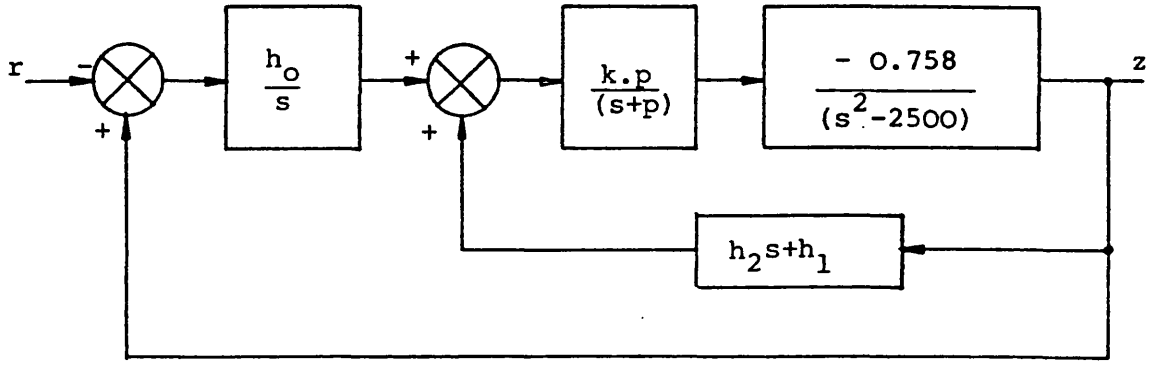

for Z_o = 0.8cm, I_o = 26.4 Amperes

Figure 6.5.2 Control loops for Z_o = 0.7cm and Z_o = 0.8cm

(a) 7mm air gap, p = 40

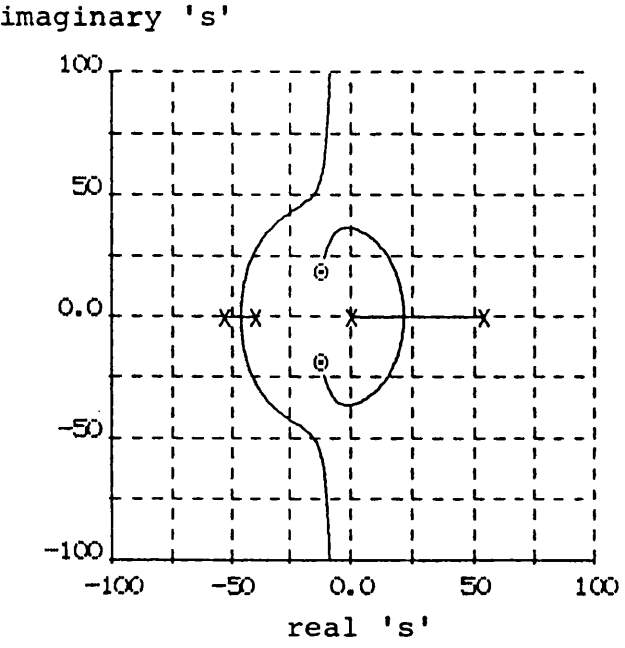

(b) 7mm air gap, no chopper

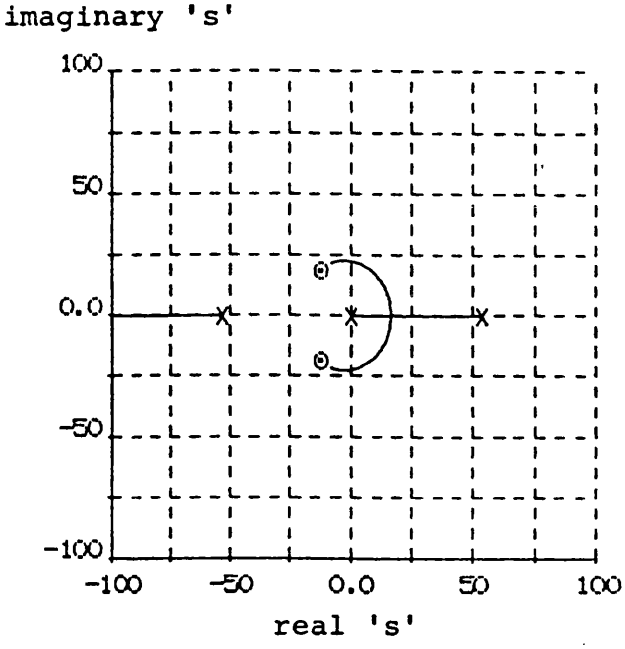

(c) 8mm air gap, p = 40

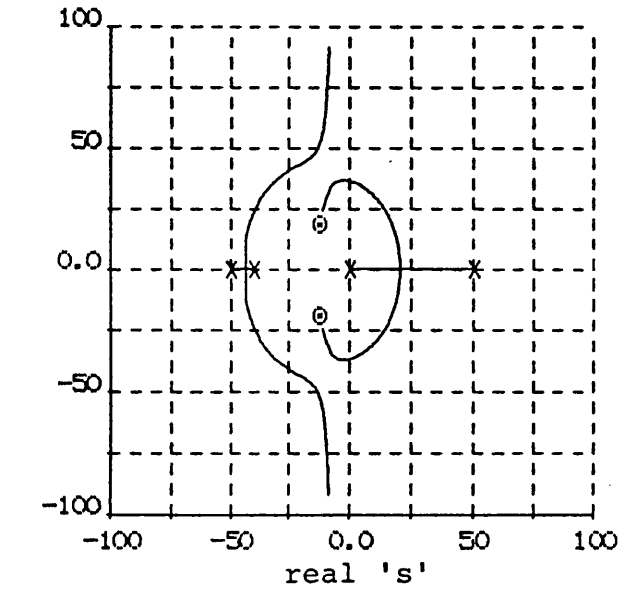

(d) 8mm air gap, no chopper

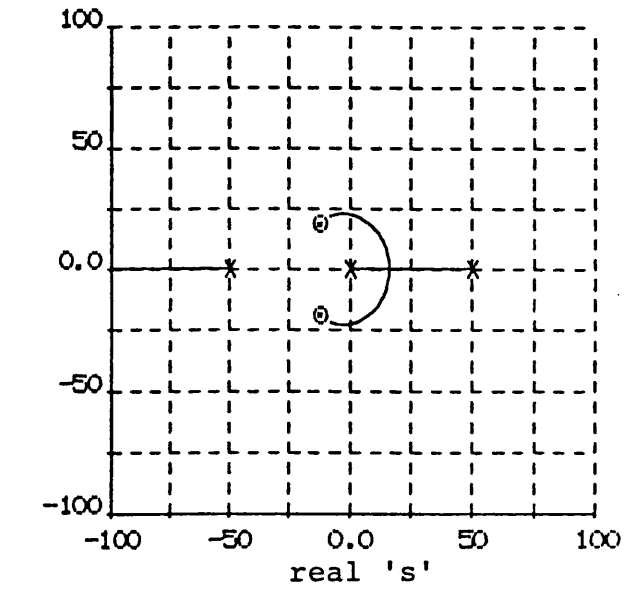

Figure 6.5.3 Root loci for 7mm and 8mm air gaps with and without the chopper pole, for h_o = 20, h_1 = 1, h_2 = 0.04, K = 10000

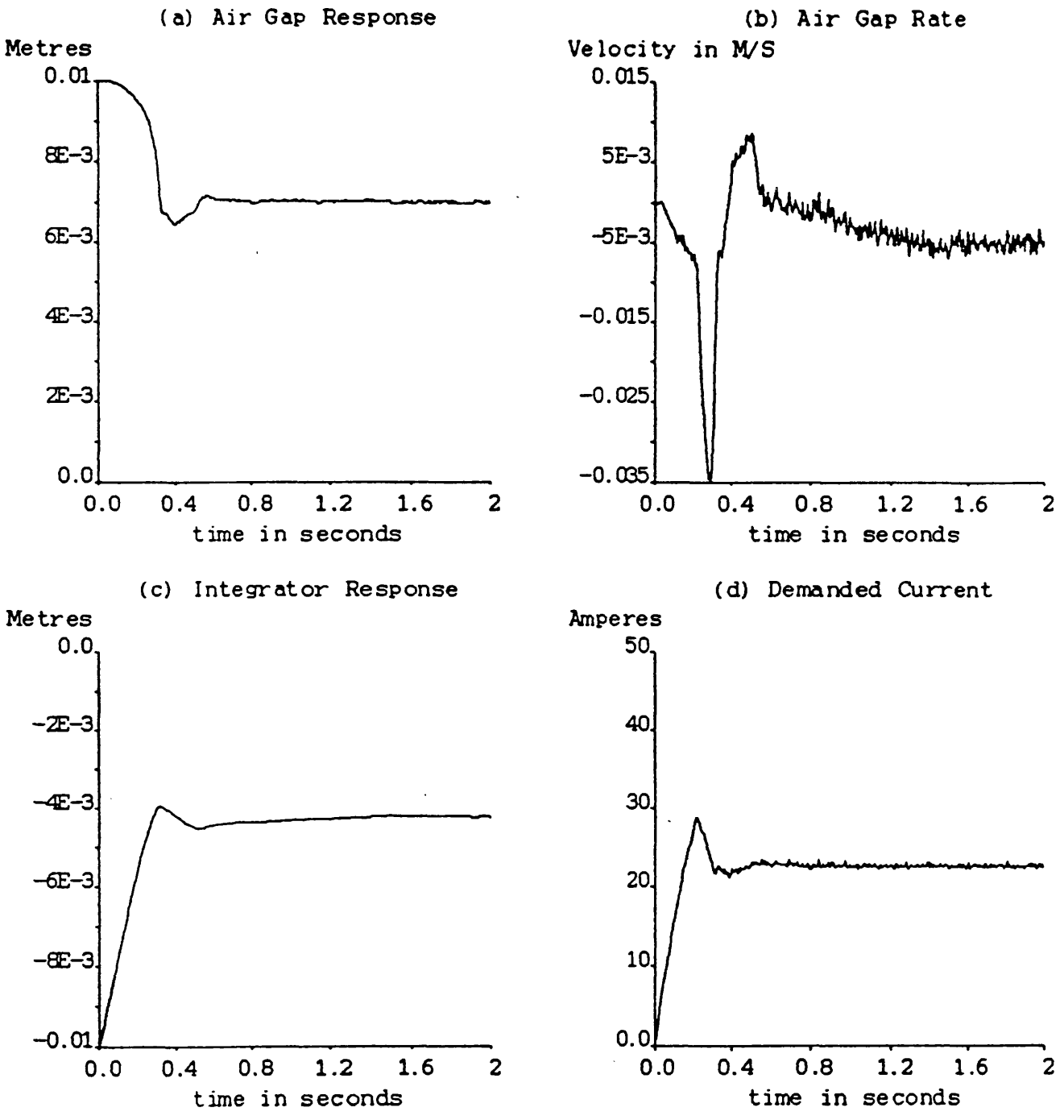

Figure 6.5.4 Levitation results for a single corner L.S.M. for an air gap of 7 mm

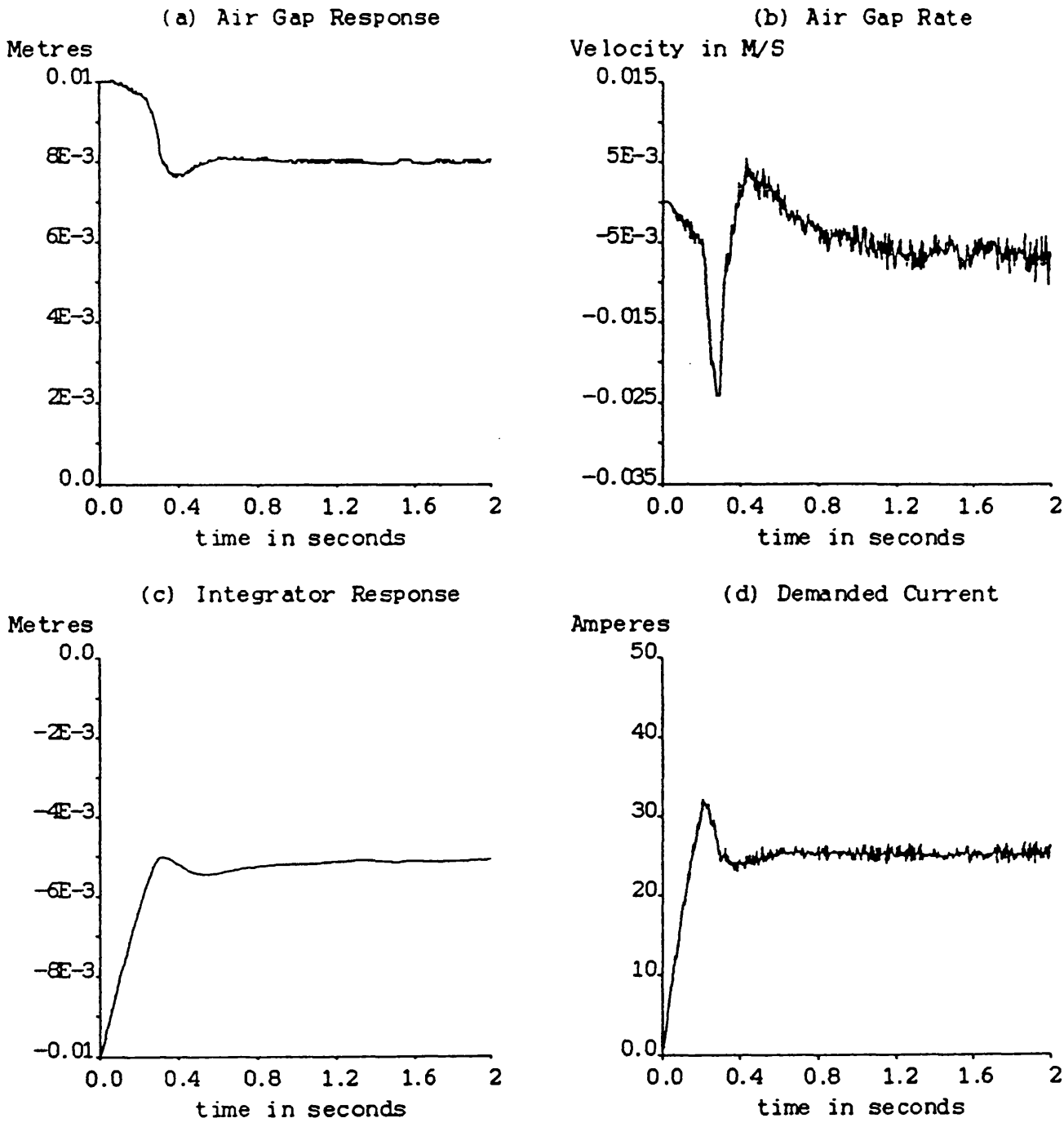

Figure 6.5.5 Levitation results for a single corner L.S.M. for an air gap of 8 mm

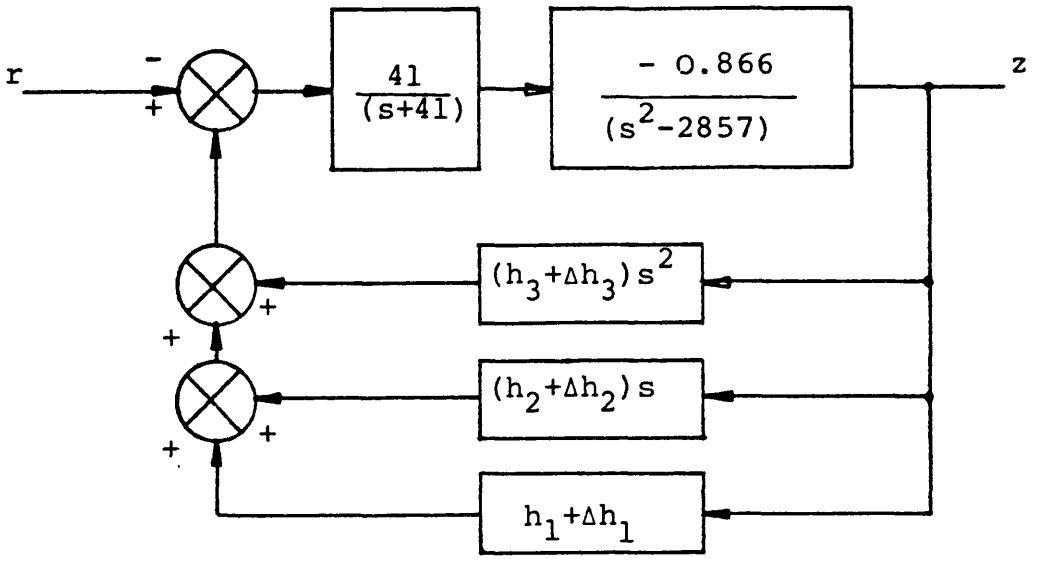

Figure 6.6.1 Basic variable structure control system for the MAGLEV vehicle

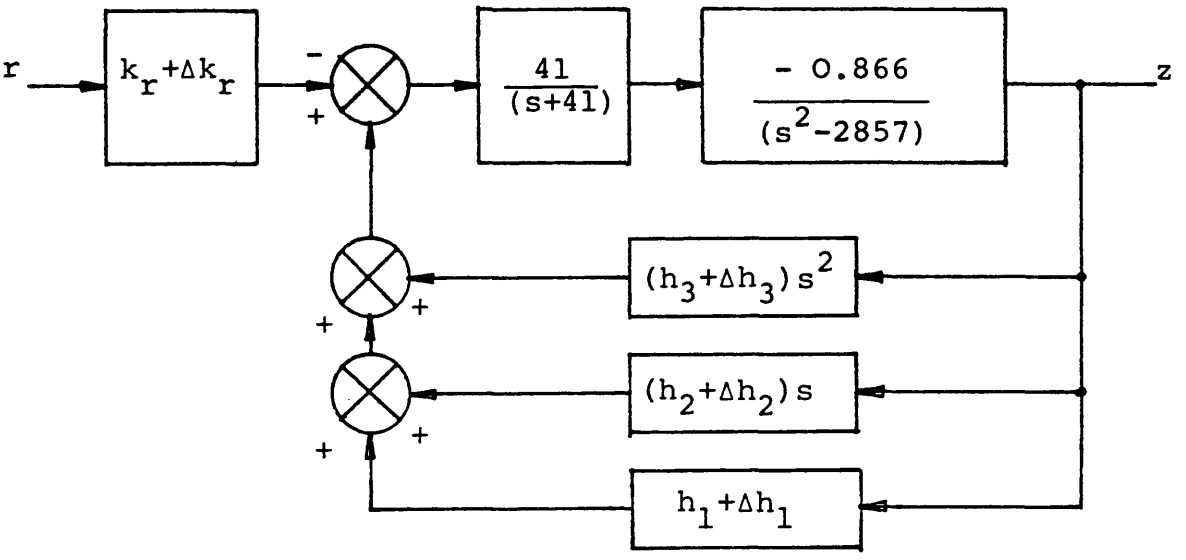

Figure 6.6.2 Variable structure control system including switching reference input gain

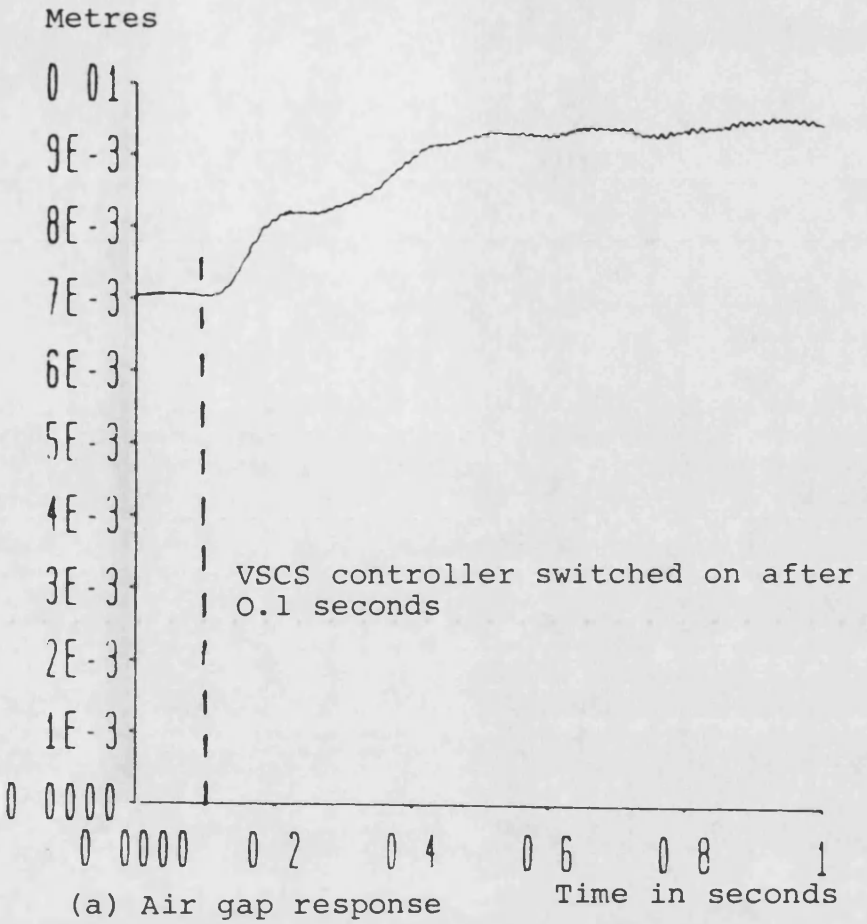

(a) Air gap response

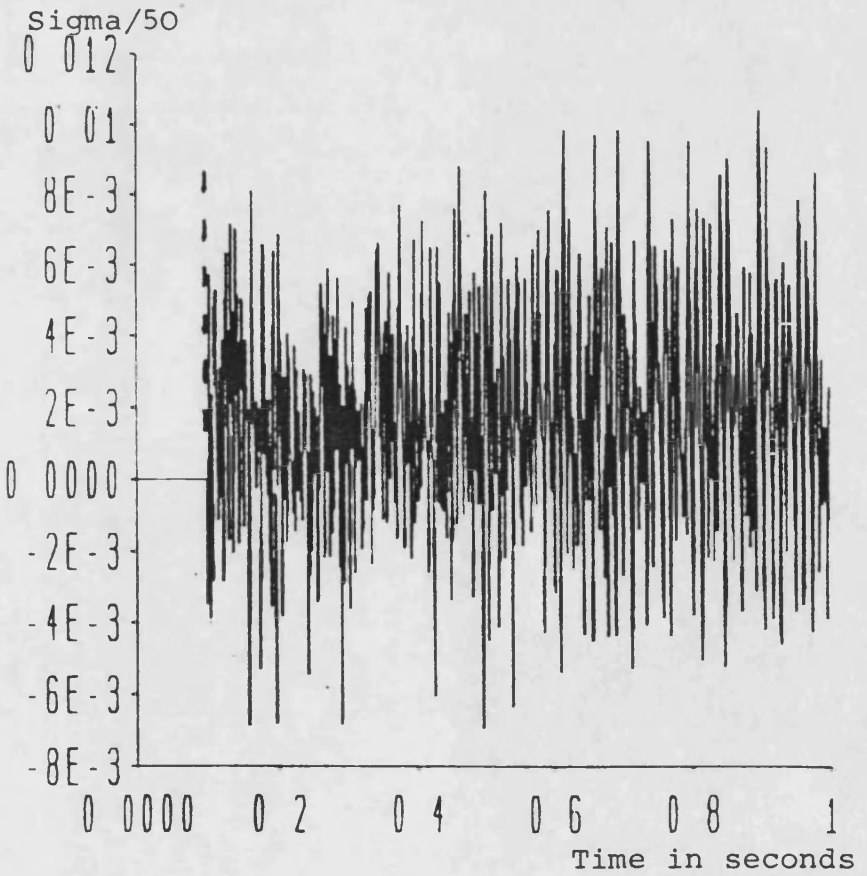

(b) Time history of sigma

Figure 6.6.3 Levitation results for a VSCS controller for ω_n = 15.0, ξ = 0.7071

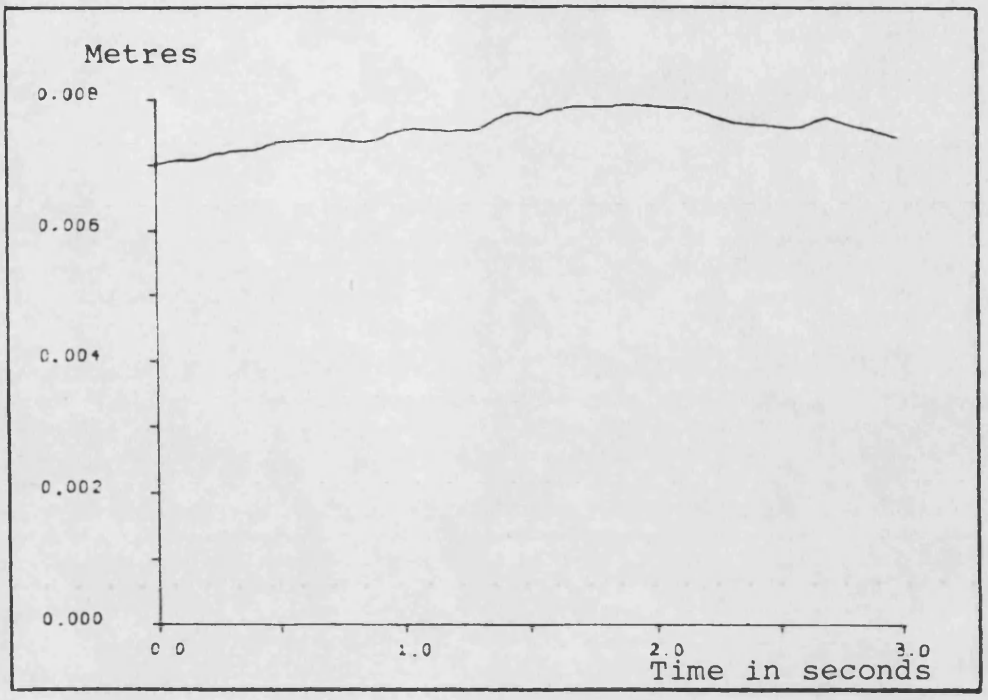

(a) Air gap response

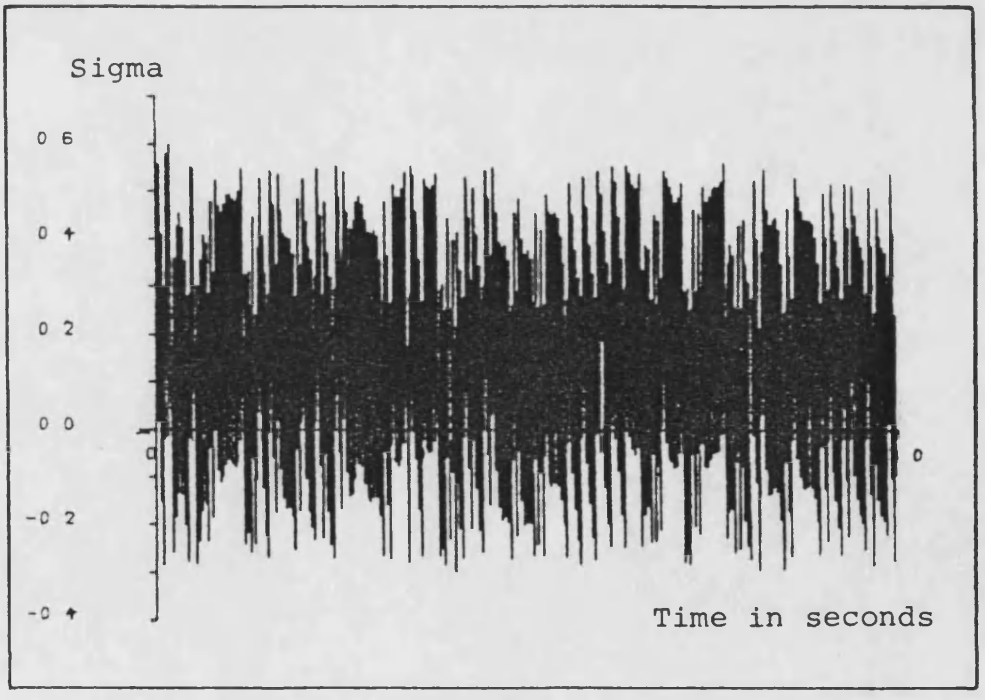

(b) Time history of sigma

Figure 6.6.4 Simulation results for a VSCS controller for ω_n = 15.0, ξ = 0.7071

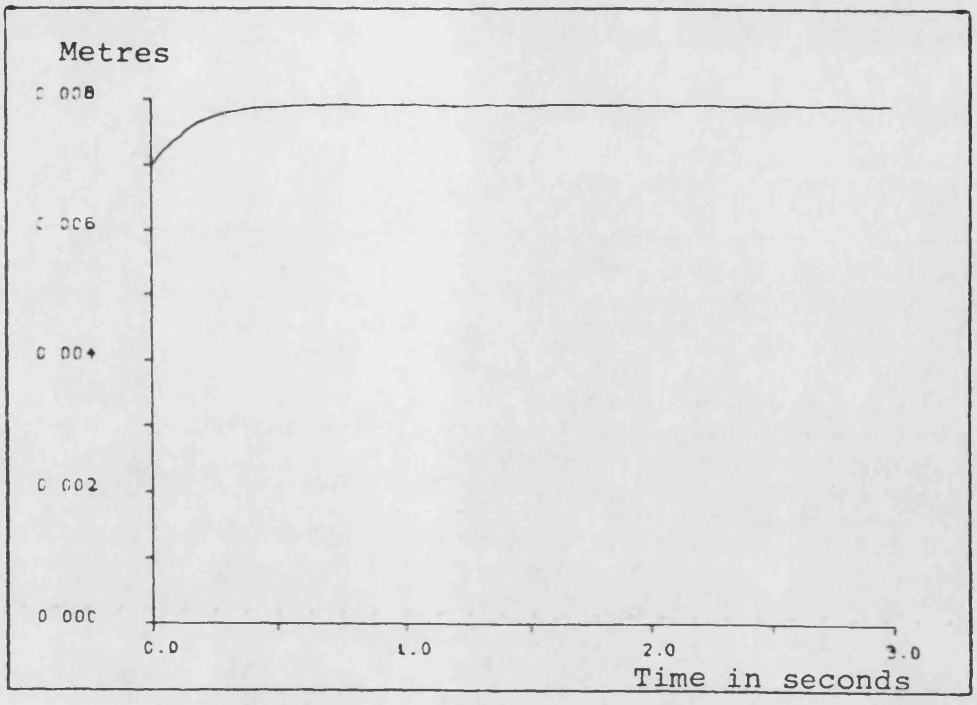

(a) Air gap response

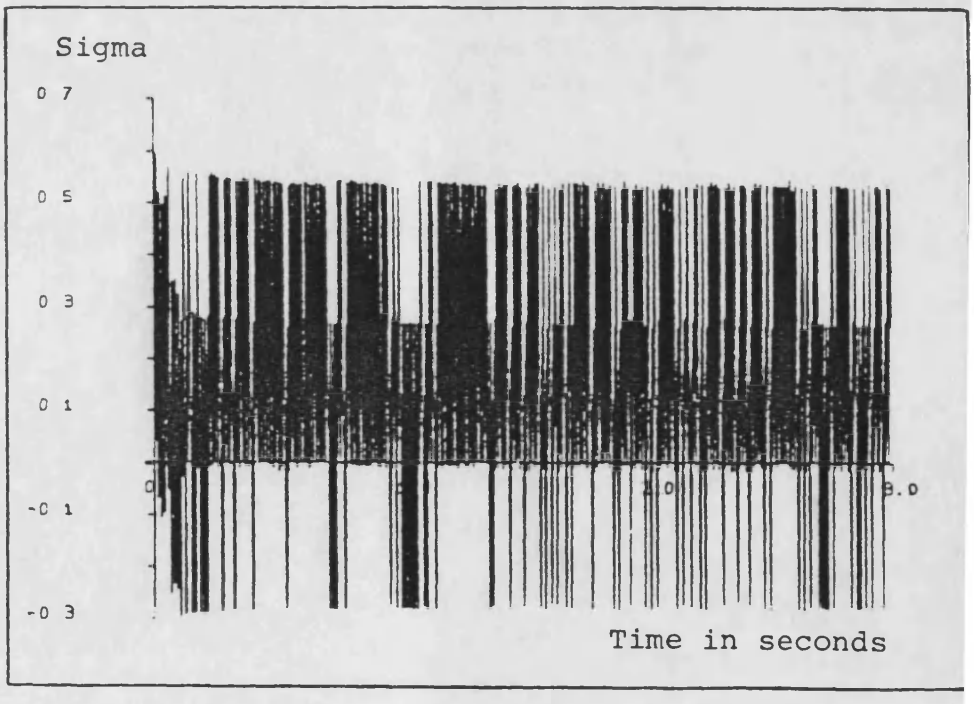

(b) Time history of sigma

Figure 6.6.5 Simulation results for a VSCS controller with digital transducer quantisation and noise removed

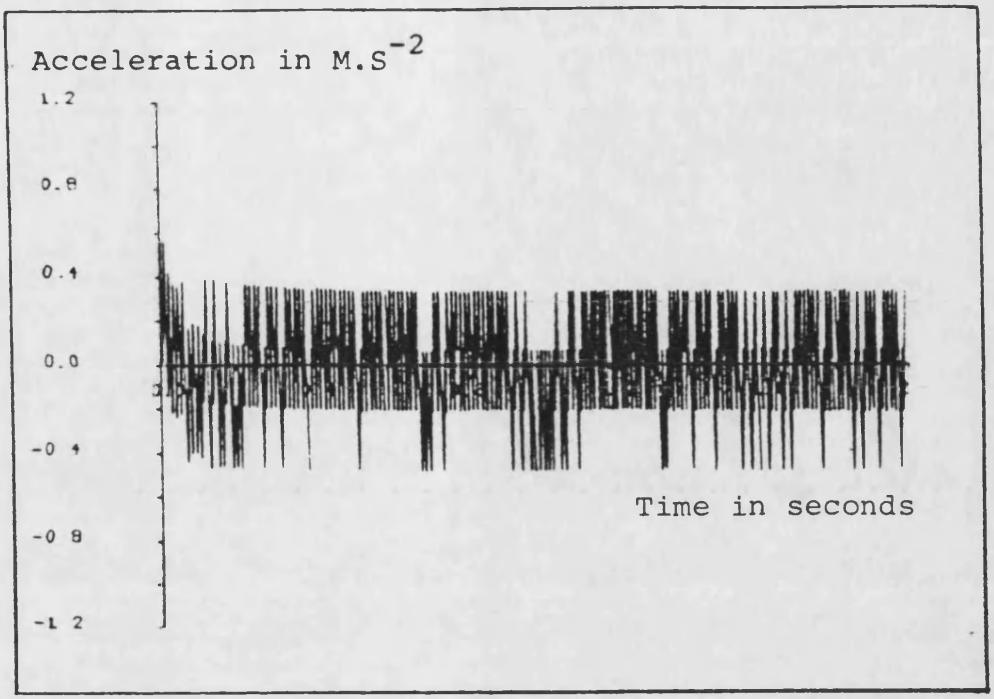

(a) Acceleration of air gap response

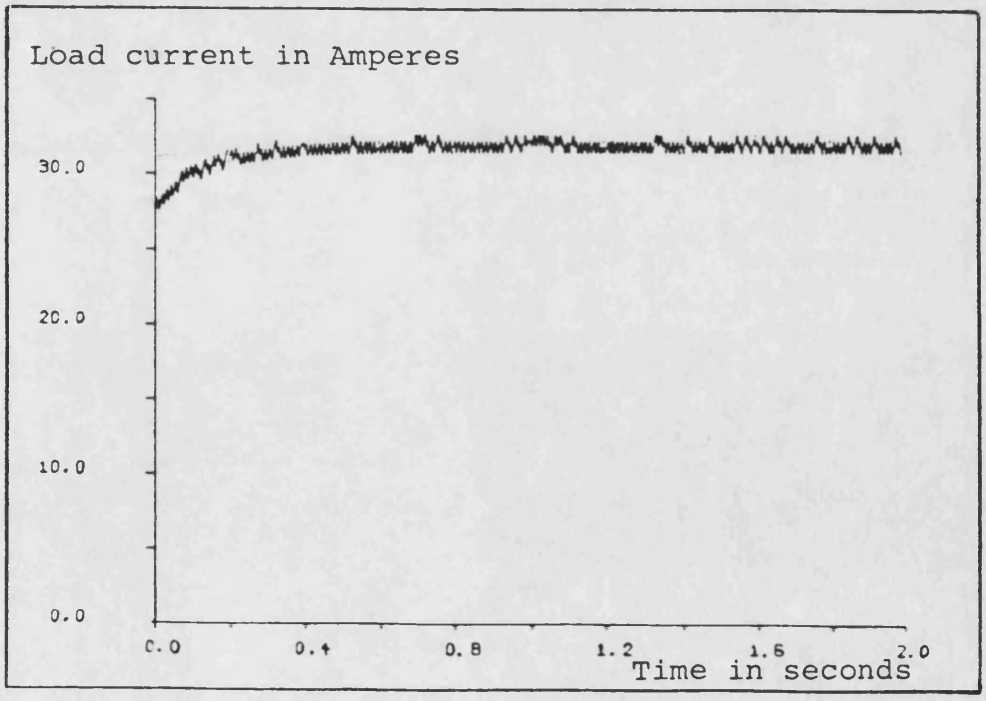

(b) Load current response

Figure 6.6.6 Simulated acceleration and chopper load current with digital transducer quantisation and noise removed

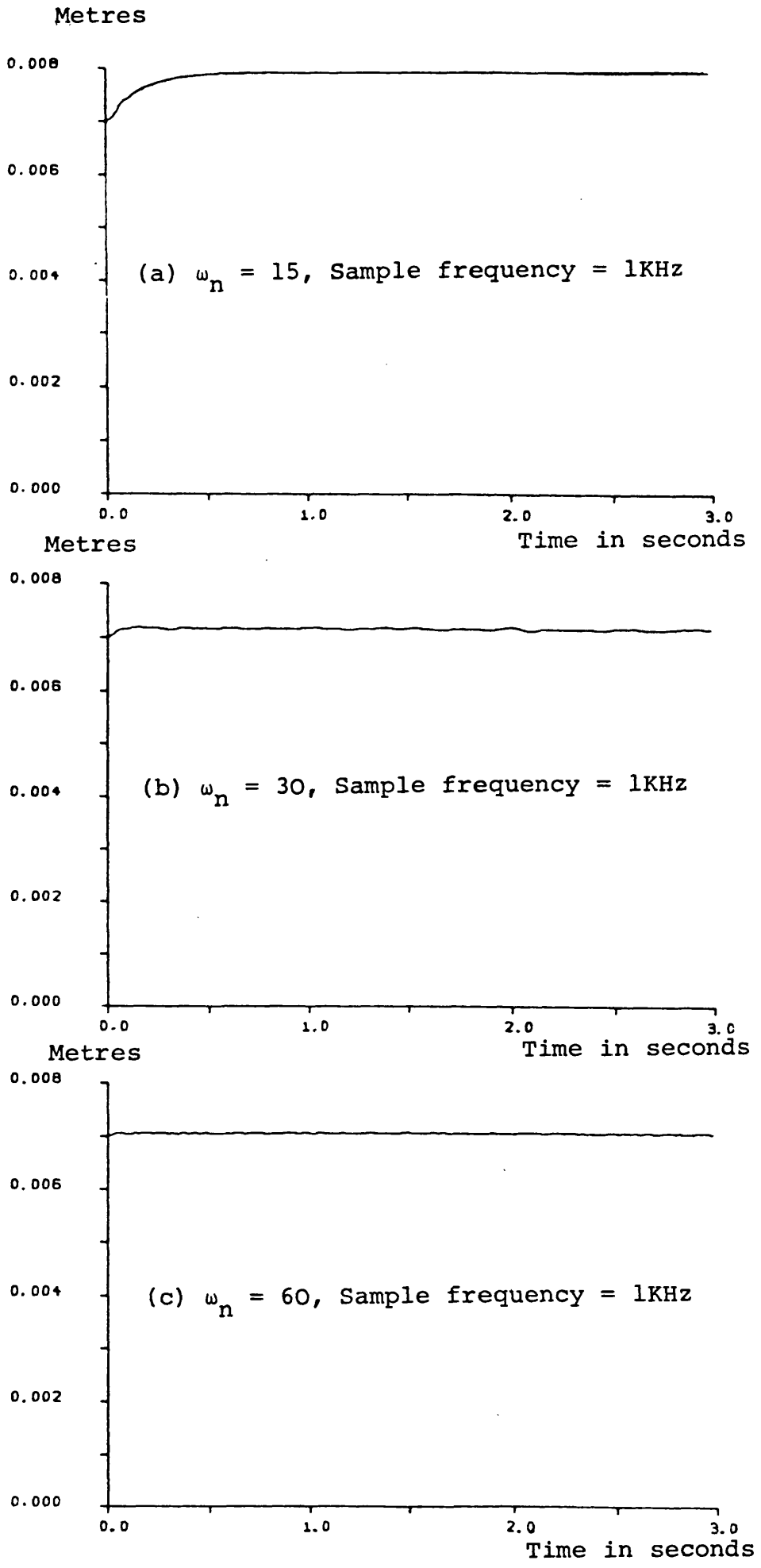

Figure 6.6.7 Simulated results showing the effect of designing for faster dynamic response

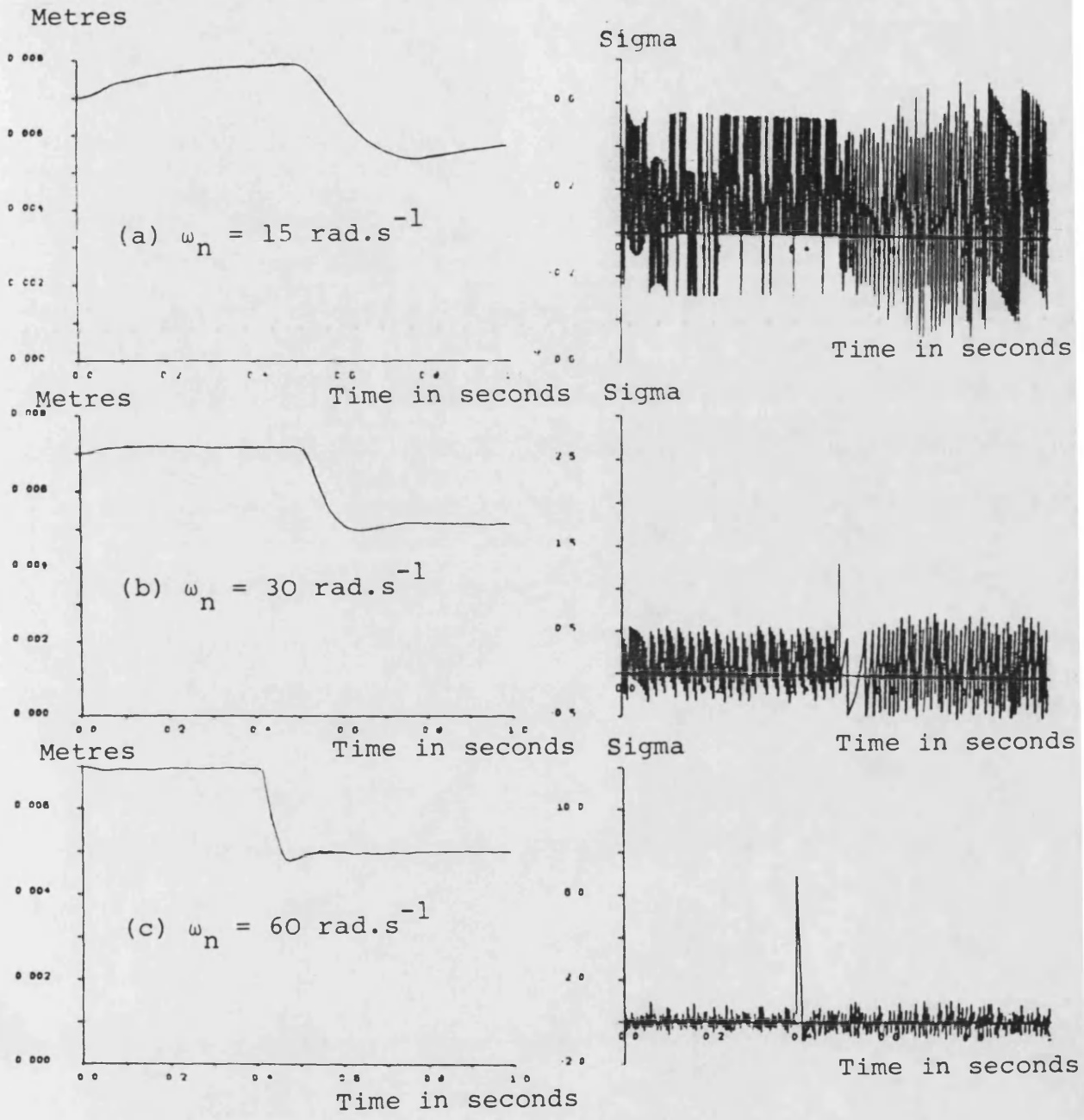

Figure 6.6.8 Simulation results showing step responses for various system dynamic response speeds

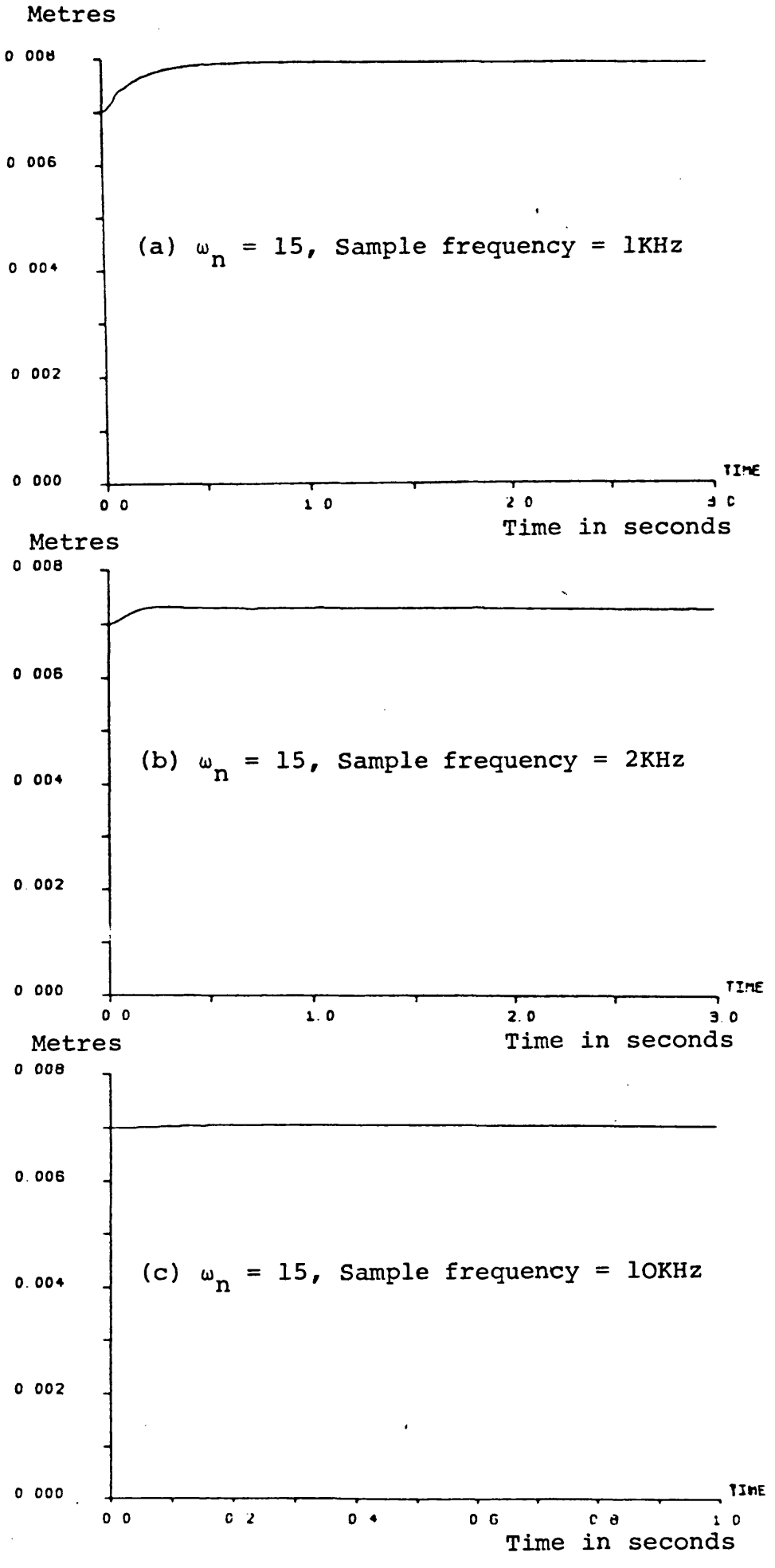

Figure 6.6.9 Simulation results showing the effect on the air gap drift of using higher sample rates for the digital controller

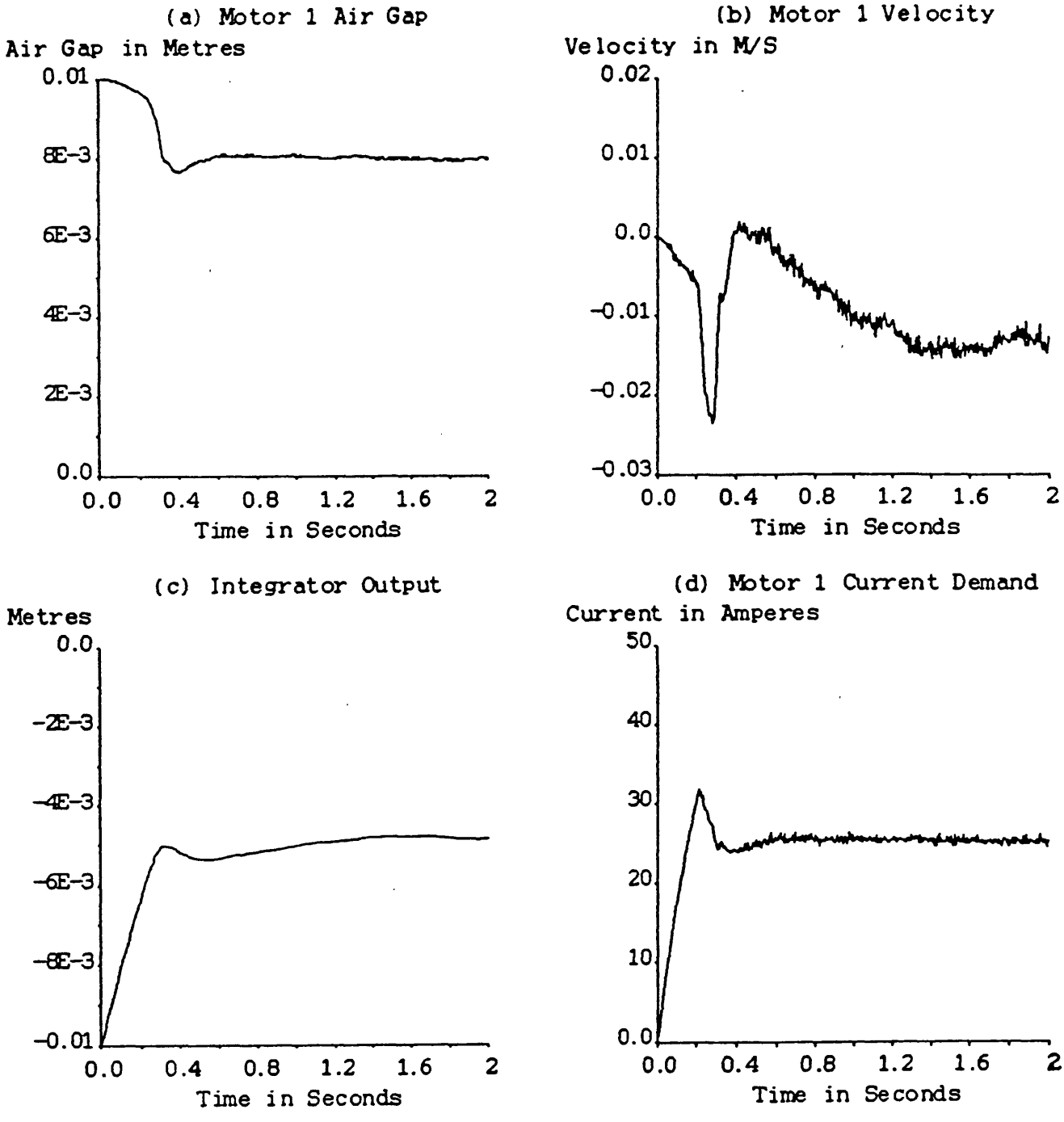

Figure 7.2.1 Motor 1 response on 'lift-off' of the two L.S.M. system

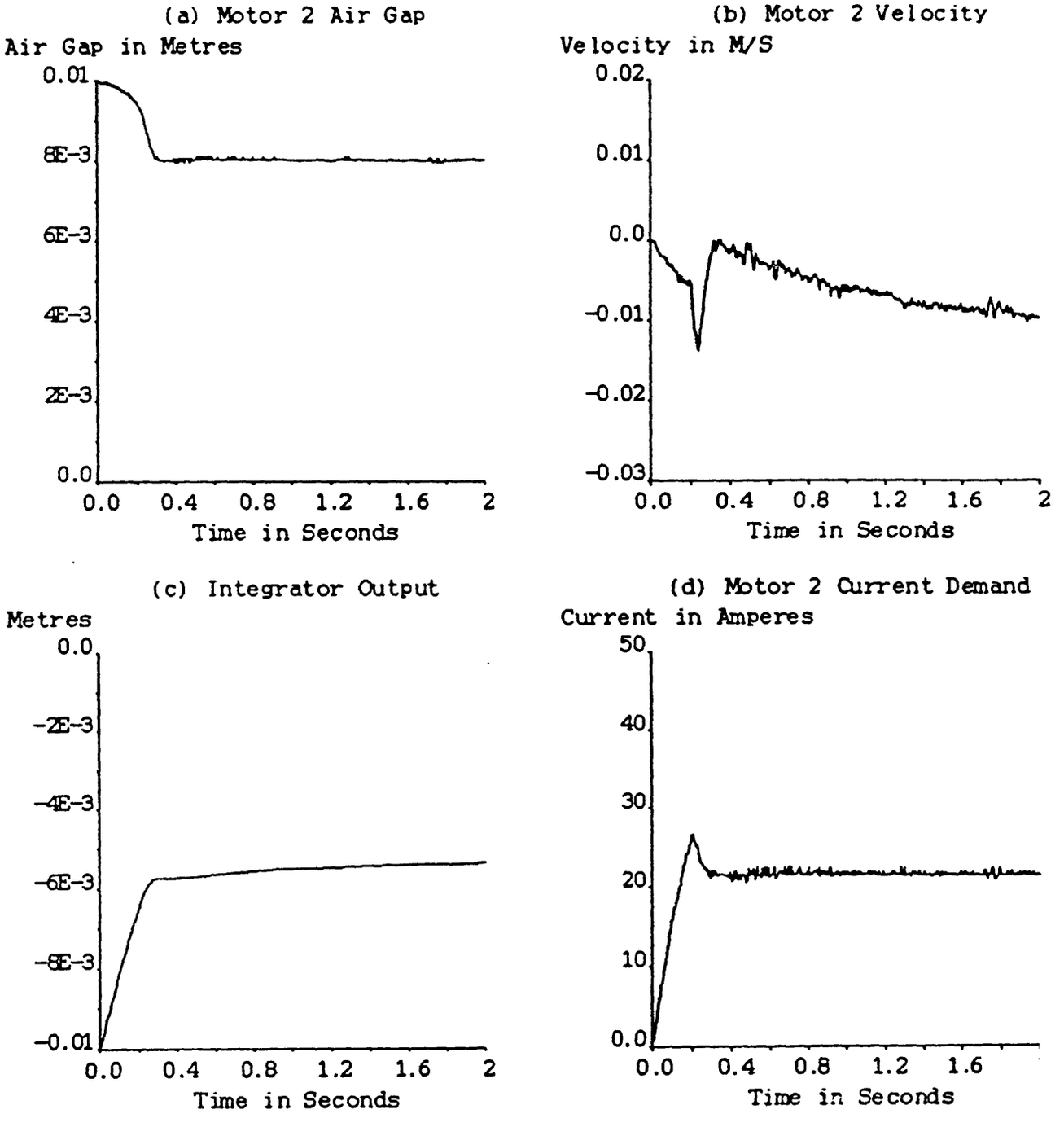

Figure 7.2.2 Motor 2 response on 'lift-off' of the two L.S.M. system

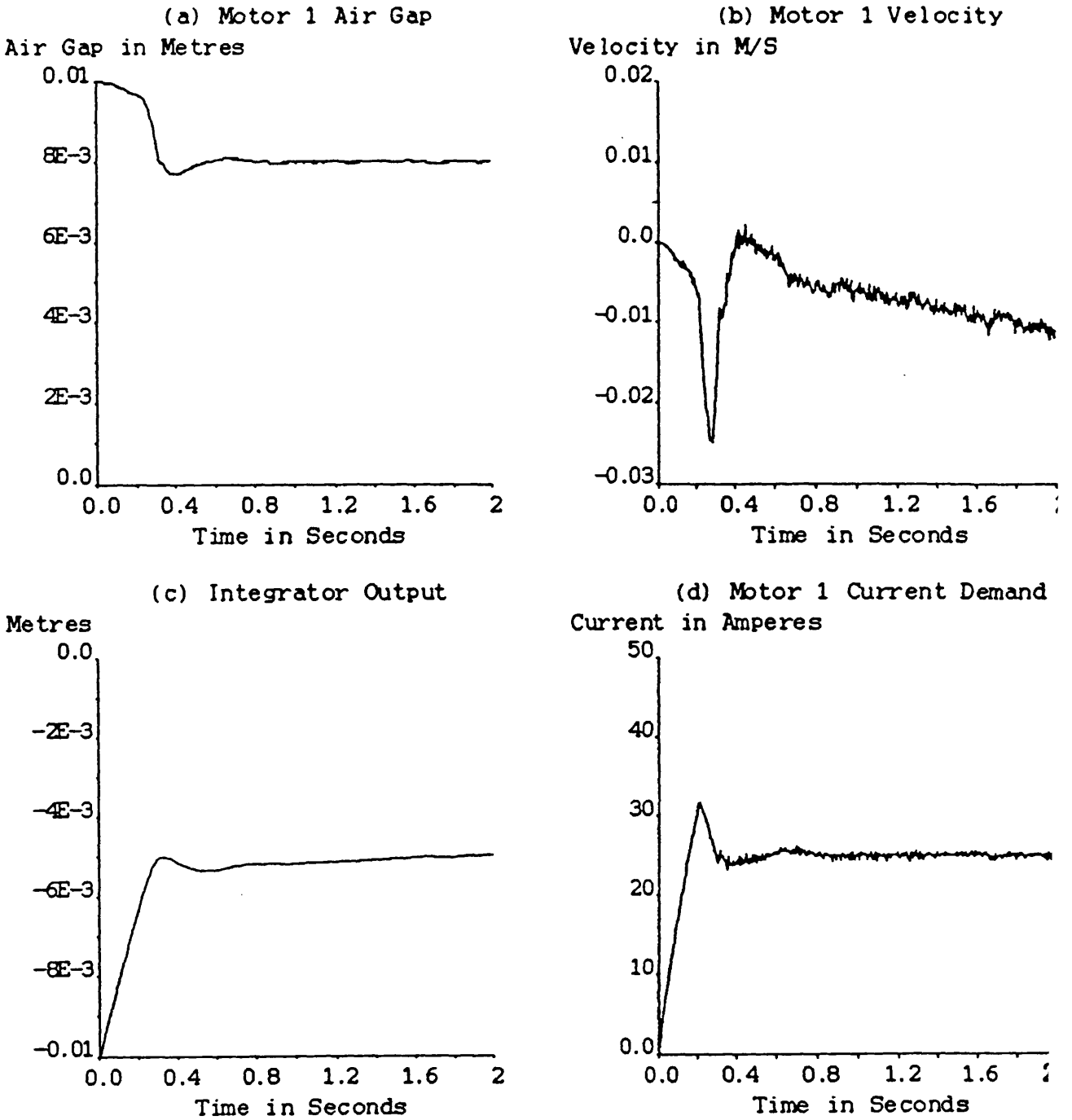

Figure 7.2.3 Motor 1 response on 'lift-off' with the pivot 5 cm towards motor 4

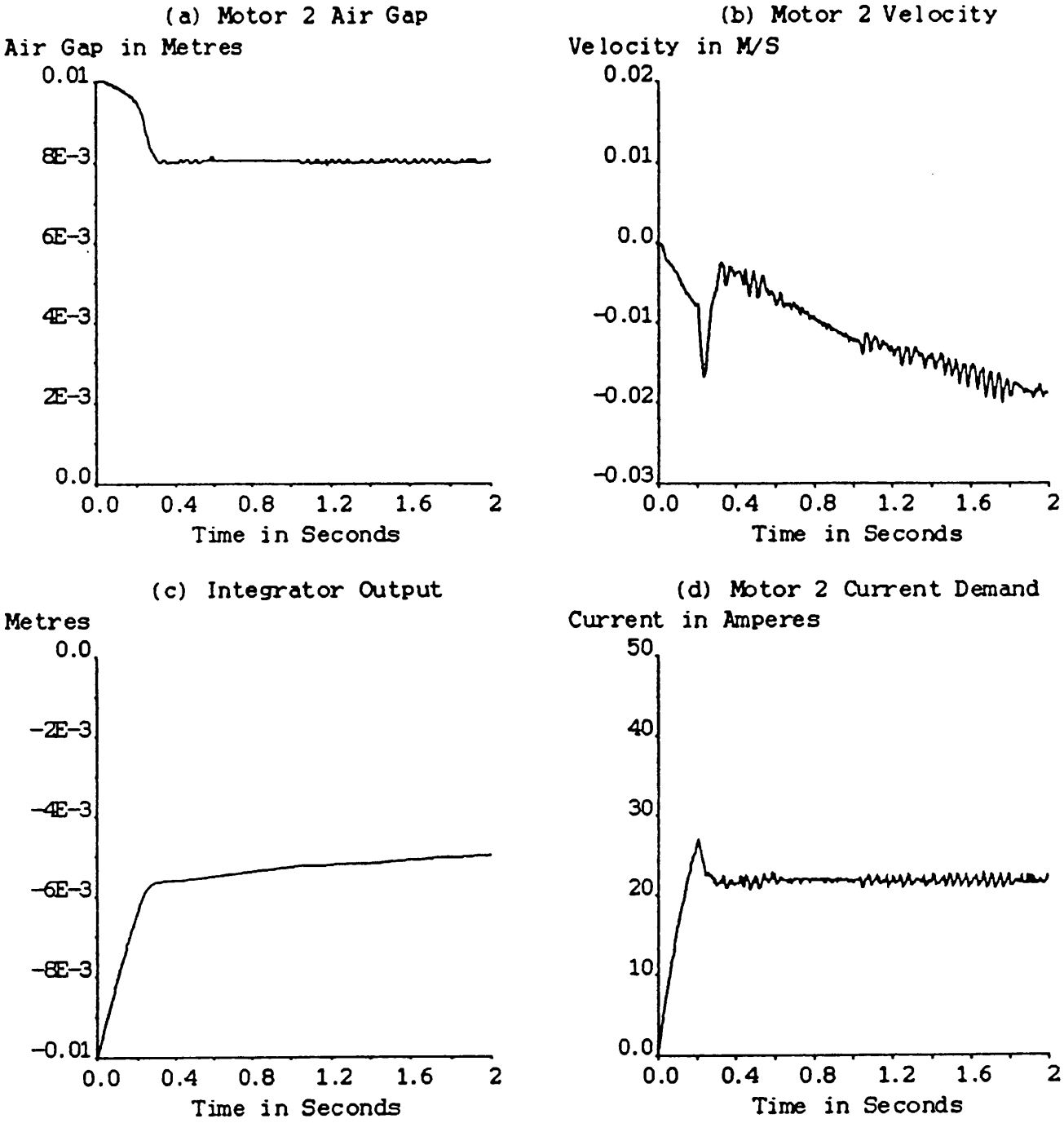

Figure 7.2.4 Motor 2 response on 'lift-off' with the pivot 5 cm towards motor 4

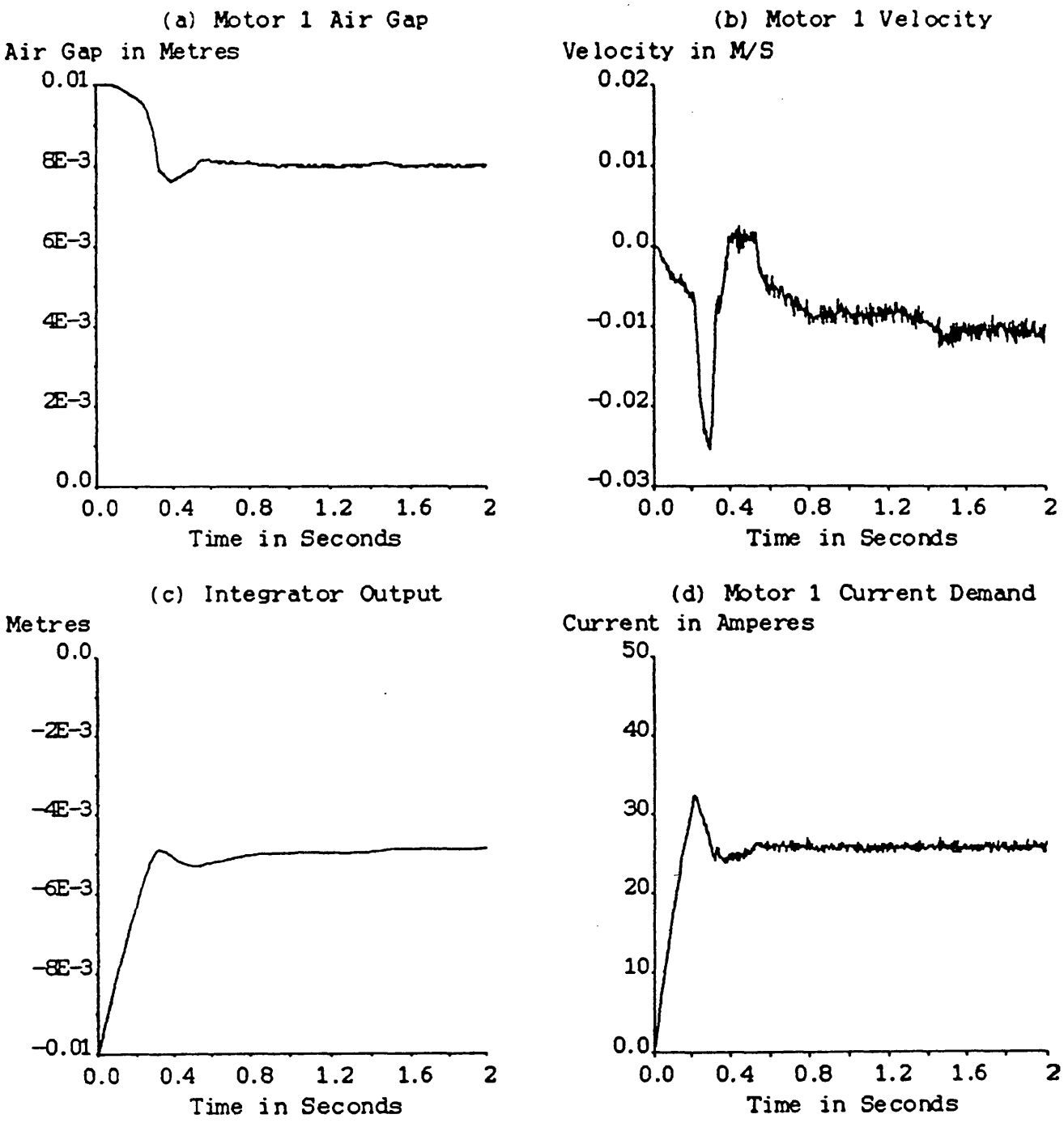

Figure 7.2.5 Motor 1 response on 'lift-off' with the pivot 5 cm towards motor 3

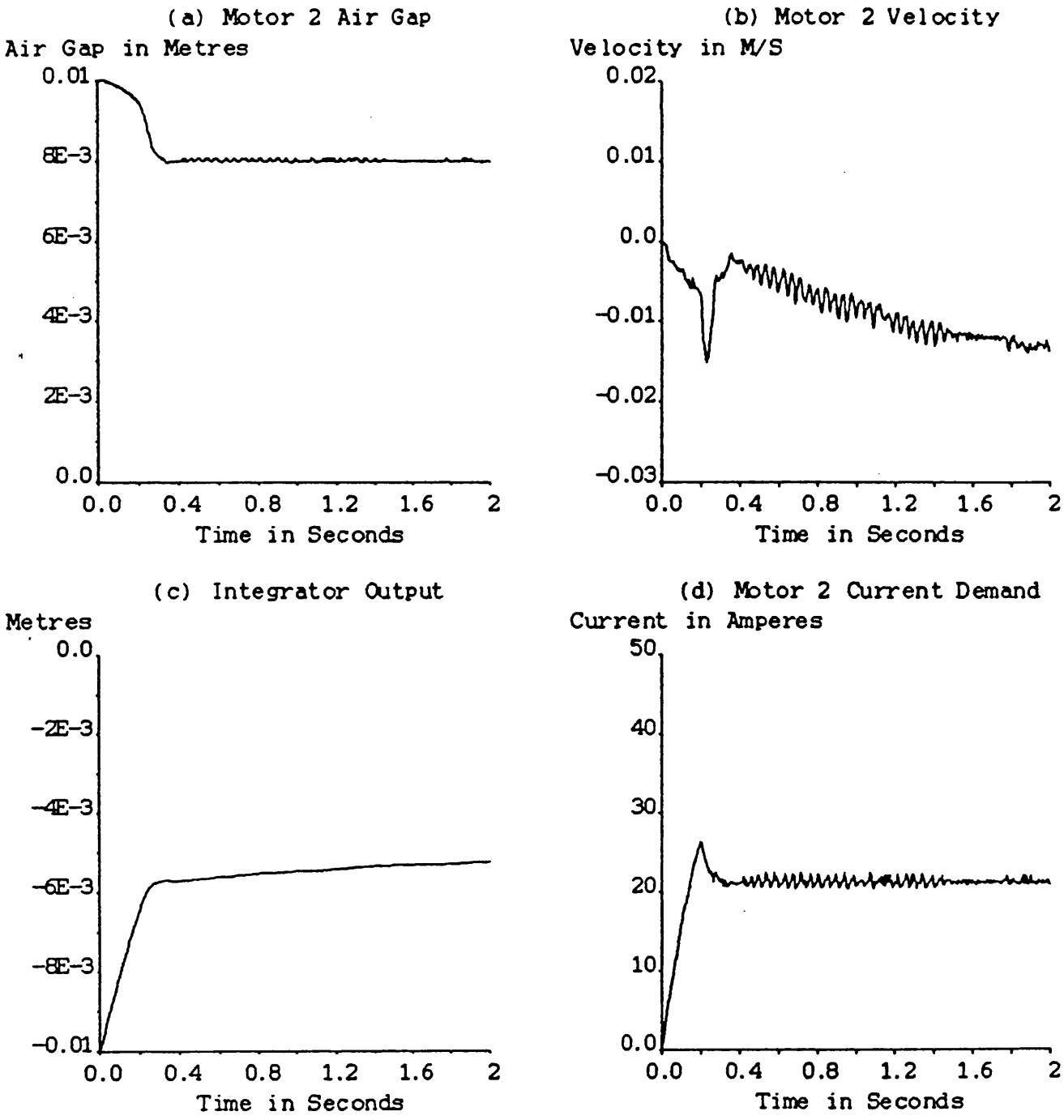

Figure 7.2.6 Motor 2 response on 'lift-off' with the pivot 5 cm towards motor 3

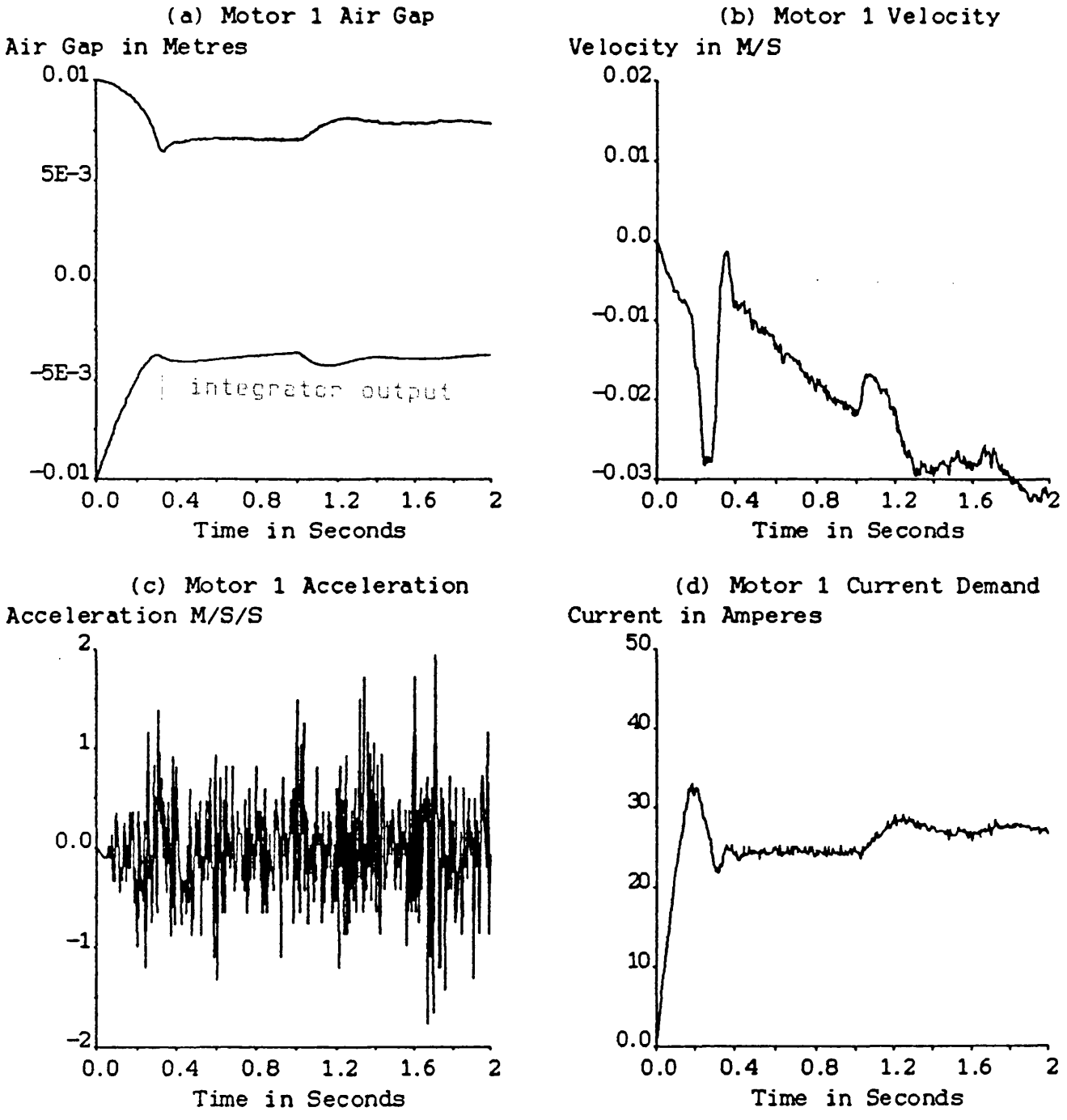

Figure 7.2.7 Motor 1 response for decoupling test of a step in motor 1 air gap of 1 mm

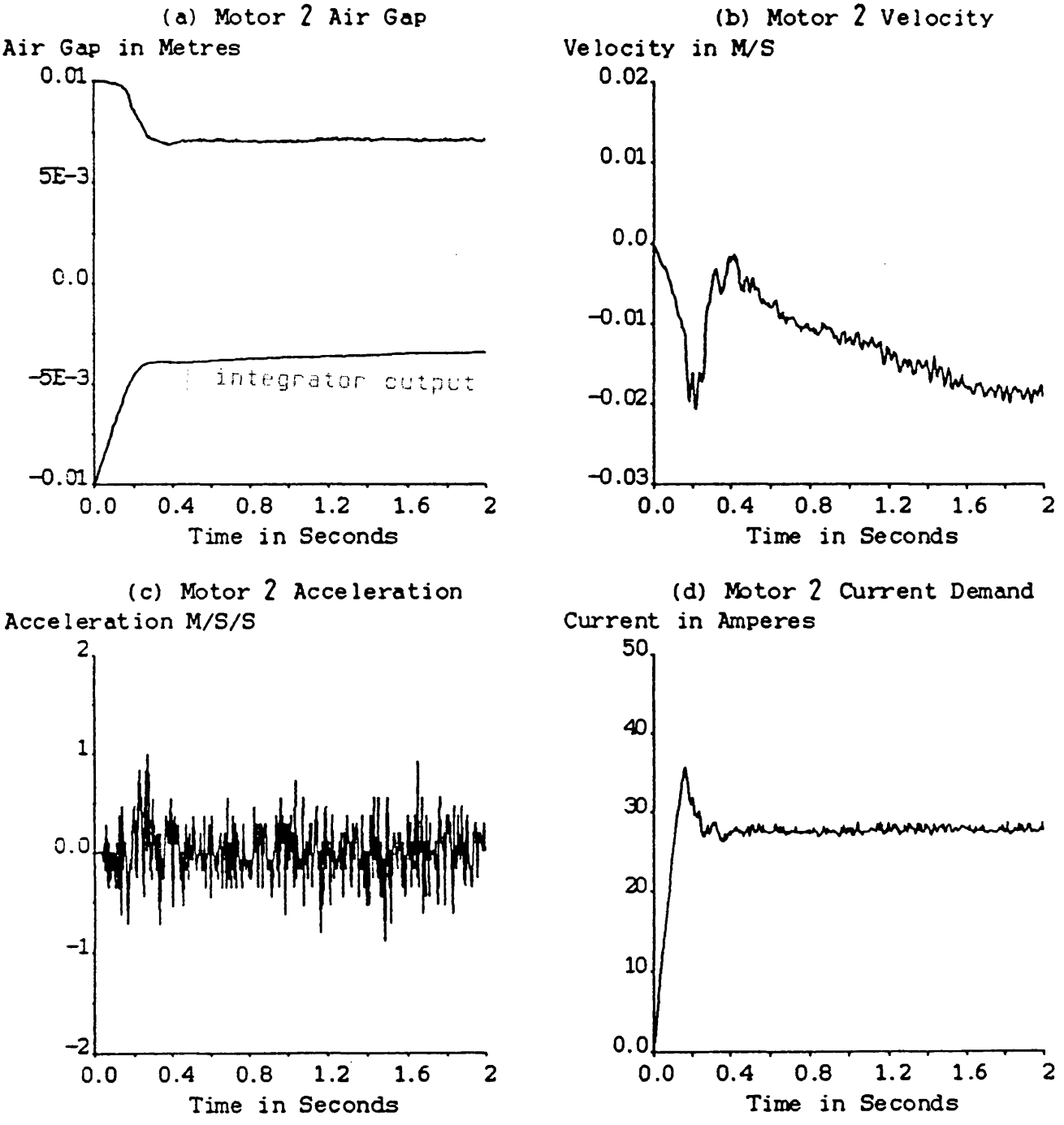

Figure 7.2.8 Motor 2 response for decoupling test of a step in motor 1 air gap of 1 mm

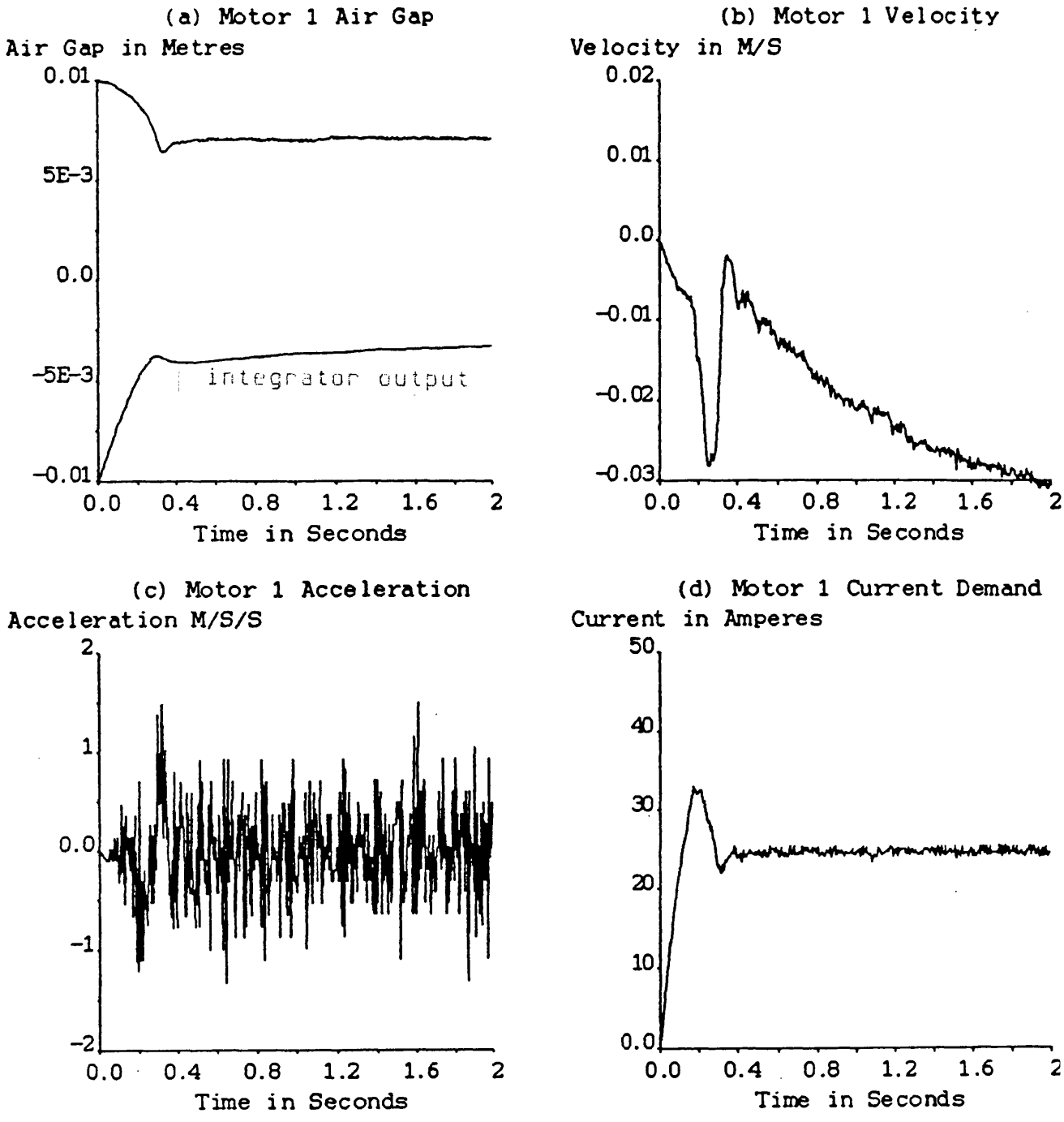

Figure 7.2.9 Motor 1 response for decoupling test of a step in motor 2 air gap of 1 mm

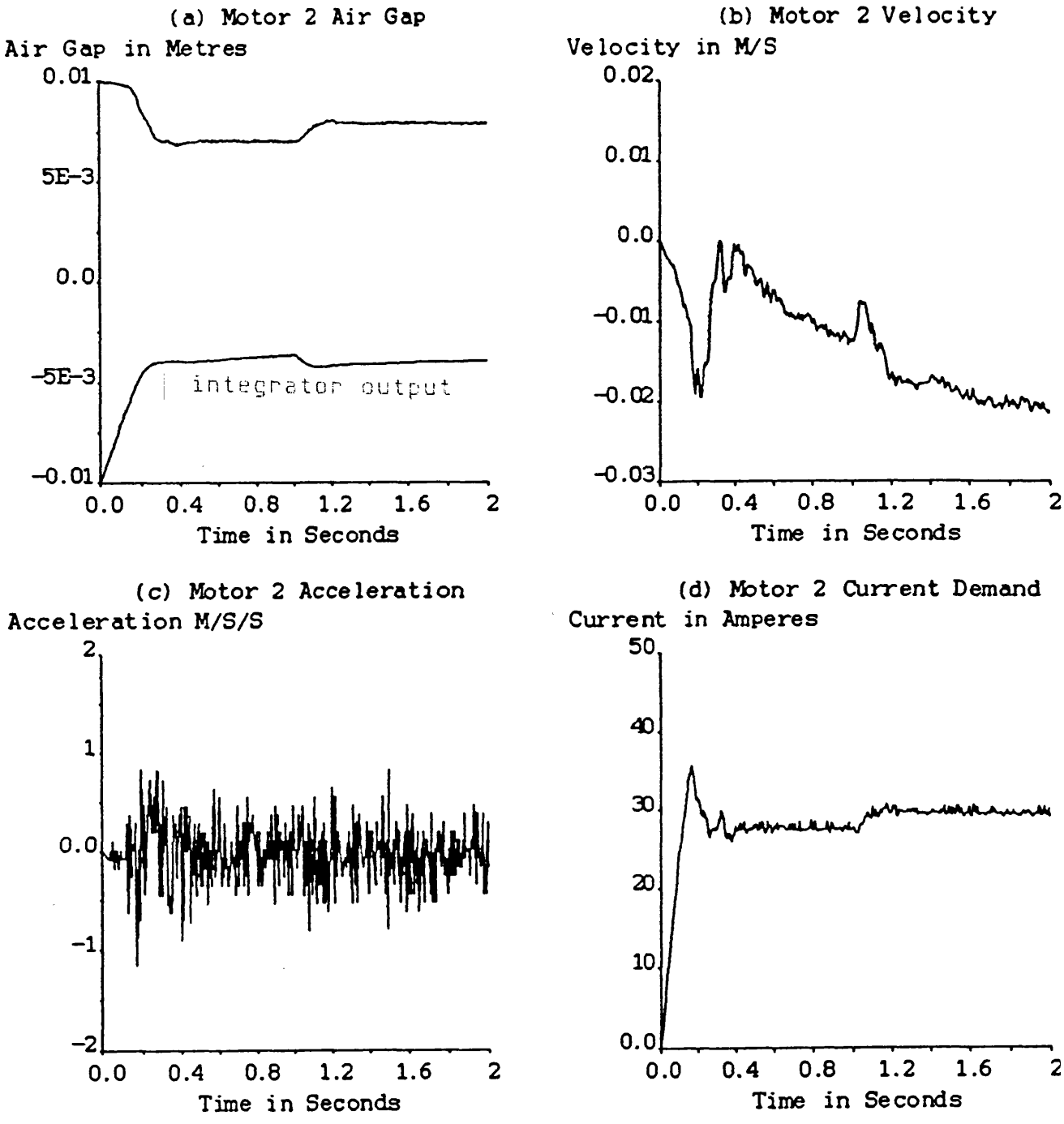

Figure 7.2.10 Motor 2 response for decoupling test of a step in motor 2 air gap of 1 mm

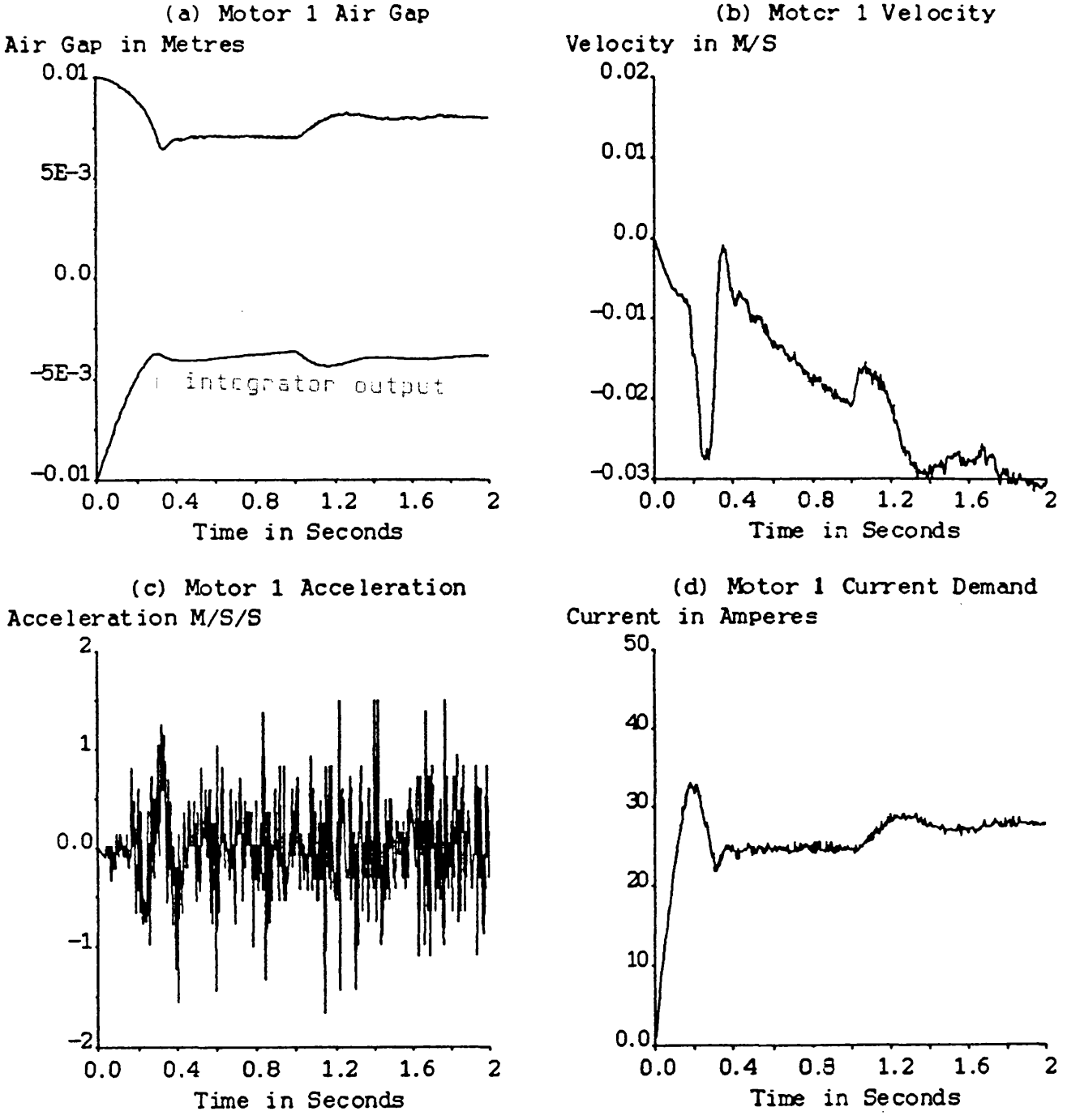

Figure 7.2.11 Motor 1 response for decoupling test of a step in both motors air gap of 1 mm

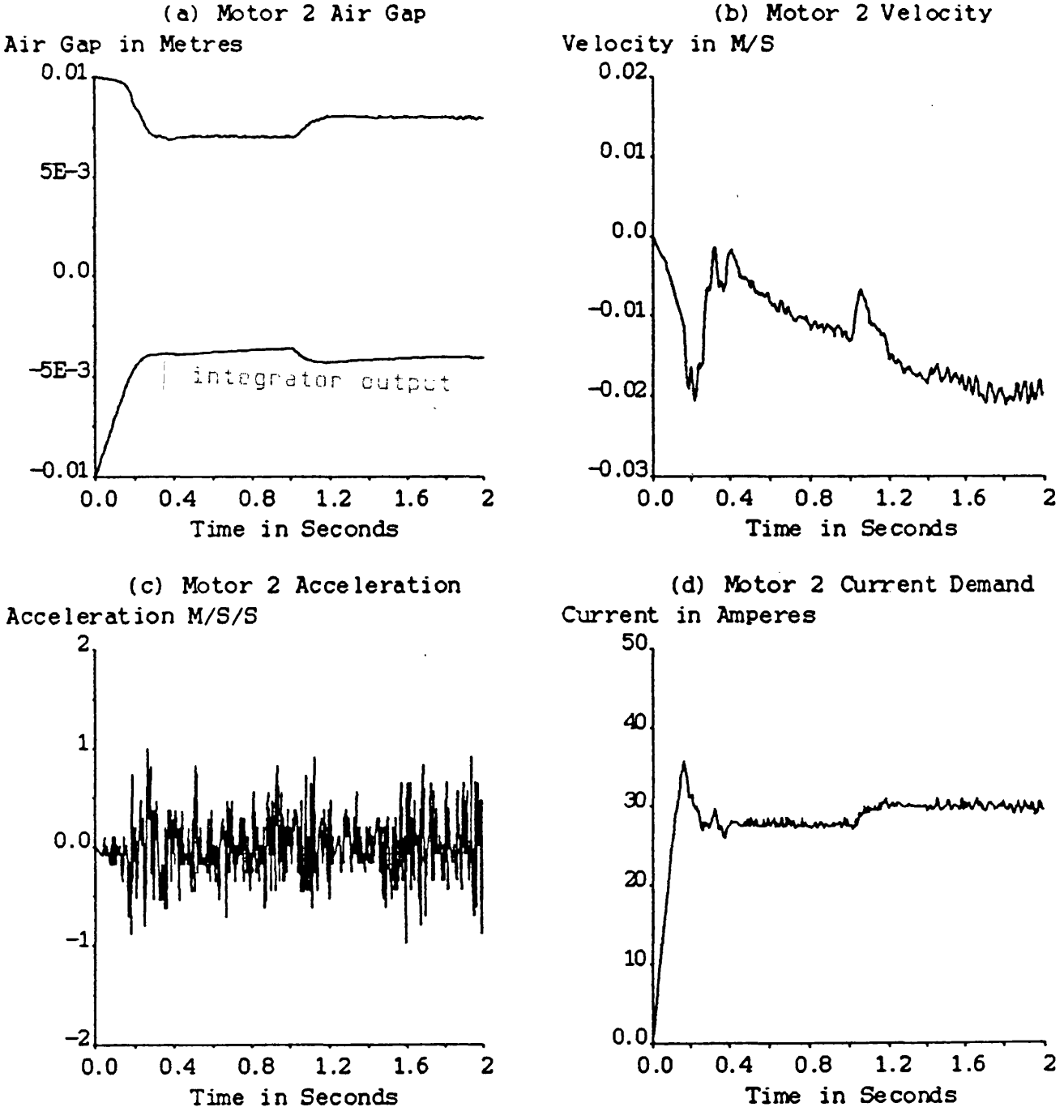

Figure 7.2.12 Motor 2 response for decoupling test of a step in both motors air gap of 1 mm

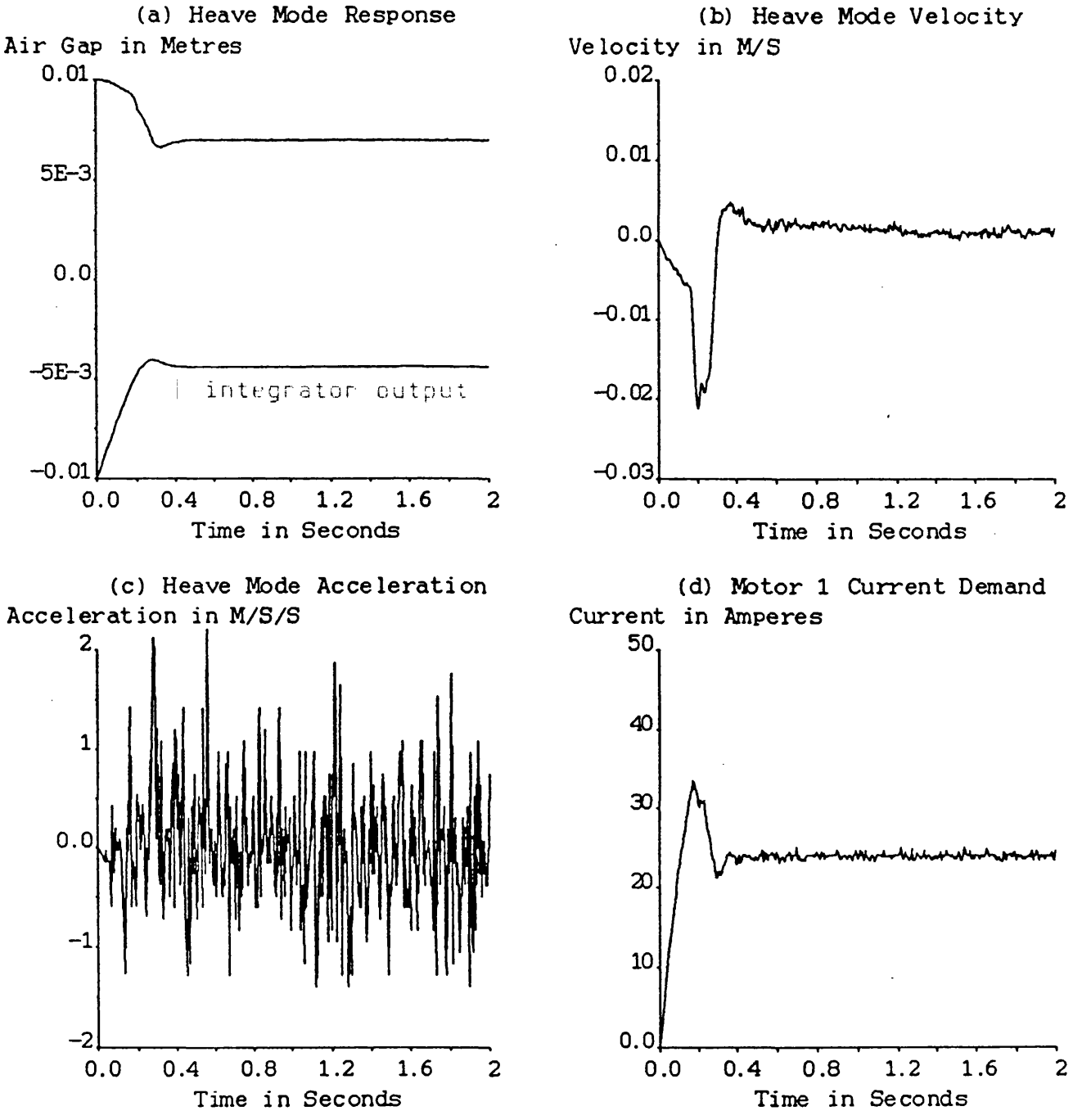

Figure 7.2.13 Heave mode response on 'lift-off' for a decoupled heave and roll controller

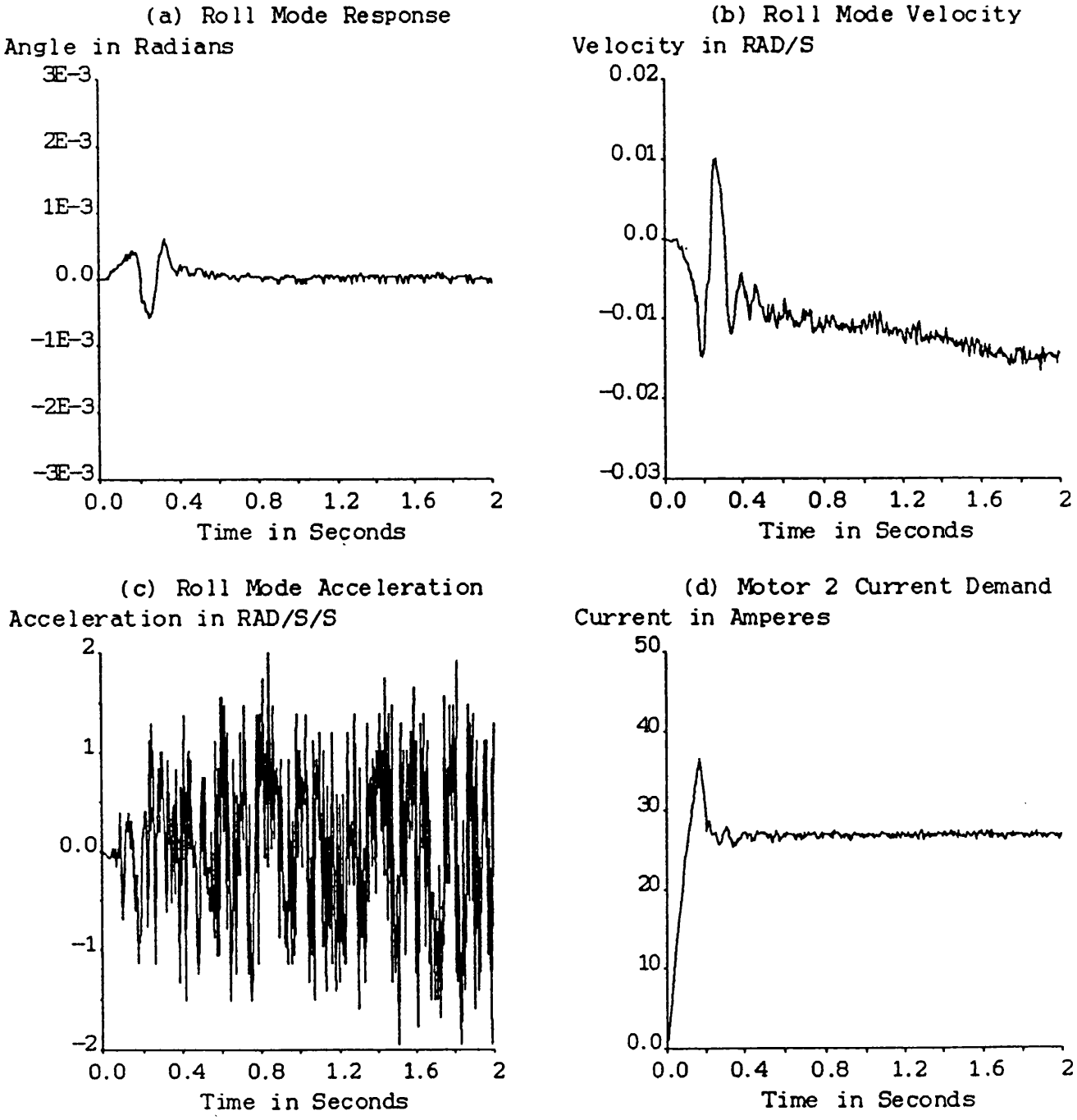

Figure 7.2.14 Roll mode response on 'lift-off' for a decoupled heave and roll controller

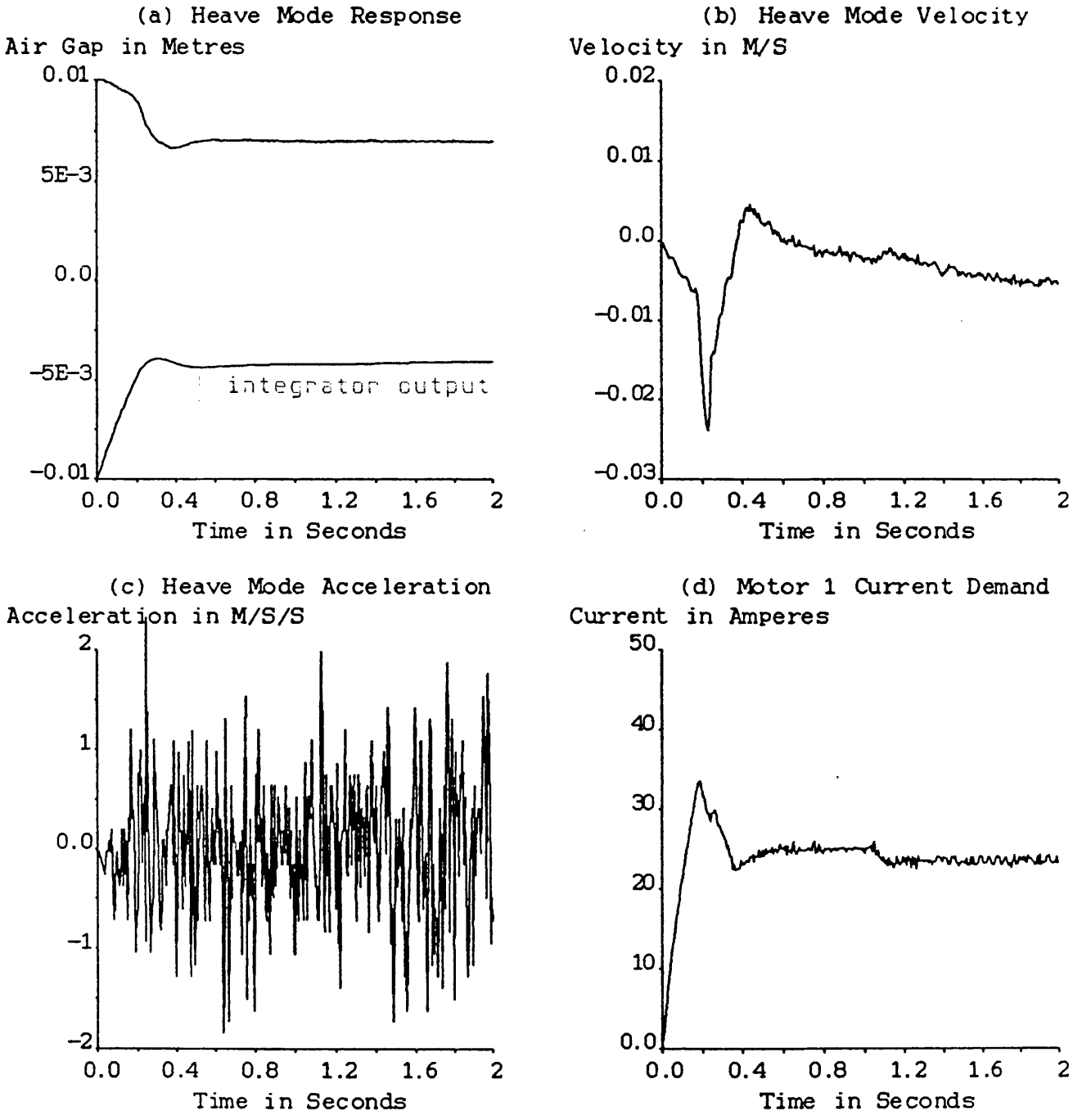

Figure 7.2.15 Heave response to a 1 milliradian roll disturbance

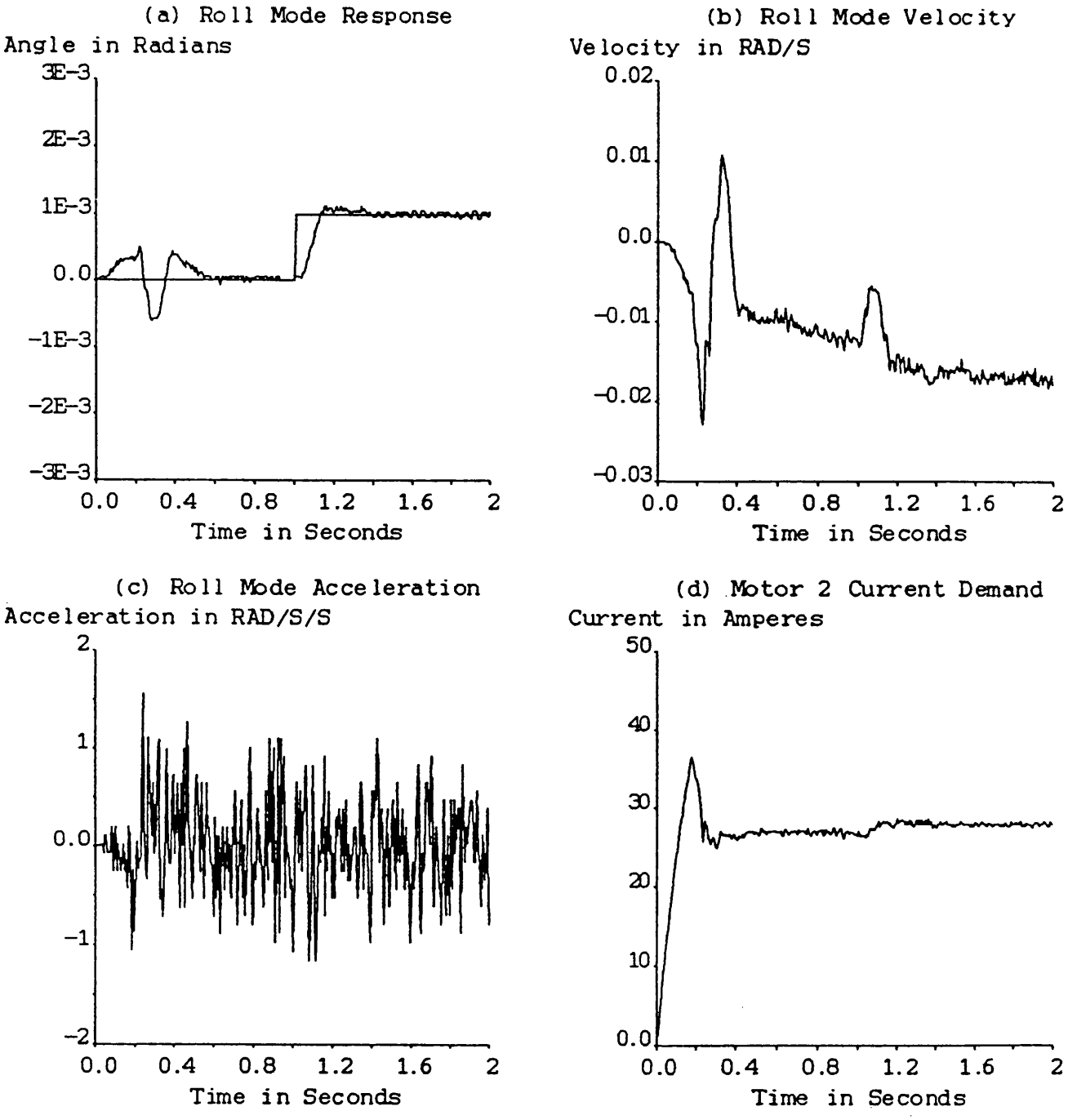

Figure 7.2.16 Roll response to a 1 milliradian roll disturbance

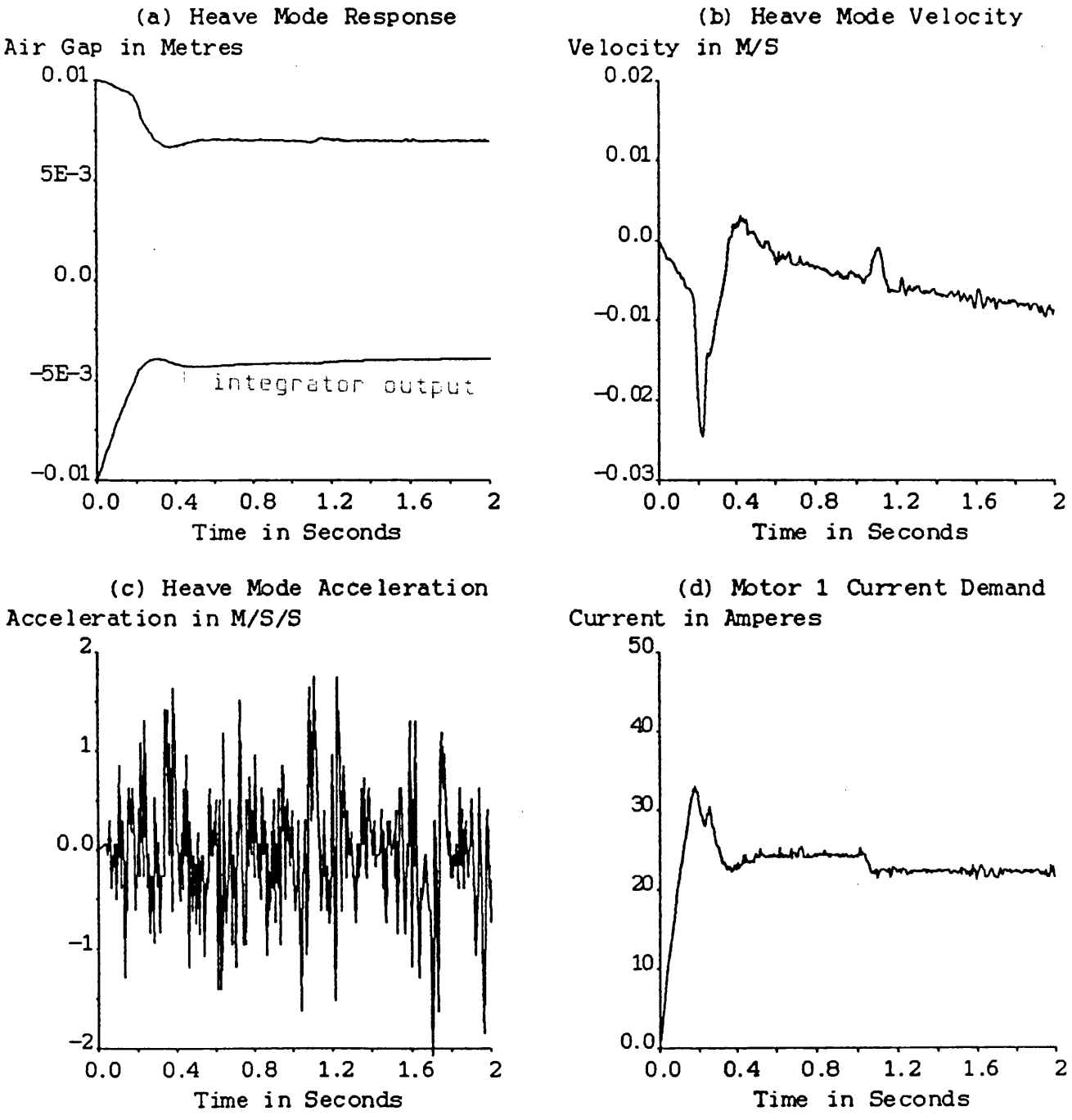

Figure 7.2.17 Heave response to a 2 milliradian roll disturbance

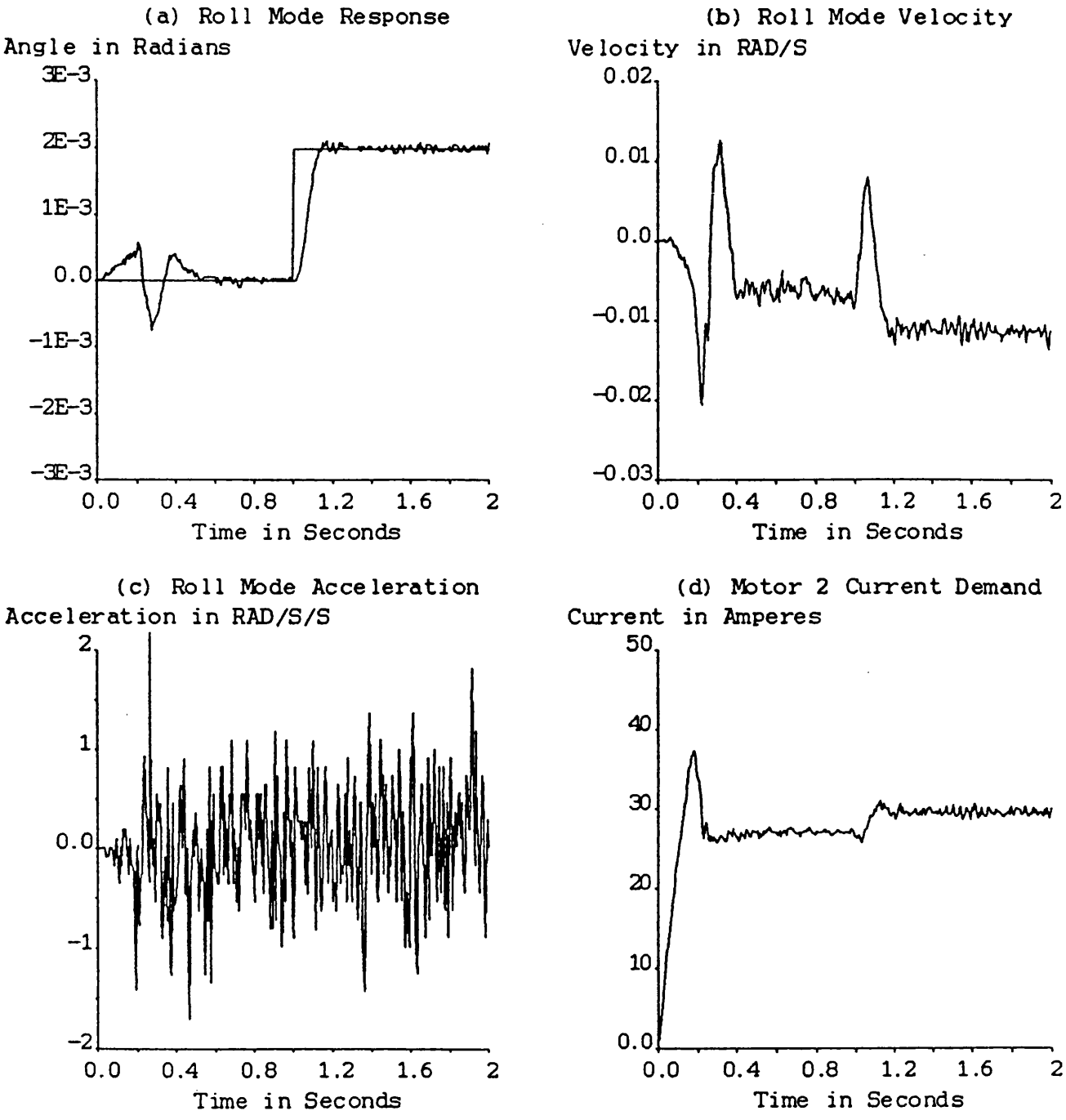

Figure 7.2.18 Roll response to a 2 milliradian roll disturbance

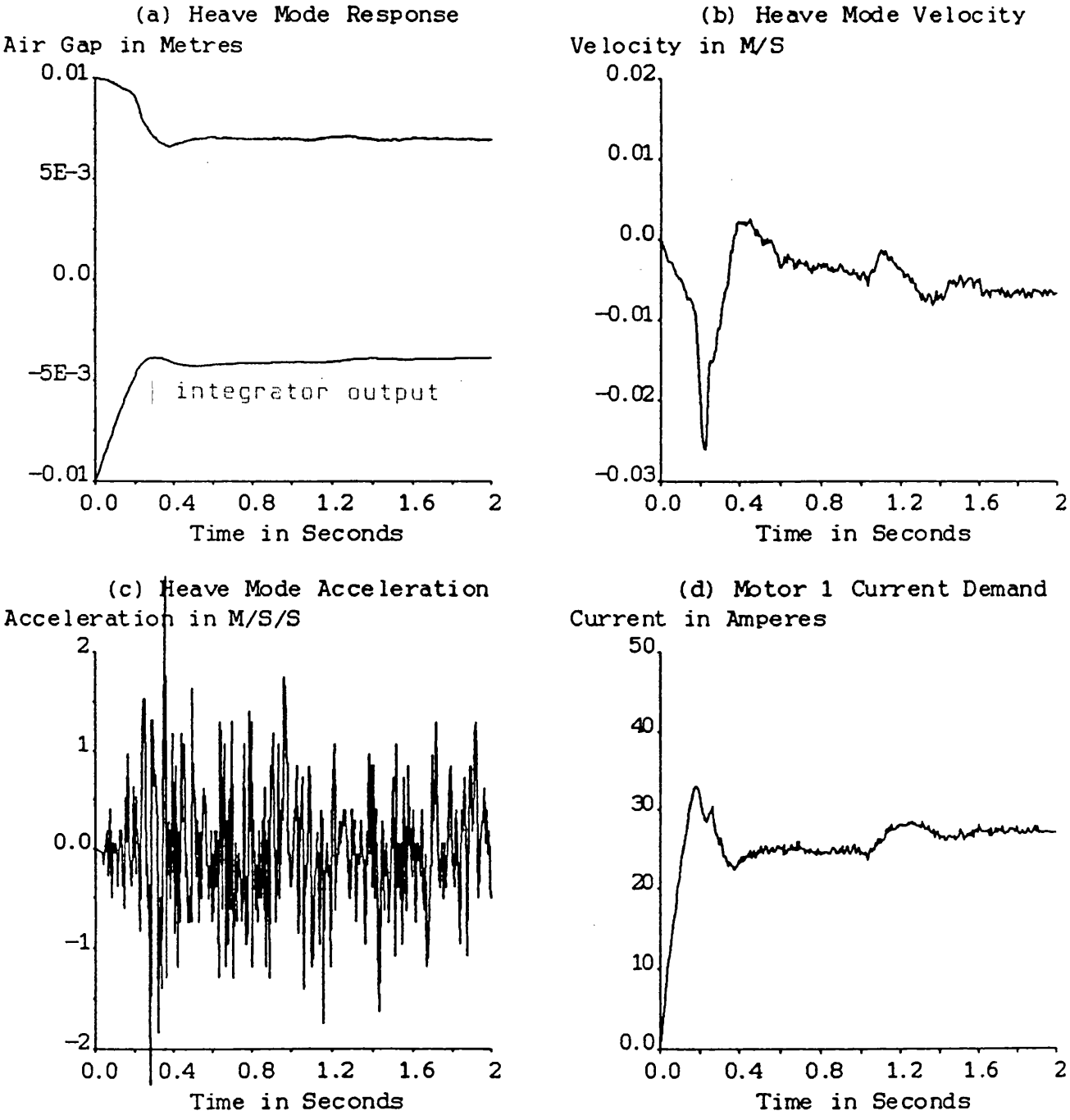

Figure 7.2.19 Heave response to a -1 milliradian roll disturbance

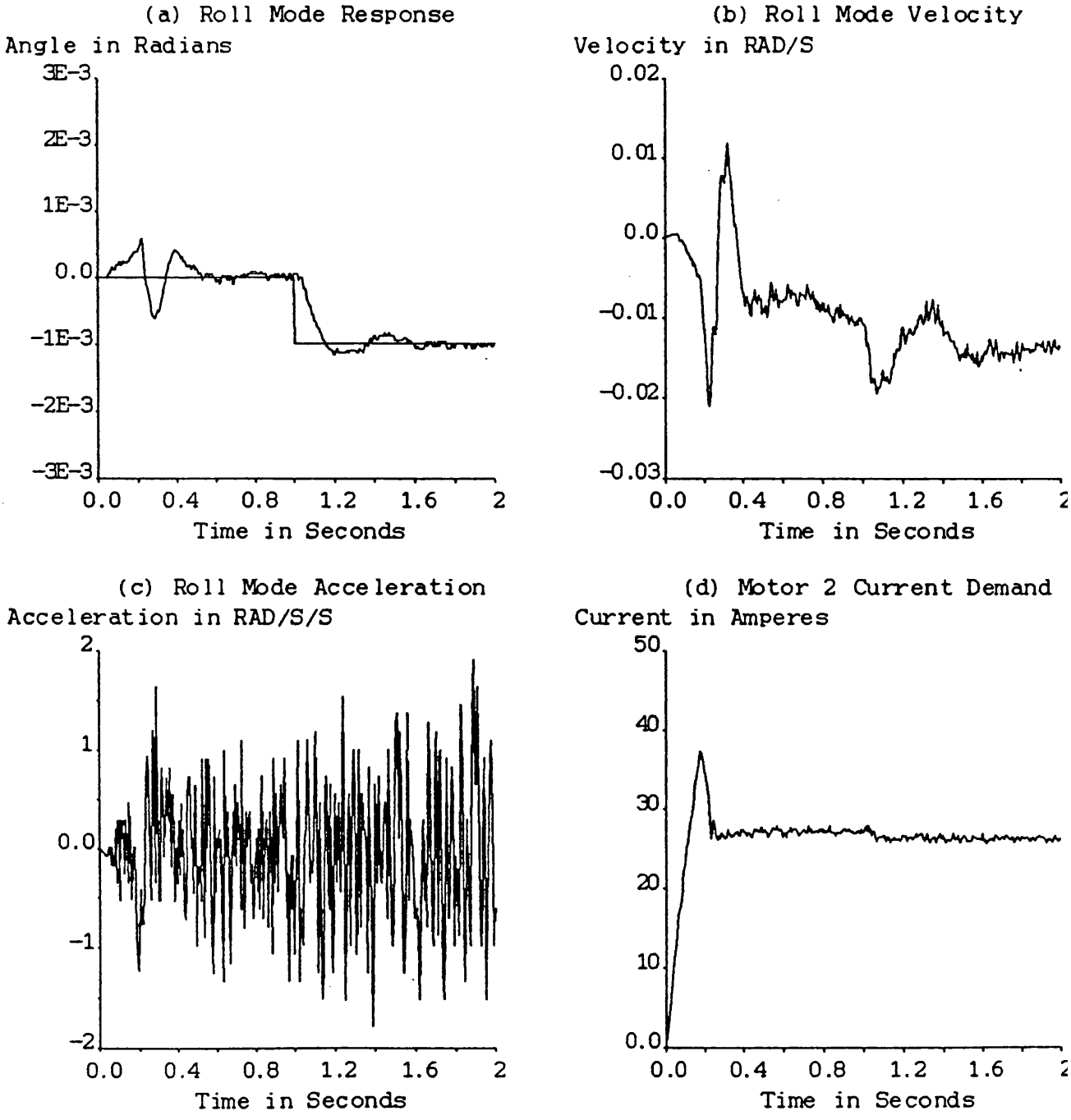

Figure 7.2.20 Roll response to a -1 milliradian roll disturbance

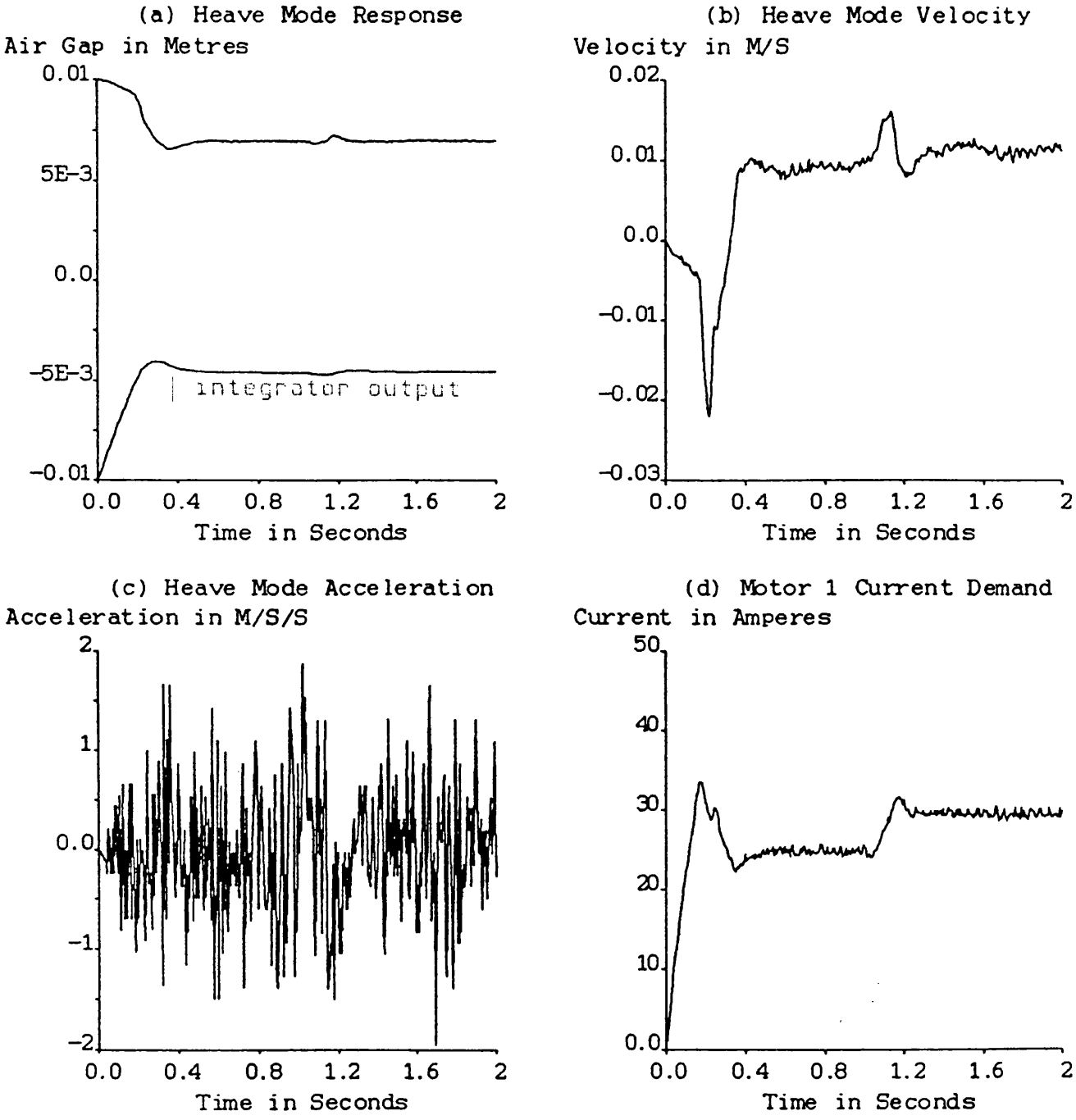

Figure 7.2.21 Heave response to a -2 milliradian roll disturbance

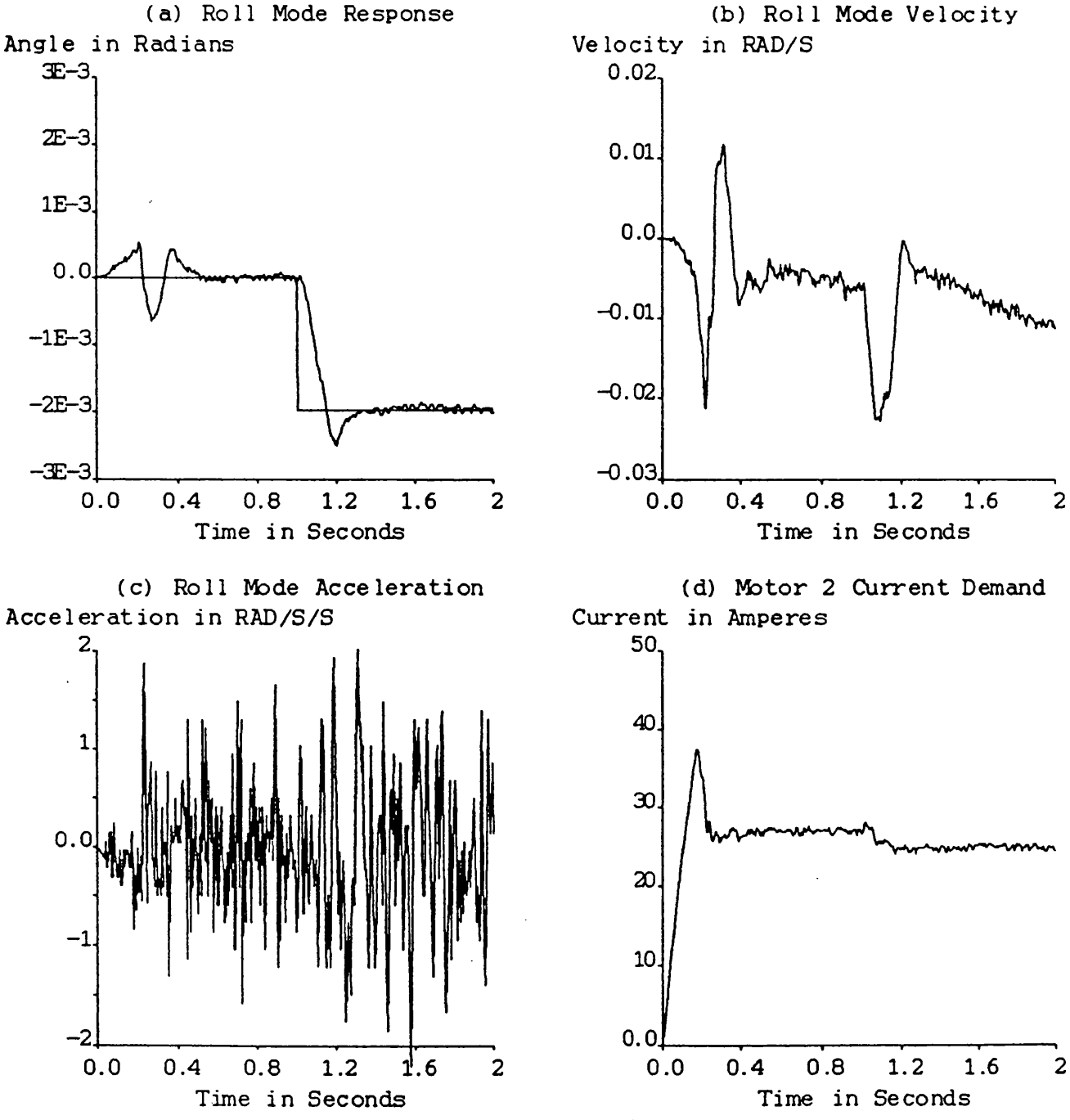

Figure 7.2.22 Roll response to a -2 milliradian roll disturbance

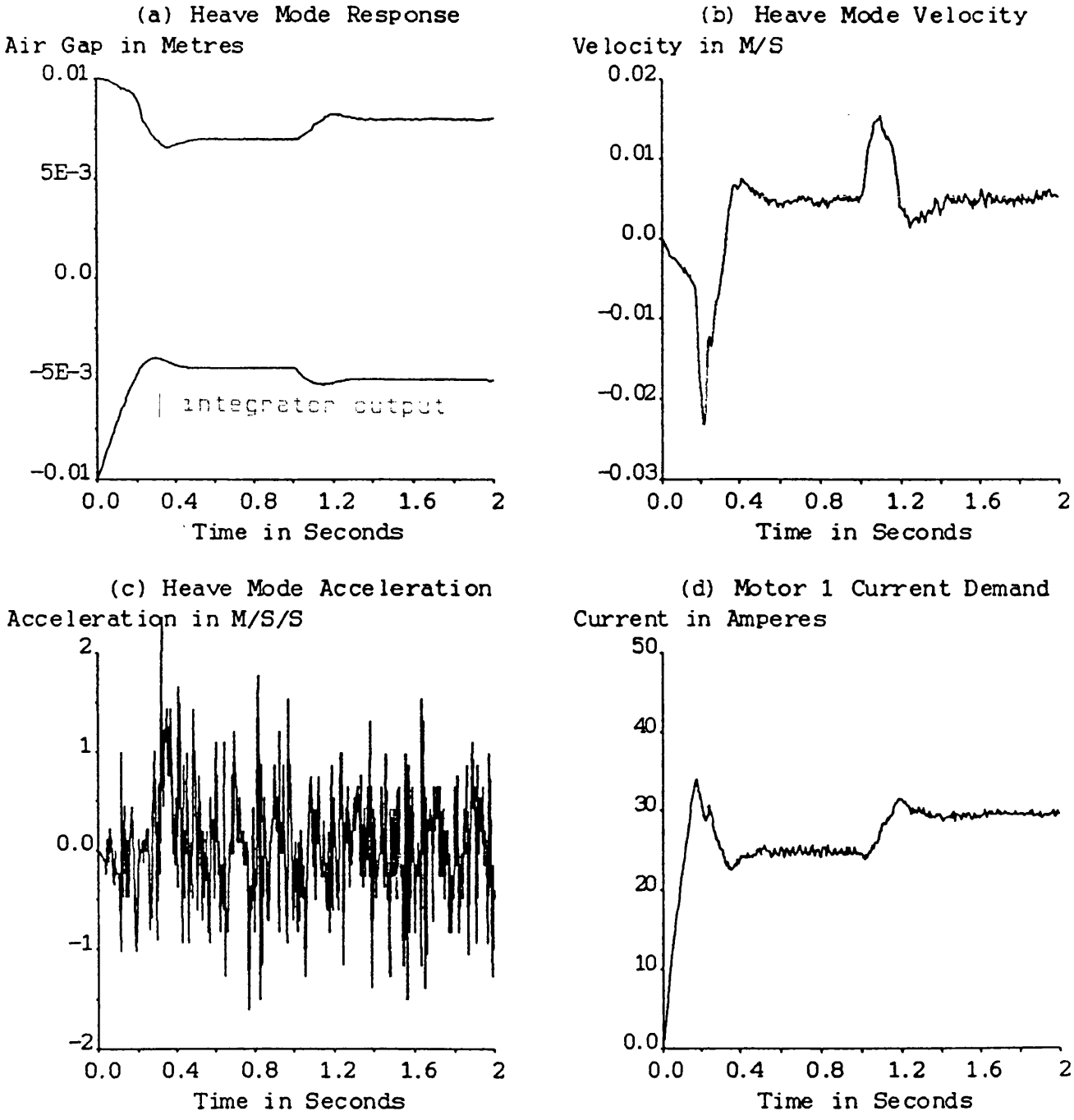

Figure 7.2.23 Heave response to a 1 millimetre heave disturbance

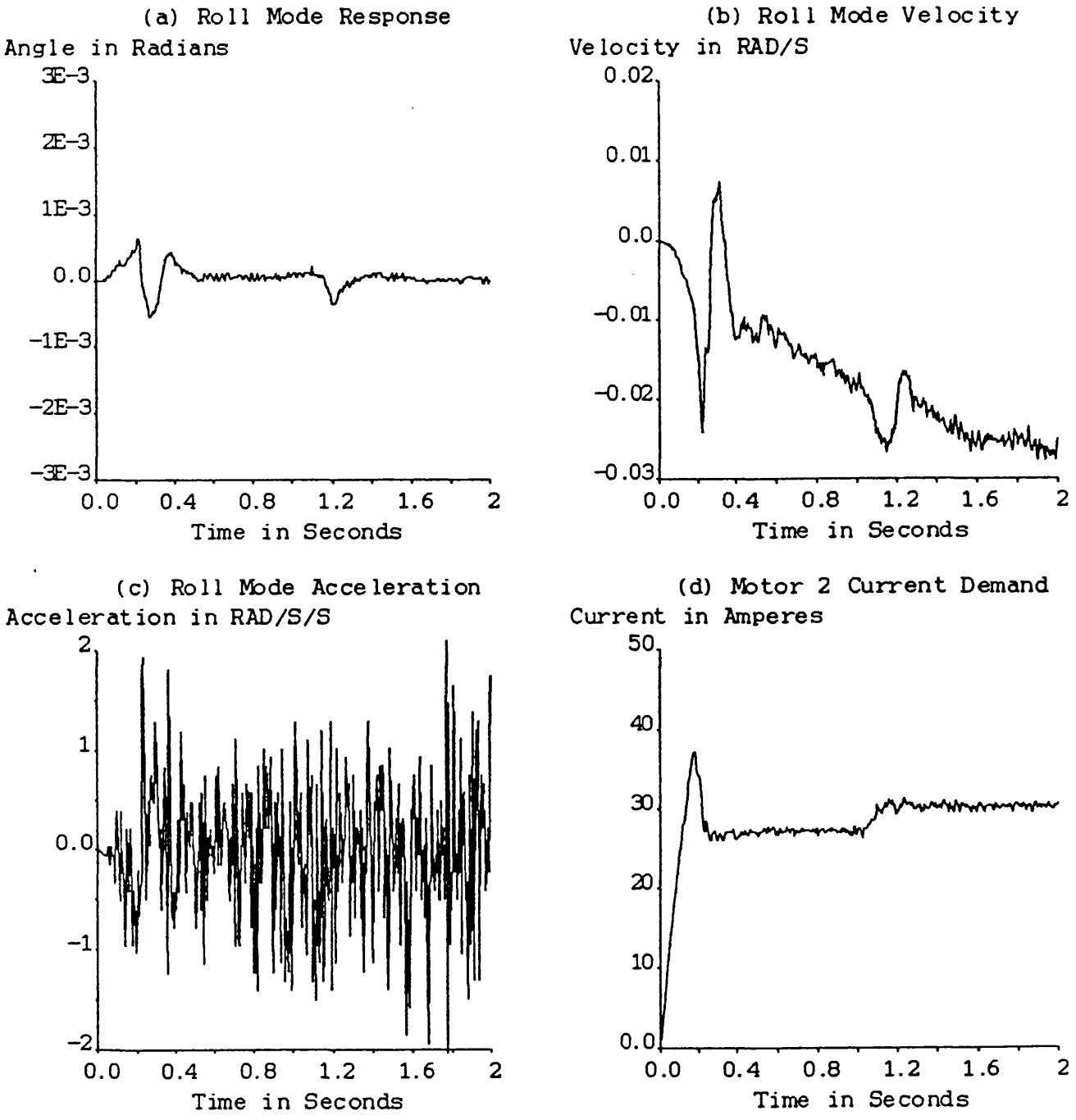

Figure 7.2.24 Roll response to a 1 millimetre heave disturbance

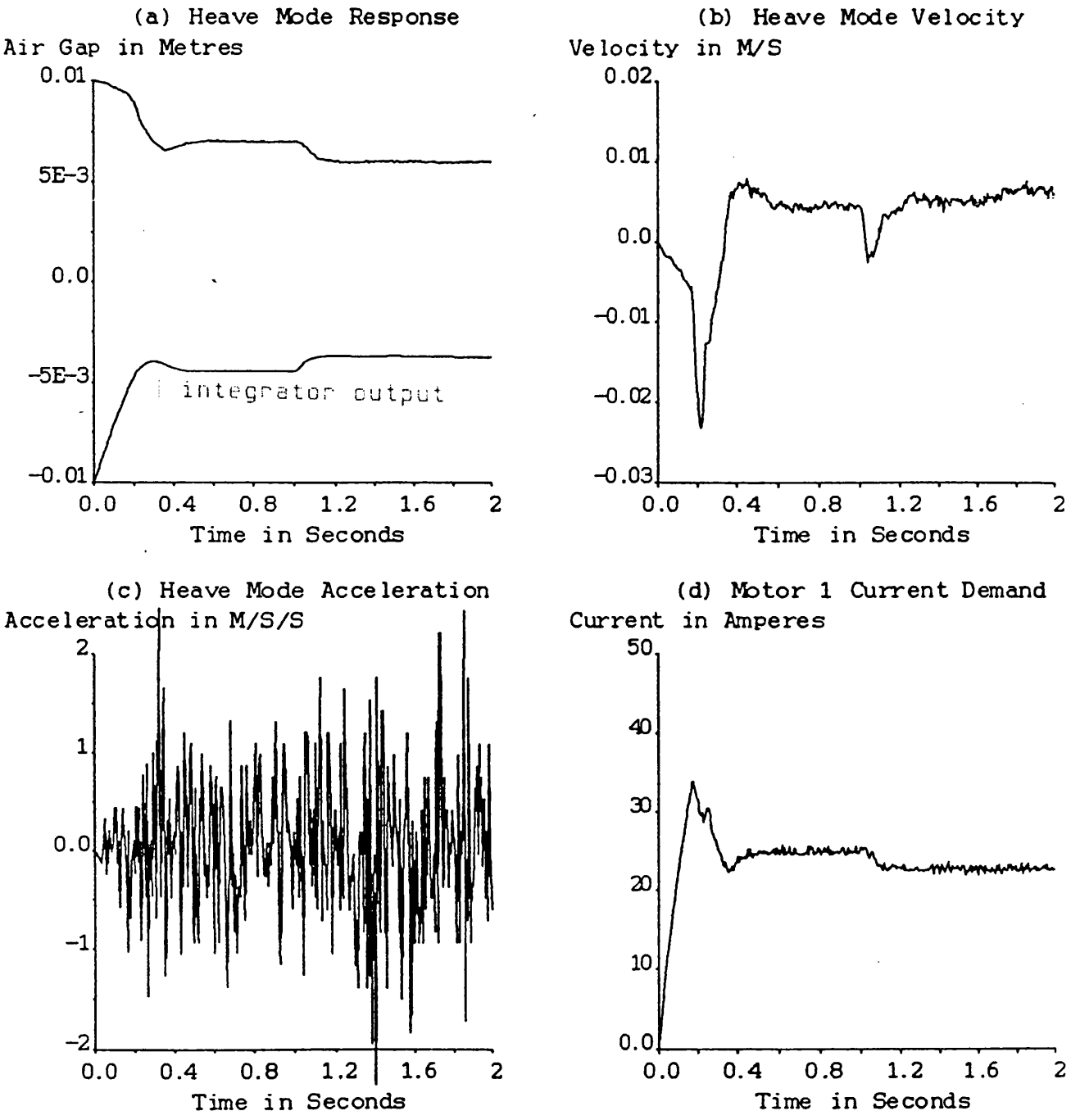

Figure 7.2.25 Heave response to a -1 millimetre heave disturbance

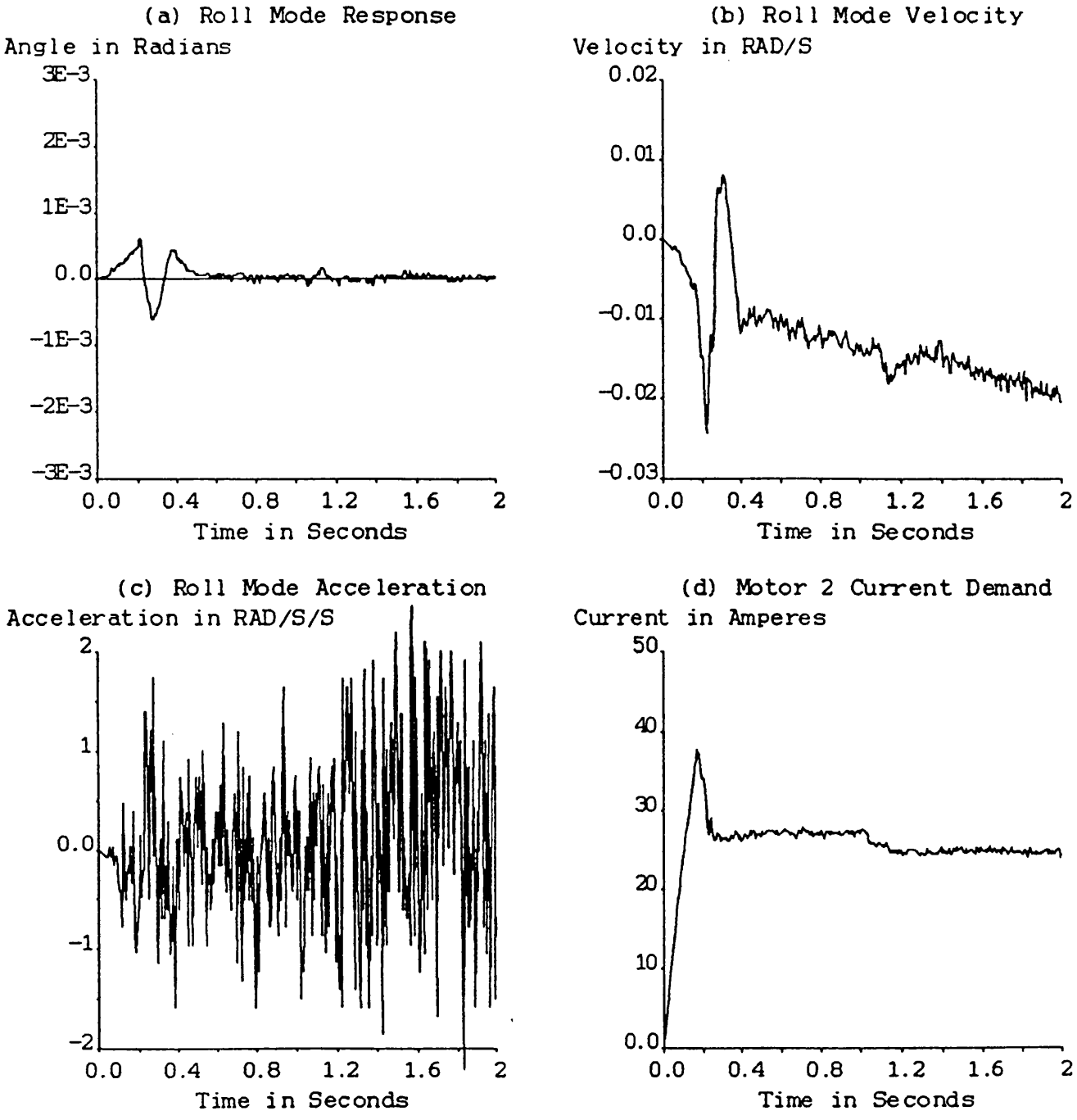

Figure 7.2.26 Roll response to a -1 millimetre heave disturbance

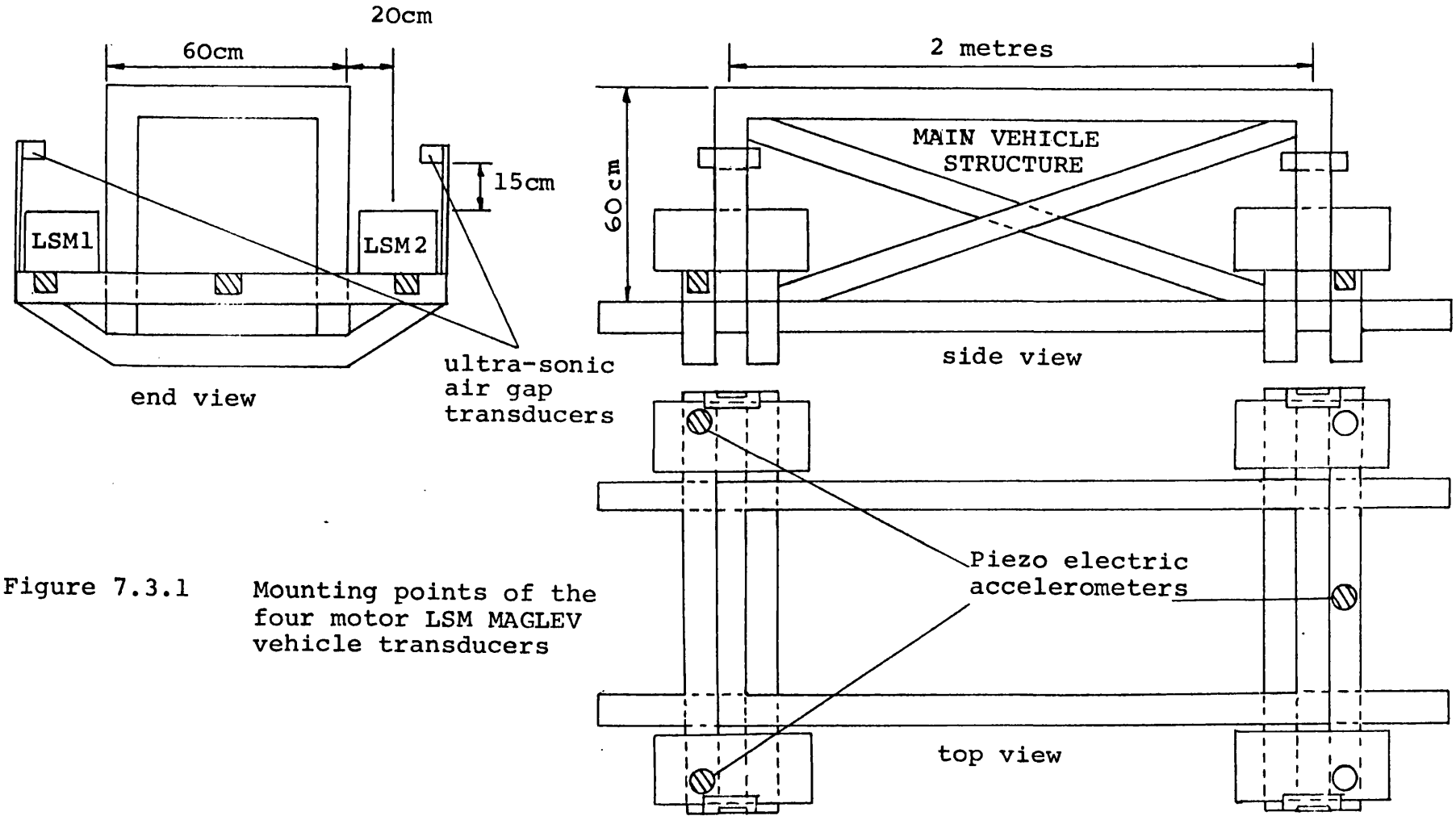

Figure 7.3.1 Mounting points of the four motor LSM MAGLEV vehicle transducers

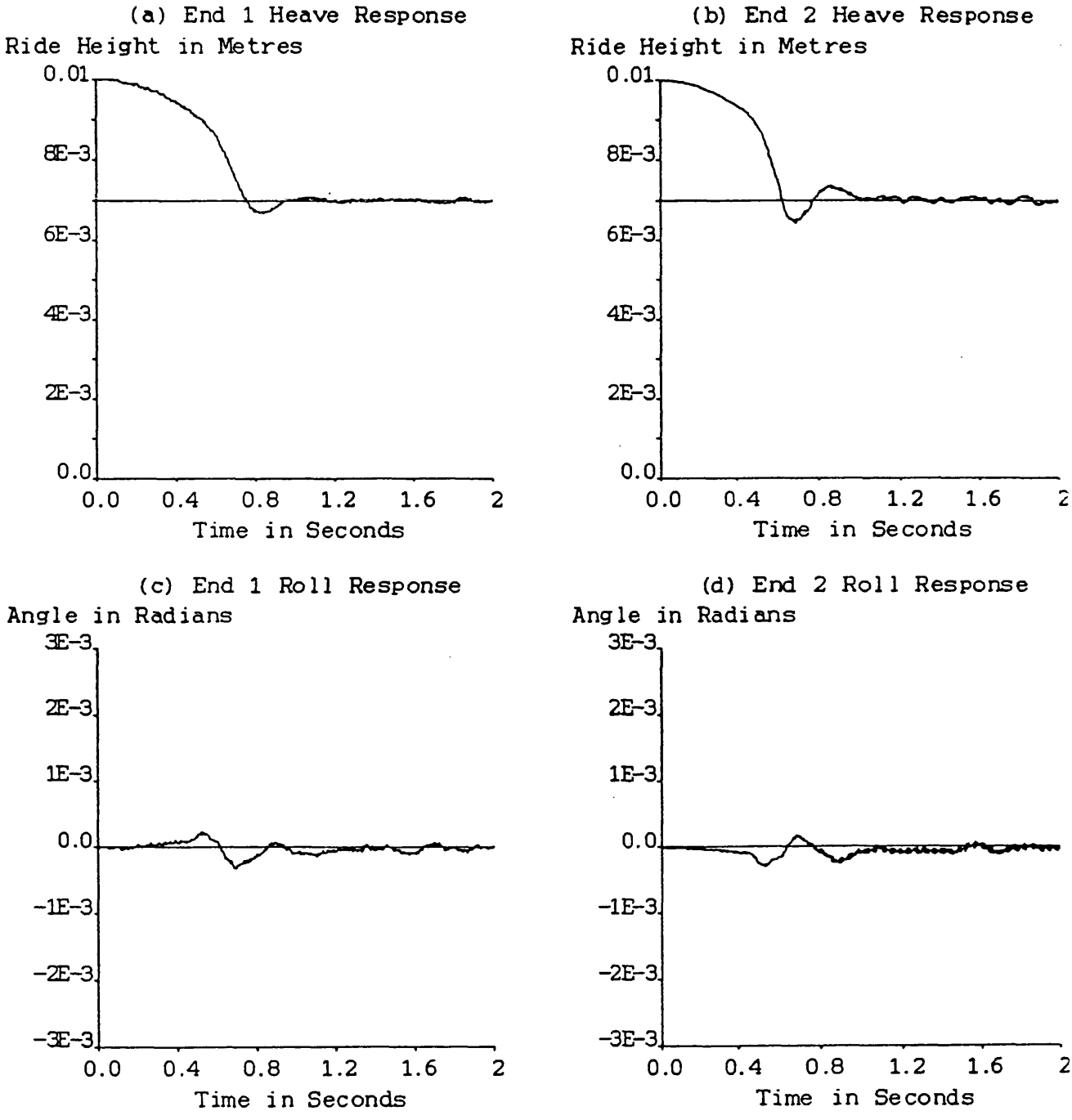

Figure 7.3.2 Heave and roll position responses for both ends of the vehicle on 'lift-off'

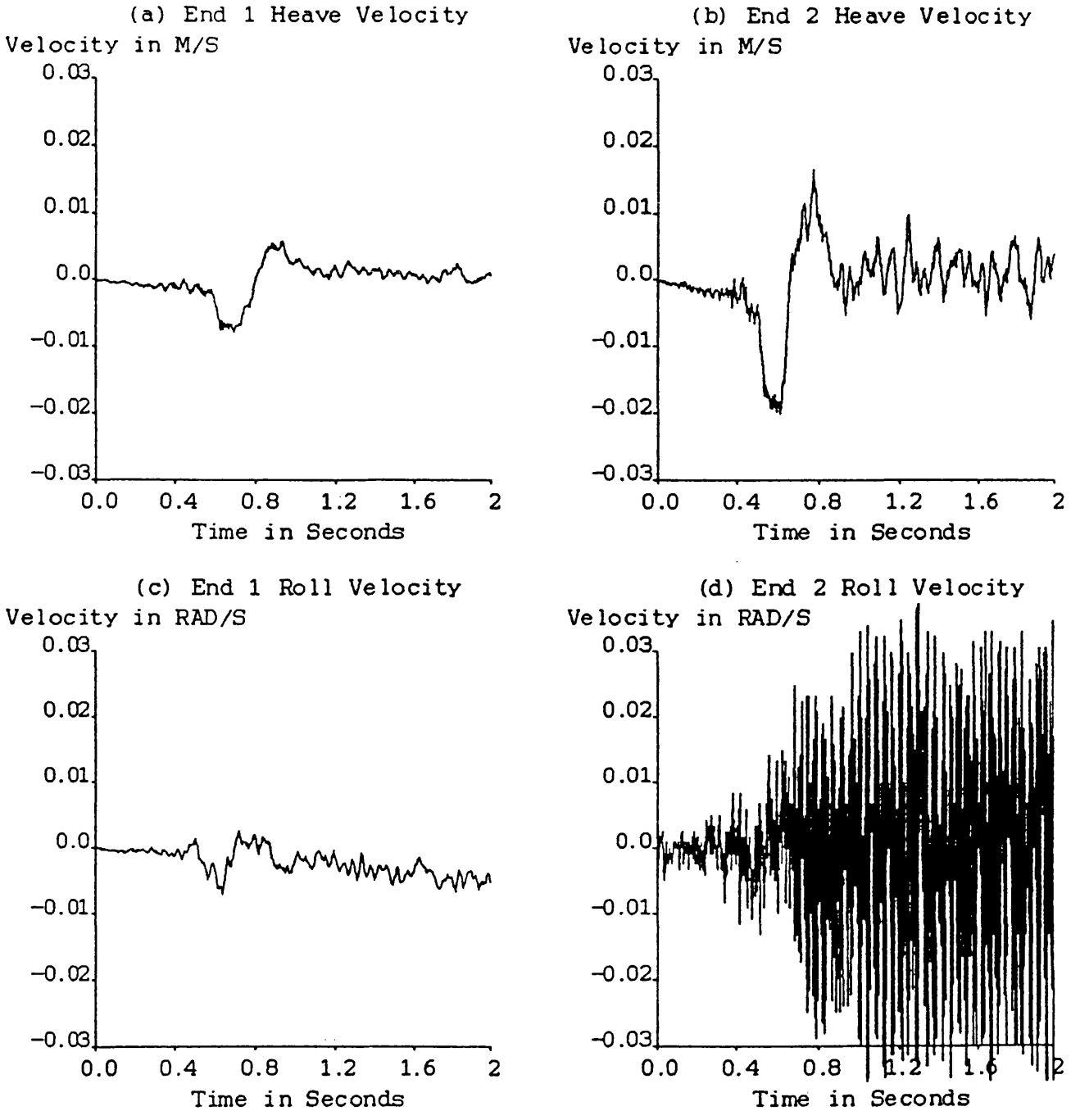

Figure 7.3.3 Heave and roll velocity responses for both ends of the vehicle on 'lift-off'

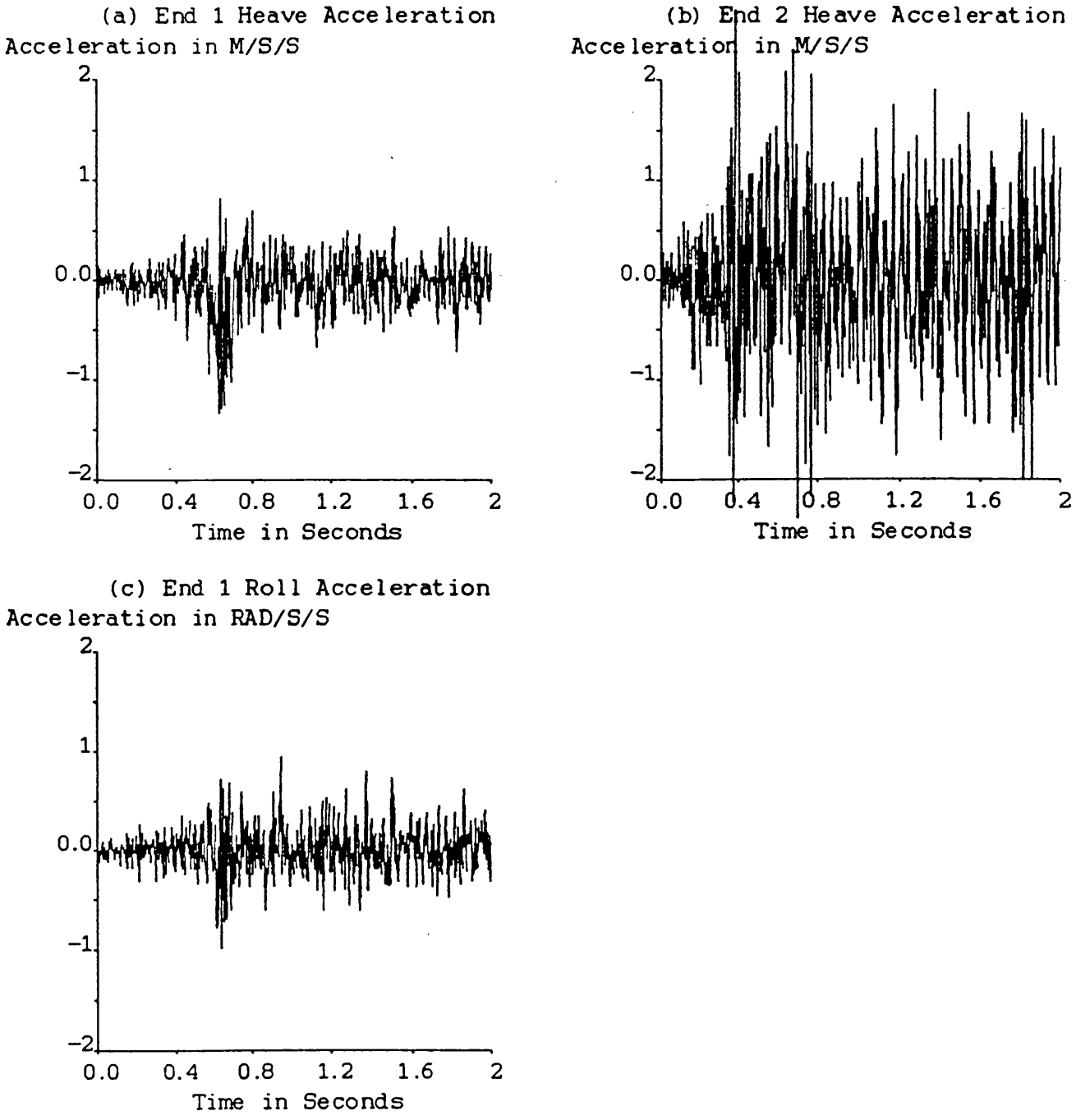

Figure 7.3.4 Heave and roll acceleration responses for both ends of the vehicle on 'lift-off'

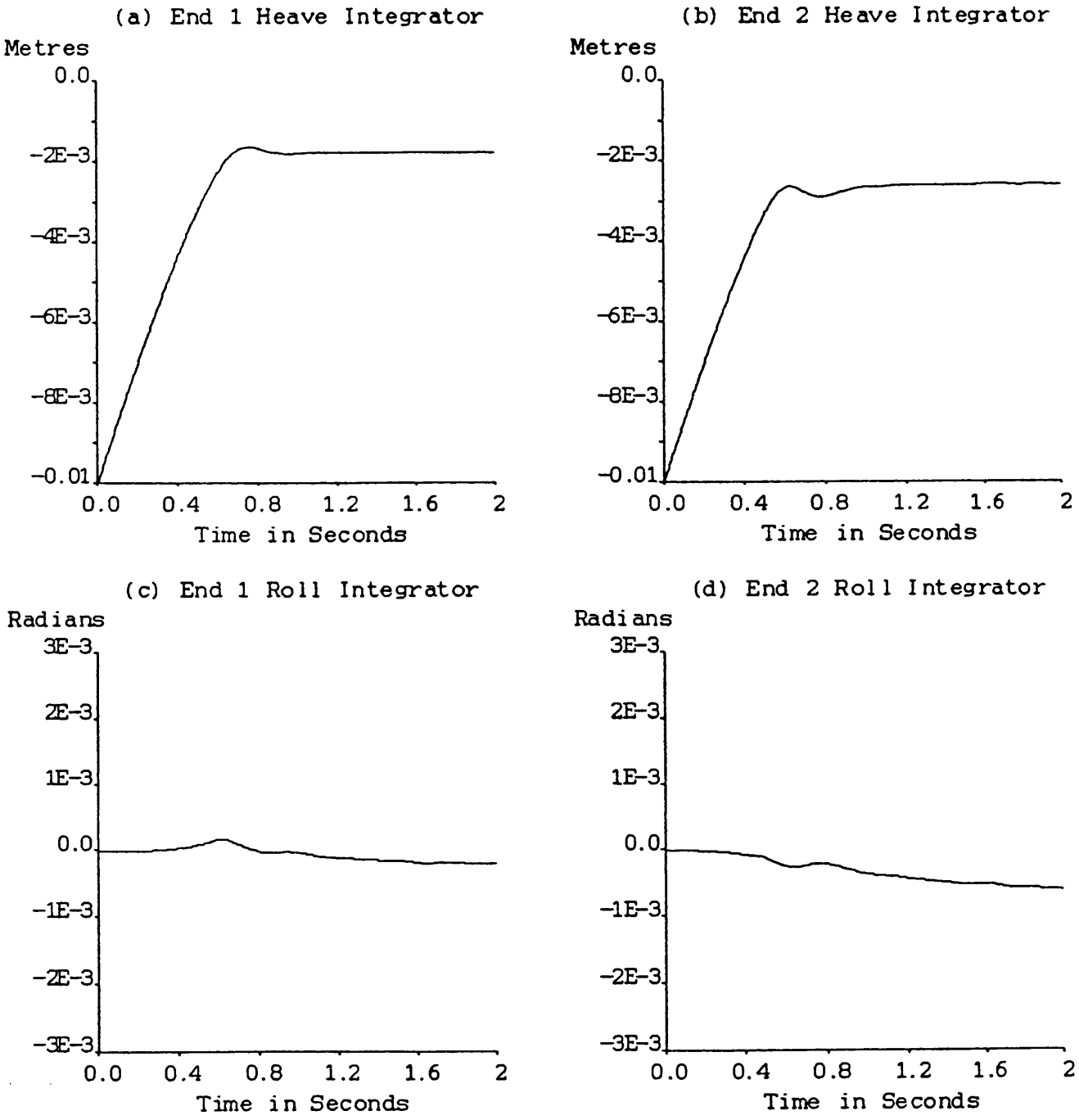

Figure 7.3.5 Heave and roll integrator responses for both ends of the vehicle on 'lift-off'

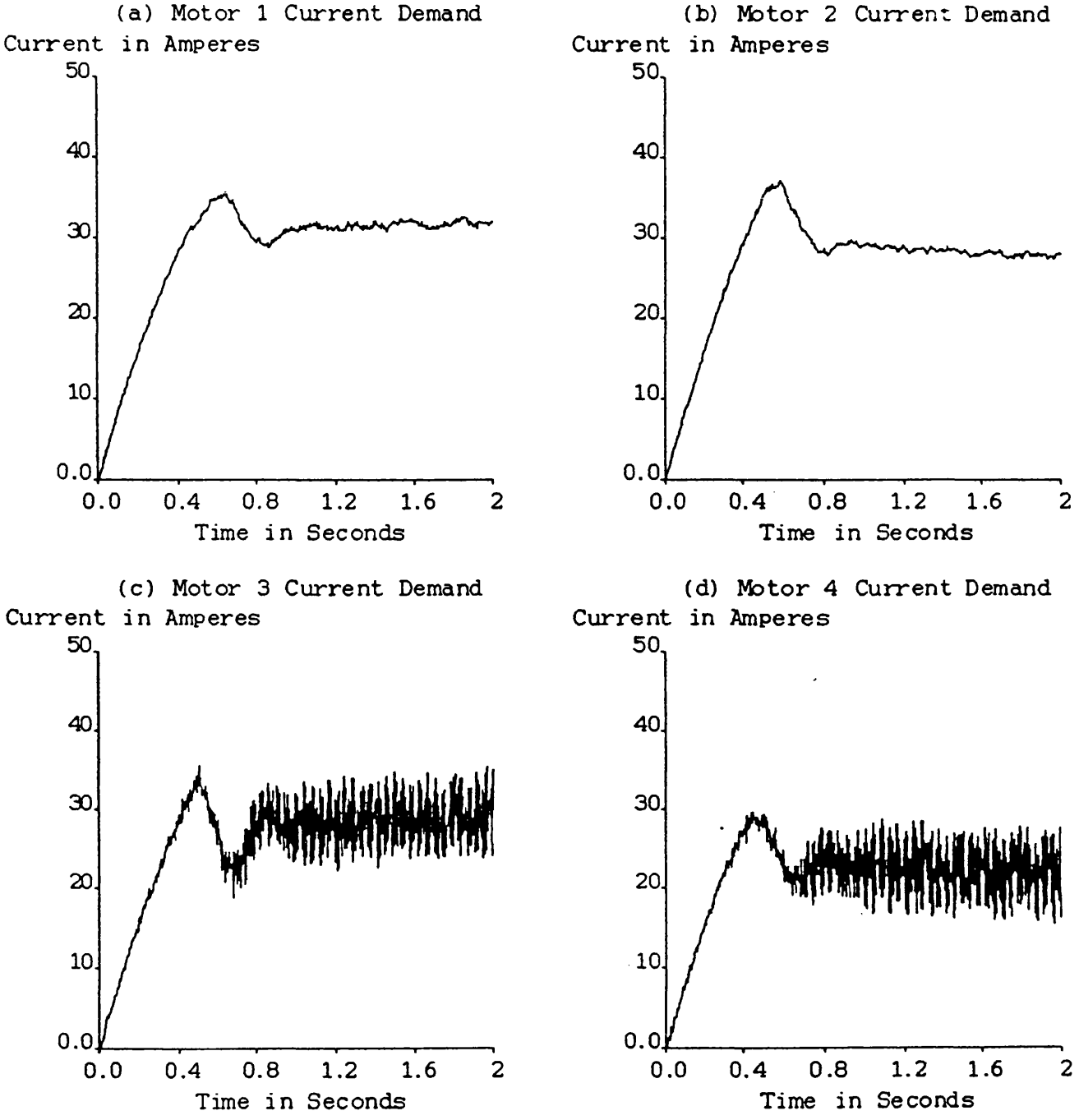

Figure 7.3.6 Heave and roll current demands for both ends of the vehicle on 'lift-off'

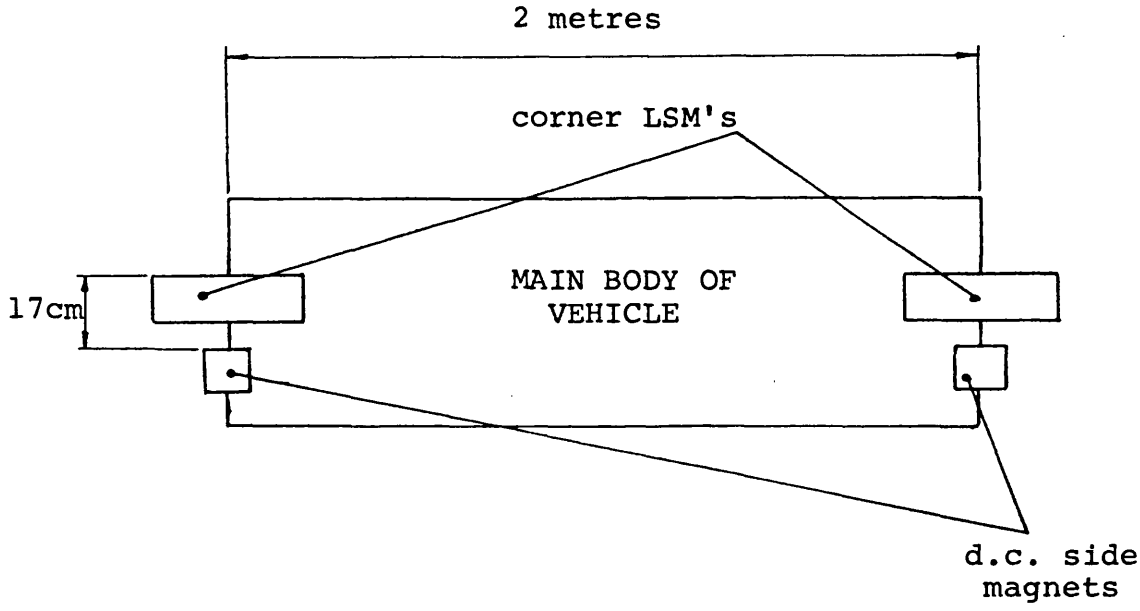

View from side of the vehicle

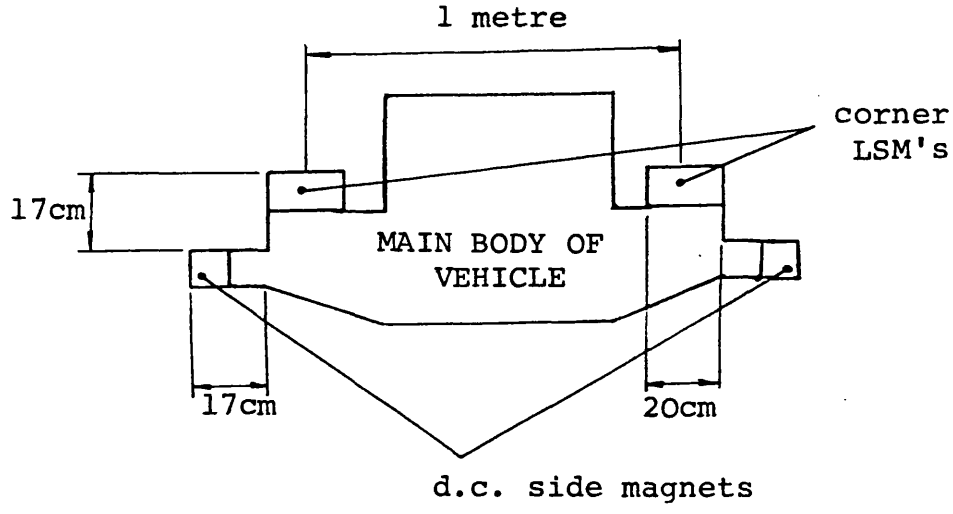

View from end of the vehicle

Figure 7.4.1 The fitting positions of the side magnets

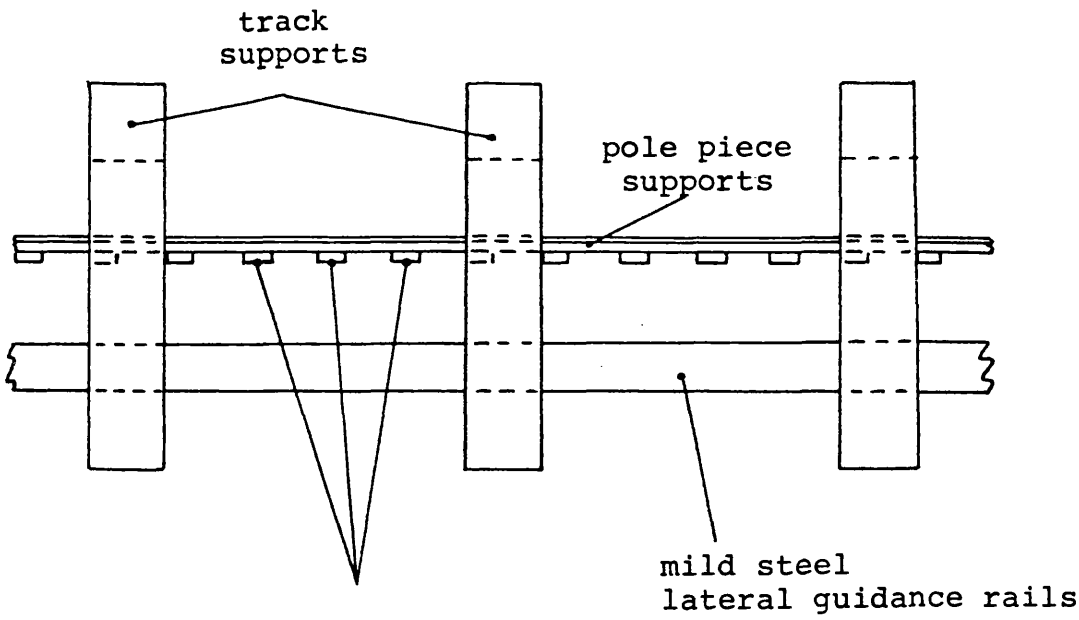

View from side of track

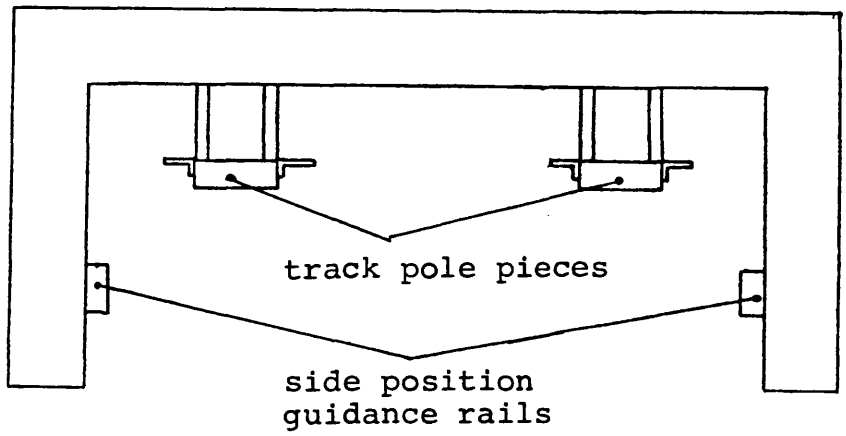

View along track

Figure 7.4.2 The fitting positions of the lateral guidance rails

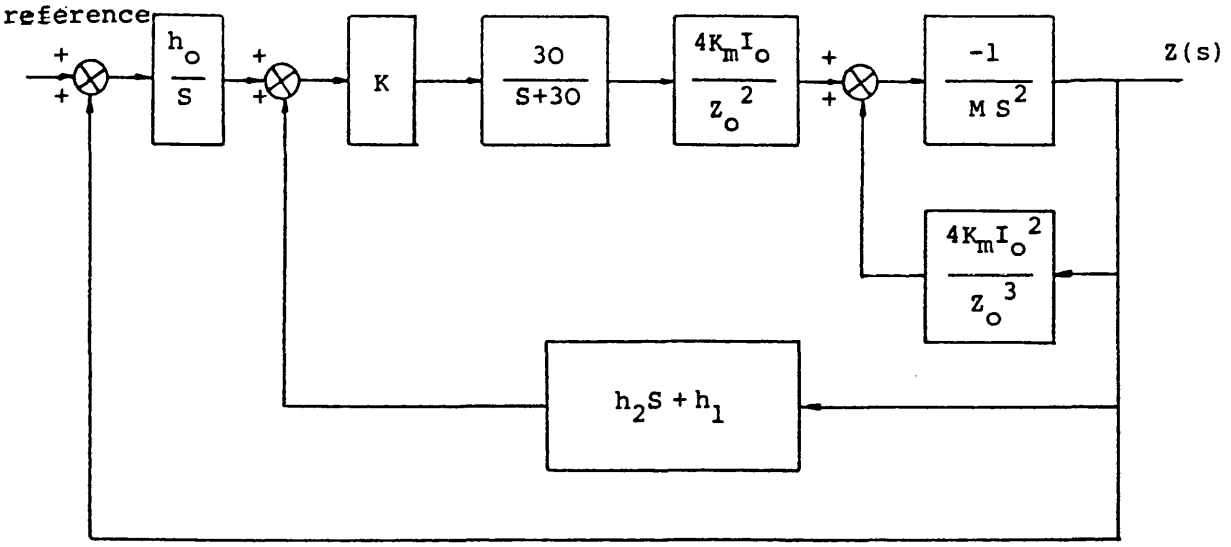

Figure 7.4.3 Linearised fourth order model of the side magnet system

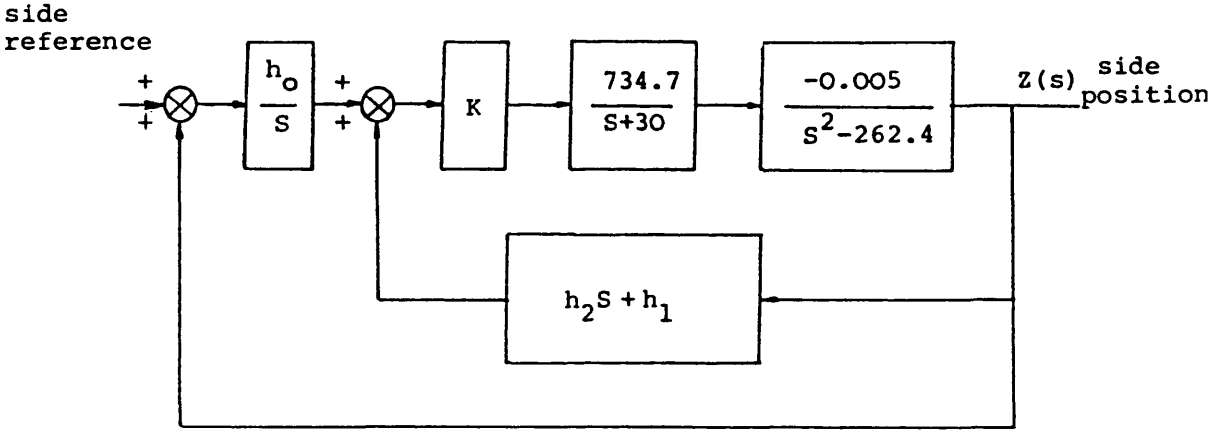

Figure 7.4.4 The side magnet system for standing current of 15 Amperes and air gaps of 7mm

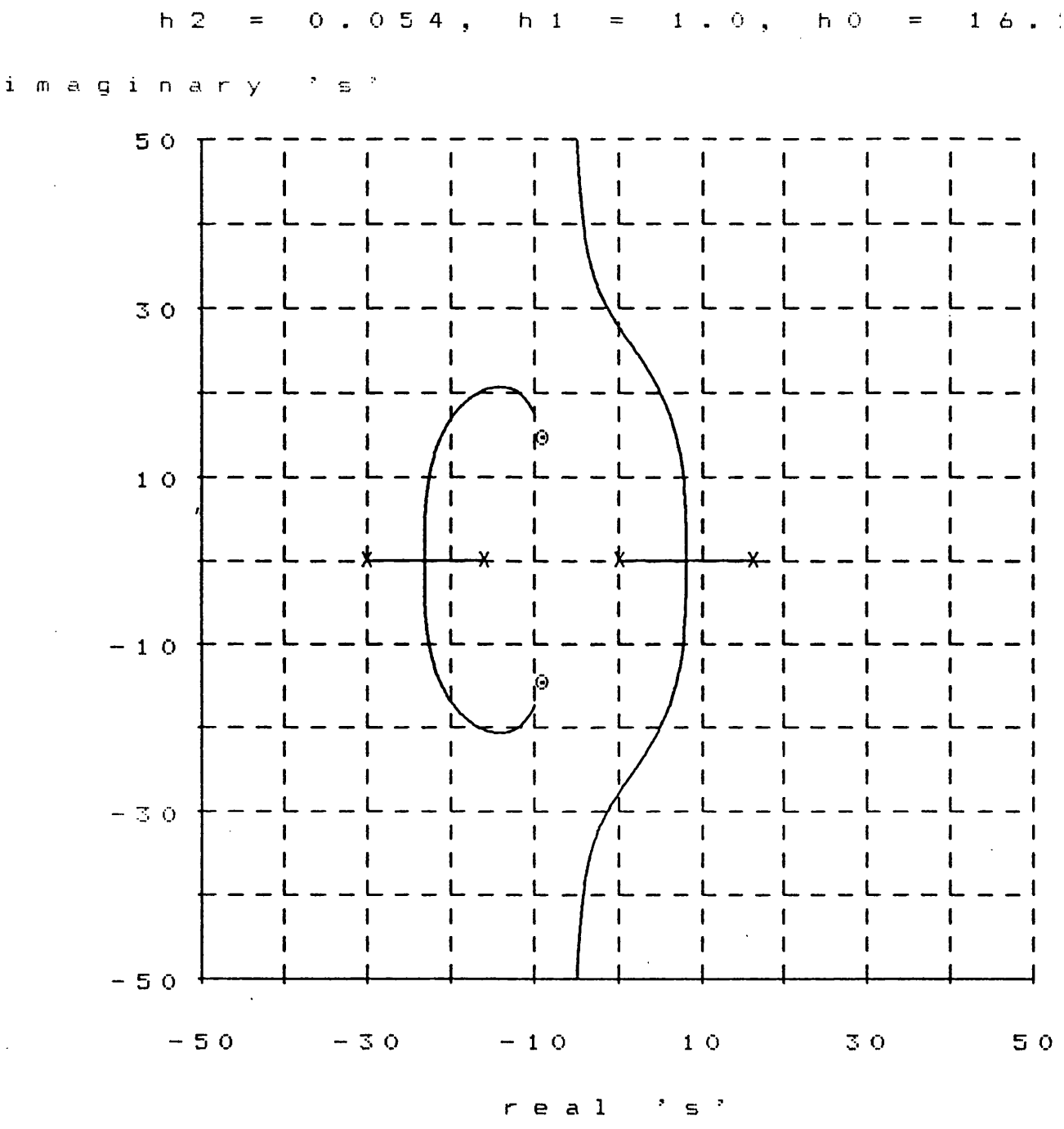

Figure 7.4.5 Root locus for design for $\omega_n = 20.0$, $\xi = 0.5$

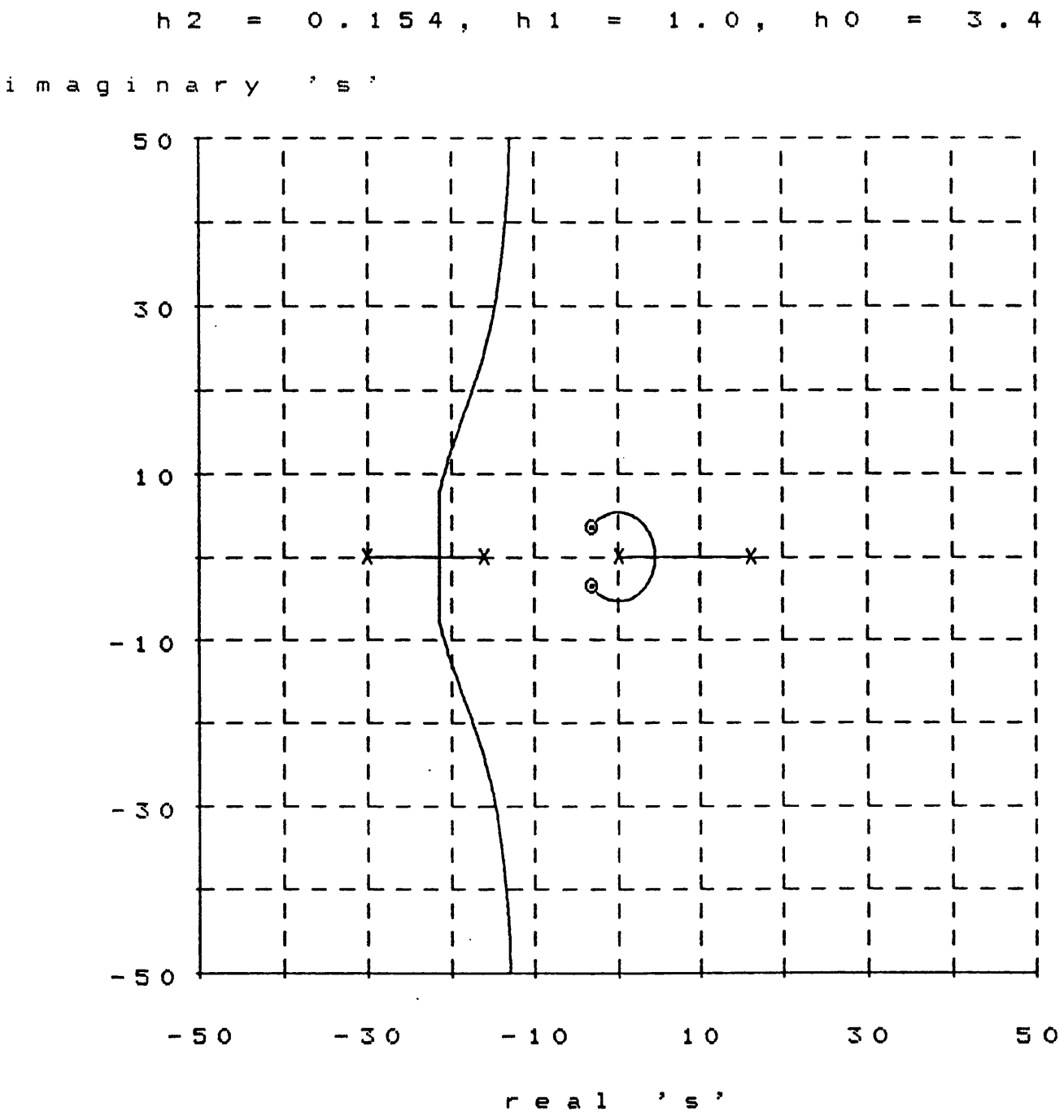

Figure 7.4.6 Root locus for design for $\omega_n = 5.0$, $\xi = 0.5$

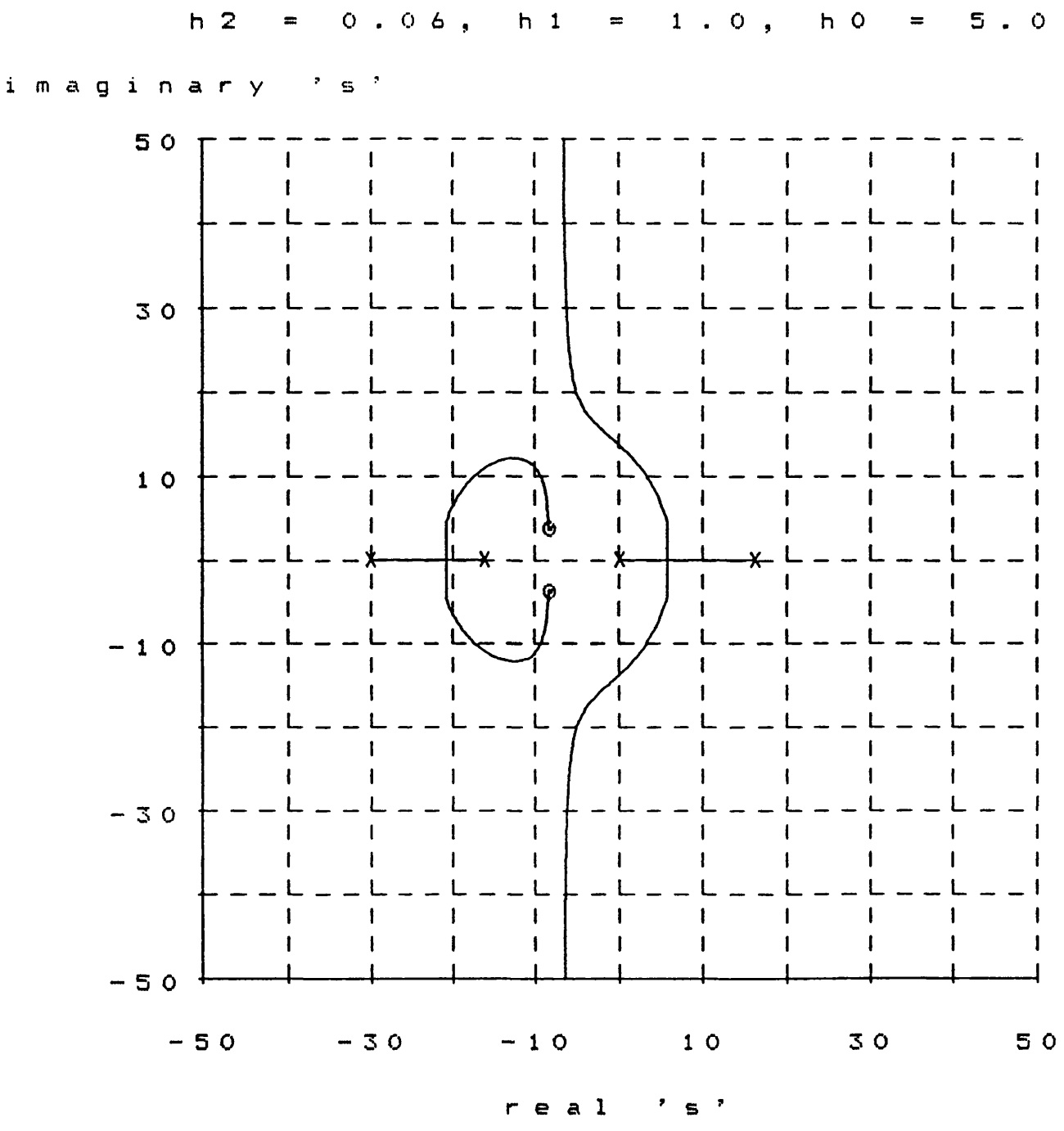

Figure 7.4.7 Root locus for h_o = 5.0, h_1 = 1.0, h_2 = 0.06

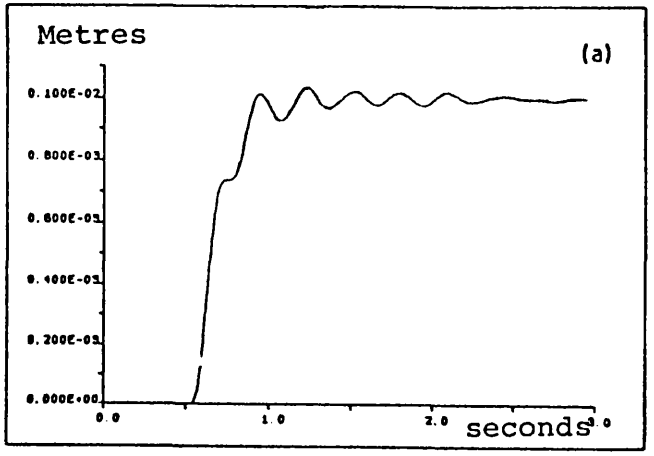

(a) Side position

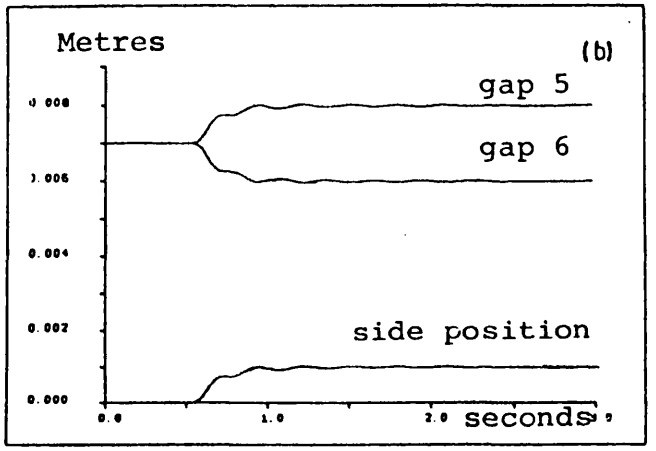

(b) Side air gaps

Simulation Results for

K = 50,000 I_o = 0·0

No Force Offset

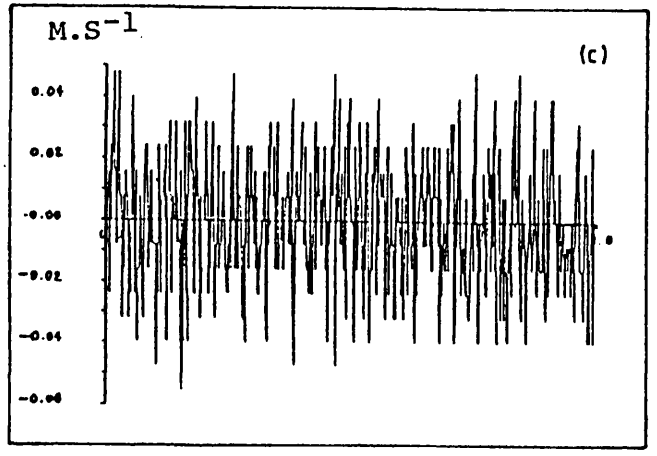

(c) Side velocity

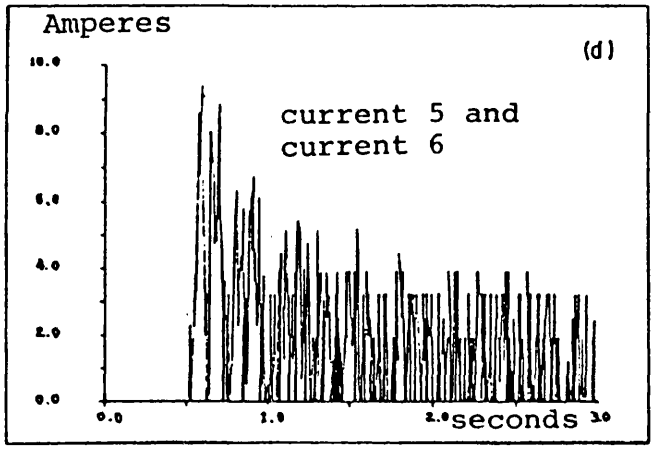

(d) Side magnet current

Figure 7.5.1 Simulation results for system 4 without current offset

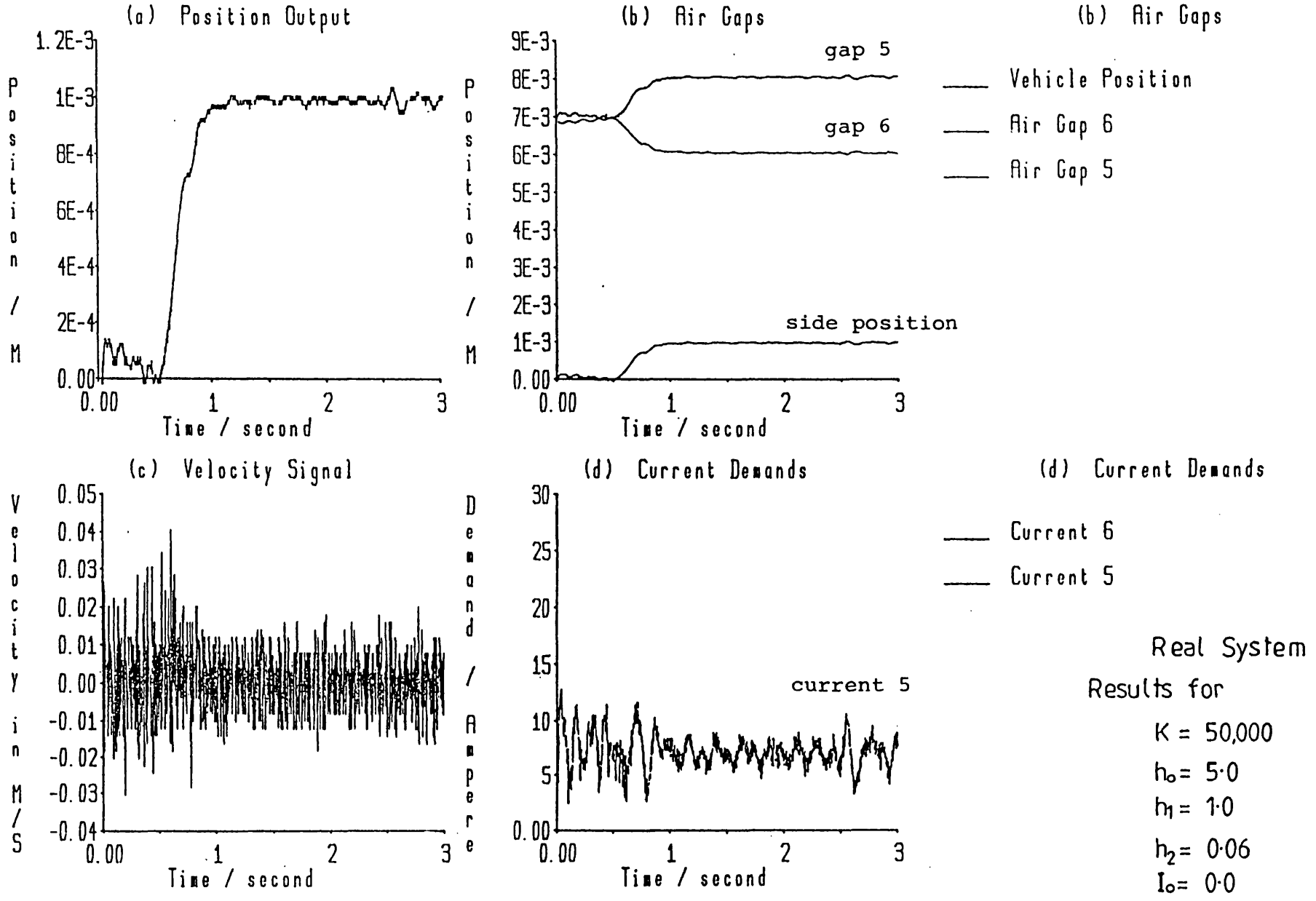

Figure 7.5.2 Real system results for system 4 showing standing current due to sloped track

(a) Side position

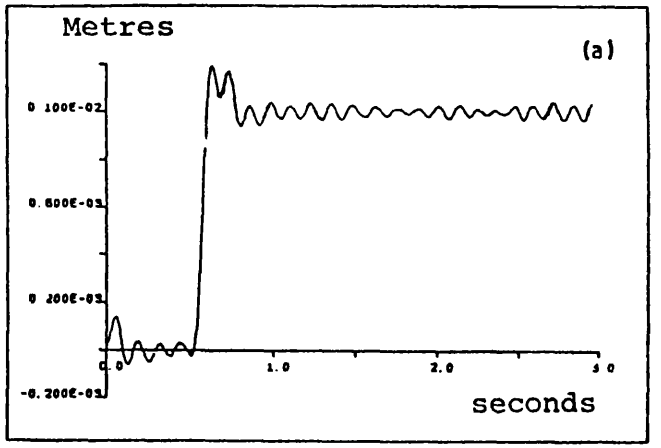

(b) Side air gaps

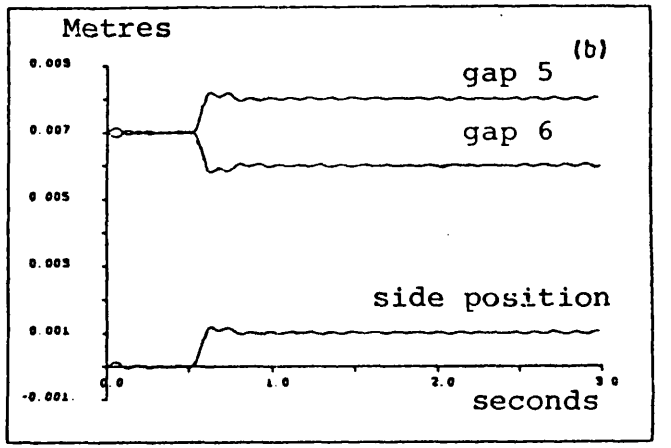

Simulation Results for

K = 16,480 I_o = 15·0

(c) Side velocity

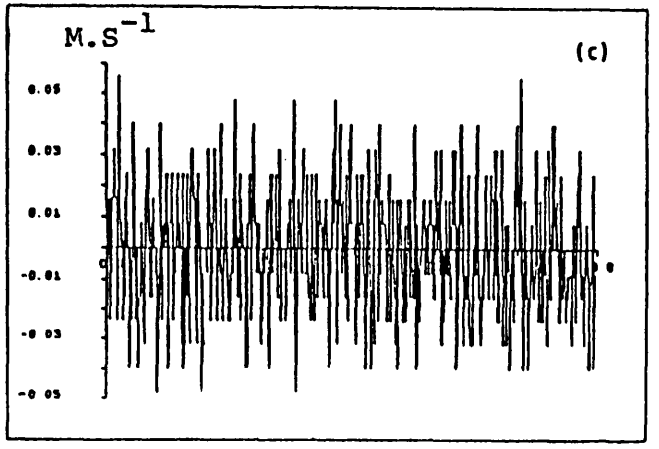

(d) Side magnet current

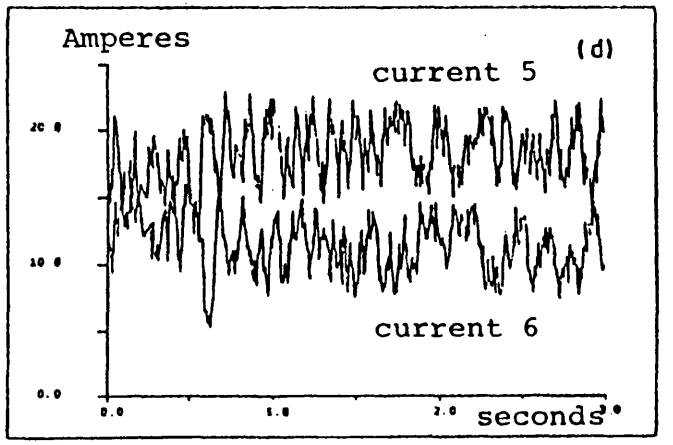

Figure 7.5.3 Simulation results for system 1 including standing current due to

(a) Side position

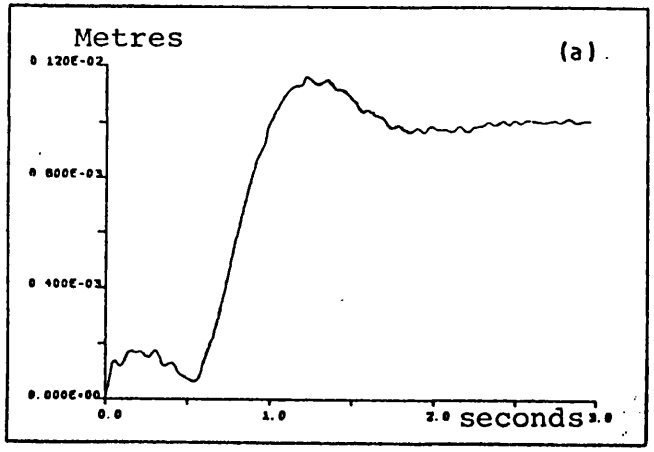

(b) Side air gaps

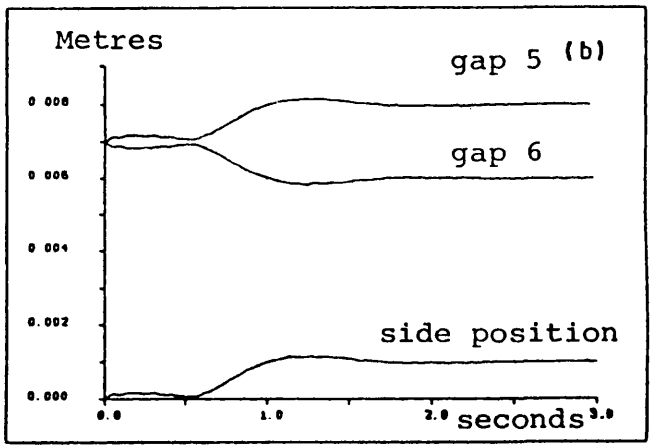

Simulation Results for

$K = 7{,}630 \quad I_o = 15{\cdot}0$

(c) Side velocity

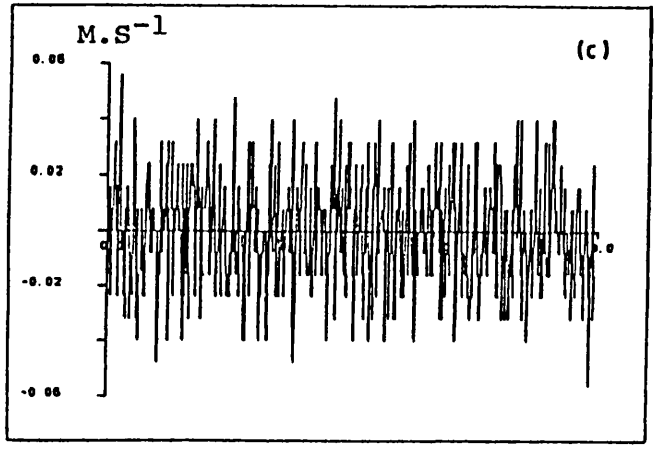

(d) Side magnet current

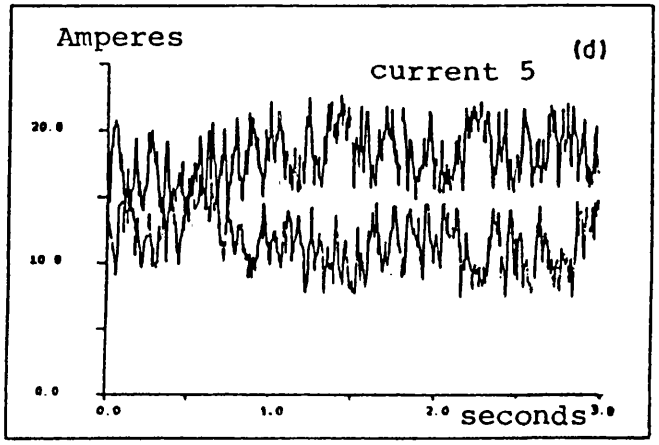

Figure 7.5.4 Simulation results for system 2 including standing current due to sloped track

(a) Side position

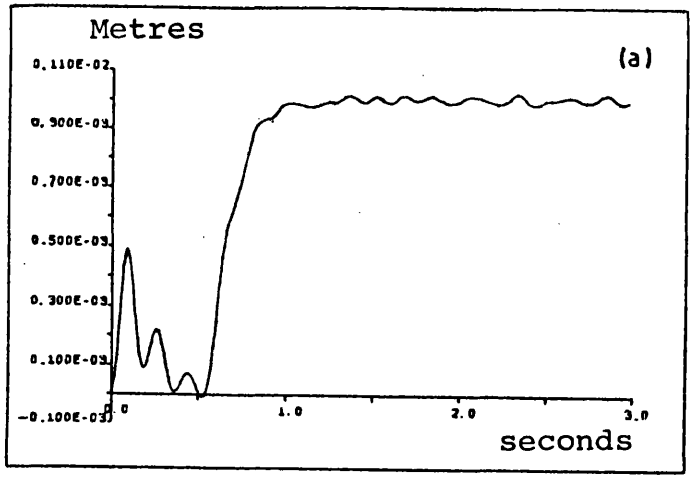

(b) Side air gaps

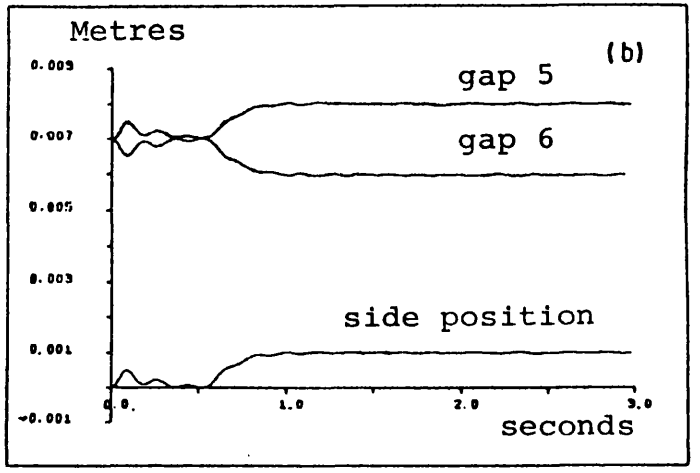

Simulation Results for
K = 25,000 I_o = 0·0

(c) Side velocity

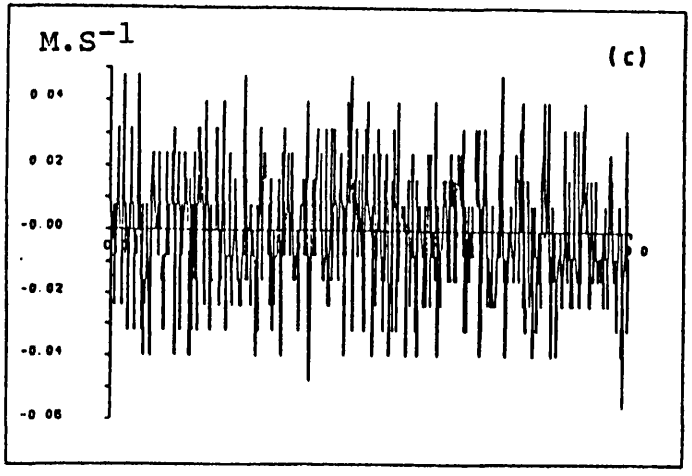

(d) Side magnet current

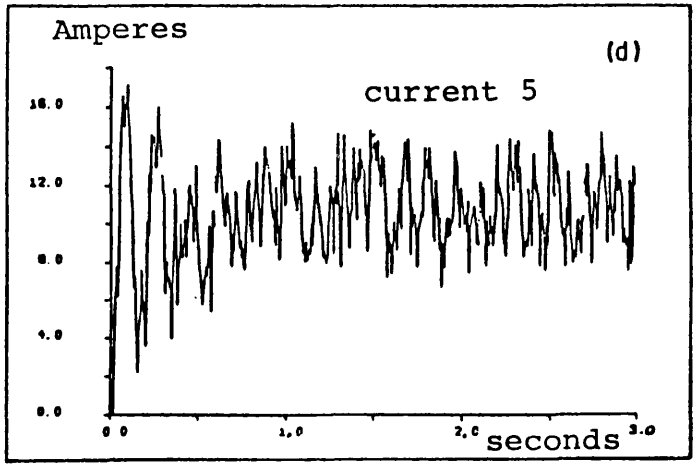

Figure 7.5.5 Simulation results for system 3 including standing current due to sloped track

(a) Side position

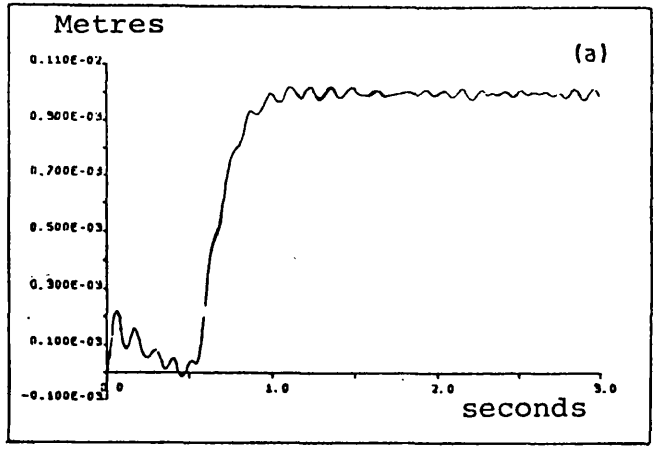

(b) Side air gaps

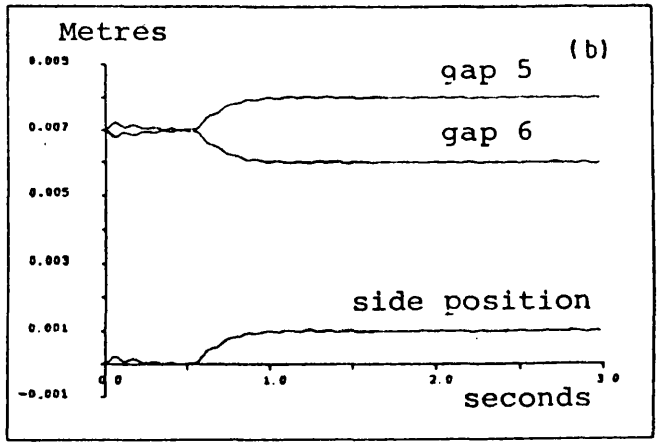

Simulation Results for
K=50,000 $I_o = 0{\cdot}0$

(c) Side velocity

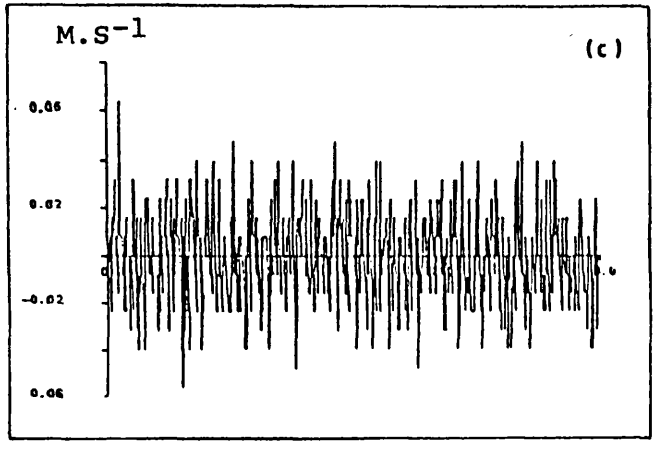

(d) Side magnet current

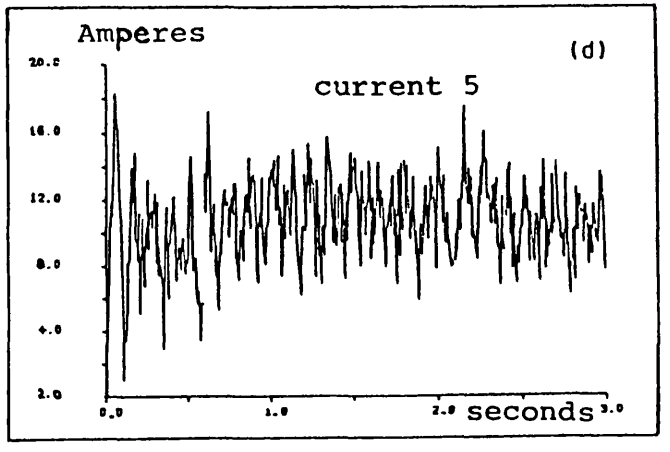

Figure 7.5.6 Simulation results for system 4 including standing current due to sloped track

(a) Side position

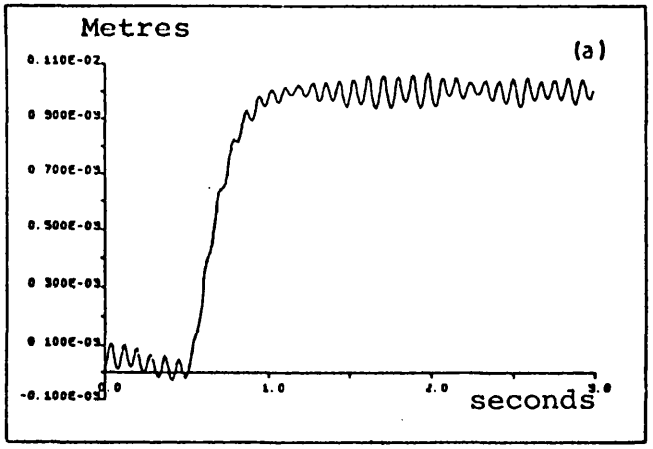

(b) Side air gaps

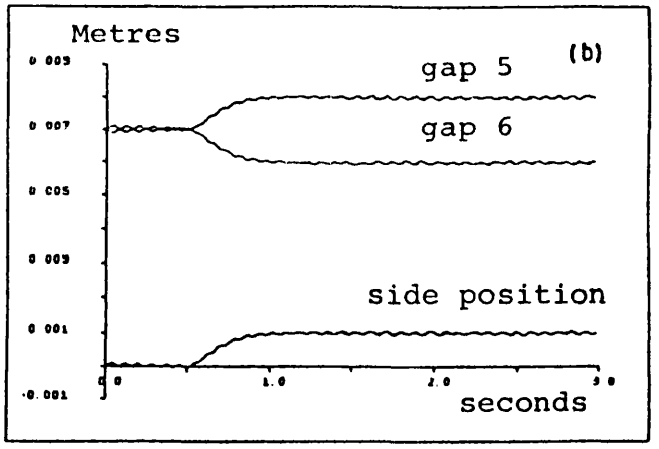

Simulation Results for
K = 100,000 I_o = 0·0

(c) Side velocity

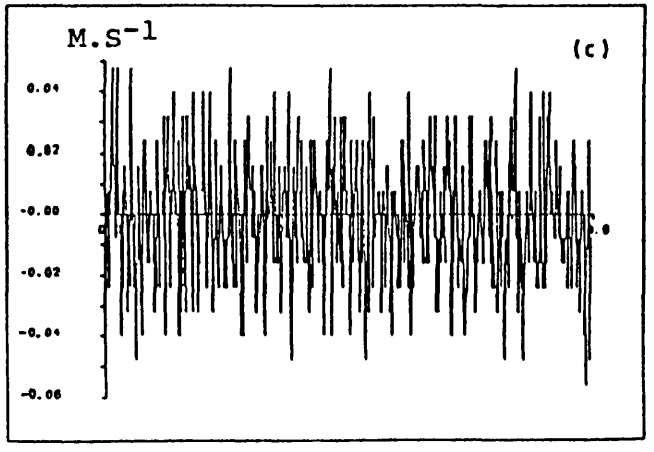

(d) Side magnet current

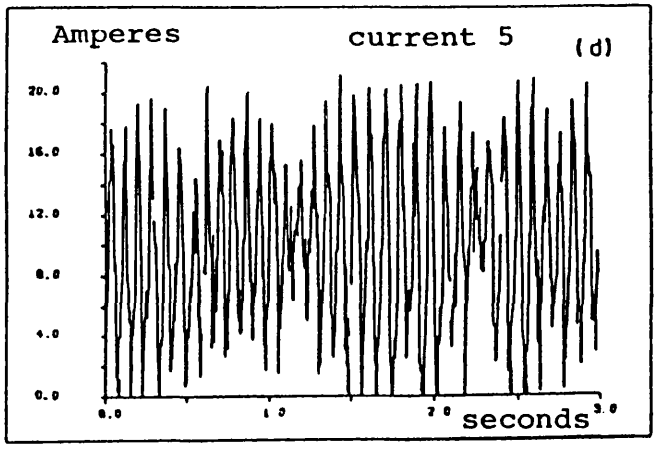

Figure 7.5.7 Simulation results for system 5 including standing current due to sloped track

(a) Side position

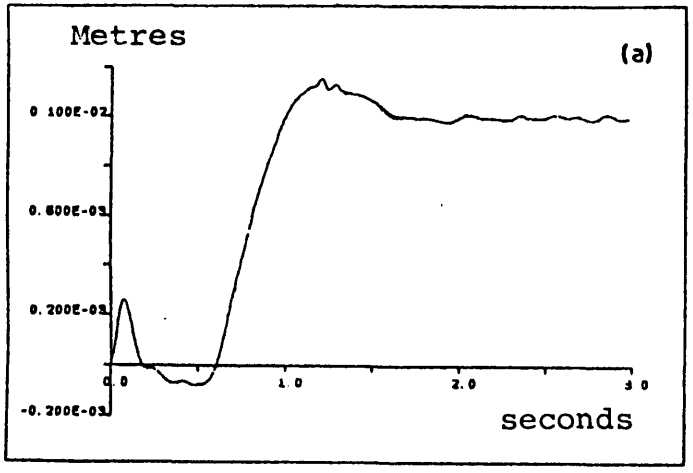

(b) Side air gaps

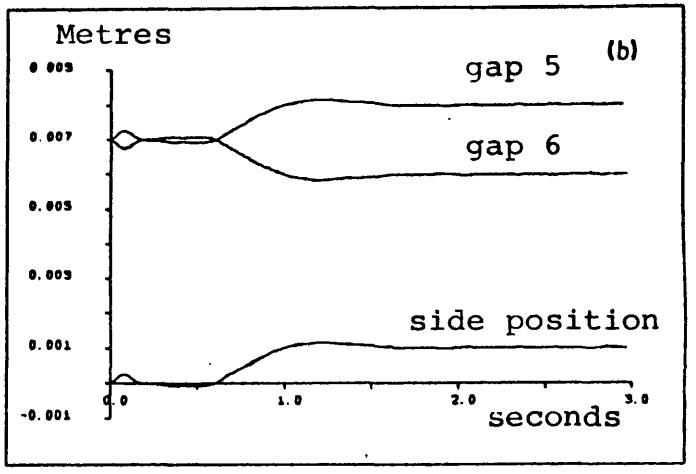

Simulation Results for

$K = 7,630 \quad I_o = 0{\cdot}0$

(c) Side velocity

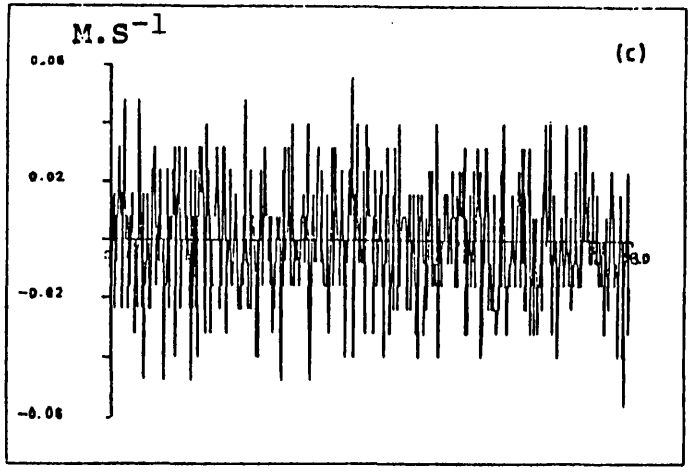

(d) Side magnet current

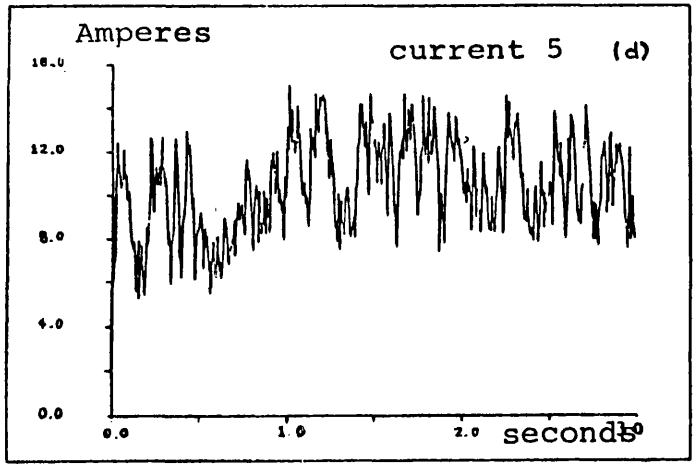

Figure 7.5.8 Simulation results for system 6 including standing current due to sloped track

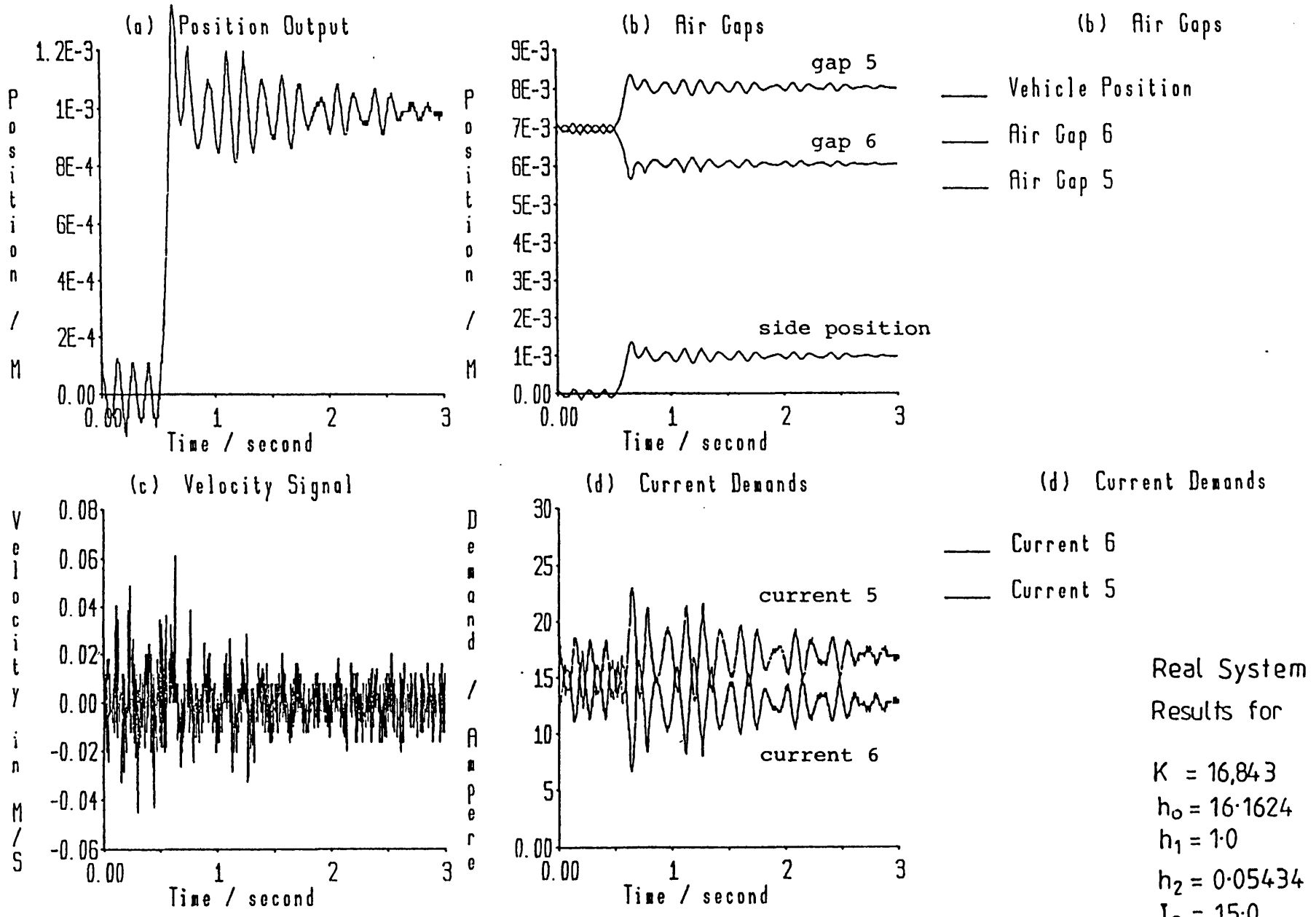

Figure 7.5.9 Real system results for system 1 including standing current due to sloped track

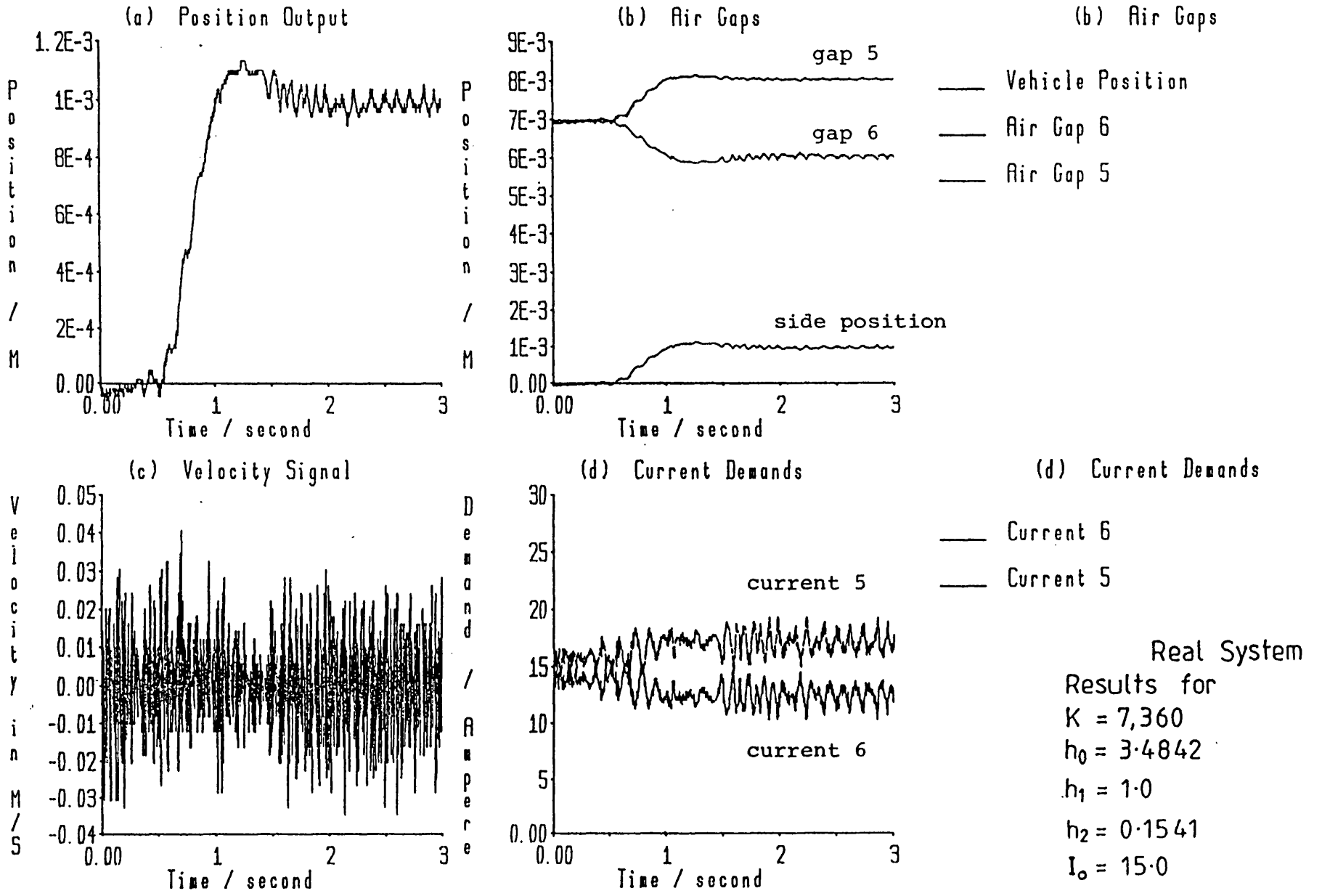

Figure 7.5.10 Real system results for system 2 including standing current due to sloped track

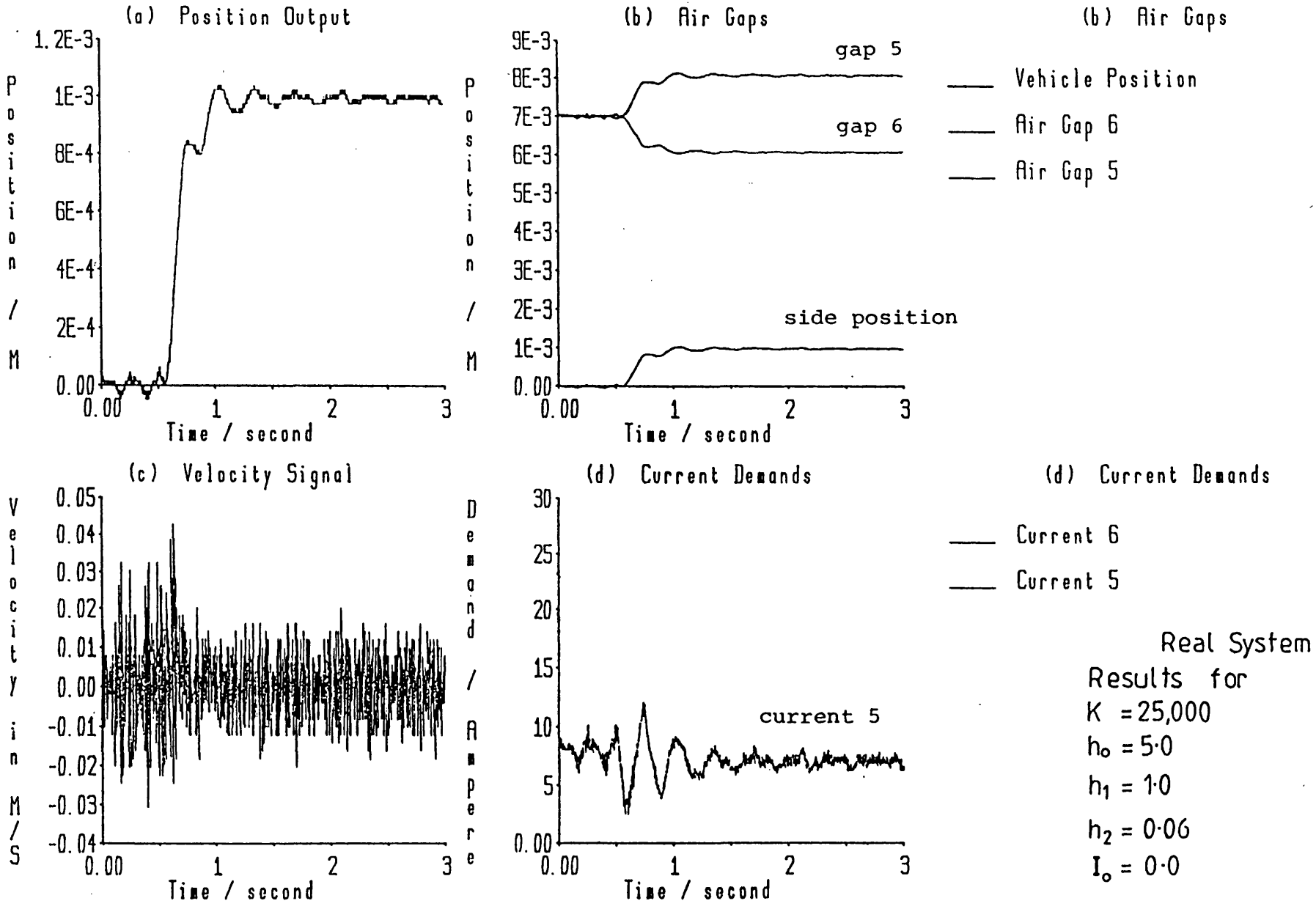

Figure 7.5.11 Real system results for system 3 including standing current due to sloped track

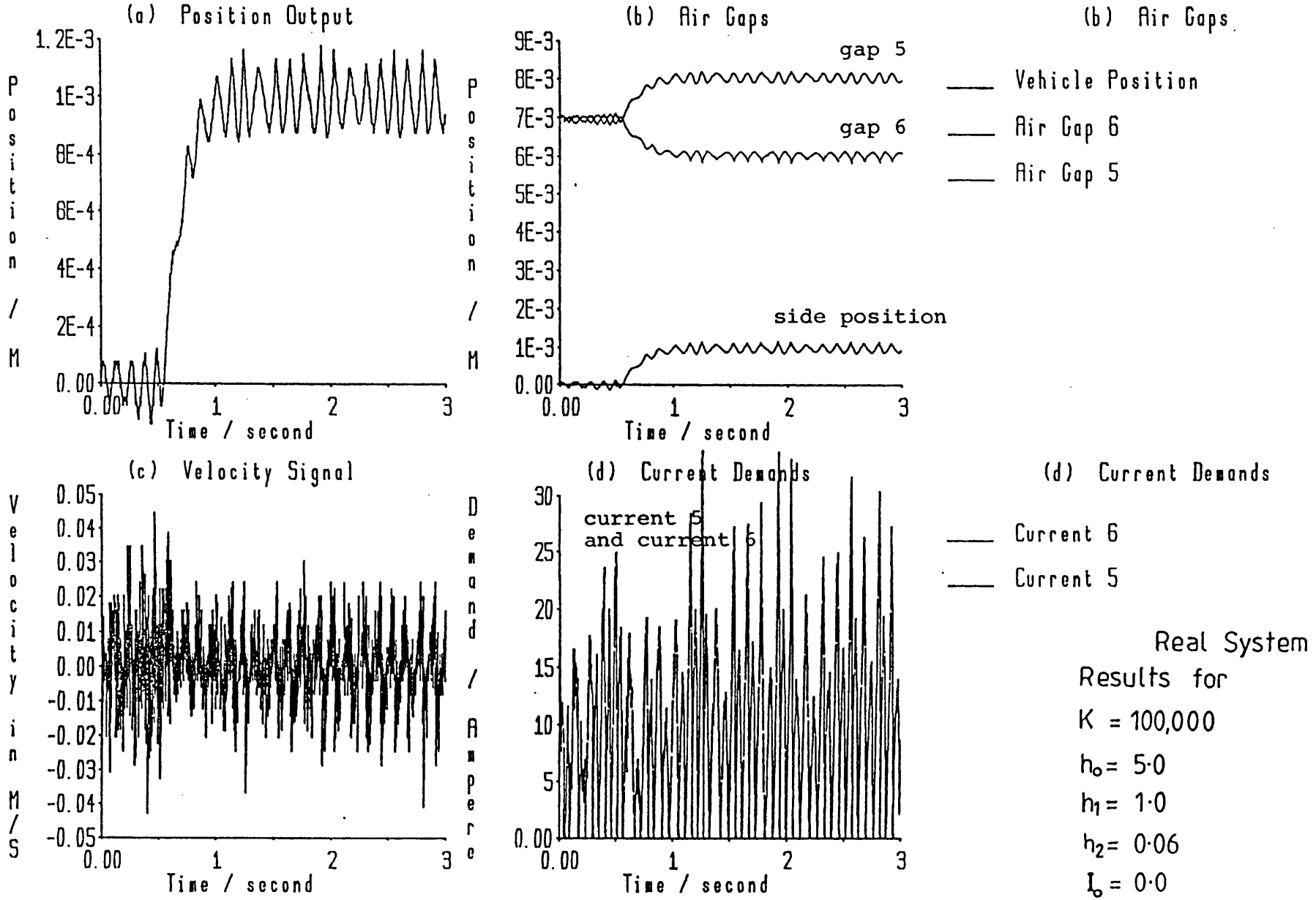

Figure 7.5.12 Real system results for system 5 including standing current due to sloped track

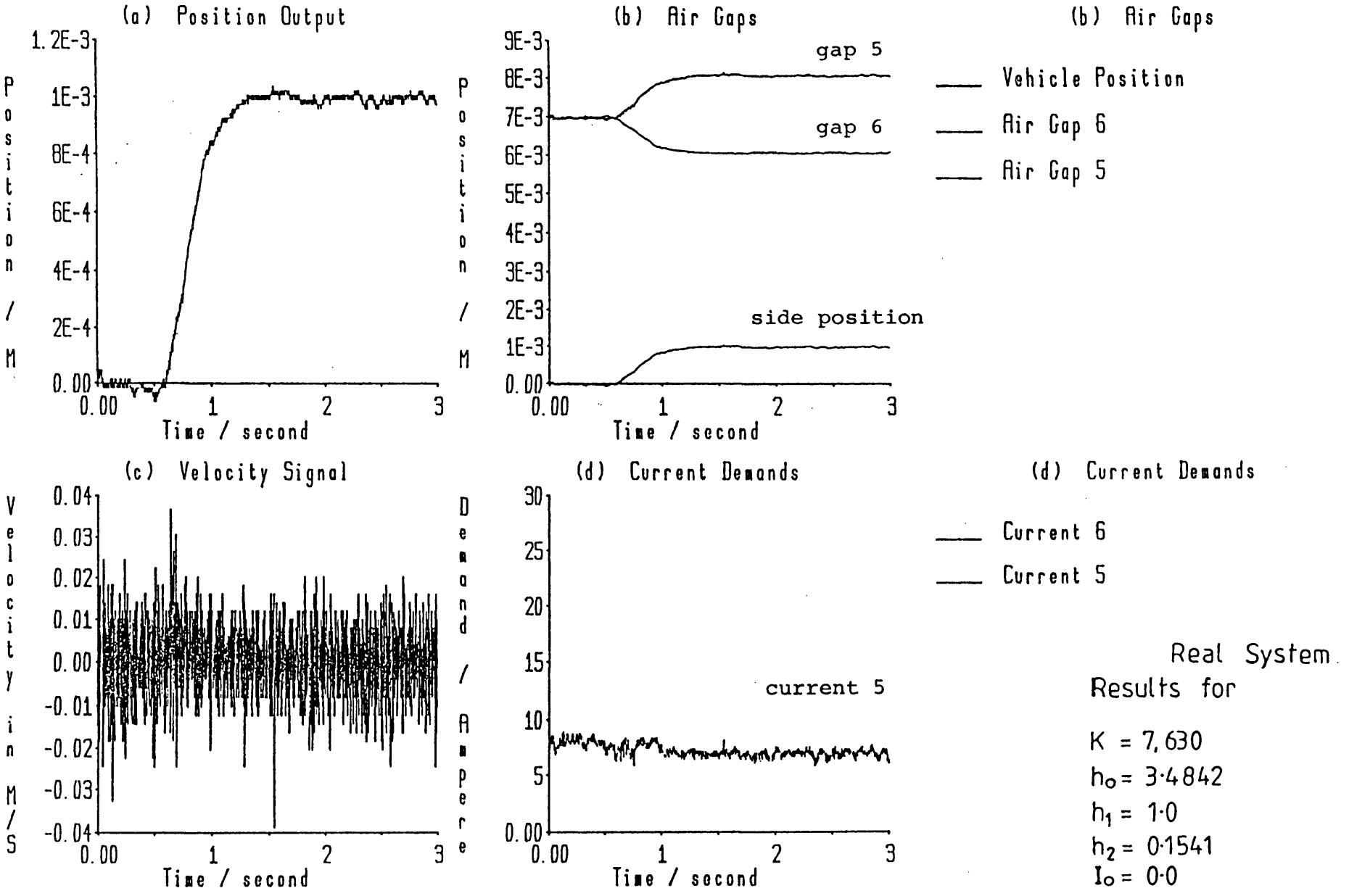

Figure 7.5.13 Real system results for system 6 including standing current due to sloped track

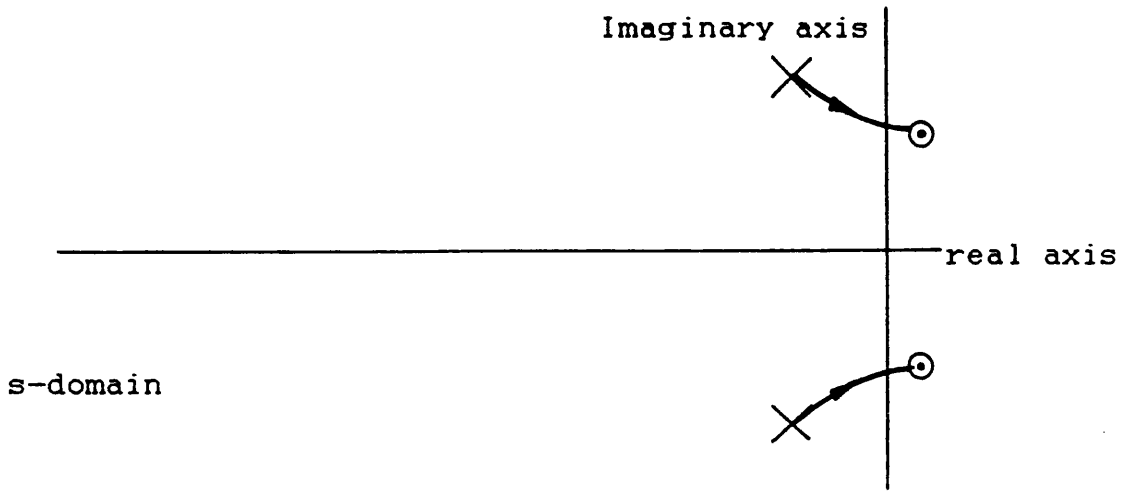

Figure 7.5.14 Root locus showing the effect of using high gain controllers in systems with flexible side rails

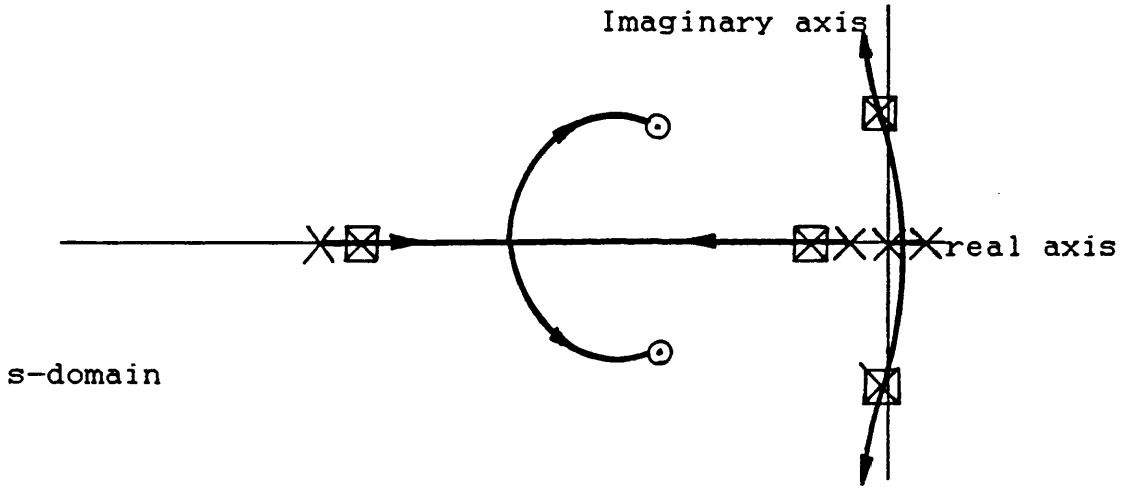

Figure 7.5.15 Root locus showing the effect of using low gain controllers in systems with zero standing current

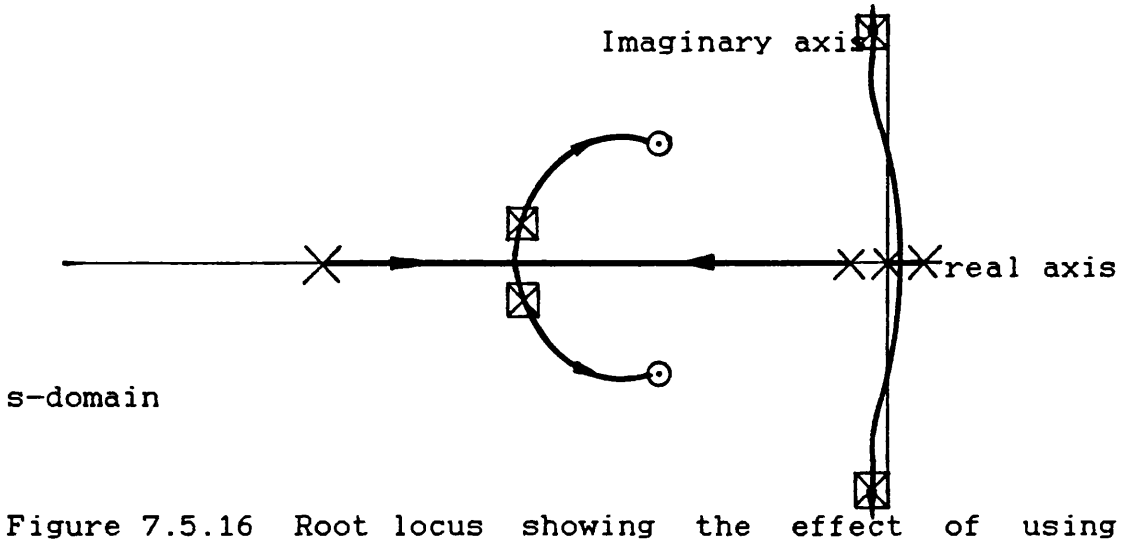

Figure 7.5.16 Root locus showing the effect of using a moderate gain gives a higher damped second dominated system